frontiers | Research Topics

Mineral solubilizing microorganisms (MSM) and their applications in nutrient availability, weathering and bioremediation

Edited by
Muhammad Zahid Mumtaz, Maqshoof Ahmad, Hassan Etesami and Adnan Mustafa

Published in
Frontiers in Microbiology
Frontiers in Soil Science

ISSN 1664-8714
ISBN 978-2-83251-618-8
DOI 10.3389/978-2-83251-618-8

About Frontiers

Frontiers is more than just an open access publisher of scholarly articles: it is a pioneering approach to the world of academia, radically improving the way scholarly research is managed. The grand vision of Frontiers is a world where all people have an equal opportunity to seek, share and generate knowledge. Frontiers provides immediate and permanent online open access to all its publications, but this alone is not enough to realize our grand goals.

Frontiers journal series

The Frontiers journal series is a multi-tier and interdisciplinary set of open-access, online journals, promising a paradigm shift from the current review, selection and dissemination processes in academic publishing. All Frontiers journals are driven by researchers for researchers; therefore, they constitute a service to the scholarly community. At the same time, the *Frontiers journal series* operates on a revolutionary invention, the tiered publishing system, initially addressing specific communities of scholars, and gradually climbing up to broader public understanding, thus serving the interests of the lay society, too.

Dedication to quality

Each Frontiers article is a landmark of the highest quality, thanks to genuinely collaborative interactions between authors and review editors, who include some of the world's best academicians. Research must be certified by peers before entering a stream of knowledge that may eventually reach the public - and shape society; therefore, Frontiers only applies the most rigorous and unbiased reviews. Frontiers revolutionizes research publishing by freely delivering the most outstanding research, evaluated with no bias from both the academic and social point of view. By applying the most advanced information technologies, Frontiers is catapulting scholarly publishing into a new generation.

What are Frontiers Research Topics?

Frontiers Research Topics are very popular trademarks of the *Frontiers journals series*: they are collections of at least ten articles, all centered on a particular subject. With their unique mix of varied contributions from Original Research to Review Articles, Frontiers Research Topics unify the most influential researchers, the latest key findings and historical advances in a hot research area.

Find out more on how to host your own Frontiers Research Topic or contribute to one as an author by contacting the Frontiers editorial office: frontiersin.org/about/contact

Mineral solubilizing microorganisms (MSM) and their applications in nutrient availability, weathering and bioremediation

Topic editors

Muhammad Zahid Mumtaz — The University of Lahore, Pakistan
Maqshoof Ahmad — The Islamia University of Bahawalpur, Pakistan
Hassan Etesami — University of Tehran, Iran
Adnan Mustafa — Brno University of Technology, Czechia

Citation

Mumtaz, M. Z., Ahmad, M., Etesami, H., Mustafa, A., eds. (2023). *Mineral solubilizing microorganisms (MSM) and their applications in nutrient availability, weathering and bioremediation*. Lausanne: Frontiers Media SA. doi: 10.3389/978-2-83251-618-8

Table of contents

frontiers | Frontiers in Microbiology

TYPE Editorial
PUBLISHED 24 January 2023
DOI 10.3389/fmicb.2023.1101426

OPEN ACCESS

EDITED AND REVIEWED BY
Jesús Navas-Castillo,
IHSM La Mayora (CSIC), Spain

*CORRESPONDENCE
Hassan Etesami
✉ hassanetesami@ut.ac.ir
Muhammad Zahid Mumtaz
✉ zahidses@gmail.com

SPECIALTY SECTION
This article was submitted to Microbe and Virus Interactions with Plants, a section of the journal Frontiers in Microbiology

RECEIVED 17 November 2022
ACCEPTED 11 January 2023
PUBLISHED 24 January 2023

CITATION
Mumtaz MZ, Ahmad M, Etesami H and Mustafa A (2023) Editorial: Mineral solubilizing microorganisms (MSM) and their applications in nutrient availability, weathering and bioremediation. *Front. Microbiol.* 14:1101426. doi: 10.3389/fmicb.2023.1101426

Editorial: Mineral solubilizing microorganisms (MSM) and their applications in nutrient availability, weathering and bioremediation

Muhammad Zahid Mumtaz[1]*, Maqshoof Ahmad[2], Hassan Etesami[3]* and Adnan Mustafa[4,5,6]

[1]Institute of Molecular Biology and Biotechnology, The University of Lahore, Lahore, Pakistan, [2]Department of Soil Science, The Islamia University of Bahawalpur, Bahawalpur, Pakistan, [3]Department of Soil Science, College of Agriculture and Natural Resources, University of Tehran, Tehran, Iran, [4]Faculty of Chemistry, Institute of Chemistry and Technology of Environmental Protection, University of Technology, Brno, Czechia, [5]Department of Agrochemistry, Soil Science, Microbiology and Plant Nutrition, Faculty of AgriSciences, Mendel University in Brno, Brno, Czechia, [6]Faculty of Science, Institute for Environmental Studies, Charles University in Prague, Prague, Czechia

KEYWORDS

plant-microbe interactions, mineral-microbe interactions, minerals solubilization, nutrients availability, bioremediation

Editorial on the Research Topic
Mineral solubilizing microorganisms (MSM) and their applications in nutrient availability, weathering and bioremediation

As the world's human population continues to grow, agricultural needs for future food supply will be one of the greatest challenges facing the agricultural community. In other words, agriculture is essential to achieve food security. Chemical fertilizers and pesticides have become a necessity in plant production to fulfill the rapid rise in population and, as a result, the increased nutritional needs. However, the unwanted and indiscriminate use of these fertilizers/pesticides causes many problems and has a negative impact on agricultural production in many countries today. In addition, soil pollution by chemical fertilizers, pesticides and heavy metals is a threat to the environment and food security due to the rapid growth of industry and agriculture and disruption of natural ecosystems by human pressures related to human population growth. Heavy metal pollution also poses many risks to the ecosystem and humans, affecting the safety of the food chain, food quality, and the ability to use land for agricultural production, which in turn affects food security. To meet this challenge, a lot of effort focusing on soil biological system and agro-ecosystem as a whole is needed to enable a better understanding of the complex processes and interactions among soil, plant and microorganisms governing the sustainability of agricultural land. Plant-associated microorganisms play a key role in solubilizing mineral substrates and contribute to the release of key nutrients from primary minerals and make essential plant elements available in soil, enhancing crop productivity (Etesami and Adl, 2020). In addition, these beneficial microbes are also involved in the degradation and/or detoxification of organic and inorganic compounds (bioremediation) present in the ecosystem (Etesami, 2018). Hence, introducing such a phytomicrobiome into the agricultural industry is an effective approach as a result of its long-term and environmentally favorable mechanisms to increase plant growth and preserve plant health and quality. In recent years, low-cost and environmentally friendly agricultural practices have received increasing attention.

This Research Topic, *Mineral-solubilizing microorganisms and their applications in nutrient availability, weathering and bioremediation*, presents one review paper and 12 original research papers, from 11 different countries (88 authors), and has papers that span the field of mineral-solubilizing microorganisms research, gives insight into ongoing topics, and provides a basis for further study on *Mineral-solubilizing microorganisms and their applications in nutrient availability, weathering and bioremediation*. Here, we summarized some of the highlights derived from the 13 articles published in this Research Topic.

Phosphorus (P) is one of the major plant nutrients, lack of which limits plant growth. Most agricultural soils contain large reserves of total P. Both P fixation and precipitation occur in soil because of the large reactivity of phosphate ions with numerous soil constituents. Developing microbial inoculants containing phosphate-solubilizing bacteria (PSB) represents an emerging biological solution to improve rhizosphere P availability (Etesami, 2020). In addition to PSB, the association of plants with mycorrhizal fungi defines a strategy to cope with P limitation (Plassard and Dell, 2010). The results of the study of Schreider et al. also provided evidence that an ectomycorrhiza has the potential to occupy fundamental niches of various P sources differing in their bioavailability, indicating that being a generalist in P nutrition can facilitate adaptation to various nutritional settings in soil.

Most publications describing isolation of PSB employed tricalcium phosphate. According to Bashan et al. (2013), tricalcium phosphate is relatively weak and unreliable as a universal selection factor for isolating and testing PSB for enhancing plant growth. A practical approach to screen true PSB is to use a combination of two or three metal-P compounds together. Janati et al. assessed several PSB strains' ability to enhance solubilization activity from rock phosphate, tricalcium phosphate, and their combination. The results of these researchers showed that the isolated bacteria had the ability to dissolve different sources of P both individually and in combination. It has been reported that the results obtained from the effect of PSB/plant growth promoting rhizobacteria (PGPR) on plant growth under axenic conditions could not be reproduced under field conditions (Smyth et al., 2011; Bashan et al., 2013). This might be occurred due to the low quality of the inoculums and/or the inability of the PSB/PGPR to compete with the indigenous population (Catroux et al., 2001) and to survive under stressful conditions (Etesami and Maheshwari, 2018). Janati et al. showed that the isolated PSB also were resistant to salinity, acidity, drought, and temperature stress, which can be used in stressful environments. Another reasons for the poor performance of agricultural bio-inocula in natural environments and in the rhizosphere of host plants could be the use of a single bacterial strain (van Veen et al., 1997). Khan M. Y. et al. showed that a multi-strain consortium of PGPR could be more effective to combat the salinity stress owing to the presence of a variety of plant growth-promoting traits (e.g., ACC-deaminase, phosphate solubilization, exopolysaccharides and siderophore). Compared to the well-known role of bacterial auxin hormone in increasing plant growth and resistance to stress, in the study of Zaheer et al., it was also found that bacterial cytokinin hormone also plays a significant role in plant growth.

It is known that rock/minerals weathering is the result of a combination of physical, chemical, and biological weathering, with organisms, particularly microorganisms, playing an important role in the early rock weathering process (Liu et al., 2020). Chen et al. provided new insights into the weathering process of carbonate rocks.

Zinc (Zn) is one of the most abundantly found heavy metals in the Earth's crust and is reported to be an essential trace metal required for the growth of living beings. However, its essentiality also runs parallel to its toxicity, which is induced through various anthropogenic sources, constant exposure to polluted sites, and other natural phenomena. Hussain et al. reviewed Zn and its properties, uses, bioavailability, toxicity, as well as the major mechanisms involved in its bioremediation from polluted soil and wastewaters. Dietary essential micronutrient (Zn, Fe, and Se) deficiency also affects a high percentage of the world population with significant health impacts. Microbial-assisted biofortification is a novel concept in the field of agricultural microbiology for nutrifying crop edibles. In the study of Upadhayay et al., the application of zinc-solubilizing bacteria caused an elevated Zn amount in the rice grain.

It has been a challenge to decontaminate industrial wastewater and soil from heavy metals and organic pollutants. Different strategies have been designed and implemented for their removal, including filtration, oxidation/reduction, reverse osmosis and electro-chemical treatment among many others, but are not the favored option due to their cost, inefficiency, and intense labor (Algieri et al., 2021). The use of bacteria possessing the ability to degrade organic pollutants, to immobilize heavy metals in soil and to promote plant growth, as single or in combination with plants, is an efficient and environmentally sustainable strategy to remediate organic pollutant and heavy metal-contaminated soils. Alotaibi et al. demonstrated that the combination of PGPR and the petroleum hydrocarbons (PHC) degradation potential of bacteria can result in an enhanced beneficial effect in phytoremediation management, which could lead to the development of innovative bacterial inoculants for plants to remediate PHC-contaminated soils. In the study of Khan M. et al., the potential of a copper (Cu)-resistant bacterium (*Bacillus altitudinis* MT422188) to remove Cu from polluted wastewater was investigated. Due to having some special features, *B. altitudinis* MT422188 was introduced as an efficient biosorbent for Cu that can be employed for Cu remediation. Xue et al. remedied copper-rich water bodies by using two-step biomineralization approach (i.e., securing the urease activity and modifying pH conditions).

In the study of Batool et al., the use of bacterial and fungal strains and zinc and iron-enriched rice husk biochar also resulted in maximum chromium [Cr(VI)] adsorption from wastewater applied to the soil by various mechanisms. In addition to bacteria and fungi, thermoacidophilic archaea also have a promising potential in bioleaching operations and metal recycling processes in regard to circular economies and waste management as investigated by Kölbl et al. To study microbial-assisted phytoremediation, the understanding the changes in the microbial community structure and the relationship between microbial community and soil environment is of utmost importance. Liu et al. studied microbial-assisted phytoremediation by exploring soil bacterial community. Their results showed that the diverse bacterial community is the result of adaptation to environmental changes.

Author contributions

All authors listed have made a substantial, direct, and intellectual contribution to the work and approved it for publication.

Conflict of interest

The authors declare that the research was conducted in the absence of any commercial or financial relationships that could be construed as a potential conflict of interest.

Publisher's note

References

Algieri, C., Chakraborty, S., and Candamano, S. (2021). A way to membrane-based environmental remediation for heavy metal removal. *Environments* 8, 52. doi: 10.3390/environments8060052

Bashan, Y., Kamnev, A. A., and De-Bashan, L. E. (2013). Tricalcium phosphate is inappropriate as a universal selection factor for isolating and testing phosphate-solubilizing bacteria that enhance plant growth: a proposal for an alternative procedure. *Biol. Fertil. Soil* 49, 465–479. doi: 10.1007/s00374-012-0737-7

Catroux, G., Hartmann, A., and Revellin, C. (2001). Trends in rhizobial inoculant production and use. *Plant Soil* 230, 21–30. doi: 10.1023/A:1004777115628

Etesami, H. (2018). Bacterial mediated alleviation of heavy metal stress and decreased accumulation of metals in plant tissues: mechanisms and future prospects. *Ecotoxicol. Environ. Saf.* 147, 175–191. doi: 10.1016/j.ecoenv.2017.08.032

Etesami, H. (2020). "Enhanced phosphorus fertilizer use efficiency with microorganisms," in *Nutrient Dynamics for Sustainable Crop Production*, ed R. S. Menna (Singapore: Springer), 215–245.

Etesami, H., and Adl, S. M. (2020). "Plant growth-promoting rhizobacteria (PGPR) and their action mechanisms in availability of nutrients to plants," in *Phyto-Microbiome in Stress Regulation*, eds M. Kumar, V. Kumar, and R. Prasad (Singapore: Springer), 147–203.

Etesami, H., and Maheshwari, D. K. (2018). Use of plant growth promoting rhizobacteria (PGPRs) with multiple plant growth promoting traits in stress agriculture: Action mechanisms and future prospects. *Ecotoxicol. Environ. Saf.* 156, 225–246. doi: 10.1016/j.ecoenv.2018.03.013

Liu, X., Koestler, R. J., Warscheid, T., Katayama, Y., and Gu, J.-D. (2020). Microbial deterioration and sustainable conservation of stone monuments and buildings. *Nat. Sustain.* 3, 991–1004. doi: 10.1038/s41893-020-00602-5

Plassard, C., and Dell, B. (2010). Phosphorus nutrition of mycorrhizal trees. *Tree Physiol.* 30, 1129–1139. doi: 10.1093/treephys/tpq063

Smyth, E. M., Mccarthy, J., Nevin, R., Khan, M. R., Dow, J. M., O'gara, F., et al. (2011). *In vitro* analyses are not reliable predictors of the plant growth promotion capability of bacteria; a Pseudomonas fluorescens strain that promotes the growth and yield of wheat. *J. Appl. Microbiol.* 111, 683–692. doi: 10.1111/j.1365-2672.2011.05079.x

van Veen, J. A., Van Overbeek, L. S., and Van Elsas, J. D. (1997). Fate and activity of microorganisms introduced into soil. *Microbiol. Mol. Biol. Rev.* 61, 121–135. doi: 10.1128/mmbr.61.2.121-135.1997

frontiers in Microbiology

ORIGINAL RESEARCH
published: 29 March 2022
doi: 10.3389/fmicb.2022.863702

In-Depth Characterization of Plant Growth Promotion Potentials of Selected Alkanes-Degrading Plant Growth-Promoting Bacterial Isolates

*Fahad Alotaibi[1,2], Marc St-Arnaud[1] and Mohamed Hijri[1,3]**

[1]*Institut de Recherche en Biologie Végétale, Département de Sciences Biologiques, Université de Montréal, Montréal, QC, Canada,* [2]*Department of Soil Science, King Saud University, Riyadh, Saudi Arabia,* [3]*African Genome Center, Mohammed VI Polytechnic University (UM6P), Ben Guerir, Morocco*

OPEN ACCESS

Edited by:
Muhammad Zahid Mumtaz, University of Lahore, Pakistan

Reviewed by:
Muhammad Yahya Khan, University of Agriculture Faisalabad, Pakistan
Muhammad Saqlain Zaheer, Khawaja Freed University of Engineering and Information Technology, Pakistan
Ashraf Kariminik, Islamic Azad University Kerman, Iran

***Correspondence:**
Mohamed Hijri
mohamed.hijri@umontreal.ca

Specialty section:
This article was submitted to Terrestrial Microbiology, a section of the journal Frontiers in Microbiology

Received: *27 January 2022*
Accepted: *24 February 2022*
Published: *29 March 2022*

Citation:
Alotaibi F, St-Arnaud M and Hijri M (2022) In-Depth Characterization of Plant Growth Promotion Potentials of Selected Alkanes-Degrading Plant Growth-Promoting Bacterial Isolates. Front. Microbiol. 13:863702. doi: 10.3389/fmicb.2022.863702

The use of plant growth-promoting rhizobacteria (PGPR) as a bioremediation enhancer in plant-assisted phytoremediation requires several steps, consisting of the screening, selection, and characterization of isolates. A subset of 50 bacterial isolates representing a wide phylogenetic range were selected from 438 morphologically different bacteria that were originally isolated from a petroleum hydrocarbon (PHC)-polluted site of a former petrochemical plant. Selected candidate bacteria were screened using six conventional plant growth-promoting (PGP) traits, complemented with the genetic characterization of genes involved in alkane degradation, as well as other pertinent functions. Finally, the bacterial isolates were subjected to plant growth promotion tests using a gnotobiotic approach under normal and stressed conditions. Our results indicated that 35 bacterial isolates (70%) possessed at least four PGP traits. Twenty-nine isolates (58%) were able to utilize *n*-hexadecane as a sole carbon source, whereas 43 isolates (86%) were able to utilize diesel as the sole carbon source. The presence of catabolic genes related to hydrocarbon degradation was assessed using endpoint PCR, with the alkane monooxygenase (*alkB*) gene found in 34 isolates, the cytochrome P450 hydroxylase (*CYP153*) gene found in 24 isolates, and the naphthalene dioxygenase (*nah1*) gene found to be present in 33 isolates. Thirty-six strains (72%) promoted canola root elongation in the growth pouch assay. After several rounds of screening, seven bacterial candidates (individually or combined in a consortium) were tested for canola root and shoot growth promotion in substrates amended by different concentrations of *n*-hexadecane (0%, 1%, 2%, and 3%) under gnotobiotic conditions. Our results showed that *Nocardia* sp. (WB46), *Pseudomonas plecoglossicida* (ET27), *Stenotrophomonas pavanii* (EB31), and *Gordonia amicalis* (WT12) significantly increased the root length of canola grown in 3% *n*-hexadecane compared with the control treatment, whereas *Nocardia* sp. (WB46) and *Bacillus megaterium* (WT10) significantly increased shoot length compared to control treatment at the same concentration of *n*-hexadecane. The consortium had a significant enhancement effect on root length compared to all isolates inoculated individually or to the control. This study demonstrates that the combination of PGPR traits and the PHC degradation

potential of bacteria can result in an enhanced beneficial effect in phytoremediation management, which could lead to the development of innovative bacterial inoculants for plants to remediate PHC-contaminated soils.

Keywords: PGPR, alkanes, rhizoremediation, plant growth promotion, bioinoculants, 1-aminocyclopropane-1-carboxylate deaminase

INTRODUCTION

Human activities related to the petroleum and gas industry, such as exploration, extraction, refining, storage, and shipping, are polluting soil and water environments with petroleum hydrocarbons (PHCs; Alotaibi et al., 2021a). Aliphatic hydrocarbons (alkanes) are saturated hydrocarbons, representing the main constituents of crude oil, and are major soil contaminants (Chénier et al., 2003; Stroud et al., 2007). Alkanes are major soil pollutants, characterized by low chemical activity, low water solubility, and higher activation energies (Labinger and Bercaw, 2002; Rojo, 2009). Hexadecane ($C_{16}H_{34}$) is present in the aliphatic fraction of crude oil and is a main component of diesel fuel (Chénier et al., 2003). Hexadecane has been used as a model compound to study alkane biodegradation because of its presence in many diesel-contaminated soils and its well-characterized biodegradability (Chénier et al., 2003; Tara et al., 2014; Shiri et al., 2015; Balseiro-Romero et al., 2017a; Garrido-Sanz et al., 2019). The presence of these compounds in the environment adversely affects plant, animal, and human health (Arslan et al., 2014). Thus, the remediation of alkane-contaminated environments is a primary goal in the field of environmental biotechnology.

The use of the usual physical and chemical methods to cope with PHC contamination have shown many limitations (Alotaibi et al., 2021a). These conventional approaches are very expensive, only work for specific organic compounds and do not often result in the complete degradation of the contaminants; in addition, they are not environmentally friendly as they contribute to greenhouse gas emissions (Kuiper et al., 2004; Pilon-Smits, 2005; Behera, 2014). On the other hand, a biological method such as phytoremediation that relies on the plant–microbe partnership is a promising strategy for the remediation of soils contaminated with aliphatic hydrocarbons. Phytoremediation requires less maintenance effort, minimizes site disturbances, and is a cost-effective and less destructive approach (Alotaibi et al., 2021a).

Plants, due to their exudates, metabolite diversity and enzymatic machinery, can adapt and alleviate stressful conditions such as the presence of hydrocarbons in soil (Pilon-Smits, 2005). However, plant growth and biomass production are often limited under such harsh conditions and subsequently phytoremediation efficiency is reduced and plant mortality is increased (Glick and Stearns, 2011). Plant growth-promoting rhizobacteria (PGPR) can be used to enhance plant growth in stressful conditions, thus enhancing phytoremediation efficiency (Tara et al., 2014; Balseiro-Romero et al., 2017a; Oleńska et al., 2020). PGPR can alleviate stress in plants and reduce the phytotoxicity of hydrocarbons *via* many mechanisms, such as reducing soil nutrient deficiencies (fixing nitrogen, solubilizing phosphorus, and enhancing iron uptake), synthesizing plant growth-promoting (PGP) hormones, suppressing ethylene production *via* 1-aminocyclopropane-1-carboxylate (ACC) deaminase (ACCD) activity (Schlaeppi and Bulgarelli, 2015; Backer et al., 2018; Oleńska et al., 2020), and by virtue of their pollutant-degrading pathways and metabolic activities (Arslan et al., 2014; Xu et al., 2018).

The development of a database and collection of bacterial isolates characterized for PGP traits and hexadecane degradation potential can assist in the selection of the most promising strains for further advancement as bioaugmentation inoculants in phytoremediation strategies for diesel-contaminated soils. In this study, 50 bacterial strains were selected from 438 morphologically different bacteria that were isolated from bulk and rhizosphere soils of plants growing in a petrochemical site contaminated with PHCs (Alotaibi et al., 2021b). The strains were selected based on the fact that they covered a wide phylogenetic affiliation range, their ability to possess various PGP activities and their wide-spectrum hydrocarbon degradation potential. We hypothesize that combined traits of PGP and hexadecane degradation potential occur in bacteria isolated from an aged petroleum-hydrocarbon polluted site. The specific objectives of this study were: to define and compare the PGP traits of selected bacterial strains qualitatively and quantitatively; to test their ability to utilize 1% (v/v) sterilized *n*-hexadecane and 1% (v/v) diesel as a sole carbon source; to screen for the presence of the stress tolerance gene (*acdS*) encoding ACCD and the dinitrogenase reductase gene (*nifH*) encoding (nitrogen fixation); to search for the presence of hydrocarbon-degrading genes (*alkB*, *CYP153*, and *nah*); and to assess their plant growth promotion potential under gnotobiotic conditions in growth pouches. The outcome of this study can be an effective approach for the developing integrated microbial inoculants for bioremediation biotechnology applications.

MATERIALS AND METHODS

Bacterial Strains

The 50 bacterial strains used in this study are a subset of a larger collection of 438 morphologically different bacteria isolated from bulk soil and the rhizosphere of *Salix purpurea* and *Eleocharis obtusa* plants growing in a site highly polluted with petroleum-hydrocarbons (Alotaibi et al., 2021b). This site is in Varennes, Quebec, Canada (45°43 N, 73°22 W), with an allocated area of approximately 5,000 m^2. These bacterial strains were selected based on their phylogenetic affiliations to cover major bacterial lineages in order to increase taxonomic, genetic and functional

TABLE 1 | List of bacterial isolates used in this study.

Isolation code	Environmental niche	Isolation medium[a]	Phylum/Family	NCBI taxonomic identity (accession number)
ST4	Bulk soil	1/10TSA	Actinobacteria/Nocardiaceae	*Rhodococcus ruber* (MZ430450)
ST15	Bulk soil	1/10TSA	Gammaproteobacteria/Pseudomonadaceae	*Pseudomonas* sp. (MZ430461)
ST25	Bulk soil	1/10TSA	Gammaproteobacteria/Xanthomonadaceae	*Stenotrophomonas nitritireducens* (MZ430471)
ST45	Bulk soil	1/10TSA	Actinobacteria/Gordoniaceae	*Gordonia amicalis* (MZ430491)
SB26	Bulk soil	B–H_amended diesel	Actinobacteria/Rhodobacteraceae	*Paracoccus* sp. (MZ430412)
SB32	Bulk soil	B–H_amended diesel	Actinobacteria/Microbacteriaceae	*Microbacterium hatanonis* (MZ430418)
SB36	Bulk soil	B–H_amended diesel	Gammaproteobacteria/Moraxellaceae	*Acinetobacter pittii* (MZ430422)
SB38	Bulk soil	B–H_amended diesel	Gammaproteobacteria/Pseudomonadaceae	*Pseudomonas stutzeri* (MZ430424)
SB39	Bulk soil	B–H_amended diesel	Actinobacteria/Microbacteriaceae	*Microbacterium oxydans* (MZ430425)
SB41	Bulk soil	B–H_amended diesel	Gammaproteobacteria/Moraxellaceae	*Acinetobacter* sp. (MZ430427)
SB45	Bulk soil	B–H_amended diesel	Gammaproteobacteria/Pseudomonadaceae	*Pseudomonas mosselii* (MZ430431)
SB49	Bulk soil	B–H_amended diesel	Betaproteobacteria/Oxalobacteraceae	*Massilia oculi* (MZ430435)
SB50	Bulk soil	B–H_amended diesel	Alphaproteobacteria/Sphingomonadaceae	*Sphingobium yanoikuyae* (MZ430436)
ET5	*Eleocharis* rhizosphere	1/10TSA	Actinobacteria/Microbacteriaceae	*Microbacterium testaceum* (MZ430211)
ET10	*Eleocharis* rhizosphere	1/10TSA	Alphaproteobacteria/Rhizobiaceae	*Rhizobium selenitireducens* (MZ430216)
ET25	*Eleocharis* rhizosphere	1/10TSA	Firmicutes/Bacillaceae	*Bacillus marisflavi* (MZ430231)
ET27	*Eleocharis* rhizosphere	1/10TSA	Gammaproteobacteria/Pseudomonadaceae	*Pseudomonas plecoglossicida* (MZ430233)
ET33	*Eleocharis* rhizosphere	1/10TSA	Betaproteobacteria/Comamonadaceae	*Delftia lacustris* (MZ430239)
ET46	*Eleocharis* rhizosphere	1/10TSA	Gammaproteobacteria/Yersiniaceae	*Serratia* sp. (MZ430252)
ET49	*Eleocharis* rhizosphere	1/10TSA	Gammaproteobacteria/Enterobacteriaceae	*Enterobacter bugandensis* (MZ430255)
EB6	*Eleocharis* rhizosphere	B–H_amended diesel	Betaproteobacteria/Burkholderiaceae	*Chitinimonas taiwanensis* (MZ430152)
EB26	*Eleocharis* rhizosphere	B–H_amended diesel	Gammaproteobacteria/Aeromonadaceae	*Aeromonas hydrophila* (MZ430172)
EB31	*Eleocharis* rhizosphere	B–H_amended diesel	Gammaproteobacteria/Xanthomonadaceae	*Stenotrophomonas pavanii* (MZ430177)
EB35	*Eleocharis* rhizosphere	B–H_amended diesel	Betaproteobacteria/Comamonadaceae	*Comamonas odontotermitis* (MZ430181)
EB37	*Eleocharis* rhizosphere	B–H_amended diesel	Actinobacteria/Microbacteriaceae	*Lysinimonas* sp. (MZ430183)
EB43	*Eleocharis* rhizosphere	B–H_amended diesel	Gammaproteobacteria/Pseudomonadaceae	*Pseudomonas entomophila* (MZ430189)
WT8	*Salix* rhizosphere	1/10TSA	Actinobacteria/Streptomycetaceae	*Streptomyces atriruber* (MZ430334)
WT10	*Salix* rhizosphere	1/10TSA	Firmicutes/Bacillaceae	*Bacillus megaterium* (MZ430336)
WT12	*Salix* rhizosphere	1/10TSA	Actinobacteria/Gordoniaceae	*Gordonia amicalis* (MZ430338)
WT17	*Salix* rhizosphere	1/10TSA	Gammaproteobacteria/Pseudomonadaceae	*Pseudomonas kilonensis* (MZ430343)
WT19	*Salix* rhizosphere	1/10TSA	Actinobacteria/Micrococcaceae	*Pseudarthrobacter siccitolerans* (MZ430345)
WT34	*Salix* rhizosphere	1/10TSA	Actinobacteria/Micrococcaceae	*Arthrobacter* sp. (MZ430360)
WT39	*Salix* rhizosphere	1/10TSA	Actinobacteria/Streptomycetaceae	*Streptomyces atratus* (MZ430365)
WB17	*Salix* rhizosphere	B–H_amended diesel	Actinobacteria/Micrococcaceae	*Paenarthrobacter nitroguajacolicus* (MZ430283)
WB23	*Salix* rhizosphere	B–H_amended diesel	Betaproteobacteria/Comamonadaceae	*Variovorax paradoxus* (MZ430289)
WB25	*Salix* rhizosphere	B–H_amended diesel	Alphaproteobacteria/Sphingomonadaceae	*Sphingomonas sanxanigenens* (MZ430291)
WB31	*Salix* rhizosphere	B–H_amended diesel	Gammaproteobacteria/Pseudomonadaceae	*Pseudomonas frederiksbergensis* (MZ430297)
WB40	*Salix* rhizosphere	B–H_amended diesel	Actinobacteria/Micrococcaceae	*Pseudarthrobacter siccitolerans* (MZ430306)
WB46	*Salix* rhizosphere	B–H_amended diesel	Actinobacteria/Nocardiaceae	*Nocardia* sp. (MZ430312)
WB48	*Salix* rhizosphere	B–H_amended diesel	Actinobacteria/Nocardiaceae	*Streptomyces umbrinus* (MZ430314)
WB49	*Salix* rhizosphere	B–H_amended diesel	Actinobacteria/Nocardioidaceae	*Nocardioides alpinus* (MZ430315)
WB51	*Salix* rhizosphere	B–H_amended diesel	Actinobacteria/Gordoniaceae	*Nocardia asteroides* (MZ430317)
WB54	*Salix* rhizosphere	B–H_amended diesel	Actinobacteria/Intrasporangiaceae	*Phycicoccus bigeumensis* (MZ430320)
SA7	Bulk soil	ACCD	Gammaproteobacteria/Enterobacteriaceae	*Pantoea agglomerans* (MZ430101)
EA5	*Eleocharis* rhizosphere	ACCD	Gammaproteobacteria/Enterobacteriaceae	*Klebsiella oxytoca* (MZ430073)
EA9	*Eleocharis* rhizosphere	ACCD	Gammaproteobacteria/Enterobacteriaceae	*Enterobacter cancerogenus* (MZ430077)
EA21	*Eleocharis* rhizosphere	ACCD	Actinobacteria/Microbacteriaceae	*Curtobacterium* sp. (MZ430089)
WA8	*Salix* rhizosphere	ACCD	Gammaproteobacteria/Erwiniaceae	*Raoultella terrigena* (MZ430128)
WA19	*Salix* rhizosphere	ACCD	Gammaproteobacteria/Enterobacteriaceae	*Citrobacter* sp. (MZ430139)
WA25	*Salix* rhizosphere	ACCD	Gammaproteobacteria/Pseudomonadaceae	*Pseudomonas thivervalensis* (MZ430145)

[a]*Isolation media abbreviations: B–H_amended diesel, Bushnell–Haas medium amended with 1% diesel; TSA, Trypticase Soy Agar; and ACCD, 1-aminocyclopropane-1-carboxylate (ACC) deaminase enrichment culture method.*

diversities. The identification of bacterial strains was performed using Sanger sequencing of the 16S rRNA gene, as described in Alotaibi et al. (2021b). The isolation source and the species affiliations of bacterial strains used in this study are summarized in **Table 1**. The bacterial strains were stored at −80°C.

Stock cultures were preserved in 20% glycerol at −80°C. When reviving bacteria, isolates were cultured in 50 ml of 1/2 strength Trypticase Soy Broth (TSB) (Difco Laboratories Inc. Detroit, Michigan, United States) at room temperature for 48 h with continuous agitation at 150 rpm on a gyratory shaker.

Screening for *in vitro* PGP Characteristics

Phosphate Solubilization

The inorganic phosphate solubilization activity of bacterial isolates was determined using both qualitative and quantitative assays as

described in Nautiyal (1999). In the qualitative assay using solid agar plates, fresh pure bacterial isolates were grown in half-strength TSB at 28°C for 48 h with continuous agitation at 150 rpm in a rotary shaker. Then, 10 µl of growing bacterial culture was spot-inoculated into the center of NBRIP (the National Botanical Institute's phosphate growth medium) agar plates containing tri-calcium phosphate as the sole inorganic phosphate source (Nautiyal, 1999). The NBRIP agar plates were incubated at 28°C for 14 days and a clear zone around inoculated colonies indicated the solubilization of inorganic phosphate. The test was replicated three times.

In the quantitative liquid assay, a loopful of pure bacterial isolates growing on 1/10 Trypticase Soy Agar (TSA) plates were inoculated into 125-ml Erlenmeyer flasks containing 50 ml freshly sterilized liquid NBRIP medium supplemented with tri-calcium phosphate as the sole inorganic phosphate source. The cultures were grown at 28°C under continuous agitation at 150 rpm in a rotary shaker for up to 14 days. Five-milliliter aliquots were centrifuged at 10,000 g for 10 min, and the supernatant was filtered through a 0.2-µm Millipore filter and used for soluble P determination using ammonium molybdate reagent (Fiske and Subbarow, 1925). The blue-color compound was measured by reading the absorbance at 650 nm using a multimode microplate spectrophometer against a standard curve KH_2PO_4. The test was replicated three times.

Indole-3-Acetic Acid Production

The production of IAA by bacterial isolates was determined using both qualitative and quantitative assays as described in Patten and Glick (2002). Bacterial isolates were first cultured overnight in 5 ml of DF salts minimal medium, and then 20 µl aliquots were transferred into 15-ml Falcon tubes containing 5 ml of DF salts minimal medium supplemented with tryptophan (1 mg ml^{-1}) as auxin precursor. Cultures were grown in a shaker (120 rpm) for 48 h at 28°C. One-milliliter aliquots of bacterial cultures were then centrifuged at 9,500 g for 2 min and 100 µl of supernatant were added to a 96-well plate, followed by the addition of 100 µl of Salkowski's reagent, and the 96-well plate was incubated in the dark for 30 min at room temperature. Bacterial isolates producing IAA were characterized by the formation of a distinct red color. To quantify IAA produced by bacterial isolates, the absorbance was measured at 535 nm using a multimode microplate spectrophotometer against a standard curve of commercial IAA (Sigma-Aldrich, United States). The test was replicated three times.

Siderophore Syntheses

Siderophore production by bacterial isolates was determined qualitatively using the Chrome-Azurol S (CAS) assay as described in Alexander and Zuberer (1991). Pure bacterial isolates were grown in half-strength TSB at 28°C for 48 h with continuous agitation at 150 rpm in a rotary shaker, and 10 µl of the growing bacterial culture was spot-inoculated into the centers of CAS-agar plates. The CAS-agar plates were incubated at 28°C for 72 h, and bacterial isolates showing an orange halo were considered positive for siderophore synthesis (Schwyn and Neilands, 1987). The test was replicated three times.

Siderophore production quantification was estimated using the CAS-Shuttle assay performed in high-throughput mode using a 96-well format, as described in Payne (1994). Briefly, bacterial strains were inoculated into an iron-deficient MM9 medium to induce siderophore production and grown at 28°C under continuous agitation. After 48 h, 100 µl of cell-free supernatant was mixed with 100 µl of CAS dye and 2 µl of shuttle solution. The 96-well plate was incubated in the dark for 15 min, and the absorbance was measured at 630 nm using a multimode microplate spectrophotometer. The test was replicated three times.

Ammonia Production

The ammonia production by bacterial isolates was evaluated in both qualitative and quantitative assays as described in Cappuccino and Sherman (1992) and as outlined in Dutta et al. (2015). The qualitative estimation of ammonia production was carried out by inoculating fresh bacterial isolates into 10-ml test tubes of peptone water (peptone 10 g. L^{-1}; NaCl 5 g. L^{-1}; 1 L dH_2O), and bacterial cultures were incubated for 72 h at 28°C. Then, 1 ml aliquots of bacterial culture were transferred to 2 ml tubes and 50 µl of Nessler's reagent [10% HgI^2; 7% KI; 50% aqueous solution of NaOH (32%)] were added to each tube. A color change of the mix to yellow indicates ammonia production, with a weak yellow indicating of small amount of production and a deep yellow being a sign of the maximum capacity of ammonia production (Marques et al., 2010). To quantify ammonia production by bacterial isolates, the absorbance was measured at 450 nm against a standard curve of ammonium sulfate using a multimode microplate spectrophotometer. The test was replicated three times.

ACCD Activity

ACCD activity was assessed by monitoring the bacterial isolate's ability to grow on DF minimal salts medium containing ACC as a sole nitrogen source (Penrose and Glick, 2003). Pure bacterial isolates were grown in half-strength TSB at 28°C for 48 h under continuous agitation at 150 rpm in a rotary shaker. A loopful of each bacterial isolate growing in liquid culture was streaked into a DF minimal salts agar plate containing 3 mM ACC solution, which was spread into the agar plate immediately prior to use. Plates were incubated at 28°C for up to 1 week. The presence of growth in the DF-ACC agar plates was considered positive. Bacterial strains were classified using a rating scale as follows: −, no growth; +, slightly growth; ++, moderate growth; and +++, heavy growth. The test was replicated three times.

ACCD activity was also confirmed *via* PCR amplification of the *acdS* gene (Blaha et al., 2006). More details regarding procedure and PCR conditions are given below.

Nitrogen Fixation

Bacterial isolates were evaluated regarding their capacity to grow on an N-deficient combined carbon medium (Rennie, 1981). Bacterial cultures were grown in half-strength TSB at 28°C for 48 h under continuous agitation at 150 rpm in a rotary

shaker. A loopful of each bacterial isolate growing in liquid culture was streaked into the N-deficient combined carbon medium agar plate and incubated at 28°C for up to 1 week. The presence of growth in the agar plates was considered positive. Bacterial strains were classified using a rating scale as follows: −, no growth; +, slightly growth; ++, moderate growth; and +++, heavy growth. The test was replicated three times.

Nitrogen fixation activity was also confirmed using PCR amplification of the *nifH* gene (Rösch et al., 2002). More details regarding the procedure and PCR conditions are given below.

Catabolic Gene Detection Using PCR Amplifications

PCR analysis was used to assess the presence of hydrocarbon-degrading genes and PGPR genes in bacterial isolates selected in this study. Primers used to detect the presence of genes and PCR conditions are presented in **Supplementary Table S1**.

PCR reactions for the analysis of the *alkB* gene were performed in a reaction volume of 25 µl, which consisted of 1× PCR Buffer (Qiagen, Toronto, Canada), 0.8 µM of each primer, 0.2 mM of dNTP mix, 0.5 mM of $MgCl_2$, 0.2 mg ml^{-1} of BSA (Amersham Biosciences, Mississauga, Canada), 1.25 U of *Taq* DNA polymerase (Qiagen, Toronto, Canada), and 1 µl purified genomic DNA (Kloos et al., 2006). For the detection of the *CYP153* gene, PCR reactions were prepared as for the *alkB* gene (Wang et al., 2010). In addition, PCR *nah* gene detection was conducted as previously described in Baldwin et al. (2003). Briefly, PCR analyses were performed in a reaction volume of 25 µl, which consisted of 1× PCR buffer, 0.5 µM of each primer, 1 µl of dNTP (Qiagen, Toronto, Canada), 0.5 mM of $MgCl_2$, 0.2 mg ml^{-1} of BSA, 1 U of *Taq* DNA polymerase, and 1 µl purified genomic DNA. For the detection of the *acdS* gene, PCR reactions were prepared as for the *nah* gene (Blaha et al., 2006). Finally, for the detection of the *nifH* gene, PCRs were performed in a reaction volume of 25 µl of 1× PCR buffer, 0.5 µM of each primer, 0.5 µl of dNTP, 0.5 µl of $MgCl_2$, 0.2 mg ml^{-1} of BSA, 1 U of *Taq* DNA polymerase, and 1 µl purified genomic DNA (Rösch et al., 2002).

The presence and length of PCR products were verified by electrophoresis with GelRed-stained 1.5% agarose gels using the Gel-Doc system (Bio-Rad Laboratories, Mississauga, Canada).

PGP Potential of Bacterial Isolates Under Gnotobiotic Conditions

Inoculum Preparation

Bacterial isolates (**Table 1**) were first grown in fresh 1/10 TSA plates and incubated for 72–96 h at 28°C. Then, pure colonies of each isolate were inoculated separately into a 500 ml Erlenmeyer flask containing 250 ml half-strength TSB medium. Bacterial isolates were incubated on a rotary shaker (150 rpm) at 28°C for 48 h (except for the following isolates, which were grown for up to 120 h at 28°C: *Rhodococcus ruber* ST4, *Sphingobium yanoikuyae* SB50, *Lysinimonas* sp. EB37, *Gordonia amicalis* WT12, *Sphingomonas* sp. WB25, *Nocardioides alpinus* WB49, *Gordonia* sp. WB51, and *Phycicoccus* sp. WB54). The optical density (OD) of bacterial cells was measured and adjusted to an OD_{600} value of 1. Bacterial suspensions were harvested *via* centrifugation (15 min at 5,000 g), washed three times in phosphate buffer saline (PBS; Difco Laboratories, Detroit, United States), and resuspended in 20 ml sterile tap water. Serial dilutions were then prepared in PBS and spread on 1/10 TSA plates, and incubated at 28°C for 72 h. This yielded cell densities of approximately 10^9 (colony-forming units) cfu ml^{-1}.

Seed Inoculation

Canola (cv. 4,187 RR) seeds were surface-sterilized by washing with ethanol (95% $v.v^{-1}$) for 30 s, followed by soaking in NaClO (2.5% $v.v^{-1}$) for 10 min under constant gentle shaking (Hynes et al., 2008). Seeds were rinsed with sterile distilled water 10 times in order to remove excess sodium hypochlorite. The seeds were then air-dried by placing them in a biosafety cabinet for 24 h. Sub-samples of surface-sterilized seeds were picked randomly and placed onto 1/10-strength TSA plates and incubated at 28°C for 24 h to further check for any contamination. Surface-sterilized seeds were soaked in 5 ml of bacterial suspension for 4 h with gentle shaking in a rotary shaker to allow the bacteria to penetrate into the seeds. For the control treatment (without bacterial inoculum), seeds were soaked in 5 ml autoclaved distilled H_2O.

Root Elongation Assay

The root elongation assays were conducted under gnotobiotic conditions using growth pouches as previously described in Lifshitz et al. (1987). Seed growth pouches (16.5 cm × 18 cm) containing chromatographic filter paper (Mega International, Minneapolis, United States) were filled with 10 ml of sterile half-strength N-free Hoagland's nutrient solution, wrapped in aluminum foil and sterilized at 121°C for 20 min prior to seeding. Ten seeds soaked in the bacterial suspension were aseptically sown inside the growth pouches and five replicate pouches were used for each treatment and for the control. After seed germination, pouches were thinned to five seeds per pouch. The pouches were wrapped with Saran plastic wrap to minimize the loss of moisture and covered with aluminum foil to prevent light from reaching plant roots. The moisture content was kept constant during the time course of the experiment *via* additions of sterile distilled water and half-strength N-free Hoagland nutrient solution, on an alternative day's basis, using aseptic techniques. The seeds were grown in growth pouches for 7 days at 28°C, with a 16/8 h day/night cycle, before the root measurements were taken.

Growth of Bacterial Isolates in MSM With (1%) *n*-Hexadecane and (1%) Diesel

Bacterial isolates were tested for their ability to utilize either 1% (v/v) filter-sterilized *n*-hexadecane or 1% (v/v) diesel in mineral salt medium (MSM) by measuring the cell density at 600 nm. Bacterial isolates were first grown in half-strength TSB at 28°C for 48 h with continuous agitation at 150 rpm. Then,

cells were collected *via* centrifugation, washed three times with PBS, and resuspended in sterile dH_2O, and 10 µl was used to inoculate MSM amended with 1% *n*-hexadecane or 1% diesel. The assay was carried out in 125 ml Erlenmeyer flasks containing 50 ml sterile MSM and the *n*-hexadecane or diesel as carbon source, incubated at 28°C under continuous agitation at 150 rpm on a rotary shaker. After a week, cells growth was measured at 600 nm and compared with a control containing no carbon source. The experiment was carried out in triplicate.

Gnotobiotic Assay Under Alkane Stress Conditions

Seven candidates that performed well in different assays were selected and tested gnotobiotically for their plant growth promotion potential under different concentrations of *n*-hexadecane (0%, 1%, 2%, and 3%).

The bacterial strains tested in this experiment were *Acinetobacter* sp. strain SB41, *Pseudomonas putida* strain ET27, *Stenotrophomonas maltophilia* strain EB31, *Bacillus megaterium* strain WT10, *G. amicalis* strain WT12, *Arthrobacter* sp. strain WT19, and *Nocardia* sp. strain WB46. The bacterial inoculum was prepared as described above.

The experiment was performed utilizing growth pouches as described above, with modifications. The ability of bacterial strains to enhance plant growth under alkane stress conditions was tested by including different concentrations of *n*-hexadecane (0%, 1%, 2%, and 3%) in the sterile half-strength N-free Hoagland nutrient solution in the growth pouches. Briefly, 10 seeds soaked in the bacterial suspension were aseptically sown inside the growth pouches and five replicated pouches were used for each treatment and control. After seed germination, pouches were thinned to five seeds per pouch. The pouches were wrapped with Saran plastic wrap to minimize the loss of moisture and covered with aluminum foil to prevent light from reaching the plant roots. The seeds were grown in growth pouches for 7 days at 28°C, with a 16/8 h day/night cycle, before the root and shoot measurements were made.

Growth of Bacterial Isolates on Different Concentrations of *n*-Hexadecane

The growth of bacterial strains was measured in sterile 50 ml MSM medium containing different concentrations of *n*-hexadecane (1%, 2%, and 3%) as the carbon source in 125 ml Erlenmeyer flasks. Bacterial cultures were grown as described in above and then the bacterial cultures were incubated at 28°C under continuous agitation at 150 rpm on a rotary shaker. Bacterial growth was determined by measuring the cell density at 600 nm every day for up to 7 days. Non-inoculated control treatments were included at each concentration. The experiment was carried out in triplicate.

Statistical Analyses

The growth pouch study was carried out in a completely randomized design. In the first growth pouch study, the data were presented as means and SDs, and the difference between treatments compared to the control were analyzed using Dunnett's test ($p = 0.05$). In the second growth pouch experiment, the differences between treatments were analyzed using one-way ANOVA at a 5% significance level with Tukey's *post-hoc* test, using JMP software (SAS Institute Inc. Cary, NC, United States). A Venn diagram was generated using *InteractiVenn* software (Heberle et al., 2015).

RESULTS

PGP Traits of Bacterial Isolates

A total of 50 bacterial isolates were screened for six different PGP traits and the presence of two genes encoding nitrogenase (*nifH*) and ACCD (*acdS*). The results of screening tests are shown in **Table 2**. Fourteen strains (28%) were able to solubilize calcium phosphate in the liquid medium (**Table 2**). Among these, several strains showed excellent P solubilization ability. *B. megaterium* strain WT10 showed the highest solubilization activity with 690.86 µg ml^{-1} calcium phosphate (**Table 2**), followed by *G. amicalis* strain WT12, *Curtobacterium* sp. strain EA21, and *Pseudomonas fluorescens* strain WT17, which were able to solubilize 567.12 µg ml^{-1}, 525.4 µg ml^{-1}, and 476.48 µg ml^{-1} calcium phosphate, respectively (**Table 2**).

Out of 50 bacterial strains, 34 strains (68%) were able to produce IAA after 48 h of incubation with a 1 mg ml^{-1} supplement of tryptophan as an auxin precursor (**Table 2**). Three bacterial strains showed the highest IAA production among all the strains, specifically *Rhizobium* sp. strain ET10, *Curtobacterium* sp. strain EA21, and *Klebsiella* sp. EA5, which produced 44.31 µg ml^{-1}, 44.13 µg ml^{-1}, and 31.32 µg ml^{-1} IAA, respectively (**Table 2**).

Twenty-four bacterial strains (48%) were able to synthesize siderophores (**Table 2**). The maximum production of siderophores by bacterial strains were observed in *Pseudomonas putida* strain ET27, *Enterobacter* sp. strain EA9, *Pseudomonas stutzeri* strain SB38, *Enterobacter cancerogenus* strain ET49, and *Pseudomonas fluorescens* strain WT17, which produced around 29% or above of siderophore units (**Table 2**).

Most of the bacterial strains under investigation were able to produce ammonia (**Table 2**). Most bacterial isolates produced ammonia in the range of 5.00 to 10.50 µmol ml^{-1} (**Table 2**). Four bacterial strains showed the maximum ammonia production among the strains, namely, *Comamonas* sp. strain EB35, *Chitinimonas* sp. strain EB6, *Microbacterium oxydans* strain SB39, and *S. maltophilia* strain EB31 (**Table 2**).

All bacterial isolates were further screened qualitatively for ACCD and N fixation, of which 34 isolates (68%) demonstrated ACCD activity and also showed the presence of an ACCD gene (*acdS*) (**Table 2**). Additionally, 28 isolates (56%) showed the ability to fix atmospheric N_2 and the presence of the N fixation gene (*nifH*) (**Table 2**).

Root Elongation Assay

The bacterial isolates were tested on canola root elongation under gnotobiotic conditions. The results indicated that the

TABLE 2 | Screening of selected bacterial strains for PGP traits.

Strain code	Identity	IAA production[a] ($\mu g\,ml^{-1}$)	Phosphate solubilization ($\mu g\,ml^{-1}$)	Siderophore production (%)	Ammonia production ($\mu mol\,ml^{-1}$)	ACC deaminase[b]	Nitrogen fixation[c]	PCR[d]	
								acdS	*nifH*
ST4	*Rhodococcus ruber*	25.93	–	–	9.59	+	+	+	+
ST15	*Pseudomonas* sp.	11.51	–	13.4	7.35	++	+	–	+
ST25	*Stenotrophomonas nitritireducens*	21.48	–	7.6	9.81	+++	–	+	–
ST45	*Gordonia amicalis*	–	–	–	–	++	+++	+	+
SB26	*Paracoccus* sp.	–	–	–	9.47	–	–	–	–
SB32	*Microbacterium hatanonis*	–	–	9.16	7.39	++	+++	–	–
SB36	*Acinetobacter pittii*	–	420.36	22.3	–	+++	+	+	+
SB38	*Pseudomonas stutzeri*	13.78	–	32.1	8.11	–	–	+	–
SB39	*Microbacterium oxydans*	6.51	–	8.2	12.51	++	–	–	–
SB41	*Acinetobacter* sp.	4.39	369.28	–	7.25	+++	++	–	+
SB45	*Pseudomonas mosselii*	19.10	–	12.3	6.42	+++	+++	+	+
SB49	*Massilia oculi*	7.67	–	17.1	7.36	–	–	–	–
SB50	*Sphingobium yanoikuyae*	15.34	–	–	5.93	++	++	+	+
ET5	*Microbacterium testaceum*	11.01	–	–	8.23	–	–	–	–
ET10	*Rhizobium selenitireducens*	44.31	–	26.7	9.05	–	+++	–	+
ET25	*Bacillus marisflavi*	–	–	–	8.61	+++	–	–	–
ET27	*Pseudomonas plecoglossicida*	11.80	424.68	36.4	7.07	+++	+++	+	+
ET33	*Delftia lacustris*	5.05	–	–	–	+++	–	+	–
ET46	*Serratia* sp.	13.47	381.51	24.8	7.06	++	+	–	+
ET49	*Enterobacter bugandensis*	9.18	–	31.1	8.59	++	++	–	+
EB6	*Chitinimonas taiwanensis*	–	–	–	13.05	++	–	–	–
EB26	*Aeromonas hydrophila*	1.67	–	–	10.50	–	–	–	–
EB31	*Stenotrophomonas pavanii*	29.44	380.79	19.6	11.46	++	+	–	+
EB35	*Comamonas odontotermitis*	–	–	14.9	13.95	+	–	+	+
EB37	*Lysinimonas* sp.	–	–	–	8.64	–	–	–	–
EB43	*Pseudomonas*	0.45	–	–	8.89	++	++	–	+
WT8	*entomophila*	0.53	72.16	–	9.16	–	–	–	–
WT10	*Streptomyces atriruber Bacillus*	–	690.86	–	9.27	–	–	–	–
WT12	*megaterium Gordonia amicalis*	0.45	567.12	–	7.97	++	+++	+	+
WT17	*Pseudomonas kilonensis*	8.41	476.48	29. 3	6.41	+++	++	+	+
WT19	*Pseudarthrobacter siccitolerans*	11.56	–	10.1	6.70	–	+	–	+
WT34	*Arthrobacter* sp.	10.32	–	–	10.34	–	–	–	–
WT39	*Streptomyces atratus*	–	–	–	5.0	–	–	–	–
WB17	*Paenarthrobacter nitroguajacolicus*	–	–	12.1	6.86	+++	++	+	+
WB23	*Variovorax paradoxus*	–	–	–	–	++	+++	+	+
WB25	*Sphingomonas sanxanigenens*	1.14	–	8.3	9.10	++	–	–	–
WB31	*Pseudomonas frederiksbergensis*	9.68	449.86	22.8	7.19	+++	++	+	+
WB40	*Pseudarthrobacter siccitolerans*	7.88	–	–	7.28	–	–	–	–
WB46	*Nocardia* sp.	1.46	–	8.2	6.67	–	–	–	–
WB48	*Streptomyces umbrinus*	–	–	–	9.05	++	+++	+	–
WB49	*Nocardioides alpinus*	8.49	–	–	9.71	–	–	–	–
WB51	*Nocardia asteroides*	–	–	–	8.60	++	++	+	+
WB54	*Phycicoccus bigeumensis*	0.24	72.16	–	9.35	–	–	–	–
SA7	*Pantoea agglomerans*	19.37	–	29.1	8.42	+++	–	+	–
EA5	*Klebsiella oxytoca*	31.32	–	18.7	7.85	+++	+++	+	+
EA9	*Enterobacter cancerogenus*	10.58	–	36.4	8.25	+++	+	+	+
EA21	*Curtobacterium* sp.	44.13	525.4	–	8.60	+++	+++	–	+
WA8	*Raoultella terrigena*	13.54	–	–	7.97	+++	++	+	+
WA19	*Citrobacter* sp.	–	338.35	–	8.42	+++	+	+	+
WA25	*Pseudomonas thivervalensis*	–	324.68	19.3	7.11	+++	+++	+	+

Values are means of three replicates ± SD. [a]*Indole-3-acetic acid.*

[b]*1-aminocyclopropane-1-carboxylate deaminase "–" means showed no growth on agar plates, "+" means showed low growth on agar plates, "++" means showed medium growth on agar plates, and "+++" means showed heavy growth on agar plates.*

[c]*The presence of growth in the agar plates was considered positive for nitrogen fixation, "–" means showed no growth on agar plates, "+" means showed low growth on agar plates, "++" means showed medium growth on agar plates, and"+++" means showed heavy growth on agar plates.*

[d]*"–" indicates the absence of PCR products and "+" indicates the presence of PCR products for the functional genes—acdS, ACCD gene and nifH, nitrogen fixation gene.*

highest canola root elongation effect was induced by the following bacterial isolates: *Curtobacterium* sp. EA21, *B. megaterium* WT10, and *Gordonia* sp. ST45, which significantly increased ($p \leq 0.05$) canola root elongation by 118%, 98%, and 86%, respectively, compared with the control treatment (**Figure 1**). Other isolates that significantly increased ($p \leq 0.05$) canola root

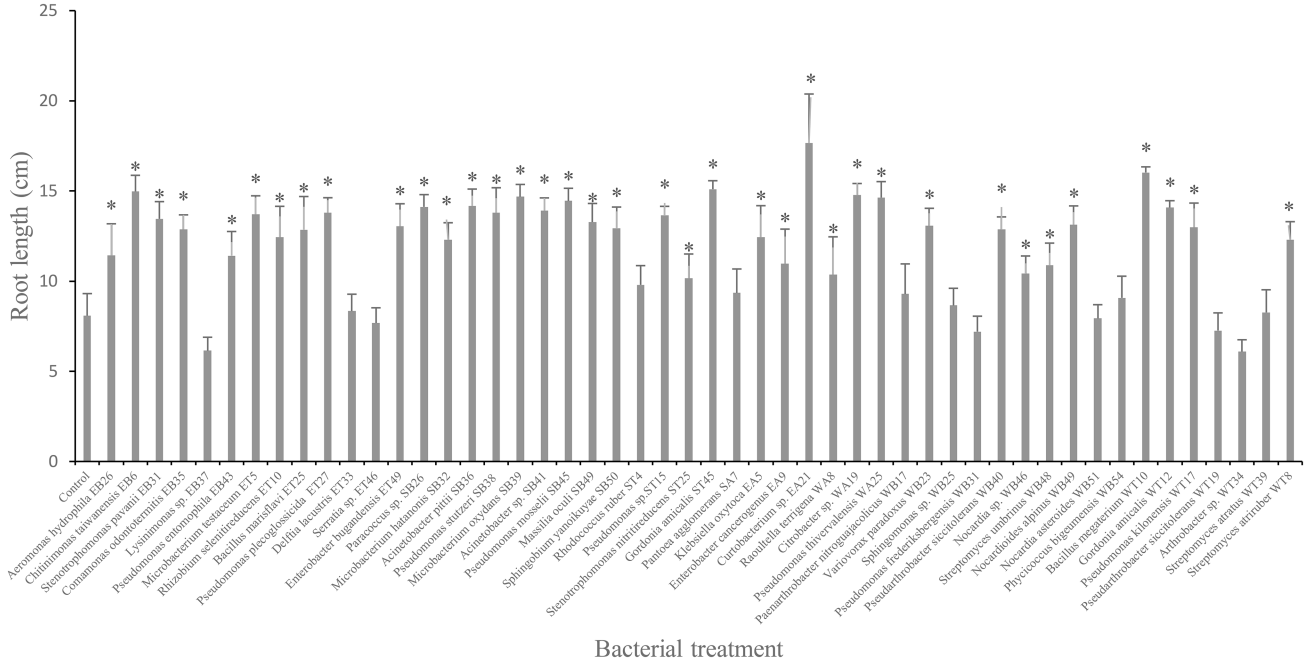

FIGURE 1 | Effect of selected plant growth-promoting rhizobacteria (PGPR) bacterial isolates on root length (cm) of canola plants measured after 7 days of growth. Error bars represent SDs and * indicates a significant difference compared to the control according to a Dunnett test, $p \leq 0.05$.

length included *Citrobacter* sp. WA19, *Pseudomonas thivervalensis* WA25, *Microbacterium oxydans* SB39, *Pseudomonas mosselii* SB45, *Pseudomonas stutzeri* SB38, *Acinetobacter pittii* SB36, *Pseudomonas putida* ET27, *S. maltophilia* EB31, *G. amicalis* WT12, *Arthrobacter* sp. WB40, and *Klebsiella* sp. EA5 (**Figure 1**). In contrast, bacterial isolates *Arthrobacter* sp. WT34, *Pseudomonas* sp. WB31 and *Gordonia* sp. WB51 tended to inhibit canola root elongation, although this effect was not significant at $p = 0.05$ (**Figure 1**).

n-Hexadecane and Diesel Degradation Potential, and Presence of *alkB*, *CYP153* and *nahA* Genes in Bacterial Isolates

n-hexadecane was used as the sole carbon source for the growth of 29 isolates (58%) (**Table 3**). Some isolates, such as *G. amicalis* ST45, *Comamonas odontotermitis* EB35, *Pseudomonas fluorescens* WT17, *Nocardia* sp. WB46, *Nocardia asteroides* WB51, and *Phycicoccus bigeumensis* WB54, showed high growth rates when they were cultivated in MSM medium supplemented with *n*-hexadecane as the sole source of carbon and energy (**Table 3**).

Similarly, 43 bacterial isolates (86%) were able to utilize diesel as the sole carbon source (**Table 3**). Isolates *R. ruber* ST4, *G. amicalis* ST45, *Comamonas odontotermitis* EB35, *B. megaterium* WT10, *G. amicalis* WT12, *Pseudomonas kilonensis* WT17, *Paenarthrobacter nitroguajacolicus* WB17, *Sphingomonas sanxanigenens* WB25, *Nocardia* sp. WB46, *Nocardia asteroides* WB51, and *Enterobacter cancerogenus* EA9 showed the highest growth rate when they were cultivated in MSM medium supplemented with diesel as the sole source for carbon and energy (**Table 3**).

The detection of the presence of functional genes related to PHC-degradation—*alkB*, *CYP153*, and *nah1*—was used to evaluate the biodegradation ability of bacterial isolates. The *alkB* gene was detected in 34 isolates (68%) by PCR amplification (**Table 3**). The *CYP153* gene was also detected in 24 isolates (48%) (**Table 3**), whereas 33 bacterial isolates (66%) possessed the *nah1* gene (**Table 3**).

Notably, five hexadecane-degrading bacterial isolates possessed all PGP traits under investigation (**Figure 2**) specifically, *Pseudomonas putida* ET27, *Serratia* sp. ET46, *S. maltophilia* EB31, *Pseudomonas fluorescens* WT17, and *Pseudomonas* sp. WB31 (**Figure 2**).

Canola Growth Promotion under *n*-Hexadecane Gradient

Further screening tests were performed on bacterial isolates in order to assess their PGP activity using canola plants in growth pouches amended or not with a gradient of *n*-hexadecane concentrations ranging from 0% as a control to 3%. Under the conditions of no hydrocarbon stress (0% *n*-hexadecane), the consortium significantly increased ($p \leq 0.05$) root length compared to all isolates inoculated individually and to the control (**Figure 3**). All bacterial isolates, except *Pseudarthrobacter siccitolerans* WT19, significantly increased ($p \leq 0.05$) their root length compared to the control treatment (**Figure 3**). The highest growth promotion was observed in inoculations with *Stenotrophomonas pavanii* EB31 and *G. amicalis* WT12 (**Figure 3**). Similarly, all bacterial treatments significantly increased ($p \leq 0.05$) the shoot lengths of canola plants compared

TABLE 3 | Ability of bacterial isolates to grow on aliphatic compounds and to possess hydrocarbon degradation genes.

Strain	Identity[a]	Isolation medium	Growth in diesel[b]	Growth in hexadecane[c]	PCR[d]		
					alkB	*CYP153*	*nah*
ST4	*Rhodococcus ruber*	1/10TSA	+++	+++	+	+	+
ST15	*Pseudomonas* sp.	1/10TSA	+	–	–	–	+
ST25	*Stenotrophomonas nitritireducens*	1/10TSA	++	–	+	–	–
ST45	*Gordonia amicalis*	1/10TSA	++++	++++	+	+	–
SB26	*Paracoccus* sp.	B–H_amended diesel	+	–	–	+	+
SB32	*Microbacterium hatanonis*	B–H_amended diesel	++	–	+	–	+
SB36	*Acinetobacter pittii*	B–H_amended diesel	–	++	+	–	+
SB38	*Pseudomonas stutzeri*	B–H_amended diesel	++	+	–	+	+
SB39	*Microbacterium oxydans*	B–H_amended diesel	+	–	+	–	–
SB41	*Acinetobacter* sp.	B–H_amended diesel	+++	++	+	–	+
SB45	*Pseudomonas mosselii*	B–H_amended diesel	++	–	–	+	+
SB49	*Massilia oculi*	B–H_amended diesel	–	+	+	–	+
SB50	*Sphingobium yanoikuyae*	B–H_amended diesel	+++	+	+	–	+
ET5	*Microbacterium testaceum*	1/10TSA	+	–	–	–	+
ET10	*Rhizobium selenitireducens*	1/10TSA	+	–	+	+	+
ET25	*Bacillus marisflavi*	1/10TSA	++	–	–	–	+
ET27	*Pseudomonas plecoglossicida*	1/10TSA	+++	+	+	+	+
ET33	*Delftia lacustris*	1/10TSA	–	+	+	–	+
ET46	*Serratia* sp.	1/10TSA	–	+	+	–	+
ET49	*Enterobacter bugandensis*	1/10TSA	+++	–	+	+	+
EB6	*Chitinimonas taiwanensis*	B–H_amended diesel	++++	+	–	+	+
EB26	*Aeromonas hydrophila*	B–H_amended diesel	+	+	+	–	–
EB31	*Stenotrophomonas pavanii*	B–H_amended diesel	++++	+++	+	+	+
EB35	*Comamonas odontotermitis*	B–H_amended diesel	+	++++	+	–	+
EB37	*Lysinimonas* sp.	B–H_amended diesel	+	–	+	–	+
EB43	*Pseudomonas entomophila*	B–H_amended diesel	+	+	+	–	–
WT8	*Streptomyces atriruber*	1/10TSA	–	–	–	–	+
WT10	*Bacillus megaterium*	1/10TSA	+++	+	+	–	–
WT12	*Gordonia amicalis*	1/10TSA	++++	++++	+	+	+
WT17	*Pseudomonas kilonensis*	1/10TSA	+++	+	–	+	–
WT19	*Pseudarthrobacter siccitolerans*	1/10TSA	+	++	+	–	+
WT34	*Arthrobacter* sp.	1/10TSA	++	+	+	–	–
WT39	*Streptomyces atratus*	1/10TSA	+	–	–	–	–
WB17	*Paenarthrobacter nitroguajacolicus*	B–H_amended diesel	++++	+	+	+	+
WB23	*Variovorax paradoxus*	B–H_amended diesel	++	+	+	–	+
WB25	*Sphingomonas sanxanigenens*	B–H_amended diesel	+++	–	+	–	–
WB31	*Pseudomonas frederiksbergensis*	B–H_amended diesel	+	+++	–	+	–
WB40	*Pseudarthrobacter siccitolerans*	B–H_amended diesel	++	++	–	–	+
WB46	*Nocardia* sp.	B–H_amended diesel	++++	++++	+	–	+
WB48	*Streptomyces umbrinus*	B–H_amended diesel	++	+	+	+	–
WB49	*Nocardioides alpinus*	B–H_amended diesel	+	–	–	+	+
WB51	*Nocardia asteroides*	B–H_amended diesel	+++	++++	+	+	+
WB54	*Phycicoccus bigeumensis*	B–H_amended diesel	–	++++	+	–	–
SA7	*Pantoea agglomerans*	ACCD	+	–	+	–	–
EA5	*Klebsiella oxytoca*	ACCD	+	–	–	+	–
EA9	*Enterobacter cancerogenus*	ACCD	+++	+	+	+	+
EA21	*Curtobacterium* sp.	ACCD	+	–	–	+	–
WA8	*Raoultella terrigena*	ACCD	++	–	+	+	+
WA19	*Citrobacter* sp.	ACCD	–	+	–	+	–
WA25	*Pseudomonas thivervalensis*	ACCD	++	+	+	+	+

[a]*Indicates 16S rDNA identity of bacterial strains with their closest type strains in GenBank.*

[b]*Indicates growth capability of bacterial strains on 1% (v:v) diesel in MSM. ++++, +++, ++, +, and –, indicating the growth capability from strong to weak with diesel as a sole carbon and energy source, measured by optical density at 600 nm, after 1 week incubation at 28°C. ++++, growth (OD600 > 1); +++, growth (OD600 > 0.6); ++, growth (0.6 > OD600 > 0.2); +, growth (OD600 < 0.2); and –, no growth.*

[c]*Indicates growth capability of bacterial strains on 1% (v:v) n-hexadecane in MSM. ++++, +++, ++, +, and –, indicating the growth capability from strong to weak with n-hexadecane as a sole carbon and energy source, measured by optical density at 600 nm, after 1 week incubation at 28°C. ++++, growth (OD600 > 1); +++, growth (OD600 > 0.6); ++, growth (0.6 > OD600 > 0.2); +, growth (OD600 < 0.2); and –, no growth.*

[d]*Indicates "–" absence of PCR products and "+" presence of PCR products for the functional genes: alkB, alkane monooxygenase; CYP153, cytochrome P450 hydroxylase; and nah, naphthalene dioxygenase.*

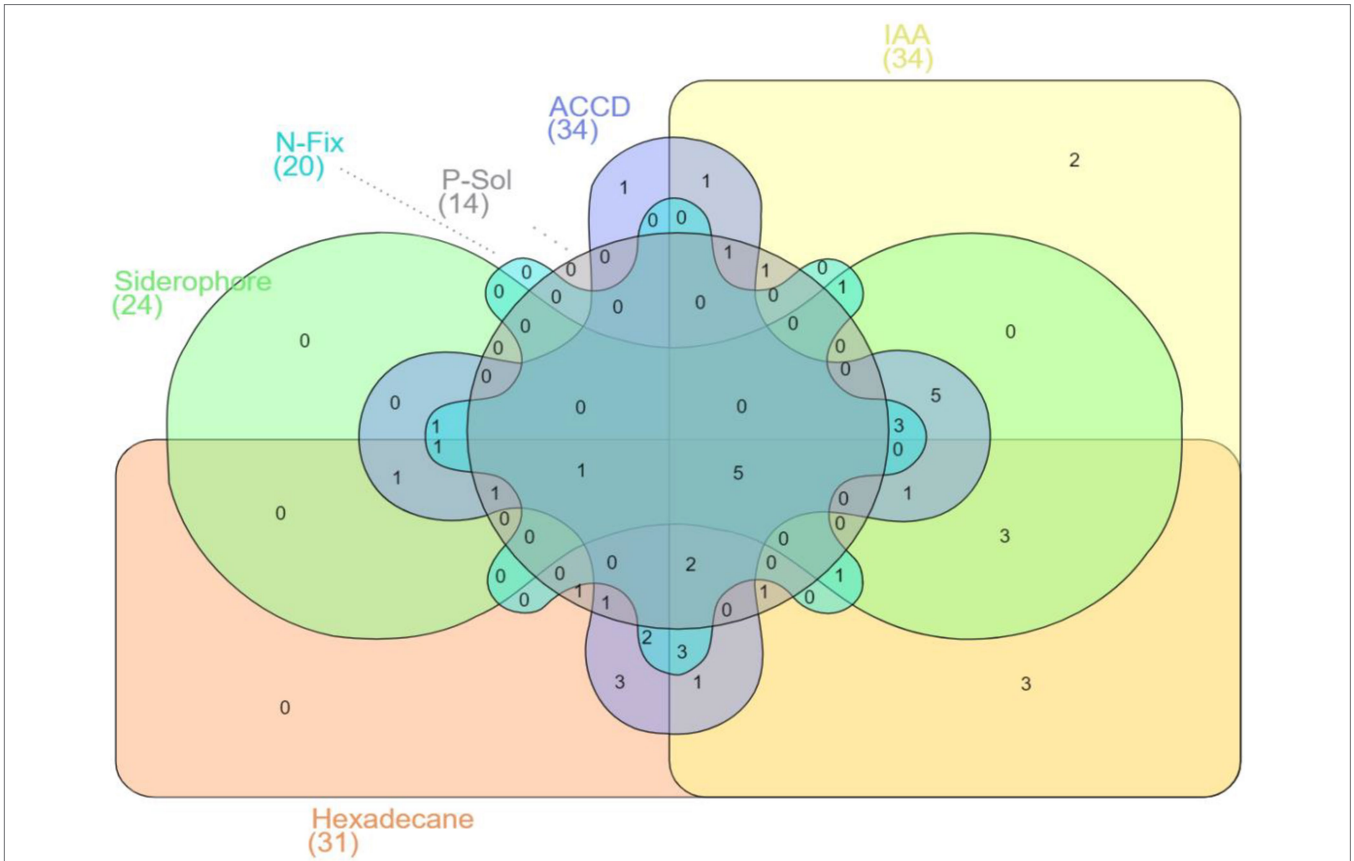

FIGURE 2 | Venn diagram representation of 50 rhizobacterial strains, showing positive results for hexadecane degradation potential and different plant growth-promoting (PGP) traits (with five strains showing positive results for all the traits under investigation).

to the control (**Figure 3**). The highest growth promotion was observed in the consortium treatment (**Figure 3**).

When canola seedlings were grown in the presence of different concentrations of *n*-hexadecane (1%, 2%, and 3%), the resultant hydrocarbon stress caused a decrease in both root length and shoot length among most of the treatments (**Figures 3–6**). For example, canola seedlings treated with *S. pavanii* EB31, *G. amicalis* WT12, and *Pseudomonas plecoglossicida* ET27 grown in the presence of 3% *n*-hexadecane stress showed shoot lengths that were decreased by up to 60% compared to seedlings inoculated with the same strains grown in the absence of the hydrocarbon (**Figures 3**, **6**). However, under 3% *n*-hexadecane amendment, all bacteria treatments significantly ($p \leq 0.05$) increased their shoot length when compared with the control treatment (**Figure 6**). The highest shoot enhancement was induced by the isolate *Nocardia* sp. WB46 and the consortium treatment (**Figure 6**).

Unlike shoot length, canola seedlings grown under different concentrations of *n*-hexadecane showed an almost 16% decrease in root length when compared with seedlings grown in the absence of the hydrocarbon (**Figures 3–6**). In the presence of 3% *n*-hexadecane stress, all bacteria treatments significantly ($p \leq 0.05$) increased root length when compared with the control treatment (**Figures 4**, **6**). The highest root growth promotion was induced by the consortium treatment of *Nocardia* sp. WB46, *P. plecoglossicida* ET27, and *S. pavanii* EB31 (**Figure 6**).

Growth of Bacterial Isolates in Different Concentrations of *n*-Hexadecane

Bacterial isolates were grown in different concentrations of *n*-hexadecane (1%, 2%, and 3%) to determine the effect of increasing concentrations on bacterial growth. The results of this experiment indicated that when the concentration of *n*-hexadecane increased, the growth rate of some hexadecane-degrading bacteria was inhibited (**Figure 7**). For example, *B. megaterium* WT10 has an OD of 0.470 in 1% *n*-hexadecane, whereas this value decreased to 0.230 in the presence of the 3% concentration of *n*-hexadecane (**Figure 7**). Similar trends were observed for *plecoglossicida* ET27, *S. pavanii* EB31, and *Acinetobacter* sp. SB41. In contrast, *Nocardia* sp. WB46 and *Pseudarthrobacter siccitolerans* WT19 showed increased bacterial growth as the *n*-hexadecane concentrations increased (**Figure 7**). For example, *Nocardia* sp. WB46 had an OD of 1.6 with 1% *n*-hexadecane, whereas its growth rate increased to 2.3 with 3% *n*-hexadecane (**Figure 7**).

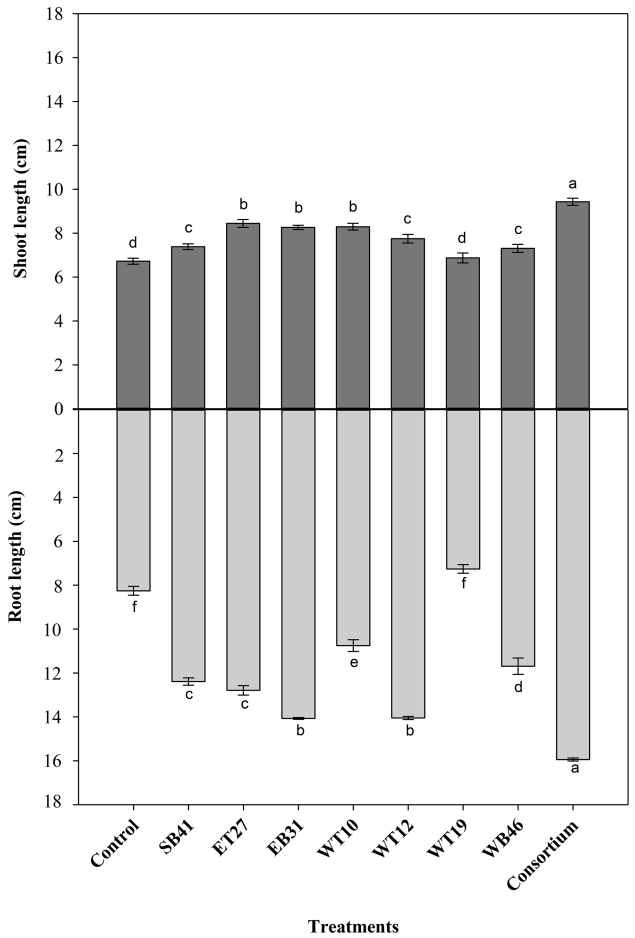

FIGURE 3 | Effect of selected PGPR bacterial strains on root and shoot length (cm) of canola plants measured after 7 days of growth in the presence of 0% *n*-hexadecane. Error bars represent SDs, and different letters indicate significance according to Tukey's *post-hoc* test at $p \leq 0.05$.

DISCUSSION

The use of plants in combination with bacteria possessing the ability to degrade PHCs and to promote plant growth is an efficient and environmentally sustainable strategy to remediate diesel-contaminated soils. High concentrations of PHCs can have phytotoxic effects on plants growing on contaminated soils (Baek et al., 2004). Therefore, the use of bacterial strains with multiple PGP and hydrocarbon degradation capabilities has crucial advantages for plants growing in such hostile environments.

To select bacterial isolates for the phytoremediation of diesel-contaminated soil, it is important to consider characteristics such as high degradation potential, the presence of alkane-degrading genes and a robust substrate affinity, as well as multiple PGP traits, such as the production of plant growth regulator substances and the ability to improve nutrient acquisition, which may enhance plant growth under contamination stress (Balseiro-Romero et al., 2017a).

We previously isolated and identified 438 PHC-degrading bacteria with multiple PGP characteristics from rhizosphere soil of *Salix purpurea* and *E. obtusa* plants growing in a highly PHC-contaminated site (Alotaibi et al., 2021b). In this study, we selected and characterized 50 bacterial isolates in depth based on their taxonomic and functional diversities and they were tested for their alkane degradation potential, PGP traits, and plant growth promotion potential under normal and stressed conditions using growth pouch assays.

PGPR regulate plant growth *via* diverse sets of mechanisms (Lugtenberg and Kamilova, 2009; Schlaeppi and Bulgarelli, 2015). In the present work, bacterial isolates exhibited several PGP traits, including P solubilization, IAA production, siderophore synthesis, ammonia production, ACCD activity, and N-fixation (**Table 2**). Ammonia production may play a role in enhancing plant growth through the accumulation of N and subsequently increasing biomass production (Marques et al., 2010). Ammonia production was the most common PGP trait observed among the strains. Similar results were reported in Dutta and Thakur (2017) in the characterization of 48 bacterial strains isolated from different tea cultivars in India. This suggest that ammonia production is among the mechanisms used by PGPR to stimulate plant growth. It has been shown that ammonia produced by PGPR supplies N to their host plants and thus promotes root and shoot elongation (Marques et al., 2010; Bhattacharyya et al., 2020).

The ability to fix nitrogen would provide a selective advantage for hydrocarbon-degrading bacteria used in phytoremediation applications, particularly in N-limited soils (Foght, 2018). Our results indicated that majority of diazotrophic bacteria belonged to *Gammaproteobacteria* (**Table 2**). In line with our findings, several reports indicate that diazotrophic bacteria predominate in PHCs-contaminated environments were affiliated to *Gammaproteobacteria* (Church et al., 2008; Radwan et al., 2010; Do Carmo et al., 2011) including taxa such as *Acinetobacter*, *Pseudomonas*, *Azotobacter*, *Stenotrophomonas*, and *Klebsiella* (Eckford et al., 2002; Dashti et al., 2009; Do Carmo et al., 2011; Foght, 2018; Alotaibi et al., 2021b). One of the constraint-limiting biodegradation activities of microbial communities in PHC-contaminated soils is the lack of sufficient nutrients especially nitrogen. Thus, application of diazotroph could offer a sustainable and efficient approach to enhance bioaugmentation and phytoremediation of PHC-contaminated soils (Dashti et al., 2009; Foght, 2018).

Bacteria capable of solubilizing inorganic forms of P may promote plant growth by improving the nutrient uptake of plants. The majority of bacterial isolates that showed P solubilization activity in this study belonged to *Proteobacteria* (**Table 2**). This corroborates previous reports about the ability of many bacterial strains isolated from plants growing in agricultural and contaminated soils and belonging to this phylum to have P solubilization abilities (Chowdhury et al., 2017; Pawlik et al., 2017; Lumactud and Fulthorpe, 2018). Iron-chelating siderophores are another important factor for PGP. PGPR produce siderophores that bind Fe^{3+} and render it available for reduction to Fe^{+2}, a preferred form for plant roots uptake (Oleńska et al., 2020). Similar results were reported previously

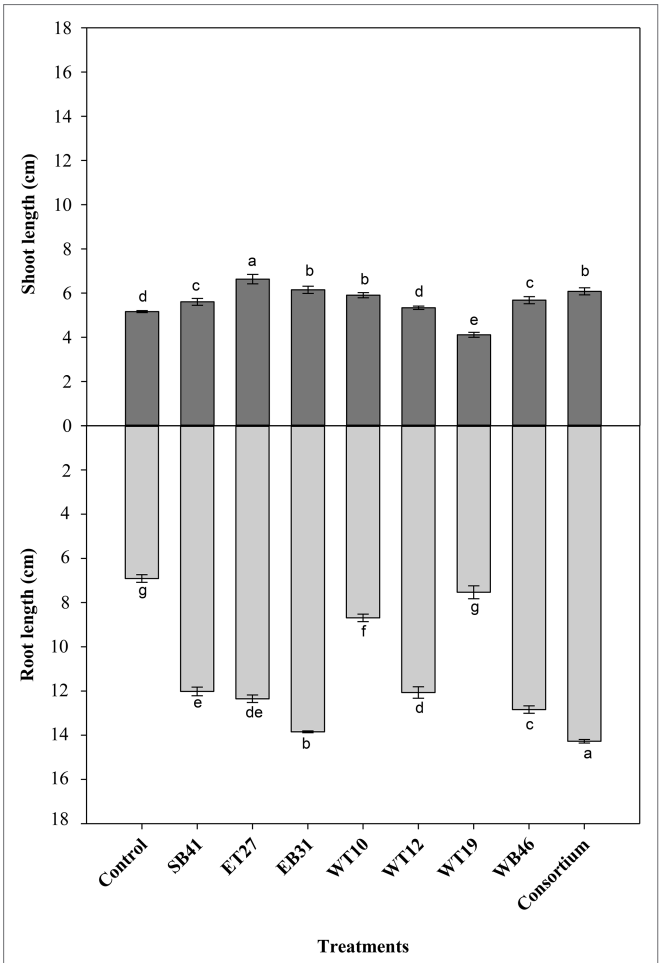

FIGURE 4 | Effect of selected PGPR bacterial strains on root and shoot length (cm) of canola plants measured after 7 days of growth in the presence of 1% *n*-hexadecane. Error bars represent SDs, and different letters indicate significance according to Tukey's *post-hoc* test at $p \leq 0.05$.

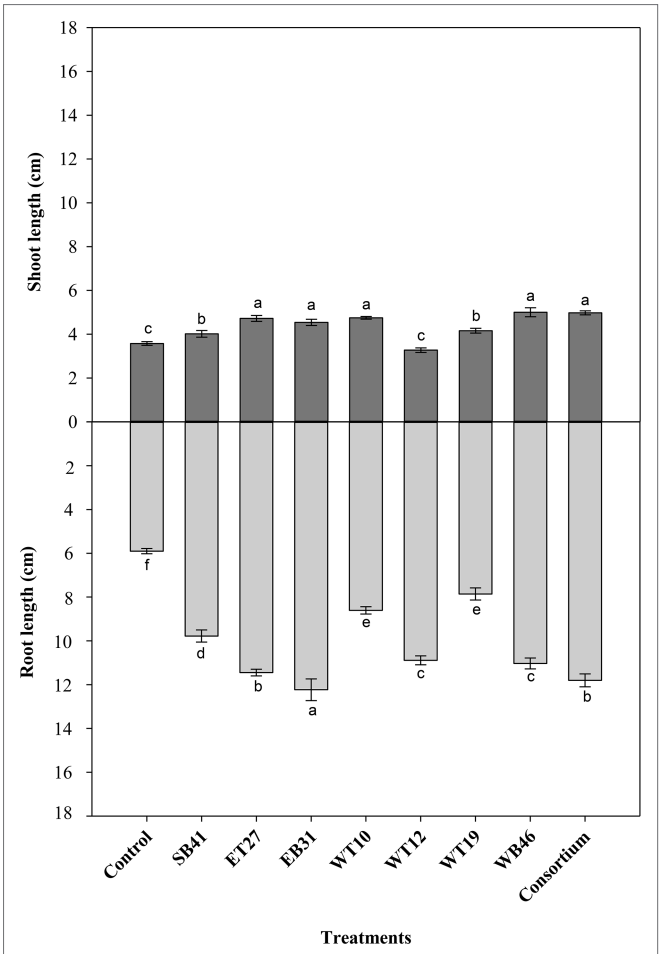

FIGURE 5 | Effect of selected PGPR bacterial strains on root and shoot length (cm) of canola plants measured after 7 days of growth in the presence of 2% *n*-hexadecane. Error bars represent SDs, and different letters indicate significance according to Tukey's *post-hoc* test at $p \leq 0.05$.

in Príncipe et al. (2007) in the characterization of PGPR isolates from saline soils. In a recent study, Eze et al. (2022) isolated a PGP and diesel-degrading bacterial consortium, dominated by *Alphaproteobacteria*, that led to a 66% increase in *Medicago sativa* biomass and resulted in 91% removal of diesel hydrocarbons in just 60 days. Functional metagenome analysis of the consortium revealed the presence of several genes responsible for PGP traits, including N-fixation, phosphate solubilization, and siderophore production (Eze et al., 2022). The prevalence of PGP genes in the consortium may account for not only the growth promotion of *M. sativa* but also their tolerance of diesel toxicity (Eze et al., 2022).

PGPR capable of lowering levels of ACC, a precursor of ethylene phyto-hormone, may stimulate growth and stress tolerance in plants under normal and stressed conditions (Glick, 2014). The high percentage of ACCD-producing bacteria in our study is in agreement with previous reports documenting the prevalence of this phenotype in various soil bacteria isolated from many stressed environments (Belimov et al., 2001; Mayak et al., 2004; Sandhya et al., 2010; Ali and Kim, 2018). Tara et al. (2014) reported that maximum bacterial population, plant biomass and hydrocarbon degradation activity were achieved for carpet grass plants growing in soil spiked with diesel and inoculated with bacterial strains (*Pseudomonas* sp. ITRH25, *Pantoea* sp. BTRH79, and *Burkholderia* sp. PsJN) possessing both alkane-degradation and ACCD activity, compared to bacterial strains possessing only alkane degradation activity.

IAA produced by PGPR is responsible for increasing root elongation, lateral root formation and root hairs, thus enhancing the water and nutrient uptake efficiency of the plant root system (Lugtenberg and Kamilova, 2009). Some recent studies have shown that rhizobacteria isolated from PHC-contaminated soil including strains of *Arthrobacter* sp., *Bacillus* sp., *Enterobacter* sp., *Rhodococcus* sp., *Pantoea* sp., *Pseudomonas* sp., *Stenotrophomonas* sp., and *Streptomyces* sp. are also PGPR-producing IAA (Pawlik et al., 2017; Balseiro-Romero et al., 2017a; Lumactud and Fulthorpe, 2018; Kidd et al., 2021). In a recent study, Li et al. (2021) reported a significant plant growth enchantment of ryegrass growing in PHC-contaminated

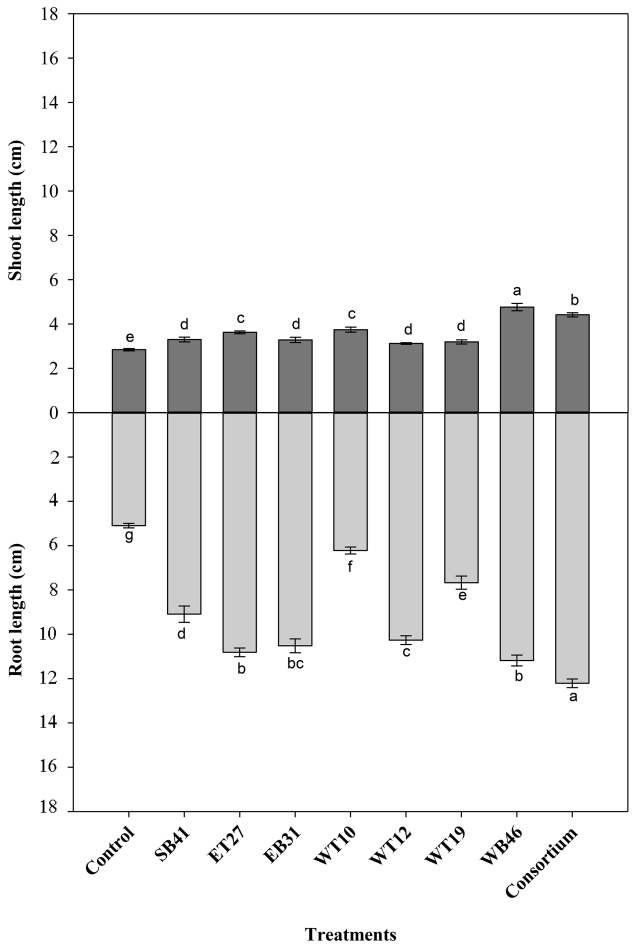

FIGURE 6 | Effect of selected PGPR bacterial strains on root and shoot length (cm) of canola plants measured after 7 days of growth in the presence of 3% *n*-hexadecane. Error bars represent SDs, and different letters indicate significance according to Tukey's *post-hoc* test at $p \leq 0.05$.

soils and co-inoculated with bacterial strains *Arthrobacter pascen* and *Bacillus cereus*, possessing both IAA production and fluoranthene (Flu) degradation traits. Additionally, the Flu concentration was enhanced in the roots and shoots of inoculated plants (Li et al., 2021). The increase in the absorption and transport of Flu into plant tissues was attributed to the effect of IAA-producing bacteria on plants growth. IAA producing microbes would increase plant growth, which may increase the production of extra root exudates and lead to a higher transpiration rate, thus improving the rate of mineralization, solubility, and transport of Flu into the plant tissues (Técher et al., 2011; Li et al., 2021).

Plant-related factors in the rhizosphere, such as the production of organic compounds in root exudates, might affect the survival and colonization of PGPR and their ability to express many PGP activities (Drogue et al., 2012; Alemneh et al., 2021). Therefore, we used a plant-based strategy for screening PGPR regarding their PGP potential. In our study, numerous bacterial strains significantly increased the root elongation of canola plants (**Figure 1**). Our results are in line with the findings of Asghar et al. (2004), who screened the effect of 100 rhizobacterial strains on the promotion of canola root growth under gnotobiotic conditions and found that 58% enhanced root growth. Several studies have suggested that the PGPR isolates that most effectively promote plant growth produce both IAA and ACCD (Glick, 2014; Balseiro-Romero et al., 2017b; Kang et al., 2019). In our study, the highest root-growth promotion effect was observed with *Curtobacterium* sp. strain EA21. This strain produced the highest amount of IAA among all strains (44.13 $\mu g\,ml^{-1}$; **Table 2**) and produced ACCD, as demonstrated by the plate assay and the positive PCR amplification result (**Table 2**). The cross-talk between IAA and ACCD is fundamental for PGPR to enhance root growth (Glick, 2014). Several studies have reported that PGPR producing IAA higher than 40 $\mu g\,ml^{-1}$ inhibited root growth and seed germination (Pawlik et al., 2017; Alemneh et al., 2021) due to the stimulation of ethylene caused by the higher amount of IAA (Glick, 2014). However, if the bacterium has both IAA and ACC deaminase activities, then the ACCD would mediate the decreasing of ethylene production, thus permitting IAA synthesis, which could continue to enhance root growth (Glick, 2014; Kang et al., 2019; Alemneh et al., 2021). Several other PGPR in our study that promoted root growth and produced both IAA and ACC deaminase included strains such as *Microbacterium oxydans* strain SB39, *Pseudomonas mosselii* strain SB45, *Pseudomonas stutzeri* strain SB38, *P. plecoglossicida* strain ET27, *S. pavanii* strain EB31, *G. amicalis* strain WT12, and *Klebsiella oxytoca* strain EA5 (**Figure 1**). Interestingly, *B. megaterium* strain WT10, which was unable to express ACCD and IAA, significantly enhanced the root growth of canola plants compared to the control treatment (**Figure 1**). Therefore, the positive effect of this strain might be related to its ability to solubilize inorganic phosphate up to 690.86 $\mu g\,ml^{-1}$ and its ammonia production (**Table 2**). Similar results were reported in Alemneh et al. (2021), who observed that several strains belonging to *Bacillus* spp. enhanced the growth and nodulation of chickpeas under gnotobiotic conditions. The improvement of plant growth was mainly related to the ability of these strains to express PGP traits other than IAA and ACCD (Alemneh et al., 2021). Interestingly, bacterial strains tested in this experiment showed growth-promoting potential for canola plants despite being isolated from different plant species. This fact suggests that these PGPR strains are non-host-specific, thus having huge potential as inoculants to promote plant growth in phytoremediation, as well as in organic agriculture.

Degradative bacteria can enhance the removal of alkanes and reduce the phytotoxicity of pollutants in soils due to their capability to possess hydrocarbon-degrading enzymes (van Beilen and Funhoff, 2007; Arslan et al., 2014). In our study, numerous bacterial strains had the potential to utilize aliphatic hydrocarbons (**Table 3**). Several authors have reported both large populations and high diversities of alkane-degrading bacteria in various habitats, ranging from marine environments to polar soils (Whyte et al., 2002; Yakimov et al., 2007; Jurelevicius et al., 2013; Lumactud et al., 2016; Pawlik et al., 2017).

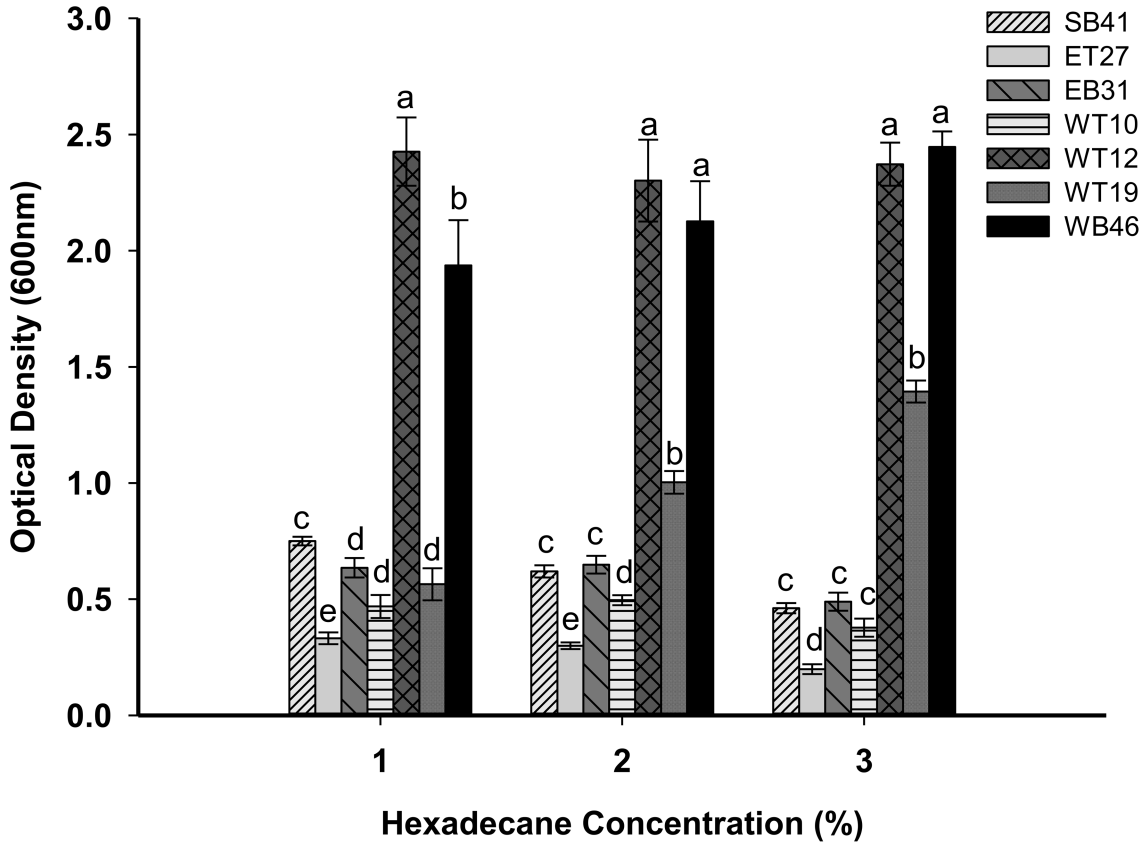

FIGURE 7 | Effect of different concentrations of *n*-hexadecane (1%, 2%, and 3%) on bacterial growth of selected bacterial strains. All strains were grown for 7 days. Error bars represent SDs, and different letters indicate significance according to Tukey's *post-hoc* test at $p \leq 0.05$.

Alkane hydroxylases (AHs) genes are responsible for the aerobic biodegradation of alkanes by bacteria (van Beilen and Funhoff, 2007). In our study, various bacterial strains harbored *AlkB* and *CYP153*-related AHs. These two AHs genes demonstrate a complementary substrate range. *AlkB* is involved in the degradation of medium-chain alkanes (C10-C20), whereas *CYP153* catalyzes the biodegradation of short-chain alkanes (C5-C16; Rojo, 2009; Ji et al., 2013; Wang and Shao, 2013). Similar results were reported by Pawlik et al. (2017), who screened 26 bacterial strains isolated from *Lotus corniculatus* and *Oenothera biennis* plants growing in a long-term polluted site, and found that 50% of these strains were equipped with *CYP153* genes.

Previous research has shown that AH genes are often associated with *Betaproteobacteria* and *Gammaproteobacteria*, particularly the *Pseudomonas* genus (van Beilen and Funhoff, 2007; Liu et al., 2014; Garrido-Sanz et al., 2019; Eze et al., 2021). In our study, AH-degrading genes were also found in strains that belonged to *Betaproteobacteria* and *Gammaproteobacteria*; in addition, members of the *Actinobacteria*, such as *Gordonia*, *Arthrobacter*, *Nocardia*, *Rhodococcus*, and *Rhodococcus*, were found to harbor these genes (**Table 3**). The wider taxonomic affiliations of bacterial strains capable of metabolizing alkanes demonstrate the potential of this culture collection for the remediation of diesel-contaminated soils.

Interestingly, several strains tested in this study had multiple *AlkB* and *CYP153* genes coexisting together (**Table 3**). The co-occurrence of multiple AHs has been reported previously in several bacterial strains, such as *Acinetobacter* sp. ADP1 (Barbe et al., 2004), *Dietzia* sp. DQ12-45-1b (Nie et al., 2011), and *Amycolicicoccus subflavus* DQS3-9A1 (Nie et al., 2014b). Undoubtedly, the coexistence of multiple AH genes in one bacterium would extend the alkane substrate range, thus enhancing the adaptation ability and subsequently the degradation potential of the host bacterium (Sun et al., 2018).

Under contaminant stress conditions (the second growth pouch experiments with various *n*-hexadecane concentrations), the inoculation of canola seeds with the selected PGPR strains either alone or in consortia generally provoked a significant increase in both the root length and shoot length of canola seedlings when compared with control plants (**Figures 3–6**). This indicates that PGPR inoculants exert a positive effect on plant growth under such stressful conditions. In agreement with our results, Balseiro-Romero et al. (2017b) reported that the inoculation of *Cytisus striatus* L. and *Lupinus luteus* L plants, grown in 1.25% diesel-contaminated soil in a pot experiment, with diesel-degrading bacterial strains with multiple PGP activities significantly improved plant growth. In the present experiment, selected hexadecane-degrading strains were

evaluated for their ability to promote the growth of canola plants under increasing hexadecane concentrations (**Table 3**). Additionally, these selected hexadecane-degrading strains possessed multiple PGP traits (**Table 2**). Among the hexadecane-degrading strains, after the consortium treatments, the actinobacterium *Nocardia* sp. strain WB46 was found to be the best plant growth promoter among all the strains assessed (**Figure 6**). This strain showed robust growth on hexadecane as a sole energy source (**Figure 7**). Genome analyses revealed that *Nocardia* sp. strain WB46 contains three copies of the *alkB* gene (unpublished data). *AlkB* is a class of alkane hydroxylase enzymes that is responsible for the microbial degradation of oil and fuel additives, as well as many other compounds (van Beilen and Funhoff, 2007; Nie et al., 2014a). *Nocardia* sp. strain WB46 was also shown to possess several PGP activities, such as IAA, siderophore, and ammonia production (**Table 2**). IAA is a phytohormone responsible for increasing root elongation and the formation of lateral root and root hairs, thus enhancing the water and nutrient uptake efficiency of plant root systems (Lugtenberg and Kamilova, 2009), whereas the production of siderophores and ammonia plays a role in enhancing plant growth by increasing the nutrient acquisition efficiency of Fe^{+2} and N, respectively (Lugtenberg and Kamilova, 2009; Marques et al., 2010).

Other hexadecane-degrading isolates, specifically *P. plecoglossicida* ET27 and *S. pavanii* EB31, exhibited excellent plant growth promotion potential (**Figure 6**). Although these two isolates do not utilize hexadecane as efficiently as *Nocardia* sp. WB46 (**Figure 7**), they were shown to possess strong PGP capabilities (**Table 2**). *Pseudomonas plecoglossicida* ET27 was able to produce all PGP traits under investigation in this study. In agreement with our results, Balseiro-Romero et al. (2017b) reported the characterization of *Pseudomonas* strain 12, which was isolated from the rhizosphere of poplar plants growing in a diesel-contaminated site. In their study, *Pseudomonas* stain 12 was able to solubilize P, produce siderophore, synthesize IAA and produce ACCD, as well as promoting plant growth when used as an inoculum to enhance the growth of plants growing in diesel-contaminated soils (Balseiro-Romero et al., 2017b). *Stenotrophomonas pavanii* EB31 was also shown to possess all PGP features. Several recent studies highlighted the potential of the members of genus *Stenotrophomonas* having multiple PGP traits to be used as inoculants in the bioremediation of PHC-contaminated soils (Pawlik et al., 2017; Lumactud and Fulthorpe, 2018; Mitter et al., 2019; Alotaibi et al., 2021b).

Interestingly, *P. plecoglossicida* ET27 and *S. pavanii* EB31 contain genes for N-fixation and alkane degradation. Earlier studies reported that other N-fixers such as *Frankia* spp. were found to harbored alkane genes in addition *nifH* gene (Rehan et al., 2016). Diazotroph capable of coupling N-fixation to hydrocarbon degradation represent a key strategy to promote plant growth in N-limited marginal lands such as PHC-contaminated soils (Foght, 2018). Thus, enhancing the efficiency of phytoremediation of PHC-contaminated soils.

Our results along with previous reports (Tara et al., 2014; Balseiro-Romero et al., 2017a,b; Kidd et al., 2021) support our hypothesis that bacteria with multiple PGP and pollutant degradation characteristics performed better than strains with only one of these traits. In addition, hexadecane-degrading activity could be considered itself a PGP feature, because pollutants have a harmful effect on plant growth and development. Given the potential for positively influencing plant growth, exploiting these bacteria is a major goal for environmental and agricultural biotechnologies (Quiza et al., 2015). Such an achievement could enhance our ability to promote efficient soil nutrient use to increase plant growth, while reducing the toxicity of PHC pollutants. Our study clearly demonstrated that some bacterial taxa exhibit traits of PGP and capacity of degradation of PH pollutants. Integration of bacterial taxa that performed better for each test, can help to develop different formulations of bioinoculants. Further compatibility and formulation tests of these bioinoculants must avoid competition between isolates and allow the maintenance of microbial propagule survival for long periods of time and assure their ability to improve the growth of plants under various field conditions.

CONCLUSION

In conclusion, the results of our study suggest that the screening of rhizobacteria for *in vitro* PGP activities, aliphatic hydrocarbon degradation potential, and root growth promotion under gnotobiotic conditions is an effective approach for the selection of efficient PGPR candidates for bioremediation biotechnology applications. After several rounds of screenings, bacterial strains *Nocardia* sp. WB46, *P. plecoglossicida* ET27 and *S. pavanii* EB31 showed the highest growth stimulation when grown under the presence of 3% *n*-hexadecane. These isolates originated from a unique site with high concentration of PHC pollution scored positive for PGP traits and hexadecane degradation potentials, indicating the potential to serve as inoculants for assisting the phytoremediation of diesel-contaminated soils. Additionally, with this culture collection in hand, a better understanding of the role of plant growth promotion in the phytoremediation of PHC-contaminated soils can be achieved through additional phenotypic and in planta characterization, whole genome sequencing, and the construction of bacterial consortia for field applications.

DATA AVAILABILITY STATEMENT

The datasets presented in this study can be found in online repositories. The names of the repository/repositories and accession number(s) can be found in the article/**Table 1**.

AUTHOR CONTRIBUTIONS

FA performed experiments and experimental design, analyzed data, and wrote the manuscript draft. MS-A contributed to conceptualization, experimental design, co-supervision, and

manuscript editing. MH contributed to concepts, design, supervision, and manuscript writing. All authors contributed to the article and approved the submitted version.

FUNDING

This study was supported by funds from Natural Sciences and Engineering Research Council of Canada (NSERC) discovery grant to MH (grant number: RGPIN-2018-04178), Genome Quebec, Genome Canada, FA was also supported by a grant from King Saud University *via* the Saudi Arabian Cultural Bureau in Ottawa which are gratefully acknowledged.

SUPPLEMENTARY MATERIAL

The Supplementary Material for this article can be found online at: https://www.frontiersin.org/articles/10.3389/fmicb.2022.863702/full#supplementary-material

REFERENCES

Alemneh, A. A., Zhou, Y., Ryder, M. H., and Denton, M. D. (2021). Large-scale screening of rhizobacteria to enhance the chickpea-mesorhizobium symbiosis using a plant-based strategy. *Rhizosphere* 18:100361. doi: 10.1016/j.rhisph.2021.100361

Alexander, D., and Zuberer, D. (1991). Use of chrome azurol S reagents to evaluate siderophore production by rhizosphere bacteria. *Biol. Fertil. Soils* 12, 39–45. doi: 10.1007/BF00369386

Ali, S., and Kim, W. C. (2018). Plant growth promotion under water: decrease of waterlogging-induced ACC and ethylene levels by ACC Deaminase-producing bacteria. *Front. Microbiol.* 9:1096. doi: 10.3389/fmicb.2018.01096

Alotaibi, F., Hijri, M., and St-Arnaud, M. (2021a). Overview of approaches to improve rhizoremediation of petroleum hydrocarbon-contaminated soils. *Appl. Microbiol.* 1, 329–351. doi: 10.3390/applmicrobiol1020023

Alotaibi, F., Lee, S.-J., St-Arnaud, M., and Hijri, M. (2021b). *Salix purpurea* and *Eleocharis obtusa* rhizospheres harbor a diverse rhizospheric bacterial community characterized by hydrocarbons degradation potentials and plant growth-promoting properties. *Plan. Theory* 10:1987. doi: 10.3390/plants10101987

Arslan, M., Afzal, M., Amin, I., Iqbal, S., and Khan, Q. M. (2014). Nutrients can enhance the abundance and expression of alkane hydroxylase CYP153 gene in the rhizosphere of ryegrass planted in hydrocarbon-polluted soil. *PLoS One* 9:e111208. doi: 10.1371/journal.pone.0111208

Asghar, H., Zahir, Z., and Arshad, M. (2004). Screening rhizobacteria for improving the growth, yield, and oil content of canola (*Brassica napus* L.). *Aust. J. Agric. Res.* 55, 187–194. doi: 10.1071/AR03112

Backer, R., Rokem, J. S., Ilangumaran, G., Lamont, J., Praslickova, D., Ricci, E., et al. (2018). Plant growth-promoting rhizobacteria: context, mechanisms of action, and roadmap to commercialization of biostimulants for sustainable agriculture. *Front. Plant Sci.* 9:1473. doi: 10.3389/fpls.2018.01473

Baek, K.-H., Kim, H.-S., Oh, H.-M., Yoon, B.-D., Kim, J., and Lee, I.-S. (2004). Effects of crude oil, oil components, and bioremediation on plant growth. *J. Environ. Sci. Health A* 39, 2465–2472. doi: 10.1081/ESE-200026309

Baldwin, B. R., Nakatsu, C. H., and Nies, L. (2003). Detection and enumeration of aromatic oxygenase genes by multiplex and real-time PCR. *Appl. Environ. Microbiol.* 69, 3350–3358. doi: 10.1128/AEM.69.6.3350-3358.2003

Balseiro-Romero, M., Gkorezis, P., Kidd, P. S., Van Hamme, J., Weyens, N., Monterroso, C., et al. (2017a). Characterization and degradation potential of diesel-degrading bacterial strains for application in bioremediation. *Int. J. Phytoremediation* 19, 955–963. doi: 10.1080/15226514.2017.1337065

Balseiro-Romero, M., Gkorezis, P., Kidd, P. S., Van Hamme, J., Weyens, N., Monterroso, C., et al. (2017b). Use of plant growth promoting bacterial strains to improve *Cytisus striatus* and *Lupinus luteus* development for potential application in phytoremediation. *Sci. Total Environ.* 581–582, 676–688. doi: 10.1016/j.scitotenv.2016.12.180

Barbe, V., Vallenet, D., Fonknechten, N., Kreimeyer, A., Oztas, S., Labarre, L., et al. (2004). Unique features revealed by the genome sequence of *Acinetobacter* sp. ADP1, a versatile and naturally transformation competent bacterium. *Nucleic Acids Res.* 32, 5766–5779. doi: 10.1093/nar/gkh910

Behera, K.K., (2014). *Phytoremediation, Transgenic Plants and Microbes, Sustainable Agriculture Reviews*. Springer, Berlin/Heidelberg, Germany, pp. 65–85.

Belimov, A. A., Safronova, V. I., Sergeyeva, T. A., Egorova, T. N., Matveyeva, V. A., Tsyganov, V. E., et al. (2001). Characterization of plant growth promoting rhizobacteria isolated from polluted soils and containing 1-aminocyclopropane-1-carboxylate deaminase. *Can. J. Microbiol.* 47, 642–652. doi: 10.1139/w01-062

Bhattacharyya, C., Banerjee, S., Acharya, U., Mitra, A., Mallick, I., Haldar, A., et al. (2020). Evaluation of plant growth promotion properties and induction of antioxidative defense mechanism by tea rhizobacteria of Darjeeling, India. *Sci. Rep.* 10, 1–19. doi: 10.1038/s41598-020-72439-z

Blaha, D., Prigent-Combaret, C., Mirza, M. S., and Moënne-Loccoz, Y. (2006). Phylogeny of the 1-aminocyclopropane-1-carboxylic acid deaminase-encoding gene acdS in phytobeneficial and pathogenic proteobacteria and relation with strain biogeography. *FEMS Microbiol. Ecol.* 56, 455–470. doi: 10.1111/j.1574-6941.2006.00082.x

Cappuccino, J. C., and Sherman, N. (1992). "Negative staining," in *Microbiology: A Laboratory Manual. 3rd Edn.* ed. J. C. C. A. N. Sherman (Redwood City: Benjamin/Cummings), 125–179.

Chénier, M. R., Beaumier, D., Roy, R., Driscoll, B. T., Lawrence, J. R., and Greer, C. W. (2003). Impact of seasonal variations and nutrient inputs on nitrogen cycling and degradation of hexadecane by replicated river biofilms. *Appl. Environ. Microbiol.* 69, 5170–5177. doi: 10.1128/AEM.69.9.5170-5177.2003

Chowdhury, M. E. K., Jeon, J., Rim, S. O., Park, Y.-H., Lee, S. K., and Bae, H. (2017). Composition, diversity and bioactivity of culturable bacterial endophytes in mountain-cultivated ginseng in Korea. *Sci. Rep.* 7, 1–10. doi: 10.1038/s41598-017-10280-7

Church, M. J., Björkman, K. M., Karl, D. M., Saito, M. A., and Zehr, J. P. (2008). Regional distributions of nitrogen-fixing bacteria in the Pacific Ocean. *Limnol. Oceanogr.* 53, 63–77. doi: 10.4319/lo.2008.53.1.0063

Dashti, N., Khanafer, M., El-Nemr, I., Sorkhoh, N., Ali, N., and Radwan, S. (2009). The potential of oil-utilizing bacterial consortia associated with legume root nodules for cleaning oily soils. *Chemosphere* 74, 1354–1359. doi: 10.1016/j.chemosphere.2008.11.028

Do Carmo, F. L., Dos Santos, H. F., Martins, E. F., van Elsas, J. D., Rosado, A. S., and Peixoto, R. S. (2011). Bacterial structure and characterization of plant growth promoting and oil degrading bacteria from the rhizospheres of mangrove plants. *J. Microbiol.* 49, 535–543. doi: 10.1007/s12275-011-0528-0

Drogue, B., Doré, H., Borland, S., Wisniewski-Dyé, F., and Prigent-Combaret, C. (2012). Which specificity in cooperation between phytostimulating rhizobacteria and plants? *Res. Microbiol.* 163, 500–510. doi: 10.1016/j.resmic.2012.08.006

Dutta, J., Handique, P. J., and Thakur, D. (2015). Assessment of culturable tea rhizobacteria isolated from tea estates of Assam, India for growth promotion in commercial tea cultivars. *Front. Microbiol.* 6:1252. doi: 10.3389/fmicb.2015.01252

Dutta, J., and Thakur, D. (2017). Evaluation of multifarious plant growth promoting traits, antagonistic potential and phylogenetic affiliation of rhizobacteria associated with commercial tea plants grown in Darjeeling, India. *PLoS One* 12:e0182302. doi: 10.1371/journal.pone.0182302

Eckford, R., Cook, F. D., Saul, D., Aislabie, J., and Foght, J. (2002). Free-living heterotrophic nitrogen-fixing bacteria isolated from fuel-contaminated Antarctic soils. *Appl. Environ. Microbiol.* 68, 5181–5185. doi: 10.1128/AEM.68.10.5181-5185.2002

Eze, M. O., Hose, G. C., George, S. C., and Daniel, R. (2021). Diversity and metagenome analysis of a hydrocarbon-degrading bacterial consortium from asphalt lakes located in Wietze, Germany. *AMB Express* 11, 1–12. doi: 10.1186/s13568-021-01250-4

Eze, M. O., Thiel, V., Hose, G. C., George, S. C., and Daniel, R. (2022). Enhancing rhizoremediation of petroleum hydrocarbons through bioaugmentation with a plant growth-promoting bacterial consortium. *Chemosphere* 289:133143. doi: 10.1016/j.chemosphere.2021.133143

Fiske, C. H., and Subbarow, Y. (1925). The colorimetric determination of phosphorus. *J. Biol. Chem.* 66, 375–400. doi: 10.1016/S0021-9258(18)84756-1

Foght, J. (2018). "Nitrogen fixation and hydrocarbon-oxidizing bacteria. Cellular ecophysiology of microbe: hydrocarbon and lipid interactions," in *Handbook of Hydrocarbon and Lipid Microbiology*. ed. K. N. Timmis (Cham: Springer), 431–448.

Garrido-Sanz, D., Redondo-Nieto, M., Guirado, M., Pindado Jiménez, O., Millán, R., Martin, M., et al. (2019). Metagenomic insights into the bacterial functions of a diesel-degrading consortium for the rhizoremediation of diesel-polluted soil. *Gene* 10:456. doi: 10.3390/genes10060456

Glick, B. R. (2014). Bacteria with ACC deaminase can promote plant growth and help to feed the world. *Microbiol. Res.* 169, 30–39. doi: 10.1016/j.micres.2013.09.009

Glick, B. R., and Stearns, J. C. (2011). Making phytoremediation work better: maximizing a plant's growth potential in the midst of adversity. *Int. J. Phytoremediation* 13(Suppl. 1), 4–16. doi: 10.1080/15226514.2011.568533

Heberle, H., Meirelles, G. V., da Silva, F. R., Telles, G. P., and Minghim, R. (2015). InteractiVenn: a web-based tool for the analysis of sets through Venn diagrams. *BMC Bioinform.* 16:169. doi: 10.1186/s12859-015-0611-3

Hynes, R. K., Leung, G. C., Hirkala, D. L., and Nelson, L. M. (2008). Isolation, selection, and characterization of beneficial rhizobacteria from pea, lentil, and chickpea grown in western Canada. *Can. J. Microbiol.* 54, 248–258. doi: 10.1139/W08-008

Ji, Y., Mao, G., Wang, Y., and Bartlam, M. (2013). Structural insights into diversity and n-alkane biodegradation mechanisms of alkane hydroxylases. *Front. Microbiol.* 4:58. doi: 10.3389/fmicb.2013.00058

Jurelevicius, D., Alvarez, V. M., Peixoto, R., Rosado, A. S., and Seldin, L. (2013). The use of a combination of alkB primers to better characterize the distribution of alkane-degrading bacteria. *PLoS One* 8:e66565. doi: 10.1371/journal.pone.0066565

Kang, S.-M., Shahzad, R., Bilal, S., Khan, A. L., Park, Y.-G., Lee, K.-E., et al. (2019). Indole-3-acetic-acid and ACC deaminase producing *Leclercia adecarboxylata* MO1 improves *Solanum lycopersicum* L. growth and salinity stress tolerance by endogenous secondary metabolites regulation. *BMC Microbiol.* 19:80. doi: 10.1186/s12866-019-1450-6

Kidd, P. S., Álvarez, A., Álvarez-López, V., Cerdeira-Pérez, A., Rodríguez-Garrido, B., Prieto-Fernández, Á., et al. (2021). Beneficial traits of root endophytes and rhizobacteria associated with plants growing in phytomanaged soils with mixed trace metal-polycyclic aromatic hydrocarbon contamination. *Chemosphere* 277:130272. doi: 10.1016/j.chemosphere.2021.130272

Kloos, K., Munch, J. C., and Schloter, M. (2006). A new method for the detection of alkane-monooxygenase homologous genes (alkB) in soils based on PCR-hybridization. *J. Microbiol. Methods* 66, 486–496. doi: 10.1016/j.mimet.2006.01.014

Kuiper, I., Lagendijk, E. L., Bloemberg, G. V., and Lugtenberg, B. J. (2004). Rhizoremediation: a beneficial plant-microbe interaction. *Mol. Plant-Microbe Interact.* 17, 6–15. doi: 10.1094/MPMI.2004.17.1.6

Labinger, J. A., and Bercaw, J. E. (2002). Understanding and exploiting C–H bond activation. *Nature* 417, 507–514. doi: 10.1038/417507a

Li, W., Zhang, Z., Sun, B., Hu, S., Wang, D., Hu, F., et al. (2021). Combination of plant-growth-promoting and fluoranthene-degrading microbes enhances phytoremediation efficiency in the ryegrass rhizosphere. *Environ. Sci. Pollut. Res.* 28, 6068–6077. doi: 10.1007/s11356-020-10937-3

Lifshitz, R., Kloepper, J. W., Kozlowski, M., Simonson, C., Carlson, J., Tipping, E. M., et al. (1987). Growth promotion of canola (rapeseed) seedlings by a strain of pseudomonas putida under gnotobiotic conditions. *Can. J. Microbiol.* 33, 390–395. doi: 10.1139/m87-068

Liu, H., Xu, J., Liang, R., and Liu, J. (2014). Characterization of the medium- and long-chain n-alkanes degrading *Pseudomonas aeruginosa* strain SJTD-1 and its alkane hydroxylase genes. *PLoS One* 9:e105506. doi: 10.1371/journal.pone.0105506

Lugtenberg, B., and Kamilova, F. (2009). Plant-growth-promoting rhizobacteria. *Annu. Rev. Microbiol.* 63, 541–556. doi: 10.1146/annurev.micro.62.081307.162918

Lumactud, R., and Fulthorpe, R. R. (2018). Endophytic bacterial community structure and function of herbaceous plants from petroleum hydrocarbon contaminated and non-contaminated sites. *Front. Microbiol.* 9:1926. doi: 10.3389/fmicb.2018.01926

Lumactud, R., Shen, S. Y., Lau, M., and Fulthorpe, R. (2016). Bacterial endophytes isolated from plants in natural oil seep soils with chronic hydrocarbon contamination. *Front. Microbiol.* 7:755. doi: 10.3389/fmicb.2016.00755

Marques, A. P., Pires, C., Moreira, H., Rangel, A. O., and Castro, P. M. (2010). Assessment of the plant growth promotion abilities of six bacterial isolates using *Zea mays* as indicator plant. *Soil Biol. Biochem.* 42, 1229–1235. doi: 10.1016/j.soilbio.2010.04.014

Mayak, S., Tirosh, T., and Glick, B. R. (2004). Plant growth-promoting bacteria confer resistance in tomato plants to salt stress. *Plant Physiol. Biochem.* 42, 565–572. doi: 10.1016/j.plaphy.2004.05.009

Mitter, E. K., Kataoka, R., de Freitas, J. R., and Germida, J. J. (2019). Potential use of endophytic root bacteria and host plants to degrade hydrocarbons. *Int. J. Phytoremediation* 21, 928–938. doi: 10.1080/15226514.2019.1583637

Nautiyal, C. S. (1999). An efficient microbiological growth medium for screening phosphate solubilizing microorganisms. *FEMS Microbiol. Lett.* 170, 265–270. doi: 10.1111/j.1574-6968.1999.tb13383.x

Nie, Y., Chi, C. Q., Fang, H., Liang, J. L., Lu, S. L., Lai, G. L., et al. (2014a). Diverse alkane hydroxylase genes in microorganisms and environments. *Sci. Rep.* 4:4968. doi: 10.1038/srep04968

Nie, Y., Liang, J., Fang, H., Tang, Y.-Q., and Wu, X.-L. (2011). Two novel alkane hydroxylase-rubredoxin fusion genes isolated from a Dietzia bacterium and the functions of fused rubredoxin domains in long-chain n-alkane degradation. *Appl. Environ. Microbiol.* 77, 7279–7288. doi: 10.1128/AEM.00203-11

Nie, Y., Liang, J. L., Fang, H., Tang, Y. Q., and Wu, X. L. (2014b). Characterization of a CYP153 alkane hydroxylase gene in a gram-positive *Dietzia* sp. DQ12-45-1b and its "team role" with alkW1 in alkane degradation. *Appl. Microbiol. Biotechnol.* 98, 163–173. doi: 10.1007/s00253-013-4821-1

Oleńska, E., Małek, W., Wójcik, M., Swiecicka, I., Thijs, S., and Vangronsveld, J. (2020). Beneficial features of plant growth-promoting rhizobacteria for improving plant growth and health in challenging conditions: a methodical review. *Sci. Total Environ.* 743:140682. doi: 10.1016/j.scitotenv.2020.140682

Patten, C. L., and Glick, B. R. (2002). Role of pseudomonas putida indoleacetic acid in development of the host plant root system. *Appl. Environ. Microbiol.* 68, 3795–3801. doi: 10.1128/AEM.68.8.3795-3801.2002

Pawlik, M., Cania, B., Thijs, S., Vangronsveld, J., and Piotrowska-Seget, Z. (2017). Hydrocarbon degradation potential and plant growth-promoting activity of culturable endophytic bacteria of *Lotus corniculatus* and *Oenothera biennis* from a long-term polluted site. *Environ. Sci. Pollut. Res.* 24, 19640–19652. doi: 10.1007/s11356-017-9496-1

Payne, S. M. (1994). Detection, isolation, and characterization of siderophores. *Methods Enzymol.* 235, 329–344. doi: 10.1016/0076-6879(94)35151-1

Penrose, D. M., and Glick, B. R. (2003). Methods for isolating and characterizing ACC deaminase-containing plant growth-promoting rhizobacteria. *Physiol. Plant.* 118, 10–15. doi: 10.1034/j.1399-3054.2003.00086.x

Pilon-Smits, E. (2005). Phytoremediation. *Annu. Rev. Plant Biol.* 56, 15–39. doi: 10.1146/annurev.arplant.56.032604.144214

Príncipe, A., Alvarez, F., Castro, M. G., Zachi, L., Fischer, S. E., Mori, G. B., et al. (2007). Biocontrol and PGPR features in native strains isolated from saline soils of Argentina. *Curr. Microbiol.* 55, 314–322. doi: 10.1007/s00284-006-0654-9

Quiza, L., St-Arnaud, M., and Yergeau, E. (2015). Harnessing phytomicrobiome signaling for rhizosphere microbiome engineering. *Front. Plant Sci.* 14:507. doi: 10.3389/fpls.2015.00507

Radwan, S., Mahmoud, H., Khanafer, M., Al-Habib, A., and Al-Hasan, R. (2010). Identities of epilithic hydrocarbon-utilizing diazotrophic bacteria from the Arabian gulf coasts, and their potential for oil bioremediation without nitrogen supplementation. *Microb. Ecol.* 60, 354–363. doi: 10.1007/s00248-010-9702-x

Rehan, M., Swanson, E., and Tisa, L. S. (2016). "Frankia as a biodegrading agent," in *Actinobacteria-Basics and Biotechnological Applications*. eds. D. Dhanasekaran and Y. Jiang (London: IntechOpen).

Rennie, R. (1981). A single medium for the isolation of acetylene-reducing (dinitrogen-fixing) bacteria from soils. *Can. J. Microbiol.* 27, 8–14. doi: 10.1139/m81-002

Rojo, F. (2009). Degradation of alkanes by bacteria. *Environ. Microbiol.* 11, 2477–2490. doi: 10.1111/j.1462-2920.2009.01948.x

Rösch, C., Mergel, A., and Bothe, H. (2002). Biodiversity of denitrifying and dinitrogen-fixing bacteria in an acid forest soil. *Appl. Environ. Microbiol.* 68, 3818–3829. doi: 10.1128/AEM.68.8.3818-3829.2002

Sandhya, V., Ali, S. Z., Grover, M., Reddy, G., and Venkateswarlu, B. (2010). Effect of plant growth promoting pseudomonas spp. on compatible solutes, antioxidant status and plant growth of maize under drought stress. *Plant Growth Regul.* 62, 21–30. doi: 10.1007/s10725-010-9479-4

Schlaeppi, K., and Bulgarelli, D. (2015). The plant microbiome at work. *Mol. Plant-Microbe Interact.* 28, 212–217. doi: 10.1094/MPMI-10-14-0334-FI

Schwyn, B., and Neilands, J. (1987). Universal chemical assay for the detection and determination of siderophores. *Anal. Biochem.* 160, 47–56. doi: 10.1016/0003-2697(87)90612-9

Shiri, Z., Kermanshahi, R., Soudi, M., and Farajzadeh, D. (2015). Isolation and characterization of an n-hexadecane degrading *Acinetobacter baumannii* KSS1060 from a petrochemical wastewater treatment plant. *Int. J. Environ. Sci. Technol.* 12, 455–464. doi: 10.1007/s13762-014-0702-0

Stroud, J., Paton, G., and Semple, K. T. (2007). Microbe-aliphatic hydrocarbon interactions in soil: implications for biodegradation and bioremediation. *J. Appl. Microbiol.* 102, 1239–1253. doi: 10.1111/j.1365-2672.2007.03401.x

Sun, J.-Q., Xu, L., Liu, X.-Y., Zhao, G.-F., Cai, H., Nie, Y., et al. (2018). Functional genetic diversity and culturability of petroleum-degrading bacteria isolated from oil-contaminated soils. *Front. Microbiol.* 9:1332. doi: 10.3389/fmicb.2018.01332

Tara, N., Afzal, M., Ansari, T. M., Tahseen, R., Iqbal, S., and Khan, Q. M. (2014). Combined use of alkane-degrading and plant growth-promoting bacteria enhanced phytoremediation of diesel contaminated soil. *Int. J. Phytoremediation* 16, 1268–1277. doi: 10.1080/15226514.2013.828013

Técher, D., Laval-Gilly, P., Henry, S., Bennasroune, A., Formanek, P., Martinez-Chois, C., et al. (2011). Contribution of *Miscanthus x giganteus* root exudates to the biostimulation of PAH degradation: an in vitro study. *Sci. Total Environ.* 409, 4489–4495. doi: 10.1016/j.scitotenv.2011.06.049

van Beilen, J. B., and Funhoff, E. G. (2007). Alkane hydroxylases involved in microbial alkane degradation. *Appl. Microbiol. Biotechnol.* 74, 13–21. doi: 10.1007/s00253-006-0748-0

Wang, W., and Shao, Z. (2013). Enzymes and genes involved in aerobic alkane degradation. *Front. Microbiol.* 4:116. doi: 10.3389/fmicb.2013.00116

Wang, L., Wang, W., Lai, Q., and Shao, Z. (2010). Gene diversity of CYP153A and AlkB alkane hydroxylases in oil-degrading bacteria isolated from the Atlantic Ocean. *Environ. Microbiol.* 12, 1230–1242. doi: 10.1111/j.1462-2920.2010.02165.x

Whyte, L. G., Schultz, A., Beilen, J. B., Luz, A. P., Pellizari, V., Labbé, D., et al. (2002). Prevalence of alkane monooxygenase genes in Arctic and Antarctic hydrocarbon-contaminated and pristine soils. *FEMS Microbiol. Ecol.* 41, 141–150. doi: 10.1111/j.1574-6941.2002.tb00975.x

Xu, X., Liu, W., Tian, S., Wang, W., Qi, Q., Jiang, P., et al. (2018). Petroleum hydrocarbon-degrading bacteria for the remediation of oil pollution under aerobic conditions: a perspective analysis. *Front. Microbiol.* 9:2885. doi: 10.3389/fmicb.2018.02885

Yakimov, M. M., Timmis, K. N., and Golyshin, P. N. (2007). Obligate oil-degrading marine bacteria. *Curr. Opin. Biotechnol.* 18, 257–266. doi: 10.1016/j.copbio.2007.04.006

Conflict of Interest: The authors declare that the research was conducted in the absence of any commercial or financial relationships that could be construed as a potential conflict of interest.

Publisher's Note: All claims expressed in this article are solely those of the authors and do not necessarily represent those of their affiliated organizations, or those of the publisher, the editors and the reviewers. Any product that may be evaluated in this article, or claim that may be made by its manufacturer, is not guaranteed or endorsed by the publisher.

frontiers | Frontiers in Soil Science

ORIGINAL RESEARCH
published: 04 April 2022
doi: 10.3389/fsoil.2022.865517

Mycorrhizal Mediated Partitioning of Phosphorus: Ectomycorrhizal (*Populus x canescens x Paxillus involutus*) Potential to Exploit Simultaneously Organic and Mineral Phosphorus Sources

Katharina Schreider[1]*, *Diana Hofmann*[2], *Jens Boy*[1], *Alberto Andrino*[1], *Aline Fernandes Figueiredo*[3], *Leopold Sauheitl*[1] and *Georg Guggenberger*[1]

[1] Institute of Soil Science, Leibniz Universität Hannover, Hannover, Germany, [2] Institute of Bio- and Geosciences, IBG-3: Agrosphere, Forschungszentrum Jülich GmbH, Jülich, Germany, [3] Institute of Physiology and Cell Biology, Tierärztliche Hochschule Hannover, Hannover, Germany

OPEN ACCESS

Edited by:
Maqshoof Ahmad,
The Islamia University of Bahawalpur, Pakistan

Reviewed by:
Rui S. Oliveira,
University of Coimbra, Portugal
Farhan Hafeez,
COMSATS University, Islamabad, Pakistan

***Correspondence:**
Katharina Schreider
schreider@ifbk.uni-hannover.de

Specialty section:
This article was submitted to Plant-Soil Interactions, a section of the journal Frontiers in Soil Science

Received: 30 January 2022
Accepted: 25 February 2022
Published: 04 April 2022

Citation:
Schreider K, Hofmann D, Boy J, Andrino A, Fernandes Figueiredo A, Sauheitl L and Guggenberger G (2022) Mycorrhizal Mediated Partitioning of Phosphorus: Ectomycorrhizal (Populus x canescens x Paxillus involutus) Potential to Exploit Simultaneously Organic and Mineral Phosphorus Sources. Front. Soil Sci. 2:865517. doi: 10.3389/fsoil.2022.865517

Many natural and anthropogenic soils are phosphorus (P) limited often due to larger P stocks sequestered in forms of low bioavailability. One of the strategies to overcome this shortage lies in the symbiosis of plants with mycorrhizal fungi, increasing the plant P uptake of these hardly accessible sources. However, little is known about mycorrhizal fungal mediated partitioning of differently available P forms, which could contribute to more efficient use of P by plants and, thereby, reduce competition for soil P. This study aimed to investigate the uptake of P from differently bioavailable P sources by ectomycorrhiza. For that, we conducted a rhizotrone study using *Populus x canescens* and its compatible ectomycorrhizal fungus *Paxillus involutus*. Four different P sources [*ortho*-phosphate (oP), adenosine monophosphate (AMP), hydroxyapatite (HAP), and oP bound to goethite (gP)] or only HAP as 1P control were supplied in separate compartments, where only the fungal partner had access to the P sources. The amount of the specific P sources was increased according to their decreasing bioavailability. In order to distinguish between the P sources, we applied ^{33}P to track its incorporation in plants by a non-destructive analysis *via* digital autoradiography. Our results show that an ectomycorrhizal plant is able to utilize all provided P sources *via* its mycorrhizal fungal associate. The acquisition timing was determined by the most bioavailable P sources, with oP and AMP over HAP and gP, and a mixed P pool over a single P source. In contrast, the magnitude was defined by the by the amount of supplied P source provision of additional nitrogen, hence AMP over oP and gP, as well as by P source complexity, with gP as the least favorable P form. Nevertheless, the results of the present study provide evidence that an ectomycorrhiza has the potential to occupy fundamental niches of various P sources differing in their bioavailability, indicating that being a generalist in P nutrition can facilitate adaptation to various nutritional settings in soil.

Keywords: adenosine monophosphate, ectomycorrhizal fungi, goethite P complex, hydroxyapatite, P availability, P diversity, radioactive labeling, resource partitioning

INTRODUCTION

Phosphorus is an essential element for the plant net primary productivity (1), but it is also limited in soils in many ecosystems [e.g., (2)], as more than 90% of P in the soil is present in different chemical forms that are not readily available to plants (3). Plants are able to take up P in the form of free phosphate (P_i) in soil solution (4). However, P_i is poorly mobile, as it interacts strongly with soil constituents and can be adsorbed onto metal oxides and clay minerals, and precipitate as (apatite-like) minerals (5, 6). In addition, P is immobilized in diverse organic forms. In young soils with parent material high in P, plants and microorganisms acquire P from primary minerals (7). However, with increasing soil development, primary minerals are getting depleted, and the plants and soil organisms recycle P from organic matter in the upper soil horizons (7, 8) or pedogenic Fe and Al oxides mainly in the subsoil (9, 10). Therefore, with increasing soil succession and associated depletion in readily available P sources, more efficient plant P uptake and recycling (8) are necessary.

The association of plants with mycorrhizal fungi defines a strategy to cope with P limitation (1). With their extraradical hyphae, the mycorrhizal symbionts are able to increase the volume of soil explored for nutrients beyond the rhizosphere (11, 12). Furthermore, mycorrhizal fungi actively contribute to P mobilization through exudation of low-molecular-weight organic anions (LMWOAs) to release P from primary and secondary minerals and release phosphatases to cleave P from organic P sources [reviewed by (1)]. The mycorrhiza associated P uptake is thereby more cost-effective, as less carbon (C) units are needed for the uptake of one unit P, while the hyphae provide a higher adsorbing length for the same infrastructural investment as compared to roots (13). Furthermore, depending on the inherent P acquiring mechanisms, mycorrhizal fungi are able to mobilize P from mineral and/or organic P sources (14, 15) and could, therefore, contribute to the necessary efficient use of different forms of P in soil. Also, ectomycorrhizal fungi showed an adaptation to a high variety of P sources such as inorganic phosphate (P_i), as well as different mineral (16) and organic P sources (17). Furthermore, the study of Zavičić et al. (18) has shown that fertilization of soils with triple phosphate negatively affected the P uptake efficiency of mycorrhizal beech compared to P uptake efficiency in P deficient soils.

According to the framework of Turner (19), the different chemical forms of P are partitioned by plants with different P acquiring adaptations to P limitation. This framework highlights the fact that mycorrhizal fungi are the key players to reduce competition for P and facilitate the co-existence of plants. Plant communities developing on soils with limited bioavailabilities of P are globally some of the most biodiverse compared with ecosystems limited in other nutrients (20, 21). Therefore, besides affecting the net primary productivity of terrestrial ecosystems, P limitation influences also the diversity and persistence of different plant species (20–22).

Progress in studying P partitioning for soil P has been achieved by examining plant responses to single P sources (23, 24) or a mixed pool of different P sources (25). The study of Andrino et al. (26, 27) investigated the mycorrhizal fungal acquisition of differently available P sources, which was determined by different amounts of C invested by the plant into the association with a mycorrhizal fungus that had access to differently available P sources. Nevertheless, the P sources were supplied as a single P source. The demonstration of the uptake of P with different bioavailabilities is challenging due to the need to differentiate one particular P source from a mixture of various P sources. Starting with Pearson and Jacobsen's (28) groundbreaking study on P uptake *via* mycorrhiza, recently, a few studies have used radioisotope labeling with ^{33}P to demonstrate differences in plant P uptake from different chemical forms of P offered as a sole P source (21) and as a mixture of different P sources (29). However, the sole contribution of ectomycorrhizal fungi in resource partitioning for P remains unclear. Hence, the aim of our study was to investigate whether an ectomycorrhizal fungus shows preferences to specific P sources of different bioavailability when offered in a mixed pool. This should help understand how the belowground nutrient P diversity shapes the mycorrhizal mediated aboveground plant biomass and P uptake. The present study addressed the following hypotheses: as the mycorrhizal fungi are essential in plant P acquisition and are known to be able to access organic and sorbed P (1, 30), we hypothesized (H1) that all P sources within the diverse P pool are available to mycorrhizal fungi, and therefore to plants, but the order and magnitude of acquisition depend on the P source complexity. We expected that the mycorrhizae would favor the readily available P_i over organic or mineral P sources, whereby the amount of each P source applied into the system was increased according to its complexity. Furthermore, in order to support the general assumption that a minor diversity in belowground resources, which can occur as a side effect of fertilization (31, 32), result in less efficient uptake of P (18), we hypothesize (H2) that mineral source (HAP) as a single P source is less available than within a pool of diverse P sources.

MATERIALS AND METHODS

Plant and Mycorrhizal Material

Poplar species *Populus x canescens* clone "Schleswig I" was used as a model plant and its functional ectomycorrhizal fungal strain MAJ of *Paxillus involutus* (33) was used as a symbiotic partner. Both were identified as functional associates which provide valuable model systems for a more robust test of nutrient acquisition and exchange models (33). The poplar plantlets were propagated on Woody Plant Medium [WPM (34)] without hormones (dephyte e.K., Langenberg, Germany) by establishing explants from the first two lateral meristems with one leaf and bud. The apical buds with 1.5 cm height were used for rooting on WPM medium but with one-third amount of sucrose and vitamins in Microboxes (O118/80, by Sac O_2, Deinze, Belgium) with a membrane for sterile gas exchange (81.35 GE day^{-1}). *P. involutus* was propagated in liquid culture of 0.2 L of modified Melin-Norkrans (MMN; ready to use salts, dephyte e.K., Langenberg, Germany) medium (33) in 0.5 L glass bottles under shaking and proliferated on 0.8 L Perlite as a carrier with 0.2 L MMN.

Preparation of the Phosphorus Sources and the Containers

To investigate mycorrhizal mediated plant P uptake from a pool of different P sources, the following chemical forms of P were tested: free *ortho*-phosphate (oP), adenosine monophosphate (AMP), hydroxyapatite (HAP), beside phosphate bound to goethite (gP) as a P adsorption complex with the Fe oxide, which is one of the most profuse and naturally occurring in soils (35). To differentiate the uptake between the different P sources, the use of radio-labeling with ^{33}P in combination with the non-destructive digital autoradiography was made. As ^{33}P labeled compounds [P33] phosphoric acid (FF-1) and [alpha-P33] AMP (FF-217) were purchased from Hartmann Analytic GmbH (Braunschweig, Germany).

To obtain the P sources oP and AMP in concentrations of 0.9 and 3.8 mg P ml^{-1}, respectively, $NaH_2PO_4 \cdot 2H_2O$ (for analysis, EMSURE®, Merck KGaA, Darmstadt, Germany) and adenosine 5′-monophosphate sodium salt (from yeast, >99%, SigmaAldrich, Merck KGaA, Darmstadt, Germany) were dissolved in deionized H_2O (dH_2O) and the pH adjusted to 5.2 using 1 M Na_2HPO_4 for oP and 1 M HCl for AMP. For labeling with ^{33}P, an aliquot of the oP and AMP solutions was spiked with 0.20 ml 74 MBq $H_3^{33}PO_4$ and 0.20 ml 74 MBq AM^{33}P, respectively. The oP and AMP were filtered using sterile syringe filter (Filtropur S, PES, 0.2 µm pore size, Sarstedt AG & Co. KG, Nümbrecht, Germany).

The HAP was produced as multistep synthesis at 25°C according to the protocol described by Wolf et al. (36). The only modification of this protocol was performed in the second step for the application of ^{33}P label, in which the 2 M H_3PO_4 solution was spiked with 0.5 ml 185 MBq $H_3^{33}PO_4$. The HAP pellet was ground with mortar and pestle and passed through a 0.20 mm sieve. The resulting ^{33}P activity of HAP accounted for 117.8 MBq g^{-1}.

To prepare the adsorption complexes of oP to goethite (gP), the procedure described by Andrino et al. (26, 27) was used with following modifications: for the loading of goethite with oP, 1 M NaH_2PO_4 solution was used. To prepare the ^{33}P labeled gP (gP-^{33}P), 24.5 ml of 1 M NaH_2PO_4 solution were spiked with 0.5 ml 185 MBq $H_3^{33}PO_4$. Always 6.2 ml 1 M NaH_2PO_4 (non-labeled or ^{33}P-labeled) and 5 g of synthetic goethite (α-FeOOH < 0.045 mm, Bayferrox® 920 Z, Lanxess Deutschland GmbH, Cologne, Germany) were mixed and filled up to 220 ml with dH_2O in centrifuge bottles (250 ml, Nalgene™, Thermo Scientific™, Waltham, Massachusetts, USA). Further steps are described in detail by Andrino et al. (26, 27) up to the step of drying the gP-^{33}P pellet. Due to the labeling with ^{33}P, gP had to be dried at 50°C in a drying oven without ventilation. After cooling down, the gP pellet was sieved through a 0.63 mm sieve. The resulting ^{33}P activity of gP accounted for 245.6 kBq g^{-1}.

Both gP and HAP (labeled and non-labeled) were sintered three times at 105°C for 30 min in a drying oven, including a subsequent incubation period at 30°C for 2 h the first two times. This step is called tyndallization and is used for fractionated sterilization without changing the mineral structure. The Raman spectrum of HAP with its phosphate typical bands (**Supplementary Figure 1**) is aligned with the spectra obtained by Wolf et al. (36), confirming the main characteristics of HAP.

To determine the P content of gP and HAP, 102 mg of each were solubilized in 10 ml 32% HCl (AnalaR NORMAPUR® for analysis, VWR International GmbH, Darmstadt, Germany), shaken on an overhead shaker for 24 h, and filtered using filter papers (thickness of 0.14 mm, a pore size of 2–3 µm; LABSOLUTE®, Th. Geyer GmbH & Co. KG, Renningen, Germany). P analysis was performed by Inductively Coupled Plasma-Optical Emission Spectrometry (ICP-OES, Varian 725-ES, City, State). In order to determine the easy desorbable P from gP and HAP, 55 mg gP or 101 mg HAP were suspended in 10 ml dH_2O, shaken on an overhead shaker for 24 h, and filtered through a filter paper (as described above). The analysis of P in the filtered solution was performed *via* ICP-OES. The P content of gP accounted to 1.04 ± 0.06 mg g^{-1} goethite ($n = 7$), of which 0.17 ± 0.01 mg P g^{-1} gP were easy desorbable, so that maximum of 16% P from P bound to goethite could be mobilized without any action of the mycorrhizal fungus. The P content of HAP accounted for 197.5 ± 5.3 mg g^{-1} HAP ($n = 3$), of which 7.1 ± 0.1 mg P g^{-1} HAP (3.6% P in HAP) were easy desorbable. According to the dissolution studies of HAP conducted by Wolf et al. (36), HAP is (independent of the synthesis temperature) otherwise stable in aqueous systems at pH values above 3.8.

All P sources were supplied in separate containers made of 5 ml SafeSeal reaction tubes. At around 2 ml height, a hole of 1 cm in diameter was burned into the tube and sealed with a combination of two types of membranes, allowing only the mycorrhizal partner to access the P sources in the P containers as described in more detail by Andrino et al. (26, 27). Briefly, a hydrophobic PTFE membrane (5 µm, Pieper Filter GmbH, Bad Zwischenahn, Germany) was installed at the P source side and a nylon mesh (20 µm, Franz Eckert GmbH, Waldkirch, Germany) at the plant root side. The containers were autoclaved (121°C, 20 min) and filled with the different labeled and non-labeled P sources under sterile conditions in a laminar flow cabinet. All containers were filled up to 3 ml with dH_2O.

Preparation of the Rhizotrone Culture Systems

A small-scaled, continuously closed rhizotrone culture system with four separate containers for the simultaneous supply of four different P sources (oP, AMP, HAP, and gP) was established to test hypothesis H1. In this 4P-^{33}P experiment, only one P source was labeled with ^{33}P before installing into a rhizotrone culture system. The overall P amount per system accounted for 13.2 mg P and was considered sufficient to sustain the system for 3 months. The specific P sources were supplied as 0.9 mg P in the form of oP, 3.8 mg P in the form of AMP, 6.2 ± 0.1 mg P in the form of HAP, and 2.3 ± 0.1 mg P as gP, whereby 223 and 368 µg P from mineral P sources HAP and gP (respectively) were easy desorbable (**Table 1**). The supplied P amounts increased with the increasing complexity of the P sources. The activity of ^{33}P (**Table 1**) accounted for 7,452 kBq per P container for oP and

TABLE 1 | Amount of P [mg], ^{33}P activity [kBq], and the calculated specific ^{33}P activity [Bq mg^{-1} P] of the different P sources applied in the P compartments in the rhizotrone systems.

P source in P compartment	4P +oP-^{33}P	4P +AMP-^{33}P	4P +HAP-^{33}P	4P +gP-^{33}P	1P +HAP-^{33}P
P [mg]	0.88	3.77	6.26 ± 0.12	2.32 ± 0.07	19.9 ± 0.4
^{33}P activity [kBq]	7,452	7,452	2,547 ± 47	638 ± 20	8,090 ± 158
specific ^{33}P activity [kBq mg^{-1} P]	8,498	1,975	407	275	407

Data indicate means ± standard deviation (n = 7). 4P experiment with simultaneous supply of four different P sources: oP, ortho-phosphate; AMP, adenosine monophosphate; gP, oP bound to goethite; HAP, synthesized hydroxyapatite; and 1P control experiment supplied with HAP.

AMP and 2,538 and 410 kBq per P container for HAP and gP (respectively) at 7.5 days post inoculation (dpi).

To test hypothesis H2, a 1HAP-^{33}P experiment was established to test the synthesized, ^{33}P labeled hydroxyapatite (1HAP-^{33}P) as a sole P source as a control to the 4P-^{33}P experiment. The P containers contained 19.9 ± 0.4 mg P in the form of HAP to provide a complex P source in surplus to ensure uptake. The activity of ^{33}P in HAP accounted for 8,080 kBq per P container at 3 dpi.

The rhizotrone culture systems used in the present study were made of square Petri dishes (10 × 10 × 2 cm, Sarstedt AG & Co. KG, Nümbrecht, Germany). The P containers were inserted 1 cm from the bottom into the rizotrones in a randomized order. Then, the rhizotrones were filled with Perlite (washed with dH_2O; autoclaved at 121°C for 20 min two times; Perligran® classic, Knauf Aquapanel GmbH, Dortmund, Germany) as nutrient-free substrate. To obtain mycorrhizal plant treatments, the substrate was inoculated with 10 vol.% of *P. involutus*-Perlite carrier. For the non-mycorrhizal plant treatments, the inoculated substrate was autoclaved one more time before use. The rooted poplar plantlets were placed on the top of the P containers and covered with an additional thin layer of Perlite. Next, the rhizotrone was covered with a thin, sterile PVC foil (10 × 10 × 0.02 cm, Modulor GmbH, Germany) to minimize radio-active shielding and afterwards sealed with hot glue. The skip for the plant stem at the top and the opening to release the excess of nutrient solution at 2 cm height from the bottom of the rhizotrone were closed with sterile cotton wool.

To keep the system sterile during the watering, the rhizotrones were equipped with a sterile syringe filter (Filtropur S, PES, 0.2 µm pore size, Sarstedt AG & Co. KG, Nümbrecht, Germany), which was connected to the rhizotrone through an autoclaved PVC pipe. From 0 dpi, the mesocosms were supplied with a Woody Plant (WPM) nutrient solution containing macro- and micro-elements without P and vitamins (WPM –P; dephyte e.K., Langenberg, Germany), which is a modification from a recipe described by Müller et al. (34) and which was balanced with KNO_3 and $(NH_4)_2SO_4$ to adjust the desired concentration of K.

For each ^{33}P labeled P source, four replicates were prepared as mycorrhizal treatments and three replicates as non-mycorrhizal treatments. To obtain no P controls with P compartments containing H_2O only, two mycorrhizal and two non-mycorrhizal rhizotrone culture systems were prepared. The plantlets were kept under a plastic cover that included moisturized protecting paper plugs for the first 2 weeks for acclimatization and, thus, for protection from lower ambient air humidity and higher UV radiation. The rhizotrones were kept in a climate chamber set at an 18/6 h day/night cycle with 20/18°C and 80% ambient humidity.

Autoradiography and Harvest of Rhizotrones and Plant Material

In the time course of the experiment, the rhizotrones were regularly exposed to phospho-imaging screens for 4 h (at 7, 21, 34, 52, 70, and 80 dpi) and 72 h (at 42 and 94 dpi) in order to monitor the transfer of ^{33}P through the ectomycorrhizal fungal partner from the P containers into the plant shoots. To do this, the whole rhizotrone surfaces, including the above-ground plants, were overlaid by phospho-imaging screens (20 × 40 cm and 35 × 43 cm; Dürr NDT GmbH & Co. KG, Germany). They were wrapped into an extra thin cover foil to protect the screens from contamination with the ^{33}P label and damage by an outflow from the rhizotrone. To ensure possibly tight contact between the plant leaves and stems and the phospho-imaging screen, a foam of a suitable thickness was placed under the plant shoots. Another foam and a heavier plate were placed from the phospho-imaging screens' backside to ensure tight contact between the rhizotrone and screen from the top side. As reference to the ^{33}P label, a set of ^{14}C polymer standards (IPcal test source array; Elysia-raytest, Straubenhardt, Germany) were used with different activities (in dpm cm^{-2}): 1,107,000, 424,000, 112,000, 41500, 13,350, and 3,950, supplemented by an activity free background. Thereby, each activity had a surface area of 1 cm^2. The exposition of rhizotrones to the phosphor-imaging screens must be in the dark. The phospho-image screens were read out immediately using an image plate scanner (CR-35 BIO, Elysia-raytest, Liège, Belgium) in sensitive mode with 100 µm resolution. Each scan is saved as a set of two raw data files which can be converted subsequently into one (e.g., JPG) data file using the Aida Image Analyser v5.0 (Elysia-raytest, Straubenhardt, Germany).

The mesocosms from 1HAP-^{33}P and 4P-^{33}P experiments were harvested at 108 dpi and between 110 and 112 dpi, respectively. The plant roots were separated from the substrate, washed, and dried with paper clothes. Fine root aliquots of up to 0.15 g of each plant were conserved in 70% ethanol to assess mycorrhization grade. The freshly harvested plant material was immediately imaged first for 4 h and afterwards for 72 h (as described above). The same imaging procedure was performed with the plant material after drying at 40°C overnight. After the last imaging, the plant material was separated into leaves, stem, and roots, and the biomass of the different plant parts was recorded.

The substrate was dried at 40°C for 96 h. The liquids in the P containers were collected in 2 ml SafeSeal reaction tubes,

weighed, and controlled for the pH using pH-indicator strips (Neutralit® pH5-10, Merck KGaA, Darmstadt, Germany; pH-Fix 0-6, Macherey-Nagel GmbH & Co. KG, Düren, Germany; and pH-Fix 0-14, Carl Roth GmbH & Co. KG, Karlsruhe, Germany). The pH-indicator stripes may not provide the most accurate result, but it offers reasonable control of changes in pH attributable to P uptake.

Quantification of ^{33}P and P and Calculation of Related Parameters

In order to quantitatively analyse the activity of ^{33}P in plant material, all parts of plant material (leaves, stem, roots) and substrates underwent thermal digestion at 480°C for a minimum of 6 h. ^{33}P, P, and nutrients were extracted using 3.6 M HNO_3. After 10 min incubation, the extracts were filtered using a folded filter (Sartorius™ FT-4-303-185, Grade 3hw, ø150 mm, 65 g m^{-2}, Sartorius AG, Goettingen, Germany). Thereafter, an aliquot of plant/substrate extracts (diluted to obtain a 2.3 M HNO_3 solution and prevent any phase separation) was mixed with 10 ml scintillation cocktail (Ultima Gold™, PerkinElmer Inc., USA) and analyzed for ^{33}P activity (dpm single program under blank correction) by liquid scintillation counting (LSC, Tri-Carb 3110TR, PerkinElmer Inc., Waltham, USA). The obtained ^{33}P activity was corrected by subtracting the background value, obtained as a blank undergoing the same extraction and preparation procedures as the plant material. The calibration/normalization of the LSC was performed daily with instrument inherent external standards. The reliability and accuracy of the ^{33}P activity data were ensured by a serial dilution of a sample extract with a high ^{33}P activity at 260 Bq at the day of measurement (**Supplementary Figure 2**). The reproducibility of measured values down to 1.5 Bq did not deviate significantly from the theoretical values. The measured values starting from 1.0 to 0.5 Bq were with 8–5% (respectively) less reproducible. ^{33}P activity values below 0.2 Bq were with 16% standard deviation less trustful, and as a consequence, excluded from data analysis.

The ^{33}P activity incorporated in different plant parts (leaves, stem, and roots) was determined as follows:

$$^{33}P\ activity\ \left[Bq\right] = \frac{\left(^{33}P\ signal\ \left[Bq\right]\ sample\ -\ ^{33}P\ signal\ \left[Bq\right]\ blanc\right) \bullet\ extract\ volume\ \left[ml\right] \bullet\ plant\ part\ biomass\ \left[g\right]}{extract\ aliqoute\ \left[ml\right] \bullet\ plant\ part\ aliqoute\ \left[g\right]} \quad (1)$$

The correction of ^{33}P activity in plant material from LSC measuring date and experiment starting date was calculated as follows:

$$^{33}P\ activity\ \left[\mathrm{Bq}\right] = \frac{^{33}P\ activity\ \left[Bq\right]}{e^{\left(\left(\frac{-\ln(2)}{25.34}\right) \bullet\ (t_0 - t_{LSC})\right)}} \quad (2)$$

Since not only the activity but also the P amounts applied with different P sources varied, we had to determine the specific activity in each P compartments containing ^{33}P labeled P source (**Table 1**) by using the following equation:

$$specific\ ^{33}P\ in\ P\ compartment\ \left[Bq\ mg^{-1}\right] = \frac{^{33}P\ \left[kBq\right]\ in\ P\ compartment\ \bullet\ 10^3}{P\ in\ P\ compartment\ \left[mg\ absolute\right]} \quad (3)$$

The recovery of ^{33}P (5) in plant material and substrate as well as the total P uptake in plant material (6) was calculated as follows:

$$^{33}P\ recovery\ [\%] = \frac{^{33}P\ \left[Bq\right]\ in\ plant\ or\ substrate}{^{33}P\ in\ P\ compartment\ \left[Bq\right]} \bullet 100\% \quad (4)$$

$$P\ uptake\ in\ plant\ \left[ug\right] = \frac{^{33}\ P\ \left[Bq\right]\ in\ plant\ \bullet\ 10^3}{specific\ ^{33}P\ \left[kBq\ mg^{-1}\right]\ in\ P\ compartment\ \bullet\ 10^3} \quad (5)$$

The analyses of total P in plant material and substrate were performed *via* ICP-OES (Varian 725-ES, Agilent Technologies, Santa Clara, United States). The standards for the calibration were prepared using the same matrix.

Assessment of Mycorrhization Grade of Mycorrhizal Plant Roots

In order to record the plants' response to mycorrhizal inoculation and the P source dependency and/or diversity, we determined the mycorrhization grade in mycorrhizal plant roots. Characteristically for successful mycorrhization of poplar roots by *P. involutus* (MAJ) is the change in root morphology, e.g., specific branching of root tips and no development of root hairs. The grade of mycorrhization of plant roots was determined using the gridline intersection method (37) as modified and described in detail by Brundrett et al. (38). Thereby, aliquots of 82 ± 27 cm of mycorrhizal and 28 ± 7 cm of non-mycorrhizal fine roots were inspected for the mycorrhizal root tips and the intersections of roots with the gridlines in triplicates (by rearranging the same root sample after each counting) using a stereo zoom microscope (45x magnification; KERN OZM-5, KERN & SOHN GmbH, Balingen, Deutschland). Mycorrhization grade was expressed as number of mycorrhizal root tips per cm^{-1} analyzed root length:

$$mycorrhization\ grade\quad [\#mycorrhizal\ root\ tips\ cm^{-1}\ root\ length] = \frac{number\ mycorrhizal\ root\ tips}{cm\ root\ length} \quad (6)$$

As expected, the fine roots of mycorrhizal plants were abundantly mycorrhized at 108 dpi (**Supplementary Figure 3**; **Supplementary Table 1**), while the non-mycorrhizal controls were not mycorrhized.

Statistical Analysis

All statical tests were performed with SPSS® Statistics 26.0 [IBM® Corporation, USA (39)] at the probability level of 0.05. All data were tested for normal distribution using the Shapiro-Wilk test and homogeneity of variances using Levene's test, where the *P*-value was calculated based on the mean. To test for significant differences in data of plant biomass, P content, and pH of P liquids (normally distributed) between mycorrhizal treatments (with two independent groups), the independent samples *t*-test was performed. To test for significant differences in data of plant biomass, plant P content, ^{33}P activity, ^{33}P recovery, and plant P uptake between the different P and mycorrhizal treatments (with more than three independent groups), the following statistical procedure was applied: a one-factorial analysis of the variances (ANOVA) with replicates was performed on normally distributed data. In case of significant differences, the Scheffé procedure (for data sets with no equal variances, as it is insensitive to violation of homogeneity of variances) or the Tukey-HSD test (for data sets with equal variances) as a *post-hoc* test were used. In case the data were not normally distributed, the Kruskal-Walis-*H*-test was used. It is a non-parametric equivalent of the One-Way ANOVA to test for significant differences between more than two groups using medians. In case of significant differences between the groups, the Mann-Witney-*U*-test was performed.

RESULTS

Distribution of Biomass and Absolute P Content in Plant Parts Differ Between Mycorrhizal and P Treatments

At the end of the experiment at 108 dpi, we determined in both experiments (4P-^{33}P and HAP-^{33}P) the biomass (**Figure 1A**) of, and the absolute P content (**Figure 1B**) in, different plant parts and substrate in order to investigate, whether these two parameters differ between the different plant parts and P pools applied into the system.

In both experiments, mycorrhizal plants developed significantly higher biomass at 108 dpi (**Figure 1A**) compared with the non-mycorrhizal plants ($P < 0.0005$). In addition, both treatments (mycorrhizal and non-mycorrhizal) had significantly ($P < 0.00001$) higher root biomass compared with the shoot biomass. Unfortunately, only two non-mycorrhizal 1HAP-^{33}P and mycorrhizal no P (H_2O) controls and only one non-mycorrhizal no P control could be harvested at the end of the experiment so that no statics could be done on these treatments.

The absolute P content (**Figure 1B**) follows almost the same trend as the plant biomass, as independent of the P species and mycorrhizal treatment, the absolute P content in plant correlated positively with the plant biomass ($R^2 = 0.64$, $P < 0.001$; **Supplementary Figure 4**). The absolute P content in mycorrhizal plants from 4P-^{33}P systems was significantly higher ($P < 0.001$) than in their non-mycorrhized counterparts. Mycorrhizal and non-mycorrhizal plants incorporated significantly more P ($P < 0.005$) in roots than in their stems and leaves. Furthermore, the P content in mycorrhizal 4P-^{33}P plants was significantly higher ($P < 0.04$) than in mycorrhizal 1HAP-^{33}P plants.

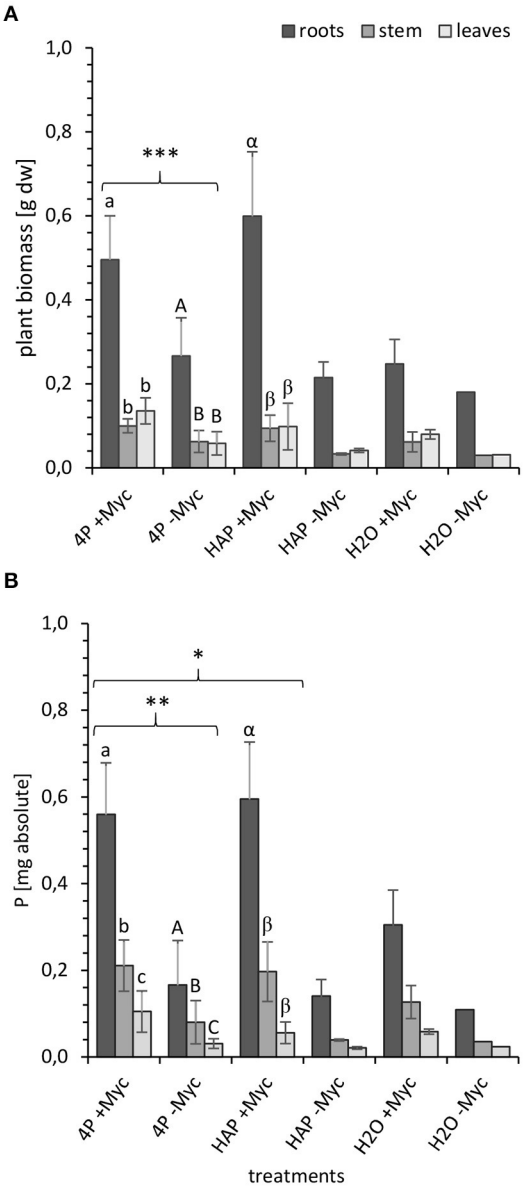

FIGURE 1 | (A) Biomass [g dry weight] and **(B)** P content [mg absolute] in different parts of mycorrhizal (+Myc) and non-mycorrhizal (-Myc) poplar plant at 108 dpi. 4P experiment with simultaneous supply of four different P sources: oP, *ortho*-phosphate; AMP, adenosine monophosphate; gP, oP bound to goethite; HAP, synthesized hydroxyapatite; and 1P control experiment supplied with HAP. The error bars show the standard deviation (4P: +Myc: $n = 16$; -Myc: $n = 12$; HAP: +Myc: $n = 4$; -Myc: $n = 2$; H_2O: +Myc: $n = 2$; -Myc: $n = 1$). The letters (a, A, α) indicate significant differences between the plant parts: **(A)** a-b and A-B: $P < 0.001$; α-β: $P < 0.003$; **(B)** a-c: $P < 0.001$; A-C and α-β: $P < 0.005$. Marking with (*) indicates significant differences between mycorrhizal and non-mycorrhizal treatments: **(A)** ***$P <$ 0.001 for whole plant and for leaves, stem, and roots); **(B)** **$P < 0.02$ for the whole plant; $P < 0.001$ for leaves, stem, and roots; *$P < 0.04$ for the whole plant; $P < 0.001$ for leaves and stem; $P < 0.01$ for roots.

The plant biomass and the P content in plants from mycorrhizal no P control systems are almost 2-fold lower than the mycorrhizal P treatments. This gain in biomass and P content of mycorrhizal P treatments accounted for 0.35 ± 0.15 g biomass and 0.38 ± 0.17 mg P. This is the gain alone from the P uptake from the P compartments.

^{33}P Incorporation in Plants and Its Distribution Between Plant Parts Differ Between P Treatments

In order to differentiate the plant P uptake from the different P sources and its partitioning in the plant, we have exposed the rhizotrone culture systems in the time course of the experiment (**Supplementary Figure 5**) as well as the harvested plants (**Figure 2**) to phospho-imaging screens for 4 and 72 h. Further, for the same reason, we determined the ^{33}P activity in harvested plants (leaves, stem, and roots) and substrate (**Figure 3**; **Supplementary Table 3**).

No incorporation of ^{33}P label in plant material was detected at 21 dpi. In contrast, the images of rhizotrone culture systems at 34 dpi revealed that the mycorrhizal fungus started to acquire the P sources oP and AMP (**Supplementary Figures 5A,B**, respectively) almost simultaneously. From HAP supplied in a pool of four different P sources (**Supplementary Figure 5C**), incorporation of ^{33}P label in plant shoots was visible for the first time at 42 dpi, while ^{33}P from HAP supplied as a single P source (**Supplementary Figure 5D**) was detectable for the first time in the plant at 94 dpi, when the rhizotrone culture systems were imaged for 72 h. No incorporation of ^{33}P label could be detected in the plant from HAP supplied as a single P source, nor from gP supplied in a pool of four different P sources at that time point.

The images of harvested plants of 4P systems with ^{33}P-labeled oP, AMP, and HAP (**Figure 3**) showed a trend in ^{33}P activity incorporated in plant: After 4 h exposing time of harvested plant material to the phospho-imaging screens, the highest ^{33}P activity was detected in 4P systems with ^{33}P-labeled AMP (**Figure 2B**), followed by oP (**Figure 2A**), and HAP (**Figure 2C**). The blue color indicates areas with high ^{33}P activity—these are the areas of roots with high intensity in the branching of the root tips (**Supplementary Figure 2**). As the main proportion of ^{33}P label in the plant is incorporated in roots, the ^{33}P incorporated in the plant from gP (**Figure 2D**) could be detected the first time in harvested plant material by exposing the dried plant to the phosphor-imaging plate for 72 h.

The quantitative analysis of ^{33}P activity (**Figure 3**) in plants showed the same trend as the images of harvested plant material. Moreover, the ^{33}P activity was significantly lower in plants from mycorrhizal gP treatments compared to the other mycorrhizal P treatments. The non-mycorrhizal P treatments were evidently lower enriched in ^{33}P than the mycorrhized counterparts, and the ^{33}P activity for the non-mycorrhizal 4P+gP-^{33}P and 1P+HAP-^{33}P treatments was even under the detection limit. When comparing different plant parts, the leaves of 4P+AMP-^{33}P treatment incorporated significantly ($P < 0.03$) more ^{33}P compared with the 4P+oP-^{33}P treatment and significantly higher amounts of ^{33}P in leaves, stem, and substrate compared with 1P+HAP-^{33}P treatment. The main proportion of ^{33}P was found in the plant roots (>57%).

^{33}P Recovery in Plant and Plant P Uptake Differ Between the Specific P Sources From a Mixed P Pool

In order to relate the ^{33}P activity incorporated in plant material to the ^{33}P activity of the initially applied P sources, we investigated the ^{33}P recovery [%] in the harvested plant (**Figure 4A**; **Supplementary Table 4**). Furthermore, in order to standardize the different ^{33}P activity added with different P amounts applied with each P source, we used the ^{33}P activity [Bq] incorporated in plant material, and the specific ^{33}P activity [kBq mg^{-1}] of the initially applied P sources to determine the plant P uptake [μg] (**Figure 4B**; **Supplementary Table 4**) from the specific ^{33}P labeled P source.

The recovery of initially applied ^{33}P in plant (**Figure 4A**) from the ^{33}P-labeled P sources accounted to a maximum of 5%. Significantly ($P < 0.03$) higher ^{33}P recovery could be observed in mycorrhizal plants grown in 4P rhizotrones with labeled AMP-^{33}P (followed by HAP-^{33}P and oP-^{33}P) compared with gP-^{33}P and single HAP-^{33}P and non-mycorrhizal treatments. Although the initial P content of 1P rhizotrone system containing labeled HAP-^{33}P as a single P source was 32% higher compared with the 4P system, the recovery of ^{33}P in plant shoots (leaves and stems) was significantly lower ($P < 0.03$) from the former as compared to the latter.

Looking at the plant ^{33}P uptake [μg] (**Figure 4B**) standardized by the initially applied P content, the uptake from HAP-^{33}P as a single P source (44 ± 66 μg P) tended to be lower than from HAP-^{33}P with the 4P system (119 ± 59 μg P), which is possibly due to the higher standard deviation in data from 1P+HAP-^{33}P treatment. Furthermore, P taken up from AMP-^{33}P (115 ± 73 μg P) and HAP-^{33}P from a mixed P pool were similar. However, the P uptake from the readily available oP-^{33}P (7.1 ± 1.6 μg P) and the more complex gP-^{33}P (0.61 ± 0.76 μg P) was significantly lower ($P < 0.03$) compared with other P treatments. Furthermore, the calculated plant P uptake from the mineral P sources HAP and gP (max. 168 μg P and 1.6 μg P, respectively) was lower compared to the easy desorbable P (max. 224 μg P from HAP and 369 μg P from gP).

DISCUSSION

The present study tested the suggestion highlighted in the framework of Turner (19) that the partitioning of different chemical P forms in the soil by plants is mediated by mycorrhizal fungi. For this purpose, we performed an experiment using an axenic rhizotrone culture system and the mycorrhizal associates of the poplar plant *P. x canescens* and the ectomycorrhizal fungus *P. involutus*. The system was supplied simultaneously with four different chemical forms of P in separate compartments so that only the mycorrhizal fungus had access to the P sources. To differentiate the mycorrhizal mediated plant P uptake between the different P sources, labeling with the radio-isotope ^{33}P was applied. Finally, the obtained results from this experiment were compared with the mycorrhizal mediated plant P uptake from

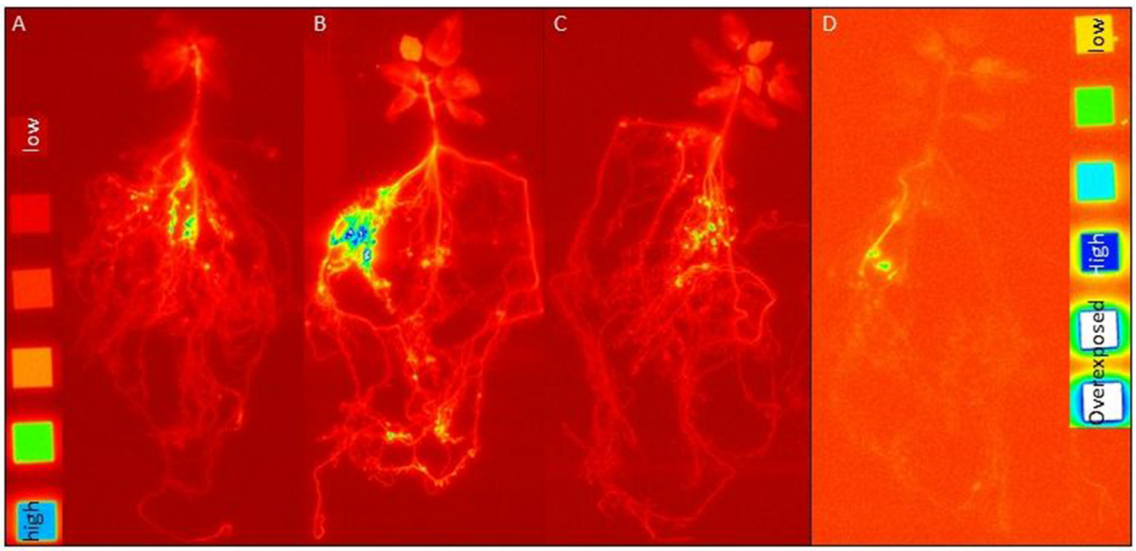

FIGURE 2 | Images of harvested plants from rhizotrone systems labeled with **(A)** ^{33}P-oP, **(B)** -AMP, and **(C)** -HAP (4 h exposing time to imaging plates; images developed at factor 2.3) as well as **(D)** ^{33}P-gP (72 h exposing time to imaging plates; images developed at factor 3.6) after 108 dpi. As reference, C-14 polymer sources were used with following activities [dpm cm^{-2}]: 1,107,000, 424,000, 112,000, 41,500, 13,350, and 3,950, supplemented by an activity free background (each activity had a surface area of 1 cm²). The blue color indicates areas with high ^{33}P activity.

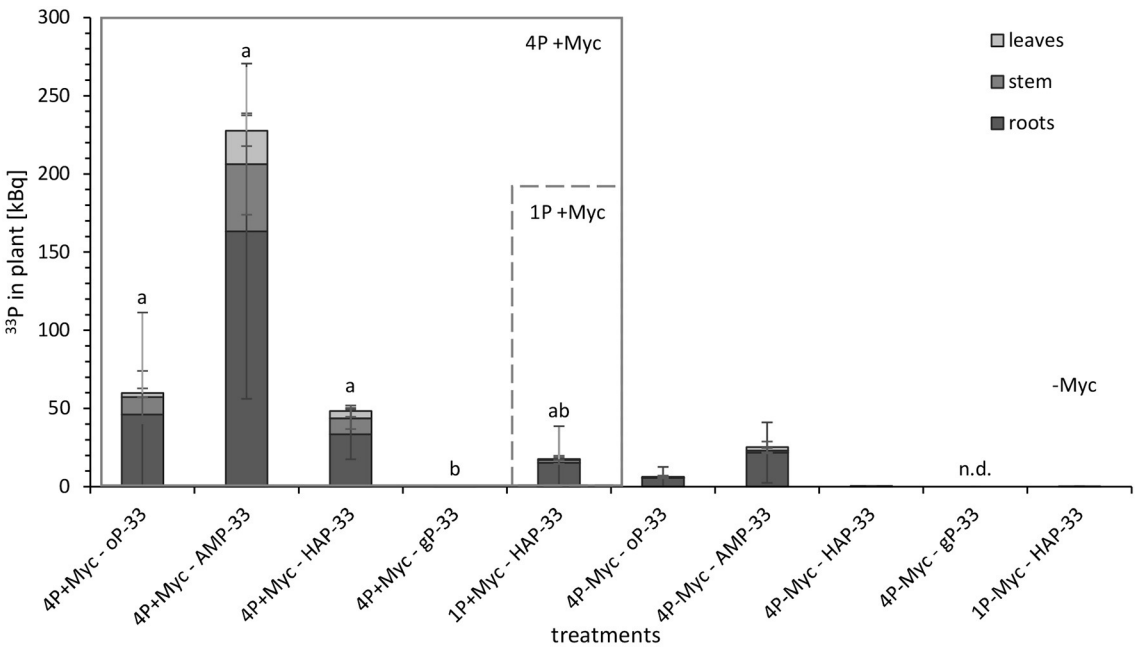

FIGURE 3 | ^{33}P activity [kBq] in different parts of mycorrhizal (+Myc) and non-mycorrhizal (-Myc) poplar plants at 108 dpi. 4P experiment with simultaneous supply of four different P sources: oP, *ortho*-phosphate; AMP, adenosine monophosphate; gP, oP bound to goethite; HAP, synthesized hydroxyapatite; and 1P control experiment supplied with HAP. The error bars show the standard deviation (4P+Myc: $n = 4$; 4P-Myc: $n = 3$; 1P+Myc: $n = 4$; 1P-Myc: $n = 2$). Data replaced by n.d. was below detection limit. The letters (a, b, c) indicate significant differences in ^{33}P activity in plant between 4p-^{33}P and 1HAP-^{33}P treatments: $P < 0.03$ (Kruskal-Wallis-*H*-test and subsequent Mann-Witney-*U*-test; see **Supplementary Table 3** for detailed information on statistical analysis).

a mineral P form supplied as a single P source in the system to support the general assumption that a minor diversity in belowground resources, e.g., due to fertilization, resulting in a reduced uptake efficiency (18). We can confirm the previous findings of Andrino et al. (26, 27), as our compartmental system using nylon and hydrophobic membranes to separate the P

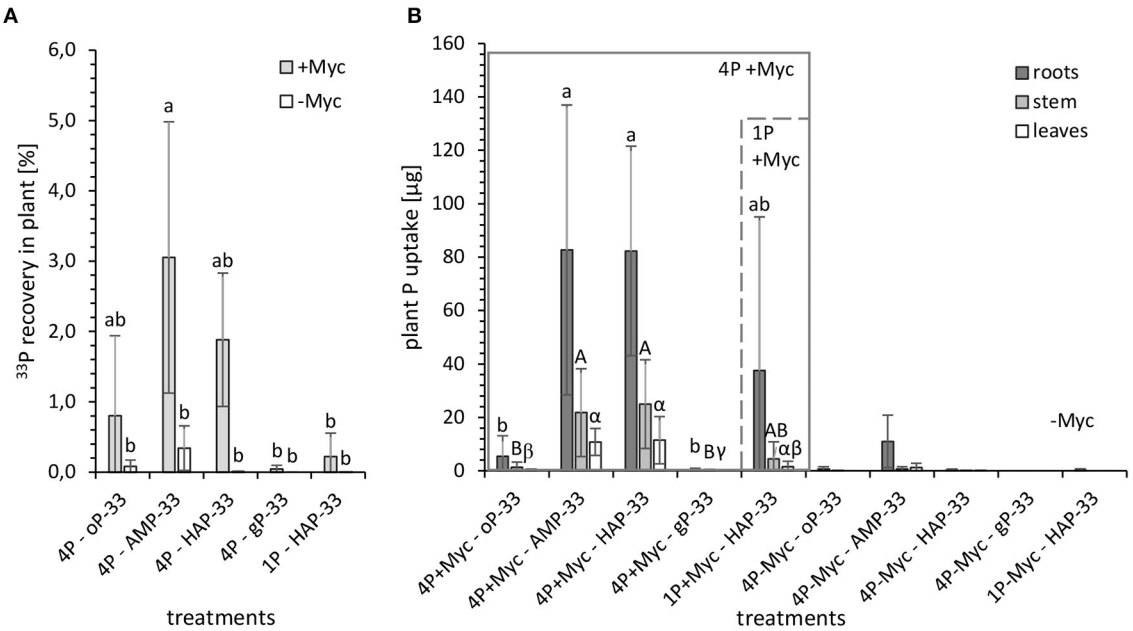

FIGURE 4 | (A) ^{33}P recovery [%] in plant and **(B)** plant P uptake [µg] from ^{33}P labeled P sources from mycorrhizal (+Myc, $n = 4$) and non-mycorrhizal (-Myc, $n = 3$ for 4P-^{33}P; and $n = 2$ for 1HAP-^{33}P) rhizotrones equipped with P containers with different P sources: 4P experiment with simultaneous supply of four different P sources: oP, *ortho*-phosphate; AMP, adenosine monophosphate; gP, oP bound to goethite; HAP, synthesized hydroxyapatite; and 1P control experiment supplied with HAP. The error bars show the standard deviation. The letters (a, A, α) indicate significant differences between the P treatments of 4P-^{33}P and 1HAP-^{33}P experiments: $P < 0.003$ (see **Supplementary Table 4** for more details).

sources from plant roots was a good choice to test mycorrhizal mediated plant P uptake. The small and negligible quantities of ^{33}P activity detected in non-mycorrhizal treatments possibly result from "leakiness" due to the process of autoclaving of the P compartments to sterilize them and create axenic conditions inside the system. After the autoclaving, the membranes could not adhere so tight anymore at some weaker spots of the P compartment, which we did not examine in this study. The autoclaving of the P compartments was chosen, as it was possible to sterilize a vast amount of P compartments simultaneously and thereby avoid the use of any chemicals and safe time of the preparation of the culture systems.

Our results confirm a successful mycorrhizal mediated plant P uptake from the P compartments, independent of the P form taken up from a pool of differently available P sources or a single P source. The mycorrhizal mediated plant P uptake from the P compartments of the P treatments resulted in the gain in plant biomass of a similar magnitude as absolute plant P content compared to the mycorrhizal no P control treatment. Also, the incorporation of the ^{33}P label (**Figures 2–4**) in mycorrhizal plants indicates a P uptake from all supplied P sources. Due to the axenic conditions prevalent in our system, we have excluded any competition with other microorganisms inhabiting the plant rhizosphere (40) and the fungal hyphosphere (41), which consume nutrients released by hyphae and root or also by feeding on hyphae (40, 42, 43), and which could reduce the control on the mycorrhizal fungal supply of P to plant. The images of harvested plants (**Figure 2**) showed areas with the highest 33P label incorporated in roots with high intensity in the branching of the root tips (**Supplementary Figure 3**), indicating that a high proportion of incorporated 33P label in the plant was detectable at the mycorrhizal fungus-root interface. This observation could result from a higher shielding of 33P by roots and shoots compared to the hyphal mantel around the root tips. In contrast to this assumption, the microradiographic localization of 33P in ectomycorrhizal poplar roots performed by Bücking and Heyser (44) has revealed that P taken up by hyphae accumulates rapidly in the hyphal mantel around the root tip and is slowly allocated through the Hartig net to the root cortical cells. Also, previous studies using excised roots detected an accumulation of P in the fungal sheet around the root tips and linked it to mycorrhizal fungal control on the amounts of P translocated to its host plant (11, 30). Nevertheless, results from experiments using excised plant roots should be handled with care, as they do not provide the same extent of a whole plant controlling its P demand and the P translocation by ECM fungus. The first successful attempt to describe the molecular processes of P transfer through the ectomycorrhizal Hartig net to plant roots under controlled conditions were made by the study of Becquer et al. (45). The H^+:P_i transporter, HcPT2, of *Hebeloma cylindrosporum* was determined not only in the extra-radical hyphae, serving for the P_i entry into the mycelium, but also in the Hartig net, aiding for the transfer of P_i to the host plant *Pinus pinaster*. Thereby, the host plant was also found to induce the expression of HcPT2, revealing that the host plant is regulating its P supply by the mycorrhizal fungus.

Nevertheless, mycorrhizal fungal P uptake preferences in an axenic system should more closely reflect the potential

capabilities (niches) (46, 47) in acquiring differently available P sources. The higher incorporation of the ^{33}P label and especially the significantly higher plant P uptake from AMP compared to oP was surprising. We have also expected that the fungus would start the P acquisition from oP, but within a week (27–34 dpi), we have detected a simultaneous uptake of oP and AMP. Nevertheless, our results cannot approve the assumption that the mycorrhizae prefer or would start to acquire the readily available oP. Free P_i has to be just taken up from the solution *via* the plasma membrane phosphate transporters at fungal hyphae (40), whereby the mycorrhizal fungus would not need to apply any acquiring mechanisms, causing no costs for the P mining. In contrast, the AMP is assumed to require a phosphomonoesterase to release the phosphate ion (P_i) (19). Previous studies provide evidence that the ectomycorrhizal fungal species *P. involutus* can produce phosphatases, which are largely surface-bound (48, 49). The phosphatase activity is considered to be induced by the substrate or a low concentration of P_i (7). Furthermore, the results of Scheerer et al. (50) have proposed that AMP (and/or ADP) or at least the nucleoside adenosine consisting of ribose and adenine could be taken up by excised roots of poplar cuttings and beech seedlings *via* some nucleotide transporters of the root, which were not indicated to date. Their assumption was built due to the uptake rates of ^{13}C and ^{15}N but also of ^{33}P of ATP tested as a P source for plant P uptake. We could not find experimental evidence for the uptake of the whole molecule of AMP or adenosine by mycorrhizal mycelium in the present literature. Still, it was already suggested by Rennenberg and Herschbach (51) that ectomycorrhizal fungi could take up organic P sources as a whole molecule. Many mycorrhizal species, including *P. involutus*, possess the ortholog of the yeast P_{org} transporter, ScGit1p (52). This transporter of *Saccharomyces cerevisiae* is upregulated under P limiting conditions and can import phospho-diesters (53). The activity of these transporters in ectomycorrhizal fungi/symbiosis was not identified to date and present a knowledge gap in the biochemistry of mycorrhizal plant P uptake. Nevertheless, this hypothesized mechanism could probably explain the mycorrhizal favoritism of AMP over oP in our study. The adenine could serve as an additional C and N source to the mycorrhizal fungal associate, reducing the dependency on C supply from the host plant.

However, the plasma membrane P_i transporters of ectomycorrhizal fungi of Basidiomecete are coupled with H^+ symporter (54). Also, the Git1p was shown to function as an H^+ symporter (55). Hence, with each imported P_i/P_{org} molecule, the P solution would lose one H^+, by which the pH in the P solution would increase. Also, the performance of Git1p was shown to drop with increasing pH (56). Likewise, in our study, the pH (**Supplementary Figure 6B**) increased significantly in harvested AMP solution of mycorrhizal treatments compared to the non-mycorrhizal treatments but also compared to the pH of 5.2 set initially. Considering the higher incorporation of the ^{33}P label from AMP, followed by oP and HAP, the pH increase in these P solutions in mycorrhizal treatments should be a consequent outcome.

On the one hand, if the activity of the Pi or Git1p transporters decreases with increasing pH, the similar plant P uptake from AMP and HAP could be explained by the pH increase in the AMP solution. We could detect the first incorporation of the 33P label in the plant from HAP only 1 week later compared to AMP and oP in the 4P system. On the other hand, HAP was supplied with a 2-fold higher P amount initially, which could indicate that besides the P source availability also the P amount of a P source is additionally essential for the choice of P uptake from a pool with different P sources by mycorrhizal fungus and its delivery to the plant. To underpin this assumption, shifts in nutritional strategies from acquisition (weathering of P rich primary minerals) to recycling (of accumulated P stocks in organic or secondary mineral P forms) were already observed from P-rich to P-poor temperate beech forests (7), suggesting that the most profuse P sources in an ecosystem are (of course depending on their bioavailability) the most favorable for the acquisition.

Inorganic P bound to metal oxides is considered not or only hardly accessible for P uptake by mycorrhizal plants and accumulating in the Lüss subsoil of forests limited in P (10). This was indebted to the high abundance of Fe and Al oxides in the Bw horizon and comprehensive adsorption of P to the mineral surface. Thus, it might not be surprising that the mycorrhizal mediated plant P uptake from gP was of the lowest magnitude compared to the other P sources supplied in the mixed pool. The desorption of P_i from goethite in H_2O is affected by sorption-desorption equilibrium and diffusion transport (35). Further, low molecular organic anions (LMWOAs) increase the release and availability of P_i sorbed to goethite *via* ligand exchange. The ectomycorrhizal fungal genera Paxillus were described to release extensive amounts of LMWOAs (57, 58). *P. involutus* was also shown to produce and exude oxalate (59–61), which is suggested to be also a key component in apatite dissolution for the P uptake by ectomycorrhizal fungi and immobilization of Ca into Ca-oxalate (62). Furthermore, it was shown for arbuscular mycorrhizae that if the P source occurs in a not dissolved form, the P is more uniformly shared between the mycorrhizal associates (26). The higher retention of P in hyphae was considered to be a response to P bioavailability (63) and enabled the arbuscular mycorrhizal fungus to invest in the growth of its hyphae to reach the not soluble P sources (64, 65). However, the plant P uptake from gP (**Figure 4B**; **Supplementary Table 4)** was lower compared to the easy desorbable P from the same P source. Nevertheless, this parameter represents the maximal desorption rate of P bound to goethite supplied in dH_2O suspended form, which was obtained by shaking the gP suspension for 24 h. In our study, the filled P compartments and the rhizotrone systems were handled with care and did not experience extensive shaking. We could instead attribute the lower P uptake from gP to its voluminous but at the same time compact consistency, which indirectly categorizes gP as a more complex P source within the mixed pool in our study. It has been suggested that ectomycorrhizal fungi can function as "biosensors" searching for nutrients from mineral sources and differentiate the mineralogy and grain sizes (61, 62). This could have lead *P. involutus* to favor HAP over gP in our study. Nevertheless, for all these reasons, we can conclude that the later and lower P incorporation in the *P. involutus* ectomycorrhizal plant could be due to the higher complexity of gP as a P source and the lower ^{33}P activity applied initially compared with other P sources.

The absolute P content in the plant and leaves of 4P treatments was significantly higher compared to the 1P treatment. This indicates that the fungus can supply the plant with more P either due to the presence of specific P forms in a mixed P pool or due to a general effect of P source diversity. To explain the latter effect of P source diversity with more favorable and readily available P sources besides the more complex P sources, we could assume that a mixed P pool might work as a "spiking" instrument to ensure an easier and faster familiarization of ectomycorrhiza to P sources with different bioavailabilities. Nevertheless, both statements are strongly supported by the significantly higher incorporation of the ^{33}P label [kBq] from AMP and its significantly higher ^{33}P recovery [%] in plant leaves compared to the 1P-HAP treatment. Higher P content in leaves of 4P plant treatments presumably allowed the earlier acquisition of HAP in 4P systems compared to the 1P system, as a higher C translocation to the HAP compartments is required to release Pi through exudation of organic anions (62). In contrast, photosynthesis is restricted under P limiting conditions (66), reducing at the same time the translocation of C to the below-ground infrastructure in order to mine the HAP patches. The lower P content in leaves of 1P treatment could result in lower photosynthetic fixation of CO_2 that consequently could result in a lower C allocation to the mycorrhizal partner for the acquisition of HAP supplied as a single P source and could explain its later uptake. Nevertheless, there was no difference in plant P uptake from HAP supplied as a single P source or with different P sources, even though the amount of P supplied with HAP as a single P source was 1/3-fold higher compared with the sum of P amounts supplied with the four different P sources in the 4P system.

CONCLUSION

In the conducted rhizotrone experiment under axenic conditions, our results indicate that the representative ectomycorrhizal fungus *P. x involutus* was able to access all P sources (oP, AMP, HAP, and gP) we have supplied with the P pool, suggesting that this ectomycorrhizal fungus can act as a generalist in P acquisition. We assume a different weighting between the ectomycorrhizal species offering a playground for further research. Nevertheless, we confirm that specialization to the acquisition of one or a few specific P sources while having access to many in order to find a niche of an appropriate resource occur as an option or need due to competition for limited soil resources (67). Ectomycorrhizal fungi, compared with other P acquiring strategies of plants, could be unequally capable of occupying a broad variety of niches (68), which could explain the dominating occurrence of ectomycorrhizal fungi in many boreal (69–71) and temperate (70, 72, 73) forest ecosystems limited in P, controlling the occurrence of other species. Our results indicate that nutrient niching is possible in one species of ectomycorrhiza and that P resource diversity improves plant nutrition, providing supporting evidence for higher functional diversity by nutrient source partitioning.

In our study, from the mixed P pool, the sources AMP and HAP (over oP) were the most favorable to ectomycorrhizal mediated plant P uptake. We conclude that the magnitude of plant P uptake from a mixed pool containing P sources of different availabilities depends on the P species itself, additional nutrients coming with the specific P sources, and the complexity of the P source. In contrast, the order of uptake of different P forms depended on their complexity (oP and AMP over HAP and gP) and supplied diversity (HAP in a pool over HAP alone).

Even though we have used one mycorrhizal fungus and one plant only, to our knowledge, we are the first in showing that the ectomycorrhizal *P. x canescens* can occupy simultaneously fundamental niches of various P sources through the mediation of its mycorrhizal fungal partner *P. involutus*, indicating that the acquisition of differently available P sources by an ectomycorrhiza can facilitate niche plasticity and adaptation to specific nutrient limiting conditions.

DATA AVAILABILITY STATEMENT

The original contributions presented in the study are included in the article, further inquiries can be directed to the corresponding author.

AUTHOR CONTRIBUTIONS

JB, KS, AA, GG, AF, and LS designed the experiment. KS prepared the plant, fungal material, everything for the rhizotrone culture systems, performed the experiment, sample, data analysis, and wrote the paper. DH synthesized the hydroxyapatite and irrigated and imaged the systems from day 10 to 88 as well as performed LSC analysis of plant extracts. JB and GG supervised the research. All authors contributed to the article and approved the submitted version.

FUNDING

We want to thank the German Federal Ministry of Education and Research for the funding of this project in the framework of the DFG-RTG 1798 Signaling at the Plant-Soil Interface. The publication of this article was funded by the Open Access fund of Leibniz Universität Hannover.

ACKNOWLEDGMENTS

The authors are thankful for the great help and guidance received by Traud Winkelmann, Maximillian Koch, Stephan Köppchen, Nina Siebers, Jens Kruse, Anne Herwig, and Viola Rünzi. The plant material (*P. x canescens* clone Schleswig I) was kindly provided by Andreas Meier-Dinkel from the Nordwestdeutsche Versuchsanstalt (Germany). The ecto-mycorrhizal fungal material, *P. involutus*, was kindly provided by Andrea Polle, Abteilung Forstbotanik und Baumphysiologie (Büsgen-Institut, Georg-August Universität Göttingen, Germany).

SUPPLEMENTARY MATERIAL

The Supplementary Material for this article can be found online at: https://www.frontiersin.org/articles/10.3389/fsoil.2022.865517/full#supplementary-material

REFERENCES

1. Plassard C, Dell B. Phosphorus nutrition of mycorrhizal trees. Invited review: part of an invited issue on tree nutrition. *Tree Physiol.* (2010) 30:1129–39. doi: 10.1093/treephys/tpq063
2. Elser JJ, Bracken MES, Cleland EE, Gruner DS, Harpole WS, Hillebrand H. Global analysis on nitrogen and phosphorus limitation of primary producers in freshwaters, marine, and terrestrial ecosystems. *Ecol Lett.* (2007) 10:1135–42. doi: 10.1111/j.1461-0248.2007.01113.x
3. Mengel K, Kirkby EA. Phosphorus. In: K Mengel, EA Kirkby, H Kosegarten, T Appel, editors, *Principles of Plant Nutrition*. Dordrecht: Springer (2001). p. 453479. doi: 10.1007/978-94-010-1009-2_9
4. Hinsinger P. Bioavailability of soil inorganic P in the rhizosphere as affected by root-induced chemical changes: a review. *Plant Soil.* (2001) 237:173–95. doi: 10.1023/A:1013351617532
5. Holford ICR. Soil phosphorus: its measurement, and its uptake by plants. *Austr J Soil Res.* (1997) 35:227–40. doi: 10.1071/S96047
6. Hinsinger P, Betencourt E, Bernard L, Brauman A, Plassard C, Shen J, et al. P for two, sharing a scarce resource: soil phosphorus acquisition in the rhizosphere of intercropped species. *Plant Physiol.* (2011) 156:1078–86. doi: 10.1104/pp.111.175331
7. Lang F, Krüger J, Amelung W, Willbold S, Frossard E, Bünemann E, et al. Soil phosphorus supply controls P nutrition strategies of beech forest ecosystems in Central Europe. *Biogeochem.* (2017) 136:5–29. doi: 10.1007/s10533-017-0375-0
8. Odum EP. The strategy of ecosystem development. *Science* (1969) 164:267–70. doi: 10.1126/science.164.3877.262
9. Walker TW, Syers JK. The fate of phosphorus during pedogenesis. *Geoderma.* (1976) 15:1–19. doi: 10.1016/0016-7061(76)90066-5
10. Klotzbücher A, Schunck F, Klotzbücher T, Kaiser K, Glaser B, Spohn M. Goethite-bound phosphorus in an acidic subsoil is not available to beech (*Fagus sylvatica* L.). *Fron Forests Glob Change.* (2020) 3:94. doi: 10.3389/ffgc.2020.00094
11. Smith SE, Read DJ. *Mycorrhizal Symbiosis*. 3rd ed. Great Britain: Academic Press (2008).
12. Owen D, Williams AP, Griffith GW, Withers PJA. Use of commercial bio-inoculants to increase agricultural production through improved phosphrous acquisition. *Appl Soil Ecol.* (2014) 86:41–54. doi: 10.1016/j.apsoil.2014.09.012
13. Jones MD, Durall DM, Tinker PB. A comparison of arbuscular and ectomycorrhizal *Eucalyptus coccifera*: growth response, phosphorus uptake efficiency and external hyphal production. *New Phytol.* (1998) 140:125–34. doi: 10.1046/j.1469-8137.1998.00253.x
14. Plassard C, Louche J, Ali MA, Duchemin M, Legname E, Cloutier-Hurteau B. Diversity in phosphorus mobilisation and uptake in ectomycorrhizal fungi. *Ann Forest Sci.* (2011) 68:33–43. doi: 10.1007/s13595-010-0005-7
15. Smith FA, Smith SE. What is the significance of the arbuscular mycorrhizal colonisation of many economically important crop plants? *Plant Soil.* (2011) 348:63–79. doi: 10.1007/s11104-011-0865-0
16. Landeweert R, Hoffland E, Finlay RD, Kuyper TW, van Breemen N. Linking plants to rock: ectomycorrhizal fungi mobilise nutrients from minerals. *Trends Ecol Evol.* (2001) 16:248–54. doi: 10.1016/S0169-5347(01)02122-X
17. Antibus RK, Sinsabaugh RL, Linkins AE. Phosphatase activities and phosphorus uptake from inositol phosphate by ectornycorrhizal fungi. *Canad J Botany.* (1992) 70:794–802. doi: 10.1139/b92-101
18. Zavišić A, Yang N, Marhan S, Kandeler E, Polle A. Forest soil phosphorus resources and fertilization affect ectomycorrhizal community composition, beech p uptake efficiency, and photosynthesis. *Front Plant Sci.* (2018) 9:463. doi: 10.3389/fpls.2018.00463
19. Turner BL. Resource partitioning for soil phosphorus: a hypothesis. *J Ecol.* (2008) 96:698–702. doi: 10.1111/j.1365-2745.2008.01384.x
20. Wassen MJ, Venterink HO, Lapshina ED, Tanneberger F. Endangered plants persist under phosphorus limitation. *Nature.* (2005) 437:547–50. doi: 10.1038/nature03950
21. Ceuleman T, Stevens CJ, Duchateau L, Jacquemyn H, Gowing DJG, Merck R, et al. Soil phosphorus constrains biodiversity across European grasslands. *Glob Change Biol.* (2014) 20:3814–22. doi: 10.1111/gcb.12650
22. Cleveland CC, Townsend AR, Taylor P, Alvarez-Clare S, Bustamante M, Chuyong G, et al. Relationships among net primary productivity, nutrients and climate in tropical rain forest: a pan-tropical analysis. *Ecol Lett.* (2011) 14:939–47. doi: 10.1111/j.1461-0248.2011.01658.x
23. Ahmad-Ramli MF, Cornulier T, Johnson D. Partitioning of soil phosphorus regulates competition between *Vaccinium vitis-idaea* and *Deschampsia cespitosa*. *Ecol Evol.* (2013) 3:4243–52. doi: 10.1002/ece3.771
24. Steidinger BS, Turner BL, Corrales A, Dalling JW. Variability in potential to exploit different organic phosphorus compounds among tropical montane tree species. *Funct Ecol.* (2014) 29:121–30. doi: 10.1111/1365-2435.12325
25. Liu X, Burslem DFRP, Taylor JD, Taylor AFS, Khoo E, Majalap-Lee N, et al. Partitioning of soil phosphorus among arbuscular and ectomycorrhizal trees in tropical and subtropical forests. *Ecol Lett.* (2018) 21:713–23. doi: 10.1111/ele.12939
26. Andrino A, Boy J, Mikutta R, Sauheitl L, Guggenberger G. Carbon investment required for the mobilization of inorganic and organic phosphorus bound to goethite by an arbuscular mycorrhiza (*Solanum lycopersicum* x *Rhizophagus irregularis*). *Fron Environm Sci.* (2019) 7:26. doi: 10.3389/fenvs.2019.00026
27. Andrino A, Guggenberger G, Sauheitl L, Burkart S, Boy J. Carbon investment into mobilization of mineral and organic phosphorus by arbuscular mycorrhiza. *Biol Fertil Soils.* (2021) 57:47–64. doi: 10.1007/s00374-020-01505-5
28. Pearson JN, Jakobsen I. The relative contribution of hyphae and roots to phosphorus uptake by arbuscular mycorrhizal plants, measured by dual labelling with ^{32}P and ^{33}P. *New Phytol.* (1993) 124:489–94. doi: 10.1111/j.1469-8137.1993.tb03840.x
29. Phoenix GK, Johnson DA, Muddimer SP, Leake JR, Cameron DD. Niche differentiation and plasticity in soil phosphorus acquisition among co-occuring plants. *Nature Plants.* (2020) 6:349–54. doi: 10.1038/s41477-020-0624-4
30. Hodge A. Accessibility of inorganic and organic nutrients for mycorrhizas. In: Johnson NC, Gehring C, Jansa J, editors. *Mycorrhizal Mediation of Soil: Fertility, Structure, and Carbon Storage*. Amsterdam: Elsevier (2017). p. 129–48.
31. Rajaniemi TK. Why does fertilization reduce plant species diversity? Testing three competition-based hypotheses. *J Ecol.* (2002) 90:316–24. doi: 10.1046/j.1365-2745.2001.00662.x
32. Rieger I, Kowarik I, Ziche D, Wellbrock N, Cierjacks A. Linkages between phosphorus and plant diversity in Central European Forest Ecosystems – complementarity or competition? *Forests.* (2019) 10:1156. doi: 10.3390/f10121156
33. Gafur A, Schutzendubel A, Langenfeld-Heyser R, Fritz E, Polle A. Compatible and incompetent *Paxillus involutus* isolates for ectomycorrhiza formation *in vitro* with poplar (*Populus* × *canescens*) differ in H_2O_2 production. *Plant Biol.* (2003) 6:91–9. doi: 10.1055/s-2003-44718
34. Müller A, Volmer K, Mishra-Knyrim M, Polle A. Growing poplars for research with and without mycorrhizas. *Fron Plant Sci.* (2013) 4:332. doi: 10.3389/fpls.2013.00332
35. Yan Y, Koopal LK, Liu F, Huang Q, Feng X. Desorption of myo-inositol hexakisphosphate and phosphate from goethite by different reagents. *J Plant Nutrit Soil Sci.* (2015) 2015:jpln.201500254. doi: 10.1002/jpln.201500254
36. Wolff J, Hofmann D, Amelung W, Lewandowski H, Kaiser K, Bol R. Rapid wet chemical synthesis for 33P-labelled hydroxyapatite – an approach for environmental research. *Appl Geochem.* (2018) 97:181–6. doi: 10.1016/j.apgeochem.2018.08.010
37. Giovannetti M, Mosse B. An evaluation of techniques for measuring vesicular arbuscular mycorrhizal infection in roots. *New Phytolog.* (1980) 84:489–500. doi: 10.1111/j.1469-8137.1980.tb04556.x
38. Brundrett M, Bougher N, Dell B, Grove T, Malajczuk N. *Working with Mycorrhizas in Forestry and Agriculture*. *ACIAR Monograph.* Canberra, ACT: Australian Centre for International Agricultural (1996). p. 32.
39. IBM Corporation. *IBM SPSS Statistics for Windows, Versions 24.0.2016 and 28.0.1.0.* Armonk, NY: IBM Corporation (2016). p. 142.
40. Becquer A, Trap J, Irshad U, Ali MA, Claude P. From soil to plant, the journey of P through trophic relationships and ectomycorrhizal association. *Fron Plant Sci.* (2014) 5:548. doi: 10.3389/fpls.2014.00548
41. Warmink JA, Nazir R, van Elsas JD. Universal and species-specific bacterial "fungiphiles" in the mycospheres of different basidiomycetous fungi. *Environm Microbiol.* (2009) 11:300–12. doi: 10.1111/j.1462-2920.2008.01767.x

42. Nazir R, Warmink JA, Boersma H, van Elsas JD. Mechanisms that promote bacterial fitness in fungal-affected soil microhabitats. *FEMS Microbiol Ecol.* (2010) 71:169–85. doi: 10.1111/j.1574-6941.2009.00807.x
43. Ballhausen MB, Vandamme P, de Boer W. Trait differentiation within the fungus-feeding (mycophagous) bacterial genus Collimonas. *PLoS ONE.* (2016) 11:e0157552. doi: 10.1371/journal.pone.0157552
44. Bücking H, Heyser W. Microautoradiographic localization of phosphate and carbohydrates in mycorrhizal roots of Populus tremula x Populus alba and the implications for transfer processes in ectomycorrhizal associations. *Tree Physiol.* (2001) 21:101–7. doi: 10.1093/treephys/21.2-3.101
45. Becquer A, Garcia K, Amenc L, Rivard C, Dore J, Trives-Segura C, et al. The Hebeloma cylindrosporum HcPT2 Pi transporter plays a key role in ectomycorrhizal symbiosis. *New Phytol.* (2018) 220:1185–99. doi: 10.1111/nph.15281
46. McKane RB, Johnson LC, Shaver GR, Nadelhoffer KJ, Rastetter EB, Fry B, et al. Resource-based niches provide a basis for plant species diversity and dominance in arctic tundra. *Nature.* (2002) 415:68–71. doi: 10.1038/415068a
47. Hutchinson GE. Homage to Santa Rosalia, or why are there so many kinds of animals? *Am Nat.* (1959) 93:145–59. doi,: 10.1086/282070
48. Alvarez M, Godoy R, Heyser W, Härtel S. Surface bound phosphatase activity in living hyphae of ectomycorrhizal fungi of Nothofagus obliqua. *Mycologia.* (2004) 96:479–87. doi: 10.2307/3762168
49. McElhinney C, Mitchell DT. Phosphatase activity of four ectomycorrhizal fungi found in a Sitka spruce–Japanese larch plantation in Ireland. *Mycol Res.* (1993) 97:725–32. doi: 10.1016/S0953-7562(09)80154-8
50. Scheerer U, Trube N, Netzer F, Rennenberg H, Herschbach C. ATP as phosphorus and nitrogen source for nutrient uptake by *Fagus sylvatica* and Populus x canescens Roots. *Front Plant Sci.* (2019) 10:378. doi: 10.3389/fpls.2019.00378
51. Rennenberg H, Herschbach C. Phosphorus nutrition of woody plants: many questions - few answers. *Plant Biol.* (2013) 15:785–8. doi: 10.1111/plb.12078
52. Plassard C, Becquer A, Garcia K. Phosphorus transport in mycorrhiza: how far are we? *Trends Plant Sci.* (2019) 24:794–801. doi: 10.1016/j.tplants.2019.06.004
53. Patton-Vogt J. Transport and metabolism of glycerophosphodiesters produced through phospholipid deacylation. *Biochim Biophys Acta.* (2007) 1771:337–42. doi: 10.1016/j.bbalip.2006.04.013
54. Nels U, Plassard C. Nitrogen and phosphate metabolism in ectomycorrhizas. *New Phytol.* (2018) 220:1047–58. doi: 10.1111/nph.15257
55. Pao SS, Paulsen IT, Saier MH. Major facilitator superfamily. *Microbiol Mol Biol Rev.* (1998) 62:1–34. doi: 10.1128/MMBR.62.1.1-34.1998
56. Almaguer C, Cheng W, Nolder C, Patton-Vogt J. Glycerophosphoinositol, a novel phosphate source whose transport is regulated by multiple factors in *Saccharomyces cerevisiae*. *J Biol Chem.* (2004) 279:31937–42. doi: 10.1074/jbc.M403648200
57. Courty PE, Franc A, Garbaye J. Temporal and functional pattern of secreted enzyme activities in an ectomycorrhizal community. *Soil Biol Biochem.* (2010) 42:2022–5. doi: 10.1016/j.soilbio.2010.07.014
58. Smith SE, Anderson IC, Smith FA. Mycorrhizal association and phosphorus acquisition: from cell to ecosystems. *Ann Plant Rev.* (2015) 48:409–40. doi: 10.1002/9781118958841.ch14
59. Lapeyrie F, Chilvers GA, Bhem CA. Oxalic acid synthesis by the mycorrhizal fungus *Paxillus involutus* (Batsch EX FR) FR. *New Phytol.* (1987) 106:139–46. doi: 10.1111/j.1469-8137.1987.tb04797.x
60. Lapeyrie F, Ranger J, Vairelles D. Phosphate-solubilizing activity of ectomycorrhizal fungi *in vitro*. *Can J Bot.* (1991) 69:342–6. doi: 10.1139/b91-046
61. Schmalenberger A, Duran AL, Bray AW, Bridge J, Bonneville S, Benning LG, et al. Oxalate secretion by ectomycorrhizal *Paxillus involutus* is mineral-specific and controls calcium weathering from minerals. *Sci Rep.* (2015) 5:12187. doi: 10.1038/srep12187
62. Leake JR, Duran AL, Hardy KE, Johnson I, Beerling DJ, Banwart SA, et al. Biological weathering in soil: the role of symbiotic root-associated fungi biosensing minerals and directing photosynthate-energy into grain-scale mineral weathering. *Mineral Mag.* (2008) 72:85–9. doi: 10.1180/minmag.2008.072.1.85
63. Ezawa T, Smith SE, Smith FAP. P metabolism and transport in AM fungi. *Plant Soil.* (2002) 244:221–30. doi: 10.1023/A:1020258325010
64. Olsson PA, Hammer EC, Wallander H, Pallon J. Phosphorus availability influences elemental uptake in the mycorrhizal fungus *Glomus intraradices*, as revealed by particle-induced X-ray emission analysis. *Appl Environ Microbiol.* (2008) 74:4144–8. doi: 10.1128/AEM.00376-08
65. Hammer EC, Pallon J, Wallander H, Olsson PA. Tit for tat? A mycorrhizal fungus accumulates phosphorus under low plant carbon availability. *FEMS Microbiol Ecol.* (2011) 76:236–44. doi: 10.1111/j.1574-6941.2011.01043.x
66. Carstensen A, Herdean A, Birkelund Schmidt S, Sharma A, Spetea C, Pribil M, et al. The impacts of phosphorus deficiency on the photosynthetic electron transport chain. *Plant Physiol.* (2018) 177:271–84. doi: 10.1104/pp.17.01624
67. Dickie IA. Host preference, niches and fungal diversity. *New Phytol.* (2007) 174:230–3. doi: 10.1111/j.1469-8137.2007.02055.x
68. McNaughton SJ, Wolf LL. Dominance and the Niche in ecological systems. *Science.* (1970) 167:131–9. doi: 10.1126/science.167.3915.131
69. Singer R, Morello JH. Ectotrophic forest tree mycorrhiza and forest communities. *Ecol.* (1960) 41:549. doi: 10.2307/1933331
70. Meyer FH. Distribution of ectomycorrhizae in native and manmade forests. In: GC Marks, TT Kozlowski, editors, *Ectomycorrhizae: Their Ecology and Physiology*. New York, NY: Academic Press (1973). p. 79–105. doi: 10.1016/B978-0-12-472850-9.50009-8
71. Read DJ. Mycorrhizas in ecosystems. *Experientia.* (1991) 47:376–91. doi: 10.1007/BF01972080
72. Moser M. Die ectotrophe Ernährungsweise an der Waldgrenze. *Mitt Forstl Bundesversuchsanst Wien.* (1967) 75:357.
73. Rosling A, Midgley MG, Cheeke T, Urbina H, Fransson P, Phillips RP. Phosphorus cycling in deciduous forest soil deffers between stands dominated by ecto- and arbuscular mycorrhizal trees. *New Phytol.* (2016) 209:1184–95. doi: 10.1111/nph.13720

Conflict of Interest: DH was employed by Institute of Bio- and Geosciences, IBG-3: Agrosphere, Forschungszentrum Jülich GmbH.

The remaining authors declare that the research was conducted in the absence of any commercial or financial relationships that could be construed as a potential conflict of interest.

frontiers | Frontiers in Microbiology

ORIGINAL RESEARCH
published: 13 April 2022
doi: 10.3389/fmicb.2022.864411

Thermoacidophilic Bioleaching of Industrial Metallic Steel Waste Product

*Denise Kölbl[1], Alma Memic[1], Holger Schnideritsch[2], Dominik Wohlmuth[2], Gerald Klösch[2], Mihaela Albu[3], Gerald Giester[4], Marek Bujdoš[5] and Tetyana Milojevic[1]**

[1] Extremophiles/Space Biochemistry Group, Department of Biophysical Chemistry, University of Vienna, Vienna, Austria, [2] voestalpine Stahl Donawitz GmbH, Leoben, Austria, [3] Graz Centre for Electron Microscopy, Graz, Austria, [4] Department of Mineralogy and Crystallography, University of Vienna, Vienna, Austria, [5] Faculty of Natural Sciences, Comenius University, Bratislava, Slovakia

OPEN ACCESS

Edited by:
Muhammad Zahid Mumtaz, University of Lahore, Pakistan

Reviewed by:
Samiullah Khan, University of Lahore, Pakistan
Basanta Kumar Biswal, National University of Singapore, Singapore
Omeid Rahmani, Islamic Azad University, Iran
Arpan Mukherjee, Precision BioSciences, United States

***Correspondence:**
Tetyana Milojevic
tetyana.milojevic@univie.ac.at

Specialty section:
This article was submitted to Microbiological Chemistry and Geomicrobiology, a section of the journal Frontiers in Microbiology

Received: *28 January 2022*
Accepted: *14 March 2022*
Published: *13 April 2022*

Citation:
Kölbl D, Memic A, Schnideritsch H, Wohlmuth D, Klösch G, Albu M, Giester G, Bujdoš M and Milojevic T (2022) Thermoacidophilic Bioleaching of Industrial Metallic Steel Waste Product. Front. Microbiol. 13:864411. doi: 10.3389/fmicb.2022.864411

The continuous deposition of hazardous metalliferous wastes derived from industrial steelmaking processes will lead to space shortages while valuable raw metals are being depleted. Currently, these landfilled waste products pose a rich resource for microbial thermoacidophilic bioleaching processes. Six thermoacidophilic archaea (*Sulfolobus metallicus, Sulfolobus acidocaldarius, Metallosphaera hakonensis, Metallosphaera sedula, Acidianus brierleyi,* and *Acidianus manzaensis*) were cultivated on metal waste product derived from a steelmaking process to assess microbial proliferation and bioleaching potential. While all six strains were capable of growth and bioleaching of different elements, *A. manzaensis* outperformed other strains and its bioleaching potential was further studied in detail. The ability of *A. manzaensis* cells to break down and solubilize the mineral matrix of the metal waste product was observed *via* scanning and transmission electron microscopy. Refinement of bioleaching operation parameters shows that changes in pH influence the solubilization of certain elements, which might be considered for element-specific solubilization processes. Slight temperature shifts did not influence the release of metals from the metal waste product, but an increase in dust load in the bioreactors leads to increased element solubilization. The formation of gypsum crystals in course of *A. manzaensis* cultivation on dust was observed and clarified using single-crystal X-ray diffraction analysis. The results obtained from this study highlight the importance of thermoacidophilic archaea for future small-scale as well as large-scale bioleaching operations and metal recycling processes in regard to circular economies and waste management. A thorough understanding of the bioleaching performance of thermoacidophilic archaea facilitates further environmental biotechnological advancements.

Keywords: thermoacidophiles, bioleaching, steel waste, archaea, metal recovery

INTRODUCTION

The mobilization of metal ions from various insoluble mineral phases has been widely used in biotechnological processes to recover useful metals (White et al., 1998; Donati and Sand, 2007; Khaing et al., 2019). However, the potential of metalliferous steel waste as a circular provider of precious metals for developing technologies has yet to be uncovered. The European Steel Association (EUROFER) states that approximately 278 million tons of steel have been produced in 2020 in Europe (15.2% of worldwide steel production), while generating millions of tons of various waste products (EUROFER, 2020). Many types of hazardous wastes, such as slags, dust, and ash, create space shortages due to their necessary deposition in landfills, contributing to the release of hazardous metalliferous wastes into our environment while leading to a depletion of valuable raw materials (Singh et al., 2013; World Steel Association, 2016).

For this study, a secondary dust waste product of the basic oxygen furnace (BOF) steelmaking process (hereafter referred to as BOF-dust) (Gara and Schrimpf, 1998; voestalpine Stahl Donawitz GmbH, Leoben, Austria) is investigated for microbial metal recovery potential by six thermoacidophilic archaeal strains. The potential of growth, metal solubilization, and the interaction of thermoacidophilic archaea with secondary dust particles was investigated to assess future implementation in high-temperature bioleaching operations. Steel waste products pose a rich resource of metal oxides that need to be recycled or reintroduced into the manufacturing system by natural microbial processes (Pawlowski et al., 1984; Krebs et al., 1997; Barbuta et al., 2015; Waste Disposal Recycling in Steel Industry, 2019). Biomining and bioleaching are well-established operations that are applied in a variety of mineral mining-associated industries and laboratory-scale operations (Bosecker, 1997; Schippers et al., 2013; Jujun et al., 2015; Banerjee et al., 2017; Blazevic et al., 2019). Additionally, microorganisms have been applied to detoxify metal-contaminated compounds derived from industrial processes such as incineration bottom ash, fly ash, slags from smelting processes, heavy metal waste from tanning factories (Batool, 2012; Igiri et al., 2018; Mäkinen et al., 2019; Srichandan et al., 2019), electronic scrap (Brandl et al., 2001), radioactive waste environments (Brim et al., 2003; Manobala et al., 2019), and many more through bioleaching.

Bioleaching is a process based on the ability of microorganisms (archaea, bacteria, fungi, etc.) to convert insoluble metals into a soluble state (Schippers et al., 2013). Usually, this process is performed by acidophilic microorganisms that are genetically equipped to oxidize Fe^{2+} into Fe^{3+} and/or reduced inorganic sulfur compounds (RISCs) at a low pH (acidophilia), preferably by growing in the unity of biofilms and frequently attaching to the mineral material, forming a reaction space (Valdés et al., 2008; Ma et al., 2017; Zhang et al., 2019). Bioleaching at elevated temperatures exploits the potential of thermoacidophilic archaea (∼70–80°C), whereas mesophilic bioleaching is performed by bacteria at lower temperatures (∼25–40°C) (Norris, 1997). Bioleaching operations executed by thermoacidophilic archaea (e.g., *Sulfolobus* spp., *Metallosphaera* spp., and *Acidianus* spp.) benefit from a more efficient mineral dissolution compared to mesophilic bacterial bioleaching (Marsh and Norris, 1983; Gericke and Pinches, 1999; Wang et al., 2014).

Since bioleaching processes of a large ore mass can generate a significant amount of exothermic heat (Beck, 1967), thermophiles such as *Acidianus brierleyi* proved themselves inherently suitable for high-temperature operations. *A. brierleyi* cells propagate chemolithotrophically by S^0 or Fe^{2+} redox chemistry (Segerer et al., 1986) and provide a higher sphalerite ($CuFeS_2$) leaching rate compared to a mesophilic bacterium *Acidithiobacillus ferrooxidans* culture (Konishi et al., 1998; Saitoh et al., 2017). Furthermore, Sulfolobales representatives, such as *Sulfolobus metallicus* (Huber and Stetter, 1991) and *Sulfolobus acidocaldarius* (Brock et al., 1972), mobilize copper, zinc, and uranium (Gautier et al., 2007), provide desulfurization strategies for coal (Shivvers and Brock, 1973; Kargi and Robinson, 1985; Tobita et al., 1994), and oxidize arsenite to arsenate in culture (Sehlin and Lindström, 1992). Great potential in industrial heap bioleaching is demonstrated by *Metallosphaera hakonensis* (Takayanagi et al., 1996) due to high Fe^{2+} oxidation rates when grown on inorganic sulfur compounds (Bromfield et al., 2011; Shiers et al., 2013). Closely related thermoacidophilic *Metallosphaera sedula* utilizes various metal-containing ores as well as organic carbon sources to feed its respiratory electron transport chain (Huber et al., 1989; Auernik and Kelly, 2010a,b). Besides inherent (chalco-)pyrite bioleaching abilities (Mikkelsen et al., 2007; Ai et al., 2019), *M. sedula* can oxidize solid triuranium octaoxide (U_3O_8) to U(VI) while feeding own bioenergetic needs (Mukherjee et al., 2012). Furthermore, *M. sedula* cells are able to biotransform the calcium-tungstate mineral *scheelite* by leaching mineral-bound tungsten into the surrounding, resulting in tungsten carbide layers on the cell surface (Blazevic et al., 2019). Precious metals from synthetic (Kölbl et al., 2017), as well as genuine extraterrestrial materials such as meteorites (ordinary chondrite NWA 1172; Martian breccia NWA 7034) are also solubilized by *M. sedula*, which creates possibilities for future asteroid biomining (Milojevic et al., 2019b, 2021). *A. manzaensis* (Yoshida et al., 2006) is an emerging thermoacidophilic bioleacher, which grows as a facultative anaerobe utilizing molecular hydrogen and elemental sulfur as electron donor under aerobic conditions by using Fe^{3+} as the electron acceptor for anaerobic growth. So far, *A. manzaensis* has merely been investigated for its chalcopyrite leaching efficiency as well as a possible acid mine drainage (AMD) bioremediation agent (Chang-Li et al., 2012; Liu et al., 2016a,b; Nie et al., 2019; Li et al., 2020). Obviously, current and future challenges in circular economy and waste management demand in-depth analyses of microorganisms with great inherent bioleaching potential.

Recent advances in these technologies (e.g., Coetzee et al., 2020; Giachino et al., 2021; Newsome and Falagán, 2021) may contribute to a great extent to the United Nations Sustainable Development Goals (specifically goal number 12), namely, to achieve sustainable and efficient use of natural resources as well as to implement an environmentally sound management of chemicals and all wastes throughout their life cycle by 2030 (United Nations General Assembly, 2015).

TABLE 1 | Detailed microbiological media composition for the six thermoacidophilic strains.

[g]	*A. manzaensis*	*A. bierleyi*	*M. sedula*	*M. hakonensis*	*S. metallicus*	*S. acidocaldarius*
$(NH_4)_2SO_4$	0.132	3.00	1.30	1.30	1.30	1.30
KH_2PO_4	0.041	0.50	0.28	0.28	0.28	0.28
$MgSO_4 \cdot 7H_2O$	0.49	0.50	0.25	0.25	0.25	0.25
$CaCl_2 \cdot 2H_2O$	0.009	-	0.07	0.07	0.07	0.07
$FeCl_3 \cdot 6H_2O$	-	-	0.02	0.02	0.02	0.02
KCl	0.052	0.10				
$Ca(NO_3)_2$	-	0.01				
Yeast extract	-	-	-	-	-	0.01 % (w/v)

In this study, the growth potential of six thermophilic archaeal strains (*S. metallicus, S. acidocaldarius, M. hakonensis, M. sedula, A. brierleyi,* and *A. manzaensis*), their ability to propagate in presence of a multimetallic waste product (BOF-dust), as well as the subsequent solubilization of metals bound to the respective BOF-dust grains is investigated. Furthermore, we focus on the bioleaching potential of *A. manzaensis,* subjecting cells to different leaching parameters (BOF-dust load, pH, and temperature), while investigating the microbial interactions with dust particles *via* scanning and transmission electron microscopy (SEM and TEM) coupled to energy-dispersive spectroscopy (EDS) analysis. In our study, we observe efficient metal solubilization from dust particles by *A. manzaensis* and explore microbial-mineral interactions associated with this case. Our results provide the first insights into laboratory-scale thermoacidophilic bioleaching associated with industrial steelmaking waste products. Integrating not well-studied bioleaching microorganisms into future circular waste management processes might open up a plethora of new applications for environmental biotechnology.

MATERIALS AND METHODS

Strains and Media Composition

A. manzaensis (NBRC 100595), *A. brierleyi* (DSMZ 1651), *S. metallicus* (DSMZ 6482), *S. acidocaldarius* (DSMZ 639), *M. hakonensis* (DSMZ 7519), and *M. sedula* (DSMZ 5348) cultures were grown aerobically in their respective media (**Table 1**). Allen's trace element solution was added to 1 L media, resulting in 1.80 mg $MnCl_2 \cdot 4H_2O$, 4.50 mg $Na_2B_4O_7 \cdot 10H_2O$, 0.22 mg $ZnSO_4 \cdot 7H_2O$, 0.05 mg $CuCl_2 \cdot 2H_2O$, 0.03 mg $Na_2MoO_4 \cdot 2H_2O$, 0.03 mg $VSO_4 \cdot 2H_2O$, and 0.01 mg $CoSO_4$ final concentration (for DSMZ 1,651; 6,482; 639; 7,519; 5,348). A solution containing 831 trace elements was added to 1 L media, resulting in a final concentration containing 1 mg $ZnSO_4 \cdot 7H_2O$, 2 mg $CuSO_2 \cdot 5H_2O$, 1 mg $MnSO_4 \cdot 5H_2O$, 0.5 mg $Na_2MoO_4 \cdot 2H_2O$, 0.5 mg $CoCl_2 \cdot 6H_2O$, 1 mg $NiCl_2 \cdot 6H_2O$, and 5 mg $FeSO_4 \cdot 7H_2O$ (for NBRC 100595). pH was adjusted with 10N H_2SO_4 according to the DSMZ/NBRC data. Cultivation of thermophilic archaea was performed as described earlier (Milojevic et al., 2019b) in 1 L modified Schott-bottle bioreactors (Duran DWK Life Sciences GmbH, Wertheim/Main, Germany), equipped with a thermocouple connected to a heating and magnetic stirring plate (RH basic 2 IKAMAG, IKA-Werke GmbH & Co. KG, Staufen, Germany) for temperature and agitation control (**Supplementary Figure S1**). Each bioreactor was equipped with three 10 ml graduated pipettes, permitting carbon dioxide and air gassing (gas flow rates 0.5 NL/min, respectively, MFC 8741, Bürkert GmbH & Co. KG, Ingelfingen, Germany) and sampling of culture. The graduated pipettes used for gassing were connected by silicon tubing to sterile 0.2 μm filters (Millex-FG Vent filter unit, Merck KGaA, Darmstadt, Germany). Graduated pipettes used for sampling were equipped with a Luer-lock system to permit sampling with sterile syringes (Soft-Ject, Henke Sass Wolf, Tuttlingen, Germany). Off-gas was forced to exit *via* a water-cooled condenser (Carl Roth GmbH & Co. KG, Karlsruhe, Germany). Respective temperatures inside the bioreactors were controlled by electronic thermocouple *via* heating and magnetic stirring plates. For chemolithotrophic growth, cultures were supplemented with 10 g/L BOF-dust. Before addition to the microbiological medium, BOF-dust samples were heat-sterilized at 180°C in a laboratory oven for a minimum of 24 h prior to autoclavation at 121°C for 20 min. Cell growth was examined *via* cell counting (Neubauer Chamber, Carl Roth GmbH & Co. KG, Karlsruhe, Germany) and the release of soluble metals into the culture medium.

Metal Release Analysis (ICP-MS)

To determine the extracellular concentrations of metal ions mobilized from the metal-containing waste product, samples of thermoacidophilic cultures were clarified by centrifugation. Cells were harvested at the early stationary growth phase for inductively coupled plasma (ICP) measurements. Samples of the resulting supernatants were filtered (0.44 μm pore size, Macherey-Nagel GmbH & Co. KG, Germany). A total of 18 elements (Fe, Cu, Ni, Zn, Cr, Cd, Mn, Ca, Mg, Al, Co, V, Ti, Sr, Pb, Mo, Ba, As) were analyzed by ICP mass spectrometry (ICP-MS). Abiotic samples (containing BOF-dust and respective microbiological media but no cells) and zero time points (at start of cultivation) were analyzed in each experiment, and their corresponding values are already subtracted in all figures presented in this study.

Wavelength-Dispersive X-Ray Fluorescence Analysis (WD-XRF)

The BOF-dust sample used in the study was analyzed using wavelength-dispersive X-ray fluorescence (WD-XRF)

spectrometer Zetium PW 5400, Panalytical and SuperQ-program. The evaluation of the measuring data was done using Uniquant program, hence the chemical composition was ascertained. In parallel, the loss of ignition of the sample was determined at 1,000°C. The results of the evaluation of the bulk elemental composition of BOF-dust *via* WD-XRF analysis are presented in **Supplementary Table S1**.

Scanning and Transmission Electron Microscopy

For scanning transmission electron microscopy coupled to energy-dispersive X-ray spectroscopy (SEM-EDS) analysis, *A. manzaensis* cells were collected, primary fixed with 2.5% glutaraldehyde (in 1 M Na-cacodylate buffer), and post-fixed for 2 h in 1% osmium tetroxide (OsO_4). Subsequently, samples were washed (1.5× PHEM-buffer) and dehydrated by a gradual ethanol series (30, 50, 70, 80, 90, 95%, abs.) and acetone (100%). Samples were dried by critical point drying (Critical Point Dryer, Leica EM CPD300, Leica Microsystems GmbH, Wetzlar, Germany), gold sputtered (JEOL JFC-2300HR from Jeol GmbH, Freising, Germany), and analyzed *via* JEOL IT300 Microscope at 20 kV acceleration voltage (Jeol GmbH, Freising, Germany). EDAX Detector (AMETER Material Analysis Division, Ametek GmbH, Weiterstadt, Germany) and energy-Dispersive X-ray spectroscope (EDX) were used for the elemental analysis at an acceleration voltage of 25 kV. Spectra and mappings with the elements of chosen areas were determined using TEAM™ EDS Analysis System (Texture and Elemental Analytical Microscopy; detector Octane Plus) program.

Sample preparation for STEM-EDS has been performed by focused ion beam (FIB) sputtering using a FEI Quanta 3D FEG instrument, equipped with an electron column hosting a field-emission electron source and an ion column hosting a Ga-liquid metal ion source (LMIS) as described earlier (Milojevic et al., 2021). Before sputtering, a Pt layer was deposited on the sample surface as a protective layer by FIB Pt deposition at 16 kV IB acceleration voltage. STEM and energy-dispersive X-ray spectrum (EDS) images were acquired from *A. manzaensis* cultures grown on BOF-dust. Elemental maps and spectra were processed with Gatan Digital Micrograph software (Gatan Inc.). Element quantification for EDS spectra was performed by using the k-factor method.

Crystal X-Ray Diffraction

The crystalline phase was collected from cultures of *A. manzaensis* grown on BOF-dust. Single crystals were mounted on loops and examined using a Bruker D8 Venture, operated with multilayer monochromator, INCOATEC microfocus sealed tube (λ (MoKα) = 0.71073 Å) and CMOS Photon Detector.

RESULTS

Microbial Growth on BOF-Dust

Six archaeal strains of the Sulfolobales order (*A. manzaensis, A. brierleyi, S. metallicus, S. acidocaldarius, M. hakonensis,* and *M. sedula)* were grown in their respective media (**Table 1**, also refer to the "Materials and methods" section) supplemented with BOF-dust to examine growth capacity and culture maintenance in conditions of a high metal content. In course of 17 days of cultivation supplemented with CO_2-gassing and BOF-dust (single portion, 10 g/L culture), microbial growth was monitored by phase-contrast/epifluorescence microscopy and metal release. Each culture was inoculated with approximately 10^6 cells/ml and during 17 days of operation time, growth of all six thermoacidophiles on BOF-dust became apparent through a 100- or 1,000-fold increase in cell densities at the final point of cultivation (**Figure 1**). *A. manzaensis* and *M. sedula* were among the highest proliferating strains with final densities of 3.5×10^9 and 3.2×10^9 cells/ml, respectively, whereas *M. hakonensis* and *S. metallicus* exhibited lowest cell densities of all six strains after 17 days of cultivation (maximum densities 1.6×10^8 and 3.7×10^8 cells/ml, respectively). *S. acidocaldarius* and *A. brierleyi* reached cell numbers (2.3×10^9 and 1.7×10^9 cell/ml, respectively) comparable to *A. manzaensis* and *M. sedula*.

Metal Release of Six Thermoacidophilic Archaea

The six aforementioned thermoacidophilic strains were tested for their potential to mobilize metals from BOF-dust particles into their respective medium (leachate solution). A comparative analysis of leached elements among thermophiles was carried out *via* ICP-MS. The most abundant elements in the microbial leachate of *A. manzaensis* were Mn, Cd, Cr, Zn, Ni, and Cu, whereas Fe, Pb, and Mn were released more efficiently by *A. brierleyi*. *M. hakonensis* was able to mobilize Mn, Zn, Cu, Fe, Cd, and Ni from the dust product, but no release of Cr or Pb could be detected. Similar to the absence of solubilized Cr in the *M. hakonensis* culture, *S. acidocaldarius* did not leach any Cr into the microbiological medium. Yet, the overall bioleaching performance of *S. acidocaldarius* is comparable to *M. sedula* and *S. metallicus,* with *S. acidocaldarius* solubilized more Mn, Zn, and Fe into the leachate solution than *M. sedula* and *S. metallicus*. Both Ni and Cd were not detected in the *S. metallicus* culture (**Figure 2**).

A. manzaensis-Mediated Bioleaching Under Various Conditions

A. manzaensis cells were subjected to further in-depth experiments due to the overall high bioleaching performance and the most outstanding Cr leaching abilities compared to other strains tested. To assess cultivation parameters for more efficient *A. manzaensis* bioleaching operations, parameters such as BOF-dust load, operation pH and temperature were examined. For future applications in bioleaching with this archaeon, exposure to higher concentrations of the multi-metallic waste product is favorable. Therefore, *A. manzaensis* cultures were fed with increasing BOF-dust concentrations (10/20/30 g/L) (**Figures 3A–C**), and subsequent metal release was investigated *via* ICP-MS. Elements, such as Fe, Zn, Mn, Mg, Cr, Cd, and Sr, were detected at elevated levels respective to increasing dust concentrations, while the release of Ca, Al, Ni, Co, V, Ti, Pb, Mo, and As did not correspond to increasing concentrations of dust in the cultures (**Figure 3A**). For aerobic growth, *A.*

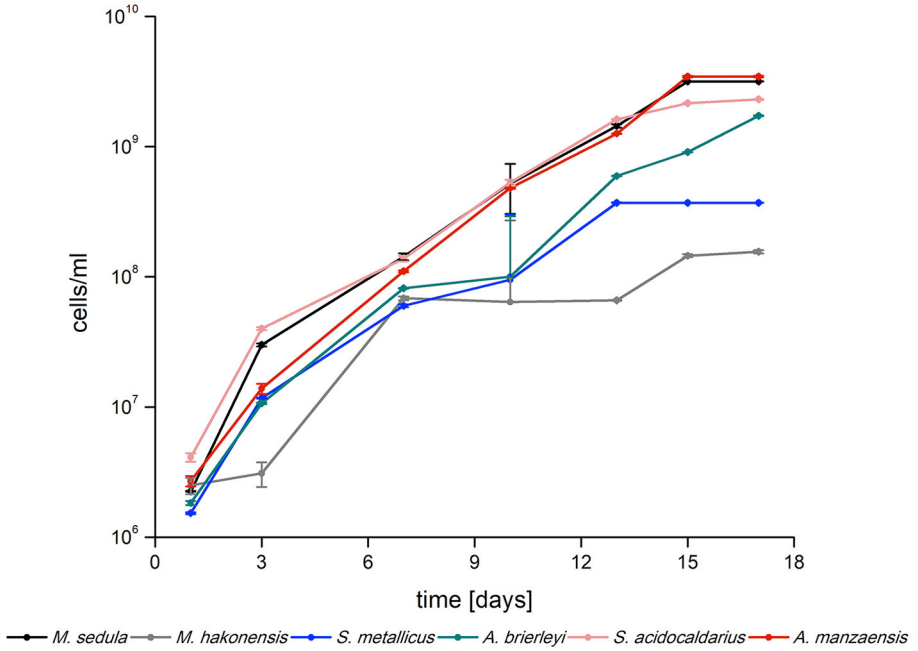

FIGURE 1 | Logarithmic growth curves of *Sulfolobus* spp., *Metallosphaera* spp., and *Acidianus* spp. grown on BOF-dust (10 g/L) over time ($n = 3$).

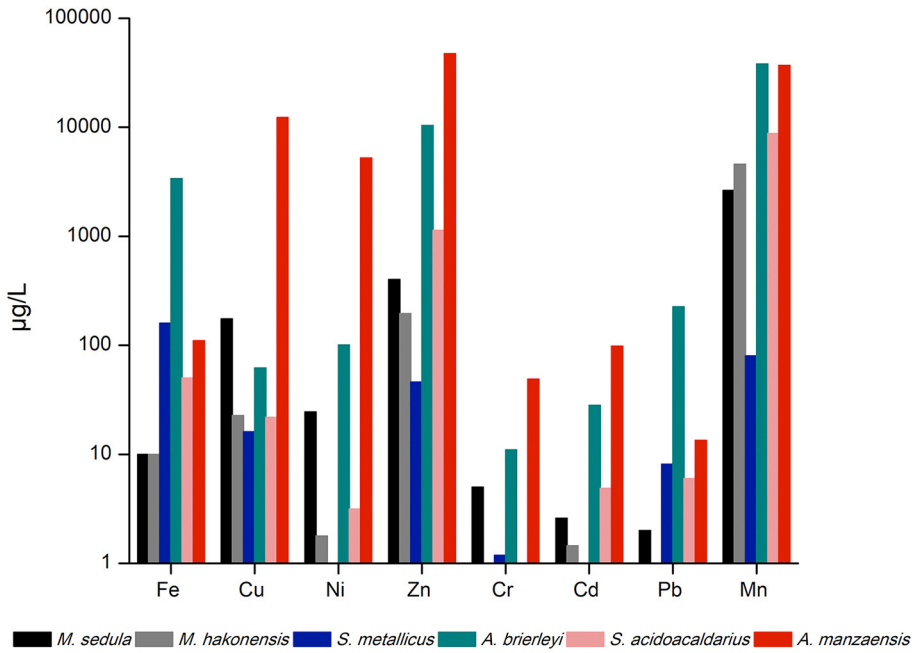

FIGURE 2 | ICP-MS analysis of released metal ions in the supernatant of thermoacidophilic cultures grown on BOF-dust (10 g/L).

manzaensis tolerates pH ranges from 1.0 to 5.0 with the optimum being around 1.2–2.0 (Yoshida et al., 2006). ICP-MS analysis for varying pH values set at 1.5, 2.0, and 2.5 points out that in a more acidic environment of pH 1.5 *A. manzaensis* cells mobilize Fe, Ni, V, Ti, and most notably Cr with the highest efficiency from dust particles into solution (**Figures 3D,E**). In contrast, a higher pH at 2.5 supports Zn, Mn, Cu, Cd, and Co bioleaching, while a neglectable change in metal mobilizing performance for all elements at pH 2.0 became apparent. Regarding operation temperature, *A. manzaensis* cells are able to

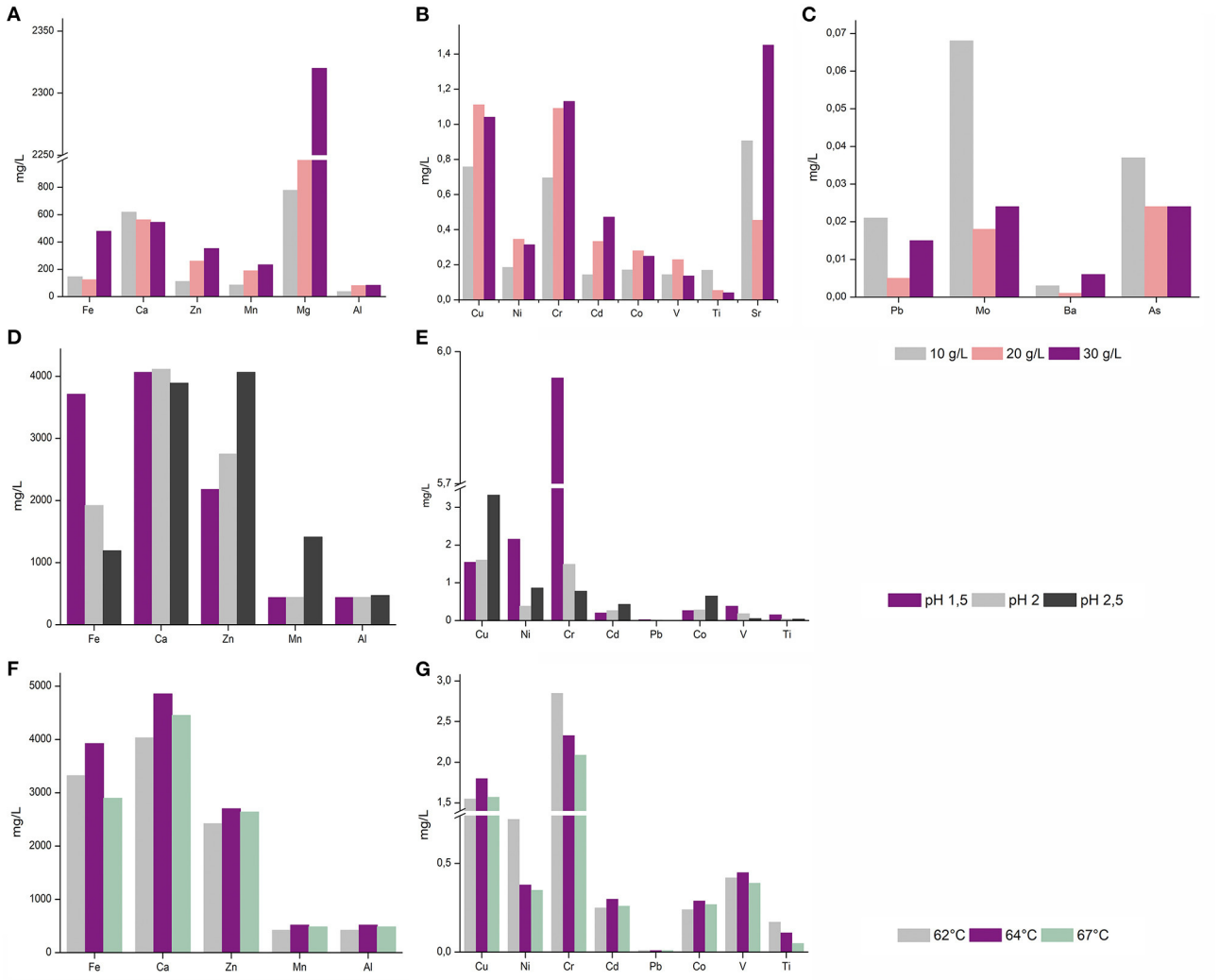

FIGURE 3 | ICP-MS analysis of released metal ions in leachate solution of *A. manzaensis* grown on BOF-dust at different parameters. **(A–C)** *A. manzaensis* grown on increasing amounts of dust (10/20/30 g/L); **(D,E)** *A. manzaensis* grown at different pH values (1.5/2.0/2.5); **(F,G)** *A. manzaensis* grown at different temperatures (62°C/64°C/67°C).

grow in a temperature range of 60–90°C (Yoshida et al., 2006), in previous bioleaching operations as well as for this study, *A. manzaensis* was cultivated at 65°C (Liu et al., 2016a,b; Nie et al., 2019). Slight temperature shifts (62°C/64°C/67°C) did not result in a significant change in bioleaching performance (**Figures 3F,G**). An operating temperature of 64°C yields slightly higher concentrations of Fe, Ca, Zn, Mn, Al, Cu, Cd, Co, and V, even though these differences are not substantial. Interestingly, the most efficient Cr leaching was achieved at 62°C, and the least efficient temperature was 67°C.

SEM Observations of Raw and Bioprocessed BOF-Dust Particles

To further investigate the interactions of *A. manzaensis* cells with BOF-dust particles, SEM was applied on unprocessed (raw, not incubated with microbial cells). BOF-dust samples as well as with BOF-dust samples after cultivation with *A. manzaensis*. SEM examination of unprocessed dust particles demonstrates that big, spherical grains with a diameter ranging from 2 to 80 μm exist among significantly smaller and finer dust grains (**Figure 4A**). A close-up SEM caption of an approximately 50-μmsized dust grain exhibits a rough and rippled surface, covered in dust debris (**Figure 4B**). After a total of 14 days of cultivation of *A. manzaensis* supplemented with 10g/L BOF-dust, observations from SEM analysis show overall small dust particles approximately 2–5 μm with various surface textures and structures (**Figures 4C–G**). The rough and rippled surface of unprocessed particles (**Figure 4B**) transformed into extremely smooth-looking structures or structures with porous or broken surface (etched) upon 14 days of cultivation (**Figures 4C–G**, **Figure 5**; **Supplementary Figures S2,S3**). Additionally, *A. manzaensis* cells appear as regular cocci

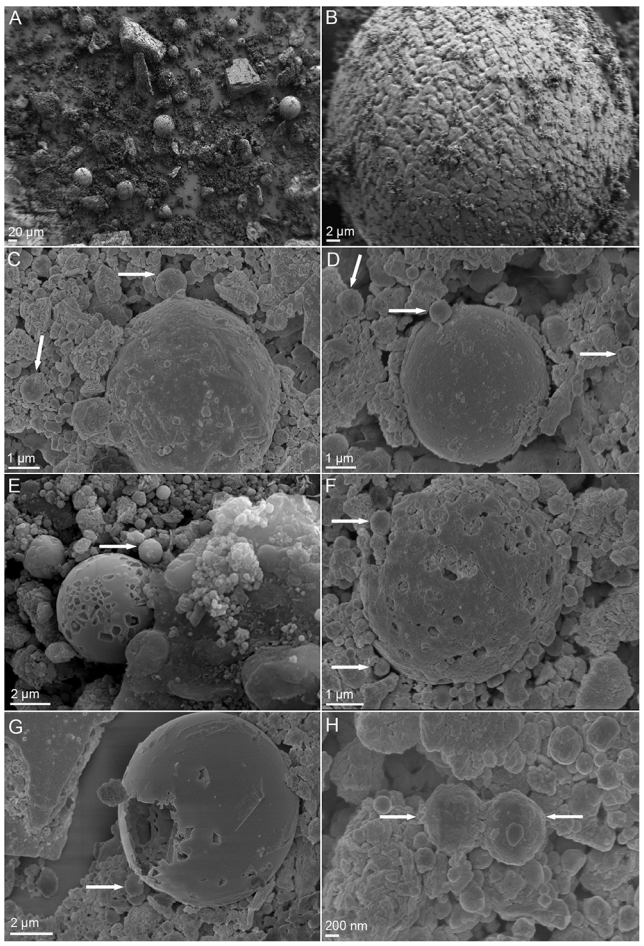

FIGURE 4 | Scanning electron microscopy (SEM) images of BOF-dust particles and cells of *A. manzaensis*. **(A)** Overview of raw, unprocessed dust sample; **(B)** Enlarged image of unprocessed dust corn particle; **(C,D)** Microbially processed sample, shown are dust corn particles with co-localized *A. manzaensis* cells. **(E–G)** Microbially processed sample, shown are dust corn particles with co-localized *A. manzaensis* cells; **(H)** Microbially processed sample, shown are dividing cells of *A. manzaensis*. White arrows indicate cells (~1 µm size). Microbially processed grains of waste dust product are bigger (up to 5–20 µm) and are shown in **(C–G)**, revealing their microbially etched surface.

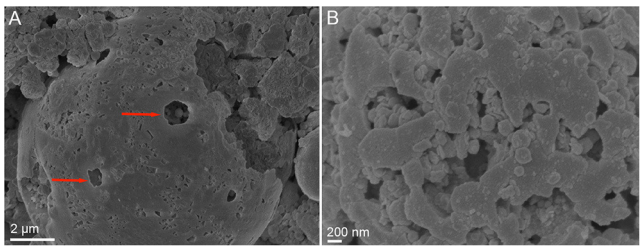

FIGURE 5 | SEM images showing the microbially etched surface of grains of waste material product bioprocessed by *A. manzaensis*. **(A)** The microbially etched pits are depicted by the red arrows. **(B)** Magnified SEM image of microbially etched surface.

that are about 0.6–1.0 µm in size, co-localizing with BOF-dust particles (**Figures 4C–H**). In **Figures 4C–G**, coccoid cells of *A. manzaensis* are shown attached or close to single grains of waste dust material (>5 µm), which have a microbially etched surface. The exemplary biotransformed grains of waste dust material are shown in **Figures 4C–G**, **Supplementary Figures S2, S3**. The magnified SEM images (**Figure 5**, **Supplementary Figure S3B**) illustrate a close-up of grains of waste product material bioprocessed by *A. manzaensis*. The red arrows in **Figure 5A** show exemplary microbially etched pits on the grain surface. Single etched pits can be bigger than 2 µm (**Figure 4G**). A cell division of *A. manzaensis* (**Figure 4H**) and cell attachment to a big grain of waste dust material (**Figure 4D**) are depicted by the white arrows. Overall, the dust grains are covered by multiple etched pits upon cultivation with *A. manzaensis*, indicating the attack of microbial cells that use the metal-bearing waste product material as a nutrient and as the energy source. Furthermore, small and round particles (around 200 nm) are highly abundant in all biogenic samples (**Figures 4**, **5**, **Supplementary Figures S2, S3**), but absent in unprocessed BOF-dust. These round-shaped nanoparticles can represent well-known extracellular vesicles that are secreted by thermoacidophilic archaea of the Sulfolobales order to catalyze metal oxidation and facilitate mineral solubilization under the energy-starving chemolithoautotrophic conditions (Johnson et al., 2018). The exemplary microbially colonized BOF-dust gains that are embedded in the network of cells and their vesicles are shown in **Supplementary Figures S2C,D**. We have also previously observed the formation of such vesicles during growth on other multimetallic materials (Milojevic et al., 2019a,b, 2021).

Analytical Spectroscopy Analysis of Microbial-Metal Interface

SEM-EDS was applied to localize element distribution among highly heterogeneous microbial-mineral content of *A. manzaensis* cultures grown on BOF-dust. Elemental EDS maps detected an abundance of Fe, S, P, Co, Pb, and Mo, which are distributed evenly among the microbially processed sample after 14 days of cultivation, whereas Cr, Mn, Al, and Mg were detected in specific spots of the same sample (**Figure 6**). For further investigations at high resolution, a thin section was produced *via* a FIB milling and examined in STEM mode. The STEM-EDS results demonstrate the content and distribution of metals and metalloids in microbial-mineral assemblages (**Figure 7**). The elemental maps show that microbial-mineral assemblages are enriched with P, Fe, Mn, Zn, and O. Biologically important elements such as S, K, and Cl are evenly distributed within a microbial-mineral assemblage. Additionally, Si and Al deposits are detected in the sample.

Moreover, the formation of crystalline material (gypsum ($CaSO_4 \times 2H_2O$) crystals) was observed in *A. manzaensis* cultures after 7 days of cultivation on BOF-dust. No crystals were detected in corresponding abiotic controls that comprise only BOF-dust and microbiological medium. Gypsum crystals were

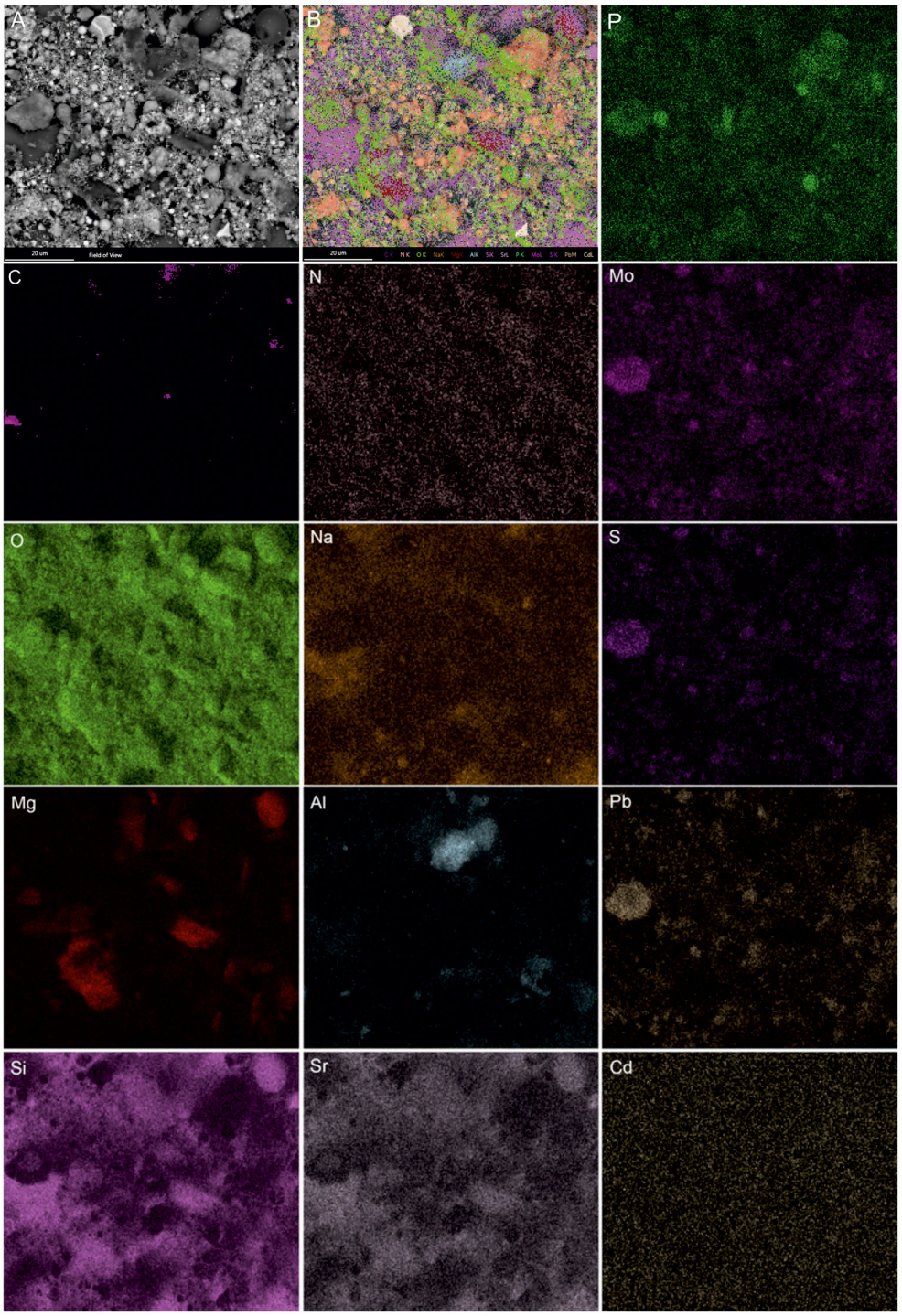

FIGURE 6 | SEM-EDS investigations of microbial-mineral assemblages formed in cultures of *A. manzaensis* grown on BOF-dust. Shown are the SEM image of a microbially processed sample used for the EDS spectrum image acquisition, composite image, and corresponding elemental distribution maps of phosphorus (P), carbon (C), nitrogen (N), molybdenum (Mo), oxygen (O), sodium (Na), sulfur (S), magnesium (Mg), aluminum (Al), lead (Pb), silicon (Si), strontium (Sr), and cadmium (Cd).

initially observed in course of light microscopy investigations (**Figure 8A**), followed by SEM-EDS analysis (**Figure 8B** and elemental maps), and subsequently analyzed *via* single-crystal X-ray diffraction (XRD) to determine the structural properties and nature of the crystals. The obtained unit cell parameters (a = 6.31Å; b = 15,25Å; c = 5,70Å; α = 90°; β = 114°) were identified as calcium sulfate dihydrate ($CaSO_4 \times 2H_2O$) (**Figure 8**), indicating the occurrence of calcium sulfate in the

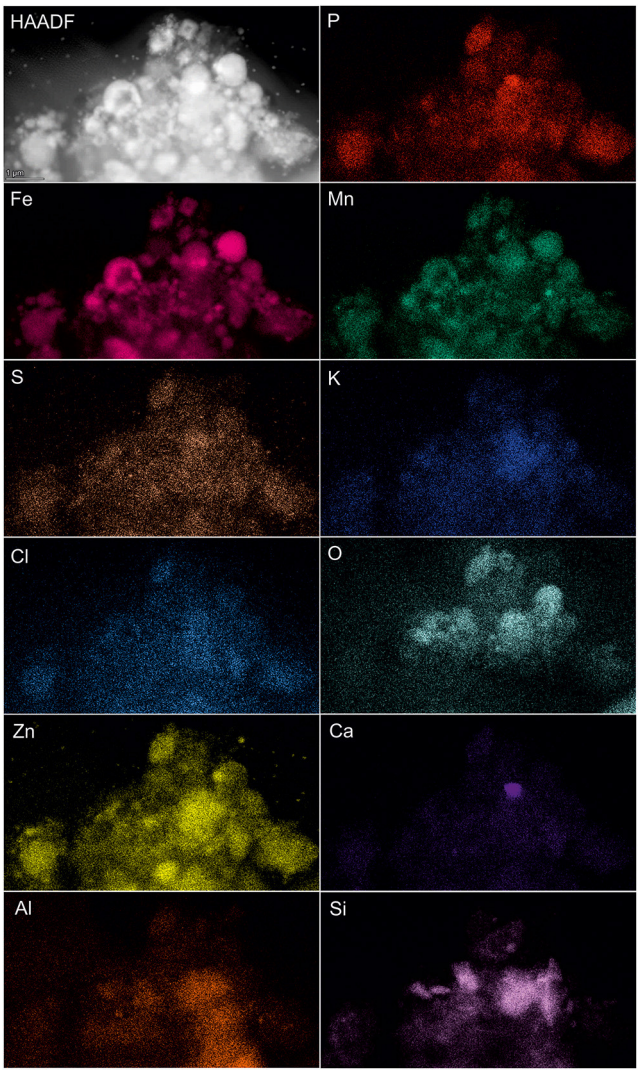

FIGURE 7 | Elemental ultrastructural analysis of microbial-mineral assemblages formed in cultures of *A. manzaensis* grown on BOF-dust. HAADF-STEM image of a microbially processed sample used for the EDS spectrum image acquisition and corresponding elemental distribution maps of phosphorus (P), iron (Fe), manganese (Mn), sulfur (S), potassium (K), chlorine (Cl), oxygen (O), zink (Zn), calcium (Ca), aluminum (Al), carbon (C), nitrogen (N), and silicon (Si).

bioleachate solution. SEM-EDS investigation of putative gypsum crystals in the microbial culture corresponds to light microscopy and XRD unit cell parameters (**Figure 8**).

DISCUSSION

All six thermoacidophilic archaeal strains cultivated for this study were able to grow chemolithotrophically on a high metal-content BOF-dust that is generated during the BOF steel production processes. Our cultivation parameters (strain-specific medium, temperature, acidity) were selected according to commonly applied cultivation parameters for each strain (refer to the "Materials and methods" section). All of the cultivated strains were able to proliferate successfully in course of 17 days. Inherent resistance to a (heavy) metalliferous environment was one of the criteria for strain selection. Previous extensive work with *M. sedula* in mineral- and metal-containing environments made this archaeon a prime candidate (Auernik and Kelly, 2010b; Blazevic et al., 2019; Milojevic et al., 2019b, 2021), along with its close relative *M. hakonensis.* Interestingly, a comparison of metal solubilization capacities of *M. hakonensis* and *M. sedula* grown on BOF-dust-supplemented medium favors *M. sedula,* which was able to extract Cr and Pb from BOF-dust grains (**Figure 2**). Silica content in BOF-dust (**Supplementary Table S1**) may be solubilized chemically by the acidic pH of the surrounding medium and is subsequently precipitated onto *M. hakonensis* cells during bioleaching operation (Usher et al., 2009). Under these circumstances, a fusion barrier can be created that consequently slows down the release of metals from dust grains (Usher et al., 2009). This phenomenon has already been observed for *M. hakonensis* in heap bioleaching operations and might be applicable to other thermoacidophilic strains (Dopson et al., 2008). Both *Metallosphaera* strains solubilize metals by attaching to their respective substrates as well as by regenerating Fe^{2+} to Fe^{3+} that is vital for chemical attack on minerals (Bromfield et al., 2011; Kölbl et al., 2017). While the growth of *S. metallicus* is inhibited by a high amount of surrounding Fe^{2+} ions (Shiers et al., 2013), proliferation on a high Fe^{3+} content (as in BOF-dust) does not seem to have significant impact on cellular propagation since *S. metallicus* cells leach metals by attaching to a mineral surface as well as by providing Fe^{3+} ions as a lixiviant (Gautier et al., 2008). Whereas *S. metallicus* grows in an obligate chemolithoautotrophic mode, its relative *S. acidocaldarius* proliferates heterotrophically (Wheaton et al., 2015). This might explain the faster generation time of *S. acidocaldarius* in course of cultivation. In this study, *S. acidocaldarius* outperformed *S. metallicus* in the growth and bioleaching of most elements except for Fe. Contradictory experimental data on lifestyle and substrate utilization (autotrophy vs. heterotrophy; oxidation of S^0) of *S. acidocaldarius* (Dworkin et al., 2006) need to be clarified by dedicated experiments in order to determine bioleaching mechanism(s). *A. manzaensis* is a facultative autotroph capable of utilizing Fe^{3+} as electron acceptor under anaerobic circumstances in contrast to the closely related *A. brierleyi* species (Yoshida et al., 2006). However, no data exist on how a high concentration of surrounding Fe^{3+} ions can influence the growth rate of *A. manzaensis*. While Fe^{3+} ions are a vital oxidizing agent in autotrophic bioleaching processes, the generation of protons by acidophilic microorganisms further supports bioleaching and keeps Fe^{3+} ions in solution (Donati and Sand, 2007). Both heterotrophs (e.g., fungi) and autotrophs (e.g., thermoacidophilic iron-oxidizing archaea) are capable of solubilizing metals from ores and minerals using different strategies and bioleaching agents (Schippers et al., 2013). In this study, all cultivated archaeal strains are chemolithotrophs (except *S. acidocaldarius*) that use a variety of inorganic energy sources, which are in turn closely intertwined with their bioleaching abilities (Donati and Sand, 2007). Chemolithotrophic production of sulfuric acid (protons) by sulfur-oxidizing thermoacidophilic archaea (*Metallosphaera* spp., *Acidianus* spp., *S. metallicus*) might

additionally support efficient metal solubilization from BOF-dust grains by maintaining a low pH during bioleaching operations.

All six thermoacidophilic archaea were able to efficiently solubilize various metals from BOF-dust grains due to their inherent bioleaching capacities. Several enzymes involved in bioleaching processes have been identified among the Sulfolobales order. *A. manzaensis* genome encodes several enzymes involved in sulfur and RISCs oxidation, including a sulfur oxygenase-reductase, thiosulfate:quinone oxidoreductase and a tetrathionate hydrolase (Ma et al., 2017). So far, no genes for iron redox chemistry in *A. manzaensis* have been annotated, which makes future biochemical characterization on genes responsible for bioleaching capacity necessary. The *fox* gene cluster responsible for iron oxidation was identified in *S. metallicus* (Bathe and Norris, 2007) and *M. sedula,* as well as the genetic presence of rusticyanin homologs (Rus) for iron oxidation and tetrathionate hydrolase (TetH) for sulfur oxidation, appear to distinguish microbes able to perform bioleaching from non-bioleaching microbes (Auernik et al., 2008). Bioleaching (and/or biomining) capacities of *M. sedula, M. hakonensis, A. brierleyi, S. metallicus,* and *S. acidocaldarius* have been examined extensively compared to *A. manzaensis*. Comparative ICP-MS analysis of all thermoacidophiles shows superiority of *A. manzaensis* in leaching of certain strategically important elements from BOF-dust, such as Cu, Ni, Zn, Cr, Cd, and Mn (**Figure 2**). Future experiments to determine iron redox (bio)chemistry in *A. manzaensis* need to be carried out to fully understand its bioleaching potential.

Refinement of the current BOF-bioleaching operation included BOF-dust load, pH, and slight temperature shifts. For most elements (Fe, Zn, Mn, Al, Cu, Ni, Cr, Cd, Co, V, Sr, Ba, Mg), a higher dust load (**Figure 3A**) equals higher amounts leached into solution. In contrast, elements such as Ti, Pb, Mo, and Al might have formed insoluble precipitates under higher dust load conditions since they seem to be underrepresented in the analyzed bioleachate solution (**Figure 3A**). Furthermore, a decrease of operation pH from 2.5 to 1.5 increased Cr, Fe, and Ni bioleaching significantly compared to a less acidic pH (**Figure 3B**). On the contrary, Zn, Mn, Co, Cd, and Cu bioleaching was enhanced at higher pH (2.5). Similar results for *A. manzaensis* copper bioleaching at different pH-values have been shown by previous experiments, where Cu dissolution increased with a less acidic pH, whereas Fe concentration dropped by pH increase which is in concordance with own measurements (Liang et al., 2014; Liu et al., 2016a). In classic metal sulfide bioleaching, Fe precipitation is usually accounted to the formation of a passivating layer (usually by jarosite), which slows down overall mineral dissolution (Klauber, 2008). Excessive implementation of mesophilic microorganisms such as *Acidithiobacillus* spp. and *Leptospirillum* spp. in commercial bioleaching operations of metal sulfides (pyrite, chalcopyrite) shows that biological leaching processes decrease with time and eventually cease due to the formation of a polysulfide ($Cu_4Fe_2S_9$) passivation layer on the mineral surface (Hackl et al., 1995; Zhao et al., 2019). Thermoacidophilic archaea such as *Acidianus* spp., *Sulfolobus* spp., and *Metallosphaera* spp. are able to significantly accelerate mineral sulfide dissolution, cope with high overall acidity and temperatures (Clark and Norris, 1996; Gericke and Pinches, 1999) and can promote a more efficient dissolution of BOF-dust grains by solubilizing metals into the leachate solution (**Figure 2**). The formation of unwanted or inhibiting bioleaching by-products formed by these processes needs to be investigated in further studies in order to enhance industrial implementation. Slight changes in bioleaching operation temperature (62°C/64°C/67°C) did not reveal any significant solubilization events; for future investigation, further temperature shifts should be examined in depth.

A. manzaensis was the most efficient strain among all other tested Sulfolobales spp. capable of chemolithotrophic growth on BOF-dust. *A. manzaensis* broke down the chemical matrix of BOF-dust grains and actively solubilized various metals into the leachate solution. Our SEM observations show the successful colonization of metal-bearing waste particles by *A. manzaensis* and their subsequent biotransformation (e.g., etched grains surface, **Figures 4C–H**, **Figure 5**, **Supplementary Figure S3**). This is in concordance with previous findings of cooperative contact/non-contact bioleaching mechanisms of *A. manzaensis* (Zhang et al., 2019). Studies of chalcopyrite bioleaching with *A. manzaensis* cells also indicate corrosion and break down of the mineral matrix with simultaneous copper solubilization after several days of cultivation (He et al., 2009; Liu et al., 2016b). Furthermore, the formation of a jarosite ($KFe_3(SO_4)_2(OH)_6$) passivation layer by *A. manzaensis* was reported from chalcopyrite bioleaching operations (Nie et al., 2019), indicating the formation of by-products during leaching processes. In our study, we observed gypsum crystals ($CaSO_4 \times 2H_2O$) after approximately 7 days of cultivation (**Figure 8**), which might be accounted for both microbial and chemical-induced processes during cultivation. A high calcium content in the BOF-dust (**Supplementary Table S1**), as well as the involvement of sulfur derived from the same product, can account for abiotic calcium sulfate formation once these elements are intensively released by *A. manzaensis* into the leachate solution. Similar to calcium sulfate, nickel and manganese sulfate formation in the leachate solution has been previously reported for *M. sedula* cultivated on multimetallic extraterrestrial material (Milojevic et al., 2019b). In this case, associated with the potential for asteroid biomining operations, nickel sulfate was proposed as a metabolic biosignature resulting from the microbial leaching activity of meteorite minerals (Milojevic et al., 2019b). In light of terrestrial industrial operations, gypsum is a naturally occurring mineral and is used in various industrial settings. Usually, gypsum is formed as a by-product of sulfide oxidation to produce sulfuric acid and is used excessively in the construction industry (Lutz et al., 2012). In contrast, a study conducted by Vogel et al. shows that biofilms of cyanobacteria and *Bacteroidetes* species are actively involved in gypsum sedimentation implicating biological involvement in its formation (Vogel et al., 2009). Despite the possibility of biological involvement, a low pH favors the growth of gypsum crystals in inorganic systems (Liu et al., 2015). Furthermore, substrates rich in Fe, Ca, Mg, or Ba combined with continuous CO_2 input in the bioreactor might precipitate as a stable red gypsum mineral through CO_2 mineral carbonation (Rahmani et al., 2016; Rahmani, 2018, 2020). As the origin of

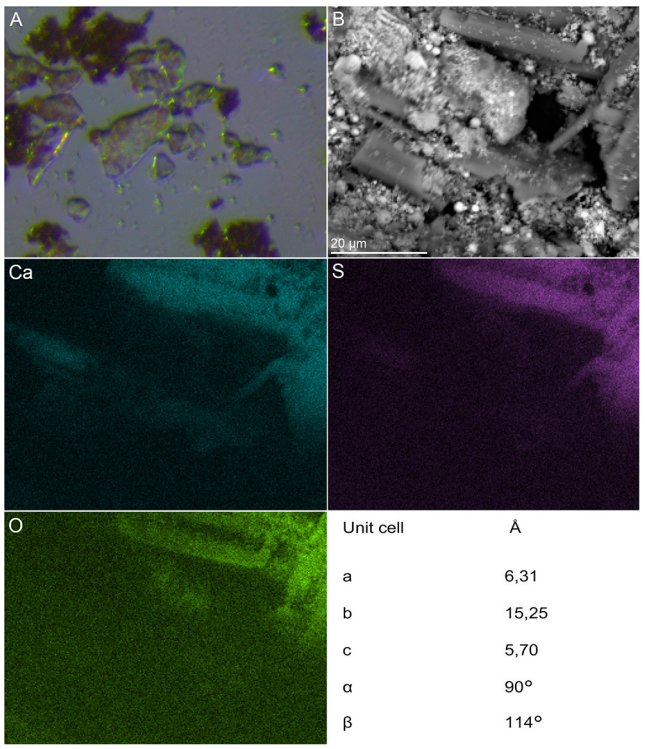

FIGURE 8 | Microscopic and spectroscopic analysis of gypsum crystals detected in *A. manzaensis* culture supplemented with BOF-dust. **(A)** Light microscopy of gypsum crystals in active culture. **(B)** SEM image of bioprocessed BOF-dust sample used for the EDS spectrum image acquisition and corresponding extracted calcium (Ca), sulfur (S), and oxygen (O) elemental maps with unit cell parameters detected with single-crystal X-ray diffraction (XRD) analysis.

gypsum crystals in this study is not resolved, more studies on its influence on bioleaching efficiency and its possible application as a useful by-product need to be executed.

First insights into laboratory-scale thermoacidophilic bioleaching associated with industrial steelmaking waste products are provided in this study. Further genetic analysis and biochemical characterization of metal-oxidizing molecular machinery of *A. manzaensis* need to be carried out to optimize this strain for future operations. A thorough screening of operation parameters in frames of scale-up processes is highly necessary to implement this technology for upcoming circular processes in order to efficiently recycle/re-feed valuable metals into industrial systems. In addition to microbial analysis on a nanometer-scale, metalliferous waste products need to be sufficiently characterized in order to assess bioleaching efficiency of each tested microorganism.

CONCLUSION

Six thermoacidophilic archaeal strains (*M. sedula, M. hakonensis, S. acidocaldarius, S. metallicus, A. brierleyi,* and *A. manzaensis*) were capable of growing when supplemented with multimetallic BOF-dust derived from a steel production plant. Furthermore, each species was able to leach a set of elements from BOF-dust grains; however, *A. manzaensis* showed the highest potential in growth and bioleaching of economically relevant elements. Electron microscopy-assisted analysis of BOF-dust grains processed by *A. manzaensis* reveals a breakdown of the dust-grains mineral matrix in course of cultivation. Additionally, the formation of gypsum crystals was observed during the cultivation process. The obtained results emphasize the utilization of thermoacidophilic archaea for future (industrial) bioleaching operations and the need to conduct more in-depth studies to optimize these processes. So far, bioleaching mechanisms have been described extensively for a handful of acidophilic bacteria (overview by Donati and Sand, 2007). To exploit the full potential of thermoacidophilic archaea, more in-depth studies need to be carried out for the future efficient bioleaching operations and for the development of environmental-friendly circular economies. Further investigations should focus on resolving the microbial-mineral interfaces of the selected thermoacidophiles grown on waste product materials down to nanometer scale. This will help understand the mechanisms of microbial interactions with metal-bearing waste product material and see the relevant cell compartments involved in the bioleaching process.

DATA AVAILABILITY STATEMENT

The original contributions presented in the study are included in the article/**Supplementary Material**, further inquiries can be directed to the corresponding author.

AUTHOR CONTRIBUTIONS

DK, AM, MA, MB, HS, and TM performed experiments. DK, AM, and TM planned and executed the cultivation of thermoacidophilic archaea, as well as performance and interpretation, of SEM-EDS experiments. MB performed ICP-MS analyses. MA and TM performed and analyzed STEM-EDS results. All authors made substantial contributions to the acquisition, analysis, and interpretation of the data described in this study. All authors critically reviewed the manuscript and approved the final version of it.

ACKNOWLEDGMENTS

We warmly thank S. Puchegger (University of Vienna, Physics Faculty Center for Nano Structure Research) for the support of electron microscopy investigations and Martina Dienstleder (Graz Centre for Electron Microscopy) for help with FIB preparation. Furthermore, we thank Daniela Gruber for the guidance of SEM-EDS analysis, which was performed at the Core Facility Cell Imaging and Ultrastructure Research, University of Vienna – member of the Vienna Life-Science Instruments (VLSI).

SUPPLEMENTARY MATERIAL

The Supplementary Material for this article can be found online at: https://www.frontiersin.org/articles/10.3389/fmicb.2022.864411/full#supplementary-material

REFERENCES

Ai, C., Yan, Z., Chai, H., Gu, T., Wang, J., Chai, L., et al. (2019). Increased chalcopyrite bioleaching capabilities of extremely thermoacidophilic Metallosphaera sedula inocula by mixotrophic propagation. *J. Ind. Microbiol. Biotechnol.* 46, 1113–1127. doi: 10.1007/s10295-019-02193-3

Auernik, K. S., and Kelly, R. M. (2010a). Impact of molecular hydrogen on chalcopyrite bioleaching by the extremely thermoacidophilic archaeon *Metallosphaera sedula*. *Appl. Environ. Microbiol.* 76, 2668–2672. doi: 10.1128/AEM.02016-09

Auernik, K. S., and Kelly, R. M. (2010b). Physiological versatility of the extremely thermoacidophilic archaeon *Metallosphaera sedula* supported by transcriptomic analysis of heterotrophic, autotrophic, and mixotrophic growth. *Appl. Environ. Microbiol.* 76, 931–935. doi: 10.1128/AEM.01336-09

Auernik, K. S., Maezato, Y., Blum, P. H., and Kelly, R. M. (2008). The genome sequence of the metal-mobilizing, extremely thermoacidophilic archaeon *Metallosphaera sedula* provides insights into bioleaching-associated metabolism. *Appl. Environ. Microbiol.* 74, 682–692. doi: 10.1128/AEM.02019-07

Banerjee, I., Burrell, B., Reed, C., West, A. C., and Banta, S. (2017). Metals and minerals as a biotechnology feedstock: engineering biomining microbiology for bioenergy applications. *Curr. Opin. Biotech.* 45, 144–155. doi: 10.1016/j.copbio.2017.03.009

Barbuta, M., Bucur, R. D., Cimpeanu, S. M., Paraschiv, G., and Bucur, D. (2015). Wastes in building materials industry. In: *Agroecology*, ed. Pilipavičius, V. (InTech). doi: 10.5772/59933

Bathe, S., and Norris, P. R. (2007). Ferrous iron- and sulfur-induced genes in *Sulfolobus metallicus*. *Appl. Environ. Microbiol.* 73, 2491–2497. doi: 10.1128/AEM.02589-06

Batool, R. (2012). Hexavalent chromium reduction by bacteria from tannery effluent. *J. Microbiol. Biotech.* 22, 547–554. doi: 10.4014/jmb.1108.08029

Beck, J. V. (1967). The role of bacteria in copper mining operations. *Biotechnol. Bioeng.* 9, 487–497. doi: 10.1002/bit.260090405

Blazevic, A., Albu, M., Mitsche, S., Rittmann, S. K.-M. R., Habler, G., and Milojevic, T. (2019). Biotransformation of scheelite CaWO4 by the extreme thermoacidophile metallosphaera sedula: tungsten–microbial interface. *Front. Microbiol.* 10, 1492. doi: 10.3389/fmicb.2019.01492

Bosecker, K. (1997). Bioleaching: metal solubilization by microorganisms. *FEMS Microbiol. Rev.* 20, 591–604. doi: 10.1111/j.1574-6976.1997.tb00340.x

Brandl, H., Bosshard, R., and Wegmann, M. (2001). Computer-munching microbes: metal leaching from electronic scrap by bacteria and fungi. *Hydrometallurgy.* 59, 319–326. doi: 10.1016/S0304-386X(00)00188-2

Brim, H., Venkateswaran, A., Kostandarithes, H. M., Fredrickson, J. K., and Daly, M. J. (2003). Engineering deinococcus geothermalis for bioremediation of high-temperature radioactive waste environments. *Appl. Environ. Microbiol.* 69, 4575–4582. doi: 10.1128/AEM.69.8.4575-4582.2003

Brock, T. D., Brock, K. M., Belly, R. T., Weiss, R. L. (1972). Sulfolobus: a new genus of sulfur-oxidizing bacteria living at low pH and high temperature. *Archiv. Mikrobiol.* 84, 54–68. doi: 10.1007/BF00408082

Bromfield, L., Africa, C.-J., Harrison, S. T. L., and van Hille, R. P. (2011). The effect of temperature and culture history on the attachment of Metallosphaera hakonensis to mineral sulfides with application to heap bioleaching. *Miner. Eng.* 24, 1157–1165. doi: 10.1016/j.mineng.2011.03.019

Chang-Li, L., Jin-Lan, X., Zhen-Yuan, N., Yi, Y., and Chen-Yan, M. (2012). Effect of sodium chloride on sulfur speciation of chalcopyrite bioleached by the extreme thermophile Acidianus manzaensis. *Bioresource Technol.* 110, 462–467. doi: 10.1016/j.biortech.2012.01.084

Clark, D. A., and Norris, P. R. (1996). Oxidation of mineral sulphides by thermophilic microorganisms. *Miner. Eng.* 9, 1119–1125. doi: 10.1016/0892-6875(96)00106-9

Coetzee, J. J., Bansal, N., and Chirwa, E. M. N. (2020). Chromium in Environment, Its Toxic Effect from Chromite-Mining and Ferrochrome Industries, and Its Possible Bioremediation. *Expo Health* 12, 51–62. doi: 10.1007/s12403-018-0284-z

Donati, E. R., and Sand, W. (2007). *Microbial Processing of Metal Sulfides*. Dordrecht: Springer.

Dopson, M., Halinen, A.-K., Rahunen, N., Boström, D., Sundkvist, J.-E., Riekkola-Vanhanen, M., et al. (2008). Silicate mineral dissolution during heap bioleaching. *Biotechnol. Bioeng.* 99, 811–820. doi: 10.1002/bit.21628

Dworkin, M., Falkow, S., Rosenberg, E., Schleifer, K.-H., and Stackebrandt, E. (2006). *The Prokaryotes*. New York, NY: Springer New York. doi: 10.1007/0-387-30743-5

EUROFER (2020). Annual Report 2020. Available online at: https://www.eurofer.eu/publications/archive/annual-report-2020. (accessed December 8, 2021)

Gara, S., and Schrimpf, S. (1998). *Behandlung von Reststoffen und Abfällen in der Eisen- und Stahlindustrie*. Wien: Bundesministerium für Umwelt, Jugend und Familie.

Gautier, V., Escobar, B., and Vargas, T. (2007). The catalytic influence of *Sulfolobus metallicus* in the bioleaching of chalcopyrite: role of attached and planktonic population. *AMR* 20–21, 354–357. doi: 10.4028/www.scientific.net/AMR.20-21.354

Gautier, V., Escobar, B., and Vargas, T. (2008). Cooperative action of attached and planktonic cells during bioleaching of chalcopyrite with Sulfolobus metallicus at 70 °C. *Hydrometallurgy.* 94, 121–126. doi: 10.1016/j.hydromet.2008.05.03

Gericke, M., and Pinches, A. (1999). Bioleaching of copper sulphide concentrate using extreme thermophilic bacteria. *Miner. Eng.* 12, 893–904. doi: 10.1016/S0892-6875(99)00076-X

Giachino, A., Focarelli, F., Marles-Wright, J., and Waldron, K. J. (2021). Synthetic biology approaches to copper remediation: bioleaching, accumulation and recycling. *FEMS Microbiol. Ecol.* 97, fiaa249. doi: 10.1093/femsec/fiaa249

Hackl, R. P., Dreisinger, D. B., Peters, E., and King, J. A. (1995). Passivation of chalcopyrite during oxidative leaching in sulfate media. *Hydrometallurgy.* 39, 25–48. doi: 10.1016/0304-386X(95)00023-A

He, H., Xia, J.-L., Yang, Y., Jiang, H., Xiao, C., Zheng, L., et al. (2009). Sulfur speciation on the surface of chalcopyrite leached by Acidianus manzaensis. *Hydrometallurgy.* 99, 45–50. doi: 10.1016/j.hydromet.2009.06.004

Huber, G., Spinnler, C., Gambacorta, A., and Stetter, K. O. (1989). Metallosphaera sedula gen, and sp. nov. represents a new genus of aerobic, metal-mobilizing, thermoacidophilic archaebacteria. *Syst. Appl. Microbiol.* 12, 38–47. doi: 10.1016/S0723-2020(89)80038-4

Huber, G., and Stetter, K. O. (1991). Sulfolobus metallicus, sp. nov., a novel strictly chemolithoautotrophic thermophilic archaeal species of metal-mobilizers. *Syst. Appl. Microbiol.* 14, 372–378. doi: 10.1016/S0723-2020(11)80312-7

Igiri, B. E., Okoduwa, S. I. R., Idoko, G. O., Akabuogu, E. P., Adeyi, A. O., and Ejiogu, I. K. (2018). Toxicity and bioremediation of heavy metals contaminated ecosystem from tannery wastewater: a review. *J. Toxicol.* 2018, e2568038. https://doi.org/10.1155/2018/2568038

Johnson, T. B., Mach, C., Grove, R., Kelly, R., Van Cott, K., and Blum, P. (2018). Secretion and fusion of biogeochemically active archaeal membrane vesicles. *Geobiology* 16, 659–673. doi: 10.1111/gbi.12306

Jujun, R., Jie, Z., Jian, H., and Zhang, J. (2015). A novel designed bioreactor for recovering precious metals from waste printed circuit boards. *Sci. Rep.* 5, 13481. doi: 10.1038/srep13481

Kargi, F., and Robinson, J. M. (1985). Biological removal of pyritic sulfur from coal by the thermophilic organism Sulfolobus acidocaldarius. *Biotechnol. Bioeng.* 27, 41–49. doi: 10.1002/bit.260270107

Khaing, S. Y., Sugai, Y., and Sasaki, K. (2019). Gold dissolution from ore with iodide-oxidising bacteria. *Sci. Rep.* 9, 4178. doi: 10.1038/s41598-019-41004-8

Klauber, C. (2008). A critical review of the surface chemistry of acidic ferric sulphate dissolution of chalcopyrite with regards to hindered dissolution. *Int. Miner. Process.* 86, 1–17. doi: 10.1016/j.minpro.2007.09.003

Kölbl, D., Pignitter, M., Somoza, V., Schimak, M. P., Strbak, O., Blazevic, A., et al. (2017). Exploring fingerprints of the extreme thermoacidophile metallosphaera sedula grown on synthetic martian regolith materials as the sole energy sources. *Front. Microbiol.* 8, 1918. doi: 10.3389/fmicb.2017.01918

Konishi, Y., Nishimura, H., and Asai, S. (1998). Bioleaching of sphalerite by the acidophilic thermophile Acidianus brierleyi. *Hydrometallurgy.* 47, 339–352. doi: 10.1016/S0304-386X(97)00057-1

Krebs, W., Brombacher, C., Bosshard, P. P., Bachofen, R., and Brandl, H. (1997). Microbial recovery of metals from solids. *FEMS Microbiol. Rev.* 20, 605–617. doi: 10.1111/j.1574-6976.1997.tb00341.x

Li, M., Huang, Y., Yang, Y., Wang, H., Hu, L., Zhong, H., et al. (2020). Heavy metal ions removed from imitating acid mine drainages with a thermoacidophilic

archaea: Acidianus manzaensis YN25. *Ecotox. Environ. Safe.* 190, 110084. doi: 10.1016/j.ecoenv.2019.110084

Liang, C., Xia, J., Nie, Z., Yu, S., and Xu, B. (2014). Effect of initial pH on chalcopyrite oxidation dissolution in the presence of extreme thermophile Acidianus manzaensis. *T. Nonferr. Metal. Soc.* 24, 1890–1897. doi: 10.1016/S1003-6326(14)63268-4

Liu, H., Xia, J., Nie, Z., Ma, C., Zheng, L., Hong, C., et al. (2016a). Bioleaching of chalcopyrite by Acidianus manzaensis under different constant pH. *Miner. Eng.* 98, 80–89. doi: 10.1016/j.mineng.2016.07.019

Liu, H., Xia, J., Nie, Z., Wen, W., Yang, Y., Ma, C., et al. (2016b). Formation and evolution of secondary minerals during bioleaching of chalcopyrite by thermoacidophilic Archaea Acidianus manzaensis. *T. Nonferr. Metal. Soc.* 26, 2485–2494. doi: 10.1016/S1003-6326(16)64369-8

Liu, K., Deng, M., and Mo, L. (2015). Influence of pH on the formation of gypsum in cement materials during sulfate attack. *Adv. Cem. Res.* 27, 487–493. doi: 10.1680/jadcr.14.00076

Lutz, H., Weitzel, H.-P., and Huster, W. (2012). Aqueous emulsion polymers. In: *Polymer Science: A Comprehensive Reference (Elsevier)* p. 479–518. doi: 10.1016/B978-0-444-53349-4.00280-6

Ma, Y., Xia, J., Yang, Y., Nie, Z., Liu, H., and Liu, L. (2017). Complete genome sequence of the extremely thermoacidophilic archaeon *Acidianus manzaensis* YN-25. *Genome Announc.* 5, e00438–17. doi: 10.1128/genomeA.00438-17

Mäkinen, J., Salo, M., Soini, J., and Kinnunen, P. (2019). Laboratory scale investigations on heap (bio)leaching of municipal solid waste incineration bottom ash. *Minerals.* 9, 290. doi: 10.3390/min9050290

Manobala, T., Shukla, S. K., Subba Rao, T., and Dharmendira Kumar, M. (2019). A new uranium bioremediation approach using radio-tolerant Deinococcus radiodurans biofilm. *J. Biosci.* 44, 122. doi: 10.1007/s12038-019-9942-y

Marsh, R. M., and Norris, P. R. (1983). Mineral sulphide oxidation by moderately thermophilic acidophilic bacteria. *Biotechnol. Lett*. doi: 10.1007/BF00130837

Mikkelsen, D., Kappler, U., Webb, R. I., Rasch, R., McEwan, A. G., and Sly, L. I. (2007). Visualisation of pyrite leaching by selected thermophilic archaea: Nature of microorganism–ore interactions during bioleaching. *Hydrometallurgy.* 88, 143–153. doi: 10.1016/j.hydromet.2007.02.013

Milojevic, T., Albu, M., Blazevic, A., Gumerova, N., Konrad, L., and Cyran, N. (2019a). Nanoscale tungsten-microbial interface of the metal immobilizing thermoacidophilic archaeon metallosphaera sedula cultivated with tungsten polyoxometalate. *Front. Microbiol.* 10. doi: 10.3389/fmicb.2019.01267

Milojevic, T., Albu, M., Kölbl, D., Kothleitner, G., Bruner, R., and Morgan, M. L. (2021). Chemolithotrophy on the Noachian Martian breccia NWA 7034 via experimental microbial biotransformation. *Commun. Earth Environ.* 2, 39. doi: 10.1038/s43247-021-00105-x

Milojevic, T., Kölbl, D., Ferrière, L., Albu, M., Kish, A., Flemming, R. L., et al. (2019b). Exploring the microbial biotransformation of extraterrestrial material on nanometer scale. *Sci. Rep.* 9, 18028. doi: 10.1038/s41598-019-54482-7

Mukherjee, A., Wheaton, G. H., Blum, P. H., and Kelly, R. M. (2012). Uranium extremophily is an adaptive, rather than intrinsic, feature for extremely thermoacidophilic Metallosphaera species. *PNAS.* 109, 16702–16707. doi: 10.1073/pnas.1210904109

Newsome, L., and Falagán, C. (2021). The microbiology of metal mine waste: bioremediation applications and implications for planetary health. *GeoHealth.* 5, e2020GH000380. doi: 10.1029/2020GH000380

Nie, Z., Zhang, W., Liu, H., Zhu, H., Zhao, C., Zhang, D., et al. (2019). Bioleaching of chalcopyrite with different crystal phases by Acidianus manzaensis. *T. Nonferr. Metal. Soc.* 29, 617–624. doi: 10.1016/S1003-6326(19)64971-X

Norris, P. (1997). Thermophiles and Bioleaching. In: *Biomining. Springer, Berlin, Heidelberg*. doi: 10.1007/978-3-662-06111-4_12

Pawlowski, L., Kotowski, M., Bolto, B. A., and McNeill, R. (1984). Reclamation of chromium from wastes. In: *Studies in Environmental Science Chemistry for Protection of The Environment.,* Pawlowski, L., Verdier, A. J., and Lacy, W. J. (Elsevier). p. 491–512. doi: 10.1016/S0166-1116(08)71256-1

Rahmani, O. (2018). Siderite precipitation using by-product red gypsum for CO2 sequestration. *J. CO2 Util.* 24, 321–327. doi: 10.1016/j.jcou.2018.01.020

Rahmani, O. (2020). An experimental study of accelerated mineral carbonation of industrial waste red gypsum for CO2 sequestration. *J. CO2 Util.* 35, 265–271. doi: 10.1016/j.jcou.2019.10.005

Rahmani, O., Kadkhodaie, A., and Highfield, J. (2016). Kinetics analysis of CO2 mineral carbonation using byproduct red gypsum. *Energy Fuels* 30, 7460–7464. doi: 10.1021/acs.energyfuels.6b00246

Saitoh, N., Nomura, T., and Konishi, Y. (2017). Bioleaching of low-grade chalcopyrite ore by the thermophilic archaean *Acidianus brierleyi*. *SSP* 262, 237–241. doi: 10.4028/www.scientific.net/SSP.262.237

Schippers, A., Hedrich, S., Vasters, J., Drobe, M., Sand, W., and Willscher, S. (2013). Biomining: Metal Recovery from Ores with Microorganisms. In: *Geobiotechnology I,* eds. Schippers, A., Glombitza, F., and Sand, W. (Berlin, Heidelberg: Springer Berlin Heidelberg), p. 1–47. doi: 10.1007/10_2013_216

Segerer, A., Neuner, A., Kristjansson, J. K., and Stetter, K. O. (1986). Acidianus infernus gen. nov., sp. nov., and acidianus brierleyi comb. nov.: facultatively aerobic, extremely acidophilic thermophilic sulfur-metabolizing archaebacteria. *Int. J. Syst. Bacteriol.* 36, 559–564. doi: 10.1099/00207713-36-4-559

Sehlin, M. H., and Lindström, B. E. (1992). Oxidation and reduction of arsenic by Sulfolobus acidocaldarius strain BC. *FEMS Microbiol. Lett.* 93, 87–92. doi: 10.1016/0378-1097(92)90494-9

Shiers, D. W., Ralph, D. E., Bryan, C. G., and Watling, H. R. (2013). Substrate utilisation by Acidianus brierleyi, Metallosphaera hakonensis and Sulfolobus metallicus in mixed ferrous ion and tetrathionate growth media. *Miner. Eng.* 48, 86–93. doi: 10.1016/j.mineng.2012.10.006

Shivvers, D. W., and Brock, T. D. (1973). Oxidation of Elemental Sulfur by Sulfolobus acidocaldarius. *J. Bacteriol.* 114, 706–710. doi: 10.1128/JB.114.2.706-710.1973

Singh, R., Gorai, A. K., and Segaran, R. G. (2013). Characterisation of LD slag of Bokaro Steel Plant and its feasibility study of manufacturing commercial "fly ash-LD slag" bricks. *IJETM* 16, 129. doi: 10.1504/IJETM.2013.050685

Srichandan, H., Mohapatra, R. K., Parhi, P. K., and Mishra, S. (2019). Bioleaching: A Bioremediation Process to Treat Hazardous Wastes. In: *Soil Microenvironment for Bioremediation and Polymer Production.* (John Wiley and Sons. Ltd) 115–129. doi: 10.1002/9781119592129.ch7

Takayanagi, S., Kawasaki, H., Sugimori, K., Yamada, T., Sugai, A., Ito, T., et al. (1996). Sulfolobus hakonensis sp. nov., a novel species of acidothermophilic archaeon. *Int. J. Syst. Bacteriol.* 46, 377–382. doi: 10.1099/00207713-46-2-377

Tobita, M., Yokozeki, M., Nishikawa, N., and Kawakami, Y. (1994). Pyrite Oxidation by Sulfolobus acidocaldarius. *Biosci. Biotechnol. Biochem.* 58, 771–772. doi: 10.1271/bbb.58.771

United Nations General Assembly (2015). Transforming our world: The 2030 agenda for sustainable development. Available online at: https://sdgs.un.org/2030agenda

Usher, K. M., Shaw, J. A., Plumb, J. J., and Saunders, M. (2009). Elemental ultrastructure of bioleaching bacteria and archaea grown on different energy sources. In: *Advanced Materials Research.* vol. 71, p. 235-238.. doi: 10.4028/www.scientific.net/AMR.71-73.235

Valdés, J., Pedroso, I., Quatrini, R., Dodson, R. J., Tettelin, H., Blake, R., et al. (2008). Acidithiobacillus ferrooxidans metabolism: from genome sequence to industrial applications. *BMC Genom.* 9, 597. doi: 10.1186/1471-2164-9-597

Vogel, M. B., Des Marais, D. J., Turk, K. A., Parenteau, M. N., Jahnke, L. L., and Kubo, M. D. Y. (2009). The role of biofilms in the sedimentology of actively forming gypsum deposits at guerrero negro, Mexico. *Astrobiology.* 9, 875–893. doi: 10.1089/ast.2008.0325

Wang, Y., Zeng, W., Qiu, G., Chen, X., and Zhou, H. (2014). A moderately thermophilic mixed microbial culture for bioleaching of chalcopyrite concentrate at high pulp density. *Appl. Environ. Microbiol.* 80, 741–750. doi: 10.1128/AEM.02907-13

Waste Disposal Recycling in Steel Industry (2019). Available online at: https://www.steel-technology.com/articles/wastedisposal. (accessed March 18, 2020)

Wheaton, G., Counts, J., Mukherjee, A., Kruh, J., and Kelly, R. (2015). The confluence of heavy metal biooxidation and heavy metal resistance: implications for bioleaching by extreme thermoacidophiles. *Minerals.* 5, 397–451. doi: 10.3390/min5030397

White, C., Shaman, A. K., and Gadd, G. M. (1998). An integrated microbial process for the bioremediation of soil contaminated with toxic metals. *Nat. Biotechnol.* 16, 572–575. doi: 10.1038/nbt0698-572

World Steel Association (2016). Fact Sheet: Steel Industry By-Products. Available online at: https://www.worldsteel.org/en/dam/jcr:b07b75c3-65d6-455e-8700-6ceb3ad3c769/Fact_By-products_2016.pdf (accessed November 2, 2021).

Yoshida, N., Nakasato, M., Ohmura, N., Ando, A., Saiki, H., Ishii, M., et al. (2006). Acidianus manzaensis sp. nov., a Novel Thermoacidophilic Archaeon Growing Autotrophically by the Oxidation of H2 with the Reduction of Fe3+. *Curr. Microbiol.* 53, 406–411. doi: 10.1007/s00284-006-0151-1

Zhang, R., Neu, T. R., Blanchard, V., Vera, M., and Sand, W. (2019). Biofilm dynamics and EPS production of a thermoacidophilic bioleaching archaeon. *New Biotechnol.* 51, 21–30. doi: 10.1016/j.nbt.2019.02.002

Zhao, H., Zhang, Y., Zhang, X., Qian, L., Sun, M., Yang, Y., et al. (2019). The dissolution and passivation mechanism of chalcopyrite in bioleaching: an overview. *Miner. Eng.* 136, 140–154. doi: 10.1016/j.mineng.2019.03.014

Conflict of Interest: GK, HS, and DW were employed by the company voestalpine Stahl Donawitz GmbH, Leoben, Austria.

The remaining authors declare that the research was conducted in the absence of any commercial or financial relationships that could be construed as a potential conflict of interest.

frontiers | Frontiers in Microbiology

ORIGINAL RESEARCH
published: 06 May 2022
doi: 10.3389/fmicb.2022.852192

FE-SEM/EDX Based Zinc Mobilization Analysis of *Burkholderia cepacia* and *Pantoea rodasii* and Their Functional Annotation in Crop Productivity, Soil Quality, and Zinc Biofortification of Paddy

Viabhav Kumar Upadhayay[1], Ajay Veer Singh[1], Amir Khan[1], Jyoti Singh[1], Navneet Pareek[2] and Alok Raghav[3]*

[1] Department of Microbiology, College of Basic Sciences and Humanities, G. B. Pant University of Agriculture and Technology, Pantnagar, India, [2] Department of Soil Science, College of Agriculture, G. B. Pant University of Agriculture and Technology, Pantnagar, India, [3] Multidisciplinary Research Unit, Department of Health Research, Ministry of Health and Family Welfare, Ganesh Shankar Vidyarthi Memorial Medical College, Kanpur, India

OPEN ACCESS

Edited by:
Adnan Mustafa, Brno University of Technology, Czechia

Reviewed by:
Vijay S. Meena, The International Maize and Wheat Improvement Center (CIMMYT), India
Usman Zulfiqar, University of Agriculture, Faisalabad, Pakistan

***Correspondence:**
Ajay Veer Singh
ajaygbpuat@gmail.com

Specialty section:
This article was submitted to Terrestrial Microbiology, a section of the journal Frontiers in Microbiology

Received: *10 January 2022*
Accepted: *15 March 2022*
Published: *06 May 2022*

Citation:
Upadhayay VK, Singh AV, Khan A, Singh J, Pareek N and Raghav A (2022) FE-SEM/EDX Based Zinc Mobilization Analysis of Burkholderia cepacia and Pantoea rodasii and Their Functional Annotation in Crop Productivity, Soil Quality, and Zinc Biofortification of Paddy. Front. Microbiol. 13:852192. doi: 10.3389/fmicb.2022.852192

The experimental study was contrived to characterize two zinc-solubilizing bacteria (ZSB), namely BMRR126 and BMAR64, and their role in zinc (Zn) biofortification of rice. These bacteria solubilized Zn profoundly, determined qualitatively by halo-zone formation on a solid medium and quantitatively in a liquid broth by AAS and SEM-EDX. The lowering of pH and contact angle assessment of the liquid broth unveiled the establishment of the acidic conditions in a medium suitable for Zn solubilization. The characterization of both isolates on the basis of 16S rRNA gene analysis was identified as *Burkholderia cepacia* and *Pantoea rodasii*, respectively. These strains were also found to have some plant probiotic traits namely phosphate solubilization, production of siderophore, indole acetic acid (IAA), exopolysaccharide (EPS), and ammonia. The field experiments were performed at two diverse locations and under all treatments; the simultaneous use of BMRR126 and BMAR64 with zinc oxide (ZnO) resulted in the highest growth and productivity of the paddy crop. The utmost Zn achievement in the grain was estimated in a treatment (T9) (25.07 mg/kg) containing a consortium of BMRR126 and BMAR64 along with ZnO for the *Terai region*. The treatment containing single ZSB bioinoculant BMRR126 (T7) showed an elevated Zn amount in the rice grain (33.25 mg/kg) for the *Katchar region*. The soil parameters (pH, EC, organic carbon, NPK, available Zn, and dehydrogenase activity) were also positively influenced under all bacterial treatments compared to the uninoculated control. Our study clearly accentuates the need for Zn solubilizing bacteria (ZSB) to provide the benefits of Zn-biofortification in different regions.

Keywords: FE-SEM/EDX, biofortification, zinc solubilizing bacteria, zinc, rice

INTRODUCTION

Agriculture is the topmost significant sector in India, besides industrial and technological developments, which contributes to a prolific role in 17.5% of the Nation's GDP (Sambasivam et al., 2020). Rice is an important edible staple crop that fulfills the nutritional requirements of an ever-growing population of the world (Val-Torregrosa et al., 2021). The addition of high-yielding rice varieties and the application of agrochemicals (fertilizers and pesticides) resulted in a significant augmentation in the rice yield (Eliazer Nelson et al., 2019; Yu et al., 2020). However, it can be predicted that rice production will be affected adversely in the near future due to some issues, such as the shrinking of rice acreage, shortage of water for proper irrigation, and higher cultivation costs. Furthermore, micronutrient dearth is the most important limiting factor for global rice productivity (Senthilkumar et al., 2021). Micronutrients, especially Zn, are required in very minute quantities and show a crucial job in the well-being of humans and plants (Sharma et al., 2013; Natasha et al., 2022). Current studies focus on the modern agricultural production of Zn-fortified food crops to curtail the negative effects of Zn-associated malnutrition among a deprived section of the global population (Kiran et al., 2022; Naeem et al., 2022). Although soils contain a huge portion of the insoluble Zn which is not accessible by plants (Moreno-Lora and Delgado, 2020), and thereby affects the amount of Zn in grains (Liu et al., 2019).

An ample range of soil factors, typically total Zn level, elevated pH, and the maximum content of calcite, organic matter, Ca, Mg, Na, phosphate, and bicarbonate also influence the Zn availability in plants (Alloway, 2009). The inadequacy of Zn exhibits various symptoms that typically become apparent within 2 to 3 weeks after seedling transplantation of rice. Symptoms may include the incidence of "brown blotches: and "streaks," which may coalesce to obscure older leaves completely, stunted growth, delay in maturity, and decline in yield (Wissuwa et al., 2006; Singh and Prasad, 2014). If we consume the rice grown on Zn scarce soil, it can lead to Zn malnutrition in humans (Rehman et al., 2012). To circumvent the issue of Zn deficiency, few methods are popular. The foremost agronomic method entails the usage of Zn fertilizers as a soil application (Liu et al., 2020) or as a foliar spray (Poblaciones and Rengel, 2017; Cakmak and Kutman, 2018). But the utilization of this method depicts environmental and economical pressure (Wissuwa et al., 2006), and Zn fertilizers convert to insoluble forms within 7 days of application (Rattan and Shukla, 1991; Hussain et al., 2018). Other methods involve three important approaches that include breeding (Swamy et al., 2016), genetic engineering (Mhatre et al., 2011; Das et al., 2020), and transgenics (Malik and Maqbool, 2020). However, all these approaches are costlier, slower, and laborious (Upadhayay et al., 2019). Studies on the functional aspects of zinc solubilizing bacteria (ZSB) can better replace these approaches (Kamran et al., 2017; Mumtaz et al., 2017; Upadhayay et al., 2021, 2022).

As a part of both the rhizo-microbiome and the phyto-microbiome, ZSB exhibits a benevolent role in maintaining plant health. The contemporary understanding of ZSB inoculants and their significance in Zn-biofortification has been imperceptibly explicated (Sharma et al., 2012; Costerousse et al., 2017; Kamran et al., 2017; Mumtaz et al., 2017; Hussain et al., 2018; Bhatt and Maheshwari, 2020; Kushwaha et al., 2020, 2021; Upadhayay et al., 2021, 2022; Prathap et al., 2022). Few studies displaying an interaction between plants and ZSB inoculants for better plant growth provided expectations to resolve the issue of Zn malnutrition in an eco-friendly manner (Ramesh et al., 2014; Kamran et al., 2017; Hussain et al., 2018; Bhatt and Maheshwari, 2020; Kushwaha et al., 2020; Bashir et al., 2021; Rezaeiniko et al., 2022; Upadhayay et al., 2022). The usage of ZSB provides an economically feasible tactic for the Zn biofortification of food crops (Upadhayay et al., 2022). The ZSB solubilizes the complex form of Zn found in the soil into a simpler form, thus giving plants access to the proper level of Zn (Saravanan et al., 2004; Kushwaha et al., 2020). Wide arrays of mechanisms involved for Zn solubilization include organic acid secretion (Costerousse et al., 2017), production of chelating agents (Singh and Prasanna, 2020), protons (Kushwaha et al., 2020), and oxidoreductive systems on cell membranes. Organic acids produced by ZSB show a downward trend in pH in the nearby soil, thus creating a suitable environment for Zn solubilization (Alexander, 1997; Wu et al., 2006; Kamran et al., 2017; Upadhayay et al., 2018, 2022). Other mechanisms include the secretion of iron-chelating agents, "siderophores," which are believed to play a key role in solubilizing micronutrients, such as Fe and Zn (Upadhayay et al., 2018, 2022).

Few studies also described the plant probiotic traits of ZSB, such as "phosphate solubilization," production of "siderophore," "phytohormones," "exopolysaccharides," "HCN," and "ammonia" (Kamran et al., 2017; Mumtaz et al., 2017; Bhatt and Maheshwari, 2020). These features make ZSB an excellent plant probiotic strain to facilitate crop growth besides providing the benefit of biofortification. Many ZSB strains namely *Acinetobacter*, *Burkholderia* (Vaid et al., 2014), *Bacillus* (Zeb et al., 2018), *Enterobacter*, and *Sphingomonas* (Wang et al., 2014) improved the Zn level in various regions of rice plant. The consortium of ZSB, which consists of the three strains, *Agrobacterium* sp., *A. lipoferum*, and *Pseudomonas* sp., showed an improvement in rice productivity in a field-based study (Tariq et al., 2007). Other prospective ZSB strains augmented Zn in the edible portion of soybean (Sharma et al., 2012), wheat (Rana et al., 2012), and maize (Mumtaz et al., 2017).

Considering the above facts, the current study was conducted to reveal the zinc oxide (ZnO) solubilization capability of two bacterial strains isolated from the rhizosphere of barnyard millet. Bacterial strains were then tested for their functional plant probiotic traits, followed by field trials conducted at two consecutive sites, especially in the "*Terai*" and "*Katchar*" regions of northern India, to illustrate the impact of the ZSB and their consortium (with and without ZnO supplementation) on growth-yield related parameters of rice crops and soil quality. Furthermore, the main objective of decoding the benefit of Zn-biofortification through estimation of Zn content in grains under the influence of ZSB was achieved.

MATERIALS AND METHODS

Soil Collection and Microorganisms

The samples of rhizospheric soil were collected from "Barnyard millet" (underutilized crop) growing at high altitudes of the Northern Himalayan regions, such as Ranichauri (30.3111°N, 78.4097°E) and Almora (29.8150°N, 79.2902°E). The carefully taken samples were tightly packed in sterilized sample collection bags and immediately brought to the microbiology laboratory for further studies. About 1 g of soil sample was serially diluted (up to 10^6) in the saline solution. About 100 μl aliquot of the diluted samples was homogeneously spread on NA (nutrient agar) medium plates. The bacterial colonies with different morphological properties were then selected after the plates had been properly incubated for 24 h at 28 ± 2°C. Afterward, the cultures of bacteria were preserved at −20°C (in glycerol stock) and in slants at 4°C for regular use.

Zinc Solubilization Bioassay

The preliminary qualitative screening for the selection of potential Zn mobilizing rhizobacteria was executed by adapting the protocol of Ramesh et al. (2014). In brief, Tris minimal medium agar plates containing 0.1% of complex zinc source i.e., "ZnO" were spot inoculated with freshly grown isolates on NA plates. The inoculated Petri plates, after sealing with the parafilm, were kept for incubation for 1 week (at 28 ± 2°C). After incubation, the appearance of the halo zone around the bacterial colonies reflected a "detecting point" for deciphering the eventuality of zinc solubilization, and the halo zone was measured in centimeters. The formation of a halo zone around bacteria is attributed due to the secretion of organic acids that lower the pH of the nearby milieu and solubilize the complex form of zinc, and this phenomenon appears in the form of a "halo zone."

Furthermore, the Zn solubilization efficiency (ZnSE) of the ZSB strains was calculated in percentage (%) by using the following formula:

$$\text{ZnSE} = \text{diameter of solubilization halo/diameter of the colony} \times 100$$

The selected ZSB were also determined for quantitative Zn mobilization in Tris-minimal liquid broth medium (with ZnO as the insoluble Zn source) by adapting the procedure of Fasim et al. (2002). In this process, 50 ml of ZnO-supplemented basal liquid medium was inoculated with 500 μl aliquots of overnight grown ZSB inoculums and kept for incubation by providing constant temperature (28 ± 2°C) for 10 days in an orbital shaker at 130 rpm while the ZnO-supplemented media without bacterial inoculation was maintained as a non-inoculated control. After proper incubation, the inoculated and uninoculated liquid broth was centrifuged at 6,100 × *g* (10 min) followed by filtration through Whatman filter paper (No. 42). The soluble Zn in the filtered suspension was evaluated by atomic absorption spectrophotometer (AAS). The pH of the suspension was also assessed by a pH meter for predicting the organic acid production in the liquid medium pertaining to Zn solubilization by following the experimental procedure of Mumtaz et al. (2017). The contact angle of the supernatant acquired from the liquid medium was also measured for observing the impact of ZSB on the inoculated broth. Contact angles were measured from the two opposite sides, which are represented as the left contact angle and right contact angle, respectively, and repeated three times.

Field Emission-Scanning Electron Microscopy/Energy Dispersive X-ray Analysis

The Zn-solubilizing behavior was also determined by Field Emission-Scanning Electron Microscope (FE-SEM) and energy dispersive X-ray (EDX). For this process, 50 ml of ZnO-amended Tris mineral-based medium was inoculated with 500 μl aliquots of fresh test bacterial culture and kept incubated at 28 ± 2°C in an orbital shaker (at 130 rpm). The ZnO-supplemented media deprived of bacterial inoculation was kept as an uninoculated control. On the 10th day after the incubation, the medium suspension of the flask was centrifuged at 10,000 rpm for 10 min. The medium suspension of the flask was centrifuged at 10,000 rpm for 10 min. After discarding the supernatant, the resulting residues were washed three times with double distilled water (DW) and dried. The dried samples were mounted on a carbon tape attached to a brass holder as per the method of Delvasto et al. (2009). The assembled samples were then sputter-coated with a carbon gold double layer. SEM and EDX-based evaluation for elements was accomplished using a JSM-7100F field emission SEM in conjunction with EDX.

Characterization of Bacterial Isolates

Various characteristics, namely colony morphology, Gram staining, cell morphology, and endospore formation, were determined by standard methods. The biochemical behaviors of the selected ZSB strains were identified using the Bergey's Manual of Determinative Bacteriology. The genomic DNA of both bacterial strains was isolated as per the method described by Bazzicalupo and Fani (1995). The 16S rRNA gene for each bacterial isolate was amplified in 100 μl reaction mixture containing 1 μl template DNA, 4 μl dNTPs (2.5 mM each), 10 μl 10X Taq DNA polymerase assay buffer, 1 μl Taq DNA polymerase enzyme (3 U/μl), water and primer (400 ng of each forward primer: 5′–CAGGCCTAACACATGCAAGTC–3′ and reverse primer: 5′– GGCGGATGTGTACAAGGC – 3′). Initial denaturation was provided at 95°C for 5 min, followed by 35 cycles of 94°C for 30 s, 50°C for 30 s, 72°C for 1.5 min, and final extension at 72°C for 7 min. The ∼1.5 kb, 16S-rDNA fragment was amplified using a thermal cycler "PTC-200 thermal cycler" (M.J. Research) and sequenced through Chromus Biotech (Bangalore, India). The identification of ZSB isolates was performed based on the 16S rRNA gene sequence homology by the MEGA6 software using a neighbor-joining method with 1,000 bootstrap replicates (Tamura et al., 2011).

In vitro Screening of PGP Traits

Phosphate Solubilization

Quantitative analysis for determining phosphate solubilization potential of both isolates was assessed by the method of

Nautiyal (1999). The fresh cultures (1 ml) of test isolates were inoculated into 50 ml of NBRIP broth. After incubation at 28 ± 2°C (120 rpm) for up to 7 days, 5 ml of the suspension was drawn out and filtered through Whatman No. 1 filter paper, which was then centrifuged at 10,000 rpm (for 20 min). After centrifugation was complete, 1 ml of cell-free suspension was mixed with 2.5 ml of Barton's reagent and the volume was made up to 50 ml by the addition of distilled water. After the development of a yellow color (10 min incubation), the OD of the suspension was recorded by a spectrophotometer and the total amount of dissolved P was determined from the standard curve.

Indole-3-Acetic Acid Synthesis

The synthesis of plant hormones, such as indole-3-acetic acid (IAA) by both strains was analyzed using Salkowski's reagent as per the protocol of Patten and Glick (2002). The bacterial cultures, grown in Luria broth (supplemented with 50 μg/ml of tryptophan) at 28 ± 2°C for 4 days, were centrifuged at 5,500 rpm for 10 min (at 4°C). About 2 ml aliquots of the supernatant were collected into fresh test tubes, followed by the addition of orthophosphoric acid (2 drops) and Salkowski's reagent (4 ml). The appearance of the pink color indicated the bacterial production of IAA in the broth medium and the OD was taken at 540 nm. The production of IAA in the broth medium was evaluated by comparison to the standard curve of IAA.

Siderophore Production

Production of siderophore (iron chelating agent) was estimated on Chrome-Azurol S (CAS) medium as presented by Schwyn and Neilands (1987). For performing this, the CAS agar plates were spot-inoculated with fresh bacterial culture. After 4 days of incubation at 28 ± 2°C, siderophore production was confirmed based on the measurement of the yellow-orange halo zone that appeared around the bacterial colony.

Production of Exopolysaccharide and Ammonia

To assess the EPS production ability of selected bacterial isolates, the 500 μl aliquot of a freshly grown bacterial suspension grown in the nutrient broth was inoculated into 50 ml of special medium for EPS production as suggested by Siddikee et al. (2011). After incubation at 28 ± 2°C for 5 days with shaking at 150 rpm, the broth was centrifuged at 10,000 × *g* (10 min). The resultant supernatant was collected in a fresh and sterile test tube, and after adding three-fold chilled absolute ethanol, the tubes were kept at 4°C overnight. The formation of the precipitation in the suspension indicated a positive result for EPS production. Once this step was completed, centrifugation was performed at 7,000 × *g* (20 min), the supernatant was discarded, and the resulting pellet was collected. The pellet was dried at 60°C for the complete disappearance of the alcohol and the dry weight of the dried residues was calculated in mg/ml. For the production of ammonia by bacterial isolates, the method of Cappuccino and Sherman (1992) was used. Vials containing peptone water (5 ml/vial) were inoculated with freshly grown bacterial cultures and incubated at 28 ± 2°C for 48 h. At the end of the incubation period, Nessler's reagent (0.5 ml) was added to each vial and kept at room temperature for at least 5 min, and the positive result was assessed by the development of a brown to yellow color.

Bacterial Culture Conditions and Consortium Preparation

The characterized ZSB isolates (BMRR126 and BMAR64) were cultured on Luria-Bertani (LB) agar plates at 28 ± 2°C for 24 h. Bacterial isolates were subcultured onto a fresh medium every 2 weeks. For the preparation of liquid cultures, the fresh colony of the bacterial culture was transferred to an LB broth medium and kept for incubation at 28 ± 2°C (for 48 h) with shaking at 200 rpm. Afterward, the broth with visible bacterial growth was spun in a centrifuge for 15 min (at 6000 × g) and the resulting bacterial pellet was suspended in sterile distilled water to achieve a concentration of 10^9 CFU/ml. This concentration of the bacterial strains was used for various *in vitro* assays. Before the preparation of the bacterial consortium, the biocompatibility of both strains was also assessed according to the method of Roshani et al. (2020). A freshly grown colony on LB agar plate from each compatible culture was inoculated into a test tube containing 10 ml of nutrient broth (NB) medium and kept at proper incubation for 24 h (with constant shaking at 120 rpm) at 28 ± 2°C. The absorbance of bacterial grown suspension was analyzed at the optimum wavelength (600 nm). Afterward, the equal culture volume {A_{600}-0.6} from both compatible bacterial cultures was dispensed to 100 ml of NB and mixed properly to build a bacterial consortium (Prasad and Babu, 2017).

In situ Field Study

Site Description and Experimental Design

The experimental study was executed at two subsequent locations in the "*Terai*" region - Breeder Seed Production Center (BPSC), GBPUA&T, Pantnagar (U.S.Nagar), Uttarakhand, India (29.0308° N, 79.4651° E) and the "*Katchar*" region - Village: Kariyamai (Budaun), Uttar Pradesh, India (28.2523° N, 78.7490° E) from July 2018 to October 2018. The soil characteristics of the experimental area in both regions are provided in **Supplementary Table 3**. The research trials were set up in a randomized block design (RBD) with three replications. The trial included nine treatments mentioned in **Table 1**.

Raising of Nursery

The preparation of nursery beds was carried out in both sites (*Terai* and *Katchar*) with the proper inclusion of drainage

TABLE 1 | Treatments used for field trial.

Labels	Treatments Description	Labels	Treatments Description
T1	Control	T6	Consortium***
T2	$ZnSO_4$*	T7	BMRR126 + ZnO
T3	ZnO**	T8	BMAR64 + ZnO
T4	BMRR126	T9	Consortium*** + ZnO
T5	BMAR64		

*$ZnSO_4$ as Zn supplement @25 kg/hectare; **ZnO as Zn supplement @60 kg/hectare; ***Consortium contains zinc solubilizing bacterial (ZSB) strains, BMRR126 and BMAR64.*

TABLE 2 | Details of trial establishment.

Particular	Details
Design	Randomized Block Design (RBD)
Crop	Rice (*Oryza sativa*)
Variety	*Pusa Basmati* 1
Number of replications	3
Number of treatment combinations	9
Total number of plots	27
Gross plot size	12 m^2
Net plot size	6.6 m^2
Spacing	15 × 20 cm

channels along the bed to drain the excess water. The seeds of the rice variety "*Pusa Basmati-1*," which were procured from the Breeder Seed Production Center, Pantnagar (Uttarakhand), India, were soaked for 48 h and kept in a moist gunny cloth for 48 h. The seeds were broadcasted uniformly on the previously established nursery beds. Adequate moisture levels were maintained by irrigation, but flooding was avoided.

Trial Establishment

Field preparation at both sites (*Terai* and *Katchar*) was commenced a week before transplanting. Some essential procedures as suggested by agricultural experts were followed to prepare the farmland for field trial. The main field was ploughed with tractor-drawn disc plough followed to obtain a good tilth, and the bunds (up to 15 cm in height) were made in dry conditions after being compacted. Each plot was 4 m long and 3 m wide, giving a total area of 12 m^2. Each plot was manually leveled and the soil was saturated prior to transplanting. The rice seedlings of 21 days old were uprooted from a nursery and thoroughly washed with water, and precautions were taken to have a lesser degree of damage to the plant roots. Uprooted seedlings were taken from the nursery to the transplanted site, followed by immersion of the roots of seedlings in the LB liquid broth of test bacterial suspensions (individual ZSB strain and consortium) with an adequate bacterial population density of approximately 10^6 to 10^7 cfu/ml as per the method of Tariq et al. (2007), Sharma et al. (2014). Inoculated seedlings (three seedlings per hill) were transplanted manually by maintaining a planting geometry of 15 cm × 20 cm. The recommended dose of fertilizers was applied before transplantation. The recommended doses of $ZnSO_4$ (@25 kg/hectare) and ZnO (@60 kg/hectare) were broadcasted into the plots according to the treatment. Irrigation, fertilization, weed management, and plant protection were performed according to standard procedures. The trials at both sites were maintained until crop harvesting. The detail of the trial establishment is given in **Table 2**.

Biometric Observation and Yield Assessment

At the time of harvest, biometric observations, such as the height of the plant, number of tillers (per hill), and dry matter accumulation were recorded. The four main yield components, such as the panicle length, the number of panicles per hill, the number of grains per panicle, and the 1,000 grain weight were also determined. The crop was harvested for decoding yield assessment, such as biological yield, grain yield, straw yield, and harvest index, when the plants attained physiological maturity. To circumvent the border effect, border rows were first harvested before net plots were harvested. After 72 h of sun drying in the field, the produce of each plot was tied into bundles (plot-wise), weighed in kg per plot with a spring balance, and then converted into q ha^{-1} for assessing the biological yield. After threshing the bundles, the grain and straw yield was recorded in kilograms per plot and then expressed in q ha^{-1}. The harvest index of each plot was calculated by the following formula:

$$\text{Harvest index} = \text{Economic yield}/\text{Biological yield} \times 100$$

Zinc Estimation in Grain

Grain samples harvested after 120 days after transplanting (DAT) of each treatment were further analyzed for Zn content according to the study by Estefan et al. (2013). In brief, 0.1 g of paddy grain samples were weighed and transferred into the flask. About 10 ml of a triacid mixture consisting of nitric acid: sulfuric acid: perchloric acid (10: 1: 4 v/v/v) were added to each flask. The flasks were then placed on a hot plate (95°C) for complete digestion. Later, 5 ml of 6N HCl was added after completion of digestion and the volume was made up to 50 ml by adding distilled water. The digested solution was filtered through a filter paper (Whatman No. 1 filter paper) and transferred to fresh storage vials. The filtered digested samples were then used to analyze the Zn content in the samples by an atomic absorption spectrophotometer (AAS).

Soil Parameters

At the time of harvest, the soil samples were collected from each plot to determine different parameters, such as pH, EC, available Zn, organic carbon (%), and available NPK. The pH and EC were determined by following the procedure of Bower and Wilcox (1965), Jackson (1967), respectively. The estimation of the available Zn in the soil of each plot was performed using the DTPA extraction method (Lindsay and Norvell, 1978). While the organic carbon content was estimated by adapting the standard protocol (rapid titration method) of Walkley and Black (1934), the availability of macronutrients, such as N, P, and K, was assessed using the procedures of Hanway and Heidel (1952), Olsen et al. (1954), Subbiah and Asija (1956), respectively. The dehydrogenase activity, which actually reflects the microbial activity in the soil, was determined by the method of Casida et al. (1964).

Cluster and Principal Component Analysis

Cluster analysis categorizes multivariate data into subgroups through a wide range of methods. By shaping multivariate data into subsets, clustering can help reveal the attributes of existing structures or patterns. Hierarchical cluster analysis for agronomical and soil parameters was accomplished to construct a dendrogram based on the mean distance between treatments using the unweighted pair group method of arithmetic means (UPGMA). Principal components analysis (PCA) is the

data reduction method relevant to quantitative data types. PCA transmutes multi-correlated variables into distinct sets of uncorrelated variables for further investigation, simplifying the complexity in high-dimensional data while preserving trends and patterns. Such new distinct sets of variables are linear amalgamations of original variables. This is based on the eigen values and mutually independent eigen vectors (principal components) arranged in the descending order of variance magnitude. Such components provide scatterplots of observations with the finest properties to examine the underlying correlation and variability. In order to estimate the relative effect of different treatments on agronomic and soil parameters, a PCA and cluster analysis were performed using the software PAST 4.03 (Hammer et al., 2001).

Statistical Analysis

Before statistical analysis, data were normalized using the Shapiro-Wilk normality test. A statistical method was used to assess the suitability of treatments for different variables, such as agronomic parameters (height of the plant, number of tillers per hill, dry matter accumulation, panicle length, the number of panicles per hill, the number of grains per panicle, 1,000 grain weight, biological yield, grain Zn content, grain yield, straw yield, and harvest index), and soil parameters (pH, EC, organic carbon content, available nitrogen, phosphorus, potassium, and Zn). Data obtained from field trials of both regions (*Terai* and *Katchar*) were subjected to statistical analysis by one-way ANOVA using OPSTAT software packages[1]. The RBD with three replicates for each treatment was used for the experiments. Treatment means were compared by the Least Significant Difference (LSD) test with a probability of 5% ($p < 0.05$). The graphs were created using GraphPad Prism 5 software (GraphPad Software, San Diego, CA, United States).

RESULTS

Zinc Solubilization Assay

A total of 62 different bacterial isolates from rhizospheric soils of millet were examined for Zn solubilization potential. Finally, two bacterial isolates i.e., BMRR126 and BMAR64, were selected based on zinc solubilizing potential. The isolate, BMRR126, showed a larger Zn solubilizing halo zone (3.17 cm) compared to BMAR64 (2.40 cm) on Tris-mineral salts medium (amended with ZnO) (**Table 3** and **Supplementary Figure 1**) but the highest solubilization efficiency (SE) was shown by BMAR64 (i.e., 1200.00%) (**Table 3**). Similarly, BMRR126 significantly augmented the Zn availability in the liquid broth amended with ZnO as compared to BMAR64 (**Table 3**). Evaluation of pH indicated a decrease in pH to a minimum of 4.38 from the initial pH of 7.2 after 1 week of incubation. The cell-free culture supernatant of BMRR126 exhibited the lowest pH value of 4.38 followed by BMAR64 with the value of 5.86. The lowering of the pH value of the inoculated broth medium shows an elevated acidity. The decreased value of the contact angle (50.23 for CA left and 51.40 for CA right) for the cell-free culture supernatant of BMRR126 compared to the uninoculated control shows the production of organic acids or other similar hydrophilic products in the cell-free suspension of the broth medium (**Figure 1** and **Table 3**). The SEM images of ZnO amended Tris-mineral salt broth medium on the 10th day after incubation of both isolates exhibited better bio mobilization of Zn over non-inoculated control (**Figure 2**). The EDX analysis of four spectra also showed a decrease in the Zn percent (%) and an increase in the carbon content in the residues of the treated samples compared to the uninoculated control (**Figure 2** and **Supplementary Table 1**).

Bacterial Characterization

Both zinc-solubilizing bacterial isolates were attributed on basis of morphological and biochemical analysis (**Supplementary Table 2**). The 16S rDNA-based analysis revealed the confirmed identification of BMRR 126 as *Burkholderia cepacia* (accession number MW843566) and BMAR64 as *Pantoea rodasii* (accession number MZ397586) (**Figure 3**). The consequences of the BLAST search of the 16S rRNA gene sequences depicted the BMRR126 isolate as closely related to *Burkholderia cepacia*. On the other hand, BMAR64 showed the highest similarity with the *Pantoea rodasii* strain Os_Ep_PSA_45 with the representation of the closest homolog, *Pantoea* sp. Strain GNH-R4.

Plant Growth Promoting Attributes

Both the bacterial isolates were further determined for different PGP traits. Isolates showed positive outcomes and gave a varying

[1]http://14.139.232.166/opstat/

TABLE 3 | Zinc solubilizing potential of BMRR126 and BMAR64 in solid medium [qualitative Zn solubilization by measuring halo zone formation and solubilization efficiency (SE)] and liquid medium (quantitative Zn estimation, pH, and contact angle analysis).

ZSB isolates	Zinc solubilizing potential			pH of broth medium	Contact angle (CA) of broth medium	
	Qualitative assay		Quantitative assay			
	halo zone (cm)	Solubilization efficiency (%)	Solubilized zinc (mg/kg)		CA left	CA right
Uninoculated control	–	–	–	7.2	58.70 ± 0.85	58.57 ± 0.82
BMRR126	3.17 ± 0.12	633.33	30.08 ± 1.54	4.38 ± 0.13	50.23 ± 0.38	51.40 ± 0.38
BMAR64	2.40 ± 0.26	1200.00	12.22 ± 0.61	5.86 ± 0.20	56.90 ± 0.58	59.23 ± 0.61

Data are represented by mean value using three replicates.

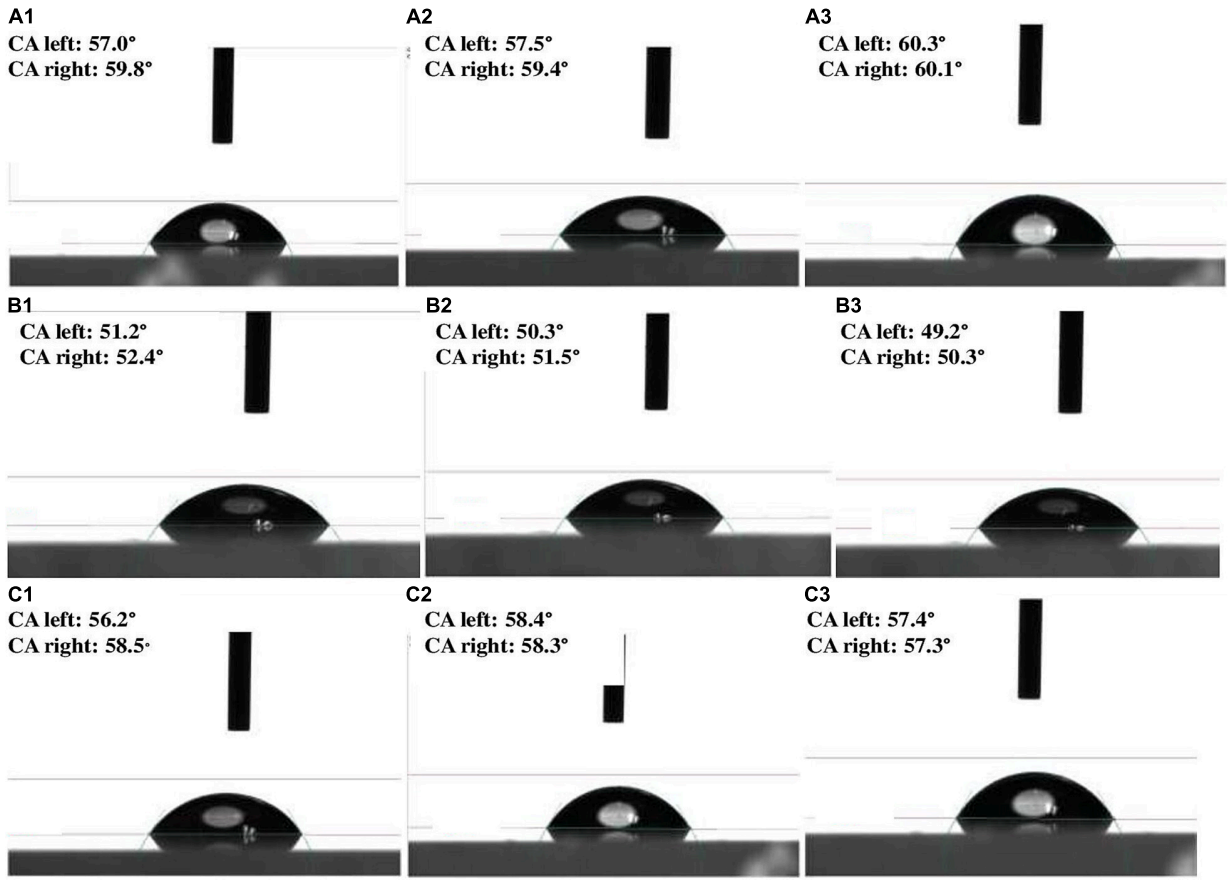

FIGURE 1 | Contact angle images depicting various level of values of broth suspension: **(A1–A3)** (uninoculated control); **(B1–B3)** (BMRR126); and **(C1–C3)** (BMAR64) inoculated broth.

degree of results for all plant growth-promoting attributes (**Table 4**). The highest halo zone formation depicting the potential of siderophore production was recorded for BMRR126 (5.87 ± 1.03 cm) followed by BMAR64 (1.57 ± 0.15 cm). The maximum phosphate solubility was determined for BMRR126 (302.67 μg/ml) followed by BMAR64 (241.67 μg/ml) after 7 days of incubation. Isolates, BMRR126 and BMAR64, produced the IAA (auxin) but the greatest potential of IAA production was observed in BMAR64 at a level of 29.82 μg/ml, followed by the isolate, BMRR126 with a range of 23.45 μg/ml in tryptophan-amended broth. In addition, isolates also showed a positive result for EPS production. Both the isolates, namely BMRR126 and BMAR64, showed different levels of EPS production of 2.80 mg/ml and 2.18 mg/ml, respectively. Moreover, the qualitative test of ammonia production was found to be positive for both isolates (BMRR126 and BMAR64).

Field Experiment and Biometric Observation

Field experiments were carried out at two subsequent locations to depict the prolific effects of ZSB strains (BMRR126 and BMAR64) and their consortium with and without Zn supplementation (ZnO). The ZSB isolates and their consortium have a positive effect on rice growth and influence plant height, number of tillers per hill, dry matter accumulation per hill, effective tillering, panicle length, number of grains per panicle, 1,000 grain weight, grain yield, and straw yield (**Tables 5**–**7**). The outcomes of the growth and yield parameters of paddy after treatments by ZSB and their consortium with and without an insoluble source of zinc (ZnO) exhibited varying levels of results. However, the least values were recorded for the uninoculated control treatment (T1). Moreover, the highest values for all the parameters were recorded for the *Katchar* region compared to the *Terai* region. Among the treatments, the maximum value of the plant height was recorded in the treatments containing ZSB inoculant, BMRR126 (137.39 cm), and consortium + ZnO (111.17 cm) for the *Katchar* region and *Terai* region, respectively. Similarly, the highest number of tillers hill^{-1} (13.27) was determined for the treatment T8 containing the bacterial strain, BMAR64, and ZnO supplementation for the *Terai* region as compared to the control (9.87). However, in the *Katchar* region, the highest number of tillers hill^{-1} (15.13) was calculated for the treatment T9 (consortium + ZnO) as compared to the control treatment (11.20).

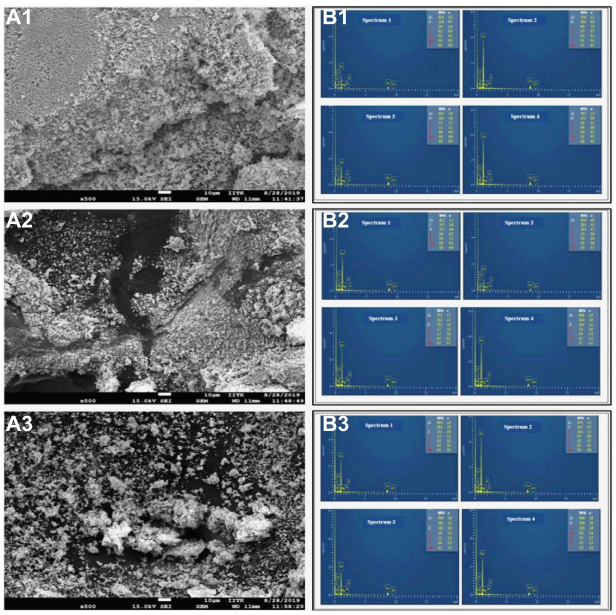

FIGURE 2 | Scanning electron micoscopy (SEM) **(A1–A3)**, typical EDX spectrum **(B1–B3)** and element quantification analysis exhibit mobility of ZnO, showing element spectrum (Wt%) of Zn (zinc) and C (carbon) by isolates, BMRR126 **(A2,B2)** and BMAR64 **(A3,B3)** in Tris mineral salt medium culture and uninoculated Tris mineral salt medium depicts the insoluble zinc (Zn) source of ZnO **(A1,B1)**.

The treatment containing the consortium and the recommended dose of ZnO (T9) showed the highest values of dry matter accumulation hill^{-1} (52.13) for the *Terai* region, while for the *Katchar* region, the treatment of the bacterial strain, BMRR126, with ZnO supplementation (T7) depicted the highest dry matter accumulation hill^{-1} (55.87 gm). Moreover, the bacterial consortium with ZnO supplementation (T9) showed the highest values of the effective tillering for both regions, i.e., *Terai* region (12.47) and *Katchar* region (13.60), in comparison to the control treatment (9.20 for the *Terai* area and 10.53 for the *Katchar* area). The highest value of the panicle length (32.95 cm) was recorded for consortium + ZnO (T9) followed by treatments containing BMRR126 + ZnO (32.44 cm) and consortium (32.31) for the *Terai* region. In contrast, the maximum value of panicle length (34.32 cm) was observed for the treatment containing BMRR126 with ZnO supplementation (T7) followed by consortium + ZnO (T9) which showed the panicle length value as 34.26 cm. For the *Terai* region, T9 (consortium + ZnO) showed the highest digits for the number of grains per panicle (179.67) in comparison with other treatments, while the bacterial strain, BMAR64 with ZnO amendment (T8) had an utmost value for grains per panicle (185.83) for the *Katchar* region. The highest grain yield (q/ha) was measured for the BMRR126 + ZnO (T7) for both the regions, *Terai* (42.52 q ha) and *Katchar* (43.59 q/ha). But treatment containing the bacterial consortium with no ZnO supplement (T6) showed a maximum value for straw yield for the *Terai* region (58.58 q/ha) and *Katchar* region (70.93 q/ha) in comparison to control treatment (52.80 q/ha for the *Terai* region and 53.65 q/ha for the *Katchar* region). Likewise, the same treatment also showed the highest value of the biological yield for both regions (99.85 q/ha for the *Terai* region and 114.07 q/ha for the *Katchar* region) compared to the control treatment (90.74 q/ha for the *Terai* region and 92.60 q/ha for the *Katchar* region).

Zinc Content Estimation in Grain

Inoculation of proficient ZSB strains and their consortium bearing massive PGP abilities not only augments plant growth but also increases the Zn micronutrient concentration in rice grains. Data about the Zn content in grains for all treatments from both trial sites are depicted in **Figure 4A**. The results from the *Terai* region revealed that the maximum Zn content (25.07 mg/kg) was observed for the treatment containing consortium with ZnO supplement (T9); there was almost 1.58-fold increment over the control (T1) which was 15.80 mg/kg. In the *Katchar* region, the highest Zn content (33.25 mg/kg) was observed for the BMRR126 + ZnO (T7), which showed a 1.72-fold increase compared to the control treatment (19.28 mg/kg). In both regions, all treatments showed significant results with a CD score of 2.83 and 2.92 for the *Terai* and *Katchar* regions, respectively (**Supplementary Table 4**). The results indicated that either single bacterial or consortium inoculation in combination with the ZnO application showed significant outcomes in providing Zn biofortification benefits *via* increasing the Zn concentration in edible parts of paddy.

Chemical Properties of Soil

Soil samples from both sites were collected from each treatment plot after the harvest of the crop for the determination of chemical properties, such as pH, EC, organic carbon, and NPK (**Table 8**). The soil pH value of the treated plots showed a lower value compared to the control. At both locations, the highest organic carbon was reported for the T7 (BMRR126 + ZnO), while the maximum P content was determined for T9 (consortium+ZnO). In addition, BMRR126 + ZnO (T7) for the *Terai* region and consortium + ZnO (T9) for the *Katchar* region showed the maximum value of N and K compared to other treatments. The data on the DTPA-extractable Zn in each treatment soil is shown in **Figure 4B**. The highest level of available Zn (1.35 mg/kg) is reported for BMRR126 + ZnO (T7) and consortium + ZnO (T9) for the *Terai* region. In contrast, BMAR64 + ZnO (T8) showed a relatively higher level of available Zn (2.10 mg/kg) for the *Katchar* region, followed by consortium + ZnO (T9) (2.09 mg/kg) and BMRR126 + ZnO (T7) (2.08 mg/kg). Furthermore, consortium + ZnO (T9) exhibited maximum DHA (dehydrogenase activity) for both *Terai* region (315.18 mgTPF/g soil/day) and *Katchar* region (463.41 mgTPF/g soil/day) (**Figure 5**).

Principal Component Analysis and Cluster Analysis

The principal component analysis allowed us to demonstrate the consequence of different treatment applications in a more cohesive mode between different variables under field

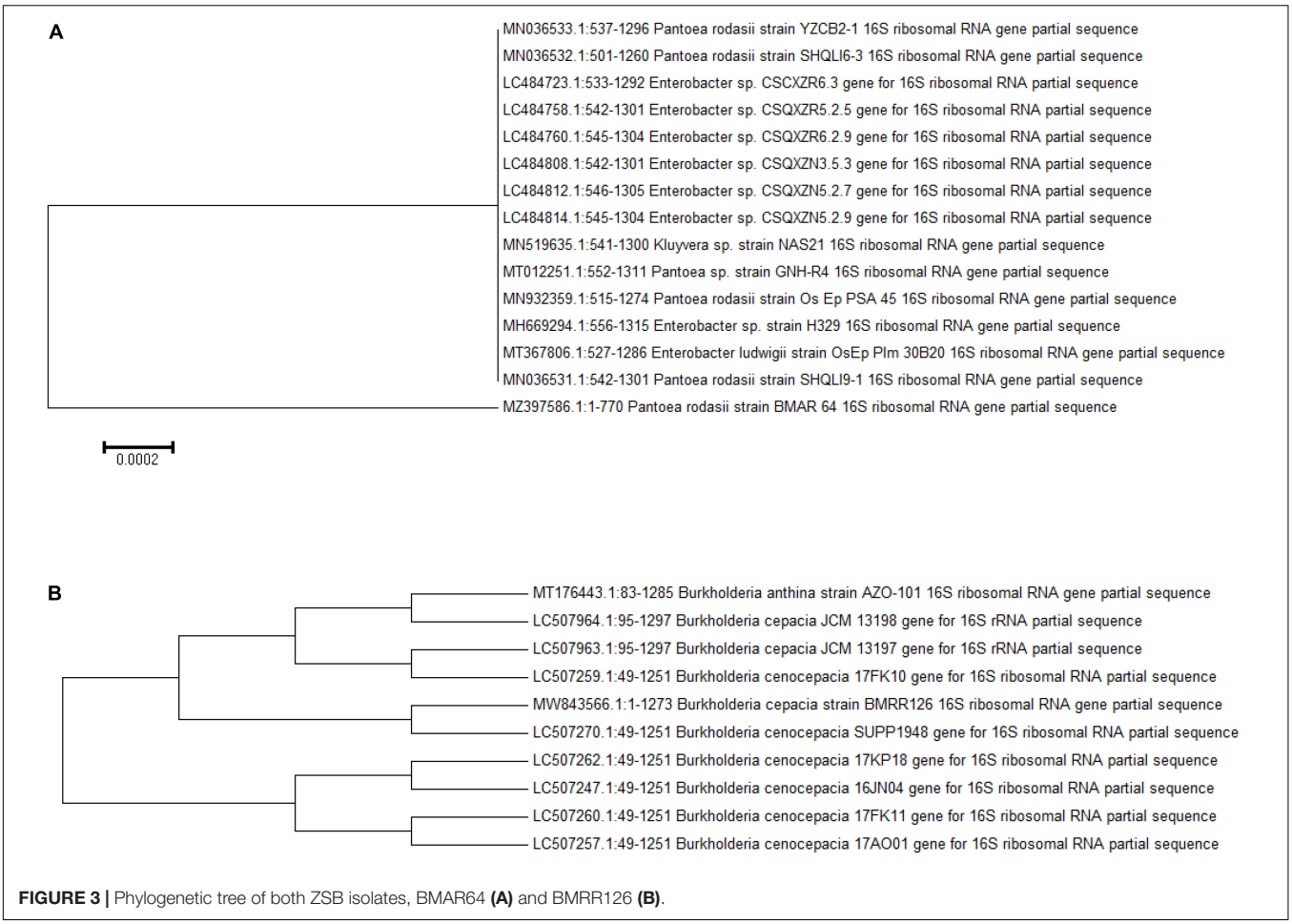

FIGURE 3 | Phylogenetic tree of both ZSB isolates, BMAR64 **(A)** and BMRR126 **(B)**.

TABLE 4 | Plant probiotic traits of potential zinc solubilizing bacterial isolates.

Isolates	Siderophore production	Phosphate solubilization	IAA production (μg/ml)	EPS Production (mg/ml)	Ammonia production
	Qualitative assay (cm)	Quantitative assay (μg/ml)			
BMRR126	5.87 ± 1.03	302.67 ± 6.03	23.45 ± 1.18	2.80 ± 0.10	+
BMAR64	1.57 ± 0.15	241.67 ± 4.73	29.82 ± 1.46	2.18 ± 0.18	+

Data are represented by mean value using three replicates.
" + " indicates positive result.

experimentation in two different regions (**Figures 6A1,A2**, **7A1,A2**). Two main components of PCAs for the agronomic parameters accounted for 93.79% of the experiment variability, i.e., PC1 for 78.14% and PC2 for 15.65%, for the *Terai* region (**Figure 6A1**). For the *Katchar* region, the PC1 and PC2 explained ∼88.45% of the total variability (PC1 for 79.01% and PC2 for 9.44%) (**Figure 6A2**). In addition, two main components of PCAs were determined for the soil-related parameters with 87.45% (PC1) and 6.74% (PC2) for the *Terai* region (**Figure 7A1**), while for the *Katchar* region, the values of PC1 and PC2 were determined as 76.97% and 10.14%, respectively (**Figure 7A2**). The concluding remarks of PCA, evidently indicate that two treatments, such as BMRR126 + ZnO (T7) and BMAR64 + ZnO (T8) in the *Terai* region, and three treatments, BMRR126 (T4), consortium (T6) and BMRR126 with ZnO supplementation (T7) in the *Katchar* region, displayed noteworthy improvement in agronomic parameters (**Figure 6**). While T4 and T7 in the *Terai* region and BMRR126 (T4) and BMAR64 with ZnO supplement (T8) in the *Katchar* region displayed noteworthy improvement in soil-related parameters. Outcomes of the cluster analysis are also similar to PCA (**Figures 6B1,B2**, **7B1,B2**). The agronomical parameters, such as the number of grains per panicle for the *Terai* region and harvest index for the *Katchar* region had the maximum coefficient value for the PC1 (0.99121) and PC2 (0.97238), respectively (**Table 9**). The soil related parameters, such as phosphorus for the *Katchar* region and nitrogen for the *Terai* region had the maximum

TABLE 5 | Effect on growth parameters (plant height, number of tillers, and dry matter accumulation) of rice at harvest stage under field experiment.

Labels	Treatments details	Plant height (in cm)		No. of tillers hill^{-1}		Dry matter (g) hill^{-1}	
		Terai region	*Katchar* region	*Terai* region	*Katchar* region	*Terai* region	*Katchar* region
T1	Control	100.66	126.85	9.87	11.20	45.60	46.26
T2	$ZnSO_4$	102.73	130.85	11.93	12.33	46.21	49.61
T3	ZnO	101.19	128.75	10.60	11.87	46.00	46.22
T4	BMRR126	105.95	137.39	12.40	13.27	49.65	51.34
T5	BMAR64	103.93	132.49	12.27	13.67	47.04	50.72
T6	Consortium*	105.09	134.79	12.73	13.47	50.04	54.28
T7	BMRR126 + ZnO	108.13	134.61	13.13	13.93	50.71	55.87
T8	BMAR64 + ZnO	105.88	134.02	13.27	14.47	47.60	53.00
T9	Consortium* + ZnO	111.17	134.87	12.80	15.13	52.13	54.73
	SE(m)±	0.93	1.02	0.65	0.58	1.53	1.28
	C.D.	2.82	3.10	1.99	1.77	NS*	3.87
	C.V.	1.54	1.34	9.41	7.68	5.49	4.32

Each value is mean of three replicates. Data were analyzed statistically at the 5% ($p < 0.05$) level of significance. Consortium contains bacterial strains, BMRR126 and BMAR64.*

TABLE 6 | Effect on growth parameters (effective tillers, panicle length, number of grains per panicle, and 1,000 grain weight) of rice at harvest stage under field experiment.

Labels	Treatments details	Effective tillers		Panicle length (in cm)		No. of grain/panicle		1000 grain weight (g)	
		Terai region	*Katchar* region	*Terai* region	*Katchar* region	*Terai* region	*Katchar* region	*Terai* region	*Katchar* region
T1	Control	9.20	10.53	28.92	30.25	130.87	142.83	16.6	18.38
T2	$ZnSO_4$	11.07	11.40	30.25	31.47	147.07	167.03	17.84	20.24
T3	ZnO	9.67	11.33	29.32	30.67	137.20	155.17	16.81	19.32
T4	BMRR126	11.20	12.67	31.14	32.70	159.93	176.90	18.56	20.94
T5	BMAR64	10.80	12.73	30.04	32.22	154.40	171.33	18.14	19.13
T6	Consortium*	11.27	13.07	32.31	33.28	169.27	177.20	18.77	20.58
T7	BMRR126 + ZnO	12.33	13.40	32.44	34.32	172.40	185.33	19.85	22.37
T8	BMAR64 + ZnO	12.20	12.93	31.81	33.03	165.07	185.83	19.6	21.1
T9	Consortium* + ZnO	12.47	13.60	32.95	34.26	179.67	184.60	20.43	21.6
	SEM ±	0.64	0.70	0.49	0.62	1.98	2.77	0.36	0.46
	C.D.	1.95	NS*	1.48	1.87	5.99	8.39	1.11	1.39
	C.V.	10.06	9.77	2.37	3.30	2.18	2.79	3.43	3.91

Each value is mean of three replicates. Data were analyzed statistically at the 5% ($p < 0.05$) level of significance. Consortium contains bacterial strains BMRR126 and BMAR64.*

coefficient value for the PC1 (0.98927) and PC2 (0.48289), respectively (**Table 10**).

DISCUSSION

"Microbial assisted biofortification" is a novel concept in the field of agricultural microbiology for nutrifying crop edibles with essential micronutrients (Zn, Fe, and Se). Zn is an indispensable element required for the maintenance of vital activities in humans, animals, and plants. The lack of this micronutrient triggers the onset of Zn malnutrition-linked ailments. In many regions of northern India, rice cultivation is being more popular among middle-income farmers as it provides the staple food for a large section of the South Asian population. India, as the second-largest rice producer, produced 112.76 million tons of rice in 2017-2018 (Sanjeeva Rao et al., 2020). At present, rice cultivation in North India is gaining popularity as these regions have all the necessary facilities, mainly irrigation systems, for rice cultivation. In fact, rice grain is the main source of calorie intake in many developing countries, but the Zn content in rice is insufficient to achieve the appropriate Zn content for human consumption (Zaman et al., 2018; Chávez-Dulanto et al., 2021). Hence, the present study reveals the incredibility of potential ZSB in improving general crop growth parameters that show the benefit of Zn biofortification of rice grain at two different state-wise regions of northern India. In the current investigation, BMRR126 and BMAR64 were recognized as competent ZSB from the rhizosphere of the barnyard millet. Rhizospheric soil is the main hub for soil-dwelling microorganisms, where a diverse range of microorganisms possibly solubilize the insoluble form of Zn and

TABLE 7 | Effect on yield parameters of rice at harvest stage under field experiment.

Labels	Treatments details	Grain yield (q/ha)		Straw yield (q/ha)		Biological yield (q/ha)		Harvest index	
		Terai region	*Katchar* region	*Terai* region	*Katchar* region	*Terai* region	*Katchar* region	*Terai* region	*Katchar* region
T1	Control	37.94	38.95	52.80	53.65	90.74	92.60	41.83	42.87
T2	$ZnSO_4$	39.67	41.77	52.48	57.52	92.15	99.28	43.08	43.99
T3	ZnO	38.53	39.23	52.29	53.41	90.82	92.64	42.44	41.18
T4	BMRR126	40.77	41.96	57.69	59.15	98.45	101.11	41.41	43.96
T5	BMAR64	38.80	39.92	55.26	59.64	94.06	99.56	41.28	43.03
T6	Consortium*	41.27	43.13	58.58	70.93	99.85	114.07	41.36	43.44
T7	BMRR126 + ZnO	42.52	43.59	55.94	67.71	98.46	111.30	43.48	41.67
T8	BMAR64 + ZnO	39.95	41.89	53.08	64.26	93.04	106.15	43.44	42.41
T9	Consortium* + ZnO	41.57	43.56	57.54	62.28	99.11	105.84	41.96	43.41
	SEM ±	0.86	0.70	3.68	2.90	3.86	2.99	1.68	0.74
	C.D.	2.62	2.12	NS*	8.79	NS*	9.06	NS*	NS*
	C.V.	3.74	2.92	11.57	8.26	7.03	5.06	6.91	2.99

Each value is mean of three replicates. Data were analyzed statistically at the 5% ($p < 0.05$) level of significance. Consortium contains bacterial strains, BMRR126 and BMAR64.*

likewise augment the crop yield (Khan et al., 2019; Upadhayay et al., 2021, 2022).

Zinc Solubilization Potential

In the current study, BMRR126 and BMAR64 were identified as the most effective Zn solubilizers. Though the strain BMRR126 showed a maximum area of halo zone illustrating Zn solubilization (3.17 cm), strain BMAR64 exhibited higher Zn SE (1200%) on ZnO supplemented medium (**Table 3**). A previous study carried out by Shaikh and Saraf (2017) also observed the solubilization of Zn on ZnO-supplemented medium, where *Exiguobacterium aurantiacum* (MS-ZT10) produced a clear zone of 31 mm in ZnO-containing medium. The possibility of Zn solubilization could be due to the stronger adhesion to insoluble metal residues (Saravanan et al., 2004). Further confirmation of Zn solubilization was evaluated in a liquid broth medium amended with ZnO as an insoluble 0.1% of Zn source. The results revealed that the potentiality of the strain, BMRR126 exerted promising Zn solubilization in comparison to strain BMAR64. These similar patterns of outcomes were also depicted by Ramesh et al. (2014), where two *Bacillus* strains (MDSR7 and MDSR14) efficiently solubilized the ZnO as an insoluble Zn compound. The decline in the pH of the inoculated liquid broth, as opposed to uninoculated broth (pH 7.2) (**Table 3**), clearly indicated the secretion of organic acids in the broth medium. The secretion of gluconic acid by ZSB was considered a prime feature for Zn solubilization (Fasim et al., 2002; Mumtaz et al., 2017; Kushwaha et al., 2020; Prathap et al., 2022; Upadhayay et al., 2022). Besides, other organic acids including oxalic, tartaric, formic, (Li et al., 2010) lactic acid, malonic acid, citric acid (Vidyashree et al., 2018a,b), and acetic acids (Mumtaz et al., 2019) which have been detected in the broth medium inoculated with ZSB, might have a probable role in the solubilization of insoluble Zn. The higher availability of elemental Zn is directly related to the acidic pH of a liquid medium, which explicates the mechanism of bacterial-assisted Zn solubilization (Desai et al., 2012). Pieces of literature have also suggested the auxiliary role of siderophore and protons produced by bacteria in Zn solubilization (Kamran et al., 2017; Hussain et al., 2018; Upadhayay et al., 2018, 2019, 2022). The lowest contact angle value which was detected for the inoculated liquid medium further illustrates the higher hydrophilicity of the liquid broth than that of the untreated control broth (**Figure 1** and **Table 3**). It was the first report based on contact angle analysis of a tiny drop of Zn-supplemented broth indicating the presence of more hydrophilic compounds, such as organic acids, which are essential for Zn solubilization. Both strains were identified as *Burkholderia cepacia* and *Pantoea rodasii* based on biochemical tests and molecular characterization, respectively (**Figure 3**). However, an inadequate number of studies are available on Zn solubilization by *Burkholderia* and *Pantoea* sp.

Field Emission-Scanning Electron Microscope/Energy Dispersive X-ray Analysis for Zinc Solubilization

The SEM-based analysis shows an effective mobilization of ZnO by both Zn solubilizing bacterial isolates compared to the control (**Figure 2**). The untreated control exhibits amorphous and dense residues of insoluble substances under SEM (**Figure 2A1**), while bacterial-treated samples showed lesser opaque "mineral residues" (**Figures 2A2,A3**). Our results were according to the findings of Gandhi and Muralidharan (2016), where the bacterium *Acinetobacter,* isolated from rice rhizosphere, efficiently mobilized ZnO observed under SEM. Elemental analysis of residues by EDX also depicted different spectra of elements, particularly, Zn and carbon (**Figures 2B1–B3** and **Supplementary Table 1**). The values of the reduced percentage of Zn from four spectra of all samples indicate that both ZSB strains have effectively solubilized Zn compared to the control. The increased carbon content in samples

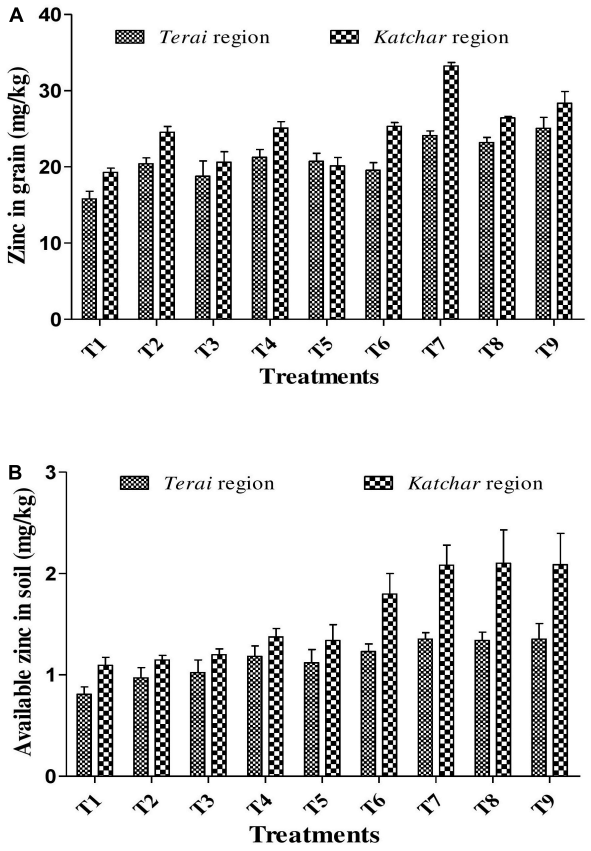

FIGURE 4 | Concentration of Zn (mg/kg) in grain **(A)** and available Zn (mg/kg) in soils **(B)** for *Terai* and *Katchar* regions.

inoculated with bacteria in all spectra indicated that organic compounds produced by bacteria may be aggregated with mineral residues.

Plant Growth Promoting Behaviors

Both bacterial strains contained some selected plant probiotic traits and showed different results under *in vitro* studies (**Table 4**). The characteristic of siderophore production shows the iron-solubilizing behavior of both isolates and enhances the value of such isolates in the form of bio-inoculants to produce Fe-fortified crops. The trait of phosphate solubilization show an imperative role of the bacterial inoculant for crop vitalization (Singh et al., 2013). Both isolates also showed varying levels of P solubilization when measured quantitatively. The highest value (302.67 μg/ml) of phosphate solubilization by isolate BMRR126 further illustrates the remarkable potential of ZSB as a "P-solubilizer." The earlier finding of Verma et al. (2020) reported "*Rhizobium radiobacter LB2*" for the phosphate solubilizing property besides being an efficient Zn solubilizer. These results are also in agreement with Mumtaz et al. (2017), Bhatt and Maheshwari (2020) who reported the phosphate solubilization potential of ZSB isolated from different sources. Isolates were also tested for IAA production and the results revealed that both ZSB strains contain the IAA production efficacy in the presence of L-tryptophan in the medium. There was considerable variation in IAA production between the ZSB isolates, ranging from 23.45 to 29.82 μg/ml in the L-tryptophan supplemented broth. In the past, a variation in the IAA production has been reported for ZSB isolates from the rhizosphere of *Chickpea and rice,* as reported by Gandhi and Muralidharan (2016), Zaheer et al. (2019), respectively. It is a well-established fact that an ample level of IAA increases plant growth and assists in the development of plant roots (Xie et al., 1996). In the present study, both ZSB isolates were evaluated for the production of EPS (exopolysaccharides), which provides help in effective root colonization. The plant facilitates the colonization of microbes by producing exudates that serve as a nutrient for bacteria in the rhizosphere (Bhattacharjee et al., 2012). In previous studies, the ZSB isolates, which demonstrate the ability to produce EPS, were used in the Zn enrichment of crops (Kamran et al., 2017; Mumtaz et al., 2017). The bacterial isolates also exhibited plant growth elevating features through the production of ammonia. This characteristic is also attributed to the plant growth-stimulating effect by plant-growth-promoting bacteria (Hayat et al., 2010; Backer et al., 2018).

Growth Parameters and Yield-Related Attributes

Outcomes of the present study revealed the remarkable influence of ZSB and their consortium along with ZnO supplement on numerous vegetative growth parameters (plant height, number of tillers per hill, and dry matter accumulation) and yield-related attributes (effective tillering per hill, panicle length, number of grains/panicle, 1,000 grain weight, grain yield, and straw yield) over uninoculated control under field study carried out at two different regions viz *Terai* and *Katchar* regions. Bacteria with diverse plant growth-promoting properties show high potential to improve plant height, dry weight, and the number of tillers, especially when applied in combination or with Zn supplementation (Vaid et al., 2014; Doni et al., 2022; Prathap et al., 2022). Maximum plant height in response to the bacterial consortium with Zn for the *Terai* region and a single bacterial inoculation (BMRR126) for the *Katchar* region indicated a microbial-assisted improvement in plant height (**Table 5**). The variation in plant height at both locations must be due to certain factors including soil type and climatic conditions. The ZSB including *Acinetobacter sp, Burkholderia cenocepacia,* and *Serratia* sp exhibited remarkable improvement in rice plant height (Idayu Othman et al., 2017; Nepomuceno et al., 2020). The effect on the number of tillers was higher when ZSB were co-inoculated with ZnO for both regions (**Table 5**). Similar results were also reported by Shakeel et al. (2015) in Basmati rice cultivars in response to co-inoculation of ZSB with Zn supplementation. Calculating effective tillering is an important feature to express grain yield and productivity in response to a given treatment. All bacterial-inoculated treatments expressed significant numbers of effective tillers (**Table 6**). Previous studies demonstrated the role of *Burkholderia* and *Acinetobacter* in considerable increment in the number of effective tillers of

TABLE 8 | Chemical properties of the experimental soils of *Terai* and *Katchar* regions.

Labels	Treatments details	pH		EC		Organic carbon (%)		Nitrogen (kg/ha)		Phosphorus (kg/ha)		Potassium (kg/ha)	
		Terai region	*Katchar* region	*Terai* region	*Katchar* region	*Terai* region	*Katchar* region	*Terai* region	*Katchar* region	*Terai* region	*Katchar* region	*Terai* region	*Katchar* region
T1	Control	7.86	7.42	0.461	0.336	0.72	0.75	220.56	267.61	16.13	19.03	114.5	138.21
T2	$ZnSO_4$	7.80	7.35	0.469	0.332	0.75	0.8	226.3	271.79	17.50	19.78	120.29	158.26
T3	ZnO	7.75	7.40	0.471	0.337	0.73	0.76	222.2	267.61	16.80	19.65	117.79	143.7
T4	BMRR126	7.62	7.30	0.335	0.281	0.79	1.12	245.21	288.51	20.01	21.81	139.81	183.27
T5	BMAR64	7.71	7.30	0.442	0.297	0.74	0.99	232.87	280.15	18.71	21.24	136.75	212.96
T6	Consortium*	7.56	7.18	0.331	0.269	0.77	0.81	226.22	284.33	19.08	21.2	144.59	150.52
T7	BMRR126 + ZnO	7.45	6.95	0.341	0.284	0.81	1.18	245.67	309.42	19.40	23.27	158.59	168.71
T8	BMAR64 + ZnO	7.64	7.23	0.348	0.295	0.77	1.1	231.37	305.24	19.28	22.03	142.13	201.67
T9	Consortium* + ZnO	7.48	6.91	0.334	0.271	0.79	0.86	238.34	317.78	20.06	23.44	155.57	226.35
	SE(m)	0.11	0.10	0.02	0.02	0.02	0.05	8.30	10.30	0.48	0.90	10.70	10.90
	C.D.	NS*	0.32	0.08	NS*	NS*	0.16	NS*	31.15	1.48	2.72	NS*	32.96
	C.V.	2.55	2.54	12.50	14.03	4.77	9.90	6.19	6.19	4.56	7.34	13.56	10.73

Each value is mean of three replicates. Data were analyzed statistically at the 5% ($p < 0.05$) level of significance. Consortium contains bacterial strains, BMRR126 and BMAR64.*

paddy (Trân Van et al., 2000; Vaid et al., 2014). The field investigation also revealed maximum values of 1,000 grain weight in response to bacteria or their consortium with ZnO supplementation (**Table 6**). Similar findings by Gandhi and Muralidharan (2016) also illustrated the effect of *Acinetobacter* with Zn supplement on increasing the 1,000 grain weight of rice. The effect of the bacterial strain, BMRR126 in combination with ZnO (T7) on the grain yield in a significant manner at different locations shows the better effectiveness of the bacterial isolate with Zn fertilizers (**Table 7**). Multitude studies decoded the enhanced grain yield in response to ZSB inoculants (Tariq et al., 2007; Vaid et al., 2014; Hussain et al., 2018; Kushwaha et al., 2020; Prathap et al., 2022). The study of Shakeel et al. (2015) illustrated the prolific effect of *Bacillus* sp on the rice plant in terms of increasing the grain yield. Bacteria play an auxiliary factor in the assimilation of nutrients from the soil, thereby increasing the grain yield and also crop biomass (Tariq et al., 2007; Suseelendra, 2012; Batool et al., 2021). The consortium of BMRR126 and BMAR64 in the paddy field gave the maximum biological yield (114.07 q/ha) for the *Katchar* region (**Table 7**). The result is similar to the result from the study of Shakeel et al., 2015, where the co-inoculation of ZSB and Zn showed an increased pattern of biological yield. In this study, results indicated that inoculation of ZSB resulted in an increase in straw yield (**Table 7**) which is supported by the results of Gandhi and Muralidharan (2016). However, the ZSB application along with ZnO showed an overall positive effect on the growth and yield of rice crops compared to a single Zn treatment containing $ZnSO_4$ and ZnO. It might be due to the steady and slow release of Zn from ZnO along with the proficient act of ZSB (Zeb et al., 2018). Somehow, the similar patterns of studies of Vaid et al. (2014), Gandhi and Muralidharan (2016), also unveiled an apparent role of ZSB in terms of improving the growth-related parameters of rice plants.

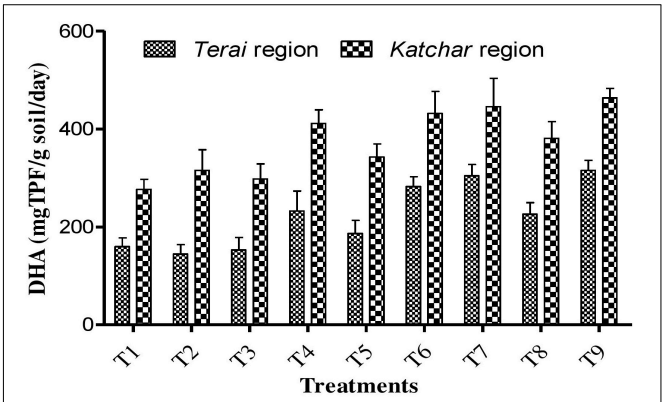

FIGURE 5 | Dehydrogenase (DHA) activity of the soils in the *Terai* and *Katchar* regions.

Zinc Content in Grain

The considerable augmentation in the Zn concentration of paddy variety, *Pusa Basmati*-1, was observed in the current study due to the effect of ZSB containing massive plant probiotic traits. Thus, the maximum Zn acquirement in the grain was determined for the treatment containing consortium and recommended dose of ZnO (T9) (for the *Terai* region) and BMRR126 + ZnO (T7) (for the *Katchar* region) (**Figure 4A**), where the application of consortium (BMRR126 and BMAR64) along with ZnO at *Terai* region and single ZSB bioinoculant BMRR126 at *Katchar* region confirm their ability of Zn solubilization. The results clearly showed that treatment with ZSB inoculants along with ZnO additives showed an improved pattern of Zn consignation in rice grains at both locations. The study by Shakeel et al. (2015), Gandhi and Muralidharan (2016) shows similar result patterns in which the ZSB shows a positive influence on the uptake of the elemental zinc in the rice grains. The key benefit of using ZSB is its dual action, firstly providing the biofortification benefits of rice to address the problem of zinc malnutrition, and secondly as a potential biofertilizer contributing to sustainable agriculture. The ZSB strains possess the plant probiotic properties to augment plant growth and improved nutrient acquisition for maintaining plant health (Upadhayay et al., 2022). The improved Zn concentration of grain is certainly influenced by ZSB

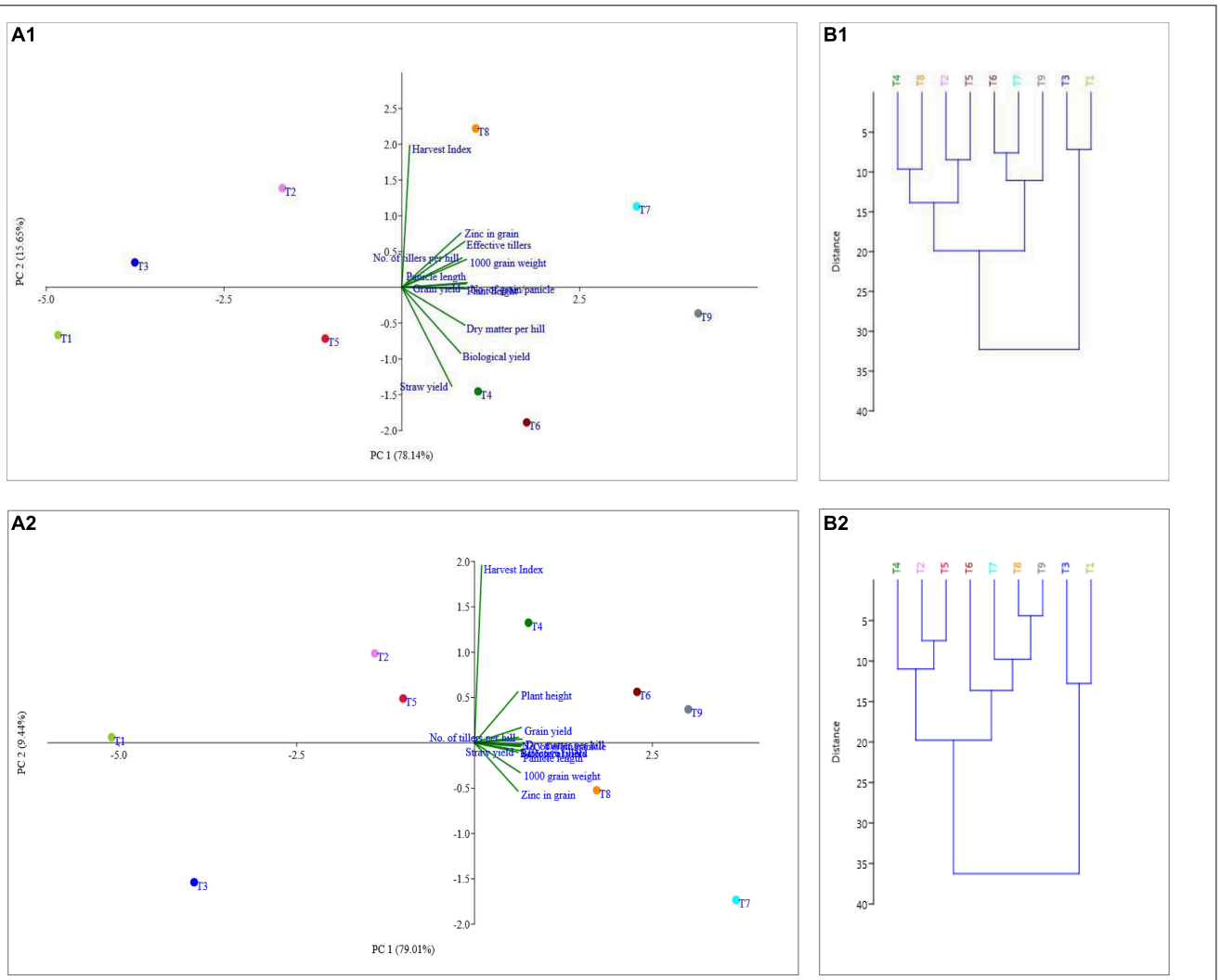

FIGURE 6 | Relative performance prognosis of different treatments on agricultural parameters (plant height, number of tillers, effective tillers, dry matter, panicle length, number of grains/panicle, 1,000 grain weight, grain yield, straw yield, biological yield, harvest index, and Zn content in grain) through cluster (**B1** for the *Terai* region and **B2** for the *Katchar* region) and principle component analysis (PCA) (**A1** for the *Terai* region and **A2** for the *Katchar* region).

inoculants, suggesting that the use of such microorganisms may offer green technological approaches for the biofortification of plants (Khan et al., 2019; Kushwaha et al., 2021). The increase in plant growth by ZSB is due to its imperative traits of root colonization (Idayu Othman et al., 2017). In our study, the augmented Zn levels in rice grain with the ZSB inoculants, BMRR126 and BMAR64, were viewed as an auxiliary tactic to curtail the Zn deficiency in cultivated rice at two consecutive locations (*Terai* region and *Katchar* region). The increased Zn content in the edible part of the plant may be due to efficient ZSB colonization, where organic acids secreted by bacteria lower the pH of the rhizospheric soil and create a favorable environment for Zn solubilization (Mumtaz et al., 2017; Hussain et al., 2018; Upadhayay et al., 2022). The finding of Zn content was consistent with previous studies using a ZSB microbial strain, such as *Bacillus* sp., enhanced Zn translocation (22–49%) in *Basmati* rice (*Basmati*-385) (Shakeel et al., 2015). Furthermore, Wang et al. (2014) deciphered that "*Enterobacter* sp. " and "*Sphingomonas* sp. " increased Zn content by 11.2% and 13.7% in polished rice, respectively.

Available Zinc in Soil

The increased level of DTPA-extractable Zn content in soils due to bacterial treatments with ZnO additives has rectified the issue of more prevalence of an inaccessible form of Zn in soil (**Figure 4B**). It is well studied that ZSB solubilizes the complex type of Zn in the soil and makes it accessible to the plant system (Ramesh et al., 2014; Kushwaha et al., 2020; Upadhayay et al., 2021). The increased level of available Zn in soil for the treatment containing bacteria and Zn supplementation might be due to the organic acid production ability of inoculated bacteria which might slowly release zinc from ZnO and other insoluble Zn forms. Plenty of previous studies documented the various organic acid producing microorganisms assisting

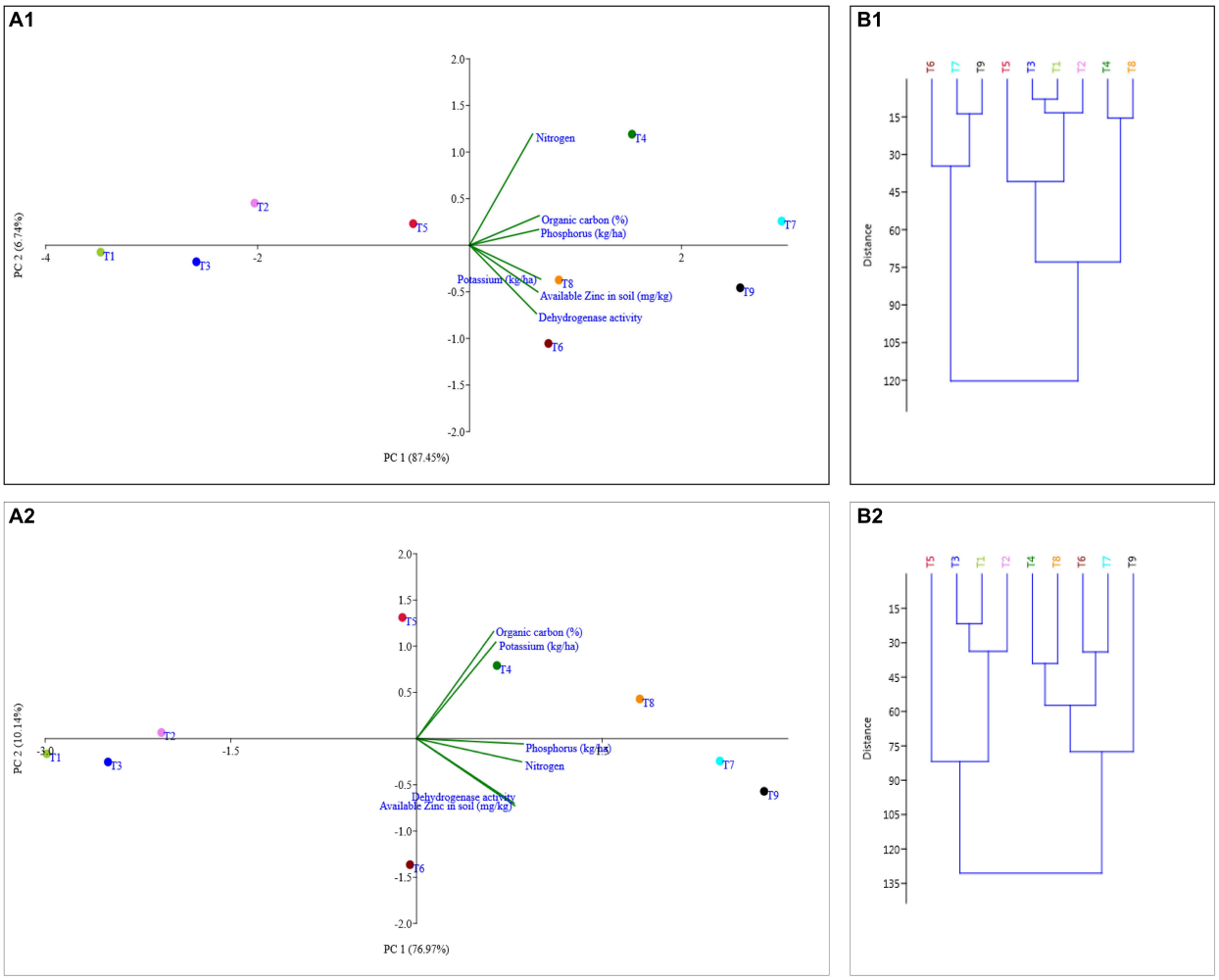

FIGURE 7 | Representation of different treatments on soil parameters (organic carbon, nitrogen, phosphorus, potassium, available zinc, and dehydrogenase activity) through cluster (**B1** for the *Terai* region and **B2** for the *Katchar* region) and PCA (**A1** for the *Terai* region and **A2** for the *Katchar* region).

in lowering the rhizospheric soil pH (Ramesh et al., 2014; Shakeel et al., 2015; Krithika and Balachandar, 2016; Kushwaha et al., 2020). Moreover, Saravanan et al. (2004), Sarathambal et al. (2010) deciphered the decline of soil pH due to the inoculation of *G. diazotrophicus, Bacillus,* and *Pseudomonas* for sufficient Zn accessibility to plant. Improved soil Zn content after bacterial inoculation can be a good indicator of microbial activity and its fruitful contribution to enhancing Zn uptake by plants.

Soil Parameters

Indeed, under field conditions, multiple external determinants come to the front and can reduce the capacity of soil bacteria to generate fertile impacts on plant growth. In field conditions, the bacterial inoculant must show competitiveness and withstand certain environmental stresses while retaining specific prolific traits. The microbiological activity in the soil should be measured using certain soil parameters, such as the available proportion of nitrogen, phosphorus, potassium, the content of organic carbon, and the determination of dehydrogenase activities. All treatments containing bacterial inoculants showed a pattern of reduced soil pH compared to no bacterial treatment (**Table 8**). The reduced soil pH may be due to the secretion of organic acids by ZSB (Fasim et al., 2002; Upadhayay et al., 2018, 2019; Kushwaha et al., 2020), and this phenomenon ultimately improves the availability of Zn in the soil (Saravanan et al., 2004; Upadhayay et al., 2022). The treatment containing BMRR126 with ZnO showed the highest organic carbon content (1.18%) in the *Katchar* region (**Table 8**). Since chemical-based fertilizers cannot increase soil organic matter, microbial inoculants improve soil organic carbon by promoting the mineralization of soil organic matter. Furthermore, Shahdi Kumleh (2020) illustrated the elevated soil organic carbon levels (1.79%) in response to bacterial inoculation in a clover rice cultivation system. Overall, a bacterial consortium with Zn supplementation, i.e., T9, showed maximum values of available nitrogen and phosphorus in the soil of both these regions (**Table 8**). BMRR126 and consortium in

TABLE 9 | Loading of coefficients of percentages of different variables of selected agronomical parameters for the first two principal components.

Variable	Principal components for the *Terai* region		Principal components for the *Katchar* region	
	PC 1	PC 2	PC 1	PC 2
Plant height	0.95826	0.023864	0.87717	0.27943
No. of tillers per hill	0.89968	0.19636	0.88837	0.029895
Dry matter per hill	0.94055	−0.25078	0.9884	−0.00893
Effective tillers	0.94076	0.3051	0.94802	−0.0143
Panicle length	0.9782	0.030622	0.98501	−0.04504
No. of grain/panicle	0.99121	−0.00974	0.96147	0.02044
1000 grain weight	0.96764	0.18626	0.92082	−0.16241
Grain yield	0.93552	−0.00529	0.94412	0.084063
Straw yield	0.74778	−0.65762	0.8781	−0.05142
Biological yield	0.87994	−0.43816	0.92305	−0.02079
Harvest Index	0.11875	0.94506	0.14513	0.97238
Zinc in grain	0.88373	0.36075	0.87716	−0.26355
% of Variance	78.14	15.65	79.01	9.44
Eigen value	9.37	1.87	9.48	1.13

TABLE 10 | Loading of coefficients of percentages of different variables of selected soil-related parameters for the first two principal components.

Variable	Principal components for the *Terai* region		Principal components for the *Katchar* region	
	PC 1	PC 2	PC 1	PC 2
Organic carbon (%)	0.95681	0.12827	0.71379	0.48229
Nitrogen	0.86659	0.48289	0.97315	−0.10445
Phosphorus (kg/ha)	0.94897	0.068391	0.98927	−0.02397
Potassium (kg/ha)	0.97747	−0.1469	0.73391	0.43436
Available Zinc in soil (mg/kg)	0.93825	−0.20242	0.90994	−0.30181
Dehydrogenase activity	0.91894	−0.29664	0.90377	−0.29104
% of Variance	87.45	6.74	76.97	10.14
Eigen value	5.24	0.40	4.61	0.60

combination with ZnO depicted the highest level of available potassium in the soil of *Terai* region (158.59 kg/ha) and *Katchar* region (226.35 kg/ha), respectively (**Table 8**). The increased dehydrogenase activity in all bacterial inoculated treatments reflects the splendid microbial activity in the soil system. A recent report by Kumawat et al. (2022) examined the nutrients and enzymatic activities in the soil and extrapolated the increased dehydrogenase activity (32.66 μg triphenylformazan g^{-1} h^{-1}) under the treatment of *Bradyrhizobium* sp., LSBR-3 and *Pseudomonas oryzihabitans* L compared to the control treatment. Microorganisms that produce organic acids facilitate the solubilization of bound phosphorus and potassium in the soil, thereby increasing the levels of these nutrients in the soil (Alori et al., 2017; Tian et al., 2021). Our study is justifiable with the previous studies in which bacterial treatments improved soil health by showing significant levels of organic carbon, nitrogen, phosphorus, and potassium (Adak et al., 2014; Reyes-Castillo et al., 2019).

Finally, we rationalize our study and present its uniqueness from other studies based on the following aspects:(i) EDX spectrum and contact angle-based analysis were new techniques used to assert the Zn-solubilization potential of bacteria isolated from rhizospheric soil of underutilized crop, i.e., barnyard millet; (ii) decoding the effects of ZSB with low-cost ZnO source input on multiple agronomic and soil parameters at two different sites.

Overall, our study showed that the agro parameters of rice crops were improved by the bacterial treatment together with the ZnO application in the soil. Similarly, bacterial inoculant in combination with soil zinc (ZnO) application increased the Zn content of grain (**Figure 4A**) in both agro-climatically different regions and proved to be a sustainable strategy for bacterial assisted grain biofortification. However, the application of $ZnSO_4$ is common as zinc fertilizer and is an important part of agronomic Zn biofortification (Xu et al., 2021). The cost of ZnO is relatively lower compared to Zn sulfate; hence the present study recommends using ZnO as a Zn supplement with ZSB to solve the purpose of Zn malnutrition in a very economically feasible way.

CONCLUSION

Zinc has a pivotal role in human health and also in crop production. The intensive cropping patterns, the rampant usage of chemical fertilizers, and a dearth of available soil zinc (Zn) results in inadequate consignation of the proper level of Zn in rice edibles and hence set forth the phenomenon of Zn malnutrition. Therefore, microbial-mediated biofortification can be a prolific tactic to counteract the issue of Zn malnutrition, as soil-dwelling ZSB acts as auxiliary natural factors to prop up plants for elevated Zn uptake from the soil system. The study was conducted to illustrate the ZnO solubilization ability of the two rhizospheric strains from the Himalayan underutilized crop, "barnyard millet." The FE-SEM-EDX-based analysis revealed a notable Zn solubilization behavior by the mobility of zinc from the ZnO residue for both isolates, i.e., BMRR126 and BMAR64. The isolates were prominent for various plant probiotic traits, such as P solubilization, production of siderophores, IAA, EPS, etc. (**Table 4**). Further, both ZSB strains were determined under the field conditions at two different sites (*Terai* region and *Katchar* region) and demonstrated their auspicious effects in terms of showing maximum growth-yield related characteristics of paddy. The bacterial consortium for the *Terai* region and a bacterial inoculant (BMRR126) for the *Katchar* region with ZnO supplementation exhibited a 1.58- and 1.72-fold increase in Zn levels of the rice grain, respectively, compared to the control (**Figure 4A**). The improved soil quality was also evident with all treatments containing bacterial inoculants (**Table 8**). By carefully monitoring all parameters, this study proposes the use of ZSB inoculants with an economically feasible Zn source, specifically ZnO, to achieve the benefits of the overall plant productivity and the benefits of Zn biofortification. The outcomes of the current investigation motivate the authors to further explore the bacterial potentiality under various agro-climatic conditions to

assess the agronomic and zinc biofortification benefits of multiple staple food crops.

DATA AVAILABILITY STATEMENT

The datasets presented in this study can be found in online repositories. The names of the repository/repositories andw accession number(s) can be found in the article/**Supplementary Material**.

AUTHOR CONTRIBUTIONS

VU wrote the original draft preparation. AVS did the conceptualization, performed the methodology and inputs for framing of manuscript, and supervised the data. AK and JS edited and reviewed the manuscript. NP validated the data. AR provided technical assistance in SEM-EDX and contact angle analysis. All authors contributed to the article and approved the submitted version.

ACKNOWLEDGMENTS

The authors gratefully acknowledge (a) the Department of Microbiology, College of Basic Sciences and Humanities, Govind Ballabh Pant University of Agriculture and Technology, Pantnagar, India, for accomplishing this research, and (b) ACMS, IIT, Kanpur for the SEM-EDX analysis.

SUPPLEMENTARY MATERIAL

The Supplementary Material for this article can be found online at: https://www.frontiersin.org/articles/10.3389/fmicb.2022.852192/full#supplementary-material

REFERENCES

Adak, T., Singha, A., Kumar, K., Shukla, S. K., Singh, A., and Kumar Singh, V. (2014). Soil organic carbon, dehydrogenase activity, nutrient availability and leaf nutrient content as affected by organic and inorganic source of nutrient in mango orchard soil. *J. Soil Sci. Plant Nutr.* 14, 394–406. doi: 10.4067/s0718-95162014005000031

Alexander, M. (1997). *Introduction to Soil Microbiology*. New York: John Wiley and Sons.

Alloway, B. J. (2009). Soil factors associated with zinc deficiency in crops and humans. *Environ. Geochem. Health* 31, 537–548. doi: 10.1007/s10653-009-9255-4

Alori, E. T., Glick, B. R., and Babalola, O. O. (2017). Microbial phosphorus solubilization and its potential for use in sustainable agriculture. *Front. Microbiol.* 8:971. doi: 10.3389/fmicb.2017.00971

Backer, R., Rokem, J. S., Ilangumaran, G., Lamont, J., Praslickova, D., Ricci, E., et al. (2018). Plant growth-promoting rhizobacteria: context, mechanisms of action, and roadmap to commercialization of biostimulants for sustainable agriculture. *Front. Plant Sci.* 9:1473. doi: 10.3389/fpls.2018.01473

Bashir, S., Basit, A., Abbas, R. N., Naeem, S., Bashir, S., Ahmed, N., et al. (2021). Combined application of zinc-lysine chelate and zinc-solubilizing bacteria improves yield and grain biofortification of maize (*Zea mays* L.). *PLoS One* 16:e0254647. doi: 10.1371/journal.pone.0254647

Batool, S., Asghar, H. N., Shehzad, M. A., Yasin, S., Sohaib, M., Nawaz, F., et al. (2021). Zinc-solubilizing bacteria-mediated enzymatic and physiological regulations confer zinc biofortification in chickpea (*Cicer arietinum* L.). *J. Soil Sci. Plant Nutr.* 21, 2456–2471. doi: 10.1007/s42729-021-00537-6

Bazzicalupo, M., and Fani, R. (1995). "The use of RAPD for generating specific DNA probes for microorganisms," in *Methods In Molecular Biology: Species diagnostics protocols: PCR and other Nucleic Acid Methods*, ed. J. P. Clapp (Totowa: Humana Press Inc.), 155–175. doi: 10.1385/0-89603-323-6:155

Bhatt, K., and Maheshwari, D. K. (2020). Zinc solubilizing bacteria (*Bacillus megaterium*) with multifarious plant growth promoting activities alleviates growth in *Capsicum annuum* L. *3 Biotech.* 10:36. doi: 10.1007/s13205-019-2033-9

Bhattacharjee, R. B., Jourand, P., Chaintreuil, C., Dreyfus, B., Singh, A., and Mukhopadhyay, S. N. (2012). Indole acetic acid and ACC deaminase-producing *Rhizobium leguminosarum* bv. *trifolii* SN10 promote rice growth, and in the process undergo colonization and chemotaxis. *Biol. Fertil. Soils* 48, 173–182. doi: 10.1007/s00374-011-0614-9

Bower, C. A., and Wilcox, L. V. (1965). "Soluble Salts," in *Methods of Soil Analysis*, eds C. A. Black, et al. (Madison: American Society of Agronomy), 933–940.

Cakmak, I., and Kutman, U. B. (2018). Agronomic biofortification of cereals with zinc: a review. *Eur. J. Soil Sci.* 69, 172–180. doi: 10.1111/ejss.12437

Cappuccino, J. C., and Sherman, N. (1992). *Microbiology: A Laboratory Manual*, third Edn. New York: Benjamin/Cumming Pub. Co.

Casida, L. E. Jr, Klein, D. A., and Santoro, T. (1964). Soil dehydrogenase activity. *Soil Sci.* 98, 371–376. doi: 10.1097/00010694-196412000-00004

Chávez-Dulanto, P. N., Thiry, A. A. A., Glorio-Paulet, P., Vögler, O., and Carvalho, F. P. (2021). Increasing the impact of science and technology to provide more people with healthier and safer food. *Food Energy Secur.* 10:e259. doi: 10.1002/fes3.259

Costerousse, B., Schönholzer-Mauclaire, L., Frossard, E., and Thonar, C. (2017). Identification of heterotrophic zinc mobilization processes among bacterial strains isolated from wheat rhizosphere (*Triticum aestivum* L.). *Appl. Environ. Microbiol.* 84, e1715–e1717. doi: 10.1128/AEM.01715-17

Das, P., Adak, S., and Lahiri Majumder, A. (2020). Genetic Manipulation for Improved Nutritional Quality in Rice. *Front. Genet.* 11:776. doi: 10.3389/fgene.2020.00776

Delvasto, P., Ballester, A., Muñoz, J. A., González, F., Blázquez, M. L., Igual, J. M., et al. (2009). Mobilization of phosphorus from iron ore by the bacterium *Burkholderia caribensis* FeGL03. *Miner. Eng.* 22, 1–9. doi: 10.1016/j.mineng.2008.03.001

Desai, S., Kumar, P., Sultana, U., Pinisetty, S., Hassan, M., Ahmed, S. K., et al. (2012). Potential microbial candidate strains for management of nutrient requirements of crops. *Afr. J. Microbiol. Res.* 6, 3924–3931. doi: 10.5897/ajmr12.224

Doni, F., Suhaimi, N. S. M., Mispan, M. S., Fathurrahman, F., Marzuki, B. M., Kusmoro, J., et al. (2022). Microbial contributions for rice production: from conventional crop management to the use of "omics" technologies. *Int. J. Mol. Sci.* 23:737. doi: 10.3390/ijms23020737

Eliazer Nelson, A. R. L., Ravichandran, K., and Antony, U. (2019). The impact of the Green Revolution on indigenous crops of India. *J. Ethn. Foods* 6:8. doi: 10.1186/s42779-019-0011-9

Estefan, G., Sommer, R., and Ryan, J. (2013). *Methods of Soil, Plant, and Water Analysis: A manual for the West Asia and North*. Beirut: International Center for Agricultural Research in the Dry Areas (ICARDA).

Fasim, F., Ahmed, N., Parsons, R., and Gadd, G. M. (2002). Solubilization of zinc salts by a bacterium isolated from the air environment of a tannery. *FEMS Microbiol. Lett.* 213, 1–6. doi: 10.1111/j.1574-6968.2002.tb11277.x

Gandhi, A., and Muralidharan, G. (2016). Assessment of zinc solubilizing potentiality of *Acinetobacter* sp. isolated from rice rhizosphere. *Eur. J. Soil. Biol.* 76, 1–8. doi: 10.1016/j.ejsobi.2016.06.006

Hammer, Ø, Harper, D. A., and Ryan, P. D. (2001). PAST: paleontological statistics software package for education and data analysis. *Palaeontol. Electron.* 4, 1–9.

Hanway, J. J., and Heidel, H. (1952). Soil analysis methods as used in Iowa state college soil testing laboratory. *Iowa State Coll. Agric. Bull.* 57, 1–31.

Hayat, R., Ali, S., Amara, U., Khalid, R., and Ahmed, I. (2010). Soil beneficial bacteria and their role in plant growth promotion: A review. *Ann. Microbiol.* 60, 579–598. doi: 10.1007/s13213-010-0117-1

Hussain, A., Zahir, Z. A., Asghar, H. N., Ahmad, M., Jamil, M., Naveed, M., et al. (2018). "Zinc solubilizing bacteria for zinc biofortification in cereals: a step toward sustainable nutritional security," in *Role of Rhizospheric Microbes in Soil*, ed. V. Meena (Singapore: Springer), 203–227. doi: 10.1007/978-981-13-0044-8_7

Idayu Othman, N. M., Othman, R., Saud, H. M., and Megat Wahab, P. E. (2017). Effects of root colonization by zinc-solubilizing bacteria on rice plant (*Oryza sativa* MR219) growth. *Agric. Nat. Resour*. 51, 532–537. doi: 10.1016/j.anres.2018.05.004

Jackson, M. L. (1967). *Soil Chemical Analysis*. New Delhi: Prentice-Hall of India Pvt. Ltd.

Kamran, S., Shahid, I., Baig, D. N., Rizwan, M., Malik, K. A., and Mehnaz, S. (2017). Contribution of zinc solubilizing bacteria in growth promotion and zinc content of wheat. *Front. Microbiol*. 8:2593. doi: 10.3389/fmicb.2017.02593

Khan, A., Singh, J., Upadhayay, V. K., Singh, A. V., and Shah, S. (2019). "Microbial biofortification: A green technology through plant growth promoting microorganisms," in *Sustainable Green Technologies for Environmental Management*, eds S. Shah, V. Venkatramanan, and R. Prasad (Singapore: Springer), 255–259. doi: 10.1007/978-981-13-2772-8_13

Kiran, A., Wakeel, A., Mahmood, K., Mubaraka, R., Hafsa, and Haefele, S. M. (2022). Biofortification of staple crops to alleviate human malnutrition: contributions and potential in developing countries. *Agronomy* 12:452. doi: 10.3390/agronomy12020452

Krithika, S., and Balachandar, D. (2016). Expression of zinc transporter genes in rice as influenced by zinc-solubilizing *Enterobacter cloacae* strain ZSB14. *Front. Plant Sci.* 7:446. doi: 10.3389/fpls.2016.00446

Kumawat, K. C., Singh, I., Nagpal, S., Sharma, P., Gupta, R. K., and Sirari, A. (2022). Co-inoculation of indigenous *Pseudomonas oryzihabitans* and *Bradyrhizobium* sp. modulates the growth, symbiotic efficacy, nutrient acquisition, and grain yield of soybean. *Pedosphere* 32, 438–451. doi: 10.1016/s1002-0160(21)60085-1

Kushwaha, P., Kashyap, P. L., Pandiyan, K., and Bhardwaj, A. K. (2020). "Zinc-solubilizing microbes for sustainable crop production: Current understanding, opportunities, and challenges," in *Phytobiomes: Current Insights and Future Vistas*, (Singapore: Springer Singapore), 281–298. doi: 10.1007/978-981-15-3151-4_11

Kushwaha, P., Srivastava, R., Pandiyan, K., Singh, A., Chakdar, H., Kashyap, P. L., et al. (2021). Enhancement in Plant Growth and Zinc Biofortification of Chickpea (*Cicer arietinum* L.) by *Bacillus altitudinis*. *J. Soil Sci. Plant Nutr*. 21, 922–935. doi: 10.1007/s42729-021-00411-5

Li, W. C., Ye, Z. H., and Wong, M. H. (2010). Metal mobilization and production of short-chain organic acids by rhizosphere bacteria associated with a Cd/Zn hyperaccumulating plant, *Sedum alfredii*. *Plant Soil* 326, 453–467. doi: 10.1007/s11104-009-0025-y

Lindsay, W. L., and Norvell, W. A. (1978). Development of a DTPA Soil Test for Zinc, Iron, Manganese, and Copper. *Soil Sci. Soc. Am. J*. 42, 421–428. doi: 10.2136/sssaj1978.03615995004200030009x

Liu, D. Y., Liu, Y. M., Zhang, W., Chen, X. P., and Zou, C. Q. (2019). Zinc uptake, translocation, and remobilization in winter wheat as affected by soil application of zn fertilizer. *Front. Plant Sci.* 10:426. doi: 10.3389/fpls.2019.00426

Liu, Y. M., Liu, D. Y., Zhang, W., Chen, X. X., Zhao, Q. Y., Chen, X. P., et al. (2020). Health risk assessment of heavy metals (Zn, Cu, Cd, Pb, As and Cr) in wheat grain receiving repeated Zn fertilizers. *Environ. Pollut*. 257:113581. doi: 10.1016/j.envpol.2019.113581

Malik, K. A., and Maqbool, A. (2020). Transgenic Crops for Biofortification. *Front. Sustain. Food Syst*. 4:571402. doi: 10.3389/fsufs.2020.571402

Mhatre, M., Srinivas, L., and Ganapathi, T. R. (2011). Enhanced iron and zinc accumulation in genetically engineered pineapple plants using soybean ferritin gene. *Biol. Trace Elem. Res*. 144, 1219–1228. doi: 10.1007/s12011-011-9092-z

Moreno-Lora, A., and Delgado, A. (2020). Factors determining Zn availability and uptake by plants in soils developed under Mediterranean climate. *Geoderma* 376:114509. doi: 10.1016/j.geoderma.2020.114509

Mumtaz, M. Z., Ahmad, M., Jamil, M., and Hussain, T. (2017). Zinc solubilizing *Bacillus* spp. potential candidates for biofortification in maize. *Microbiol. Res.* 202, 51–60. doi: 10.1016/j.micres.2017.06.001

Mumtaz, M. Z., Barry, K. M., Baker, A. L., Nichols, D. S., Ahmad, M., Zahir, Z. A., et al. (2019). Production of lactic and acetic acids by *Bacillus* sp. ZM20 and *Bacillus cereus* following exposure to zinc oxide: A possible mechanism for Zn solubilization. *Rhizosphere* 12:100170. doi: 10.1016/j.rhisph.2019.100170

Naeem, A., Aslam, M., Ahmad, M., Asif, M., Yazici, M. A., Cakmak, I., et al. (2022). Biofortification of diverse Basmati rice cultivars with iodine, selenium, and zinc by individual and cocktail spray of micronutrients. *Agronomy* 12:49. doi: 10.3390/agronomy12010049

Natasha, N., Shahid, M., Bibi, I., Iqbal, J., Khalid, S., Murtaza, B., et al. (2022). Zinc in soil-plant-human system: A data-analysis review. *Sci. Total Environ*. 808:152024. doi: 10.1016/j.scitotenv.2021.152024

Nautiyal, C. S. (1999). An efficient microbiological growth medium for screening phosphate solubilizing microorganisms. *FEMS Microbiol. Lett*. 170, 265–270. doi: 10.1016/S0378-1097(98)00555-2

Nepomuceno, R. A., Brown, C. B. P., Gargarino, A. M., Pedro, M. S., and Brown, M. B. (2020). Growth Enhancement of Rice (*Oryza sativa* L.) by Zinc-Solubilizing Bacteria Isolated from Vesicular-Arbuscular Mycorrhizal Root Inoculant (VAMRI). *Philipp. J. Crop Sci*. 45, 34–40.

Olsen, S. R., Cole, C. V., Watandbe, F., and Dean, L. (1954). *Estimation of Available Phosphorus in Soil by Extraction with sodium Bicarbonate. USDA Circular 939*. Washington D.C: U.S. Government Printing Office.

Patten, C. L., and Glick, B. R. (2002). Role of *Pseudomonas putida* indole acetic acid in development of the host plant root system. *Appl. Environ. Microbiol*. 68, 3795–3801. doi: 10.1128/aem.68.8.3795-3801.2002

Poblaciones, M. J., and Rengel, Z. (2017). Combined foliar selenium and zinc biofortification in field pea (*Pisum sativum*): accumulation and bioavailability in raw and cooked grains. *Crop Pasture Sci*. 68, 265–271. doi: 10.1071/CP17082

Prasad, A. A., and Babu, S. (2017). Compatibility of *Azospirillum brasilense* and *Pseudomonas fluorescens* in growth promotion of groundnut (*Arachis hypogea* L.). *An. Acad. Bras. Cienc.* 89, 1027–1040. doi: 10.1590/0001-3765201720160617

Prathap, S., Thiyageshwari, S., Krishnamoorthy, R., Prabhaharan, J., Vimalan, B., Gopal, N. O., et al. (2022). Role of zinc solubilizing bacteria in enhancing growth and nutrient accumulation in rice plants (*Oryza sativa*) grown on zinc (Zn) deficient submerged soil. *J. Soil Sci. Plant Nutr*. 22, 971–984. doi: 10.1007/s42729-021-00706-7

Ramesh, A., Sharma, S. K., Sharma, M. P., Yadav, N., and Joshi, O. P. (2014). Inoculation of zinc solubilizing *Bacillus aryabhattai* strains for improved growth, mobilization and biofortification of zinc in soybean and wheat cultivated in Vertisols of central India. *Appl. Soil Ecol*. 73, 87–96. doi: 10.1016/j.apsoil.2013.08.009

Rana, A., Joshi, M., Prasanna, R., Shivay, Y. S., and Nain, L. (2012). Biofortification of wheat through inoculation of plant growth promoting rhizobacteria and cyanobacteria. *Eur. J. Soil Biol*. 50, 118–126. doi: 10.1016/j.ejsobi.2012.01.005

Rattan, R. K., and Shukla, L. M. (1991). Influence of different zinc carriers on the utilization of micronutrients by rice. *J. Indian Soc. Soil Sci*. 39, 808–810.

Rehman, H. U., Aziz, T., Farooq, M., Wakeel, A., and Rengel, Z. (2012). Zinc nutrition in rice production systems: A review. *Plant Soil* 361, 203–226. doi: 10.1007/s11104-012-1346-9

Reyes-Castillo, A., Gerding, M., Oyarzúa, P., Zagal, E., Gerding, J., and Fischer, S. (2019). Plant growth-promoting rhizobacteria able to improve NPK availability: selection, identification and effects on tomato growth. *Chil. J. Agric. Res.* 79, 473–485. doi: 10.4067/s0718-58392019000300473

Rezaeiniko, B., Enayatizamir, N., and Norouzi Masir, M. (2022). Changes in soil zinc chemical fractions and improvements in wheat grain quality in response to zinc solubilizing bacteria. *Commun. Soil Sci. Plant Anal*. 53, 622–635. doi: 10.1080/00103624.2021.2017962

Roshani, Khan, A., Singh, A. V., Upadhayay, V. U., and Prasad, B. (2020). Development of potential microbial consortia and their assessment on wheat (*Triticum aestivum*) seed germination. *Environ. Ecol*. 38, 6–16.

Sambasivam, V. P., Thiyagarajan, G., Kabir, G., Ali, S. M., Khan, S. A. R., and Yu, Z. (2020). Selection of winter season crop pattern for environmental-friendly agricultural practices in India. *Sustainability* 12:4562. doi: 10.3390/su12114562

Sanjeeva Rao, D., Neeraja, C. N., Madhu Babu, P., Nirmala, B., Suman, K., Rao, L. V. S., et al. (2020). Zinc biofortified rice varieties: challenges, possibilities, and progress in India. *Front. Nutr*. 7:26. doi: 10.3389/fnut.2020.00026

Sarathambal, C., Thangaraju, M., Paulraj, C., and Gomathy, M. (2010). Assessing the Zinc solubilization ability of *Gluconacetobacter diazotrophicus* in maize

rhizosphere using labelled (65)Zn compounds. *Indian J. Microbiol.* 50, 103–109. doi: 10.1007/s12088-010-0066-1

Saravanan, V. S., Subramoniam, S. R., and Raj, S. A. (2004). Assessing in vitro solubilization potential of different zinc solubilizing bacterial (ZSB) isolates. *Braz. J. Microbiol*. 35, 121–125. doi: 10.1590/S1517-83822004000100020

Schwyn, B., and Neilands, J. B. (1987). Universal chemical assay for the detection and determination of siderophores. *Anal. Biochem*. 160, 47–56. doi: 10.1016/0003-2697(87)90612-9

Senthilkumar, K., Sillo, F. S., Rodenburg, J., Dimkpa, C., Saito, K., Dieng, I., et al. (2021). Rice yield and economic response to micronutrient application in Tanzania. *Field Crops Res*. 270:108201. doi: 10.1016/j.fcr.2021.108201

Shahdi Kumleh, A. (2020). Effect of plant growth promoting rhizobacteria (PGPRs) on soil chemical properties in a clover-rice cropping system. *J. Water Soil Res. Conserv*. 9, 89–104. Available online at: https://www.sid.ir/en/journal/ViewPaper.aspx?id=862392

Shaikh, S., and Saraf, M. (2017). Biofortification of *Triticum aestivum* through the inoculation of zinc solubilizing plant growth promoting rhizobacteria in field experiment. *Biocatal. Agric. Biotechnol*. 9, 120–126. doi: 10.1016/j.bcab.2016.12.008

Shakeel, M., Rais, A., Hassan, M. N., and Hafeez, F. Y. (2015). Root associated *Bacillus* sp. improves growth, yield and zinc translocation for basmati rice (*Oryza sativa*) varieties. *Front. Microbiol*. 6:1286. doi: 10.3389/fmicb.2015.01286

Sharma, A., Patni, B., Shankhdhar, D., and Shankhdhar, S. C. (2013). Zinc - An Indispensable Micronutrient. *Physiol. Mol. Biol. Plants* 19, 11–20. doi: 10.1007/s12298-012-0139-1

Sharma, A., Shankhdhar, D., Sharma, A., and Shankhdhar, S. C. (2014). Growth promotion of the rice genotypes by pgprs isolated from rice rhizosphere. *J. Soil Sci. Plant Nutr*. 14, 505–517. doi: 10.4067/s0718-95162014005000040

Sharma, S. K., Sharma, M. P., Ramesh, A., and Joshi, O. P. (2012). Characterization of zinc-solubilizing *Bacillus* isolates and their potential to influence zinc assimilation in soybean seeds. *J. Microbiol. Biotechnol*. 22, 352–359. doi: 10.4014/jmb.1106.05063

Siddikee, M. A., Glick, B. R., Chauhan, P. S., Yim, W. J., and Sa, T. (2011). Enhancement of growth and salt tolerance of red pepper seedlings (*Capsicum annuum* L.) by regulating stress ethylene synthesis with halotolerant bacteria containing 1-aminocyclopropane-1-carboxylic acid deaminase activity. *Plant Physiol. Biochem*. 49, 427–434. doi: 10.1016/j.plaphy.2011.01.015

Singh, A. V., Chandra, R., and Goel, R. (2013). Phosphate solubilization by *Chryseobacterium* sp. and their combined effect with N and P fertilizers on plant growth promotion. *Arch. Agron. Soil Sci*. 59, 641–651. doi: 10.1080/03650340.2012.664767

Singh, D., and Prasanna, R. (2020). Potential of microbes in the biofortification of Zn and Fe in dietary food grains. A review. *Agron. Sustain. Dev*. 40:15. doi: 10.1007/s13593-020-00619-2

Singh, M. K., and Prasad, S. K. (2014). Agronomic aspects of zinc biofortification in rice (*Oryza sativa* l.). *Proc. Natl. Acad. Sci. India Sect. B Biol.* Sci. 84, 613–623. doi: 10.1007/s40011-014-0329-4

Subbiah, B. V., and Asija, G. L. (1956). A rapid procedure for estimation of available nitrogen in soils. *Curr. Sci*. 25, 259–260.

Suseelendra, D. (2012). Potential microbial candidate strains for management of nutrient requirements of crops. *Afr. J. Microbiol. Res*. 6:17. doi: 10.5897/ajmr12.224

Swamy, B. P. M., Rahman, M. A., Inabangan-Asilo, M. A., Amparado, A., Manito, C., Chadha-Mohanty, P., et al. (2016). Advances in breeding for high grain Zinc in Rice. *Rice* 9:49. doi: 10.1186/s12284-016-0122-5

Tamura, K., Peterson, D., Peterson, N., Stecher, G., Nei, M., and Kumar, S. (2011). MEGA5: molecular evolutionary genetics analysis using maximum likelihood, evolutionary distance, and maximum parsimony methods. *Mol. Biol. Evol*. 28, 2731–2739. doi: 10.1093/molbev/msr121

Tariq, M., Hameed, S., Malik, K. A., and Hafeez, F. Y. (2007). Plant root associated bacteria for zinc mobilization in rice. *Pak. J. Bot*. 39, 245–253.

Tian, J., Ge, F., Zhang, D., Deng, S., and Liu, X. (2021). Roles of phosphate solubilizing microorganisms from managing soil phosphorus deficiency to mediating biogeochemical P cycle. *Biology* 10:158. doi: 10.3390/biology10020158

Trân Van, V., Berge, O., Ngô Kê, S., Balandreau, J., and Heulin, T. (2000). Repeated beneficial effects of rice inoculation with a strain of *Burkholderia vietnamiensis* on early and late yield component in low fertility sulphate acid soils of Vietnam. *Plant Soil* 21, 273–284. doi: 10.1023/a:1014986916913

Upadhayay, V. K., Singh, A. V., and Khan, A. (2022). Cross talk between zinc-solubilizing bacteria and plants: A short tale of bacterial-assisted zinc biofortification. *Front. Soil Sci*. 1:788170. doi: 10.3389/fsoil.2021.788170

Upadhayay, V. K., Singh, A. V., Khan, A., and Pareek, N. (2021). Influence of zinc solubilizing bacterial co-inoculation with zinc oxide supplement on rice plant growth and Zn uptake. *Pharm. Innovat*. 10, 113–116.

Upadhayay, V. K., Singh, A. V., and Pareek, N. (2018). An insight in decoding the multifarious and splendid role of microorganisms in crop biofortification. *Int. J. Curr. Microbiol. Appl. Sci*. 7, 2407–2418. doi: 10.20546/ijcmas.2018.706.286

Upadhayay, V. K., Singh, J., Khan, A., Lohani, S., and Singh, A. V. (2019). "Mycorrhizal mediated micronutrients transportation in food based plants: A biofortification strategy," in *Mycorrhizosphere and Pedogenesis*, eds A. Varma and D. Choudhary (Singapore: Springer), 1–24. doi: 10.1007/978-981-13-6480-8_1

Vaid, S. K., Kumar, B., Sharma, A., Shukla, A. K., and Srivastava, P. C. (2014). Effect of zinc solubilizing bacteria on growth promotion and zinc nutrition of rice. *Soil. Sci. Plant Nutr*. 14, 889–910. doi: 10.4067/s0718-95162014005000071

Val-Torregrosa, B., Bundó, M., and San Segundo, B. (2021). Crosstalk between nutrient signalling pathways and immune responses in rice. *Agriculture* 11:747. doi: 10.3390/agriculture11080747

Verma, M., Singh, A., Dwivedi, D. H., and Arora, N. K. (2020). Zinc and phosphate solubilizing *Rhizobium radiobacter* (LB2) for enhancing quality and yield of loose leaf lettuce in saline soil. *J. Environ. Sustain*. 3, 209–218. doi: 10.1007/s42398-020-00110-4

Vidyashree, D. N., Muthuraju, R., and Panneerselvam, P. (2018a). Evaluation of zinc solubilizing bacterial (ZSB) strains on growth, yield and quality of tomato (*Lycopersicon esculentum*). *Int. J. Curr. Microbiol. App. Sci*. 7, 1493–1502. doi: 10.20546/ijcmas.2018.704.168

Vidyashree, D. N., Muthuraju, R., Panneerselvam, P., and Mitra, D. (2018b). Organic acids production by zinc solubilizing bacterial isolates. *Int. J. Curr. Microbiol. App. Sci*. 7, 626–633. doi: 10.20546/ijcmas.2018.710.070

Walkley, A. J., and Black, I. A. (1934). Estimation of soil organic carbon by the chromic acid titration method. *Soil Sci*. 37, 29–38. doi: 10.1097/00010694-193401000-00003

Wang, Y., Yang, X., Zhang, X., Dong, L., Zhang, J., Wei, Y., et al. (2014). Improved plant growth and Zn accumulation in grains of rice (*Oryza sativa* L.) by Inoculation of endophytic microbes Isolated from a Zn hyperaccumulator, *Sedum alfredii* H. *J. Agric. Food Chem*. 62, 1783–1791. doi: 10.1021/jf404152u

Wissuwa, M., Ismail, A. M., and Yanagihara, S. (2006). Effects of zinc deficiency on rice growth and genetic factors contributing to tolerance. *Plant Physiol*. 142, 731–741. doi: 10.1104/pp.106.085225

Wu, S. C., Luo, Y. M., Cheung, K. C., and Wong, M. H. (2006). Influence of bacteria on Pb and Zn speciation, mobility and bioavailability in soil: A laboratory study. *Environ. Pollut*. 144, 765–773. doi: 10.1016/j.envpol.2006.02.022

Xie, H., Pasternak, J. J., and Glick, B. R. (1996). Isolation and characterization of mutants of the plant growth-promoting Rhizobacterium *Pseudomonas putida* GR12-2 that overproduce indoleacetic acid. *Curr. Microbiol*. 32, 67–71. doi:10.1007/s002849900012

Xu, M., Liu, M., Si, L., Ma, Q., Sun, T., Wang, J., et al. (2021). Spraying high concentrations of chelated zinc enhances zinc biofortification in wheat grain. *J. Sci. Food Agric*. doi: 10.1002/jsfa.11705 [Epub online ahead of print].

Yu, S., Ali, J., Zhang, C., Li, Z., and Zhang, Q. (2020). Genomic breeding of green super rice varieties and their deployment in Asia and Africa. *Theor. Appl. Genet*. 133, 1427–1442. doi: 10.1007/s00122-019-03516-9

Zaheer, A., Malik, A., Sher, A., Mansoor Qaisrani, M., Mehmood, A., Ullah Khan, S., et al. (2019). Isolation, characterization, and effect of phosphate-zinc-solubilizing bacterial strains on chickpea (*Cicer arietinum* L.) growth. *Saudi J. Biol. Sci*. 26, 1061–1067. doi: 10.1016/j.sjbs.2019.04.004

Zaman, Q. Uz, Aslam, Z., Yaseen, M., Ihsan, M. Z., Khaliq, A., Fahad, S., et al. (2018). Zinc biofortification in rice: leveraging agriculture to moderate hidden hunger in developing countries. *Arch. Agron. Soil Sci*. 64, 147–161. doi: 10.1080/03650340.2017.1338343

Zeb, H., Hussain, A., Naveed, M., Ditta, A., Ahmad, S., Jamshaid, M. U., et al. (2018). Compost enriched with ZnO and Zn-solubilising bacteria improves

yield and Zn-fortification in flooded rice. *Ital. J. Agron.* 13, 10–316. doi: 10.4081/ija.2018.1295

Conflict of Interest: The authors declare that the research was conducted in the absence of any commercial or financial relationships that could be construed as a potential conflict of interest.

Publisher's Note: All claims expressed in this article are solely those of the authors and do not necessarily represent those of their affiliated organizations, or those of the publisher, the editors and the reviewers. Any product that may be evaluated in this article, or claim that may be made by its manufacturer, is not guaranteed or endorsed by the publisher.

frontiers | Frontiers in Microbiology

ORIGINAL RESEARCH
published: 19 May 2022
doi: 10.3389/fmicb.2022.886041

Cytokinin Production by *Azospirillum brasilense* Contributes to Increase in Growth, Yield, Antioxidant, and Physiological Systems of Wheat (*Triticum aestivum* L.)

Muhammad Saqlain Zaheer[1], Hafiz Haider Ali[2]*, Muhammad Arslan Iqbal[3], Kehinde O. Erinle[4], Talha Javed[5,6], Javaid Iqbal[7], Makhdoom Ibad Ullah Hashmi[8], Muhammad Zahid Mumtaz[9], Ehab A. A. Salama[10], Hazem M. Kalaji[11,12], Jacek Wróbel[13] and Eldessoky S. Dessoky[14]*

[1] Department of Agricultural Engineering, Khwaja Fareed University of Engineering and Information Technology, Rahim Yar Khan, Pakistan, [2] Sustainable Development Study Center (SDSC), Government College University, Lahore, Pakistan, [3] District Headquarter Hospital, Muzaffargarh, Pakistan, [4] School of Agriculture, Food and Wine, The University of Adelaide, Adelaide, SA, Australia, [5] College of Agriculture, Fujian Agriculture and Forestry University, Fuzhou, China, [6] Department of Agronomy, University of Agriculture, Faisalabad, Pakistan, [7] Department of Entomology, Muhammad Nawaz Shareef (MNU) University of Agriculture, Multan, Pakistan, [8] Department of Chemical Engineering, Khwaja Fareed University of Engineering and Information Technology, Rahim Yar Khan, Pakistan, [9] Institute of Molecular Biology and Biotechnology (IMBB), The University of Lahore, Lahore, Pakistan, [10] Agricultural Botany Department, Faculty of Agriculture Saba Basha, Alexandria University, Alexandria, Egypt, [11] Department of Plant Physiology, Institute of Biology, Warsaw University of Life Sciences SGGW, Warsaw, Poland, [12] Institute of Technology and Life Sciences - National Research Institute, Raszyn, Poland, [13] Department of Bioengineering, West Pomeranian University of Technology in Szczecin, Szczecin, Poland, [14] Department of Biology, College of Science, Taif University, Taif, Saudi Arabia

Plant growth-promoting rhizobacteria are known to associate with several cereal crops. The rhizobacterium exerts its function by synthesizing diverse arrays of phytohormones, such as cytokinin (Ck). However, it is difficult to determine the plant growth promotion when a bacterium produces many different kinds of phytohormones. Therefore, to assess the involvement of Ck in growth promotion and activation of antioxidant and physiological systems, we set up this experiment. Wheat seeds (*Triticum aestivum* L.) were inoculated with *Azospirillum brasilense* RA−17 (which produces zeatin type Ck) and RA−18 (which failed to produce Ck). Results showed that seed inoculation with RA−17 significantly improved growth and yield-related parameters compared with RA−18. The activity of enzymes, proline contents, and endogenous hormonal levels in wheat kernels were improved considerably with RA−17 than with RA−18. Strain RA−17 enhanced grain assimilation more than strain RA−18 resulting in a higher crop yield. These results suggest that microbial Ck production may be necessary for stimulating plant growth promotion and activating antioxidant and physiological systems in wheat.

Keywords: bacteria, cytokinin, hormones, rhizosphere, wheat

OPEN ACCESS

Edited by:
Maqshoof Ahmad, The Islamia University of Bahawalpur, Pakistan

Reviewed by:
Liziane Cristina Campos Brusamarello-Santos, Federal University of Paraná, Brazil
Ernesto Garcia-Pineda, Universidad Michoacana de San Nicolás de Hidalgo, Mexico

****Correspondence:***
Muhammad Saqlain Zaheer
msaqlainzaheer@gmail.com
Hafiz Haider Ali
haider3993@gmail.com

Specialty section:
This article was submitted to Terrestrial Microbiology, a section of the journal Frontiers in Microbiology

Received: *28 February 2022*
Accepted: *13 April 2022*
Published: *19 May 2022*

Citation:
Zaheer MS, Ali HH, Iqbal MA, Erinle KO, Javed T, Iqbal J, Hashmi MIU, Mumtaz MZ, Salama EAA, Kalaji HM, Wróbel J and Dessoky ES (2022) Cytokinin Production by Azospirillum brasilense Contributes to Increase in Growth, Yield, Antioxidant, and Physiological Systems of Wheat (Triticum aestivum L.). Front. Microbiol. 13:886041. doi: 10.3389/fmicb.2022.886041

INTRODUCTION

Rhizobacteria play a vital role in ecosystem services. The bacterial population around plant roots is more versatile in nutrients solubilization, transformation, and mobilization (Hussain et al., 2013; Sabir et al., 2013), thus increasing plant growth (Qureshi et al., 2012; Liu et al., 2019). It is carried out by synthesizing diverse arrays of plant hormones. such as auxin, cytokinin (Ck), gibberellin, abscisic acid (ABA), and indole-3-acetic acid (IAA) (Ahmed and Hasnain, 2020; Ortiz-Castro et al., 2020). Microbe-derived phytohormones influence plant growth parameters and have been well studied (Arshad and Frankenberger, 1991; Zafar et al., 2012; Farooq and Bano, 2013; Xu et al., 2018). Phytohormones improve the metabolic functions of plants, influence root exudation, alter gene expressions, cell division, xylem processes, root development, and different signaling processes (Campos et al., 2019; Mushtaq et al., 2019).

Cytokinins play a significant role in plant growth promotion in different mechanistic ways, such as cell division, chlorophyll accumulation, expansion of leaves, by delaying leaf senescence, and etioplasts conversion to the chloroplast (Angeli et al., 2001; Zafar et al., 2012; Zwack and Rashotte, 2013). Both plants and microorganisms produce Cks, which differ in types and activity (Akhtar et al., 2020). Cerný et al. (2010) noticed that the different kinds of proteins and phosphor-proteins are present in the chloroplast, a direct singling chain responsible for the CK actions in the chloroplast. Rhizobacterial inoculation with the seeds was independent of specific hormone signaling. For example, López-Bucio et al. (2007) reported that *Bacillus megaterium* inoculation enhanced biomass and stimulated the growth of roots in auxin mutant Arabidopsis by auxin and ethylene-independent signaling system. Ortíz-Castro et al. (2008) found reduced growth-promoting effects in Arabidopsis inoculation with *B. megaterium*. They suggested that crop growth stimulation by the microbe may require an intact Ck signaling pathway. Rice seedling inoculation with a Ck-mutant *Magnaporthe oryzae* did not show distinct growth and development features until an exogenous source of Ck was applied (Chanclud et al., 2016).

Wheat (*Triticum aestivum* L.) is a significant food source for human consumption. For decades, improving growth and increasing yield have been the major interest among wheat breeders (Sears, 1997; Zaheer et al., 2021b). It has been suggested that wheat production needs to be increased by an estimated 60% to meet market demand in the next 10 years (Zaheer et al., 2019a). Interactions between (Ck producing) rhizobacteria and wheat is crucial for promoting growth and increasing yield. Zaheer et al. (2019a) reported that Ck plays a vital role in improving wheat yield. Its production with the rhizobacteria strain can be more beneficial for the physiological processes of the wheat plant. The use of specific bacterial strains that can produce more Ck in the plant can benefit the wheat plant's internal metabolic and growth improvement processes. Little study is available for those rhizobacteria that can make Ck, so there is a need to investigate the Ck-producing bacteria and their effect on plant growth (Sarkar et al., 2018).

In this study, carried out in the field, wheat seeds were inoculated with a strain of Ck (zeatin)-producing bacteria, *Azospirillum brasilense*, and its effects on wheat growth, physiological and antioxidant systems were compared to inoculation with a Ck non-producing strain of the same bacteria. We hypothesize that Ck-producing bacteria, compared with non-producing bacteria, are more beneficial for wheat growth and yield improvement and upregulation of physiological and antioxidant systems.

MATERIALS AND METHODS

Bacterial Strains and Preparation of Wheat Seeds

Cytokinin producing (RA−17) and non-producing (RA−18) strains of *A. brasilense* were obtained from the soil lab of the Ayub Agricultural Research Institute, Faisalabad. Ck production was confirmed before being used for the experiments (**Figure 1**). Surface sterilized seed with ethanol (70%) and sodium hypochlorite of an approved wheat variety "Galaxy−2013" were used in the experiment. Seeds were inoculated with either the Ck producing or non-producing strain (10×10^8 CFU ml^{-1} obtained at exponential growth phase) following the procedure reported by Fukami et al. (2016).

Plant Growth Conditions

Field experiments were conducted in the semi-arid region of Bahawalpur from 2017 to 2018. The experimental plots size was 5×5 m. The soil was loamy, having 0.61% organic matter, 8.1 pH, 249 μS cm^{-1} electrical conductivity, 7.08 ppm available P, 112 ppm available K, and 34% saturation percentage. The Galaxy−2013 wheat variety, released by Punjab Seed Corporation in 2013 and mostly grown in the area of Bahawalpur, was used for the experiment.

To compare the effects of Ck-producing strains with non-producing strains on wheat growth and physiological parameters, three treatments, uninoculated control (T_0), inoculation with Ck producing (T_1), and non-Ck producing (T_2) *A. brasilense*, were arranged in Randomized Complete Block Design (RCBD). Wheat seeds (according to the treatments) were sown on 15 November 2017. According to the recommendations, recommended fertilizers (120-60-60 NPK kg/ha) and four irrigation schemes (3 Acr inches) were applied. Briefly, 3 feet was the inter-plot distance in all replications.

Measured Parameters

Physiological parameters were determined using 20 plants from each plot with three replications and an average. Different growth and yield-related parameters were measured by standard procedures (Bremner, 1965; Tkachuk, 1966; Ullah et al., 2018). Crop growth rate (CGR) and relative growth rate (RGR) were calculated by the formula described by Karimi and Siddique (1991), and net assimilation rate (NAR) was obtained by following the procedure of Vernon and Allison (1963). The leaf area index (LAI) was noticed using the digital leaf area meter, and the chlorophyll meter was used to detect the chlorophyll content. An infrared gas analyzer (IRGA) was used to notice the stomatal conductance and photosynthetic rate. Epicuticular wax was determined by following the approach described by

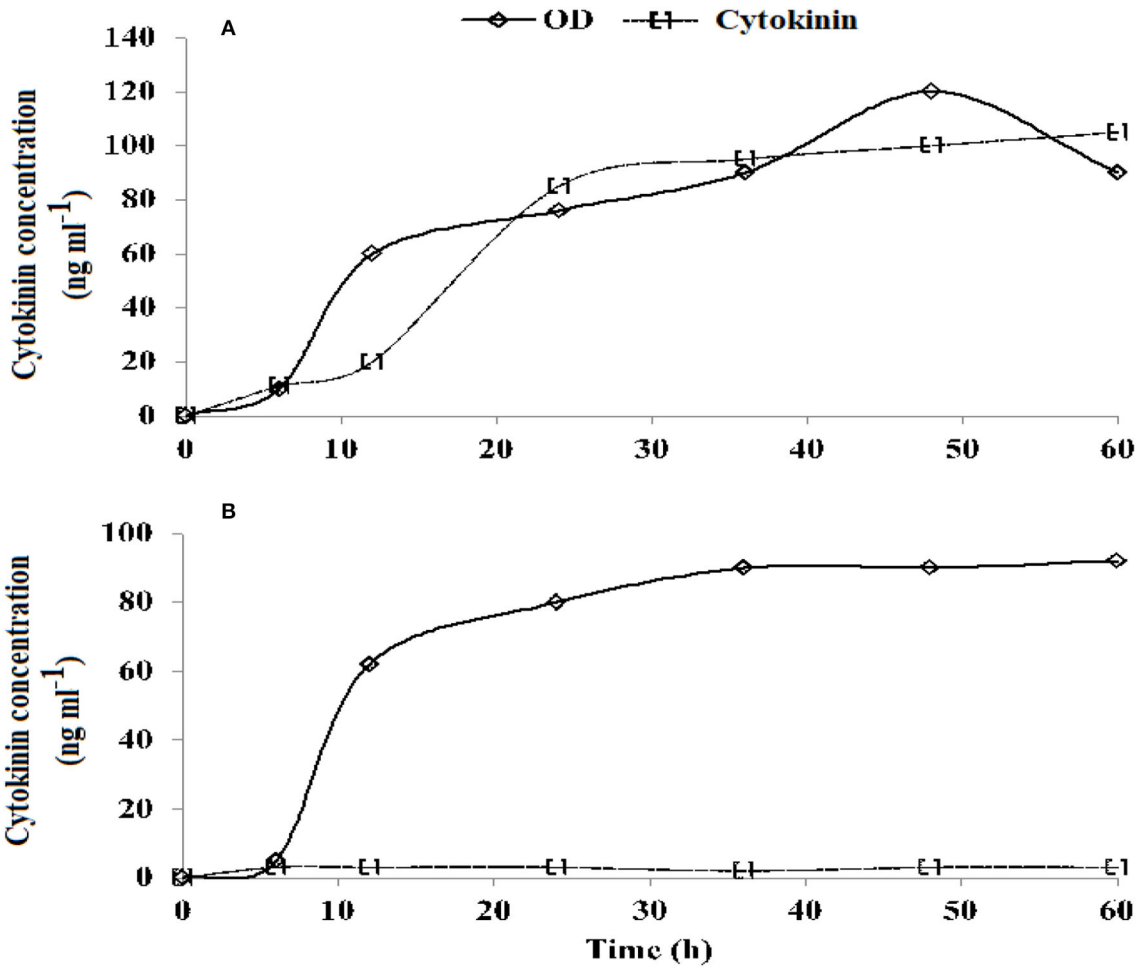

FIGURE 1 | Growth curve (OD, optical density) and cytokinin (Ck accumulation) of a cultured medium of *Azospirillum brasilense* RA−17 **(A)** and RA−18 **(B)**.

Silva-Fernandes et al. (1964). Relative water content (RWC) of a leaf was measured according to Barrs and Weatherley (1962) equation:

$$\text{RWC (\%)} = (\text{Fresh weight} - \text{dry weight}) / (\text{turgid weight} - \text{dry weight}) \times 100$$

According to Kudoyarova et al. (2014), levels of endogenous hormones in kernels of wheat were noticed. Proline content determined in wheat leaves by the ninhydrin method as reported by Bates et al. (1973). The activity of antioxidant enzymes, such as Ascorbate peroxidase (APX), catalase (CAT), Peroxidase (POD), and superoxide dismutase (SOD) was determined according to Nakano and Asada (1981), Vanacker et al. (2000), Ghanati et al. (2002), and Beyer and Fridovich (1987), respectively.

Statistical Analysis

Data from three experiments were analyzed using Fisher's test, and least significant difference (LSD) was used to compare treatments at a 95% probability level (Steel et al., 1997).

RESULTS

Azospirillum brasilense strain RA−17 produced an increasingly higher concentration of Ck, while the RA−18 strain consistently delivered a very low concentration of Ck (**Figure 1**).

Growth and Yield-Related Parameters

Relative growth rate (**Figure 2**) and net assimilation rate (**Figure 2**) were higher in wheat plants inoculated with Ck-producing than non-producing strain at tillering, flag leaf, milking, and maturity stages, and were lowest in the uninoculated plants. RGR was highest at the tillering stage and was about two-folds higher than at the flag leaf stage, about four-folds higher than at the milking stage, and six-folds higher than at the maturity stage. NAR was highest at the flag leaf stage and was about two-folds higher than at tillering and milking stages, which did not differ, but was four–six-folds more increased than at the maturity stage.

At tillering stage, the LAI did not differ between plants inoculated with Ck-producing and non-producing bacterial strains but it was lowest in the uninoculated plants (**Figure 2**).

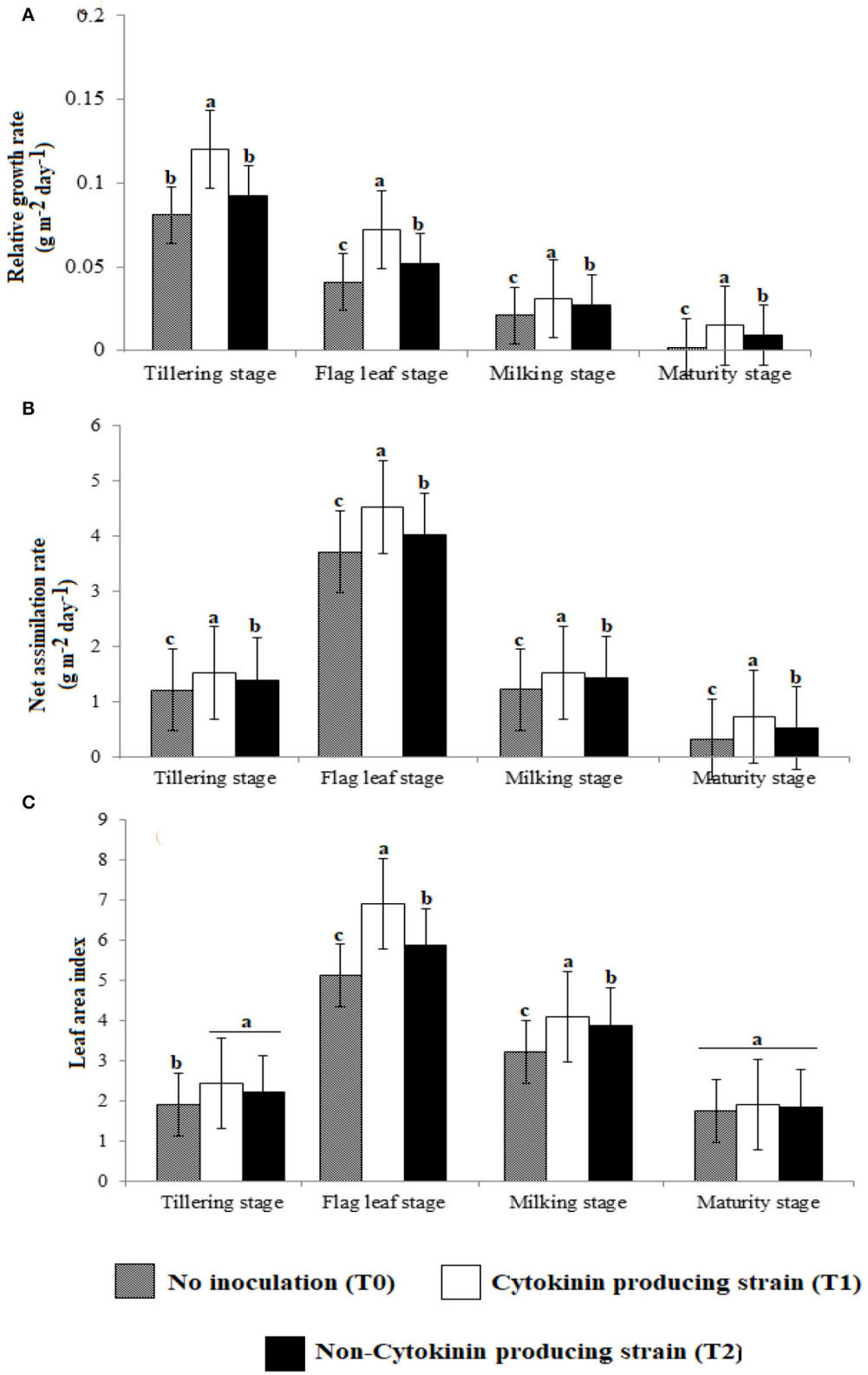

FIGURE 2 | Effect of Ck-producing *A. brasilense* RA−17 and non-producing *A. brasilense* RA−18 on **(A)** Relative growth rate (RGR), **(B)** Net assimilation rate (NAR), and **(C)** Leaf area index (LAI) of wheat plants. Different letters are significantly other in each column ($p \leq 0.05$), and the different letter shows a significant difference in treatments at a 5% probability level.

TABLE 1 | Effect of cytokinin producing *Azospirillum brasilense* RA−17 (T_1) and non-producing *A. brasilense* RA−18 (T_2) on crop growth rate (CGR, g m^{-2} day^{-1}) of wheat.

Treatment	Tillering stage	Flag leaf stage
T_0 (control)	1.73 c	6.33 c
T_1	2.15 a	9.58 a
T_2	1.94 b	8.44 b

The different letter shows a significant difference in treatments at a 5% probability level.

TABLE 2 | Effect of cytokinin (Ck)-producing *A. brasilense* RA−17 (T_1) and non-producing *A. brasilense* RA−18 (T_2) on plant height (cm) and yield parameters of wheat.

Treatments	Plant height (cm)	Spike length (cm)	Number of spikelets per spike	Number of grains per spike	1,000-grain weight (g)	Grain yield (kg/ha)
T_0 (Control)	83.33 c	8.88 c	14.23 c	24.34 c	37.7 c	3,850 c
T_1	88.34 a	11.19 a	19.23 a	28.54 a	44.12 a	4,666 a
T_2	85.53 b	10.06 b	18.55 b	26.52 b	41.56 b	4,182 b

The different letter shows a significant difference in treatments at a 5% probability level.

TABLE 3 | Effect of cytokinin-producing *A. brasilense* RA−17 (T_1) and non-producing *A. brasilense* RA−18 (T_2) on proline content, epicuticular wax, stomatal conductance, and photosynthetic rate of wheat at flag leaf stage.

Treatments	Epicuticular wax (g cm^{-2})	Stomatal conductance (mmol m^{-2} s^{-1})	Photosynthetic rate (μ mol m^{-2} s^{-1})
T_0 (control)	0.007 c	266.33 c	7.84 c
T_1	0.009 a	290.66 a	11.45 a
T_2	0.008 b	279.00 b	9.84 b

The different letter shows a significant difference in treatments at a 5% probability level.

However, at the flag leaf and milking stage, LAI was more significant with the Ck-producing than non-producing strain and was lowest in the uninoculated plants. LAI was highest at the flag leaf stage and was about two-folds higher than at the milking stage. A non-significant difference was noticed in LAI at the maturity of all treatments.

Crop growth rate at tillering and flag leaf stages was greater in wheat plants inoculated with the Ck-producing than non-producing strain, and it was lowest in the uninoculated plants (**Table 1**). CGR was about four-folds higher in wheat at the flag leaf stage than at the tillering stage. All growth and yield-related parameters were more significant with the Ck-producing than non-producing bacterial strain and were lowest in the uninoculated plants (**Table 2**).

Physiological and Photosynthetic Parameters in Wheat Leaves

Epicuticular wax, stomatal conductance, photosynthetic rate (**Table 3**), and chlorophyll contents (**Figure 3**) were greater with the Ck-producing than non-producing bacterial strain and were lowest in the uninoculated plants. RWC did not differ between plants inoculated with Ck-producing and non-producing bacterial strains but was lowest in the uninoculated plants (**Figure 4**).

Proline and Antioxidant Enzymes

Antioxidant enzyme activities and proline content (**Figures 5**, **6**) were greater in those wheat plants that were inoculated with the Ck-producing compared with the non-producing strain and were lowest in the uninoculated plants. Generally, enzyme activities were highest at the anthesis stage and lowest at tillering stage.

Endogenous Hormone Levels in Kernels

The concentration of endogenous hormones in kernels of wheat was highest in wheat plants inoculated with the Ck-producing strain than non-producing strain and was lowest in the uninoculated plants (**Figure 7**). Zeatin riboside, IAA, and ABA levels increased from 3 to 18 days after anthesis and decreased sharply after (**Figures 7A–C**). Gibberellin level was high at the early grain filling stage and then decreased continually for 15 days and then increased from 15 to 18 days and then decreased again until 27.

DISCUSSION

Influence of Ck-Producing Strain on Wheat Growth Parameters

Azospirillum spp. are known to be associated with several cereal crops (Ibrahim et al., 2016; Chávez-Herrera et al., 2018; Zaheer et al., 2021a). In this study, inoculation of wheat seed with strains of *A. brasilense* increased plants' growth parameters (plant height, CGR, RGR, NAR, and LAI) at different developmental stages than in uninoculated control. Seed inoculation with rhizobacteria has improved plant growth performance by releasing phytohormones, such as IAA, Ck, and gibberellins (Lakshmanan et al., 2013). For example, in grapevines, *A. brasilense* Sp245 enhanced the root and vegetative development (Bartolini et al., 2017), cucumber seedlings (Pereyra et al., 2010), and wheat plants (Spaepen et al., 2008) by producing IAA, and *A. brasilense* improved growth and photosynthetic parameters in wheat by producing Cks (Afzal et al., 2014; Zaheer et al., 2019b).

However, in this study, wheat inoculation with strain RA−17 produced a higher level of Ck significantly increased growth parameters compared with strain RA−18. Cks are phytohormones that influence plant growth and development by cell division, expansion of leaves, delay leaf senescence, etioplasts conversion to chloroplasts, and chlorophyll accumulation in leaves (Zafar et al., 2012; Zwack and Rashotte, 2013). Ck-producing *Magnaporthe oryzae* aided plant nutrient mobilization, increased photosynthetic levels and activated salicylic acid-mediated defense response in rice (Chanclud et al., 2016). Whereas, the Ck-mutant with a deleted Ck synthesizing gene did not show distinct growth and development features until an exogenous source of Ck was applied. In a study by Esquivel-Cote et al. (2010), inoculation of tomato seeds with a

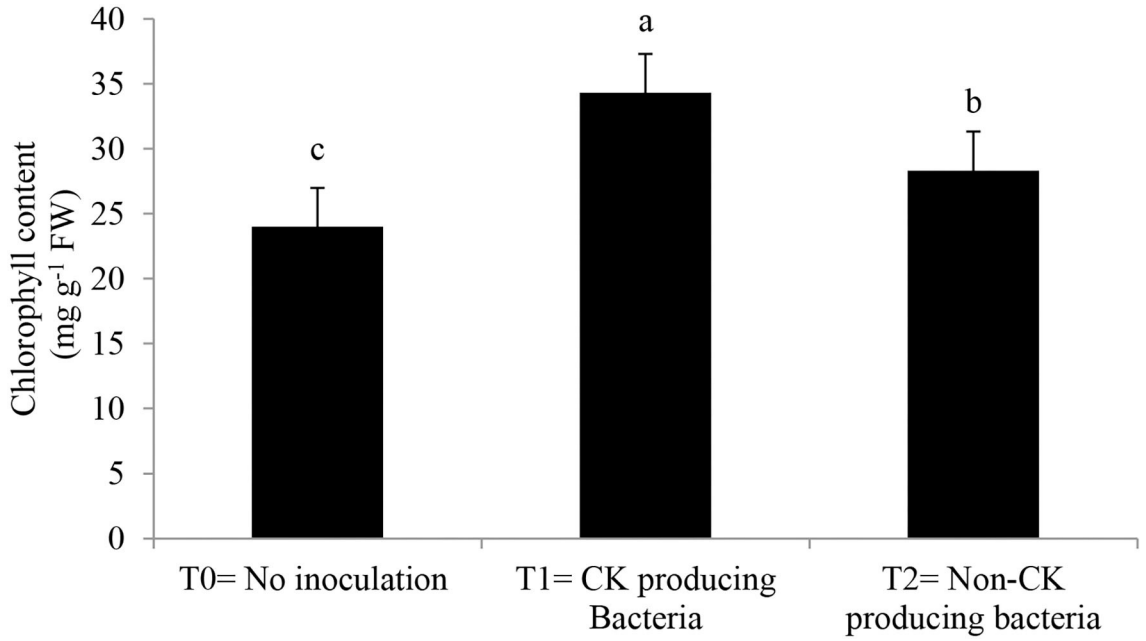

FIGURE 3 | Effect of Ck producing *A. brasilense* RA−17 and non-producing *A. brasilense* RA−18 on relative chlorophyll content (mg g^{-1} FW) of wheat. T0 = no inoculation; T1 = Ck producing strain, and T2 = non-Ck producing bacterial strains. The different letter shows a significant difference in treatments at a 5% probability level.

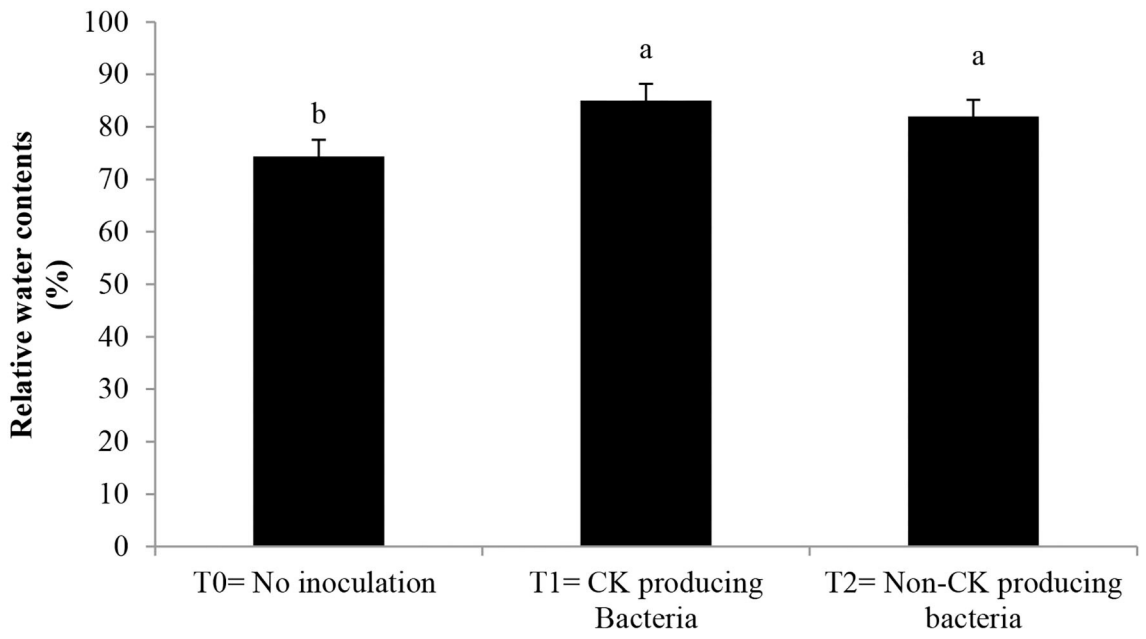

FIGURE 4 | Effect of Ck producing *A. brasilense* RA−17 and non-producing *A. brasilense* RA−18 on relative water content (RWC, %) of wheat. T0 = no inoculation; T1 = Ck producing strain, and T2 = non-Ck producing bacterial strains. The different letter shows a significant difference in treatments at a 5% probability level.

higher Ck-producing *Azospirillum* strain, *A. lipoferum* AZm5, enhanced RGR and increased leaf area, thus resulting in an increased photosynthetic surface, compared with a low-Ck producing strain VS9. However, they found that NAR did not increase due to nitrogen deprivation, which was reversed after the supply of N-fertilizer.

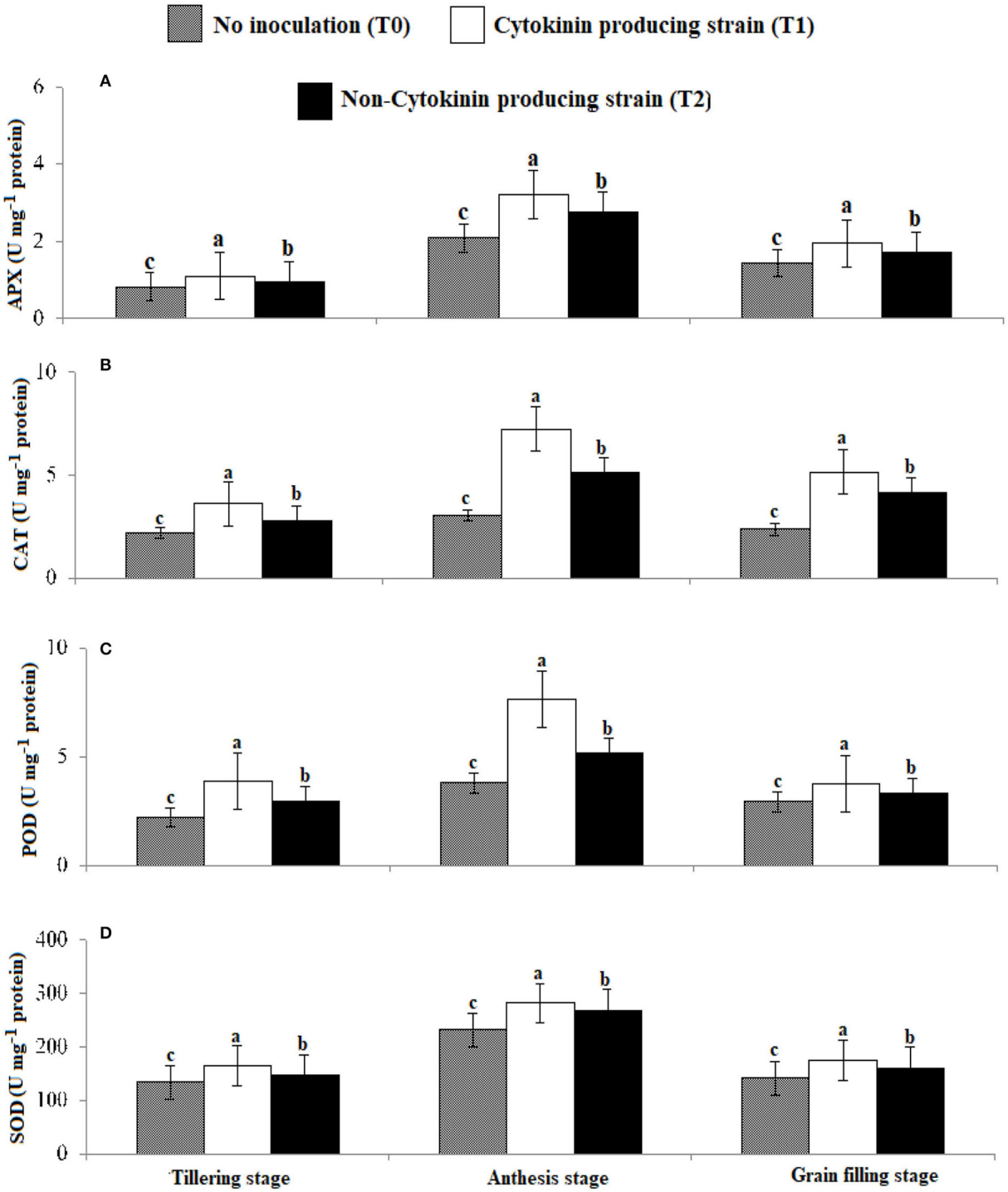

FIGURE 5 | Effect of Ck-producing *A. brasilense* RA−17 and non-producing *A. brasilense* RA−18 on antioxidant enzymes activities (U mg^{-1} protein) of wheat. The different letter shows a significant difference in treatments at a 5% probability level.

Influence of Ck-Producing Strain on Wheat Yield Parameters

All yield-promoting parameters are more significant with the Ck-producing than non-producing strain and were lowest in the uninoculated plants. Yield improvement in rhizobacteria-inoculated plants is due to improved water uptake and nutrient availability (Liu et al., 2019). In Panda et al. (2018), Ck significantly improved grain filling by increasing the expression

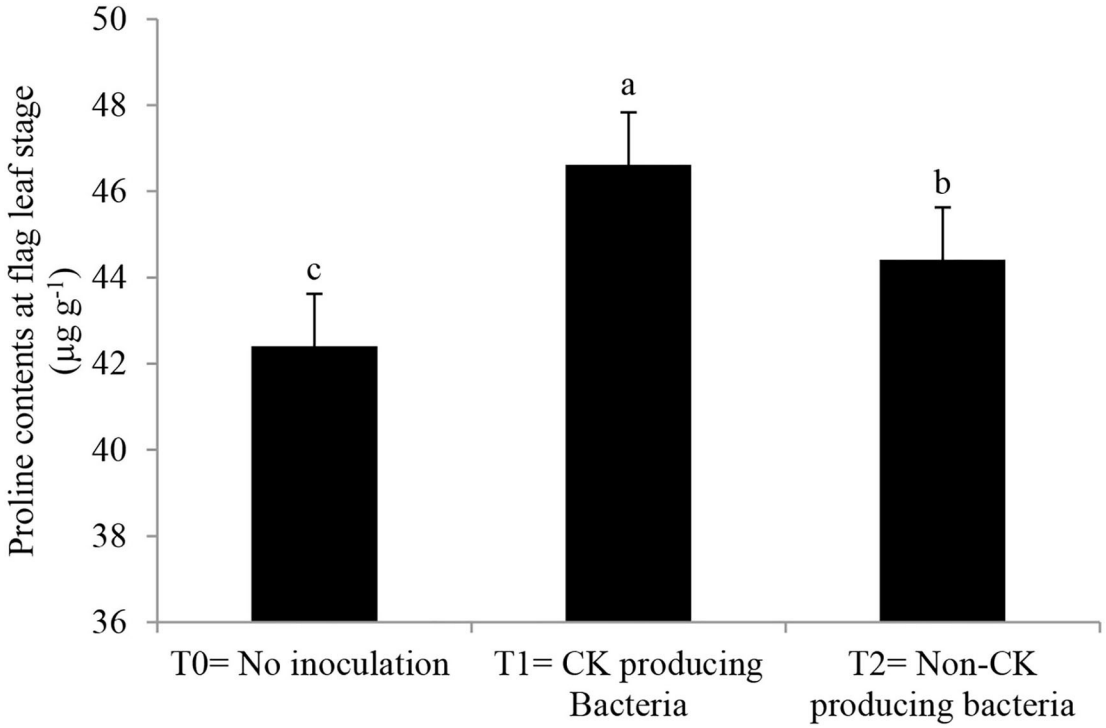

FIGURE 6 | Effect of Ck-producing *A. brasilense* RA−17 and non-producing *A. brasilense* RA−18 on proline content at flag leaf stage of wheat. The different letter shows a significant difference in treatments at a 5% probability level.

of cell cycle regulators in the spike's basal spikelets, leading to enhancement in grain filling. Mohapatra et al. (2011) showed the growth promotion effect of Ck in rice with the improving grain filling in rice panicles. Ck production by rhizobia was also shown to enhance the growth of different crops (Hayat et al., 2008). Barley inoculation with Ck-producing *A. brasilense* Sp246 increased yield and related parameters compared with the uninoculated control (Ozturk et al., 2003). Saber et al. (2012) also reported higher grains in wheat inoculated with plant growth-promoting rhizobacteria that lead to a higher yield.

Influence of Ck-Producing Strain on Proline Content and Antioxidant Enzyme Activities

Inoculating wheat seeds with the Azospirillum strains increased proline content and antioxidant enzyme activity (APX, CAT, POD, and SOD) more than in uninoculated plants. However, inoculation with high Ck-producing *Azospirillum* strain AR−17 than strain AR−18 increased the accumulation of these metabolites, particularly at anthesis. Rhizobacteria produce different metabolites to enhance stress tolerance and remove the adverse effects of reactive oxygen species (ROS) in plants (Madhaiyan et al., 2006; Raheem et al., 2018; Zaheer et al., 2021a). Synthesis of proline is increased by upregulation of the P5CS gene in the presence of Ck and ABA in plants (Vacheron et al., 2013). Different Ck-producing rhizobacterial strains have been noted to increase proline content under salt stress in soybean (Naz et al., 2009). Higher activities of APX, CAT, POD, and SOD were noticed at tillering, anthesis, and grain filling stages with the strain AR−17 than strain AR−18. As opined by Naseem et al. (2014), Ck can modulate defense signaling by activating antioxidant enzymes. Argueso et al. (2012) demonstrated that higher levels of Ck increased immune defenses in Arabidopsis. They showed that the enhanced levels of Ck gave higher protection in wild Arabidopsis plants. Ghorbanpour et al. (2013) and El-Esawi et al. (2018) reported that rhizobacterial inoculation of *Hyoscyamus niger* improves antioxidant enzymes activities, thus activating the plant defense mechanism. Chang et al. (2016) observed that levels of antioxidant enzymes increased in plants when Ck level was also increased.

Influence of Ck-Producing Strain on Endogenous Hormone Levels in Wheat Kernels

Inoculation with Ck-producing *Azospirillum* strain AR−17 increased the contents of zeatin riboside, gibberellin, IAA, and ABA, compared with strain AR−18, in wheat kernels and was lowest in the uninoculated plants. Higher hormonal contents in the kernels have been noted to significantly increase grain filling percentage (Yang et al., 2000; Zhang et al., 2010) and also regulate the sink size of the kernels (Yang et al., 2003). However, a study of Ck application in wheat kernels is limited. Yang et al. (2016) found that the contents of zeatin riboside, gibberellin, IAA, and ABA were significantly correlated with grain-filling rate. Production of endogenous hormones is essential for the regulation of kernel development. For example, zeatin maximizes the endosperm cell division, and increases sink capacity, thus

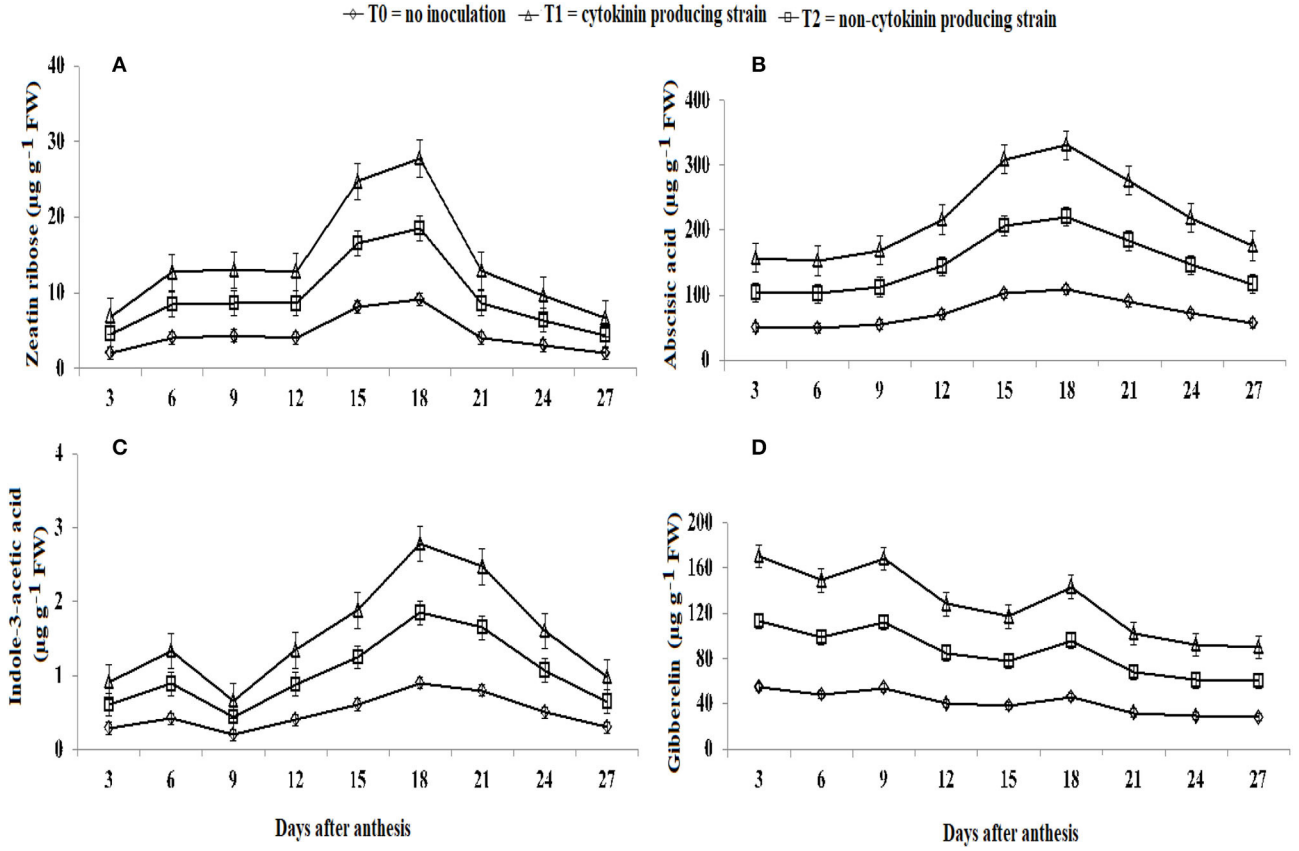

FIGURE 7 | Effect of Ck-producing *A. brasilense* RA−17 and non-producing *A. brasilense* RA−18 on levels of endogenous hormones (µg g^{-1} FW) in wheat kernels.

increasing assimilating accumulation (Yang et al., 2002). An increase in IAA content could reverse the reduction in grain weight (Yan et al., 2005). This suggests that Ck could sustain a more active photosynthetic period, thus transferring more assimilates to the grains during the grain filling stage, (Chen et al., 2010), and finally increase yield.

CONCLUSION

Azospirillum brasilense inoculation with the wheat seed significantly affected the wheat crop's growth, yield, and physiological parameters. Ck-producing *A. brasilense* is more beneficial for the growth, yield, antioxidant, and physiological systems of wheat than the non-Ck-producing *A. brasilense*. Ck producing *A. brasilense* is very effective for higher antioxidant enzyme activities and growth hormones production in wheat crops.

DATA AVAILABILITY STATEMENT

The original contributions presented in the study are included in the article/supplementary material, further inquiries can be directed to the corresponding author/s.

AUTHOR CONTRIBUTIONS

MZ, MM, and KE planned and executed the field experiment. HA and MI supervised the investigation. MZ, MM, KE, and MI participated in a write-up and review of the manuscript. MZ, TJ, and JI performed the antioxidant analysis. MH, ES, HK, JW, and ED reviewed the article and performed a revision of the manuscript. All authors made critically reviewed the manuscript, approved the final version, substantial contributions to the acquisition, analysis, and interpretation of the data described in this study.

FUNDING

The current work was funded by Taif University Researchers Supporting Project number (TURSP−2020/85), Taif University, Taif, Saudi Arabia.

ACKNOWLEDGMENTS

The authors extend their sincere appreciation to the Taif University Researchers Supporting Project number (TURSP-2020/85), Taif University, Taif, Saudi Arabia for supporting the current research.

REFERENCES

Afzal, J., Zia-ul-hassan, N., Depar, M., Arshad, S.S., Rao, I., and Shah, A.N. (2014). Wheat response to acc-deaminasefluorescent pseudomonads with varying phosphate solubilizing activity on a phosphorus deficient soil. *J. Anim. Plant Sci*. 24, 1834–1839.

Ahmed, A., and Hasnain, S. (2020). Extraction and evaluation of indole acetic acid from indigenous auxin- producing rhizosphere bacteria. *J. Anim. Plant Sci*. 30, 1024–1036. doi: 10.36899/JAPS.4, 0117.

Akhtar, S. S., Mekureyaw, M. F., Pandey, C., and Roitsch, T. (2020). Role of cytokinins for interactions of plants with microbial pathogens and pest insects. *Front. Plant Sci*. 10, 1777.

Angeli, S. D., Lauri, P., Dewitte, W., Onckelen, H. V., and Caboni, E. (2001). Factors affecting in vitro shoot formation from vegetative shoot apices of apple and relationship between organogenic response and cytokinin localisation. *Plant Biosyst*. 135, 95–100. doi: 10.1080/11263500112331350700

Argueso, C. T., Ferreira, F. J., Epple, P., To, J. P. C., Hutchison, C. E., Schaller, G. E., et al. (2012). Two-component elements mediate interactions between cytokinin and salicylic acid in plant immunity. *PLoS Genet*. 8, e1002448. doi: 10.1371/journal.pgen.1002448

Arshad, M., and Frankenberger, W. (1991). Microbial production of plant hormones. *Plant Soil*. 133, 1–8. doi: 10.1007/BF00011893

Barrs, H. D., and Weatherley, P. E. (1962). A re-examination of the relative turgidity technique for estimating water deficit in leaves. *Aust. J. Biol. Sci*. 15, 413–428. doi: 10.1071/BI9620413

Bartolini, S., Carrozza, G. P., Scalabrelli, G., and Toffanin, A. (2017). Effectiveness of *Azospirillum brasilense* Sp245 on young plants of *Vitis vinifera* L. *Open Life Sci*. 12, 365–372. doi: 10.1515/biol−2017-0042

Bates, L. S., Waldren, R. P., and Teare, I. D. (1973). Rapid determination of free proline for water-stress studies. *Plant Soil*. 39, 205–207. doi: 10.1007/BF00018060

Beyer, W. F., and Fridovich, I. (1987). Assaying for superoxide dismutase activity: some large consequences of minor changes in conditions. *Anal. Biochem*. 161, 559–566.

Bremner, J. M. (1965). "Total nitrogen and inorganic forms of nitrogen," in *Methods of Soil Analysis,* eds v C.A. Black (Madison, Wisconsin American Society of Agronomy), pp. 1149–1237.

Campos, F. V., Oliveira, J. A., Pereira, M. G., and Farnese, F. S. (2019). Nitric oxide and phytohormone interactions in the response of Lactuca sativa to salinity stress. *Planta*. 250, 1475–1489. doi: 10.1007/s00425-019-03236-w

Cerný, M., Dyčka, F., Bobál'ová J., and Brzobohatý, B. (2010). Early cytokinin response proteins and phosphoproteins of Arabidopsis thaliana identified by proteome and phosphoproteome profiling. *J. Exp. Bot*. 62, 921–937.

Chanclud, E., Kisiala, A., Emery, N. R. J., Chalvon, V., Ducasse, A., Romiti-Michel, C., et al. (2016). Cytokinin production by the rice blast fungus is a pivotal requirement for full virulence. *PLoS Pathog*. 12, e1005457. doi: 10.1371/journal.ppat.1005457

Chang, Z., Liu, Y., Dong, H., Teng, K., Han, L., and Zhang, X. (2016). Effects of cytokinin and nitrogen on drought tolerance of creeping bentgrass. *PLoS ONE*. 11, e0154005. doi: 10.1371/journal.pone.0154005

Chávez-Herrera, E., Hernández-Esquivel, A. A., Castro-Mercado, E., and García-Pineda, E. (2018). Effect of *Azospirillum brasilense* Sp245 lipopolysaccharides on wheat plant development. *J. Plant Growth Regul*. 37, 859–866. doi: 10.1007/s00344-018-9782–2

Chen, J. B., Liang, Y., Hu, X. Y., Wang, X. X., Tan, F. Q., Zhang, H. Q., et al. (2010). Physiological characterization of 'stay green' wheat cultivars during the grain filling stage under field growing conditions. *Acta. Physiol. Plant*. 32, 875–882.

El-Esawi, M. A., Alaraidh, I. A., Alsahli, A. A., Alamri, S. A., Ali, M. A., and Alayafi, A. A. (2018). (2018). *Bacillus firmus* (SW5) augments salt tolerance in soybean (*Glycine max* L.) by modulating root system architecture, antioxidant defense systems and stress-responsive genes expression. *Plant Physiol. Biochem*. 132, 375–384. doi: 10.1016/j.plaphy.09, 026.

Esquivel-Cote, R., Ramírez-Gama, R. M., Tsuzuki-Reyes, G., Orozco-Segovia, A., and Huante, P. (2010). *Azospirillum lipoferum* strain AZm5 containing 1-aminocyclopropane−1-carboxylic acid deaminase improves early growth of tomato seedlings under nitrogen deficiency. *Plant Soil*. 337, 65–75. doi: 10.1007/s11104-010-0499-7

Farooq, U., and Bano, A. (2013). Screening of indigenous bacteria from rhizosphere of maize (Zea mays L.) For their plant growth promotion ability and antagonism against fungal and bacterial pathogens. *J. Anim. Plant Sci*. 23, 1642–1652.

Fukami, J., Nogueira, M. A., Araujo, R. S., and Hungria, M. (2016). Accessing inoculation methods of maize and wheat with *Azospirillum brasilense*. *AMB Exp*. 6, 3. doi: 10.1186/s13568-015-0171-y

Ghanati, F., Morita, A., and Yokota, H. (2002). Induction of suberin and increase of lignin content by excess boron in tabacco cell. *Soil Sci. Plant Nutr*. 48, 357–364.

Ghorbanpour, M., Hatami, M., and Khavazi, K. (2013). Role of plant growth promoting rhizobacteria on antioxidant enzyme activities and tropane alkaloid production of Hyoscyamus niger under water deficit stress. *Turk. J. Biol*. 37, 350–360. doi: 10.3906/biy−1209–12

Hayat, S., Hasan, S. A., Fariduddin, Q., and Ahmad, A. (2008). Growth of tomato (*Lycopersicon Asculentum*) in response to salicylic acid under water stress. *J. Plant Interact*. 3, 297–304. doi: 10.1080/17429140802320797

Hussain, M. I., Asghar, H. N., Arshad, M., and Shahbaz, M. (2013). Screening of multi-traits rhizobacteria to improve maize growth under axenic conditions. *J. Anim. Plant Sci*. 23, 514–520.

Ibrahim, A., Shahid, A. A., Noreen, S., and Ahmad, A. (2016). Physiological changes against meloidogyne incognita in rhizobacterial treated eggplant under organic conditions. *J. Anim. Plant Sci*. 26, 805–813.

Karimi, M. M., and Siddique, K. H. M. (1991). Crop growth and relative growth rates of old and modern wheat cultivars. *Aust. J. Agric. Res*. 42, 13–20. doi: 10.1071/AR9910013

Kudoyarova, G. R., Melentiev, A. L., Martynenko, E. V., Timergalina, L. N., Arkhipova, T. N., and Shendel, G. V. (2014). VCytokinin producing bacteria stimulate amino acid deposition by wheat roots. *Plant Physiol. Biochem*. 83, 285–291. doi: 10.1016/j.plaphy.08, 015.

Lakshmanan, V., Castaneda, R., Rudrappa, T., and Bais, H. P. (2013). Root transcriptome analysis of Arabidopsis thaliana exposed to beneficial *Bacillus subtilis* FB17 rhizobacteria revealed genes for bacterial recruitment and plant defense independent of malate efflux. *Planta*. 238, 657–668. doi: 10.1007/s00425-013–1920–2

Liu, X., Jiang, X., He, X., Zhao, W., Cao, Y., Guo, T., et al. (2019). Phosphate-solubilizing pseudomonas sp. strain p34-l promotes wheat growth by colonizing the wheat rhizosphere and improving the wheat root system and soil phosphorus nutritional status. *J. Plant Growth Regul*. 38, 1314–1324. doi: 10.1007/s00344-019-09935-8

López-Bucio, J., Campos-Cuevas, J. C., Hernández-Calderón, E., Velásquez-Becerra, C., Farías-Rodríguez, R., Macías-Rodríguez, L. I., et al. (2007). *Bacillus megaterium* rhizobacteria promote growth and alter root-system architecture through an auxin-and ethylene-independent signaling mechanism in Arabidopsis thaliana. *Mol. Plant Microbe. In*. 20, 207–217.

Madhaiyan, M., Poonguzhali, S., Ryu, J., and Sa, T. (2006). Regulation of ethylene levels in canola (*Brassica campestris*) by 1-aminocyclopropane−1-carboxylate deaminase-containing Methylobacterium fujisawaense. *Planta*. 224, 268–278. doi: 10.1007/s00425-005-0211-y

Mohapatra, P. K., Panigrahi, R., and Turner, N. C. (2011). Physiology of spikelet development on the rice panicle: is manipulation of apical dominance crucial for grain yield improvement? *Adv. Agron*. 110, 333–360. doi: 10.1016/B978-0–12-385531–2.00005-0

Mushtaq, S., Shafiq, M., Ashraf, T., Haider, M. S., Ashfaq, M., and Ali, M. (2019). Characterization of plant growth promoting activities of bacterial endophytes and their antibacterial potential isolated from citrus. *J. Anim. Plant Sci*. 29, 978–991.

Nakano, Y., and Asada, K. (1981). Hydrogen peroxide is scavenged by ascorbate-specific peroxidase in spinach chloroplasts. *Plant Cell Physiol*. 22, 867–880.

Naseem, M., Kunz, M., and Dandekar, T. (2014). Probing the unknowns in cytokinin-mediated immune defense in Arabidopsis with systems biology approaches. *Bioinformatics boil. Insights*. 8, 35–44. doi: 10.4137/BBI.S13462

Naz, I., Bano, A., and Ul-Hassan, T. (2009). Isolation of phytohormones producing plant growth promoting rhizobacteria from weeds growing in Khewra salt range, Pakistan and their implication in providing salt tolerance to *Glycine max* L. *Afr. J. Biotechnol*. 8, 5762–5768. doi: 10.5897/AJB09.1176

Ortiz-Castro, R., Campos-García, J., and López-Bucio, J. (2020). *Pseudomonas putida* and *Pseudomonas fluorescens* influence arabidopsis root system

architecture through an auxin response mediated by bioactive cyclodipeptides. *J. Plant Growth. Regul*. 39, 254–265. doi: 10.1007/s00344-019-09979-w

Ortíz-Castro, R., Valencia-Cantero, E., and López-Bucio, J. (2008). Plant growth promotion by *Bacillus megaterium* involves cytokinin signaling. *Plant Signal. Behav*. 3, 263–265. doi: 10.4161/psb.3.4.5204

Ozturk, A., Caglar, O., and Sahin, F. (2003). Yield response of wheat and barley to inoculation of plant growth promoting rhizobacteria at various levels of nitrogen fertilization. J. Plant Nutr. *Soil Sci*. 166, 262–266.

Panda, B. B., Sekhar, S., Dash, S. K., Behera, L., and Shaw, B. P. (2018). Biochemical and molecular characterisation of exogenous cytokinin application on grain filling in rice. *BMC Plant Biol*. 18, 89. doi: 10.1186/s12870-018–1279-4

Pereyra, C. M., Ramella, N. A., Pereyra, M. A., Barassi, C. A., and Creus, C. M. (2010). Changes in cucumber hypocotyl cell wall dynamics caused by Azospirillum brasilense inoculation. *Plant Physiol. Biochem*. 48, 62–69. doi: 10.1016/j.plaphy.10, 001.

Qureshi, M. A., Ahmad, Z. A., Akhtar, N., Iqbal, A., Mujeeb, F., and Shakir, M. A. (2012). Role of phosphate solubilizing bacteria (PSB) in enhancing p availability and promoting cotton growth. *J. Anim. Plant Sci*. 22, 204–210.

Raheem, A., Shaposhnikov, A., Belimov, A. A., Dodd, I. C., and Ali, B. (2018). Auxin production by rhizobacteria was associated with improved yield of wheat (*Triticum aestivum* L.) under drought stress. *Arch. Agron. Soil Sci*. 4, 574–587.

Saber, Z., Pirdashti, H., Esmaeili, M., Abbasian, A., and Heidarzadeh, A. (2012). Response of wheat growth parameters to co-inoculation of plant growth promoting rhizobacteria (PGPR) and different levels of inorganic nitrogen and phosphorus. *World Appl. Sci. J*. 16, 213–219.

Sabir, S., Asghar, H. N., Kashif, S. U. R., Khan, M. Y., and Akhtar, M. J. (2013). Synergistic effect of plant growth promoting rhizobacteria and Kinetin on maize. *J. Anim. Plant Sci*. 23, 1750–1755.

Sarkar, J., Chakraborty, B., and Chakraborty, U. (2018). Plant growth promoting rhizobacteria protect wheat plants against temperature stress through antioxidant signalling and reducing chloroplast and membrane injury. *J. Plant Growth Regul*. 37, 1396–1412. doi: 10.1007/s00344-018-9789-8

Sears, R. G. (1997). "Strategies for improving wheat grain yield," in *Wheat: Prospects for Global Improvement. Developments in Plant Breeding*, eds Braun HJ, Altay F, Kronstad WE, Beniwal SPS, McNab A. (Dordrecht: Springer), p. 3.

Silva-Fernandes, A. M., Baker, E. A., and Martin, J. T. (1964). Studies of plant cuticle VI. The isolation and fractionation of cuticular waxes. *Ann. Appl. Biol*. 53, 43–58. doi: 10.1111/j.1744-7348.1964.tb03779.x

Spaepen, S., Dobbelaere, S., Croonenborghs, A., and Vanderleyden, J. (2008). Effects of *Azospirillum brasilense* indole-3-acetic acid production on inoculated wheat plants. *Plant Soil*. 312, 15–23. doi: 10.1007/s11104-008-9560–1

Steel, R. G. D., Torrie, J. H., and Dickey, D. A. (1997). *Principles and Procedures of Statistics, A Biometrical Approach (3rd ed.)*. New York, NY: Book *Co,* pp. 352–358.

Tkachuk, R. (1966). Factor of conversion of nitrogen to protein. *Cereal Chemistr*. 43, 207–203.

Ullah, I., Ali, N., Durrani, S., Shabaz, M. A., Hafeez, A., Ameer, H., et al. (2018). Effect of different nitrogen levels on growth, yield and yield contributing attributes of wheat. *Int. J. Sci. and Eng. Res*. 9, 595–602. doi: 10.14299/ijser.09, 01.

Vacheron, J., Desbrosses, G., Bouffaud, M. L., Touraine, B., Moënne-Loccoz, Y., Muller, D., et al. (2013). Plant growth-promoting rhizobacteria and root system functioning. *Front. Plant Sci*. 4, 356. doi: 10.3389/fpls.2013.00356

Vanacker, H., Carver, T. L. W., and Foyer, C. M. (2000). Early H_2O_2 accumulation in mesophyll cells leads to induction of glutathione during the hyper sensitive response in the barley-powdery mildew interaction. *Plant Physiol*. 123, 1289–1300. doi: 10.1104/pp.123.4.1289

Vernon, A., and Allison, J. (1963). A method of calculating net assimilation rate. *Nature*. 200, 814. doi: 10.1038/200814a0

Xu, L., Wu, C., Oelmuller, R., and Zhang, W. (2018). Role of phytohormones in piriformospora indica-induced growth promotion and stress tolerance in plants: more questions than answers. *Front. Microbiol*. 9, 1646. doi: 10.3389/fmicb.2018.01646

Yan, J., Cao, L. P., Zhang, W., Chen, J. X., and Wu, X. C. (2005). Effected on endogenous hormone and grain filling characteristic under soil water stress. *J. Shihezi Univ*. 23, 30–38.

Yang, D., Li, Y., Shi, Y., Cui, Z., Luo, Y., Zheng, M., et al. (2016). Exogenous cytokinins increase grain yield of winter wheat cultivars by improving stay-green characteristics under heat stress. *PLoS One*. 11, e0155437. doi: 10.1371/journal.pone.0155437

Yang, J. C., Peng, S. B., Visperas, R. M., Sanico, A. L., Zhu, Q. S., and Gu, S. L. (2000). Grain filling pattern and cytokinin content in the grains and roots of rice plants. *Plant Growth. Regul*. 30, 261–270.

Yang, J. C., Zhang, J. H., Wang, Z. Q., and Zhu, Q. S. (2003). Hormones in the grains in relation to sink strength and postanthesis development of spikelets in rice. *Plant Growth Regul*. 41, 185–195. doi: 10.1023/B:GROW.0000007503.95391.38

Yang, J. C., Zhang, J. H., Wang, Z. Q., Zhu, Q. S., and Liu, L. J. (2002). Abscisic acid and cytokinins in the root exudates and leaves and their relationship to senescence and remobilization of carbon reserves in rice subjected to water stress during grain filling. *Planta*. 215, 645–652. doi: 10.1007/s00425-002-0789–2

Zafar, M., Abbasi, M. K., Khan, M. A., Khaliq, A., Sultan, T., and Aslam, M. (2012). Effect of plant growth-promoting rhizobacteria on growth, nodulation and nutrient accumulation of lentil under controlled conditions. *Pedosphere*. 22, 848–859. doi: 10.1016/S1002-0160(12)60071-X

Zaheer, M. S., Ali, H. H., Erinle, K. O., Wani, S. H., Okon, O. G., Nadeem, M. A., et al. (2021a). Inoculation of Azospirillum brasilense and exogenous application of trans-zeatin riboside alleviates arsenic induced physiological damages in wheat (*Triticum aestivum*). *Environ. Sci. Pollut. Res*. 17, 106. doi: 10.1007./s11356-021-18106-w

Zaheer, M. S., Ali, H. H., Soufan, W., Iqbal, R. M., Habib-ur-Rahman, J., et al. (2021b). Potential effects of biochar application for improving wheat (*Triticum aestivum* L.) growth and soil biochemical properties under drought stress conditions. *Land* 10, 1125. doi: 10.3390/land10111125

Zaheer, M. S., Raza, M. A. S., Saleem, M. F., Erinle, K. O., Iqbal, R., and Ahmad, S. (2019b). Effect of rhizobacteria and cytokinins application on wheat growth and yield under normal vs drought conditions. *Comm. Soil Sci. Plant Anal*. 50, 2521–2533. doi: 10.1080/00103624.2019.1667376

Zaheer, M. S., Raza, M. A. S., Saleem, M. F., Khan, I. H., Ahmad, S., Iqbal, R., et al. (2019a). Investigating the effect of *Azospirillum brasilense* and *Rhizobium pisi* on agronomic traits of wheat (*Triticum aestivum* L.). *Arch. Agron. Soil Sci*. 65, 1554–1564. doi: 10.1080/03650340.2019.1566954

Zhang, H., Chen, T. T., Wang, Z. Q., Yang, J. C., and Zhang, J. H. (2010). Involvement of cytokinins in the grain filling of rice under alternate wetting and drying irrigation. *J. Exp. Bot*. 61, 3719–3733. doi: 10.1093/jxb/erq198

Zwack, P. J., and Rashotte, A. M. (2013). Cytokinin inhibition of leaf senescence. *Plant Signal. Behav*. 8, e24737. doi: 10.4161/psb.24737

Conflict of Interest: The authors declare that the research was conducted in the absence of any commercial or financial relationships that could be construed as a potential conflict of interest.

Publisher's Note: All claims expressed in this article are solely those of the authors and do not necessarily represent those of their affiliated organizations, or those of the publisher, the editors and the reviewers. Any product that may be evaluated in this article, or claim that may be made by its manufacturer, is not guaranteed or endorsed by the publisher.

frontiers | Frontiers in Microbiology

ORIGINAL RESEARCH
published: 19 May 2022
doi: 10.3389/fmicb.2022.878000

Harnessing the Potential of *Bacillus altitudinis* MT422188 for Copper Bioremediation

Maryam Khan[1], Muhammad Kamran[2], Roqayah H. Kadi[3], Mohamed M. Hassan[4], Abeer Elhakem[5], Haifa Abdulaziz Sakit ALHaithloul[6], Mona H. Soliman[7,8], Muhammad Zahid Mumtaz[1], Muhammad Ashraf[1] and Saba Shamim[1]**

[1]Institute of Molecular Biology and Biotechnology, The University of Lahore, Lahore, Pakistan, [2]School of Agriculture, Food and Wine, The University of Adelaide, Adelaide, SA, Australia, [3]Department of Biology, College of Science, University of Jeddah, Jeddah, Saudi Arabia, [4]Department of Biology, College of Science, Taif University, Taif, Saudi Arabia, [5]Department of Biology, College of Sciences and Humanities, Prince Sattam Bin Abdulaziz University, Al-Kharj, Saudi Arabia, [6]Biology Department, College of Science, Jouf University, Sakaka, Saudi Arabia, [7]Botany and Microbiology Department, Faculty of Science, Cairo University, Giza, Egypt, [8]Biology Department, Faculty of Science, Taibah University, Al-Sharm, Yanbu El-Bahr, Saudi Arabia

OPEN ACCESS

Edited by:
Adnan Mustafa,
Brno University of Technology,
Czechia

Reviewed by:
Sajid Ali,
Yeungnam University,
South Korea
M. Oves,
King Abdulaziz University,
Saudi Arabia
Khalid Z. Elwakeel,
Jeddah University,
Saudi Arabia
Muhammad Amjad Ali,
University of Agriculture, Faisalabad,
Pakistan

***Correspondence:**
Mohamed M. Hassan
m.khyate@tu.edu.sa
Saba Shamim
sabashamimgenetics@gmail.com

Specialty section:
This article was submitted to Terrestrial Microbiology, a section of the journal Frontiers in Microbiology

Received: 17 February 2022
Accepted: 05 April 2022
Published: 19 May 2022

Citation:
Khan M, Kamran M, Kadi RH, Hassan MM, Elhakem A, Sakit ALHaithloul HA, Soliman MH, Mumtaz MZ, Ashraf M and Shamim S (2022) Harnessing the Potential of Bacillus altitudinis MT422188 for Copper Bioremediation. Front. Microbiol. 13:878000. doi: 10.3389/fmicb.2022.878000

The contamination of heavy metals is a cause of environmental concern across the globe, as their increasing levels can pose a significant risk to our natural ecosystems and public health. The present study was aimed to evaluate the ability of a copper (Cu)-resistant bacterium, characterized as *Bacillus altitudinis* MT422188, to remove Cu from contaminated industrial wastewater. Optimum growth was observed at 37°C, pH 7, and 1 mm phosphate, respectively. Effective concentration 50 (EC_{50}), minimum inhibitory concentration (MIC), and cross-heavy metal resistance pattern were observed at 5.56 mm, 20 mm, and Ni > Zn > Cr > Pb > Ag > Hg, respectively. Biosorption of Cu by live and dead bacterial cells in its presence and inhibitors 1 and 2 (DNP and DCCD) was suggestive of an ATP-independent efflux system. *B. altitudinis* MT422188 was also able to remove 73 mg/l and 82 mg/l of Cu at 4th and 8th day intervals from wastewater, respectively. The presence of Cu resulted in increased GR (0.004 ± 0.002 $Ug^{-1}FW$), SOD (0.160 ± 0.005 $Ug^{-1}FW$), and POX (0.061 ± 0.004 $Ug^{-1}FW$) activity. Positive motility (swimming, swarming, twitching) and chemotactic behavior demonstrated Cu as a chemoattractant for the cells. Metallothionein (MT) expression in the presence of Cu was also observed by SDS-PAGE. Adsorption isotherm and pseudo-kinetic-order studies suggested Cu biosorption to follow Freundlich isotherm as well as second-order kinetic model, respectively. Thermodynamic parameters such as Gibbs free energy ($\Delta G°$), change in enthalpy ($\Delta H° = 10.431$ kJ/mol), and entropy ($\Delta S° = 0.0006$ kJ/mol/K) depicted the biosorption process to a feasible, endothermic reaction. Fourier Transform Infrared Spectroscopy (FTIR), Scanning Electron Microscopy (SEM), and Energy-Dispersive X-Ray Spectroscopy (EDX) analyses revealed the physiochemical and morphological changes in the bacterial cell after biosorption, indicating interaction of Cu ions with its functional groups. Therefore, these features suggest the potentially effective role of *B. altitudinis* MT422188 in Cu bioremediation.

Keywords: copper bioremediation, biosorption, industrial wastewater, isotherm, thermodynamics

INTRODUCTION

Heavy metals are one of the most persistent pollutants found on Earth due to their non-biodegradability and tendency to accumulate in the environment, causing harm to our natural ecosystems in the process (Gaur et al., 2021). There are many sources of heavy metals which can take root from natural and anthropogenic origins, with the former including soil run-off, volcanic eruptions, weathering, and erosion (Soltani-Gerdefaramarzi et al., 2021), whereas the latter are anthropogenic sources that stem from several industrial processes such as ore mining, combustion of fossil fuels, and the production of alloys, steel, plastic, dyes, and pigments, respectively (Selvi et al., 2019). Like soil and surface resources, water resources too tend to get contaminated by heavy metals, due to their closeness to industries which require large amounts of water for cooling and other processes, which ultimately enhances the precipitation of heavy metal ions onto the water bed once they enter the closest source (Briffa et al., 2020).

Among many heavy metals that are specifically categorized on the basis of their essentiality and non-essentiality to living organisms, copper (Cu) is an essential metal for biological systems as it is required for the function of various significant processes in prokaryotes and eukaryotes (Oves et al., 2016). It is a soft metal which conducts both heat and electricity, and belongs to the group IB in the Periodic Table of elements, in between nickel (Ni) and zinc (Zn). It is naturally found as a mineral, bound with other elements in the form of sulfides, oxides, and carbonates (Crichton and Pierre, 2001). Though found in two oxidation states in nature, it is usually found in its monovalent form (Cu^{+}), which is required by various organisms for essential biological functions, as well as a co-factor for many enzymes, albeit in low concentrations, as elevated levels of Cu tend to induce cellular toxicity and can result in cell death (Zhao et al., 2010). Increasing levels of Cu in our environment have resulted in its pollution, which has since been aggravated due to many anthropogenic and natural factors (Izydorczyk et al., 2021; Covre et al., 2022).

Extensive research for mitigating excessive levels of heavy metals in the environment has brought about several methods for combating environmental pollution, as their accumulation poses a grave danger to sensitive ecosystems of the world (Minnikova et al., 2017). Over the years, many physical and chemical methods of remediation have been developed and critically evaluated, but not all were deemed to be sufficiently efficacious (Sayqal and Ahmed, 2021). The need for cheaper, feasible, and environmentally friendly methods was imperative, due to which the focus shifted toward other forms of adsorbents to remove heavy metals from water (Sulaiman et al., 2021). Biological agents, such as plants, algae, and microorganisms were found to be better suited for heavy metal remediation (Elwakeel et al., 2012; El-Liethy et al., 2018; Elgarahy et al., 2020), but the latter appeared to be more beneficial as they improved metal solubility due to the production of organic acids and/or by modification of soil texture due to the production of polysaccharides (Wang et al., 2017; Alves et al., 2022). Microorganisms such as bacteria are considered to be efficacious agents of bioremediation due to their generally well-known resistance mechanisms, and for their tendency to survive and endure extreme environments (Jain et al., 2011; Saeed et al., 2022). Bacterial consortia of several species such as *Alcaligenes faecalis*, *Staphylococcus aureus*, *Streptococcus lactis*, *Micrococcus luteus*, and *Enterobacter aerogenes* was reported to remove various heavy metals such as copper, cadmium, lead, and zinc from wastewaters (Silambarasan and Abraham, 2013). Furthermore, *Bacillus* sp. have also been well-reported as efficient agents of bioremediation from soil and wastewaters over the years (Joo et al., 2010; Kamika and Momba, 2013; Singh et al., 2014; Wierzba, 2015; Babar et al., 2021). *Bacillus* sp. are considered to be potentially effective in removing heavy metals from contaminated sources of soil and water, based on prior knowledge that Gram-positive bacteria are able to resist a much higher quantity of heavy metals than Gram-negative bacteria (Nwinyi et al., 2014). Furthermore, carboxyl group in the peptidoglycan layers of the bacterial cell wall serve a key role in the uptake of heavy metals, due to which *Bacillus* sp. are potential candidates for the bioremediation of Cu and its compounds (Igiri et al., 2018).

This study aimed to investigate the bioremediation potential of a Cu-resistant bacterium isolated from contaminated industrial wastewaters. The bacterium was also evaluated for its growth characteristics, antioxidative, motility and chemotactic behavior, as well as for the presence of metallothioneins. Fourier Transform Infrared Spectroscopy (FTIR), Scanning Electron Microscopy (SEM), and Energy-Dispersive X-Ray Spectroscopy (EDX) analyses were employed to study physicochemical changes to bacterial cells pre and post Cu biosorption.

MATERIALS AND METHODS

Collection of Samples

The wastewater samples ($n = 10$) were collected from 10 different industrial sites each at Kalashah Kaku and Muridke, which are well-known industrial areas in Sheikhupura, Punjab, Pakistan (geographically located at 31° 72′ 50″ North, 74° 26′ 77″ East and 31° 80′ 95″ North, 74° 25′ 34″ East), respectively. Samples were obtained in sterilized containers, after which some of their physical and chemical characteristics *viz.*, pH, concentration of Cu ions, and temperature were checked and noted.

Isolation and Purification of Selected Bacterial Strain

All the samples were proceeded on Luria-Bertani (LB) agar medium (tryptone 1%; yeast extract 1%; sodium chloride 0.5%; agar 1.5%). Prior to spreading each sample, Cu (0.1 mm) was added (100 µl) after which incubation was done at 37°C for 24 h. The process was repeated until pure bacterial strains were isolated.

Abbreviations: APOX, Ascorbate Peroxidase; CAT, Catalase; DCCD, N, N-Dicyclohexylcarbodiimide; DNP, 2,4-Dinitrophenol; EDX, Energy-Dispersive X-Ray Spectroscopy; FTIR, Fourier Transform Infrared Spectroscopy; GR, Glutathione Reductase; MIC, Minimum Inhibitory Concentration; MT, Metallothionein; OD, Optical Density; POX, Peroxidase; PVP, Polyvinylpyrrolidone; ROS, Reactive Oxygen Species; rRNA, Ribosomal RNA; SDS-PAGE, Sodium Dodecyl Sulphate-Polyacrylamide Gel Electrophoresis; SEM, Scanning Electron Microscopy; SOD, Superoxide Dismutase.

Determination of Minimum Inhibitory Concentration

The purified cultures were streaked on sterile plates of minimal salt medium (1.0 g/l NH_4Cl; 0.001 g/l $CaCl_2.H2O$, 0.2 g/l $MgSO_4.7H_2O$, 0.5 g/l K_2HPO_4, 0.001 g/l $FeSO_4.7H_2O$, 5.0 g/l sodium acetate, 1 g/l yeast extract, final pH adjusted to 7.0; Pattanapipitpaisal et al., 2001), supplemented with different concentrations of Cu (0.1–35 mm). The plates were incubated overnight and the process was repeated until the concentration inhibiting the growth of the most resistant isolate was determined (Shamim, 2014). The isolate was then selected for further study.

Characterization of Selected Bacterial Strain

The chosen strain was identified by observing several parameters such as colony morphology, Gram staining, and other biochemical tests (Cheesbrough, 2006), after which its molecular characterization was confirmed by 16S rRNA sequencing from Macrogen®, South Korea.

Determination of Cross Heavy Metal Resistance

The resistance to other heavy metals was also investigated by test-tube dilution method. Minimal salt broth medium (supplemented with phosphate and sodium succinate) was prepared and autoclaved in test-tubes, to which 1% of fresh bacterial culture was added in aseptic conditions. Variable concentrations of metal ions were added until the concentration at which the bacterial growth was inhibited for every metal was obtained (Shamim, 2014).

Determination of Optimal Growth Parameters

The optimal conditions for growth parameters such as temperature, pH, and phosphate concentration were investigated with regard to the chosen bacterial strain. Fresh bacterial cells (1%) in sterile broth media were incubated overnight at varying temperatures (10, 15, 20, 25, 37, 40, 40, 50, 55°C). For the determination of pH, various pH values (5–9) were adjusted for each set, whereas for optimal phosphate concentration, freshly inoculated cells were supplemented with phosphate concentrations ranging from 0.1–5.0 mm prior to their incubation at 37°C. Growth of bacterial cells was observed (OD_{578}nm) after successful overnight incubation (Shamim and Rehman, 2012).

Determination of EC_{50} and Effect of Cu on Bacterial Growth

The half maximal effective concentration (EC_{50}) was calculated by administering several concentrations of Cu to fresh bacterial cells (1%) in minimal salt broth medium (pH 7). The samples were incubated at 37°C and optical density was determined after subsequent time periods (OD = 578 nm; Pepi et al., 2008). The growth pattern of cells with and without Cu was also investigated (Shamim et al., 2014). In the experimental setup, Cu (0.1 mm) was supplemented to fresh cultured cells (1%) once they reached logarithmic phase (OD_{578} = 0.3–0.4) while no Cu was added to the control. Growth in each setup was noted at every hour by drawing an aliquot of culture (1 ml) for absorbance at 578 nm.

Cu Uptake Studies

Uptake of Cu by Live Bacterial Cells

Purified bacterial cells (1%) were inoculated in sterile minimal salt medium (pH 7), followed by the addition of Cu (10 mg/l) at logarithmic phase (OD = 578 nm). The flask was placed in a shaking incubator for 30 min to achieve acclimatization phase. In the next step, aliquot (15 ml) was drawn from the setup after regular hourly intervals and was harvested *via* centrifugation for 10 min at 15,000 rpm. Washing of cell pellets was done thrice with EDTA (0.5 M) and Milli-Q® water, while supernatants were collected separately. The water collected from washing was used to analyze the amount of Cu ions adsorbed onto the bacterial surface, while the cell pellets (acid digested; 0.2 N HNO_3) were evaluated for intracellular accumulation of Cu. All three samples (supernatants, acid digested pellets, water obtained from washing) were then investigated for Cu by atomic absorption spectrometry (AAS) analysis (228.8 nm). The overall % increase and decrease in the concentration of Cu (accumulation, uptake and adsorption) was calculated and presented in the form of graphs (Shamim et al., 2014).

Effect of Inhibitors on the Uptake of Cu by Live Bacterial Cells

Three experimental setups were prepared as before. The first set consisted of live bacterial cells, Cu ions (10 mg/l) and 2,4-Dinitrophenol (DNP, Sigma-Aldrich; 1 mm; 1st inhibitor), while the second setup consisted of live cells, Cu ions and N, N-Dicyclohexylcarbodiimide (DCCD, Sigma-Aldrich; 100 µm; 2nd inhibitor). DNP acts as an uncoupler of the mitochondrial membrane by blocking electron transport, while DCCD is a metabolic inhibitor which blocks ATPase and modifies the carboxyl group. In the third setup, the uptake of Cu ions was evaluated in the presence of both inhibitors (Shamim et al., 2014). All three setups were analyzed by AAS analysis (228.8 nm).

Uptake of Cu by Dead Bacterial Cells

Upon achieving log phase, live cells in the medium were killed by autoclaving. In the next step, Cu was added in the medium (10 mg/l), followed by incubation, growth determination and AAS analysis at hourly intervals as before (Shamim et al., 2014).

Cu Removal Efficacy by Pilot-Scale Study

The efficacy of Cu removal by bacterial cells was evaluated by pilot-scale study. Regular tap water (10 l), and industrial effluents (including Cu; 10 l) were taken in one and two large-sized plastic containers, respectively, to which bacterial culture (1.5 l) was then added to tap water, and one of the effluent containers, respectively. Cu (10 mg/l) was then added to all three containers. Samples were then harvested (15,000 rpm; 10 min) after 4 and 8 day intervals, after which the supernatants were used to evaluate the percentage (%) removal of Cu (Shamim and Rehman, 2012).

Estimation of Antioxidative Enzymes

For the preparation of enzyme extract, inoculation of fresh bacterial cells in medium was performed, followed by incubation at 37°C for 24 h. The next day, Cu (10 mg/l) was added to

the medium which was then incubated again overnight. Control was run parallel to the experimental setup, where no Cu was introduced to the bacterial cells. After sufficient growth, bacterial cells were harvested and extraction buffer [50 mm NaH_2PO_4 (pH 7.5); 1% PVP; 0.5% Triton X-100; 1 mm EDTA] was added to obtained pellet under low temperature (4°C), after the suspension was centrifuged again (Shamim et al., 2014). The supernatant was then accumulated in a sterile falcon tube and was labelled as the enzyme extract, which was then utilized to evaluate the expression of various antioxidative enzymes such as glutathione reductase (GR; Rao et al., 1996), peroxidase (POX; Reuveni et al., 1992), superoxide dismutase (SOD; Beauchamp and Fridovich, 1971), catalase (CAT; Luck, 1965), and ascorbate peroxidase (APOX; Nakano and Asada, 1987).

Metallothionein Profiling

The profiling of metallothioneins was carried out using SDS-PAGE. Bacterial cells (1%) supplemented with Cu (0.1 mm) as well as control were incubated overnight. After 24 h, pellets were obtained by centrifuging cells in the medium. The supernatant was discarded and the pellet obtained was dried thoroughly and homogenized in 1X gel-loading buffer. Protein marker and bacterial samples were loaded into resolving gel (12%) and stacking gel (5%) and the electrophoresis apparatus (Bio-Rad, United States) was supplied with electrical current from the power supply. The protein bands were subsequently visualized by using staining and de-staining solutions (Laemmli, 1970). The quantitative estimation of protein was also performed using Bradford assay (Bradford, 1976).

Evaluation of Bacterial Motility and Chemotaxis in the Presence of Cu

Three patterns of bacterial motility (swimming, swarming, and twitching) were evaluated in the presence and absence of Cu on 0.1, 0.3, and 1.0% of agar, respectively (Murray et al., 2010). Bacterial chemotaxis with and without the supplementation of Cu was also evaluated according to Adler (1973).

Cu Adsorption Isotherm and Kinetic Studies

Isotherm Models

Two isotherm models (Langmuir and Freundlich) were used to determine the suitable mode of biosorption. The Langmuir adsorption isotherm model assumes the biosorption occurs as a monolayer, and was calculated using the following formulae (Wierzba, 2015):

$$\frac{Ce}{q_e} = \frac{Ce}{q_{\max}} + \frac{1}{bq_{\max}} \quad (1)$$

where C_e, q_e is the amount of metal ions in solution and adsorbed at equilibrium state, respectively, whereas q_{max}, and b denotes the Langmuir and adsorption constant, respectively.

The Freundlich adsorption isotherm model assumes heterogeneous biosorption, with binding taking place as a multi-layer of ions stacked onto bacterial cells, and is denoted by the following formulae (Joo et al., 2010):

$$\ln q_e = \ln k_f + \frac{1}{n} \ln Ce \quad (2)$$

where constants of Freundlich isotherm model are represented by K_f and n, respectively.

Kinetic Parameters

The kinetic parameters of Cu biosorption were studied by pseudo-first and second-order kinetic models (Lagergren, 1898; Aksu, 2001), using the following formulae:

$$\ln\left(q_e - q_t\right) = \ln q_e - k_1 t \quad (3)$$

$$\frac{t}{q_t} = \frac{1}{k_2\left(q_e^2\right)} + \frac{t}{q_e} \quad (4)$$

where q_e and q_t represent adsorption of metals ions adsorbed at equilibrium level, and t, k_1 and k_2 denote time and constants of first- and second-order kinetics, respectively.

Thermodynamic Parameters

Gibbs free energy change (ΔG°), enthalpy change (ΔH°), and entropy change (ΔS°) were calculated using the following formulae:

$$\Delta G° = -RT \ln K_D \quad (5)$$

where the constants R, T represent universal gas constant, and temperature (Kelvin), respectively.

Fourier Transform Infrared Spectroscopy Analysis

In order to determine the interaction of bacterial cells with Cu in the medium, FTIR was performed. Samples were prepared by harvesting bacterial cells (24 h) which were previously supplemented with Cu (10 mg/l) as well as control. Samples homogenized in deionized water were then subjected to FTIR analysis in the mid IRF region of 500–4,000/cm^{-1} (Bruker; Deokar et al., 2013).

Scanning Electron Microscopy and Energy-Dispersive X-Ray Spectroscopy Analysis

Bacterial characteristics before and after Cu biosorption were analyzed by SEM, coupled with EDX. Samples were prepared according to the method of Khan et al. (2016), which were then fixed and dehydrated using fixing agent and alcohol. The samples were then freeze-dried and were coated with gold for SEM-EDX analysis (JEOL, Japan).

Statistical Analysis

The experimental and control setups were carried out thrice, accompanied with controls in similar experimental conditions. Standard error, mean and standard deviation were estimated using SPSS (IBM; V. 27.0).

RESULTS

Purification, Screening and Selection of Cu-Resistant Isolate

In the present study, 25 bacterial isolates were obtained from wastewater samples. From these isolates, the most resistant strain was chosen for its minimum inhibitory concentration, which was demonstrated to be 20 mm for Cu. The selected isolate, labelled as SMK-08, also exhibited resistance to varying concentrations of several other heavy metals. The cross heavy metal resistance pattern was observed in the following order; Ni (25 mm) > Zn (20 mm) > Cr (18 mm) > Pb (12 mm) > Ag (10 mm) > Hg (5 mm).

Characterization of Cu-Resistant Isolate

The selected bacterial isolate was identified (morphologically and biochemically) and characterized using 16S rRNA ribotyping, which elucidated the isolate SMK-08 as *Bacillus altitudinis*, which was submitted to GenBank under the accession number MT422188.

Optimal Growth Parameters, Growth in Presence of Cu and EC_{50}

Several growth parameters such as pH, phosphate concentration, and temperature of *B. altitudinis* MT422188 were observed to be pH 7, 1 mm phosphate, and 37°C, which were noted for further experimental setups. The growth curve indicated that the presence of Cu lowered the rate of growth than normal but did not stop it altogether, as shown in **Figure 1**. The effective concentration (EC_{50}) for Cu was observed to be 5.56 mm, depicting that this was the maximal dose at which half the bacterial cells could survive. To validate the results, optical density was obtained (OD = 578 nm) and plotted on the same graph, which demonstrated decline in cellular growth (**Figure 2**).

Cu Biosorption Studies

Cu Uptake by Live Bacterial Cells

Cu adsorption onto the bacterial surface was observed to be maximum at 9th h (1.52 mg/l), which was also indicated by decrease in Cu present in the medium from 2nd h The intracellular accumulation of Cu increased from 3rd h, with maximum uptake at 9th h (0.37 mg/l). Bacterial cells entered logarithmic phase when added to the medium, whereupon the addition of Cu into aqueous medium, the growth of cells slowly increased from 1st to 5th h, with sharp increase from the 6th to 9th h (**Figure 3A**).

Cu Uptake by Live Bacterial Cells in the Presence of Inhibitors

When inhibitor 1 (DNP) was added to the medium in the presence of Cu, the amount of extracellular Cu in the medium decreased from the original concentration (10 mg/l) in the 1st h to 9.75 ± 0.05 mg/l in the 9th h, which was suggestive of Cu uptake by bacterial cells. The adsorption of Cu onto bacterial cell surface started in the 3rd h (0.1 mg/l) but continued to increase slowly till 9th h (0.19 mg/l). Intracellular accumulation of Cu commenced from 6th h (0.01 mg/l), and continued to increase at regular intervals till 9th h (0.05 mg/l). The growth of bacterial cells dipped between 1st and 2nd h due to acclimatation, but an overall increase was observed after cells entered logarithmic phase (**Figure 3B**). In the case of inhibitor 2 (DCCD), once the bacterial cells were introduced in the medium, growth dipped at 2nd h, but sharply increased at 7th h Cu adsorption started at 3rd h (0.05 mg/l) which increased at regular intervals up until 9th h (0.16 mg/l). Intracellular accumulation of Cu commenced from 6th (0.01 mg/l) to 9th h (0.05 mg/l), which was due to the action of DCCD and resulted in the slow but active uptake of Cu from the medium (**Figure 3C**). In the presence of Cu and both inhibitors in the same experimental setup, the adsorption and intracellular accumulation were found to be decreased than the other sets, but the cells were still regulating uptake of Cu, starting at the 6th h till 9th h (0.02 mg/l). Cu adsorption also started at 2nd h, with only 0.02 mg/l adsorbed at 9th h (**Figure 3D**).

Cu Uptake by Dead Bacterial Cells

The dead bacterial cells were not able to grow exponentially in the growth medium as they were inactivated *via* heat. Due to no active uptake process, most of the metal remained in the medium, but the surface of dead bacterial cells provided enough surface area for adsorption onto bacterial cells, which started in 2nd h (0.01 mg/l) and continued till 9th h (0.06 mg/l; **Figure 3E**).

Cu Removal Efficacy by Pilot-Scale Study

Bacillus altitudinis MT422188 cells was able to remove 73 mg/l and 82 mg/l at 4 and 8 day intervals, respectively, from distilled water which contained Cu, whereas the bacterial cells removed 52 and 68 mg/l at day 4 and 8, respectively, from industrial effluent. On the other hand, the original microbial flora of the industrial effluent removed 18 and 28 mg/l at day 4 and 8, respectively, demonstrating that *B. altitudinis* MT422188 is more efficient in removing Cu, as shown in **Figure 4**.

Estimation of Antioxidative Enzymes

In *B. altitudinis* MT422188, expression of antioxidative enzymes with and without Cu yielded the increased expression of GR, SOD, and POX. CAT and APOX activity were not induced in either the control or experimental setup (**Table 1**).

Metallothionein Profiling by SDS-PAGE

In bacterial sample (control) without Cu, the induction of several proteins was observed (100, 51, 35, 30, 27, 15, 14, and 12 kDa), whereas in the experimental sample, the presence of Cu elucidated protein of molecular weight 70 kDa among other proteins, suggesting the presence of metallothionein (**Figure 5**).

Bacterial Motility and Chemotaxis in the Presence of Cu

The motility experiments demonstrated remarkable patterns of bacterial movement. Swimming and swarming pattern enabled

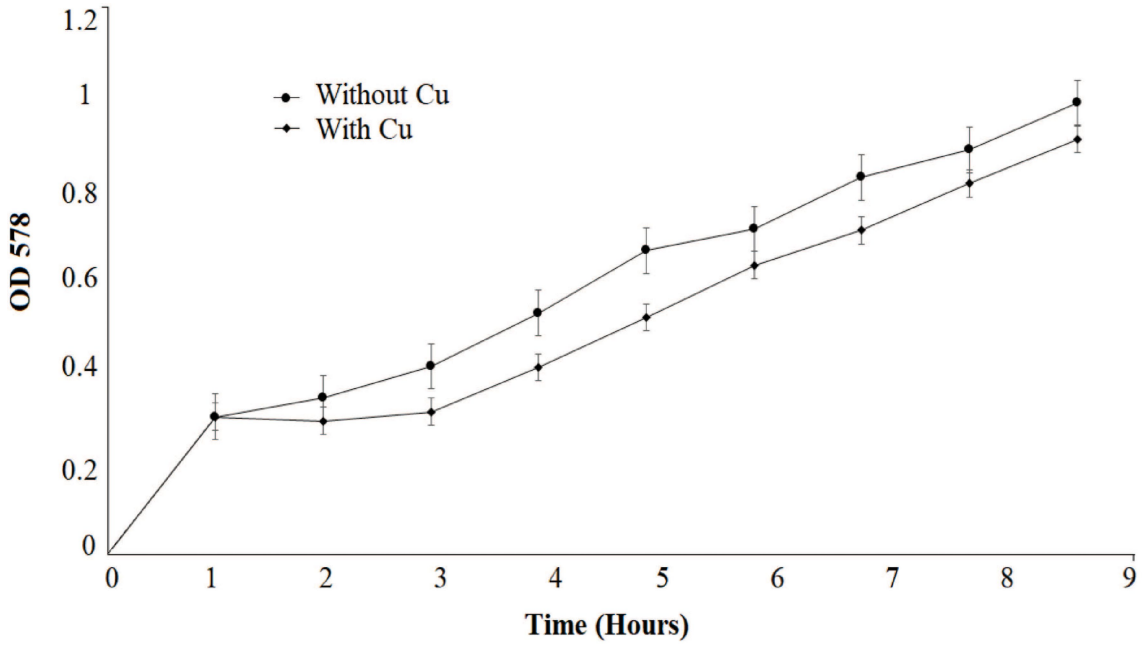

FIGURE 1 | Growth pattern of *Bacillus altitudinis* MT422188 with Cu (0.1 mm) and control.

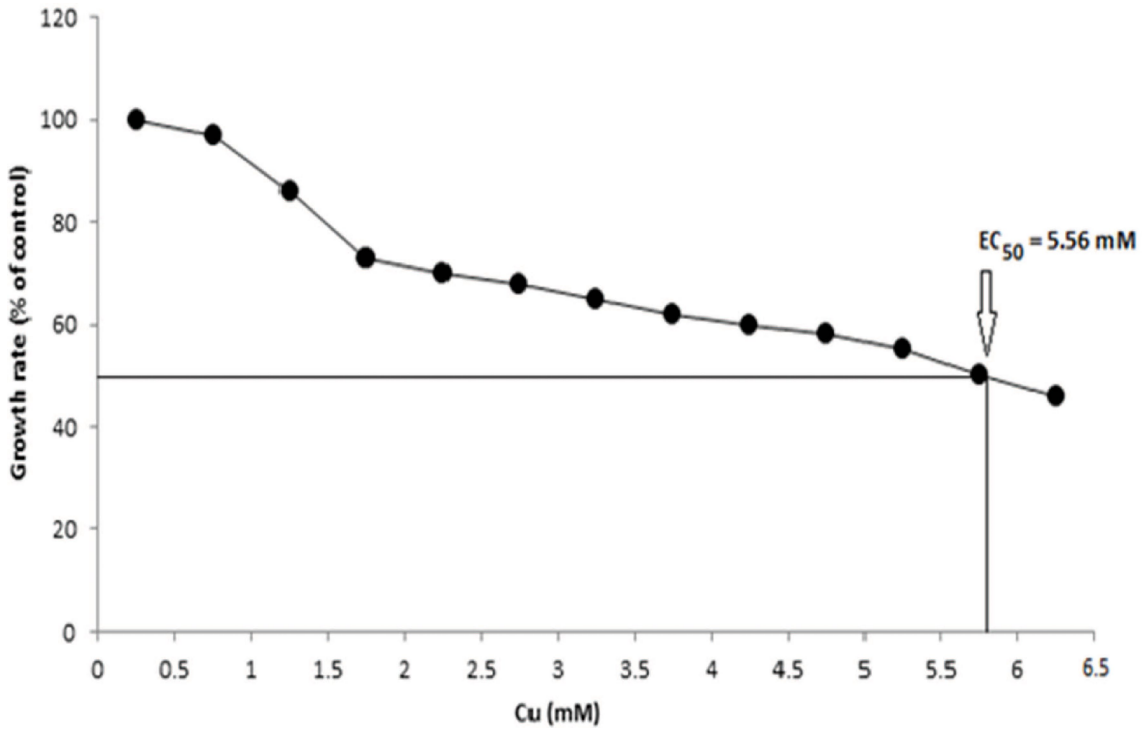

FIGURE 2 | EC_{50} of *B. altitudinis* MT422188 with Cu.

the bacterial cells to cover the entire agar plate, indicating the cells moved freely in the presence of Cu (**Figures 6A,B**). Twitching motility, however, was less pronounced (**Figure 6C**). Chemotaxis experiments demonstrated that Cu acted as a chemoattractant for *B. altitudinis* cells, which subsequently activates bacterial flagellar movements resulting in motion toward Cu ions (**Figure 7**).

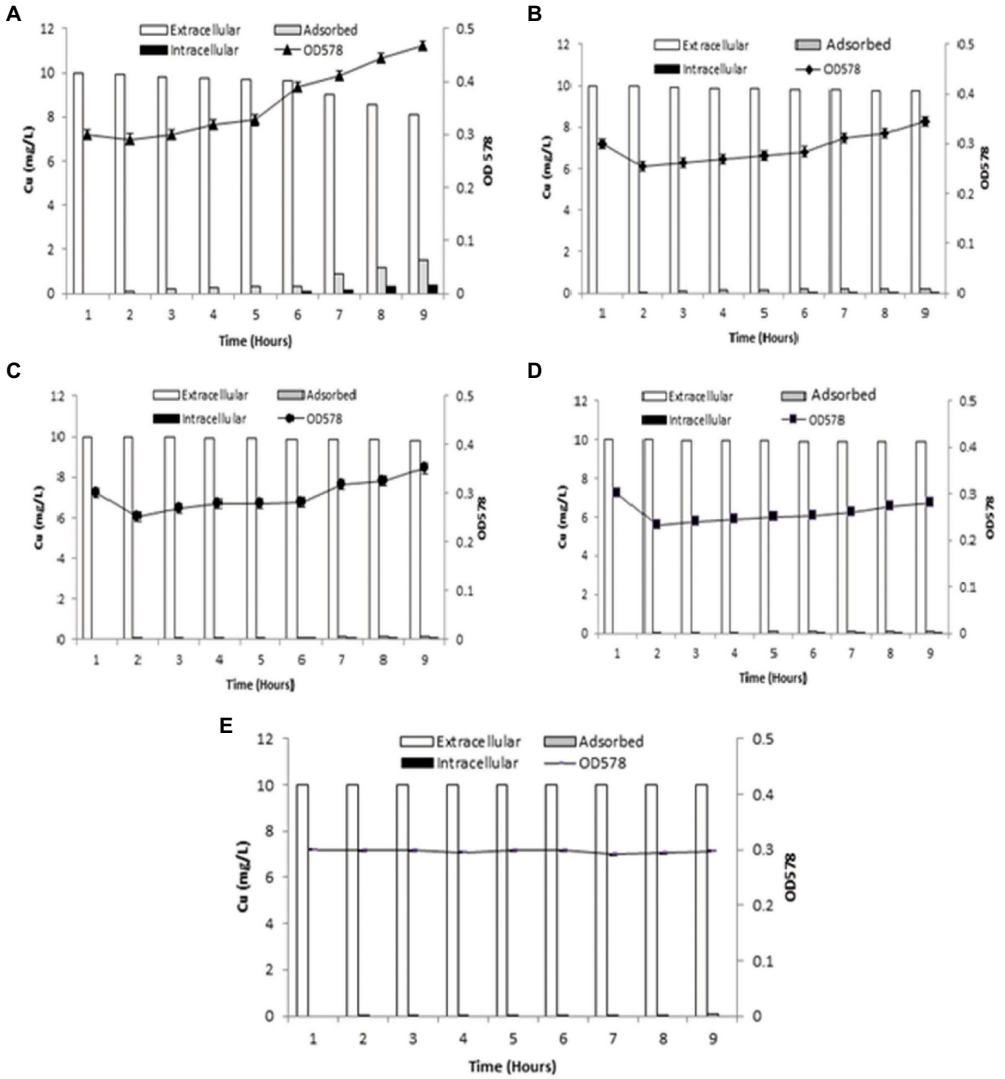

FIGURE 3 | Graphs demonstrating biosorption by *B. altitudinis* MT422188 **(A)** for Cu (10 mg/l; **B**) for Cu (10 mg/l) and DNP (1 mm; **C**) for Cu (10 mg/l) and DCCD (100 μm; **D**) for Cu (10 mg/l), DNP (1 mm) and DCCD (100 μm; **E**) for dead cells and Cu (10 mg/l).

Cu Adsorption Isotherm and Kinetic Order Studies

Isotherm Models

Two isotherm models were applied for investigating adsorption of Cu ions onto bacterial cells. The correlation coefficient (R^2) values of Langmuir isotherm were in the range of 0.90–0.95, which was less than the R^2 values of the Freundlich isotherm (0.955–0.999; **Table 2**), which is why the latter was the suitable model for our work.

Kinetic Parameters

The parameters of pseudo-first- and second-order kinetics are given in **Table 3**. Graphs for first-order were plotted with ln (qe-qt) and qt on the *y*- and *x*-axis, respectively. Correlation coefficients (R^2) for first-order were in the range of 0.9993–0.997, but the values of the experimental and calculated coefficient (q_{exp} and q_{cal}) were not in tandem with the values of the equilibrium constant (q_e). In the case of pseudo-second order, the R^2 values were in the range of 0.98–0.99, and the equilibrium constants were also in agreement to the experimental and calculated constants, which therefore implicated the pseudo-second-order to be better fitted for our study (**Table 3**).

Thermodynamic Parameters

Gibbs free energy (ΔG°) for 10, 25, 37, and 45°C was calculated to be −9.3719, −9.64062, −9.6609, and −4.1655 kJ/mol, respectively. The entropy change (ΔS°) was demonstrated to be 0.0006 kJ/mol/K, while the enthalpy change (ΔH°) was observed to be 10.431 kJ/mol (**Table 4**).

Fourier Transform Infrared Spectroscopy Analysis

The FTIR peaks elucidated several functional groups which interacted with Cu ions. The peak of 1637.22 cm^{-1} demonstrated

C═O stretching of amide I, as well as the C═O peptide bond of carboxyl groups, whereas peaks of 3279.39 cm^{-1} was characteristic of hydroxyl, amine, and carboxyl groups in the control, which was determined with the help of peak shifts in experimental and control samples.

Scanning Electron Microscopy and Energy-Dispersive X-Ray Spectroscopy Analysis

SEM analysis represented changes in the bacterial cellular morphology and shape after the addition of Cu, where the cells appeared to be a bit flattened and elongated in shape, as compared to bacterial cells which grew without the addition of Cu (**Figures 8A,B**). EDX analysis represented Cu to be part of the main elements which interacted with the bacterial cell (**Figures 9A,B**).

DISCUSSION

The sources of heavy metal contamination in the environment have increased in the past few decades, giving rise to many grave predicaments in nature. It has been a challenge to decontaminate industrial wastewater and soil from heavy metals. Different strategies have been designed and implemented for their removal, including filtration, oxidation/reduction, reverse osmosis and electro-chemical treatment among many others, but are not the favored option due to their cost, inefficiency, and intense labor (Algieri et al., 2021). This research work was carried out to investigate the bioremediation ability of chosen bacterial isolate for removing Cu from contaminated wastewaters. In this study, the chosen strain was identified as *Bacillus altitudinis* MT422188, which was isolated from the industrial areas of Kala Shah Kaku and Muridke, known for their miscellaneous industries and contamination of surrounding areas. It was affirmed in a previous study that a major share of bacteria isolated from heavy metal contaminated environments are Gram positive in nature, and are particularly members of the genus *Bacillus* (Aka and Babalola, 2017).

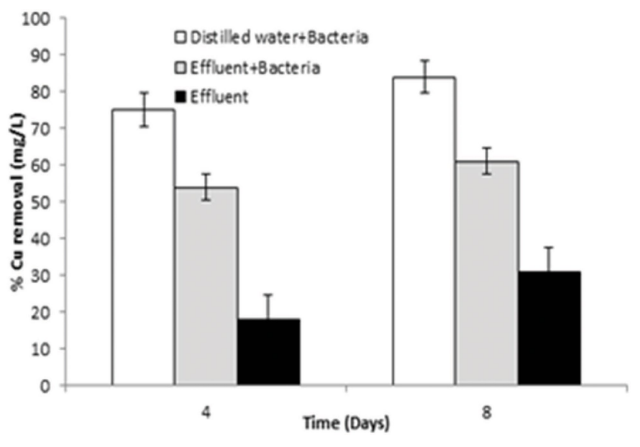

FIGURE 4 | Graph of pilot scale study for biosorption of Cu (10 mg/l) by *B. altitudinis* MT422188 after 4 and 8 days, respectively.

Cu-resistant bacteria isolated from various sources have been previously reported (Rathi and Nandabalan, 2017; Bhardwaj et al., 2018; Irawati and Tahya, 2021). In our study, the minimum inhibitory concentration (MIC) of *B. altitudinis* MT422188 for Cu was observed to be 20 mm, which was in agreement with the results of Mustapha and Halimoon (2015). The cross metal resistance behavior was also investigated (Ni > Zn > Cr > Pb > Ag > Hg). Rohini and Jayalakshmi (2015) reported the resistance of *Bacillus cereus* against Cu and more heavy metals. *B. subtilis* was reported to be capable of tolerating Cr and Cu upto 20 and 80 mm, respectively (Khusro et al., 2014). *Bacillus* sp. was found to have a high tolerance to many metals, with the most resistance observed against Cu at 12.5 mm, in a study conducted by Esertaş et al. (2020). Similar observations for *Bacillus* sp. were reported in another study (Singh and Chopra, 2014; Gillard et al., 2019). Prior to conducting further experimentation, the growth parameters such as pH, temperature, and phosphate concentration of *B. altitudinis* MT422188 were studied, where it demonstrated favorable growth at pH 7, 37°C, and 1 mm phosphate, respectively. *B. licheniformis* was also reported to demonstrate optimum growth at 37°C and pH 7 (Sher et al., 2021). pH has a pronounced effect on the solubility of heavy metal ions and the charge on the cell surface, which aids greatly in removing the former from contaminated media (Jin et al., 2018), and optimal pH (4–8) is reported to be significantly associated with all biomass forms (Sánchez-Clemente et al., 2020). The growth curves of *B. altitudinis* MT422188 were studied in the presence and absence of Cu, where its presence extended the lag phase of the bacterial cells for a short period of time and did not stop the growth, but resulted in its overall decrease (**Figure 1**). Similar growth characteristics were observed in *B. licheniformis* in the study of Sher et al. (2021). No effect of Cu on the final growth of *B. stearothermophilus* cells was observed when it was added to medium in a study (Bubela, 1973). In another study, *Bacillus* sp. demonstrated remarkable growth pattern in the absence of Cu, but the overall growth was observed to be decreased in the presence of increasing Cu concentrations (Khan et al., 2017), which was also evident from the findings of our study. Cu ions did not affect growth of *B. thuringiensis* cells greatly, indicating that they survived and grew in low concentrations

TABLE 1 | Expression of antioxidative enzymes of *Bacillus altitudinis* MT422188 with and without Cu.

Experiment	GR ($Ug^{-1}FW$)	POX ($Ug^{-1}FW$)	SOD ($Ug^{-1}FW$)	APOX ($Ug^{-1}FW$)	CAT ($Ug^{-1}FW$)
B. altitudinis with Cu	0.004 ± 0.002	0.061 ± 0.004	0.160 ± 0.005	–	–
B. altitudinis without Cu	0.001 ± 0.003	0.003 ± 0.001	0.091 ± 0.003	–	–

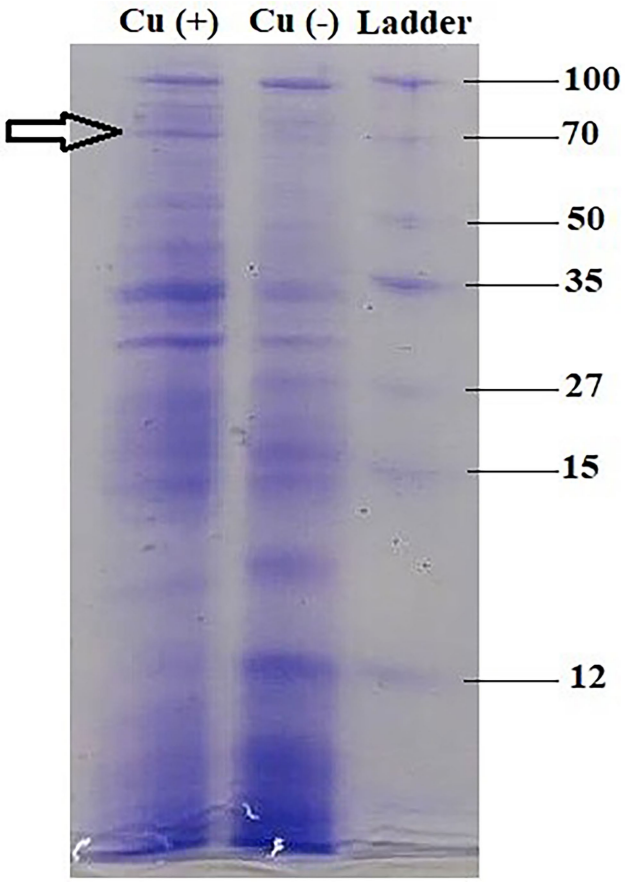

FIGURE 5 | Metallothionein profiling of *B. altitudinis* MT422188 *via* SDS-PAGE.

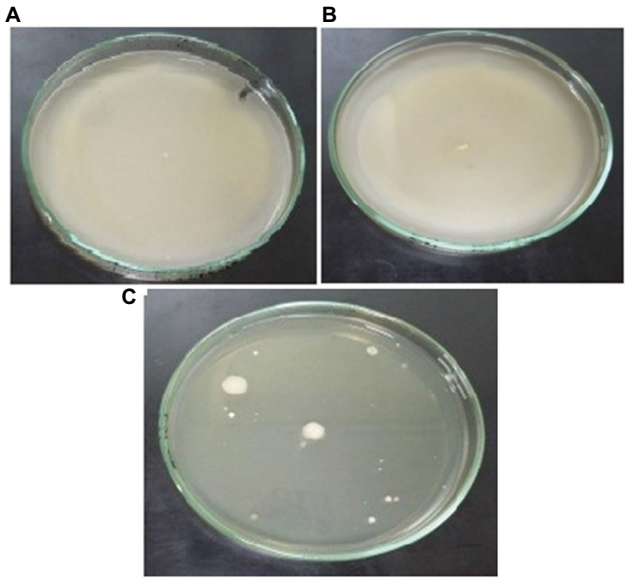

FIGURE 6 | Motility patterns of **(A)** swimming, **(B)** swarming, and **(C)** twitching behavior of *B. altitudinis* MT422188 with Cu (10 mg/l).

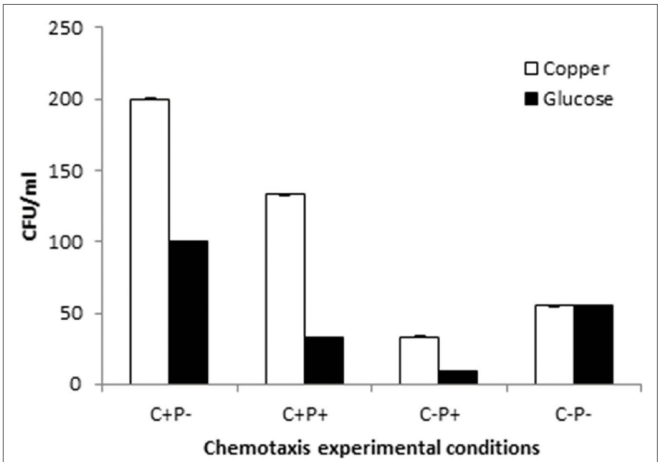

FIGURE 7 | Chemotactic pattern of *B. altitudinis* MT422188 in 4 different setups with Cu and control (glucose). (+) = Cu present, (–) = Cu absent, C = capillary, and P = pond.

of the metal (Liu et al., 2020). The half maximal effective concentration (EC_{50}) is considered to be the initial concentration of the metal ions at which the activity of the bacterial cells in the presence of metal is comparable to that of 50% of the control culture in the absence of the metal. Due to this aspect, EC_{50} is a determinative parameter that defines the toxicity of metals with respect to bacterial cells. In this study, EC_{50} of *B. altitudinis* for Cu was 5.56 mm, demonstrating that this was the dose at which 50% of the bacterial cells would survive in the presence of Cu (**Figure 2**). Utgikar et al. (2001) reported the EC_{50} for Cu in their study to be <0.1 mm.

The biosorption studies depicted that in the case of Cu, the amount of extracellular Cu from the medium decreased proportionally from 7th h onwards, particularly due to the increased adsorption of Cu onto the bacterial cells, as well as some of the Cu being accumulated at intracellular level by bacterial cells, indicating that some of Cu was used for the performance of their essential functions. Growth of bacterial cells also noticeably increased after the first 6 h (**Figure 3A**). When DNP (inhibitor 1) was added to the medium containing Cu and bacterial cells, less pronounced but still eminent uptake was observed as there was some decrease in total Cu present in the medium. Adsorption of Cu also occurred, albeit slowly, from the 3rd to 9th h, while intracellular accumulation of Cu took place in the last 3 h (**Figure 3B**). DCCD (inhibitor 2) reduced the uptake of Cu from the medium but did not halt it altogether. Adsorption commenced from the 3rd h which continued till 9th h, while the intracellular accumulation was the same as in the case of DNP (**Figure 3C**). In the presence of both inhibitors and Cu, the bacterial growth rate was reduced. The adsorption and accumulation were also decreased but still occurred nevertheless, indicating that an ATP independent efflux system was employed by *B. altitudinis* MT422188 (**Figure 3D**). The most commonly reported Cu efflux system in bacterial species is encoded by the *copZA* operon, which

TABLE 2 | Cu adsorption isotherm model constants of *B. altitudinis* MT422188.

Experiments	Langmuir isotherm			Freundlich isotherm		
	q_{max}	b	R^2	n	K_f	R^2
Live cells + Cu	4.504	0.0015	0.9515	1.83	1.574	0.9999
Live cells + Cu + DNP	4.699	0.0025	0.9058	1.828	1.545	0.9999
Live cells + Cu + DCCD	3.381	0.0006	0.9206	1.752	1.536	0.997
Live cells + Cu + DNP + DCCD	1.594	0.0005	0.9331	1.75	1.535	0.9996
Dead cells + Cu	9.19	0.0482	0.9237	2.069	0.676	0.9557

TABLE 3 | Pseudo-order (first and second) kinetic model constants for *B. altitudinis* MT422188 biosorption.

Experiments	Pseudo first-order				Pseudo second-order		
	q_{exp}	k_1	q_{cal}	R^2	k_2	q_{cal}	R^2
Live cells + Cu	9.11	0.052	2.612	0.9995	0.434	8.438	0.989
Live cells + Cu + DNP	8.88	0.051	2.581	0.9936	0.669	10.44	0.9883
Live cells + Cu + DCCD	8.57	0.0512	2.542	0.9999	1.836	9.8619	0.9974
Live cells + Cu + DNP + DCCD	8.14	0.0535	2.485	0.9998	0.658	10.537	0.9884
Dead cells + Cu	2.11	0.2141	1.383	0.9978	0.5594	10.706	0.9881

TABLE 4 | Thermodynamic parameters for *B. altitudinis* MT422188 biosorption.

Thermodynamic parameters			ΔG° (kJ/mol)			
	ΔH° (kJ/mol)	ΔS°(kJ/mol/K)	10°C (283.15 K)	25°C (298.15 K)	37°C (310.15 K)	45°C (318.15 K)
Values	10.431	0.0006	−9.3719	−9.64062	−9.6609	−4.1655

is essential for inducing resistance to excessive levels of Cu. CueR is a protein which regulates cytosolic Cu and the operon encoding both Cu chaperones and ATPases for efflux, respectively (Gaballa and Helmann, 2003). CopZ serves the key role as chaperone for delivering Cu to CopA, a CPx-type ATPase, whereas CopB in the operon is responsible for Cu efflux and detoxification (Smaldone and Helmann, 2007; **Figure 10**).

In many studies, live or dead biosorbents have been used to deduce their efficiency in removing heavy metals from contaminated environments. It has been reported that rendering a bacterial biosorbent inactive by heat (autoclaving) strengthens its efficacy of biosorption (Paul et al., 2012). Therefore, passive uptake seems to be the major mechanism of biosorption in killed cells, as compared to the active uptake in live cells, respectively (Shamim et al., 2014). In this study, the killed cells of *B. altitudinis* MT422188 were able to remove Cu ions from the environment (**Figure 3E**), the findings of which were consistent with the study findings of Todorova et al. (2019) and Hu et al. (2020). In the pilot scale study, *B. altitudinis* MT422188 was able to remove 73 mg/l and 82 mg/l at 4 and 8 day intervals, which demonstrated its biosorption ability to be efficient in removing Cu (**Figure 4**). *B. cereus* has been reported to effectively remove more than 40 and 50% of Cu from industrial effluents (Raj et al., 2018).

Environmental factors like heavy metal stress can act as key inducers of ROS production, which are directly associated with cell death due to the alteration of intracellular redox stats of the cell (Franco et al., 2009). This increased level of ROS species in the cell can induce a state of "oxidative stress" which can be triggered by toxic concentrations of heavy metal ions and metalloids anions in the cell (Kumagai and Sumi, 2007). In order to combat this, high concentrations of heavy metal ions stimulate the increase in the activity of defense antioxidative enzymes, of which SOD and CAT are the first responders (Choudhary et al., 2007). The presence of divalent or monovalent heavy metal cations, including Cu, can induce the production of ROS through Fenton and Haber-Weiss reactions (Gunther et al., 1995). In our study, the increased activities of SOD, POX, and GR in the presence of Cu was indicative that Cu acted as a stress of *B. altitudinis* MT422188 cells, while CAT and APOX demonstrated no activity (**Table 1**). High concentrations of heavy metals are reported to trigger oxidative and non-oxidative stress, suggesting increased levels of ROS in metal stressed bacterial cells (Steunou et al., 2020). Cu-Zn SODs were previously thought to be specific to eukaryotes but are now reported to be present in many bacterial species, including *Bacillus* (Argüello et al., 2013). It is pertinent to note that the presence of Cu may have possibly induced the

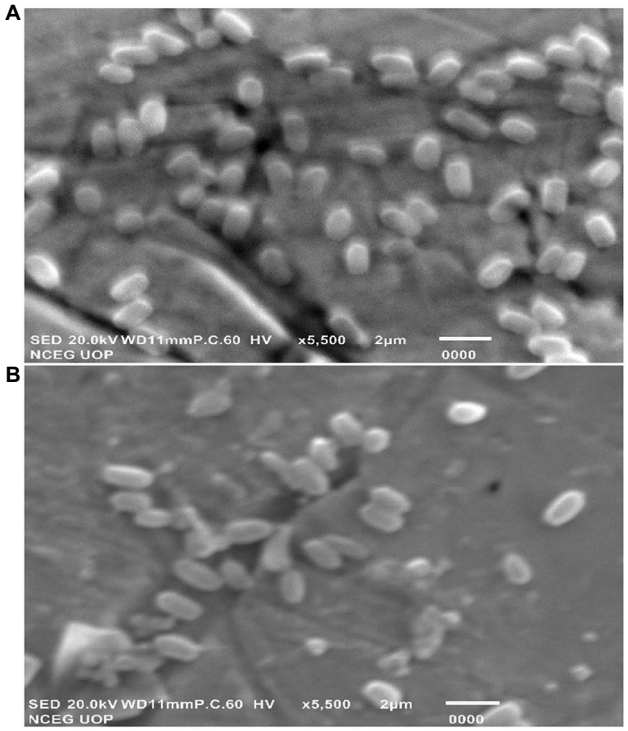

FIGURE 8 | SEM micrographs of *B. altitudinis* MT422188 **(A)** with **(B)** without Cu.

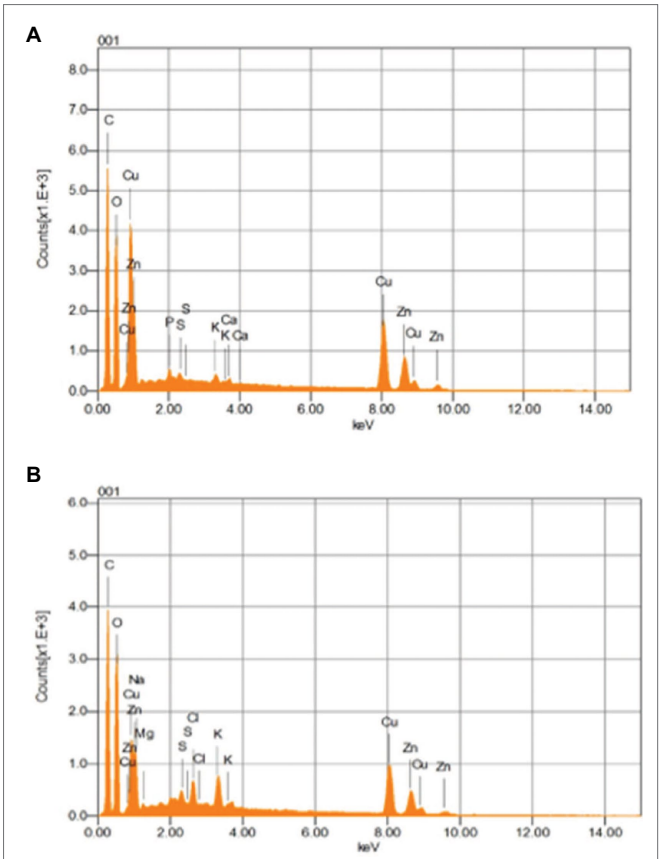

FIGURE 9 | EDX images of *B. altitudinis* MT422188 in **(A)** with **(B)** without Cu.

enhanced activity of Cu-Zn SOD in our study. The study findings of Wiesemann et al. (2013) demonstrated elevated SOD activity for mitigating ROS-mediated stress in cells. Another study demonstrated increased CAT activity in the face of elevated H_2O_2 stress (Behera et al., 2014), while Latef et al. (2020) reported the elevated POX activity and decreased CAT activity during oxidative stress, respectively. Metallothioneins (MTs) are proteins that are low in weight and abundant in cysteine, which also bind to heavy metal ions with remarkable avidity, and aid in regulating high toxic metal concentrations as well as metal homeostasis (Gadd, 2010). It is reported to be found in many microorganisms including bacteria and fungi, as well as eukaryotes such as plants, animals, and human beings (Chaturvedi et al., 2012). The findings of our study elucidated the presence of a 70 kDa MT protein in *B. altitudinis* MT422188 in the presence of Cu (**Figure 5**). Another study also reported the role of MT in removing metal ions from the environment *via* sequestration (Mulik et al., 2018). Copper homeostasis involves sequestration, efflux or detoxification as shown in **Figure 11**. Although essential for the cellular processes, concentrations of Cu^{2+} above 10 µm becomes toxic for the microbial cell. The detoxification mechanisms (Rohini and Jayalakshmi, 2015) are mentioned in **Figure 11**. During efflux mechanism, CopZ acts as chaperone and converts Cu^{2+} to Cu^{+} which ultimately enters the cells *via* CopA protein. CopB protein is associated with ATPase which is energy dependent and helps in Cu^{+} efflux out of the cell (Alotaibi et al., 2021; **Figure 10**). To the best of our knowledge, copper sequestration by MTs as well as uptake and efflux mechanisms regulated by copZA operon are apparently involved in copper homeostasis in *B. altitudinis*, as observed in our study.

Motility, particularly in bacteria, is generated by flagellae which enable bacteria to move forward through various movements. There are six different types of movements which cause bacterial motility, such as swimming, swarming, twitching, gliding, sliding, and darting, of which the first two are caused by flagellar movements (Prabhakaran et al., 2016). In our study, swimming, swarming, and twitching patterns of *B. altitudinis* MT422188 were found to be positive in the presence of Cu, which resulted in enhanced motile behavior in bacterial cells (**Figures 6A–C**). Enhanced motility was also observed in *Bacillus* sp. in the presence of Cu (Singh et al., 2014). In another study, the positive motility and chemotactic behavior of *B. safensis* was reported in the presence of manganese (Mn) ions (Ran et al., 2020). Chemotaxis is a process which involves the regulation of movement away or toward the concentration gradient of specific stimuli or stresses, acting either as attractant and repellent factors, respectively (Vladimirov and Sourjik, 2009). Chemotaxis in bacteria is regulated *via* a chemo-sensory pathway which involves several key proteins which initiate the movement away or toward an external stimulus. In this study, Cu acted as a chemoattractant for the cells, meaning that bacterial cells in

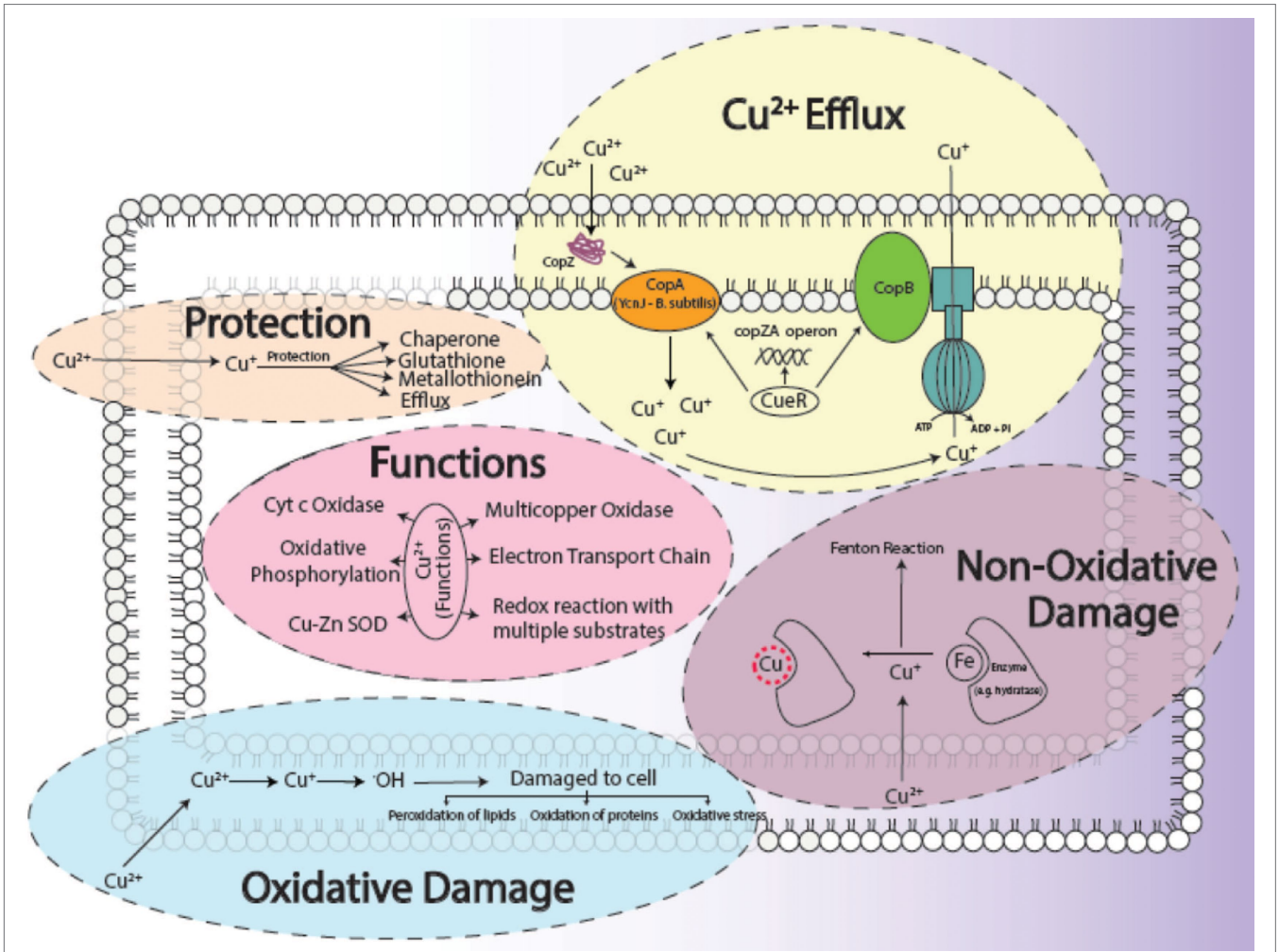

FIGURE 10 | General aspects of copper metabolism in bacterial cells, where it acts as a causative agent for copper-mediated oxidative stress (Ladomersky and Petris, 2015), non-oxidative stress, its efflux (Alotaibi et al., 2021), its major functions (Bondarczuk and Piotrowska-Seget, 2013) in the cell as well as how a cell protects (Giachino and Waldron, 2020) itself from its harmful effects. The conversion of Cu^{2+} to Cu^{+} results in the production of ·OH ions, which damages the cells. The replacement of Fe with Cu^{+} initiates the Fenton reaction which ultimately harms the survival of the cell.

solution tended to move toward Cu ions, which initiated flagellar motions of movement in *B. altitudinis* MT422188 (**Figure 7**).

For the determination of suitable adsorption isotherm, the biosorption data were examined with two mathematical models (**Table 2**). The study findings indicated biosorption was well-fitted by the Freundlich model ($R^2 \geq 0.98$). The Langmuir isotherm model suggests that the process of adsorption is homogenous which occurs at specific sites in the adsorbent, while the Freundlich model suggests the adsorption occurs on a heterogenous surface with varying levels of biosorption affinities. The binding sites with a remarkably stronger binding energy tend to be involved primarily, followed by the exponential decline in the adsorptive energy until the whole process is completed (Pandhare et al., 2013). The Freundlich intensity constant (n) is regarded to be independent of the metal ion concentration, where $n > 1$, $1/n < 1$, $1/n > 1$ are suggestive of adsorption in favorable conditions, normal adsorption, and co-operative adsorption, respectively. In our study, the value of n was found to be greater than 1, which indicated the favorable biosorption of Cu ions. The results were in agreement with other studies which was also reported the Freundlich isotherm model to be well-fitted for *Bacillus* sp. (Liu et al., 2013; Kanamarlapudi and Muddada, 2019). In another study, the same model was also observed to be opted by *Lactobacillus fermentum* for the biosorption of Cu ions (Kargar and Shirazi, 2020). The study of kinetic parameters is important for the examination of the binding processes which can aid in elucidating reaction pathways and their mechanisms of action for subsequent biosorption. In order to determine the kinetic parameters of Cu for *B. altitudinis*, the pseudo-order (first and second) kinetics were investigated (**Table 3**), which demonstrated pseudo-second-order kinetics to be more suitable for our results than the former. Yang et al. (2017) also described the pseudo-second-order to be well-fitted with their study of Cu biosorption. Change in free energy, enthalpy and entropy ($\Delta G°$, $\Delta H°$, and $\Delta S°$, respectively) were calculated in this study in order to

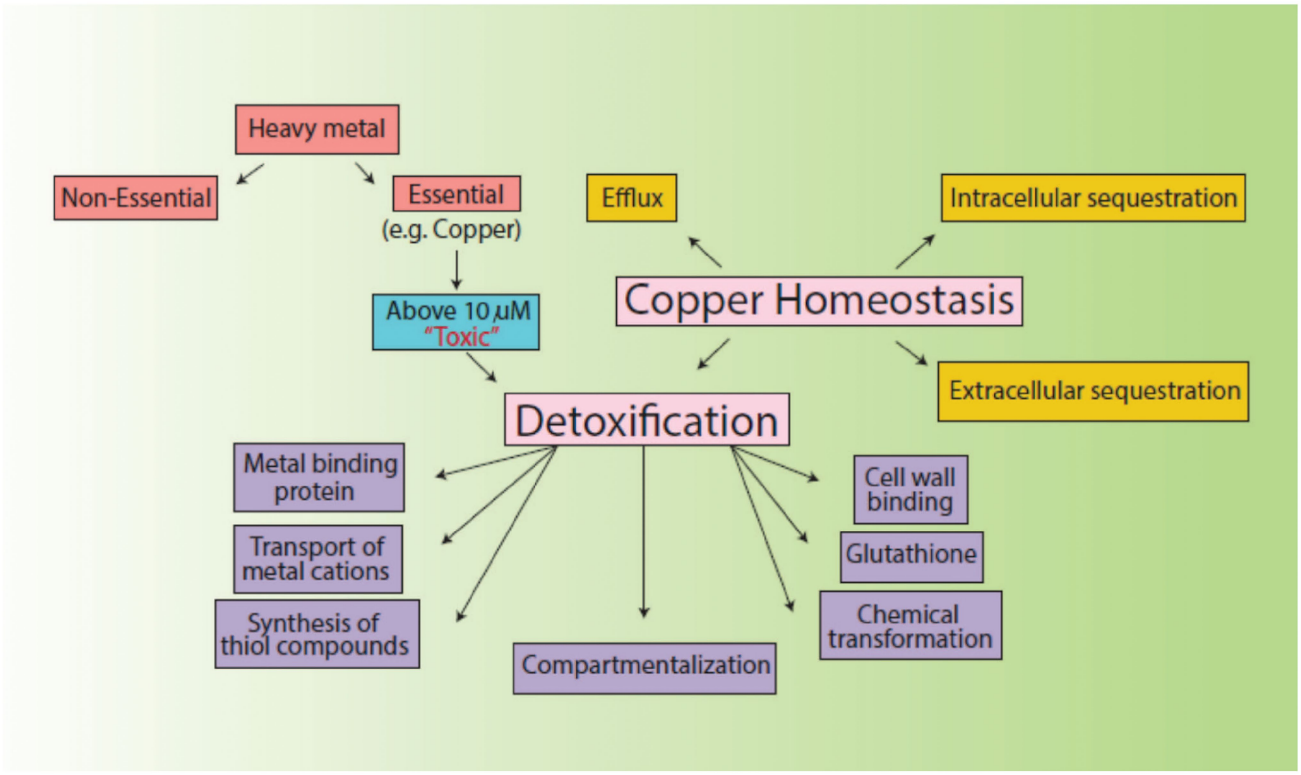

FIGURE 11 | Mechanisms of copper homeostasis and detoxification.

evaluate the thermodynamic patterns of Cu biosorption onto *B. altitudinis* cells. ΔG° was observed to be −9.3719, −9.64062, −9.6609, and −4.1655 kJ/mol, respectively (**Table 4**). The negative values of free energy change were suggestive of the thermodynamically feasible nature of the biosorption process. The enthalpy change (ΔH°) was found to be 10.431 kJ/mol, which indicated that Cu biosorption by *B. altitudinis* MT422188 was an endothermic process. ΔS° demonstrated the reaction to be feasible due to increased randomness at solid–liquid interface, which also agreed with the works of Kaparapu and Prasad (2018) and Sonawdekar and Gupte (2020).

The interaction of Cu with bacterial cell was investigated by FTIR. Peaks after Cu biosorption demonstrated slight shift in various functional groups such as hydroxyl (═OH) and carboxyl (−C═O). These peaks were indicative of Cu ion adsorption onto bacterial cells, with the cell membrane and its functional groups playing a significant part in the binding of metal ions, respectively. Many studies reported similar bands of biosorption peaks (Yang et al., 2017; Palanivel et al., 2020). SEM and EDX analyses yielded the physicochemical changes in bacterial cells in the presence of Cu, which was analyzed through SEM micrographs. These changes after Cu biosorption pertained to structural changes in bacterial cells, which were noted to be irregular and more flattened in shape as compared to cells prior Cu biosorption, as shown in **Figures 8A,B**. Changes in the shape of bacterial cells in response to metal ions has been reported previously by Yang et al. (2017). The changes in bacterial cells in the presence of Cu were also observed by EDX analysis, where sharp, intensified peaks in the range of 0–2 keV and at 8 keV corresponded to the presence of Cu signals in the spectrum, which was less pronounced in the control sample (**Figures 9A,B**). Our study findings were in agreement with Matilda et al. (2021).

CONCLUSION

This research work was conducted to investigate a Cu-resistant bacterium for its potentially efficient ability to remove Cu from polluted wastewater. The selected bacterial isolate SMK-08, identified as *Bacillus altitudinis*, was observed to optimally grow at pH 7, 1 mm phosphate, and 37°C, while its EC_{50} (for Cu) was observed to be 5.56 mm. Biosorption studies indicated the efflux and uptake of Cu in bacterial cells to be an ATP independent process, whereas in the pilot scale study the efficient removal of Cu by *B. altitudinis* MT422188 (73 mg/l and 82 mg/l of Cu at 4 and 8 day intervals) was indicative of its efficacy. Chemotaxis and motility demonstrated positive chemoattractant behavior by *B. altitudinis* MT422188 cells for Cu. GR, SOD, and POX activity in bacterial cells was elevated in the presence of copper, while no expression of CAT and APOX activity was observed in either the presence or absence of Cu. Isotherm study demonstrated the Freundlich model to be the closest fit to the study, while the pseudo-second-order was suited in the kinetics of the study. The thermodynamic parameters depicted the overall process of

biosorption to be spontaneous and feasible. FTIR demonstrated interaction of bacterial −OH and −C═O groups with Cu after biosorption, while the SEM and EDX analyses were indicative of the interactions of Cu ions with the bacterial cell wall and other components, resulting in physicochemical changes. Taking these properties presented in our study into consideration, it could be stated that *B. altitudinis* MT422188 is an efficient biosorbent for Cu, and can be employed for its remediation.

DATA AVAILABILITY STATEMENT

The datasets presented in this study can be found in online repositories. The names of the repository/repositories and accession number(s) can be found in the article/supplementary material.

AUTHOR CONTRIBUTIONS

MK performed all the experimentations, writing-review, and editing. MK, RK, MH, AE, and HS performed data analysis, validation, writing–review and editing, and resources. MZ helped in execution and validation of the experimentations. MA facilitated critical review on pre-publication stages. SS conceived and designed the experimental strategies and was the main supervisor of the whole project. All authors contributed to the article and approved the submitted version.

FUNDING

This research was funded by Taif University Researchers Supporting Project number (TURSP - 2020/59), Taif University, Taif, Saudi Arabia.

ACKNOWLEDGMENTS

The authors extend their appreciation to Taif University, Taif, Saudi Arabia for funding current work under Taif University Researchers Supporting Project number (TURSP - 2020/59).

REFERENCES

Adler, J. (1973). A method for measuring chemotaxis and use of the method to determine optimum conditions for chemotaxis by *Escherichia coli*. *J. Gen. Microbiol.* 74, 77–91. doi: 10.1099/00221287-74-1-77

Aka, R. J. N., and Babalola, O. O. (2017). Identification and characterization of Cr-, Cd-, and Ni-tolerant bacteria isolated from mine tailings. *Biorem. J.* 21, 1–19. doi: 10.1080/10889868.2017.1282933

Aksu, Z. (2001). Equilibrium and kinetic modeling of cd (II) biosorption by *C. vulgaris* in batch system: effect of temperature. *Sep. Purif. Technol.* 21, 285–294. doi: 10.1016/S1383-5866(00)00212-4

Algieri, C., Chakraborty, S., and Candamano, S. (2021). A way to membrane-based environmental remediation for heavy metal removal. *Environment* 8, 52–71. doi: 10.3390/environments8060052

Alotaibi, B. S., Khan, M., and Shamim, S. (2021). Unraveling the underlying heavy metal detoxification mechanisms of bacillus species. *Microorganisms* 9, 1628–1659. doi: 10.3390/microorganisms9081628

Alves, D. A. S., Botelho, A. B. Jr., Espinosa, D. C. R., Tenório, J. A. S., and Baltazar, M. P. G. (2022). Copper and zinc adsorption from bacterial biomass – possibility of low-cost industrial wastewater treatment. *Environ. Technol.*, 1–10. doi: 10.1080/09593330.2022.2031312

Argüello, J. M., Raimunda, D., and Padilla-Benavides, T. (2013). Mechanisms of copper homeostasis in bacteria. *Front. Cell. Infect. Microbiol.* 3:73. doi: 10.3389/fcimb.2013.00073

Babar, Z., Khan, M., Chotana, G. A., Murtaza, G., and Shamim, S. (2021). Evaluation of the potential role of *Bacillus altitudinis* MT422188 in nickel bioremediation from contaminated industrial effluents. *Sustain. For.* 13:53. doi: 10.3390/su13137353

Beauchamp, C., and Fridovich, I. (1971). Superoxide dismutase: improved assays and an assay applicable to acrylamide gels. *Anal. Biochem.* 44, 276–287. doi: 10.1016/0003-2697(71)90370-8

Behera, M., Dandapat, J., and Rath, C. C. (2014). Effect of heavy metals on growth response and antioxidant defense protection in *Bacillus cereus*. *J. Basic Microbiol.* 54, 1201–1209. doi: 10.1002/jobm.201300805

Bhardwaj, R., Gupta, A., and Garg, J. K. (2018). Impact of heavy metals on inhibitory concentration of *Escherichia coli*-a case study of river Yamuna system, Delhi. *India. Environ. Monit. Assess.* 190, 674–691. doi: 10.1007/s10661-018-7061-0

Bondarczuk, K., and Piotrowska-Seget, Z. (2013). Molecular basis of active copper resistance mechanisms in gram-negative bacteria. *Cell Biol. Toxicol.* 29, 397–405. doi: 10.1007/s10565-013-9262-1

Bradford, M. M. (1976). A rapid and sensitive method for the quantitation of microgram quantities of protein utilizing the principle of protein-dye binding. *Anal. Biochem.* 72, 248–254. doi: 10.1006/abio.1976.9999

Briffa, J., Sinagra, E., and Blundell, R. (2020). Heavy metal pollution in the environment and their toxicological effects on humans. *Heliyon.* 6, e04691–e04626. doi: 10.1016/j.heliyon.2020.e04691

Bubela, B. (1973). Effect of copper on the growth of *Bacillus stearothermophilus*. *Zentralblatt für Bakteriologie, Parasitenkunde, Infektionskrankheiten und Hygiene Zweite naturwissenschaftliche Abteilung: Mikrobiologie der Landwirtschaft der Technologie und des Umweltschutzes* 128, 274–284. doi: 10.1016/S0044-4057(73)80013-9

Chaturvedi, A. K., Mishra, A., Tiwari, V., and Jha, B. (2012). Cloning and transcript analysis of type 2 metallothionein gene (SbMT 2) from extreme halophyte *Salicornia brachiata* and its heterologous expression in *E. coli*. *Gene* 499, 280–287. doi: 10.1016/j.gene.2012.03.001

Cheesbrough, M. (2006). *District Laboratory Practice in Tropical Countries*. United Kingdom: Cambridge University Press.

Choudhary, M., Jetley, U. K., Khan, M. A., Zutsh, I. S., and Fatma, T. (2007). Effect of heavy metal stress on proline, malondialdehyde, and superoxide dismutase activity in the cyanobacterium *Spirulina platensis*-S5. *Ecotoxicol. Environ. Saf.* 66, 204–209. doi: 10.1016/j.ecoenv.2006.02.002

Covre, W. P., Ramos, S. J., Pereira, W. V. D. S., Souza, E. S., Martins, G. C., Teixeira, O. M. M., et al. (2022). Impact of copper mining wastes in the Amazon: properties and risks to environment and human health. *J. Hazard. Mater.* 421, 126688–126613. doi: 10.1016/j.jhazmat.2021.126688

Crichton, R. R., and Pierre, J. L. (2001). Old iron, young copper: From Mars to Venus. *Biometals* 14, 99–112. doi: 10.1023/A:1016710810701

Deokar, A. R., Lin, L. Y., Chang, C. C., and Ling, Y. C. (2013). Single-walled carbon nanotube coated antibacterial paper: preparation and mechanistic study. *J. Mater. Chem. B* 1, 2639–2646. doi: 10.1039/C3TB20188K

Elgarahy, A. M., Elwakeel, K. Z., Mohammad, S. H., and Elshoubaky, G. A. (2020). Multifunctional eco-friendly sorbent based on marine brown algae and bivalve shells for subsequent uptake of Congo red dye and copper(II) ions. *J. Environ. Chem. Eng.* 8:103915. doi: 10.1016/j.jece.2020.103915

El-Liethy, M. A., Elwakeel, K. Z., and Ahmed, M. S. (2018). Comparison study of Ag(I) and au(III) loaded on magnetic thiourea-formaldehyde as disinfectants for water pathogenic microorganism's deactivation. *J. Environ. Chem. Eng.* 6, 4380–4390. doi: 10.1016/j.jece.2018.06.028

Elwakeel, K. Z., El-Sadik, H. A., Abdel-Razek, A. S., and Beheary, M. S. (2012). Environmental remediation of thorium(IV) from aqueous medium onto

Cellulosimicrobium cellulans isolated from radioactive wastewater. *Desalin. Water Treat.* 46, 1–9. doi: 10.1080/19443994.2012.677405

Esertaş, Ü. Z. U., Uzunalioğlu, E., Güzel, S., Bozdeveci, A., and Karaoglu, S. A. (2020). Determination of bioremediation properties of soil-borne bacillus sp. 5O5Y11 and its effect on the development of Zea mays in the presence of copper. *Arch. Microbiol.* 202, 1817–1829. doi: 10.1007/s00203-020-01900-4

Franco, R., Sanchez-Olea, R., Reyes-Reyes, E. M., and Panayiotidis, M. I. (2009). Environmental toxicity, oxidative stress and apoptosis. *Ménage à Trois. Mutat. Res.* 674, 3–22. doi: 10.1016/j.mrgentox.2008.11.012

Gaballa, A., and Helmann, J. D. (2003). *Bacillus subtilis* CPx-type ATPases: characterization of Cd, Zn, Co and cu efflux systems. *Biometals* 16, 497–505. doi: 10.1023/A:1023425321617

Gadd, G. M. (2010). Metals, minerals and microbes: geomicrobiology and bioremediation. *Microbiology* 156, 609–643. doi: 10.1099/mic.0.037143-0

Gaur, V. K., Sharma, P., Gaur, P., Varjani, S., Ngo, H. H., Guo, W., et al. (2021). Sustainable mitigation of heavy metals from effluents: toxicity and fate with recent technological advancements. *Bioengineered.* 12, 7297–7313. doi: 10.1080/21655979.2021.1978616

Giachino, A., and Waldron, K. J. (2020). Copper tolerance in bacteria requires the activation of multiple accessory pathways. *Mol. Microbiol.* 114, 377–390. doi: 10.1111/mmi.14522

Gillard, B., Chatzievangelou, D., Thomsen, L., and Ullrich, M. S. (2019). Heavy-metal resistant microorganisms in deep-sea sediments disturbed by mining activity: an application toward the development of experimental *in vitro* systems. *Front. Mar. Sci.* 4:462. doi: 10.3389/fmars.2019.00462

Gunther, M. R., Hanna, P. M., Mason, R. P., and Cohen, M. S. (1995). Hydroxyl radical formation from cuprous ion and hydrogen peroxide: a spin-trapping study. *Arch. Biochem. Biophys.* 316, 515–522. doi: 10.1006/abbi.1995.1068

Hu, X., Cao, J., Yang, H., Li, D., Qiao, Y., Zhao, J., et al. (2020). Pb^{2+} biosorption from aqueous solutions by live and dead biosorbents of the hydrocarbon-degrading strain *Rhodococcus* sp. HX-2. *PLoS One* 15, e0226557–e0226524. doi: 10.1371/journal.pone.0226557

Igiri, B. E., Okoduwa, S. I. R., Idoko, G. O., Akabuogu, E. P., Adeyi, A. O., and Ejiogu, I. K. (2018). Toxicity and bioremediation of heavy metals contaminated ecosystem from tannery wastewater: a review. *J Toxicol.* 2018, 1–16. doi: 10.1155/2018/2568038

Irawati, W., and Tahya, C. Y. (2021). Copper removal by *Enterobacter cloacae* strain IrSuk1, *Enterobacter cloacae* strain IrSuk4a, and *Serratia nematodiphila* strain IrSuk13 isolated from Sukolilo River-Indonesia. *IOP Conf Ser: Mater. Sci. Eng.* 1053:012038. doi: 10.1088/1757-899X/1053/1/012038

Izydorczyk, G., Mikula, K., Skrzypczak, D., Moustakas, K., Witek-Krowiak, A., and Chojnacka, K. (2021). Potential environmental pollution from copper metallurgy and methods of management. *Environ. Res.* 197, 111050–111011. doi: 10.1016/j.envres.2021.111050

Jain, P. K., Gupta, V. K., Guar, R. K., Lowry, M., Jaroli, D. P., and Chauhan, U. K. (2011). Bioremediation of petroleum oil contaminated soil and water. *Res. J. Environ. Toxicol.* 5, 1–26. doi: 10.3923/rjet.2011.1.26

Jin, Y., Luan, Y., Ning, Y., and Wang, L. (2018). Effects and mechanisms of microbial remediation of heavy metals in soil: a critical review. *Appl. Sci.* 8, 1336–1353. doi: 10.3390/app8081336

Joo, J. H., Hassan, S. H. A., and Oh, S. E. (2010). Comparative study of biosorption of Zn^{2+} by *Pseudomonas aeruginosa* and *Bacillus cereus*. *Int. Biodeterior. Biodegrad.* 64, 734–741. doi: 10.1016/j.ibiod.2010.08.007

Kamika, I., and Momba, M. N. (2013). Assessing the resistance and bioremediation ability of selected bacterial and protozoan species to heavy metals in metal-rich industrial wastewater. *BMC Microbiol.* 13, 28–42. doi: 10.1186/1471-2180-13-28

Kanamarlapudi, S. L. R. K., and Muddada, S. (2019). Structural changes of *Bacillus subtilis* biomass on biosorption of iron (II) from aqueous solutions: isotherm and kinetic studies. *Pol. J. Microbiol.* 68, 549–558. doi: 10.33073/pjm-2019-057

Kaparapu, J., and Prasad, M. K. (2018). Equilibrium, kinetics and thermodynamic studies of cadmium(II) biosorption on *Nannochloropsis oculata*. *Appl. Water Sci.* 8, 179–187. doi: 10.1007/s13201-018-0810-y

Kargar, H. M., and Shirazi, S. H. (2020). *Lactobacillus fermentum* and *lactobacillus plantarum* bioremediation ability assessment for copper and zinc. *Arch. Microbiol.* 202, 1957–1963. doi: 10.1007/s00203-020-01916-w

Khan, A. L., Bilal, S., Halo, B. A., Al-Harrasi, A., Khan, A. R., Waqas, M., et al. (2017). *Bacillus amyloliquefaciens* BSL16 improves phytoremediation potential of *Solanum lycopersicum* during copper stress. *J. Plant Interact.* 12, 550–559. doi: 10.1080/17429145.2017.1397203

Khan, Z., Rehman, A., Hussain, S. Z., Nisar, M. A., Zulfiqar, S., and Shakoori, A. R. (2016). Cadmium resistance and uptake by bacterium, *salmonella enterica* 43C, isolated from industrial effluent. *AMB Express* 6, 54–69. doi: 10.1186/s13568-016-0225-9

Khusro, A., Raj, J. P. P., and Panicker, S. G. (2014). Multiple heavy metals response and antibiotic sensitivity pattern of *Bacillus subtilis* strain KPA. *J. Chem. Pharm. Res.* 6, 532–538.

Kumagai, Y., and Sumi, D. (2007). Arsenic: signal transduction, transcription factor, and biotransformation involved in cellular response and toxicity. *Annu. Rev. Pharmacol. Toxicol.* 47, 243–262. doi: 10.1146/annurev.pharmtox.47.120505.105144

Ladomersky, E., and Petris, M. J. (2015). Copper tolerance and virulence in bacteria. *Metallomics* 7, 957–964. doi: 10.1039/c4mt00327f

Laemmli, U. K. (1970). Cleavage of structural proteins during the assembly of the head of bacteriophage T4. *Nature* 227, 680–685. doi: 10.1038/227680a0

Lagergren, S. (1898). Zur theorie der sogenannten adsorption gel€oster stoffe, Kungliga Svenska Vetenskapsakademiens. *Hand* 24, 1–39.

Latef, A. A. H. A., Zaid, A., Abo-Baker, A. A., Salem, W., and Alhmad, M. F. A. (2020). Mitigation of copper stress in maize by inoculation with *Paenibacillus polymyxa* and Bacillus circulans. *Plan. Theory* 9, 1513–1531. doi: 10.3390/plants911151

Liu, Y. G., Liao, T., He, Z. B., Li, T. T., Wang, H., Hu, X. J., et al. (2013). Biosorption of copper(II) from aqueous solution by *Bacillus subtilis* cells immobilized into chitosan beads. *T. Nonferr. Metal. Soc. China.* 23, 1804–1814. doi: 10.1016/s1003-6326(13)62664-3

Liu, Z., Xie, J., Deng, Z., Wang, M., Dang, D., Luo, S., et al. (2020). Enhancing the insecticidal activity of new *bacillus thuringiensis* X023 by copper ions. *Microb. Cell Factories* 19, 195–204. doi: 10.1186/s12934-020-01452-8

Luck, F. H. (1965). "Catalase," in *Methods of Enzymatic Analysis*. ed. H. U. Bergmeyer (New York: Academic Press), 885–894.

Matilda, C. S., Mannully, S. T., Rao, V. P., and Shanthi, C. (2021). Chromium binding *Bacillus cereus* VITSH1-a promising candidate for heavy metal clean up. *Lett. Appl. Microbiol.* 72, 517–525. doi: 10.1111/lam.13441

Minnikova, T. V., Denisova, T. V., Mandzhieva, S. S., Kolesnikov, S. I., Minkina, T. M., Chaplygin, V. A., et al. (2017). Assessing the effect of heavy metals from the Novocherkassk power station emissions on the biological activity of soils in the adjacent areas. *J. Geochem. Explor.* 174, 70–78. doi: 10.1016/j.gexplo.2016.06.007

Mulik, A., Bhola, J., and Bhadekar, R. (2018). Protein profiling and antioxidant enzyme activity of cadmium and lead tolerant *Kocuria* sp. BRI 36. *Int. J. Appl. Eng. Res.* 13, 8357–8363.

Murray, T. S., Ledizet, M., and Kazmierczak, B. I. (2010). Swarming motility, secretion of type 3 effectors and biofilm formation phenotypes exhibited within a large cohort of *Pseudomonas aeruginosa* clinical isolates. *J. Med. Microbiol.* 59, 511–520. doi: 10.1099/jmm.0.017715-0

Mustapha, M. U., and Halimoon, N. (2015). Screening and isolation of heavy metal tolerant bacteria in industrial effluent. *Procedia Environ. Sci.* 30, 33–37. doi: 10.1016/j.proenv.2015.10.006

Nakano, Y., and Asada, K. (1987). Purification of ascorbate peroxidase in spinach chloroplasts: its activation in ascorbate depleted medium and reactivation by monodehydroascorbate radical. *Plant Cell Physiol.* 28, 131–140. doi: 10.1093/oxfordjournals.pcp.a077268

Nwinyi, O. C., Kanu, I. A., Tunde, A., and Ajanaku, K. O. (2014). Characterization of diesel degrading bacterial species from contaminated tropical ecosystem. *Braz. Arch. Biol. Technol.* 57, 789–796. doi: 10.1590/S1516-8913201402250

Oves, M., Khan, M. S., Qari, A. H., Felemban, M. N., and Almeelbi, T. (2016). Heavy metals: biological importance and detoxification strategies. *J. Bioremed. Biodegr.* 7, 334–349. doi: 10.4172/2155-6199.1000334

Palanivel, T. M., Sivakumar, N., Al-Ansari, A., and Victor, R. (2020). Bioremediation of copper by active cells of *pseudomonas stutzeri* LA3 isolated from an abandoned copper mine soil. *J. Environ. Manag.* 253, 109706–109707. doi: 10.1016/j.jenvman.2019.109706

Pandhare, G., Trivedi, N., Pathrabe, R., and Dawande, S. (2013). Adsorption of cadmium (II) and lead 644 (II) from a stock solution using neem leaves powder as a low-cost adsorbent. *Int. J. Innov. Res. Sci. Eng. Technol.* 2, 5752–5761.

Pattanapipitpaisal, P., Brown, N. L., and Macaskie, L. E. (2001). Chromate reduction and 16S rRNA identification of bacteria isolated from a Cr(VI)-contaminated site. *Appl. Microbiol. Biotechnol.* 57, 257–261. doi: 10.1007/s002530100758

Paul, M. L., Samuel, J., Chandrasekaran, N., and Mukherjee, A. (2012). Comparative kinetics, equilibrium, thermodynamic and mechanistic studies on biosorption of hexavalent chromium by live and heat killed biosorbent of *Acinetobacter junii* VITSUKMW2, an indigenous chromite mine isolate. *Chem. Eng. J.* 187, 104–113. doi: 10.1016/j.cej.2012.01.106

Pepi, M., Heipieper, H. J., Fischer, J., Ruta, M., Volterrani, M., and Focardi, S. E. (2008). Membrane fatty acids adaptive profile in the simultaneous presence of arsenic and toluene in *bacillus* sp. ORAs2 and *pseudomonas* sp. ORAs5 strains. *Extremophiles* 12, 343–349. doi: 10.1007/s00792-008-0147-9

Prabhakaran, P., Ashraf, M. A., and Aqma, W. S. (2016). Microbial stress response to heavy metals in the environment. *RSC Adv.* 6, 109862–109877. doi: 10.1039/C6RA10966G

Raj, A. S., Muthukumar, P. V., Bharathiraja, B., and Priya, M. (2018). Comparative biosorption capacity of copper and chromium by *Bacillus cereus*. *Int. J. Eng. Technol.* 7, 442–444. doi: 10.14419/ijet.v7i3.34.19355

Ran, X., Long, H., Tian, Q., Wang, J., You, L., Huang, S., et al. (2020). Mechanism of manganese oxidization of *bacillus safensis* strain ST7 isolated from the soil of mineral area. *Res. Square.* 2020, 1–33. doi: 10.21203/rs.3.rs-46834/v1

Rao, M. V., Paliyath, G., and Ormrod, D. P. (1996). Ultraviolet-B and ozone induced biochemical changes in antioxidative enzymes of *Arabidopsis thaliana*. *Plant Physiol.* 110, 125–136. doi: 10.1104/pp.110.1.125

Rathi, M., and Nandabalan, Y. K. (2017). Copper-tolerant rhizosphere bacteria-characterization and assessment of plant growth promoting factors. *Environ. Sci. Pollut. Res. Int.* 24, 9723–9733. doi: 10.1007/s11356-017-8624-2

Reuveni, R., Shimoni, M., Karchi, Z., and Kuch, J. (1992). Peroxidase activity as a biochemical marker for resistance of muskmelon *Cucumis melo* to *Pseudopernospora cubensis*. *Phytopathology* 82, 749–753. doi: 10.1094/Phyto-82-749

Rohini, B., and Jayalakshmi, S. (2015). Bioremediation potential of *Bacillus cereus* against copper and other heavy metals. *Int. J. Adv. Res. Biol. Sci.* 2, 200–209.

Saeed, M. U., Hussain, N., Sumrin, A., Shahbaz, A., Noor, S., Bilal, M., et al. (2022). Microbial bioremediation strategies with wastewater treatment potentialities: a review. *Sci. Total Environ.* 818:151754. doi: 10.1016/j.scitotenv.2021.151754

Sánchez-Clemente, R., Guijo, M. I., Nogales, J., and Blasco, R. (2020). Carbon source influence on extracellular pH changes along bacterial cell-growth. *Gen. Dent.* 11, 1292–1309. doi: 10.3390/genes11111292

Sayqal, A., and Ahmed, O. B. (2021). Advances in heavy metal bioremediation: An overview. *Appl. Bionics Biomech.* 2021:1609149. doi: 10.1155/2021/1609149

Selvi, A., Rajasekar, A., Theerthagiri, J., Ananthaselvam, A., Sathishkumar, K., Madhavan, J., et al. (2019). Integrated remediation processes toward heavy metal removal/recovery from various environments-A review. *Front. Environ. Sci.* 7:66. doi: 10.3389/fenvs.2019.00066

Shamim, S. (2014). Comparative analysis of metal resistance, accumulation and antioxidant enzymes in *Cupriavidus metallidurans* CH34 and *pseudomonas putida* mt 2 during cadmium stress. PhD Thesis. Department of Microbiology and Molecular Genetics, University of the Punjab, Pakistan.

Shamim, S., and Rehman, A. (2012). Cadmium resistance and accumulation potential of *Klebsiella pneumoniae* strain CBL-1 isolated from industrial wastewater. *Pak. J. Zool.* 44, 203–208.

Shamim, S., Rehman, A., and Qazi, M. H. (2014). Cadmium resistance mechanism in the bacteria *Cupriavidus metallidurans* CH34 and *pseudomonas putida* mt2. *Arch. Environ. Contam. Toxicol.* 67, 149–157. doi: 10.1007/s00244-014-0009-7

Sher, S., Sultan, S., and Rehman, A. (2021). Characterization of multiple metal resistant *bacillus licheniformis* and its potential use in arsenic contaminated industrial wastewater. *Appl. Water Sci.* 11, 69–75. doi: 10.1007/s13201-021-01407-3

Silambarasan, S., and Abraham, J. (2013). Biosorption and characterization of metal tolerant bacteria isolated from Palar river basin Vellore. *J. Sci. Res.* 6, 125–131. doi: 10.3329/jsr.v6i1.14678

Singh, P. P., and Chopra, A. K. (2014). Removal of Zn2+ and Pb2+ using new isolates of *bacillus* spp. PPS03 and *Bacillus subtilis* PPS04 from paper mill effluents using indigenously designed bench-top bioreactor. *J. Appl. Nat. Sci.* 6, 47–56. doi: 10.31018/jans.v6i1.374

Singh, A. K., Dhanjal, S., and Cameotra, S. S. (2014). Surfactin restores and enhances swarming motility under heavy metal stress. *Colloids Surf. B: Biointerfaces* 116, 26–31. doi: 10.1016/j.colsurfb.2013.12.035

Smaldone, G. T., and Helmann, J. D. (2007). CsoR regulates the copper efflux operon copZA in *Bacillus subtilis*. *Microbiology* 153, 4123–4128. doi: 10.1099/mic.0.2007/011742-0

Soltani-Gerdefaramarzi, S., Ghasemi, M., and Ghanbarian, B. (2021). Geogenic and anthropogenic sources identification and ecological risk assessment of heavy metals in the urban soil of Yazd, Central Iran. *PLoS One* 16, e0260418–e0260414. doi: 10.1371/journal.pone.0260418

Sonawdekar, S., and Gupte, A. (2020). Biosorption of copper(II) and cadmium(II) by *Bacillus cereus* sys1 isolated from oil-contaminated site. *SN Appl. Sci.* 2, 1254–1262. doi: 10.1007/s42452-020-3062-z

Steunou, A. S., Babot, M., Bourbon, M. L., Tambosi, R., Durand, A., Liotenberg, S., et al. (2020). Additive effects of metal excess and superoxide, a highly toxic mixture in bacteria. *Microb. Biotechnol.* 13, 1515–1529. doi: 10.1111/1751-7915.13589

Sulaiman, S., Azis, R. S., Ismail, I., Man, H. C., Yusof, K. F. M., Abba, M. U., et al. (2021). Adsorptive removal of copper (II) ions from aqueous solution using a magnetite nano-adsorbent from mill scale waste: synthesis, characterization, adsorption and kinetic modelling studies. *Nanoscale Res. Lett.* 16, 168–185. doi: 10.1186/s11671-021-03622-y

Todorova, K., Velkova, Z., Stoytcheva, M., Kirova, G., Kostadinova, S., and Gochev, V. (2019). Novel composite biosorbent from *Bacillus cereus* for heavy metals removal from aqueous solutions. *Biotechnol. Biotechnol. Equip.* 33, 730–738. doi: 10.1080/13102818.2019.1610066

Utgikar, V. P., Chen, B. Y., Chaudhary, N., Tabak, H. H., Haines, J. R., and Govind, R. (2001). Acute toxicity of heavy metals to acetate-utilizing mixed cultures of sulfate-reducing bacteria: EC100 and EC50. *Environ. Toxicol. Chem.* 20, 2662–2669. doi: 10.1002/etc.5620201202

Vladimirov, N., and Sourjik, V. (2009). Chemotaxis: how bacteria use memory. *Biol. Chem.* 390, 1097–1104. doi: 10.1515/BC.2009.130

Wang, L., Ji, B., Hu, Y., Liu, R., and Sun, W. (2017). A review on in situ phytoremediation of mine tailings. *Chemosphere* 184, 594–600. doi: 10.1016/j.chemosphere.2017.06.025

Wierzba, S. (2015). Biosorption of lead (II), zinc (II) and nickel (II) from industrial wastewater by *Stenotrophomonas maltophilia* and *Bacillus subtilis*. *Pol. J. Chem. Technol.* 17, 79–87. doi: 10.1515/pjct-2015-0012

Wiesemann, N., Mohr, J., Grosse, C., Herzberg, M., Hause, G., Reith, F., et al. (2013). Influence of copper resistance determinants on gold transformation by *Cupriavidus metallidurans* strain CH34. *J. Bacteriol.* 195, 2298–2308. doi: 10.1128/JB.01951-12

Yang, Y., Hu, M., Zhou, D., Fan, W., Wang, X., and Huo, M. (2017). Bioremoval of Cu^{2+} from CMP wastewater by a novel copper-resistant bacterium *Cupriavidus gilardii* CR3: characteristics and mechanisms. *RSC Adv.* 7, 18793–18802. doi: 10.1039/c7ra01163f

Zhao, S. L., Liu, Q., Qi, Y. T., and Duo, L. (2010). Responses of root growth and protective enzymes to copper stress in turfgrass. *Acta Biol. Cracov. Ser. Bot.* 52, 7–11. doi: 10.2478/v10182-010-0017-5

Conflict of Interest: The authors declare that the research was conducted in the absence of any commercial or financial relationships that could be construed as a potential conflict of interest.

Publisher's Note: All claims expressed in this article are solely those of the authors and do not necessarily represent those of their affiliated organizations, or those of the publisher, the editors and the reviewers. Any product that may be evaluated in this article, or claim that may be made by its manufacturer, is not guaranteed or endorsed by the publisher.

frontiers | Frontiers in Microbiology

REVIEW
published: 31 May 2022
doi: 10.3389/fmicb.2022.900740

Zinc Essentiality, Toxicity, and Its Bacterial Bioremediation: A Comprehensive Insight

Sarfraz Hussain[1†], Maryam Khan[2†], Taha Majid Mahmood Sheikh[3], Muhammad Zahid Mumtaz[2], Talha Ali Chohan[2], Saba Shamim[2*] and Yuhong Liu[1*]*

[1]*Key Laboratory of Integrated Regulation and Resource Development on Shallow Lakes of Ministry of Education, College of Environment, Hohai University, Nanjing, China,* [2]*Institute of Molecular Biology and Biotechnology, The University of Lahore, Lahore, Pakistan,* [3]*Institute of Plant Protection, Jiangsu Academy of Agriculture Sciences, Nanjing, China*

OPEN ACCESS

Edited by:
Maqshoof Ahmad, The Islamia University of Bahawalpur, Pakistan

Reviewed by:
Ajay Kumar, Agricultural Research Organization (ARO), Israel
Pooja Sharma, National University of Singapore, Singapore

***Correspondence:**
Taha Majid Mahmood Sheikh
tahamajid1705@yahoo.com
Saba Shamim
sabashamimgenetics@gmail.com
Yuhong Liu
yhliu@hhu.edu.cn

[†]These authors have contributed equally to this work

Specialty section:
This article was submitted to Terrestrial Microbiology, a section of the journal Frontiers in Microbiology

Received: *21 March 2022*
Accepted: *09 May 2022*
Published: *31 May 2022*

Citation:
Hussain S, Khan M, Sheikh TMM, Mumtaz MZ, Chohan TA, Shamim S and Liu Y (2022) Zinc Essentiality, Toxicity, and Its Bacterial Bioremediation: A Comprehensive Insight. Front. Microbiol. 13:900740. doi: 10.3389/fmicb.2022.900740

Zinc (Zn) is one of the most abundantly found heavy metals in the Earth's crust and is reported to be an essential trace metal required for the growth of living beings, with it being a cofactor of major proteins, and mediating the regulation of several immunomodulatory functions. However, its essentiality also runs parallel to its toxicity, which is induced through various anthropogenic sources, constant exposure to polluted sites, and other natural phenomena. The bioavailability of Zn is attributable to various vegetables, beef, and dairy products, which are a good source of Zn for safe consumption by humans. However, conditions of Zn toxicity can also occur through the overdosage of Zn supplements, which is increasing at an alarming rate attributing to lack of awareness. Though Zn toxicity in humans is a treatable and non-life-threatening condition, several symptoms cause distress to human activities and lifestyle, including fever, breathing difficulty, nausea, chest pain, and cough. In the environment, Zn is generally found in soil and water bodies, where it is introduced through the action of weathering, and release of industrial effluents, respectively. Excessive levels of Zn in these sources can alter soil and aquatic microbial diversity, and can thus affect the bioavailability and absorption of other metals as well. Several Gram-positive and -negative species, such as *Bacillus* sp., *Staphylococcus* sp., *Streptococcus* sp., and *Escherichia coli*, *Pseudomonas* sp., *Klebsiella* sp., and *Enterobacter* sp., respectively, have been reported to be promising agents of Zn bioremediation. This review intends to present an overview of Zn and its properties, uses, bioavailability, toxicity, as well as the major mechanisms involved in its bioremediation from polluted soil and wastewaters.

Keywords: zinc, bioremediation, pollution, wastewater, heavy metal, toxicity

INTRODUCTION

The surge in anthropogenic activities has exacerbated the problem of heavy metal pollution in the world, which, due to their indefinite persistence in the environment, are non-degradable pollutants and can be detrimental for living beings at high levels (Witkowska et al., 2021). Zinc (Zn) is one of the most profusely abundant transition elements in the Earth's crust and is also reported to be an essential trace element for all living organisms (Roohani et al., 2013; Jarosz et al., 2017; Lee, 2018). It is a significant component of various proteins, acting as a cofactor or coenzyme of more

than 300 enzymes (Rahman and Karim, 2018), and is attributable to the activity and regulation of various enzymes, proteins, DNA and DNA binding proteins, immunity, as well as cell metabolism. It also aids in suppressing the generation of free radicals and reactive oxygen species (ROS), which accentuates protein stability and the function of antioxidative enzymes (Narayanan et al., 2020). In nature, it exists as a divalent cation (Zn^{2+}), thus interacting with various negatively charged ions (CO_3^{-}, OH^{-}, $C_2O_4^{2-}$). Zn was first reported to be essential for the growth of microorganisms in 1869 (Raulin, 1869), much earlier than plants and animals (Todd et al., 1933; Prasad et al., 1963). It was not until the 1960s that Zn was established to be essential for humans as well, prior to which it was not known that its deficiency would cause detrimental effects to human health (Prasad, 2017). In humans, Zn serves the elemental role in the production of hormones and their receptors (Chasapis et al., 2012; Roohani et al., 2013). It is reported that the cumulative concentration of Zn in the human body amounts to approximately 2–3 gm, more than 80% of which is apportioned in the bone and muscles. During transportation within the body, enzymes like superoxide dismutase and carbonic anhydrase in the red blood cells carry the largest quantity of Zn in the bloodstream (Vallee and Falchuk, 1993). However, majority of transported Zn is bound to albumin in plasma, with approximate concentration of 12–16 μm (Rink and Gabriel, 2000). Furthermore, the regulation of Zn in the human body is closely associated with normal levels of cellular proliferation, apoptosis and differentiation (Haase and Rink, 2014a), and the production of cytokines and antibodies, thus serving a significant role in the homeostasis of innate and adaptive immune systems (Haase and Rink, 2014b; Weyh et al., 2022). The supplementation of Zn has also been recommended for the reduction of viral activity, as well as the amelioration of tissue damage and inflammation in many viral infections, including COVID-19 (Asl et al., 2021; Rodelo et al., 2022). The consumption of Zn in humans is typically dependent upon dietary intake, which is varied according to age and gender. According to the German Nutrition Society, the consumption of 1.5 mg/day for infants (0–4 months), 11 and 14 mg/day for adolescent males and females (15–19 years) has been advised, while for adult males and females (ages 19 or older), the average allowance of intake is recommended to be 11–16 and 7–10 mg/day (variable by phytate intake), respectively, by The Food and Nutrition Board, United States (Otten et al., 2006; Rodelo et al., 2022). Thus, deficiency of Zn can be an important factor in creating nutritional imbalance and can adversely impact human health, where it can be a precursor in the development of certain medical ailments, including immune dysregulation, impaired immunity, increased vulnerability to infection, lymphopenia, common cold, epilepsy, acne, Wilson's disease, and neurological diseases, such as schizophrenia, Parkinson's, and Alzheimer's disease (Irving et al., 2003; Walker and Black, 2004; Prasad, 2013). Zn intake and its excess is also reported to be associated with the modulation of gastrointestinal flora and immune systems (Skalny et al., 2021). In this light, it is also important to note that excessive intake of this element can have negative effects, such as disturbances in the levels of other elements, particularly copper, which can subsequently result in copper deficiency anemia, reduction in the copper-dependent enzymes, and cholesterol metabolism dysregulation (Terrin et al., 2020; Brzóska et al., 2021).

In literature, there are various reports which demonstrate the adverse effects caused by excessive micronutrient exposure, including exposure to Zn, causing disturbance to the homeostasis of various biological systems (Hynninen et al., 2010; Potocki et al., 2012). At higher concentrations, Zn can cause toxicity in cells, which can often result in the disruption of essential biological functions triggered by blocking protein thiols through mismetallation with other metals (Marchetti, 2013; Chandrangsu et al., 2017). In the environment, emissions of vast quantities of Zn due to natural and anthropogenic sources has enabled its unmitigated entry into food chains, resulting in biomagnification in living organisms. Bioremediation is feasible and efficient method for the removal of these toxic quantities from contaminated soil and wastewater sources, thus offering a new perspective on the utilization of heavy metal-resistant bacteria through sustainable development (Sharma et al., 2021).

This review aims to compile and present the chemical and physical properties of Zn, its uses, the effects of its toxicity, as well as summarize and highlight the potential mechanism of resistance in bacteria which enable them as promising agents of bioremediation of heavy metals, such as Zn.

PHYSICAL AND CHEMICAL PROPERTIES OF ZINC

Zinc is represented by the symbol "Zn," with an atomic number and weight of 30 and 65.38 gm, respectively. It was discovered and recognized as a metal for the first time in 1746 by German chemist Andreas Sigismund Marggraf (National Center for Biotechnology Information, 2022). It belongs to group XII (known formerly as II-B) of the periodic table (Period number 4, element group number 12, block "d"; Jensen, 2003), and is a brittle, lustrous, bluish-white metal which is solid at room temperature. When heated at temperatures above 110°C, it readily becomes malleable and ductile and is generally considered to be a moderately reactive metal in terms of its reactivity with oxygen and other metals (**Table 1**; Wuana and Okieimen, 2011). It acts as a strong reducing agent, and in hydrolytic reactions, acts as a Lewis acid in catalyzing reactions, thereby being associated with various metalloenzymes, DNA binding, and regulatory proteins, as well as transcription factors (Cerasi et al., 2013). Zn naturally occurs as a mineral sphalerite (ZnS) and has five stable isotopes (^{64}Zn, ^{66}Zn, ^{67}Zn, ^{68}Zn, and ^{70}Zn) in nature, from which ^{64}Zn is the major isotope in terms of natural abundance (Audi et al., 2017).

Zn does not generally act as a typical metal, as it does not have an 8-electron octet rather an 18-electron shell upon

Abbreviations: ATP, Adenosine 5′-triphosphate; CDF, Cation diffusion facilitator; DNA, Deoxyribonucleic acid; IFN-γ, Interferon gamma; IL-1α, Interleukin 1 alpha; IL-1β, Interleukin 1 beta; IL-2, Interleukin-2; IL-6, Interleukin-6; NADPH, Reduced nicotinamide adenine dinucleotide phosphate; NF-κB, Nuclear factor kappa B; NK, Natural killer; RNA, Ribonucleic acid; RND, Resistance nodulation division; ROS, Reactive oxygen species; SARS, Severe acute respiratory syndrome; TLR, Toll-like receptor; TNFR, Tumor necrosis factor receptors; TNF-α, Tumor necrosis factor α.

TABLE 1 | Description of various physical parameters of Zn.

Physical parameters	Zn properties
Atomic number	30
Density at room temperature (gcm^{-3})	7.134
Atomic weight (mass)	65.39
Relative abundance in Earth's crust (%)	8×10^{-3}
Melting point (°C)	419.53°C
Boiling point (°C)	907°C
Heat of vaporization (kJ/mol)	295.8
Specific heat capacity ($J\,kg^{-1}\,K^{-1}$)	388
Heat of transformation, (J/gram atom)	1,966
Crystal structure;	
α-Zn	
β-Zn	Cubic (face-centered) Tetragonal
Van der Waals radius (nm)	0.138
Ionic radius (nm)	0.074
Isotopes	5 (stable)
Electronic shell	[Ar] $3d^{10}\ 4s^2$
Energy of first ionization ($kJ\,mol^{-1}$)	904.5
Energy of second ionization ($kJ\,mol^{-1}$)	1723
Energy of third ionization ($kJ\,mol^{-1}$)	3832.687

the loss of its outermost two electrons, rendering it less reactive than other metals. However, since it undergoes neither oxidation nor reduction, it forms a stable metal ion in biological matrices where the redox potential is in constant flux (Graf, 1997). It has an oxidation state of 2+, and readily forms compounds with ammonia, cyanide, and halide ions. When compared to the metal itself, Zn dust is reported to be more reactive and pyro-phoric due to its large surface area. Selective compounds of Zn (chloride and sulfate) are water soluble, whereas other compounds (sulfide, carbonate, phosphate, oxide) are observed to be insoluble or slightly soluble in water (Habashi, 2013). It is capable of displacement of all metals beneath its position in the electrochemical series, and can also displace gold from cyanide solution, the latter of which is a large-scale industrial process (Robinson and Pohl, 2013). The surface of the metal is prone to rapid corrosion, ultimately forming an encapsulant layer of Zn carbonate after reacting with atmospheric carbon dioxide (Holleman et al., 1985), though it can be removed by the corroding action of strong acids (HCl, H_2SO_4; Porter, 1994).

IMMUNOMODULATORY FUNCTIONS OF ZINC

Zinc and Its Role in Innate and Adaptive Immunity

Sufficient consumption and uptake of Zn is vital for the regulation and optimal function of innate and adaptive immunity in human beings (Bonaventura et al., 2015). In innate immunity, Zn serves an elemental role in maintaining the activity of NADPH oxidase found in neutrophil granulocytes (Hasegawa et al., 2000; DeCoursey et al., 2003). Thus, the lack of Zn uptake and its subsequent deficiency could beget decreased production and killing potential of ROS (Bonaventura et al., 2015). Furthermore, Zn deficiency mediates the induction of decreased adhesion and chemotactic behavior in neutrophil and monocyte granulocytes and impairs the function and maturation phase of macrophages (Shankar and Prasad, 1998). Pertaining to its role in natural killer cells (NK cells), a deficit of Zn in the body could reduce overall NK cell count in blood, where the decreased chemotactic and lytic behavior of infected or cancer cells has also been observed (Rajagopalan et al., 1995; Rajagopalan and Long, 1998).

In the case of adaptive immunity, the presence of Zn is fundamental in the generation, maturation, and activity of T cells (Fraker and King, 2004). This is due to its significance in the elemental composition of thymulin, a hormone produced in the thymus which promotes the development of pre-T lymphocytes into mature lymphocytes (Dardenne and Pleau, 1994; Saha et al., 1995), which can be inhibited in the case of Zn deficiency, resulting in thymus atrophy and decreased T-cell count (King et al., 2005). Moreover, Zn deficiency can negatively affect T cell and cytokines (such as IL-2 and IFN-γ) production (Bădulici et al., 1994; Prasad et al., 1997). Apart from T-cell maturation, Zn also aids in the cell differentiation process, where it was observed that a deficiency of Zn demonstrated a decrease in $CD4^+$ T cells, which ultimately results in the disruption of $CD4^+/CD8^+$ cells ratio, which is a characteristic sign of immune dysfunction (Beck et al., 1997; Sheikh et al., 2010).

Immunomodulatory Effects of Zinc

Apart from its effect on the functions of selective immune cells, the uptake of Zn is affiliated with the general regulation of the entire immune system, where various studies have demonstrated that elevated levels of oxidative stress and inflammation are all associated with a deficiency of Zn in the body (Wong et al., 2015, 2019; Gammoh and Rink, 2017). In *in vivo* models, the supplementation of Zn was observed to induce the production, maturation, and stability of function in regulatory T cells (Rosenkranz et al., 2016, 2017). Moreover, lack of Zn in the body can aggravate cases of chronic inflammation, which can elevate the expression of pro-inflammatory markers, such as IL-1α, IL-1β, and IL-6 in several inflammatory disease (Yazar et al., 2005). This aspect of Zn significance as a micronutrient is therefore essential for the positive downregulation of disease pathogenesis and molecular pathways, such as NF-κB signaling pathway, which significantly regulates apoptosis, immune and inflammatory responses, as well as the expression of pro-inflammatory cytokines (Jarosz et al., 2017). In addition, Zn also importantly affects the expression of Zn finger proteins which are known to suppress the expression of TNFR- and TLR-initiated NF-κB signaling pathways (Gammoh and Rink, 2017).

Zinc and Infections

Over the years, studies have reported the importance of Zn in the alleviation of viral infections, which is mainly associated with the entry of virus particles into the host cells, and their subsequent fusion and replication, as well as translation and emission of virus proteins in the host (Ishida, 2019; Read et al., 2019). In a

study, it was reported that supplementing Zn at the recommended dose (>75 mg/day) remarkably aided in the reduction of severity of colds (Maares and Haase, 2020). In elder adults, the supplementation of Zn (45 mg/day of Zn gluconate) was observed to reduce the number of infections, as well as strengthen their immune system *via* the marked increase in the concentration of Zn in the plasma, along with the lowered production of oxidative stress markers and TNF-α (Prasad et al., 2007). More recent research findings demonstrate the ability of Zn to aid in the inhibition of RNA polymerase of SARS virus, *via* the reduction of viral replication (Te Velthuis et al., 2010), which are suggestive of Zn to be potentially effective against SARS-CoV-2, and COVID-19 (Skalny et al., 2020; Weyh et al., 2022).

BIOAVAILABILITY OF ZINC

Plants tend to uptake Zn from soil because of which its deficiency is reported to be a significant abiotic stress factor affecting more than 40% of agricultural lands worldwide. Several plant species are reported to be Zn-efficient (rich in Zn), such as carrot, rye, cashew nuts, wheat, sunflower, pea, oats, and alfalfa (Hambidge et al., 2010). Other good sources of Zn include beef, and dairy products, such as milk, eggs, and cheese (Hacisalihoglu, 2020). Though it is well established that the presence of high phytate ions in the diet can ultimately hinder the absorption of several essential minerals like Ca, Fe, and Zn (Castro-Alba et al., 2019), improved absorption of Zn was observed when dairy products were consumed in combination with other foods with high phytate (e.g., bread, tortillas, and rice), which seemed to be associated with the presence and beneficial effects of citrate and phosphopeptides in dairy products (Shkembi and Huppertz, 2021). Zn absorption occurs within the small intestine in its ionized form which is formed when Zn is released from consumed foods. However, this ionized form may then be able to form inhibiting complexes with ligands of organic acids, such as phytates, amino acids, and phosphates, inadvertently affecting its solubility and absorption (Krebs, 2000). The presence of citrate, a low molecular weight ligand found in human milk which binds with Zn, and casein phosphopeptides, which are phosphorylated peptides released upon the digestion of casein which can also bind to Zn, in dairy products has thus been hypothesized to improve Zn absorption by preventing it from binding and forming complexes with phytate ions (Miquel and Farré, 2007). However, there have been some reports which state otherwise (Pécoud et al., 1975; Sandström and Cederblad, 1980; Flanagan et al., 1985; Wood and Zheng, 1990). The availability of Zn from mixed- or vegetable-based diets is reported to be more than 20% (Hacisalihoglu and Blair, 2020). The use of Zn supplements is widespread, though not necessarily mandatory for fulfilling dietary Zn requirements. In a normal and healthy host, the choice of Zn salt used is insignificant (Tran et al., 2004), though the amount of Zn absorbed from supplements is more greater than absorption from diet. Furthermore, despite the beneficial effect of Zn consumption on the immune system, excessive intake can result in its toxicity (Maares and Haase, 2020).

ZINC TOXICITY

Heavy metals are known to persist in the human body as well as the environment, with various environmental sources being attributable for their wide availability (Haiyan and Stuanes, 2003; Nadal et al., 2005). They can usually be exposed to humans through inhalation, ingestion, and dermal contact (of contaminated soil and water), as well as consumption of contaminated produce (Hough et al., 2004; Baastrup et al., 2008; Mari et al., 2009; Man et al., 2020). In order to ensure public safety and health, it is essential to identify and mitigate these sources of exposure (Hu and Dong, 2011). Zn is one of the most readily available heavy metals found in soil, where its excessive levels may exert a phytotoxic effect which can drastically affect crop quality and yield, respectively, and even pose a health risk to humans upon consumption due to the accumulation of Zn through absorption or deposition (Wang et al., 2005; Baran, 2012, 2013; Bolan et al., 2014). Furthermore, excess levels of Zn in soil also contribute to the inhibition and alteration of soil microorganisms (Olaniran et al., 2013), due to its bioavailability in the form of ionic Zn and as part of organo-metallic complexes, which have been previously determined (Pueyo et al., 2004; Anju and Banerjee, 2011; Fedotov et al., 2012; Agnieszka et al., 2014; Kim et al., 2015; Baran et al., 2018). Therefore, efficient methods of heavy metal remediation are crucial for the alleviation of Zn toxicity in order to preserve soil microorganisms and their biodiversity, as well as plant and human health (Guarino et al., 2020).

Zn is a biologically essential element for the human body, which is significantly required for the normal function and regulation of several enzymes and other proteins. However, excess levels of Zn can act as toxic, which can induce conditions of acute toxicity for living beings (Lindholmer, 1974; Wu et al., 2011; Wadige et al., 2014). According to the Environmental Protection Agency, United States, the Zn toxicity concentration in the case of freshwater aquatic life is 120 μg/l (for short- and long-term hazardous concentration), while the ranges for human health amount to 7,400 and 26,000 μg/l, respectively (for drinking water + consumable aquatic living beings, and consumable living beings only; US EPA, 2009; Li et al., 2019). In humans, Zn toxicity mainly occurs in either of three ways; oral, dermal, and inadvertent inhalation (Toxicological Profile for Zinc, 2005). As most of Zn toxicity cases are reported to be acute, prognosis are often good with complete recovery by treatment, such as chelation therapy or medication (Qu et al., 2012). One of the most common causes of acute Zn toxicity is the over-consumption of dietary Zn supplements. This also creates an imbalance for copper bioavailability, which can subsequently lead to its deficiency. This mechanism can likely be attributable to Zn-induced formation of copper-binding metallothioneins (Sandstead, 2013).

Other reasons include the unpremeditated consumption of dental products rich in Zn, as well as Zn contaminated food and drinks, which can result in acute gastrointestinal illness, with vomiting, nausea, and epigastric pain as the major symptoms. Inhalation of smoke and fumes containing Zn usually occurs in the case of exposure to industrial processes, such as

galvanization. Furthermore, Zn-containing smoke bombs are the major sources of inhalation toxicity, primarily in soldiers and armed forces (Freitag and Caduff, 1996). However, in two reports, there was no scientific evidence that the respiratory distress was mainly attributable to Zn (Johnson and Stonehill, 1961; Zerahn et al., 1999). Inhalation of Zn fumes can induce metal fume fever, which is one of its most widely caused and reported effects (**Figure 1**). It is an acute condition originating in cases of industrial exposure (Zn smelting, welding, and galvanization) in the presence of metal fumes (particular size <1 μm; Vogelmeier et al., 1987). Although a non-life-threatening condition, it can manifest several symptoms in the case of acute exposure which include nausea, muscle fatigue, chest pain, cough, breathing distress, and fever (Rohrs, 1957; Putila and Guo, 2011). With accurate treatment, these symptoms can be cured completely within a matter of days (Martin et al., 1999; Plum et al., 2010). Excessive consumption of Zn can also result in gastrointestinal distress, with several symptoms, such as vomiting, nausea, cramps, diarrhea, and epigastric pain. This can also arise from ingesting Zn from food and drinks stored in galvanized containers, where the acidic nature of the food or drinks enables the liberation of Zn from the galvanized coating layer (Brown et al., 1964). Ingestion of Zn sulphate tablets was also reported to induce gastrointestinal stress symptoms in healthy subjects (Haase et al., 2008). Additionally, other compounds, such as Zn gluconate and oxide, are also observed to induce similar effects on human gastrointestinal health (Callender and Gentzkow, 1937; Lewis and Kokan, 1998; Liu et al., 2006). In human health, though Zn is well-reported to be essential for the regulation of most biological functions, its excessive levels are implicated in the causation and development of prostate cancer (Zaichick et al., 1997; Costello and Franklin, 1998), which is associated with regulating Zip1, a Zn transporter attributed to its accumulation and acquisition in prostate cells (Costello et al., 1999; Franklin et al., 2005). Though men having a moderate to high level of Zn intake may be reported to face a lower risk of prostate cancer, exceedingly high concentrations or perpetual Zn intake can result otherwise (Jarrard, 2005; Plum et al., 2010).

ZINC IN THE ENVIRONMENT

In the environment, the persistence of Zn is the culmination of both natural and anthropogenic sources, the latter of which can arise from various sources (Hanahan and Weinberg, 2000). These sources can significantly contaminate water sources when industrial waste is discharged into river streams and water lines, where microbial and marine life get exposed. Industrial wastewaters can also be released into soils and irrigative lands where this contaminated water can enable Zn to leach into soils and affect soil microbial diversity and pH (Gautam et al., 2016).

Zn is the one of the most abundant elements (23rd in rank) found in the Earth's crust, with an average of about 78 mg/kg (Alloway, 2008). It is deemed requisite for modern times, as it is one of most utilized metals alongside iron (Fe), aluminum (Al), and copper (Cu) in the world in terms of tonnage. Sphalerite,

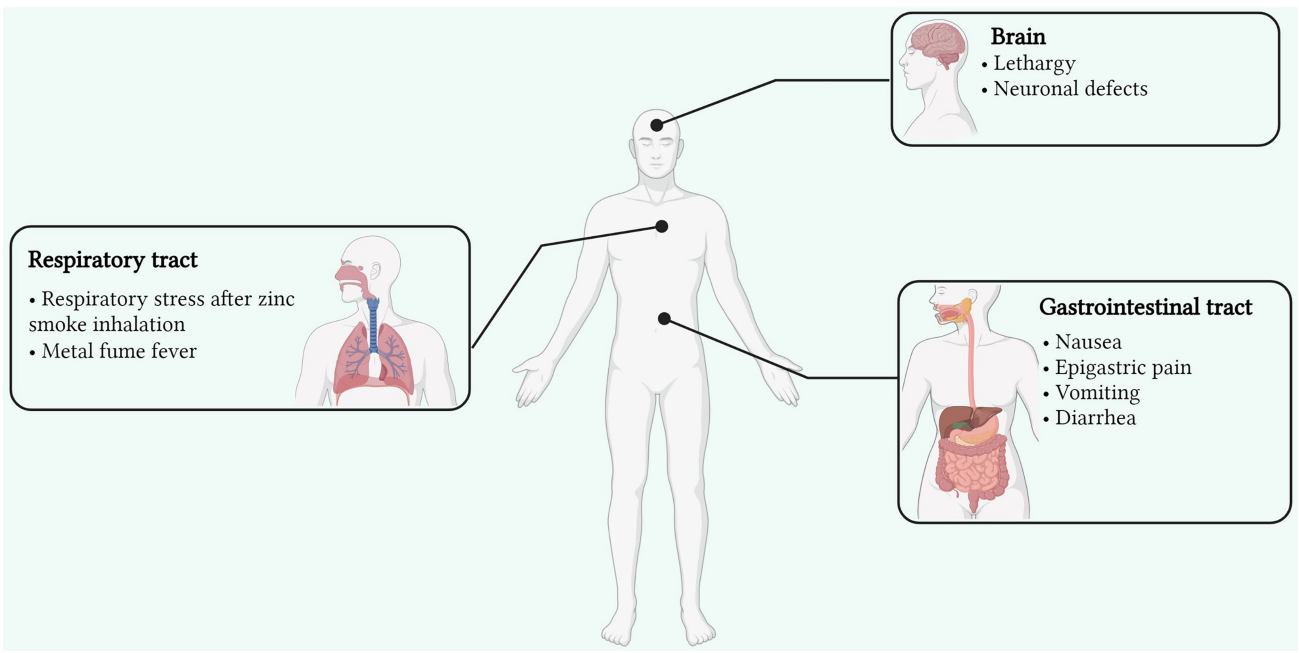

FIGURE 1 | Signs and symptoms of Zn toxicity affecting various organs and sites of the human body (Created with BioRender). Zn toxicity can occur *via* three primary routes; oral, dermal, and inadvertent inhalation. Though reversible, its toxicity can affect the respiratory and gastrointestinal tracts as well as the brain with various side effects. Inhalation of Zn fumes can induce metal fume fever arising from fume inhalation in industries, manifesting several symptoms in the case of acute exposure which include nausea, muscle fatigue, chest pain, cough, breathing distress, and fever.

Zn's primary ore, is among the most principal ores in the world. Zn mine global production was reported to increase in 2021 from that of its predecessor year, where production was observed to be halted due to lockdown restrictions (International Lead and Zinc Study Group, 2020). Therefore, in 2021, production reached approximately 14.13 million tons which resulted in a production surplus (Guo and Feng, 2013). The identified Zn resources are reported to amount to more than 1.8 billion tons in the world, with China being the second largest country in the world in terms of extracting, importing, and consumption of Zn (Li et al., 2019; U.S. Geological Survey, 2022). The natural introduction of Zn in soils is attributable to natural phenomenon of parent rock erosion and weathering. The exchangeability and bioavailability of Zn (in Zn^{2+} form) is dependent upon the pH of the soil, where adsorption and desorption into soil organic matter takes place (Mertens and Smolders, 2013). However, at high concentration of Zn, non-specific sorption to clay as well as mineral precipitation are primary and there is little or no correlation to pH. Typical concentrations of Zn in the soil range from 10–300 $mg\,kg^{-1}$ (White, 1993). Zn concentration is reported to be richer in soils formed from basic rocks (e.g., basalt) as compared to acid rocks (e.g., granite; Vinogradov, 1959). Furthermore, Zn content is found to be comparatively greater in heavier soils than lighter ones (Frank et al., 1976). Other sources may likely include atmospheric deposition through natural sources like volcanic ash, forest fires, and dust (Nriagu, 1989), along with man-made sources, such as combustion of fossil fuels, galvanization, tire and railing rust, motor oil, cement, tar production, and hydraulic fluid (Imseng et al., 2019). In soil, Zn can occur in either of these five forms; water soluble, complexed, chelated, adsorbed, or exchangeable; where these forms can vary in terms of uptake, dissemination, and strength and are regulated by several factors, such as pH, and the concentration of other ions, such as Fe and manganese (Mn; Deb, 1992). Moreover, the availability of Zn to plants in the soil is contingent on clay, carbonate, and total Zn content, redox, and moisture conditions, microbial activity in soil, as well as the concentration of micro- and macro-nutrients (Mandal et al., 1993; Alloway, 2008). In soils formed from limestone, the chemisorption of Zn onto calcium carbonate aids the formation of Zn hydroxycarbonate which ultimately inhibits its availability to surrounding plants. Moreover, Zn readily adsorbs to kaolinite and illite types of clay in the presence of high pH conditions (Farrah and Pickering, 1977). The formation of poorly soluble Zn sulfide is facilitated by the oxidation of organic matter in the case of Zn sedimentation, which also decreases the availability of Zn to plants (Sandstead, 2013). In the atmosphere, Zn is usually found in its oxidized form, and particles containing Zn can range up to 5 mm in size. In freshwaters, the pH range most often favors the adsorption of Zn, where its binding to organic matter is facilitated by pH above 6. Normal concentration of Zn in surface and groundwater may be <10 μg/l and about 10–40 μg/l (Elinder, 1986; Sandstead, 2013). Industrial uses of Zn span a wide range of applications, including galvanization, production of brass, bronze, Zn-based alloys, metal-coating, paint, dyes, and pigments (Incharoensakdi and Kitjaharn, 2002; Wu et al., 2017).

ZINC RESISTANCE MECHANISMS AND BIOREMEDIATION

The worldwide dilemma of environmental pollution has been aggravated by the incessant usage of heavy metals in various industries. According to the US EPA, more than 40% of industrial wastewaters are reported to be contaminated with heavy metals and organic pollutants (Sharma et al., 2018). To tackle this worsening situation, many physical, chemical, and biological methods have been introduced over the years to successfully remove these pollutants from wastewater. Physical and chemical methods have since been proven to be exorbitant and unfeasible at large-scale applications (Wang and Chen, 2009). In this regard, developing and promoting biological methods to alleviate toxic levels of heavy metals was imperative. Therefore, the introduction of novel approaches has unlocked the usage of biological sources (microorganisms, plants as well as algae) to combat this problem (Ahemad and Malik, 2012). Plants have evolved to adapt numerous defense mechanisms against the exposure of excess heavy metals, including complexation, chelation with metallothioneins, and migration with ligands *via* plasma membrane channels (Cunningham et al., 1995; Wei et al., 2021). This mechanism is known as phytoremediation. Furthermore, bacteria, yeast, fungi, protozoa, and algae that grow despite the harsh environment of industrial wastewaters have evolved to harbor various resistance mechanisms that can aid in their survival (Zahoor and Rehman, 2009). Bioremediation is the process which employs the use of biological agents for the removal of heavy metals from various environments, particularly effluents and wastewaters, which has since been hailed as a cheaper, more efficient method than chemical and physical ones (Timková et al., 2018). As the problem of pollution is getting more pronounced all over the world, more and more importance is being given to detoxification methods of effluents prior to their release (Shamim and Rehman, 2012). In soil, excessive levels of heavy metals may induce alteration to soil microbial diversity and selective survival in soil microbes (Berendonk et al., 2015; Epelde et al., 2015). This can be mitigated by adapting an efficient strategy for the evolution of microbes, based on encoded genetic mechanisms, a phenomenon found in several bacterial strains which survive in heavy metal-polluted areas (Aka and Babalola, 2017). Therefore, bacteria can be utilized for remediating heavy metals from polluted areas (Chen et al., 2018). Though many efforts regarding heavy metal resistance mechanisms in bacteria are majorly focusing upon single isolated strains, a comprehensive elucidation of resistance mechanisms on the whole, contaminated areas, and the feasibility of such strategies are crucial for the optimization of bioremediation (Chen et al., 2019).

Mechanisms of Zinc Homeostasis in Bacteria

Intracellular concentrations of Zn are regulated through its homeostasis, where the use of a Zn regulator enables cells to regulate the transcriptional expression of Zn transporters which facilitate its import and export to and from the cell. This mechanism employed by cells is driven by conditions of Zn

toxicity (efflux) and starvation (uptake) across the bacterial cell membrane (Capdevila et al., 2016). In bacteria, general resistance mechanisms pertain to both Gram-negative and -positive bacteria, with many agents overlapping in many species for a particular metal. These general mechanisms can aid in metal resistance through various ways, such as efflux, sequestration, chelation, and uptake. For Zn, several of these mechanisms are widely reported in many bacterial species. The intracellular regulation (uptake and efflux) of Zn^{2+} ions across the cell membrane is mediated by Zur/SlyA/MarR family and the MerR (ZntR) and ArsR/SmtB families, respectively (Mikhaylina et al., 2018). Zur is a member of the Fur family, which represses znuABC (an ABC transporter which facilitates Zn^{2+} ions uptake) under normal concentrations of Zn^{2+} in the cell (Hantke, 2001). However, in conditions of Zn^{2+} scarcity, Zur reverses its functions and induces the transporter to uptake Zn^{2+} from the outer environment. Moreover, it activates the transcription of a P-type ATPase which mediates the efflux of Zn^{2+} out of the cell under conditions of its toxicity (Capdevila et al., 2016). In *Streptococcus pneumoniae*, CzcD, a member of the CDF family, acts as major resistance determinant for Zn (**Figure 2**; Suryawati, 2018).

Mechanisms of Zinc Uptake in Bacteria

In order to control Zn homeostasis, bacterial cells are able to enable the import and export of Zn ions *via* Zn uptake systems. In most bacterial species, two highly specified uptake systems are found to act in conditions of extreme toxicity (low-affinity uptake system) and extreme scarcity (high-affinity uptake systems), respectively, both of which are used in different conditions. In moderate conditions inside the cell, low-affinity uptake transporters are used to maintain levels of Zn (Hantke, 2001). The ABC family, comprised of three regulatory proteins (ZnuA, ZnuB, and ZnuC) is attributable to high-affinity uptake of Zn in the cell (Patzer and Hantke, 1999) and is a member of the ATP-binding cassette transporter family of the ZnuABC and AdcABC/ZitSPQ type. ZnuA is a soluble protein which resides in the outer membrane of the bacterial cell, whereas ZnuB is the protein which is found in the inner membrane and interacts with ZnuA. The third protein, ZnuC, regulates the breakdown of ATP, thus contributing to the uptake and efflux of the metal. Reports suggest that the deletion of ZnuA, ZnuB, and/or ZnuC or *znuABC* in different bacterial species can result in the decreased uptake of Zn (Porcheron et al., 2013). Though much is known about this high-affinity uptake system, very little is reported about the other uptake system (Chandra et al., 2007). In *Bacillus subtilis*, the uptake of Zn^{2+} is regulated majorly by Zur family, but another uptake system known as ZosA (which is a P-type ATPase) was also reported to be active in conditions of oxidative stress (Suryawati, 2018; **Figure 2**; **Table 2**).

Mechanisms of Zinc Efflux in Bacteria

In conditions of Zn toxicity, the expression of efflux systems in bacterial cells aids in the prevention of overabundance of Zn (Guilhen et al., 2013). In bacteria, three families of exporters; cation diffusion facilitator (CDF), Resistance nodulation division (RND) efflux pumps, and P-type ATPases are majorly reported to be involved in metal export out of bacterial cells (Kolaj-Robin et al., 2015). Among these families, the CDF family is one of the most commonly found protein families in living beings. In *Escherichia coli*, ZitB and YiiP proteins, members of the CDF family, are transporters which regulate the efflux of Zn^{2+} ions *via* using the energy generated through the uptake of H^{+} ions (Porcheron et al., 2013). Another member of the CDF family, ZntA, reported to mediate resistance against Zn^{2+} ions in *Staphylococcus aureus*, is a well-known Zn transporter (Singh et al., 1999). In *Caulobacter crescentus*, the czrCBA system is the major efflux facilitator for Cd^{2+} and Zn^{2+} ions (Valencia et al., 2013). The Czc determinant confers resistance *via* efflux against various metals, such as Co^{2+}, Zn^{2+}, and Cd^{2+} ions in *Alcaligenes eutrophus* (Nies et al., 1989). This efflux system is a cation/proton antiporter system which enables the efflux of cations from the cell, and consists of three structural genes (*czcABC*) which in turn encode three regulatory proteins of the efflux pump CzcA, CzcB, and CzcD (Nies, 1992). Moreover, efflux of Zn^{2+} ions in *B. subtilis* is mediated by CadA, which is a CPx-type ATPase efflux system (Gaballa et al., 2002). P-type ATPase family is reported to be found in both eukaryotes and bacteria, though they are generally well-defined in the latter. These transporters are regulated either by MerR/ZntR or ArsR/SmtB family members, which are often found to be working in close association with other metal transport proteins (Hantke, 2001). P-type ATPases regulate the transportation of metal ions across the bacterial cell membrane by utilizing the energy of ATP hydrolysis (Apell, 2004). A good example of P-type ATPase is ZntA in *E. coli*, which is regulated by MerR-like regulator *via* the attachment of apo-ZntR dimer to the promotor region of zntA, repressing its transcription (Porcheron et al., 2013). This phenomenon takes place when intracellular Zn concentration exceed sub-toxicity levels (Khan et al., 2002). The RND family is majorly found in Gram-negative bacteria which is involved in the active efflux of antibiotics and other therapeutic agents. These systems have large periplasmic domains and in many bacterial species are known to form complexes with extracellular channels and adaptor proteins (Nikaido and Takatsuka, 2009). In *C. crescentus*, CzrCBA is known to export cadmium and Zn ions from cytoplasm of cells (Valencia et al., 2013). The export of Zn and other metal ions in *Ralstonia metallidurans* is facilitated by CzcABC system, which is regulated by CzcS/CzcR two-component regulatory system (Anton et al., 1999; Hantke, 2001; Blencowe and Morby, 2003; Blindauer, 2015; Suryawati, 2018; **Figure 2**).

Zinc Bioremediation by Bacteria

The bioremediation of Zn from various environments has been reported in various studies over the years. *Brevibacterium* sp. was effective in removing Zn from polluted environments, even in concentrations as low as 0.1 mm (Taniguchi et al., 2000). The biosorption potential of *Delftia tsuruhatensis* for Zn and lead (Pb) was also reported in a study

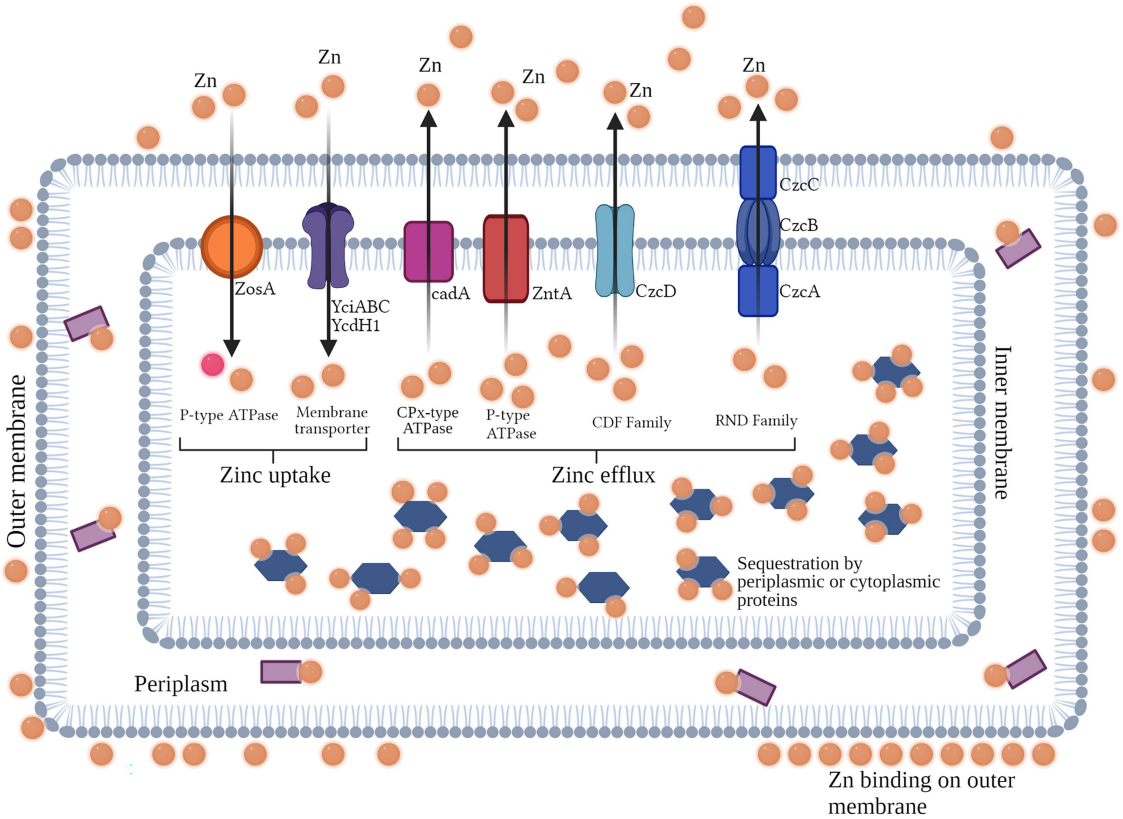

FIGURE 2 | Overview of the general resistance mechanisms for Zn found in Gram-negative and -positive bacteria (Created with BioRender). In Gram negative and positive bacteria, general resistance mechanisms aid in efflux, sequestration, chelation, and metal uptake for their survival in toxic or scarce conditions. For the metal Zn, uptake in Gram positive bacteria from the outer environment is facilitated by P-type ATPase (ZosA), and Zn membrane transporters. For efflux of Zn ions out of the cell, CDF and RND efflux pumps (Czc determinants found in both Gram positive and negative bacteria), as well as CPx-type (CadA in Gram positive bacteria) and P-type ATPases (ZntA in both Gram positive and negative bacteria) are majorly involved. Moreover, intracellular or periplasmic proteins can bind to Zn inside the cell.

TABLE 2 | Genes involved in Zn resistance in Gram-positive and Gram-negative bacterial species.

Gene	Toxic ion(s)	Bacteria
czcA, *czcB*, and *czcC*	Zn, Cd, Co	*Ralstonia eutropha*
czrCBA	Zn, Cd	*Pseudomonas aeruginosa*
zntA	Zn, Co	*Staphylococcus aureus, Escherichia coli, Ralstonia metallidurans*
smtAB	Zn, Cd	*Synechococcus* sp.
ycdH operon	Zn	*Bacillus subtilis*
yciC operon		
cadCA, cadB	Zn, Cd	*Staphylococcus aureus*

(Bautista-Hernandez et al., 2012). Bacterial consortia of several species, such as *Alcaligenes faecalis, Staphylococcus aureus, Streptococcus lactis, Micrococcus luteus,* and *Enterobacter aerogenes,* was reported to remove various heavy metals, such as copper (Cu), cadmium (Cd), Pb, and Zn from wastewaters (Silambarasan and Abraham, 2013). *Pseudomonas putida*, another Gram-negative bacterium, was reported to demonstrate highest ability of Zn removal among other isolates in a study, whereas *Bacillus subtilis* was the most effective among Gram-positive bacteria, respectively (Kamika and Momba, 2013). *Rhodobacter capsulatus* was reported to efficiently remove Zn from polluted environments with the help of its wild-type strain and an enclosed plasmid which conferred resistance (Magnin et al., 2014). *Bacillus licheniformis* and *Salmonella typhi* were reported to remove more than 90% of Zn from contaminated samples, whereas *Pseudomonas fluorescens* and *E. coli* were effective in removing more than 96 and 93% of Zn, respectively (Basha and Rajaganesh, 2014). *P. fluorescens* and *P. putida* were also observed to be good bioremediation agents for many heavy metals, including Zn (Upadhyay and Srivastava, 2014; Ahmady-Asbchin et al., 2015; Naz et al., 2016). In a similar study, several bacterial species, such as *P. aeruginosa*, *S. aureus*, *E. coli, Proteus vulgaris,* and *Klebsiella pneumoniae,* were evaluated for their heavy metal removal ability, where their mixed consortium was able to remediate more than 90% of Zn. Among pure isolates, *P. aeruginosa* was effective in removing the largest quantity of Zn from contaminated medium (53.9%), as well as other heavy metals (Oaikhena et al., 2016). Among Gram-positive bacteria,

TABLE 3 | Zn biosorption and metal uptake ability of various Gram-positive and Gram-negative bacterial species, as reported in different studies.

Bacterial strains	Initial metal concentration	Metal uptake	References
Bacillus firmus	100 mg/l	61.8%	Salehizadeh and Shojaosadati, 2003
B. subtilis D_{215}	100 mg/l	63.73%	Sabae et al., 2006
Bacillus jeotgali	75 mg/l	30%	Green-Ruiz et al., 2008
B. cereus	0–200 mg/l	66.6 mg/g	Joo et al., 2010
Pseudomonas sp.	1 mm	49.8%	Kumaran et al., 2011
Delftia tsuruhatensis	–	0.207 mmoL/g	Bautista-Hernández et al., 2012
Pseudomonas sp. *SN7*	1.6 mM	29 mg/g	Ahemad and Malik, 2012
Pseudomonas sp. *SN28*		25 mg/g	
Pseudomonas sp. *SN30*		26 mg/g	
Geobacillus thermodenitrificans	0.5 g/l	18 mg/l	Babák et al., 2012
Geobacillus thermocatenulatus.		24 mg/l	
Exiguobacterium sp. ZM-2	25–200 mg/l	78.2%	Alam and Ahmad, 2013
B. licheniformis	0.1 mg/l	53%	Kamika and Momba, 2013
B. licheniformis	–	96.14%	Basha and Rajaganesh, 2014
Salmonella typhi		91.78%	
P. fluorescens		96.14%	
Escherichia coli		93.27%	
Alcaligenes faecalis	–	39%	Silambarasan and Abraham, 2013
Staphylococcus aureus		41%	
Streptococcus lactis		38%	
Micrococcus luteus		41%	
Enterobacter aerogenes		67%	
Bacillus sp. (KF710041)	–	73.29%	Singh and Chopra, 2014
B. subtilis (KF710042)		78.15%	
Rhodobacter capsulatus	10 mg/l	164 mg/g	Magnin et al., 2014
B. subtilis	178 mg/l	49.7 mg/l	Wierzba, 2015
P. aeruginosa	100 mg/l	46.1 mg/g	Ahmady-Asbchin et al., 2015
P. aeruginosa	7 mg/l	53.9%	Oaikhena et al., 2016
S. aureus		90.1% (Mix culture)	
Escherichia coli			
Proteus vulgaris			
Klebsiella pneumoniae			
B. megaterium EMCC 1013	1 mg/ml	88%	El-barbary and El-badry, 2018
Rhizobium leguminosarum EMCC1130		85%	
Serratia sp.	1,000 mg/kg	<90%	Kour et al., 2019
Streptomyces K11 strain	–	36%	Sedlakova-Kadukova et al., 2019
Stenotrophomonas maltophilia XZN4	20 g/l	91.6%	Huang et al., 2020
Oceanobacillus profundus	2 mg/ml	54%	Mwandira et al., 2020
Sporosarcina pasteurii	4 mmol/l	70.36%	Ghorbanzadeh et al., 2022
Urease-producing isolate		71.46%	
L-asparaginase-producing isolate	8 mmol/l	97.32%	

Staphylococcus epidermidis was also reported to be effective in removing Zn (<80%) as well as other heavy metals from contaminated water (Nwagwu et al., 2017). *Streptomyces* sp. also demonstrated to remove Zn under controlled conditions (Sedlakova-Kadukova et al., 2019). Another study revealed *Serratia* sp. to be effective in tolerating high concentrations of Zn. High values of biosorption (more than 90%) were observed under Zn stress, which also aided in growth augmentation of plant roots, shoots, and chlorophyll content (Kour et al., 2019). Furthermore, the bioremediation of Zn by various *Bacillus* sp. from soil and wastewaters has been well-reported in various studies over the years (Joo et al., 2010; Singh and Chopra, 2014; Wierzba, 2015; Huang et al., 2020; **Table 3**). A recent study also sought out to investigate Zn removal efficacy of *Sporosarcina pasteurii* from contaminated soils, where urease-producing isolates and *S. pasteurii* had removal ability of more than 70%, and L-asparaginase-producing isolate had the ability to remove more than 90% Zn in solution (Ghorbanzadeh et al., 2022).

CONCLUSION

Zn is the one of the major elements (23rd) found in the Earth's crust, with an average concentration of approximately 78 mg/kg. After Fe, Al, and Cu, it is the major metal used in the world, in terms of tonnage. Zn is regarded as a biologically essential element for living beings. It is reported to be imperatively required for the normal functioning of major enzymes and proteins. It is also reported to be effective in combating viral infections and strengthening the immune system against them, which involves the inhibition of the entry, fusion, replication, translation, and emission of virus particles into and out of the host cells. However, excess levels

of Zn can act as toxic, which can induce conditions of acute toxicity for living beings. For its mitigation from the environment, bioremediation is a comparatively cheaper, more efficient, and effective method employed for the removal of heavy metals from various environments, like effluents and wastewaters. In bacteria, general resistance mechanisms (such as efflux, uptake, sequestration, and chelation) are found in Gram-negative and -positive bacteria which aid in the removal of heavy metals, such as Zn, from polluted environments. However, these resistance mechanisms need to be investigated on a molecular level so that these species could be manipulated for industrial applications, as one of the drawbacks of bioremediation is its inability to be reproduced from lab scale to large scale. This review focuses on the uses, toxicity, and bioremediation of Zn with special insight into its chemical and physical properties as well as its role in nutrition and immunity. Further innovative aspects of Zn remediation and toxicity can aid in the elucidation of resistance mechanisms, as well as Zn bioavailability.

AUTHOR CONTRIBUTIONS

All authors contributed equally in this manuscript. All authors read and approved the submitted version.

ACKNOWLEDGMENTS

This study was financially supported by the Science and Technology Major Project of Inner Mongolia (No. ZDZX2018054), China, the National Natural Science Funds of China (31370474), and the Jiangsu Province Postdoctoral Excellence Program (2022ZB155). Special thanks also go to the three reviewers for their very useful comments and suggestions.

REFERENCES

Agnieszka, B., Tomasz, C., and Jerzy, W. (2014). Chemical properties and toxicity of soils contaminated by mining activity. *Ecotoxicology* 23, 1234–1244. doi: 10.1007/s10646-014-1266-y

Ahemad, M., and Malik, A. (2012). Bioaccumulation of heavy metals by zinc resistant bacteria isolated from agricultural soils irrigated with wastewater. *J. Bacteriol.* 2, 12–21. doi: 10.3923/bj.2012.12.21

Ahmady-Asbchin, S., Safari, M., and Tabaraki, R. (2015). Biosorption of Zn(II) by *Pseudomonas aeruginosa* isolated from a site contaminated with petroleum. *Desalin. Water Treat.* 54, 3372–3379. doi: 10.1080/19443994.2014.913202

Aka, R. J. N., and Babalola, O. O. (2017). Identification and characterization of Cr-, cd-, and Ni-tolerant bacteria isolated from mine tailings. *Biorem. J.* 21, 1–19. doi: 10.1080/10889868.2017.1282933

Alam, M. Z., and Ahmad, S. (2013). Multi-metal biosorption and bioaccumulation by *Exiguobacterium* sp. ZM-2. *Ann. Microbiol.* 63, 1137–1146. doi: 10.1007/s13213-012-0571-z

Alloway, B. J. (2008). *Zinc in Soils and crop Nutrition.* Brussels, Belgium and Paris: International fertilizer Industry Association and International Zinc Association, 135.

Anju, M., and Banerjee, D. K. (2011). Associations of cadmium, zinc, and lead in soils form lead and zinc mining area as studied by single and sequential extractions. *Environ. Monit. Assess.* 176, 67–85. doi: 10.1007/s10661-010-1567-4

Anton, A., Grosse, C., Reissmann, J., Pribyl, T., and Nies, D. H. (1999). CzcD is a heavy metal ion transporter involved in regulation of heavy metal resistance in *Ralstonia* sp. strain CH34. *J. Bacteriol.* 181, 6876–6881. doi: 10.1128/JB.181.22.6876-6881.1999

Asl, S. H., Nikfarjam, S., Majidi Zolbanin, N., Nassiri, R., and Jafari, R. (2021). Immunopharmacological perspective on zinc in SARS-CoV-2 infection. *Int. Immunopharmacol.* 96, 107630–107617. doi: 10.1016/j.intimp.2021.107630

Audi, G., Kondev, F. G., Wang, M., Huang, W. J., and Naimi, S. (2017). The NUBASE2016 evaluation of nuclear properties. *Chin. Phys. C.* 41:30001. doi: 10.1088/1674-1137/41/3/030001

Apell, H. J. (2004). How do P-type ATPases transport ions?. Bioelectrochemistry (Amsterdam, Netherlands), 63, 149–156. doi: 10.1016/j.bioelechem.2003.09.021

Baastrup, R., Sørensen, M., Balstrøm, T., Frederiksen, K., Larsen, C. L., and Tjønneland, A. (2008). Arsenic in drinking-water and risk for cancer in Denmark. *Environ. Health Persp.* 116, 231–237. doi: 10.1289/ehp.10623

Babák, L., Šupinová, P., Zichová, M., Burdychová, R., and Vítová, E. (2012). Biosorption of cu, Zn and Pb by thermophilic bacteria - effect of biomass concentration on biosorption capacity. *Acta Univ. Agric. Silvic. Mendelianae Brun.* 60, 9–18. doi: 10.11118/actaun201260050009

Bădulici, S., Chirulescu, Z., Chirilă, P., Chirilă, M., and Roşca, A. (1994). Treatment with zincum metallicum CH5 in patients with liver cirrhosis—preliminary study. *Rom. J. Intern. Med.* 32, 215–219.

Baran, A. (2012). Assessment of zinc content and mobility in maize. *Ecol. Chem. Eng. A.* 19, 699–706. doi: 10.2428/ecea.2012.19(07)069

Baran, A. (2013). Assessment of *Zea mays* sensitivity to toxic content of zinc in soil. *Pol. J. Environ. Stud.* 22, 77–83.

Baran, A., Wieczorek, J., Mazurek, R., Urbański, K., and Klimkowicz-Pawlas, A. (2018). Potential ecological risk assessment and predicting zinc accumulation in soils. *Environ. Geochem. Health* 40, 435–450. doi: 10.1007/s10653-017-9924-7

Basha, S. A., and Rajaganesh, K. (2014). Microbial bioremediation of heavy metals from textile industry dye effluents using isolated bacterial strains. *Int. J. Curr. Microbiol. App. Sci.* 3, 785–794.

Bautista-Hernandez, D. A., Ramirez-Burgos, I. L., Duran-Paramo, E., and Fernandez-Linares, L. (2012). Zinc and lead biosorption by *Delftia tsuruhatensis*: A bacterial strain resistant to metals isolated from mine tailings. *J. Water Resour. Protect.* 4, 207–216. doi: 10.4236/jwarp.2012.44023

Bautista-Hernández, D., Ramírez-Burgos, L., Duran-Páramo, E., and Fernández-Linares, L. (2012). Zinc and lead biosorption by Delftia tsuruhatensis: A bacterial strain resistant to metals isolated from mine tailings. *J. Water Resour. Protect.* 04, 207–216. doi: 10.4236/jwarp.2012.44023

Beck, F. W., Prasad, A. S., Kaplan, J., Fitzgerald, J. T., and Brewer, G. J. (1997). Changes in cytokine production and T cell subpopulations in experimentally induced zinc-deficient humans. *Am. J. Phys.* 272, E1002–E1007. doi: 10.1152/ajpendo.1997.272.6.E1002

Berendonk, T. U., Manaia, C. M., Merlin, C., Fatta-Kassinos, D., Cytryn, E., Walsh, F., et al. (2015). Tackling antibiotic resistance: The environmental framework. *Nat. Rev. Microbiol.* 13, 310–317. doi: 10.1038/nrmicro3439

Blencowe, D. K., and Morby, A. P. (2003). Zn(II) metabolism in prokaryotes. *FEMS Microbiol. Rev.* 27, 291–311. doi: 10.1016/S0168-6445(03)00041-X

Blindauer, C. A. (2015). Advances in the molecular understanding of biological zinc transport. *Chem. Commun.* 51, 4544–4563. doi: 10.1039/C4CC10174J

Bolan, N., Kunhikrishnan, A., Thangarajan, R., Kumpiene, J., Park, J., Makino, T., et al. (2014). Remediation of heavy metal(loid)s contaminated soils - to mobilize or to immobilize? *J. Hazard. Mater.* 266, 141–166. doi: 10.1016/j.jhazmat.2013.12.018

Bonaventura, P., Benedetti, G., Albarède, F., and Miossec, P. (2015). Zinc and its role in immunity and inflammation. *Autoimmun. Rev.* 14, 277–285. doi: 10.1016/j.autrev.2014.11.008

Brown, M. A., Thom, J. V., Orth, G. L., Cova, P., and Juarez, J. (1964). Food poisoning involving zinc contamination. *Arch. Environ. Health* 8, 657–660. doi: 10.1080/00039896.1964.10663736

Brzóska, M. M., Kozłowska, M., Rogalska, J., Gałażyn-Sidorczuk, M., Roszczenko, A., and Smereczański, N. M. (2021). Enhanced zinc intake protects against oxidative stress and its consequences in the brain: A study in an *in vivo* rat model of cadmium exposure. *Nutrients* 13, 478–504. doi: 10.3390/nu13020478

Callender, G. R., and Gentzkow, C. J. (1937). Acute poisoning by the zinc and antimony content of limeade prepared in a galvanized iron can. *Mil. Surg.* 80, 67–71.

Capdevila, D. A., Wang, J. F., and Giedroc, D. P. (2016). Bacterial strategies to maintain zinc metallostasis at the host-pathogen interface. *J. Biol. Chem.* 291, 20858–20868. doi: 10.1074/jbc.R116.742023

Castro-Alba, V., Lazarte, C. E., Bergenståhl, B., and Granfeldt, Y. (2019). Phytate, iron, zinc, and calcium content of common Bolivian foods and their estimated mineral bioavailability. *Food Sci. Nutr.* 7, 2854–2865. doi: 10.1002/fsn3.1127

Cerasi, M., Ammendola, S., and Battistoni, A. (2013). Competition for zinc binding in the host-pathogen interaction. *Front. Cell. Infect. Microbiol.* 3: 108. doi: 10.3389/fcimb.2013.00108

Chandra, B. R., Yogavel, M., and Sharma, A. (2007). Structural analysis of ABC-family periplasmic zinc binding protein provides new insights into mechanism of ligand uptake and release. *J. Mol. Biol.* 367, 970–982. doi: 10.1016/j.jmb.2007.01.041

Chandrangsu, P., Rensing, C., and Helmann, J. D. (2017). Metal homeostasis and resistance in bacteria. *Nat. Rev. Microbiol.* 15, 338–350. doi: 10.1038/nrmicro.2017.15

Chasapis, C. T., Loutsidou, A. C., Spiliopoulou, C. A., and Stefanidou, M. E. (2012). Zinc and human health: An update. *Arch. Toxicol.* 86, 521–534. doi: 10.1007/s00204-011-0775-1

Chen, Y., Jiang, Y., Huang, H., Mou, L., Ru, J., Zhao, J., et al. (2018). Long-term and high-concentration heavy-metal contamination strongly influences the microbiome and functional genes in Yellow River sediments. *Sci. Total Environ.* 637, 1400–1412. doi: 10.1016/j.scitotenv.2018.05.109

Chen, J., Li, J., Zhang, H., Shi, W., and Liu, Y. (2019). Bacterial heavy-metal and antibiotic resistance genes in a copper tailing dam area in northern China. *Front. Microbiol.* 10:1916. doi: 10.3389/fmicb.2019.01916

Costello, L. C., and Franklin, R. B. (1998). Novel role of zinc in the regulation of prostate citrate metabolism and its implications in prostate cancer. *Prostate* 35, 285–296. doi: 10.1002/(sici)1097-0045(19980601)35:4<285::aid-pros8>3.0.co;2-f

Costello, L. C., Liu, Y., Zou, J., and Franklin, R. B. (1999). Evidence for a zinc uptake transporter in human prostate cancer cells which is regulated by prolactin and testosterone. *J. Biol. Chem.* 274, 17499–17504. doi: 10.1074/jbc.274.25.17499

Cunningham, S. D., Berti, W. R., and Huang, J. W. W. (1995). Phytoremediation of contaminated soils. *Trends Biotechnol.* 13, 393–397.

Dardenne, M., and Pleau, J. M. (1994). Interactions between zinc and thymulin. *Metal. Bas. Drugs.* 1, 233–239. doi: 10.1155/MBD.1994.233

Deb, D. L. (1992). Development of seoil and plant analytical methods for micronutrients and sulphur in Sri Lanka. GCPF/SRI/047/NET field document No. 11. 16.

DeCoursey, T. E., Morgan, D., and Cherny, V. V. (2003). The voltage dependence of NADPH oxidase reveals why phagocytes need proton channels. *Nature* 422, 531–534. doi: 10.1038/nature01523

El-barbary, T. A. A., and El-Badry, M. A. (2018). Bioremediation potential of Zn(II) by different bacterial species. *Saudi J. Biomed. Res.* 3, 144–150. doi: 10.21276/sjbr.2018.3.4.3

Elinder, C. G. (1986). *Handbook on the Toxicology of Metals*. Amsterdam: Elsevier Science Publishers.

Epelde, L., Lanzén, A., Blanco, F., Urich, T., and Garbisu, C. (2015). Adaptation of soil microbial community structure and function to chronic metal contamination at an abandoned Pb-Zn mine. *FEMS Microbiol. Ecol.* 91, 1–11. doi: 10.1038/nature01523

Farrah, H., and Pickering, W. F. (1977). Influence of clay-solute interactions on aqueous heavy metals ion levels. *Water Air Soil Pollut.* 8, 189–197. doi: 10.1007/BF00294042

Fedotov, P. S., Koerdel, W., Miro, M., Peijnenburg, W. J. G. M., Wennrich, R., and Huang, P. M. (2012). Extraction and fraction methods for exposure assessment of trace metals, metalloids and hazardous organic compounds in terrestrial environments. *Crit. Rev. Environ. Sci. Technol.* 42, 1117–1171. doi: 10.1080/10643389.2011.556544

Flanagan, P. R., Cluett, J., Chamberlain, M. J., and Valberg, L. S. (1985). Dual-isotope method for determination of human zinc absorption: The use of a test meal of Turkey meat. *J. Nutr.* 115, 111–122. doi: 10.1093/jn/115.1.111

Fraker, P. J., and King, L. E. (2004). Reprogramming of the immune system during zinc deficiency. *Annu. Rev. Nutr.* 24, 277–298. doi: 10.1146/annurev.nutr.24.012003.132454

Frank, R., Ishida, K., and Suda, P. (1976). Metals in agricultural soils of Ontario. *Can. J. Soil Sci.* 56, 181–196. doi: 10.4141/cjss76-027

Franklin, R. B., Feng, P., Milon, B., Desouki, M. M., Singh, K. K., Kajdacsy-Balla, A., et al. (2005). hZIP1 zinc uptake transporter down regulation and zinc depletion in prostate cancer. *Mol. Cancer* 4, 32–45. doi: 10.1186/1476-4598-4-32

Freitag, A., and Caduff, B. (1996). ARDS caused by military zinc fumes exposure. *Schweiz. Med. Wochenschr.* 126, 1006–1010.

Gaballa, A., Wang, T., Ye, R. W., and Helmann, J. D. (2002). Functional analysis of the *Bacillus subtilis* Zur regulon. *J. Bacteriol.* 184, 6508–6514. doi: 10.1128/JB.184.23.6508-6514.2002

Gammoh, N. Z., and Rink, L. (2017). Zinc in infection and inflammation. *Nutrients* 9, 624–649. doi: 10.3390/nu9060624

Gautam, P. K., Gautam, R. K., Banerjee, S., Chattopadhyaya, M. C., and Pandey, J. D. (2016). "Heavy metals in the environment: fate, transport, toxicity and remediation technologies," in *Heavy Metals*. ed. D. Pathania (New York: Nava Science Publishers, Inc.), 101–130.

Ghorbanzadeh, N., Ghanbari, Z., Farhangi, M. B., and Rad, M. K. (2022). Zinc bioremediation in soil by two isolated L-asparaginase and urease producing bacteria strains. *Appl. Geochem.* 140:105271. doi: 10.1016/j.apgeochem.2022.105271

Graf, G. G. (1997). "Zinc," in *Handbook of Extractive Metallurgy*. ed. F. Habashi (Weinheim: Wiley-VCH), 641–688.

Green-Ruiz, C., Rodriguez-Tirado, V., and Gomez-Gil, B. (2008). Cadmium and zinc removal from aqueous solutions by *Bacillus jeotgali*: pH, salinity and temperature effects. *Bioresour. Technol.* 99, 3864–3870. doi: 10.1016/j.biortech.2007.06.047

Guarino, F., Improta, G., Triassi, M., Cicatelli, A., and Castiglione, S. (2020). Effects of zinc pollution and compost amendment on the root microbiome of a metal tolerant poplar clone. *Front. Microbiol.* 11:1677. doi: 10.3389/fmicb.2020.01677

Guilhen, C., Taha, M. K., and Veyrier, F. J. (2013). Role of transition metal exporters in virulence: the example of *Neisseria meningitidis*. *Front. Cell. Infect. Microbiol.* 3:102. doi: 10.3389/fcimb.2013.00102

Guo, C. Q., and Feng, J. C. (2013). Zinc market analysis and outlook. *China Nonferr. Metals.* 2, 44–45.

Haase, H., Overbeck, S., and Rink, L. (2008). Zinc supplementation for the treatment or prevention of disease: current status and future perspectives. *Exp. Gerontol.* 43, 394–408. doi: 10.1016/j.exger.2007.12.002

Haase, H., and Rink, L. (2014a). Multiple impacts of zinc on immune function. *Metallomics* 6, 1175–1180. doi: 10.1039/c3mt00353a

Haase, H., and Rink, L. (2014b). Zinc signals and immune function. *Biofactors* 40, 27–40. doi: 10.1002/biof.1114

Habashi, F. (2013). "Zinc, physical and chemical properties", in *Encyclopedia of Metalloproteins*, ed. Kretsinger, R. H., Uversky, V. N., and Permyakov, E. A. (New York, NY, Springer).

Hacisalihoglu, G. (2020). Zinc (Zn): The last nutrient in the alphabet and shedding light on Zn efficiency for the future of crop production under suboptimal Zn. *Plants* 9, 1471–1480. doi: 10.3390/plants9111471

Hacisalihoglu, G., and Blair, M. (2020). Current advances in zinc in soils and plants: implications for zinc efficiency and biofortification studies. *Achiev. Sustain. Crop Nutr.* 76, 337–353. doi: 10.19103/AS.2019.0062.16

Haiyan, W., and Stuanes, A. O. (2003). Heavy metal pollution in air-water-soil-plant system of Zhuzhou City, Hunan Province. *China. Water Air Soil Pollut.* 147, 79–107. doi: 10.1023/A:1024522111341

Hambidge, K. M., Miller, L. V., Westcott, J. E., Sheng, X., and Krebs, N. F. (2010). Zinc bioavailability and homeostasis. *Am. J. Clin. Nutr.* 91, 1478S–1483S. doi: 10.3945/ajcn.2010.28674I

Hanahan, D., and Weinberg, R. A. (2000). The hallmarks of cancer. *Cell* 100, 57–70. doi: 10.1016/s0092-8674(00)81683-9

Hantke, K. (2001). Bacterial zinc transporters and regulators. *Biometals* 14, 239–249. doi: 10.1023/a:1012984713391

Hasegawa, H., Suzuki, K., Suzuki, K., Nakaji, S., and Sugawara, K. (2000). Effects of zinc on the reactive oxygen species generating capacity of human neutrophils and on the serum opsonic activity *in vitro*. *Luminescence* 15, 321–327. doi: 10.1002/1522-7243(200009/10)15:5<321::AID-BIO605>3.0.CO;2-O

Holleman, A. F., Wiberg, E., and Wiberg, N. (1985). "Zink," in *Lehrbuch der Anorganischen Chemie*. ed. A. F. Holleman (Germany: Walter de Gruyter), 91–100.

Hough, R. L., Breward, N., Young, S. D., Crout, N. M. J., Tye, A. M., Moir, A. M., et al. (2004). Assessing potential risk of heavy metal exposure from consumption of home-produced vegetables by urban populations. *Environ. Health Persp.* 112, 215–221. doi: 10.1289/ehp.5589

Hu, J., and Dong, Z. (2011). Development of lead source-specific exposure standards based on aggregate exposure assessment: Bayesian inversion from biomonitoring information to multipathway exposure. *Environ. Sci. Technol.* 46, 1144–1152. doi: 10.1021/es202800z

Huang, J., Wang, J., and Jia, L. (2020). Removal of zinc (II) from livestock and poultry sewage by a zinc (II) resistant bacteria. *Sci. Rep.* 10:21027. doi: 10.1038/s41598-020-78138-z

Hynninen, A., Tönismann, K., and Virta, M. (2010). Improving the sensitivity of bacterial bioreporters for heavy metals. *Bioeng Bugs.* 1, 132–138. doi: 10.4161/bbug.1.2.10902

Imseng, M., Wiggenhauser, M., Müller, M., Keller, A., Frossard, E., Wilcke, W., et al. (2019). The fate of Zn in agricultural soils: A stable isotope approach to anthropogenic impact, soil formation and soil-plant cycling. *Environ. Sci. Technol.* 53, 4140–4149. doi: 10.1021/acs.est.8b03675

Incharoensakdi, A., and Kitjaharn, P. (2002). Zinc biosorption from aqueous solution by a halotolerant cyanobacterium Aphanothece halophytica. *Curr. Microbiol.* 45, 261–264. doi: 10.1007/s00284-002-3747-0

International Lead and Zinc Study Group. (2020) *ILZSG Session/Forecasts: Lisbon*, Portugal: International Lead and Zinc Study Group press release.

Irving, J. A., Mattman, A., Lockitch, G., Farrell, K., and Wadsworth, L. D. (2003). Element of caution: A case of reversible cytopenias associated with excessive zinc supplementation. *CMAJ* 169, 129–131.

Ishida, T. (2019). Review on the role of Zn^{2+} ions in viral pathogenesis and the effect of Zn^{2+} ions for host cell-virus growth inhibition. *Am. J. Biomed. Sci. Res.* 2, 28–37. doi: 10.34297/AJBSR.2019.02.000566

Jarosz, M., Olbert, M., Wyszogrodzka, G., Młyniec, K., and Librowski, T. (2017). Antioxidant and anti-inflammatory effects of zinc. Zinc-dependent NF-κB signaling. *Inflammopharmacology* 25, 11–24. doi: 10.1007/s10787-017-0309-4

Jarrard, D. F. (2005). Does zinc supplementation increase the risk of prostate cancer? *Arch. Ophthalmol.* 123, 102–103. doi: 10.1001/archopht.123.1.102

Jensen, W. B. (2003). The place of zinc, cadmium, and mercury in the periodic table. *J. Chem. Ed.* 80, 952–961. doi: 10.1021/ed080p952

Johnson, F. A., and Stonehill, R. B. (1961). Chemical pneumonitis from inhalation of zinc chloride. *Dis. Chest* 40, 619–624. doi: 10.1378/chest.40.6.619

Joo, J. H., Hassan, S. H., and Oh, S. E. (2010). Comparative study of biosorption of Zn^{2+} by *Pseudomonas aeruginosa* and *Bacillus cereus*. *Int. Biodeter. Biodegrad.* 64, 734–741. doi: 10.1016/j.ibiod.2010.08.007

Kamika, I., and Momba, M. N. (2013). Assessing the resistance and bioremediation ability of selected bacterial and protozoan species to heavy metals in metal-rich industrial wastewater. *BMC Microbiol.* 13, 28–42. doi: 10.1186/1471-2180-13-28

Khan, S., Brocklehurst, K. R., Jones, G. W., and Morby, A. P. (2002). The functional analysis of directed amino-acid alterations in ZntR from *Escherichia coli*. *Biochem. Biophys. Res. Commun.* 299, 438–445. doi: 10.1016/s0006-291x(02)02660-8

Kim, R. Y., Yoon, J. K., Kim, T. S., Yang, J. E., Owens, G., and Kim, K. R. (2015). Bioavailability of heavy metals in soils: definitions and practical implementation: a critical review. *Environ. Geochem. Health* 37, 1041–1061. doi: 10.1007/s10653-015-9695-y

King, L. E., Frentzel, J. W., Mann, J. J., and Fraker, P. J. (2005). Chronic zinc deficiency in mice disrupted T cell lymphopoiesis and erythropoiesis while B cell lymphopoiesis and myelopoiesis were maintained. *J. Am. Coll. Nutr.* 24, 494–502. doi: 10.1080/07315724.2005.10719495

Kolaj-Robin, O., Russell, D., Hayes, K. A., Pembroke, J. T., and Soulimane, T. (2015). Cation diffusion facilitator family: structure and function. *FEBS Lett.* 589, 1283–1295. doi: 10.1016/j.febslet.2015.04.007

Kour, R., Jain, D., Bhojiya, A. A., Sukhwal, A., Sanadhya, S., Saheewala, H., et al. (2019). Zinc biosorption, biochemical and molecular characterization of plant growth-promoting zinc-tolerant bacteria. 3. *Biotech* 9, 421–438. doi: 10.1007/s13205-019-1959-2

Krebs, N. F. (2000). Overview of zinc absorption and excretion in the human gastrointestinal tract. *J. Nutr.* 130, 1374S–1377S. doi: 10.1093/jn/130.5.1374S

Kumaran, N. S., Sundaramanicam, A., and Bragadeeswaran, S. (2011). Adsorption studies on heavy metals by isolated cyanobacterial strain (nostoc sp.) from uppanar estuarine water, southeast coast of India. *J. Appl. Sci. Res.* 7, 1609–1615.

Lee, S. R. (2018). Critical role of zinc as either an antioxidant or a prooxidant in cellular systems. *Oxidative Med. Cell. Longev.* 2018, 1–11. doi: 10.1155/2018/9156285

Lewis, M. R., and Kokan, L. (1998). Zinc gluconate: acute ingestion. *J. Toxicol. Clin. Toxicol.* 36, 99–101. doi: 10.3109/15563659809162595

Li, X. F., Wang, P. F., Feng, C. L., Liu, D. Q., Chen, J. K., and Wu, F. C. (2019). Acute toxicity and hazardous concentrations of zinc to native freshwater organisms under different pH values in China. *Bull. Environ. Contam. Toxicol.* 103, 120–126. doi: 10.1007/s00128-018-2441-2

Lindholmer, C. (1974). Toxicity of zinc ions to human spermatozoa and the influence of albumin. *Andrologia* 6, 7–16. doi: 10.1111/j.1439-0272.1974.tb01583.x

Liu, C. H., Lee, C. T., Tsai, F. C., Hsu, S. J., and Yang, P. M. (2006). Gastroduodenal corrosive injury after oral zinc oxide. *Ann. Emerg. Med.* 47:296. doi: 10.1016/j.annemergmed.2005.09.020

Maares, M., and Haase, H. (2020). A guide to human zinc absorption: general overview and recent advances of *in vitro* intestinal models. *Nutrients* 12, 762–805. doi: 10.3390/nu12030762

Magnin, J. P., Gondrexon, N., and Willison, J. C. (2014). Zinc biosorption by the purple non-sulfur bacterium *Rhodobacter capsulatus*. *Can. J. Microbiol.* 60, 829–837. doi: 10.1139/cjm-2014-0231

Man, Y. B., Sun, X. L., Zhao, Y. G., Lopez, B. N., Chung, S. S., Wu, S. C., et al. (2020). Health risk assessment of abandoned agricultural soils based on heavy metal contents in Hong Kong, the world's most populated city. *Environ. Int.* 36, 570–576. doi: 10.1016/j.envint.2010.04.014

Mandal, B., Mandal, L. N., and Ali, M. H. (1993). "Chemistry of zinc Availability in Submerged Soils in Relation to zinc Nutrition of rice crop," in *Proceedings of the Workshop on Micronutrients*, Bhubaneswar, India, 240–253.

Marchetti, C. (2013). Role of calcium channels in heavy metal toxicity. *ISRN Toxicol.* 2013, 1–9. doi: 10.1155/2013/184360

Mari, M., Nadal, M., Schuhmacher, M., and Domingo, J. L. (2009). Exposure to heavy metals and PCDD/fs by the population living in the vicinity of a hazardous waste landfill in Catalonia, Spain: health risk assessment. *Environ. Int.* 35, 1034–1039. doi: 10.1016/j.envint.2009.05.004

Martin, C. J., Le, X. C., Guidotti, T. L., Yalcin, S., Chum, E., Audette, R. J., et al. (1999). Zinc exposure in Chinese foundry workers. *Am. J. Ind. Med.* 35, 574–580. doi: 10.1016/j.envint.2009.05.004

Mertens, J., and Smolders, E. (2013). "Zinc", in *Heavy Metals in Soils: Trace Metals and Metalloids in Soils and their Bioavailability* (Dordrecht;, Springer) Brian J. Alloway 465–493.

Mikhaylina, A., Ksibe, A. Z., Scanlan, D. J., and Blindauer, C. A. (2018). Bacterial zinc uptake regulator proteins and their regulons. *Biochem. Soc. Trans.* 46, 983–1001. doi: 10.1042/BST20170228

Miquel, E., and Farré, R. (2007). Effects and future trends of casein phosphopeptides on zinc bioavailability. *Trends Food Sci. Technol.* 18, 139–143. doi: 10.1016/j.tifs.2006.11.004

Mwandira, W., Nakashima, K., Kawasaki, S., Arabelo, A., Banda, K., Nyambe, I., et al. (2020). Biosorption of Pb (II) and Zn(II) from aqueous solution by *Oceanobacillus profundus* isolated from an abandoned mine. *Sci. Rep.* 10:21189. doi: 10.1038/s41598-020-78187-4

Nadal, M., Bocio, A., Schuhmacher, M., and Domingo, J. (2005). Trends in the levels of metals in soils and vegetation samples collected near a hazardous waste incinerator. *Arch. Environ. Contam. Tox.* 49, 290–298. doi: 10.1007/s00244-004-0262-2

Narayanan, S. E., Rehuman, N. A., Harilal, S., Vincent, A., Rajamma, R. G., Behl, T., et al. (2020). Molecular mechanism of zinc neurotoxicity in Alzheimer's disease. *Environ. Sci. Pollut. Res.* 27, 43542–43552. doi: 10.1007/s11356-020-10477-w

National Center for Biotechnology Information. (2022) PubChem element summary for atomic number 30, zinc. https://pubchem.ncbi.nlm.nih.gov/element/Zinc (Accessed on February 18, 2022).

Naz, T., Khan, M. D., Ahmed, I., Rehman, S. U., Rha, E. S., Malook, I., et al. (2016). Biosorption of heavy metals by *Pseudomonas* species isolated from sugar industry. *Toxicol. Ind. Health* 32, 1619–1627. doi: 10.1177/0748233715569900

Nies, D. H. (1992). Resistance to cadmium, cobalt, zinc, and nickel in microbes. *Plasmid* 27, 17–28. doi: 10.1016/0147-619x(92)90003-s

Nies, D. H., Nies, A., Chu, L., and Silver, S. (1989). Expression and nucleotide sequence of a plasmid determined divalent cation efflux system from *Alcaligenes eutrophus*. *Proc. Natl. Acad. Sci. U. S. A.* 86, 7351–7355. doi: 10.1073/pnas.86.19.7351

Nikaido, H., and Takatsuka, Y. (2009). Mechanisms of RND multidrug efflux pumps. *Biochim. Biophys. Acta* 1794, 769–781. doi: 10.1016/j.bbapap.2008.10.004

Nriagu, J. O. (1989). A global assessment of natural sources of atmospheric trace metals. *Nature* 338, 47–49. doi: 10.1038/338047a0

Nwagwu, E. C., Yilwa, V. M., Egbe, N. E., and Onwumere, G. B. (2017). Isolation and characterization of heavy metal tolerant bacteria from Panteka stream, Kaduna, Nigeria and their potential for bioremediation. *Afr. J. Biotech.* 16, 32–40. doi: 10.5897/AJB2016.15676

Oaikhena, E. E., Makaije, D. B., Denwe, S. D., Namadi, M. M., and Haroun, A. A. (2016). Bioremediation potentials of heavy metal tolerant bacteria isolated from petroleum refinery effluent. *Am. J. Environ. Protect.* 5, 29–34. doi: 10.11648/j.ajep.20160502.12

Olaniran, A. O., Balgobind, A., and Pillay, B. (2013). Bioavailability of heavy metals in soil: impact on microbial biodegradation of organic compounds and possible improvement strategies. *Int. J. Mol. Sci.* 14, 10197–10228. doi: 10.3390/ijms140510197

Otten, J. J., Pitzi Hellwig, J., and Meyers, L. D. (2006). *Dietary Reference Intakes*. Washington, DC, USA: National Academies Press.

Patzer, S. I., and Hantke, K. (1999). SufS is a NifS-like protein, and SufD is necessary for stability of the [2Fe-2S] FhuF protein in *Escherichia coli*. *J. Bacteriol.* 181, 3307–3309. doi: 10.1128/JB.181.10.3307-3309.1999

Pécoud, A., Donzel, P., and Schelling, J. L. (1975). Effect of foodstuffs on the absorption of zinc sulfate. *Clin. Pharmacol. Ther.* 17, 469–474. doi: 10.1002/cpt1975174469

Plum, L. M., Rink, L., and Haase, H. (2010). The essential toxin: impact of zinc on human health. *Int. J. Environ. Res. Public Health* 7, 1342–1365. doi: 10.3390/ijerph7041342

Porcheron, G., Garenaux, A., Proulx, J., Sabri, M., and Dozois, C. M. (2013). Iron, copper, zinc, and manganese transport and regulation in pathogenic Enterobacteria: correlations between strains, site of infection and the relative importance of the different metal transport systems for virulence. *Front. Cell. Infect. Microbiol.* 3:90. doi: 10.3389/fcimb.2013.00090

Porter, F. C. (1994). *Corrosion Resistance of zinc and zinc Alloys*. United States: CRC Press.

Potocki, S., Rowinska-Zyrek, M., Witkowska, D., Pyrkosz, M., Szebesczyk, A., Krzywoszynska, K., et al. (2012). Metal transport and homeostasis within the human body: toxicity associated with transport abnormalities. *Curr. Med. Chem.* 19, 2738–2759. doi: 10.2174/092986712800609698

Prasad, A. S. (2013). Discovery of human zinc deficiency: its impact on human health and disease. *Adv. Nutr.* 4, 176–190. doi: 10.3945/an.112.003210

Prasad, A. S. (2017). Discovery of zinc for human health and biomarkers of zinc deficiency. Molecular, genetic, and nutritional aspects of major and trace minerals. *Adv. Nutr.* 4, 176–190. doi: 10.3945/an.112.003210

Prasad, A. S., Beck, F. W. J., Bao, B., Fitzgerald, J. T., Snell, D. C., Steinberg, J. D., et al. (2007). Zinc supplementation decreases incidence of infections in the elderly: effect of zinc on generation of cytokines and oxidative stress. *Am. J. Clin. Nutr.* 85, 837–844. doi: 10.1093/ajcn/85.3.837

Prasad, A. S., Beck, F. W., Grabowski, S. M., Kaplan, J., and Mathog, R. H. (1997). Zinc deficiency: changes in cytokine production and T-cell subpopulations in patients with head and neck cancer and in noncancer subjects. *Proc. Assoc. Am. Phys.* 109, 68–77.

Prasad, A. S., Miale, A., Farid, Z., Schulert, A., and Sandstead, H. H. (1963). Zinc metabolism in patients with the syndrome of iron deficiency anemia, hypogonadism and dwarfism. *J. Lab. Clin. Med.* 61, 537–549.

Pueyo, M., Lopez-Sanchez, J. F., and Rauret, G. (2004). Assessment of $CaCl_2$, $NaNO_3$, and NH_4NO_3 extraction procedures for the study of cd, cu, Pb and Zn extractability in contaminated soils. *Anal. Chim. Acta* 504, 217–226. doi: 10.1016/j.aca.2003.10.047

Putila, J. J., and Guo, N. L. (2011). Association of arsenic exposure with lung cancer incidence rates in the United States. *PLoS One* 6, 1–7. doi: 10.1371/journal.pone.0025886

Qu, C. S., Ma, Z. W., Yang, J., Liu, Y., Bi, J., and Huang, L. (2012). Human exposure pathways of heavy metals in a lead-zinc mining area, Jiangsu province, China. *PLOS One* 7, 1–11. doi: 10.1371/journal.pone.0046793

Rahman, M. T., and Karim, M. M. (2018). Metallothionein: A potential link in the regulation of zinc in nutritional immunity. *Biol. Trace Elem. Res.* 182, 1–13. doi: 10.1007/s12011-017-1061-8

Rajagopalan, S., and Long, E. O. (1998). Zinc bound to the killer cell-inhibitory receptor modulates the negative signal in human NK cells. *J. Immunol.* 161, 1299–1305.

Rajagopalan, S., Winter, C. C., Wagtmann, N., and Long, E. O. (1995). The Ig-related killer cell inhibitory receptor binds zinc and requires zinc for recognition of HLA-C on target cells. *J. Immunol.* 155, 4143–4146.

Raulin, J. (1869). Chemical studies on vegetation. *Ann. Des. Sci. Nat.* 11, 93–99.

Read, S. A., Obeid, S., Ahlenstiel, C., and Ahlenstiel, G. (2019). The role of zinc in antiviral immunity. *Adv. Nutr.* 10, 696–710. doi: 10.1093/advances/nmz013

Rink, L., and Gabriel, P. (2000). Zinc and the immune system. *Proc. Nutr. Soc.* 59, 541–552. doi: 10.1017/s0029665100000781

Robinson, N. J., and Pohl, E. (2013). "Zinc sensors in Bacteria," in *Encyclopedia of Metalloproteins*. eds. R. H. Kretsinger, V. N. Uversky and E. A. Permyakov (NY, Springer: New York).

Rodelo, C. G., Salinas, R. A., Armenta JaimeArmenta, E., Armenta, S., Galdámez-Martínez, A., Castillo-Blum, S. E., et al. (2022). Zinc associated nanomaterials and their intervention in emerging respiratory viruses: journey to the field of biomedicine and biomaterials. *Coord. Chem. Rev.* 457, 214402–214431. doi: 10.1016/j.ccr.2021.214402

Rohrs, L. C. (1957). Metal-fume fever from inhaling zinc oxide. *A.M.A. Arch. Ind. Health* 16, 42–47. doi: 10.1001/archinte.1957.00260070058005

Roohani, N., Hurrell, R., Kelishadi, R., and Schulin, R. (2013). Zinc and its importance for human health: An integrative review. *J. Res. Med. Sci.* 18, 144–157.

Rosenkranz, E., Hilgers, R.-D., Uciechowski, P., Petersen, A., Plümäkers, B., and Rink, L. (2017). Zinc enhances the number of regulatory T cells in allergen-stimulated cells from atopic subjects. *Eur. J. Nutr.* 56, 557–567. doi: 10.1007/s00394-015-1100-1

Rosenkranz, E., Maywald, M., Hilgers, R.-D., Brieger, A., Clarner, T., Kipp, M., et al. (2016). Induction of regulatory T cells in Th1-/Th17-driven experimental autoimmune encephalomyelitis by zinc administration. *J. Nutr. Biochem.* 29, 116–123. doi: 10.1016/j.jnutbio.2015.11.010

Sabae, S. Z., Hazaa, M., Hallim, S. A., Awny, N. M., and Daboor, S. M. (2006). Bioremediation of Zn+2, cu+2 and Fe+2 using *Bacillus subtilis* D215 and *Pseudomonas putida* biovar A D225. *Biosci. Res.* 3, 189–204.

Saha, A. R., Hadden, E. M., and Hadden, J. W. (1995). Zinc induces thymulin secretion from human thymic epithelial cells *in vitro* and augments splenocyte and thymocyte responses *in vivo*. *Int. J. Immunopharmacol.* 17, 729–733. doi: 10.1016/0192-0561(95)00061-6

Salehizadeh, H., and Shojaosadati, S. A. (2003). Removal of metal ions from aqueous solution by polysaccharide produced from *Bacillus firmus*. *Water Res.* 37, 4231–4235. doi: 10.1016/S0043-1354(03)00418-4

Sandstead, H. H. (2013). Human zinc deficiency: discovery to initial translation. *Adv. Nutr.* 4, 76–81. doi: 10.3945/an.112.003186

Sandström, B., and Cederblad, A. (1980). Zinc absorption from composite meals II. Influence of the main protein source. *Am. J. Clin. Nutr.* 33, 1778–1783. doi: 10.1093/ajcn/33.8.1778

Sedlakova-Kadukova, J., Kopcakova, A., Gresakova, L., Godany, A., and Pristas, P. (2019). Bioaccumulation and biosorption of zinc by a novel *Streptomyces* K11 strain isolated from highly alkaline aluminium brown mud disposal site. *Ecotoxicol. Environ. Saf.* 167, 204–211. doi: 10.1016/j.ecoenv.2018.09.123

Shamim, S., and Rehman, A. (2012). Cadmium resistance and accumulation potential of *Klebsiella pneumoniae* strain CBL-1 isolated from industrial wastewater. *Pak. J. Zool.* 44, 203–208.

Shankar, A. H., and Prasad, A. S. (1998). Zinc and immune function: The biological basis of altered resistance to infection. *Am. J. Clin. Nutr.* 68, 447S–463S. doi: 10.1093/ajcn/68.2.447S

Sharma, P., Kumar, S., and Pandey, A. (2021). Bioremediated techniques for remediation of metal pollutants using metagenomics approaches: A review. *J. Environ. Chem. Eng.* 9:105684. doi: 10.1016/j.jece.2021.105684

Sharma, S., Tiwari, S., Hasan, A., Saxena, V., and Pandey, L. M. (2018). Recent advances in conventional and contemporary methods for remediation of heavy metal contaminated soils. 3. *Biotech* 8, 216–234. doi: 10.1007/s13205-018-1237-8

Sheikh, A., Shamsuzzaman, S., Ahmad, S. M., Nasrin, D., Nahar, S., Alam, M. M., et al. (2010). Zinc influences innate immune responses in children with enterotoxigenic *Escherichia coli*-induced diarrhea. *J. Nutr.* 140, 1049–1056. doi: 10.3945/jn.109.111492

Shkembi, B., and Huppertz, T. (2021). Influence of dairy products on bioavailability of zinc from other food products: A review of complementarity at a meal level. *Nutrients* 13, 4253–4263. doi: 10.3390/nu13124253

Silambarasan, S., and Abraham, J. (2013). Biosorption and characterization of metal tolerant bacteria isolated from Palar river basin Vellore. *J. Sci. Res.* 6, 125–131. doi: 10.3329/jsr.v6i1.14678

Singh, P. P., and Chopra, A. K. (2014). Removal of Zn^{2+} and Pb^{2+} using new isolates of *Bacillus* spp. PPS03 and *Bacillus subtilis* PPS04 from paper mill effluents using indigenously designed bench-top bioreactor. *J. Appl. Nat. Sci.* 6, 47–56. doi: 10.31018/jans.v6i1.374

Singh, V. K., Xiong, A., Usgaard, T. R., Chakrabarti, S., Deora, R., Misra, T. K., et al. (1999). ZntR is an autoregulatory protein and negatively regulates the chromosomal zinc resistance operon *znt* of *Staphylococcus aureus*. *Mol. Microbiol.* 33, 200–207. doi: 10.1046/j.1365-2958.1999.01466.x

Skalny, A. V., Aschner, M., Lei, X. G., Gritsenko, V. A., Santamaria, A., Alekseenko, S. I., et al. (2021). Gut microbiota as a mediator of essential and toxic effects of zinc in the intestines and other tissues. *Int. J. Mol. Sci.* 22, 13074–13090. doi: 10.3390/ijms222313074

Skalny, A. V., Rink, L., Ajsuvakova, O. P., Aschner, M., Gritsenko, V. A., Alekseenko, S. I., et al. (2020). Zinc and respiratory tract infections: perspectives for COVID-19. *Int. J. Mol. Med.* 46, 17–26. doi: 10.3892/ijmm.2020.4575

Suryawati, B. (2018). Zinc homeostasis mechanism and its role in bacterial virulence capacity. *AIP Conf. Proceed.* 2021:070021. doi: 10.1063/1.5062819

Taniguchi, J., Hemmi, H., Tanahashi, K., Amano, N., Nakayama, T., and Nishino, T. (2000). Zinc biosorption by a zinc resistant bacterium, *Brevibacterium* sp. strain HZM-1. *Appl. Microbiol. Biotechnol.* 54, 581–588. doi: 10.1007/s002530000415

Te Velthuis, A. J. W., van den Worm, S. H. E., Sims, A. C., Baric, R. S., Snijder, E. J., and van Hemert, M. J. (2010). Zn^{2+} inhibits coronavirus and arterivirus RNA polymerase activity in vitro and zinc ionophores block the replication of these viruses in cell culture. *PLoS Pathog.* 6, e1001176–e1001110. doi: 10.1371/journal.ppat.1001176

Terrin, G., Boscarino, G., Chiara, M. D., Iacobelli, S., Faccioli, F., Greco, C., et al. (2020). Nutritional intake influences zinc levels in preterm newborns: An observational study. *Nutrients* 12, 529–538. doi: 10.3390/nu12020529

Timková, I., Sedláková-Kaduková, J., and Pristaš, P. (2018). Biosorption and bioaccumulation abilities of *Actinomycetes*/*Streptomycetes* isolated from metal contaminated sites. *Separations* 5, 54–68. doi: 10.3390/separations5040054

Todd, W. R., Elvehjem, C. A., and Hart, E. B. (1933). Zinc in the nutrition of the rat. *Am. J. Phys.* 107, 146–156. doi: 10.1152/ajplegacy.1933.107.1.146

Toxicological profile for zinc. (2005). *Agency for Toxic Substances and Disease Registry Division of Toxicology and Environmental Medicine* GA, USA: Atlanta.

Tran, C. D., Miller, L. V., Krebs, N. F., Lei, S., and Hambidge, K. M. (2004). Zinc absorption as a function of the dose of zinc sulfate in aqueous solution. *Am. J. Clin. Nutr.* 80, 1570–1573. doi: 10.1093/ajcn/80.6.1570

U.S. Geological Survey. (2022). Mineral Commodity Summaries, 2022. U.S. Geological Survey, 202

Upadhyay, A., and Srivastava, S. (2014). Mechanism of zinc resistance in a plant growth promoting *Pseudomonas fluorescens* strain. *World J. Microbiol. Biotechnol.* 30, 2273–2282. doi: 10.1007/s11274-014-1648-6

US EPA (2009). *National Recommended water Quality Criteria*. Washington DC: Office of Water, Office of Science and Technology.

Valencia, E. Y., Braz, V. S., Guzzo, C., and Marques, M. V. (2013). Two RND proteins involved in heavy metal efflux in *Caulobacter crescentus* belong to separate clusters within Proteobacteria. *BMC Microbiol.* 13, 79–91. doi: 10.1186/1471-2180-13-79

Vallee, B. L., and Falchuk, K. H. (1993). The biochemical basis of zinc physiology. *Physiol. Rev.* 73, 79–118. doi: 10.1152/physrev.1993.73.1.79

Vinogradov, A. P. (1959). *The Geochemistry of rare and Dispersed Chemical Elements in Soils*. New York: Consultants Bureau.

Vogelmeier, C., Konig, G., Bencze, K., and Fruhmann, G. (1987). Pulmonary involvement in zinc fume fever. *Chest* 92, 946–948. doi: 10.1378/chest.92.5.946

Wadige, C. P. M., Taylor, A. M., Maher, W. A., and Krikowa, F. (2014). Bioavailability and toxicity of zinc from contaminated freshwater sediments: linking exposure-dose-response relationships of the freshwater bivalve *Hyridella australis* to zinc-spiked sediments. *Aquat. Toxicol.* 156, 179–190. doi: 10.1016/j.aquatox.2014.08.012

Walker, C. F., and Black, R. E. (2004). Zinc and the risk for infectious disease. *Annu. Rev. Nutr.* 24, 255–275. doi: 10.1146/annurev.nutr.23.011702.073054

Wang, J., and Chen, C. (2009). Biosorbents for heavy metals removal and their future. *Biotechnol. Adv.* 27, 195–226.

Wang, X., Sato, T., Xing, B., and Tao, S. (2005). Health risks of heavy metals to the general public in Tianjin, China via consumption of vegetables and fish. *Sci. Total Environ.* 350, 28–37. doi: 10.1016/j.scitotenv.2004.09.044

Wei, Z., Gu, H., Le, Q. V., Peng, W., Lam, S. S., Yang, Y., et al. (2021). Perspectives on phytoremediation of zinc pollution in air, water and soil. *Sustain. Chem. and Pharm.* 24:100550. doi: 10.1016/j.scp.2021.100550

Weyh, C., Krüger, K., Peeling, P., and Castell, L. (2022). The role of minerals in the optimal functioning of the immune system. *Nutrients* 14:4. doi: 10.3390/nu14030644

White, C. L. (1993). *Zn in Soils and Plants*. Dordrecht, The Netherlands, Kulwer Academic Publishers.

Wierzba, S. (2015). Biosorption of lead(II), zinc (II) and nickel(II) from industrial wastewater by *Stenotrophomonas maltophilia* and *Bacillus subtilis*. *Pol. J. Chem. Technol.* 17, 79–87. doi: 10.1515/pjct-2015-0012

Witkowska, D., Słowik, J., and Chilicka, K. (2021). Heavy metals and human health: possible exposure pathways and the competition for protein binding sites. *Molecules* 26, 6060–6076. doi: 10.3390/molecules26196060

Wong, C. P., Dashner-Titus, E. J., Alvarez, S. C., Chase, T. T., Hudson, L. G., and Ho, E. (2019). Zinc deficiency and arsenic exposure can act both independently or cooperatively to affect zinc status, oxidative stress, and inflammatory response. *Biol. Trace Elem. Res.* 191, 370–381. doi: 10.1007/s12011-019-1631-z

Wong, C. P., Rinaldi, N. A., and Ho, E. (2015). Zinc deficiency enhanced inflammatory response by increasing immune cell activation and inducing IL6 promoter demethylation. *Mol. Nutr. Food Res.* 59, 991–999. doi: 10.1007/s12011-019-1631-z

Wood, R. J., and Zheng, J. J. (1990). Milk consumption and zinc retention in postmenopausal women. *J. Nutr.* 120, 398–403. doi: 10.1093/jn/120.4.398

Wu, T., Bi, X., Li, Z., Sun, G., Feng, X., Shang, L., et al. (2017). Contaminations, sources, and health risks of trace metal(loid)s in street dust of a small city impacted by artisanal Zn smelting activities. *Int. J. Environ. Res. Public Health* 14, 961–980. doi: 10.3390/ijerph14090961

Wu, F. C., Feng, C. L., Cao, Y. J., Zhang, R. Q., Li, H. X., and Zhao, X. L. (2011). Study on the toxicity characteristics and water quality of fresh water by zinc. *Asian J. Ecotoxicol.* 6, 367–382.

Wuana, R. A., and Okieimen, F. E. (2011). Heavy metals in contaminated soils: A review of sources, chemistry, risks and best available strategies for remediation. *Int. Sch. Res. Not.* 2011, 1–20. doi: 10.5402/2011/402647

Yazar, M., Sarban, S., Kocyigit, A., and Isikan, U. E. (2005). Synovial fluid and plasma selenium, copper, zinc, and iron concentrations in patients with rheumatoid arthritis and osteoarthritis. *Biol. Trace Elem. Res.* 106, 123–132. doi: 10.1385/BTER:106:2:123

Zahoor, A., and Rehman, A. (2009). Isolation of Cr (VI) reducing bacteria from industrial effluents and their potential use in bioremediation of chromium containing wastewater. *J. Environ. Sci.* 21, 814–820. doi: 10.1016/S1001-0742(08)62346-3

Zaichick, V., Sviridova, T. V., and Zaichick, S. V. (1997). Zinc in the human prostate gland: normal, hyperplastic and cancerous. *Int. Urol. Nephrol.* 29, 565–574. doi: 10.1007/BF02552202

Zerahn, B., Kofoed-Enevoldsen, A., Jensen, B. V., Mølvig, J., Ebbehøj, N., Johansen, J. S., et al. (1999). Pulmonary damage after modest exposure to zinc chloride smoke. *Respir. Med.* 93, 885–890. doi: 10.1016/S0954-6111(99)90054-9

Conflict of Interest: The authors declare that the research was conducted in the absence of any commercial or financial relationships that could be construed as a potential conflict of interest.

Publisher's Note: All claims expressed in this article are solely those of the authors and do not necessarily represent those of their affiliated organizations, or those of the publisher, the editors and the reviewers. Any product that may be evaluated in this article, or claim that may be made by its manufacturer, is not guaranteed or endorsed by the publisher.

frontiers | Frontiers in Microbiology

TYPE Original Research
PUBLISHED 05 August 2022
DOI 10.3389/fmicb.2022.926037

OPEN ACCESS

EDITED BY
Adnan Mustafa,
Brno University of Technology, Czechia

REVIEWED BY
Wensheng Qin,
Lakehead University,
Canada
Anil K. Choudhary,
Indian Council of Agricultural Research (ICAR), India

*CORRESPONDENCE
Jiayao Zhuang
nlzjiayao@njfu.edu.cn

SPECIALTY SECTION
This article was submitted to Terrestrial Microbiology, a section of the journal Frontiers in Microbiology

RECEIVED 22 April 2022
ACCEPTED 11 July 2022
PUBLISHED 05 August 2022

CITATION
Liu C, Zhuang J, Wang J, Fan G, Feng M and Zhang S (2022) Soil bacterial communities of three types of plants from ecological restoration areas and plant-growth promotional benefits of *Microbacterium invictum* (strain X-18). *Front. Microbiol.* 13:926037. doi: 10.3389/fmicb.2022.926037

Soil bacterial communities of three types of plants from ecological restoration areas and plant-growth promotional benefits of *Microbacterium invictum* (strain X-18)

Chao Liu[1], Jiayao Zhuang[1]*, Jie Wang[1], Guohua Fan[1], Ming Feng[1] and Shutong Zhang[2]

[1]Collaborative Innovation Center of Sustainable Forestry in Southern China of Jiangsu Province, Nanjing Forestry University, Nanjing, China, [2]China National Chemical Construction Investment Group Co., Ltd, Beijing, China

Microbial-assisted phytoremediation promotes the ecological restoration of high and steep rocky slopes. To determine the structure and function of microbial communities in the soil in response to changes in soil nutrient content, the bacterial communities of rhizospheric soil from three types of plants, i.e., *Robinia pseudoacacia*, *Pinus massoniana*, *and Cynodon dactylon*, were analyzed using Illumina sequencing technology. High-quality sequences were clustered at the 97% similarity level. The dominant genera were found to be *RB41*, *Gemmatimonas*, *Sphingomonas*, *Bradyrhizobium,* and *Ellin6067*. The Tukey HSD (honestly significant difference) test results showed that the abundance of *RB41* and *Gemmatimonas* were significantly different among three types of plants ($p<0.01$). The relative abundances of *RB41* (13.32%) and *Gemmatimonas* (3.36%) in rhizospheric soil samples from *R. pseudoacacia* were significantly higher than that from *P. massoniana* (0.16 and 0.35%) and *C. dactylon* (0.40 and 0.82%), respectively. The soil chemical properties analyses suggested that significant differences in rhizospheric soil nutrient content among the three plant types. Especially the available phosphorus, the content of it in the rhizospheric soil of *R. pseudoacacia* was about 280% (*P. massoniana*) and 58% (*C. dactylon*) higher than that of the other two plants, respectively. The soil bacterial communities were further studied using the correlation analysis and the Tax4Fun analysis. A significant and positive correlation was observed between *Gemmatimonas* and soil nutrient components. Except total nitrogen, the positive correlation between *Gemmatimonas* and other soil nutrient components was above 0.9. The outcomes of these analyses suggested that *Gemmatimonas* could be the indicator genus in response to changes in the soil nutrient content. Besides, the genes involved in metabolism were the major contributor to soil nutrients. This study showed that soil nutrients affect the soil bacterial community structure and function. In addition, pot experiments showed that *Microbacterium invictum* X-18 isolated from the rhizospheric soil of *R. pseudoacacia* significantly improved soil nutrient content and increased *R. pseudoacacia* growth. A significant increase in the numbers of nodules of

R. pseudoacacia and an increase of 28% in plant height, accompanied by an increase of 94% in available phosphorus was measured in the *M. invictum* X-18 treatment than the control treatment.

KEYWORDS

phytoremediation, bacterial communities, soil nutrient, sequencing technology, bioinoculant, plant-growth promotion

Highlights

- Studying microbial-assisted phytoremediation by exploring soil bacterial community.
- Response of bacterial community to changes in soil nutrients.
- Combination of sequencing and isolation culture technology.
- *Gemmatimonas* and *Microbacterium invictum* X-18 belong to the similar key indicator taxa.
- *Gemmatimonas* and *Microbacterium invictum* X-18 are beneficial for soil and plants.

Introduction

Human activities have led to the destruction of the mountains resulting in multiple high and steep rocky slopes, adversely affecting the ecological environment and landscape (Wang et al., 2020; Han et al., 2021). Thus, the restoration of the ecological environment in these areas is gaining considerable momentum. However, fragile ecological functions and poor soil nutrient conditions in these areas hinder the long-term and stable survival of plants. Thus, phytoremediation in these areas is challenging. External-soil spray seeding is widely used in such areas for ecological restoration, even then, the fertility of the soil substrate is limited, and failures of ecological restoration are not uncommon. In order to improve soil conditions on high and steep rocky slopes, microbial-assisted phytoremediation is being explored.

Soil microbes are active components of processes such as litter decomposition and soil mineralization. Certain microbes can improve soil quality, promote plant growth, and enhance phytoremediation efficiency by accelerating the weathering of rocks and promoting the production of mineral nutrients and phytohormones (Li et al., 2020; Jia et al., 2021; Tian et al., 2021). In addition, previous studies have demonstrated that bacterial community structure and diversity reflect changes in soil ecology (Su et al., 2018). Thus, understanding the changes in the bacterial community structure and the relationship between bacterial community and soil environment is of utmost importance to study microbial-assisted phytoremediation.

Legumes are commonly used as the protective species to restore high and steep rocky slopes. Legumes are highly resistant to stress and can rebuild degraded ecological functions and restore soil nutrient conditions (Sun et al., 2020). To explore the soil microbial community and its possible ecological functions, soil bacterial communities in *Robinia pseudoacacia, Pinus massoniana,* and *C. dactylon* rhizospheric soil from high and steep rocky slopes in the Yueyang, Hunan, China, were analyzed using Illumina sequencing technology that cultivation-independent. In addition, the soil bacteria were screened, and their soil improvement and plant-growth potential were explored.

Materials and methods

Sample collection and soil nutrient analysis

The study site is located on the high and steep rocky slopes on the side of Yueyang Avenue in Yueyang, Hunan, China, where external-soil spray seeding was applied to restore the ecological environment 7 years ago (Supplementary Figure S1). The dominant plant species in the experimental site included *R. pseudoacacia* (R), *P. massoniana* (P), and *C. dactylon* (C), all of which are commonly used plants in phytoremediation. The rhizospheric soil was collected, and three samples (each sample at least 5–10 m away from other plants) were collected for each plant type. Each sample was transported to the laboratory for processing within 24 h. Semi-micro Kjeldahl method was used to determine total nitrogen (TN; Liu et al., 1996; Falco and Magni, 2004), molybdenum-antimony anti-colorimetric method with NaOH melting was used to determine total phosphorus (TP), flame photometry with NaOH melting was used to determine total potassium (TK), alkaline hydrolysis diffusion method was used to determine hydrolyzed nitrogen (HN), molybdenum-antimony anti-colorimetric method with $NaHCO_3$ extraction to determine available phosphorus (AP), flame photometry with NH_4OAc extraction to determine available potassium (AK), and pH meter to determine pH.

DNA extraction and sequencing

Soil samples were sieved through a 0.075 mm screen, ground, and then lysed using the soil homogenate. Microbial DNA was extracted using the HiPure Soil DNA Kits (Magen, Guangzhou, China) according to the manufacturer's protocols. The 16S rDNA target region of the ribosomal RNA gene was amplified *via* PCR (95°C for 5 min, followed by 30 cycles at 95°C for 1 min, 60°C for 1 min, and 72°C for 1 min, and a final extension at 72°C for 7 min) using 341F primer (5'-CCTACGGGNGGCWGCAG-3′) and 806R primer (5′- GGACTACHVGGGTATCTAAT-3′) targeting the V3-V4 region. PCR reactions were performed in triplicates. 50 µl PCR mixture containing 10 µl of 5 × Q5@ Reaction Buffer, 10 µl of 5 × Q5@ High GC Enhancer, 1.5 µl of 2.5 mm dNTPs, 1.5 µl of each primer (10 µm), 0.2 µl of Q5@ High-Fidelity DNA Polymerase, and 50 ng of template DNA. Related PCR reagents were from New England Biolabs, United States. AMPure XP beads were used to purify the second round of amplified products. ABI StepOnePlus Real-Time PCR System (Life Technologies, produced in the United States) was used for quantification, and sequencing was performed on the computer based on the PE250 mode pooling of Novaseq 6000.

Processing of sequencing data

Raw reads were assigned to samples based on their unique barcode, and the barcode sequence was truncated using the lima application (version 2.0.1) of the Pbbioconda package (Pacific Biosciences). This was followed by the analysis of subreads to generate CCS (Circular Consensus Sequencing) reads using PacBio's open-source software suite Smart Link (version 7.0) with the following parameters: minfullpass = 3, minPredictedAccuacy = 0.99. Primer sequences were trimmed using cutadapt (version 2.10; Martin, 2011). The files generated by the PacBio platform were then used for amplicon size filtering to remove sequences outside the expected amplicon size (minlength 1.3 kb, maxlength 1.7 kb). Reads with the same continuous base number > 8 were considered low-quality reads and thus removed. The clean reads thus obtained were clustered into operational taxonomic units (OTUs) of ≥97% similarity using UPARSE (version 9.2.64) pipeline (Edgar et al., 2011). All chimeric reads were removed using the UCHIME algorithm to obtain clean reads for further analysis. The sequence with the highest abundance was selected as a representative sequence within each cluster.

Soil microbes' isolation, identification, and growth-promoting benefits

To study the beneficial microbes in the soil, culturable strains were isolated from the rhizospheric soil of *R. pseudoacacia* with relatively high soil nutrients. Soil samples were diluted and smeared on NA (Nutrient Agar). The agar plates were incubated at 28°C for 3 days. Morphologically distinct colonies were further sub-cultured to obtain a pure culture. The pure cultures were maintained on NA slants at 4°C in a refrigerator.

Since the sample site was phosphorus-deficient, bacterial cultures from these samples were screened for phosphorus solubilizing function. All strains were inoculated on *Monkina* agar at 28°C. The agar plates inoculated with phosphate solubilizing strains exhibited the formation of halos (zone of solubilization) around the colonies after 7 days of incubation. The diameter of the halos (D) around the microbial colonies (d) was measured, and D/d was calculated. Based on D/d, five phosphate solubilizing strains were selected for pot experiments.

To explore the growth-promoting benefits of soil microbes, the phosphate solubilizing bacteria were inoculated into the seedlings of *R. pseudoacacia*, respectively. The seeds of *R. pseudoacacia* plants were surface-sterilized and allowed to germinate for 3 days at 20°C and relative humidity of 60%. Later, the three healthy seedlings were planted in each pot, including mixed matrix soil (Jiangsu Xingnong Matrix Technology Co., Ltd). One month later, only one seedling was allowed to grow per pot, and it was ensured that the growth of seedlings in each pot was identical. Bacterial inoculum was prepared by culturing bacteria in NA. Colonies of each strain were added to a 100 ml Erlenmeyer flask containing 30 ml LB (Luria-Bertani) broth (10 g peptone, 5 g yeast, 5 g NaCl, 1,000 ml deionized water, pH 7.2), incubated at 30°C, and 180 r/min for 12 h. The absorbance of the bacterial suspension was measured (UV-8000 T, Shanghai Metash Instruments Co., Ltd) at 600 nm (18). Inoculum cultures were adjusted to get a final absorbance of 0.8 ~ 1.2. The inoculums were sealed and stored in a refrigerator at 4°C for later use. For inoculation, the stored suspension of the inocula was diluted 100X, and 60 ml of the resulting diluted sample was applied to the soil. The pots were divided into one control group and five inoculation groups, three replicates for each group, and placed in a greenhouse. Subsequently, the control group was added to the sterile LB broth, and the other inoculation groups, including five bacteria, were added with the same concentration of bioinoculant for each strain, respectively.

Three months later, the plants were sampled and analyzed. For plants, vernier calipers and tape were used to measure the ground diameter and height of the seedlings. Root scanners were used to measure the leaf area (ten upper, middle, and lower leaves were selected from each pot to measure the leaf area). The plants were dried to measure the above-ground and under-ground biomass. For potting soil, the Mettler toledo pH meter was used to measure soil's pH value (water: soil ratio was 5: 1). The alkaline hydrolysis diffusion method was used to determine HN. The molybdenum-antimony anti-colorimetric method with $NaHCO_3$ extraction was used to determine AP. The strain demonstrating the best plant-growth-promoting and soil improvement benefits was selected and was subjected to 16S rDNA analysis and morphological characteristics for identification.

Statistical analysis

To illustrate the microbial diversity of rhizospheric soil in different vegetation types, the alpha diversity (including Chao1, Simpson, and Shannon indices) was quantified based on OTU abundance. The abundance statistics of each taxonomy were visualized using Krona (version 2.6; Ondov et al., 2011). The stacked bar plot of the community composition was visualized in the R project ggplot2 package (Wickham and Chang, 2015). The pvclust package of R with the default settings was used for cluster analysis using Ward's cluster method. Heat maps and networks of correlation coefficients were generated using Omicsmart, a dynamic real-time interactive online platform for data analysis[1]. Analysis of function difference between groups was calculated by Welch's *t*-test, Wilcoxon rank test, Kruskal-Wallis H test, and Tukey's HSD test in the R project Vegan package (version 2.5.3; Oksanen et al., 2010).

Results

Rhizosphere soil nutrient

In the current study, the rhizospheric soil nutrients, i. e., N (nitrogen), P (phosphorus), and K (potassium; Table 1), were analyzed. The results of soil nutrients analyses showed that the N and K content was in normal level, and that of P was slightly lower in rhizospheric soil samples from three plants as per the 'Environmental Quality Standard for Soil' of China (Author, n.d.). It indicated that soil in sample sites was P deficient. In general, the total rhizospheric soil nutrient content from *R. pseudoacacia* was higher than that of *P. massoniana* and *C. dactylon*. The available rhizospheric soil nutrient content of *R. pseudoacacia* was significantly higher than that of *P. massoniana* and *C. dactylon*. Different plant species exhibited different rhizospheric soil nutrient content, and the rhizospheric soil nutrient content of *R. pseudoacacia* was higher than other plant species.

Effects of soil nutrients on bacterial communities

The bacterial communities of nine rhizospheric soil samples were analyzed using Illumina sequencing technology. The atypical rhizospheric soil samples collected from *R. pseudoacacia* were removed. The dataset of eight samples consisted of 837,739 unique 16S rDNA gene tags (Table 2). The OTUs per sample ranged from 2088 to 2,542. The α-diversity (Chao 1, Shannon, and Simpson) analysis assessed the bacterial abundance in rhizospheric soil samples (Table 2). Chao1 index evaluated the total number of OTUs in all the rhizospheric soil samples, demonstrating the species richness of the microbial communities. Shannon and Simpson indices reflected the richness and uniformity of the microbial communities and indicated that the α-diversity of both *R. pseudoacacia* and *C. dactylon* was higher than that of *P. massoniana*, which had a lower soil nutrient content.

Bacterial community structure in soil samples at the genus level is demonstrated in Figure 1A. *RB41*, *Gemmatimonas*, *Sphingomonas*, *Bradyrhizobium,* and *Ellin6067* were found to be the dominant genera in the rhizospheric soil samples. Tukey HSD test method was used to detect the significance of species differences at the genus level (Figure 1B). The relative abundances of *RB41* (13.32%) and *Gemmatimonas* (3.36%) in rhizospheric soil samples from *R. pseudoacacia* were significantly higher than that from *P. massoniana* (0.16 and 0.35%) and *C. dactylon* (0.40 and 0.82%), respectively. Furthermore, the relative abundances of *RB41* and *Gemmatimonas* were significantly different among the

1 http://www.omicsmart.com

TABLE 1 The rhizospheric soil nutrient content of *Robinia pseudoacacia, Pinus massoniana, and Cynodon dactylon.*

Samples	TN	TP	TK	HN	AP	AK	pH
	(g/kg, dry weight)			(mg/kg, dry weight)			
R. pseudoacacia	3.65 ± 0.04a	0.13 ± 0.01a	26.78 ± 0.54a	241.32 ± 38.23a	0.057 ± 0.006a	162.48 ± 1.21a	5.65 ± 0.22a
P. massoniana	1.90 ± 0.08b	0.07 ± 0.01b	21.37 ± 0.69ab	136.32 ± 16.64b	0.015 ± 0.001c	110.87 ± 1.10c	5.08 ± 0.17b
C. dactylon	3.13 ± 0.06a	0.10 ± 0.01a	23.13 ± 0.56a	196.84 ± 23.19ab	0.036 ± 0.001b	135.68 ± 1.10b	5.12 ± 0.13ab

The values "a, b, c" represent the standard deviation. Different letters represent significant differences. TN, Total nitrogen; TP, Total phosphorus; TK, Total potassium; HN, Hydrolyzable nitrogen; AP, Available phosphorus; and AK, Available potassium.

TABLE 2 α-diversity of bacteria from the soil samples *distance < 0.03.*

Samples	Unique tags	Number of OTUs	α-diversity		
			Chao1	Shannon	Simpson
R. pseudoacacia	118,357	2,447	2,622	8.67	0.9907
P. massoniana	90,533	2,233	2,495	8.66	0.991
C. dactylon	109,808	2,506	2,722	9.02	0.9944

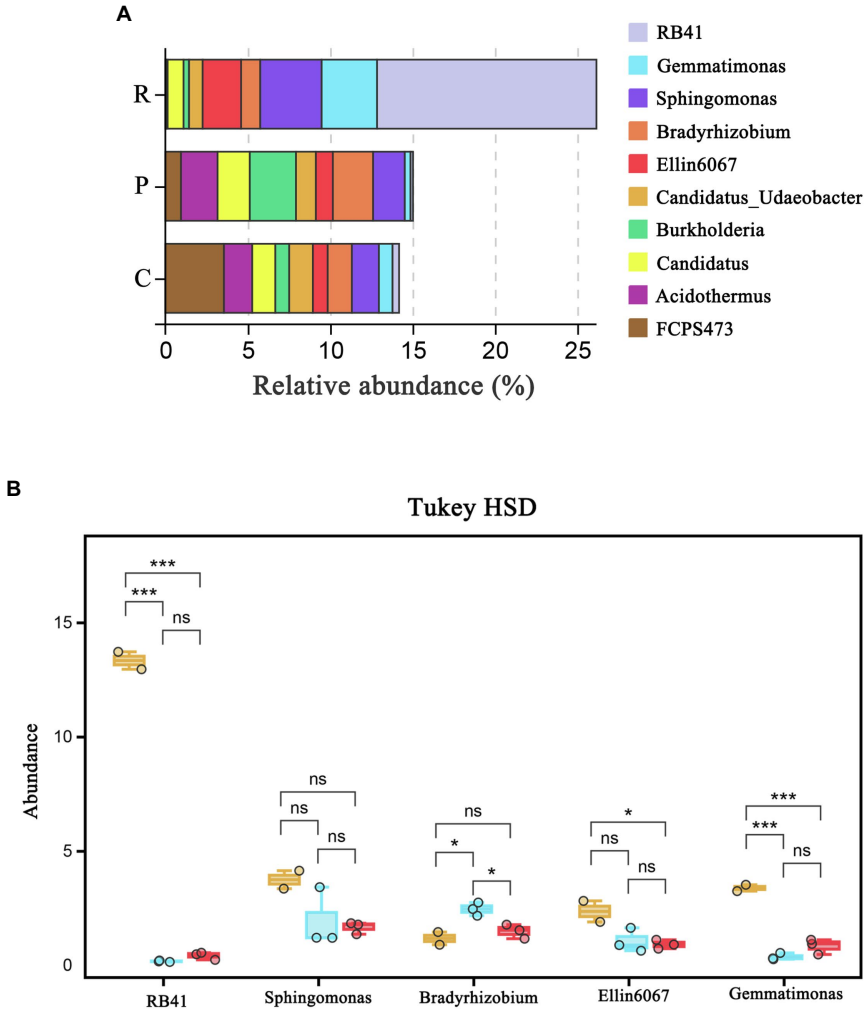

FIGURE 1
The bacterial community structure at the genus level: **(A)** Tukey HSD test at genus level with 95% confidence intervals and **(B)** *$p<0.05$; ***$p<0.01$. R, P, C represent *Robinia pseudoacacia*, *Pinus massoniana*, and *Cynodon dactylon*, respectively.

three plant types ($p<0.01$), indicating that *RB41* and *Gemmatimonas* may be correlated to the difference in rhizospheric soil nutrient content.

The correlation analysis validated the correlation between soil nutrients and soil bacterial community (Figure 2). Bacterial genera, *RB41*, *Gemmatimonas*, and *Ellin6067*, were positively correlated to soil nutrient content ($0.05<p<0.5$). Compared with *RB41* and *Ellin6067*, a significant and positive correlation was observed between *Gemmatimonas* and soil nutrient components. It indicated that *Gemmatimonas* might be most relevant to the rhizosphere soil nutrient difference.

The functional abundance of bacterial communities of rhizospheric soil from three types of plants were identified using 16S rDNA gene amplicon data and Tax4Fun (Figure 3). Several predicted pathways were significantly enriched ($p<0.5$) in the bacterial communities of rhizospheric soil from *R. pseudoacacia*, specifically genes associated with metabolism (carbohydrate metabolism, amino acid metabolism, energy metabolism,

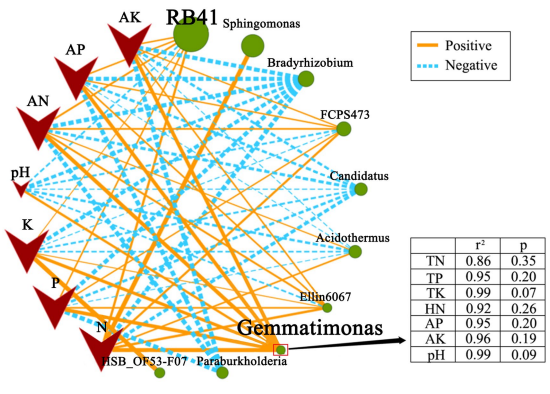

FIGURE 2
Correlation network map illustrating the correlation between soil nutrient and soil bacterial community at the genus level. Nodes represent genus and soil nutrient, lines represent correlations, and the thickness of the line represents the degree of correlation ($0.05<p<0.5$).

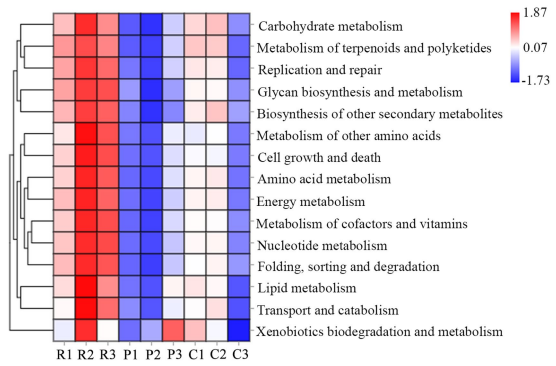

FIGURE 3
Heat map cluster and abundance of microbial functions at the genus level. R, P, and C represent *Robinia pseudoacacia*, *Pinus massoniana*, and *Cynodon dactylon*, respectively.

biosynthesis of another secondary metabolism, and so on), genetic information processing (replication and repair, folding, sorting, and degradation), and environmental information processing (cell growth and death, transport, and catabolism). In addition, almost all the secondary sub-classification pathways in metabolism were significantly enriched in the *R. pseudoacacia* rhizospheric soil bacterial communities. Besides, the abundance of bacterial metabolic functions in the rhizospheric soil of different plants was distinct due to differences in nutrient content. The results showed that vigorous microbial metabolism is associated with a higher soil nutrient content.

The 16S sequence of rhizospheric soil samples was deposited in the NCBI (The National Center for Biotechnology Information) database with the number PRJNA757370.

Isolation, identification, and benefits of X-18 of soil microbes

Since the study site was phosphorus-deficient, phosphate solubilizing bacteria were screened in the current study. As shown in Table 3, five phosphate solubilizing bacteria were screened from the rhizospheric soil of *R. pseudoacacia*.

According to the results of the pot experiment, X-18 exhibited the highest efficacy for plant-growth promotion. X-18 was identified as *Microbacterium invictum* (Figure 4; accession number MN586282). The X-18 isolate was deposited at the CCTCC (China Center for Type Culture Collection) with the accession number M2019236. Plant growth characteristics and soil nutrient concentration are demonstrated in Table 4. Compared with the control, the dry weight of the root of the X-18 inoculated plants significantly increased by 122%, ground diameter by 22%, plant height by 28%, and average leaf area by 18%. In addition, the number and total weight of nodules also increased significantly. With a significant increase of 55.34 and 93.67% ($p < 0.05$) compared to the control, HN and AP of potted soil inoculated with X-18 were 113.52 mg/kg and 2.599 mg/kg, respectively.

TABLE 3 Phosphorus-dissolving effect of phosphate solubilizing bacteria.

Name	D/d (organic phosphorus)	D/d (inorganic phosphorus)
X-4	3.61	2.13
X-8	/	2.60
X-11	3.06	4.54
X-14	3.47	2.81
X-18	3.62	2.87

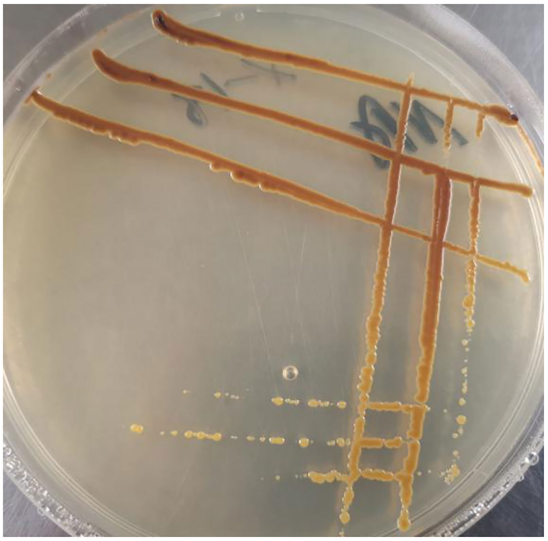

FIGURE 4
Microbacterium invictum X-18.

Discussion

Soil nutrient and soil bacterial community

In the present study, the rhizospheric soil from *R. pseudoacacia* was found to contain an increased level of total and available rhizospheric soil nutrients compared to *P. massoniana* and *C. dactylon* (Table 1). Besides, the α-diversity of soil bacteria from *R. pseudoacacia* and *C. dactylon* was higher than that of *P. massoniana* ($p < 0.05$; Table 2). These results are consistent with the previous findings that the diverse bacterial community is the result of the physiological or evolutionary adaptation of microbes to the environment (Wang et al., 2021).

The above analysis indicated that *Gemmatimonas* might be the key genus in response to changes in the soil nutrient content. *Gemmatimonas* demonstrated strong positive associations with soil nutrient transformations, and thus it emerged as the key taxa beneficial for plant growth (Li et al., 2017). According to the previous studies, *Gemmatimonas* can dissolve insolubilized P and convert it into P for plant growth. *Gemmatimonas* was found to

TABLE 4 Effects of X-18 on plant and soil.

Groups (Sample)	Soil (potted)			Plant (above ground)			Plant (underground)		
	HN (mg/kg)	AP (mg/kg)	pH	Ground diameter (m)	Plant height (m)	Average leaf area (m^2)	Number of nodules	Total nodules weight(g)	Dry weight(g)
CK	73.08 ± 2.52b	1.342 ± 0.039b	5.35 ± 0.026b	$4.75 \times 10^{-3} \pm 0.07$b	$40.04 \times 10^{-2} \pm 1.56$c	$4.353 \times 10^{-4} \pm 0.12$b	0	/	0.23 ± 0.05b
X-18	113.52 ± 2.61a	2.599 ± 0.022a	5.17 ± 0.015a	$5.81 \times 10^{-3} \pm 0.20$a	$51.20 \times 10^{-2} \pm 0.31$a	$5.131 \times 10^{-4} \pm 0.19$a	5	0.0083 ± 0.0007a	0.51 ± 0.02a

The values "a, b" represent the standard deviation. Different letters represent significant differences. HN, Hydrolyzable nitrogen and AP, available phosphorus.

be more abundant in the rhizospheric soil of healthy plants than in diseased soil (She et al., 2016), indicating its disease-suppressing properties. Besides, *Gemmatimonas* can solubilize insoluble elements, induce plant stress resistance or produce antifungal antibiotics (Mahanty et al., 2017; Shang and Liu, 2020; Akinola et al., 2021; Zhu et al., 2021). In the present study, *Gemmatimonas* was the dominant genus in the rhizospheric soil from three plant types, accounting for up to 3.36% of all OTUs from *R. pseudoacacia*. However, only 0.35 and 0.82% of all OTUs in the rhizospheric soil from *P. massoniana* and *C. dactylon* were *Gemmatimonas*. The correlation analysis showed that *Gemmatimonas* is significantly and positively correlated with all soil nutrient factors (Figure 3). Overall, if *Gemmatimonas* is beneficial to improving soil nutrients, more experiments will be necessary to understand the functional mechanism of these soil bacteria.

Microbes participating in the process of soil nutrient transformations are all connected through genes (Castaneda and Barbosa, 2017; Chen et al., 2019; Srour et al., 2020). In the present study, Tax4Fun was applied to infer the differences in the dominant functional traits dominating through 16S rDNA gene data. Genes involved in metabolism, including "carbohydrate metabolism," "amino acid metabolism," "energy metabolism," and so on, were significantly more abundant in soil with high nutrients than in low nutrient conditions (Figure 4). It suggested that the function of the microbial community significantly contributed to responses to nutrient changes in the soil environment.

The benefits of *Microbacterium invictum* X-18

Microbacterium invictum X-18 significantly increased the nutrient content of potted soil. Similarly, the number and weight of nodules, root dry weight, plant height, ground diameter, and average leaf area of X-18 inoculated plants significantly increased compared to the control group ($p < 0.05$). Sang et al. (2014) reported that *Microbacterium* sp. exhibited phosphate solubilizing activity to promote plant growth. Ribeiro et al. (2021) also showed that *Microbacterium* sp. can promote plant growth by increasing the production of IAA, siderophore, ACC deaminase, and decarboxylase. These results indicate that the mechanism of *Microbacterium* sp. to promote plant growth may improve soil nutrient content and increase the production of auxins, enzymes, and so on.

Accordingly, in the current study, it revealed that both *M. invictum* X-18 and *Gemmatimonas* belong to the similar taxa, which are beneficial to increase soil nutrient content and plant growth.

Conclusion

In this study, the rhizospheric soil bacterial community structure from three types of plants based on cultivation-independent Illumina sequencing technology was analyzed. We observed that *Gemmatimonas* is the indicator genus to assess soil nutrient changes. The results showed that the diverse bacterial community is the result of adaptation to environmental changes. *M. invictum* X-18 in soil improvement and plant-growth promotion was validated through the plate culture experiment and pot experiment. Compared with the control, the nodule, dry weight and plant height inoculated with X-18 increased significantly. The current study demonstrated a novel thought of using two approaches to explore key microbial taxa in response to changes in the soil environment. *M. invictum* X-18 strain identified in this study will be beneficial to promote the development of microbial-assisted phytoremediation technology. These work proved the feasibility and efficiency of microbial-assisted phytoremediation. It provides strain and theoretical guidance for improving the phytoremediation efficiency of barren areas.

Data availability statement

The data presented in the study are deposited in the NCBI repository, accession number PRJNA757370 (https://dataview.ncbi.nlm.nih.gov/object/PRJNA757370).

Author contributions

JZ enabled and supervised this research and conceived of the study. CL designed the experiments, conducted data analysis, and wrote the manuscript. CL, JW, GF, MF, and SZ performed the experiments. All authors contributed to the article and approved the submitted version.

Funding

This work was funded by the National Key R&D Program of China (2017YFC0505500 and 2017YFC0505506).

Conflict of interest

SZ was employed by China National Chemical Construction Investment Group Co., Ltd.

The remaining authors declare that the research was conducted in the absence of any commercial or financial relationships that could be construed as a potential conflict of interest.

Publisher's note

Supplementary material

The Supplementary material for this article can be found online at: https://www.frontiersin.org/articles/10.3389/fmicb.2022.926037/full#supplementary-material

References

Akinola, S., Ayangbenro, A., and Babalola, O. (2021). Metagenomic insight into the community structure of maize-Rhizosphere Bacteria as predicted by different environmental factors and their functioning within plant proximity. *Microorganisms* 9:1419. doi: 10.3390/microorganisms90

Author, X. (n.d.). Environmental Quality Standard for Soil' of China (GB15618-2018).

Castaneda, L., and Barbosa, O. (2017). Metagenomic analysis exploring taxonomic and functional diversity of soil microbial communities in Chilean vineyards and surrounding native forests. *PeerJ* 5:e3098. doi: 10.7717/peerj.3098

Chen, J., Shen, W., Xu, H., Li, Y., and Luo, T. (2019). The composition of nitrogen fixing microorganisms correlates With soil nitrogen content During reforestation: A comparison Between legume and non-legume plantations. *Front. Microbiol.* 10:508. doi: 10.10.3389/fmicb.2019.00508

Edgar, R., Haas, B., Clemente, J., Quince, C., and Knight, R. (2011). UCHIME improves sensitivity and speed of chimera detection. *Bioinformatics* 27, 2194–2200. doi: 10.1093/bioinformatics/btr381

Falco, G., and Magni, P. (2004). Sediment grain size and organic carbon distribution in the cabras lagoon (Sardinia, western mediterranean). *Chem. Ecol.* 20, 367–377. doi: 10.1080/02757540310001629189

Han, C., Gao, Z., Wu, Z., Huang, J., Liu, Z., Zhang, L., et al. (2021). Restoration of damaged ecosystems in desert steppe open-pit coal mines: effects on soil nematode communities and functions. *Land Degrad. Dev.* 32, 4402–4416. doi: 10.1002/ldr.4045

Jia, Z., Meng, M., Li, C., Zhang, B., Zhai, L., Liu, X., et al. (2021). Rock-solubilizing microbial inoculums have enormous potential as ecological remediation agents to promote plant growth. *Forests* 12:357. doi: 10.3390/f12030357

Li, Y., Adams, J., Shi, Y., Wang, H., He, J., and Chu, H. (2017). Distinct soil microbial communities in habitats of differing soil water balance on the Tibetan plateau. *Sci. Rep.* 7:407. doi: 10.1038/srep46407

Li, C., Jia, Z., Peng, X., Zhai, L., Zhang, B., Liu, X., et al. (2020). Functions of mineral-solubilizing microbes and a water retaining agent for the remediation of abandoned mine sites. *Sci. Total Environ.* 761:143215. doi: 10.1016/j.scitotenv.2020.143215

Liu, G., Jiang, N., Zhang, L., and Liu, Z., (1996). *Soil Physical and Chemical Analysis and Description of Soil Profiles*. Beijing: China Standard Methods Press.

Mahanty, T., Bhattacharjee, S., Goswami, M., Bhattacharyya, P., Das, B., Ghosh, A., et al. (2017). Biofertilizers: a potential approach for sustainable agriculture development. *Environ. Sci. Pollut. Res. Int.* 24, 3315–3335. doi: 10.1007/s11356-016-8104-0

Martin, M. (2011). Cutadapt removes adapter sequences from high-throughput sequencing reads. *EMBnet J.* 17:200. doi: 10.14806/ej.17.1.200

Oksanen, J., Blanchet, F., and Kindt, R., (2010). Vegan: community ecology package. R package version. R package, version. 23.

Ondov, B., Bergman, N., and Phillippy, A. (2011). Interactive metagenomic visualization in a web browser. *BMC Bioinform.* 12:385. doi: 10.1186/1471-2105-12-385

Ribeiro, I. D. A., Bach, E., Moreira, F., Mvller, A. R., Rangel, C. P., and Passaglia, L. (2021). Antifungal potential against Sclerotinia sclerotiorum (Lib.) de Bary and plant growth promoting abilities of Bacillus isolates from canola (*Brassica napus* L.) roots. *Microbiol. Res.* 248:126754. doi: 10.1016/j.micres

Sang, H., Mayank, A., and Se, C. (2014). Isolation and characterization of plant growth promoting endophytic diazotrophic bacteria from Korean rice cultivars. *Microbiol. Res.* 169, 83–98. doi: 10.1016/j.micres.06.003

Shang, J., and Liu, B. (2020). Application of a microbial consortium improves the growth of Camellia sinensis and influences the indigenous rhizosphere bacterial communities. *J. Appl. Microbiol.* 130, 2029–2040. doi: 10.1111/jam.14927

She, S., Niu, J., Zhang, C., Xiao, Y., Chen, W., Dai, L., et al. (2016). Significant relationship between soil bacterial community structure and incidence of bacterial wilt disease under continuous cropping system. *Arch. Microbiol.* 199, 267–275. doi: 10.1007/s00203-016-1301-x

Srour, A., Ammar, H., Subedi, A., Pimente, M., Cook, R., Bond, J., et al. (2020). Microbial communities associated With long-term tillage and fertility treatments in a corn-soybean cropping system. *Front. Microbiol.* 11:1363. doi: 10.3389/fmicb.01363

Su, X., Li, Y., Yang, B., and Li, Q. (2018). Effects of plant diversity on soil microbial community in a subtropical forest. *J. Ecol.* 37, 2254–2261. doi: 10.13292/j.1000-4890.201808.014

Sun, Q., Liu, Y., Liu, H., and Dumroese, R. K. (2020). Interaction of biochar type and rhizobia inoculation increases the growth and biological nitrogen fixation of *Robinia pseudoacacia* seedlings. *Forests* 11:711. doi: 10.3390/f11060711

Tian, D., Su, M., Zou, X., Zhang, L., Tang, L., Geng, Y., et al. (2021). Influences of phosphate addition on fungal weathering of carbonate in the red soil from karst region. *Sci. Total Environ.* 755:142570. doi: 10.1016/j.scitotenv.2020.142570

Wang, M., Liu, Q., and Pang, X. (2020). Evaluating ecological effects of roadside slope restoration techniques: A global meta-analysis. *J. Environ. Manag.* 281:111867. doi: 10.1016/j.jenvman

Wang, S., Zuo, X., Awada, T., Medima, E., Feng, K., Yue, P., et al. (2021). Changes of soil bacterial and fungal community structure along a natural aridity gradient in desert grassland ecosystems. *Inner Mongolia. Catena* 2021:205. doi: 10.1016/j.catena

Wickham, H., and Chang, W., (2015). ggplot2: An implementation of the grammar of graphics. http://CRAN.R-project.org/package=ggplot2. R package version 1.

Zhu, Y., Shao, T., Zhou, Y., Zhang, X., and Rengel, Z. (2021). 2021. Periphyton improves soil conditions and offers a suitable environment for rice growth in coastal saline alkali soil. *Land Degrad. Dev.* 32, 2775–2788. doi: 10.1002/ldr.3944

frontiers | Frontiers in Microbiology

TYPE Original Research
PUBLISHED 12 September 2022
DOI 10.3389/fmicb.2022.990329

OPEN ACCESS

EDITED BY
Maqshoof Ahmad,
The Islamia University of Bahawalpur, Pakistan

REVIEWED BY
Fasih Ullah Haider,
South China Botanical Garden (CAS), China
Zafar Iqbal,
Research Associate, Pakistan
Muhammad Adeel,
Beijing Normal University, Zhuhai, China
Muhammad Zahid Mumtaz,
The University of Lahore, Pakistan

*CORRESPONDENCE
Waqas-ud-Din Khan
dr.waqasuddin@gcu.edu.pk
Zhenjie Du
imdzj11@caas.cn

SPECIALTY SECTION
This article was submitted to Terrestrial Microbiology, a section of the journal Frontiers in Microbiology

RECEIVED 09 July 2022
ACCEPTED 15 August 2022
PUBLISHED 12 September 2022

CITATION
Batool M, Rahman Su, Ali M, Nadeem F, Ashraf MN, Harris M, Du Z and Khan W-u-D (2022) Microbial-assisted soil chromium immobilization through zinc and iron-enriched rice husk biochar. *Front. Microbiol.* 13:990329. doi: 10.3389/fmicb.2022.990329

Microbial-assisted soil chromium immobilization through zinc and iron-enriched rice husk biochar

Masooma Batool[1], Shafeeq ur Rahman[2,3], Muhammad Ali[1], Faisal Nadeem[4], Muhammad Nadeem Ashraf[5], Muhammad Harris[6], Zhenjie Du[7,8]* and Waqas-ud-Din Khan[1]*

[1]Sustainable Development Study Centre, Government College University, Lahore, Pakistan, [2]School of Environment and Civil Engineering, Dongguan University of Technology, Dongguan, China, [3]MOE Laboratory for Earth Surface Processes, College of Urban and Environmental Sciences, Peking University, Beijing, China, [4]Department of Soil Science, University of the Punjab, Lahore, Pakistan, [5]Institute of Soil & Environmental Sciences, University of Agriculture, Faisalabad, Pakistan, [6]Department of Environmental Sciences, University of Lahore, Lahore, Pakistan, [7]Farmland Irrigation Research Institute, Chinese Academy of Agricultural Sciences, Xinxiang, China, [8]Water Environment Factor Risk Assessment Laboratory of Agricultural Products Quality and Safety, Ministry of Agriculture and Rural Affairs, Xinxiang, China

Soil chromium toxicity usually caused by the tannery effluent compromises the environment and causes serious health hazards. The microbial role in strengthening biochar for its soil chromium immobilization remains largely unknown. Hence, this study evaluated the effectiveness of zinc and iron-enriched rice husk biochar (ZnBC and FeBC) with microbial combinations to facilitate the chromium immobilization in sandy loam soil. We performed morphological and molecular characterization of fungal [*Trichoderma harzianum* (F1), *Trichoderma viride* (F2)] and bacterial [*Pseudomonas fluorescence* (B1), *Bacillus subtilis* (B2)] species before their application as soil ameliorants. There were twenty-five treatments having ZnBC and FeBC @ 1.5 and 3% inoculated with bacterial and fungal isolates parallel to wastewater in triplicates. The soil analyses were conducted in three intervals each after 20, 30, and 40 days. The combination of FeBC 3%+F2 reduced the soil DTPA-extractable chromium by 96.8% after 40 days of incubation (DAI) relative to wastewater. Similarly, 92.81% reduction in chromium concentration was achieved through ZnBC 3%+B1 after 40 DAI compared to wastewater. Under the respective treatments, soil Cr(VI) retention trend increased with time such as 40 > 30 > 20 DAI. Langmuir adsorption isotherm verified the highest chromium adsorption capacity (41.6 mg g^{-1}) with FeBC 3% at 40 DAI. Likewise, principal component analysis (PCA) and heat map disclosed electrical conductivity-chromium positive, while cation exchange capacity-chromium and pH-organic matter negative correlations. PCA suggested the ZnBC-bacterial while FeBC-fungal combinations as effective Cr(VI) immobilizers with >70% data variance at 40 DAI. Overall, the study showed that microbes + ZnBC/FeBC resulted in low pH, high OM, and CEC, which ultimately played a role in maximum Cr(VI) adsorption from wastewater applied to the soil. The study also revealed the interrelation and alternations in soil dynamics with pollution control treatments.

Based on primitive soil characteristics such as soil metal concentration, its acidity, and alkalinity, the selection criteria can be set for treatments application to regulate the soil properties. Additionally, FeBC with *Trichoderma viride* should be tested on the field scale to remediate the Cr(VI) toxicity.

KEYWORDS

doped biochar, wastewater (WW), fungi and bacteria, phylogenetic analysis, heat map analysis

Introduction

Heavy metals such as chromium Cr(VI), arsenic (As), and lead (Pb) are generally released from processing and manufacturing industries (Wang et al., 2020). Chromium exists in natural environment as H_2CrO_4 at pH <1, $HCrO_4^-$ at pH < 6, and CrO_4^{2-} at pH > 6.0 (Xia et al., 2019). Chromium is highly toxic and mutagenic due to its oxidization characteristics to the intracellular components of living organisms (Wei et al., 2022). Chromium [Cr(VI)] has 1,000 times more cellular toxicity potential compared to Cr(III) (Shahid et al., 2017). The Cr(VI) threatens the threshold limits of land and aquatic systems due to its high stability, persistence, and solubility nature (Chen et al., 2015). It is translocated from the soil to the plant body through sulfate and phosphate transporters (Ao et al., 2022). In plants, Cr(VI) damages protein structure and minerals (K, Fe, Ca, Mn, and Mg) balance (Srivastava et al., 2021). The Cr(VI) metal has a high capacity of bioaccumulation in the human body through the food chain (Azeez et al., 2021). Ahmad et al. (2012) also mentioned Cr(VI) induced cytotoxicity in human. For developing countries such as Pakistan, inadequate investment and advanced technology to treat concentrated industrial effluents always remained serious challenges (Abriz and Golezani, 2021). Some conventional metal removal methods such as the use of ferric salts, red mud, and inorganic clays have previously been reported; however, the application of inorganic materials leads to the formation of stable metal compounds having less mobility and accessibility to plants (Choo et al., 2020). Nevertheless, associated costs, production of secondary pollutants, and minimal metal removal rate remained the major constraints (Wang et al., 2020).

Biochar (BC) is a black carbonaceous compound produced from bio-wastes under anoxic conditions (Haider et al., 2021). Accessibility and variety of raw materials for biochar

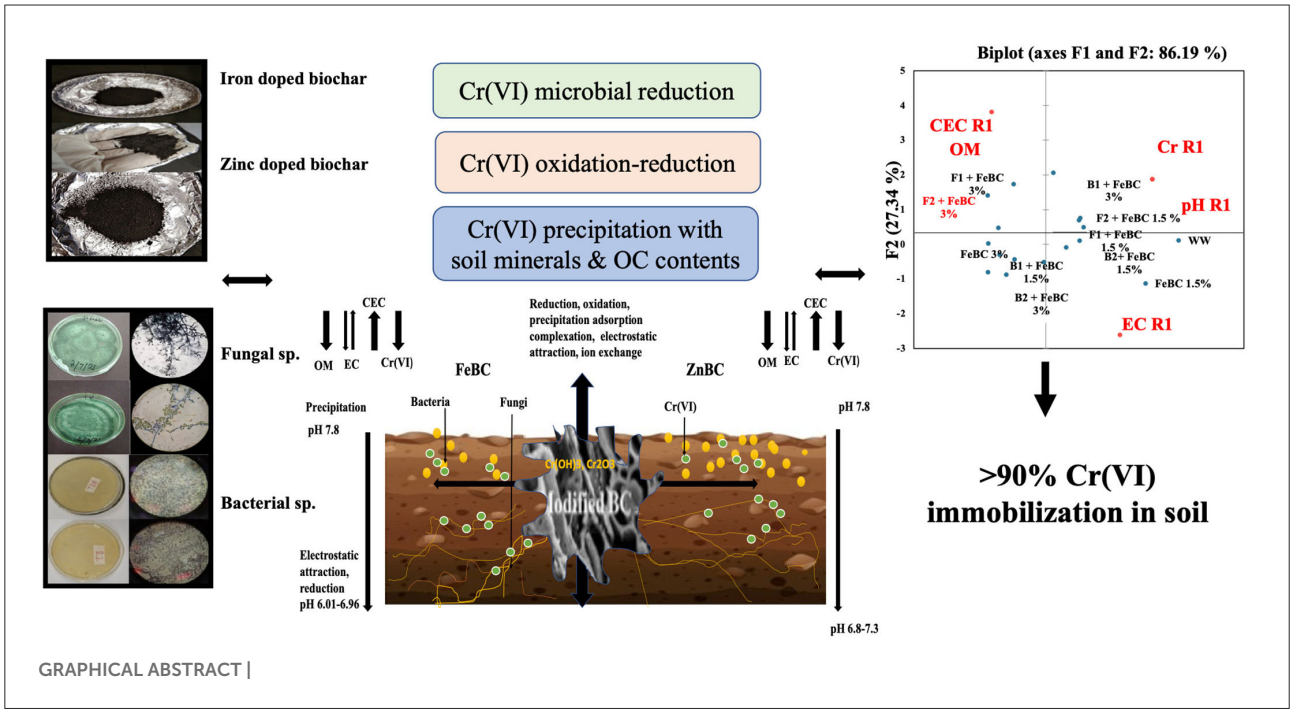

GRAPHICAL ABSTRACT |

manufacturing make it an ideal adsorbent and an inexpensive soil fertility booster material (Dai et al., 2018). Biochar characteristics depend on the type of organic raw material, BC surface area, porosity, and magnetism [metal cations (Fe, Zn, etc.) enriched form] properties (Zhang et al., 2020). Rice husk (550–650°C) BC has a honeycomb-like structure with a low atomic H/C O/C ratio and volatile matter which contributes to its soil ameliorant properties (Pariyar et al., 2019). Through metal doping mechanisms, BC chemistry, reactivity, surface energy, and complex stability can be enhanced suitably to bring multiple grades of interaction among BC and soil components (Liu et al., 2019b; Moradi et al., 2019). In a study, wheat straw Fe-enriched BC (600°C) was added to Cr(VI)-laden soil (Lyu et al., 2018). At acidic pH, iron-sulfide (FeS) disassociated with Fe^{2+} and S^{2-} ions, and Fe(II) as a natural reductant reduced Cr(VI) to Cr(III) with a subsequent increase in Fe–Cr co-precipitates [(Fe, Cr) $(OH)_3$]. The analysis on X-ray photoelectron spectroscopy (XPS) showed the disappearance of Fe°, and the appearance of Cr_2O_3 and Fe_2O_3 peaks confirmed Cr(VI) reduction by Fe° released electrons. In the same context, Li et al. (2018) showed that granular-activated carbonaceous BC enriched with zinc oxide (ZnO) resulted in a 5 times higher metal (Pb^{2+}) removal rate compared to activated BC only. Magnetic BC (Fe/Zn enriched) produced (400°C) from rice husk expressed ~10 times higher Pb^{2+} adsorption capacity than simple BC (Seleiman et al., 2020).

The acidification-based enrichment process makes BC a soil pH-reducing agent (Moradi et al., 2019). The chromium oxide species such as negatively charged chromate ions (CrO^{2-}; CrO_4^{2-}) are readily adsorbed at low pH (Zhang et al., 2018a). Contrarily, at high pH levels, OH^- species and Cr(VI) anionic species competitively interact for positively charged compounds (Gomes, 2016). The soil physicochemical properties such as organic matter (OM), pH, and electrical conductivity (EC) strongly influence the heavy metals immobilization by ion exchange, surface coagulation, sorption, chelation, and precipitation mechanisms; however, the bonding nature varies with metal characteristics (Saffari et al., 2016). Similarly, biologically modified systems through metabolism or bioaccumulation pathways contribute to metal adsorption and detoxification. Microbial phospholipid fatty acid (PLFA) studies revealed that bacteria and fungi vary in their soil OM degradation patterns through which their pollution remediation potential can be determined (Xu et al., 2018). The endophytes such as *Trichoderma* sp. develop mutual chemistry with soil dwellers (other bacterial and fungi) and release metabolites facilitating metal detoxification. Fungal mycelia usually excrete glomalin protein, which reduces the metal bioavailability (Shakya et al., 2016). Furthermore, fungal hyphae, spores, and vesicles work as exclusion barriers (Khan et al., 2020). Bacteria generally reduce the metal content by their metabolic pathways and primarily enhance the soil fertility and organic constituents' bioavailability through OM degradation (Hashem et al., 2019). Naggar et al. (2020) reported *Pseudomonas* sp. (*alcaliphila* NEWG strain) use for Cr(VI) removal (96.33%) from aqueous solution (pH 7) within 48 h of the incubation period. He et al. (2020) combined *ureolytic* bacteria with *P. fluorescence* for remediation of polluted soils and achieved 83% removal of Pb and cadmium (Cd) metals. Heavy metals accumulation by *P. fluorescence* appeared to be highly pH-dependent as it showed efficient metal removal at acidic pH (Lopez et al., 2000). Alotaibi et al. (2021) referred to the chromate reductase (ChrR) enzyme-producing Cr-resistant *Bacillus* sp. to reduce toxic Cr(VI) to Cr(III) with a 95% efficiency level. In another study, *B. subtilis* mediated ~96% Cd and 65% Cr pollution in edible radish parts relative to control (Wang et al., 2014). *B. subtilis* improved the antioxidant enzymes production in the Alfalfa plant and enhanced the nutrient cycling in the amended soil. The same species enhanced 29.4% alfalfa growth, whereas 139% Cd metal immobilization was observed in treated soil relative to control (Li et al., 2021). These microbial species are benign and have never been reported as pathogenic organisms (Quintieri et al., 2020; Su et al., 2020).

Although various studies mentioned the BC–microbial association in removing metal toxicity from different mediums such as aqueous solutions and soil (Han et al., 2016; Huang et al., 2017; Khan et al., 2020), however, few studies are available on enriched BC–microbial associations in remediation of tannery wastewater (WW) impacted soil (Batool et al., 2022; Meki et al., 2022). Based on microbial strains efficacy, bacterial species including *P. fluorescence* (B1) and *B. subtilis* (B2), and fungal sp. of genus Trichoderma including *T. harzianum* (F1) and *T. viride* (F2) were exclusively selected for the proposed study.

We hypothesized that the FeBC and ZnBC in combination with fungal and bacterial isolates could remediate soil Cr(VI) pollution. Primarily, the research was conducted to evaluate the effects of Cr(VI) polluted WW on soil physicochemical properties in control and how microbial–BC application improved these properties at different intervals. Similarly, the microbial–BC role in soil Cr(VI) removal was assessed through principal component analysis–heat map and Cr(VI) adsorption kinetics.

Materials and methods

Wastewater collection for soil spiking

The WW effluent was collected from the Siddique leather works (Pvt.) industry, Lahore (latitude: 31°37'48.05"N; longitude: 74°12'59.94"E), Pakistan. The composite WW samples were collected during November 2021 and preserved at −4°C until the experimentation. Before application to soil, WW was filtered through the filter paper (Whatman no. 42) to remove the suspended particles. Then, Cr(VI) concentration was analyzed through a multi-sequential Atomic Absorption

Spectrophotometer (Thermo Scientific iCE 3000 AAS, USA) by following Syuhadah's et al. (2015) guidelines. The Cr(VI) metal concentration in WW was 523.18 ppm considered for soil spiking.

Morphological and molecular characterization of microbial isolates

T. harzianum (F1) (accession code: FCBP-SF-1277), T. *viride* (F2) (accession code: FCBP-SF-644), *P. fluorescence* (B1) (accession code: FCBP-SB-0188), and *B. subtilis* (B2) (accession code: FCBP-SB-0189) cultures were acquired from the First Fungal Culture Bank of Pakistan (FCBP), University of the Punjab, Lahore.

Fungal species (F1, F2) were re-inoculated and maintained on Malt extract agar (10 g Malt extract, 10 g agar, 500 ml distilled water). The pH of the medium was adjusted to 6.5 with sodium hydroxide (NaOH). Fungal cultures were incubated at 26–28°C for 7 days (Baral et al., 2018). The purified culture morphological characterization was made by colony morphology and microscopic studies (Table 2; Sempere and Santamarina, 2011; Lagree et al., 2018). Finally, the pure cultures were stored at −4°C.

Fungal DNA was isolated by following the optimized Cetyl trimethylammonium bromide (CTAB) method (Doyle and Doyle, 1987) confirmed in gel electrophoresis (Inglis et al., 2018). PCR amplification was done with universal primers ITS 1 (5′TCCGTAGGTGAACCTGCGG3′) and ITS 4 (5′TCCTCCGCTTATTGATATGC3′). PCR-amplified product was sent for sequencing to Genetix: Gene Insight Experts Laboratory in Lahore (Gulberg-3), Pakistan. Through Sanger technology, obtained sequences were analyzed through BLAST (Basic Local Alignment Search Tool), and a phylogenetic tree was developed by MEGA-X software with the reference sequences from NCBI database to compare their genetic variation (Figure 2).

Bacterial cultures were re-inoculated on Lauria Bertin agar (Tryptone 5 g, yeast extract 2.5 g, NaCl 5 g, and agar 6 g in 500 ml d.H_2O) medium (Loutfi et al., 2020). The plates were incubated at 34°C for 24 h. Morphological characterization of bacterial isolates was done by gram staining test, UV light test, colony morphology, and microscopic studies at 100X (Smith and Hussey, 2005; Moyes et al., 2009). Purified bacterial cultures were stored in 20% glycerol solution at −4°C (Howard, 1956). DNA of bacterial isolates was extracted by the phenol-chloroform method by following an optimized DNA extraction protocol (Holben, 1994). To confirm extracted DNA presence, gel electrophoresis (1% agarose gel with 1 X TAE buffer), PCR amplification (Supplementary Figure 1), and PCR product gel electrophoresis steps were followed (Riffiani et al., 2015). PCR amplification was performed by 16S rRNA primers. The amplified product was gel sequenced, and result sequences after BLAST analysis were processed for alignment and phylogenetic analysis by MEGA-X software.

The freshly grown fungal culture plates were added with 200 ml of d.H_2O, and spores-enriched water was collected for pouring into treatment cups as 1 ml per 10 g of soil (David and Davidson, 2014). However, the bacterial broth cultures were prepared for direct application as 1 ml per 10 g of soil (Lederberg and Lederberg, 1952).

Biochar preparation and characterization

Rice husk (oven-dried at 80°C for 24 h) grounded samples were pyrolyzed in a furnace (TF-1200X; Hefei Ke Jing Materials Technology Co. Ltd, China) at 550°C with 10°C/min heat rate (Dad et al., 2020). Then, the pyrolyzed material (BC product) was passed through a 2-mm sieve. For Fe and Zn enrichment on BC, the procedure was adopted as given in our following manuscripts (Dad et al., 2020; Taqdees et al., 2022). The physicochemical properties of enriched rice husk BC (ZnBC and FeBC) are listed in Table 1.

Soil sample characterization

The soil used in this experiment was purchased from Malik nursery, Lahore, Pakistan. The physicochemical properties of the soil used in this experiment are given in Table 1. Soil texture was determined using the hydrometer method as described by Gee and Or (2002). Soil cation exchange capacity (CEC) was checked by the ammonium acetate extraction method (Ellen et al., 2001). For soil Cr(VI) metal content analyses, the diethylenetriamine penta-acetic acid (DTPA) metal-extraction method was followed (Lindsay and Norvell, 1978). Soil OM contents were quantified by the acid digestion (Walkley-black method) method (Nelson and Sommers, 1996). Soil pH and EC were checked with pH meter (smart CHEM-LAB Laboratory Analyser, VWR International Pty Ltd., Australia) (Rhoades, 1996) and EC meter (San ++, Skalar Analytical B.V., the Netherlands) (Hesse, 1971).

Experimental setup and design

The research elements (Zn/Fe doped BC, microbial formulations, soil, and WW) were prepared as described in the above sections for pot (height: 15.2 cm; width 9.5 cm (circumference) and bottom 6.2 cm) fil before incubation trial. ZnBC and FeBC were measured as 1.5 and 3% rates with 60 g of Bhal soil as per pot. The 25 treatments such as WW (control), B1 (*P. fluorescence*), B2 (*B. subtilis*), F1 (*T. harzianum*), F2 (*T. viride*), ZnBC1.5%, ZnBC 3%, FeBC1.5%, FeBC3%, B1 +

TABLE 1 Soil and biochar physicochemical properties (Mean ± S.D).

Materials characterization	Type	Pyrolysis temperature	Texture	pH	EC (dS/m)	CEC [cmol (+)/Kg]	OM%	Cr mg kg^{-1}
Bhal soil	Loamy sand	–	Sand 75% Loam 18% Clay 7%	7.80 ± 0.3	0.8 ± 0.01	4.21 ± 0.4	0.8 ± 0.1	0.02 ± 0.001
Enriched-Biochar	ZnBC	550°C/min	–	4.7 ± 0.4	0.36 ± 0.02	14.9 ± 0.9	3.5 ± 0.6	–
	FeBC	10°C/min	–	2.67 ± 0.1	0.1134 ± 0.001	19.9 ± 1.2	8 ± 0.99	–

ZnBC1.5%, B1 + ZnBC3%, B1 + FeBC1.5%, B1 + FeBC3%, B2 + ZnBC1.5%, B2 + ZnBC3%, B2 + FeBC1.5%, B2 + FeBC3%, F1 + ZnBC1.5%, F1 + ZnBC3%, F1 + FeBC1.5%, F1 + FeBC3%, F2 + ZnBC 1.5%, F2 + ZnBC 3%, F2 + FeBC1.5%, and F2 + FeBC 3% were applied in pots (3 replicates each) for 3 assessment periods (20, 30, and 40 days). All the treatments were mixed under sterilized conditions to avoid spore contamination. Finally, WW (100% conc.; 40 ml) was applied to all the pots. Plastic pots were placed in the growth chamber at Sustainable Agriculture Laboratory, Sustainable Development Study Center (SDSC) Government College University, Lahore, under the uniform conditions (such as average temperature 25–30°C and humidity < 20–40%).

Soil post-harvest physicochemical parameter analyses

Soil samples were harvested after 20, 30, and 40 days of incubation (DAI). Each time, soil Cr(VI) concentration (Lindsay and Norvell, 1978; Figure 4), pH (Rhoades, 1996; Figure 5), OM content (Nelson and Sommers, 1996; Figure 6), EC (Hesse, 1971; Figure 7), and CEC (Richards, 1954; FAO, 1990; Figure 8) were determined. Similarly, the confirmation of viable fungal and bacterial spores in soil samples was performed by adopting the same procedures for re-isolation and characterization of the microbes as discussed in Section Morphological and Molecular Characterization of Microbial Isolates (Figure 3).

Isotherm kinetic models

The Cr(VI) concentration adsorbed by adsorbents (unit mass) such as ZnBC and FeBC in soil was determined by the concentration difference (Manzoor et al., 2013; Shah et al., 2016). The mathematical expression was as follows:

$$q = (Cf - Ci) \times (V/1000)/m$$

Ci: Cr(VI) initial concentration (mg kg^{-1}); Cf: Cr(VI) final concentration (mg kg^{-1}); V: extractant volume (ml); m: adsorbent mass (g).

To calculate the percentage (%) metal removal, the control value was taken as an initial metal concentration (Ci) relative to treatments added as follows:

$$C = Ci - Cf/Ci \times 100$$

Langmuir and Freundlich's adsorption isotherm models were applied on Cr(VI) metal adsorption data (triplicate sets mean values) to distinguish ZnBC and FeBC adsorption capacities over time (Manzoor et al., 2013). The Langmuir linear equation (Equation 1) and Freundlich isotherm log equation (Equation 2) mathematical expressions are given

$$Ce/qe = 1/qmaxK_l + Ce/qmax \quad (1)$$

$$Log\ qe = 1/n\ (Log\ Cf) + Log\ Kf \quad (2)$$

Qe: Metal ions [Cr(VI)] sorbed (g kg^{-1}); K_l: Langmuir constant; Kf and 1/n: Freundlich constants.

Statistical and co-linearity analyses (PCA, heat map)

The data were statistically analyzed by completely randomized design (CRD) using Sigma-plot (14.5 version) and Statistix@ 8.1 software (Tallhase software package, USA) to segregate the treatments based on the least significant difference (LSD) test (Liu et al., 2020). Further to evaluate the co-linearity and co-association of variables, principal component analysis (PCA–Pearson correlation) was applied to data sets (organized as ZnBC and FeBC treatments) with mean values for 20, 30, and 40 DAI by XLSTAT 2021 tool (Addinsoft-New York, USA). Finally, for all the treatment variables, a heat map was generated through the "*Metabo-analyst*" statistic analyses online website (https://www.metaboanalyst.ca/) to visually distinguish interval-wise changes in soil properties under metal stress and treatment additions individually.

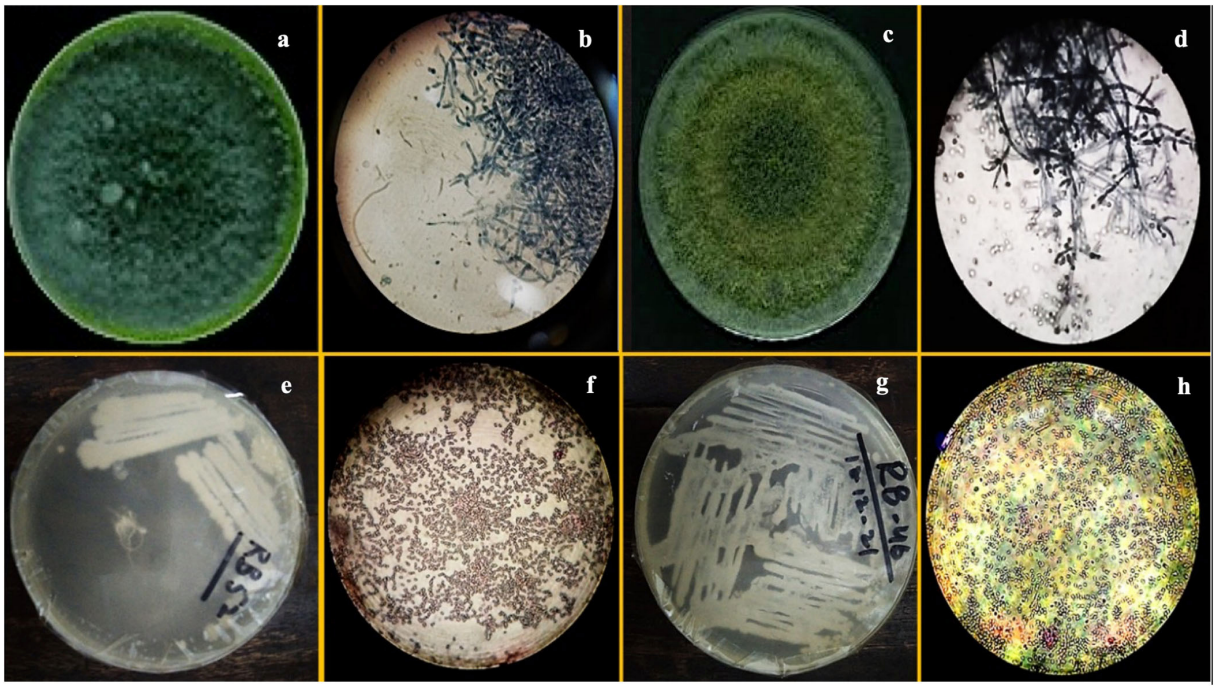

FIGURE 1
Images of pure culture T. *harzianum* **(a)** inoculated plate **(b)** microscopic study, pure culture T. *Viride* **(c)** inoculated plate **(d)** microscopic study; images of pure culture *Azotobacter nigricans* sp. **(e)** inoculated plate **(f)** microscopic study and pure cultures *Trichococcus* sp. **(g)** inoculated plate **(h)** microscopic study.

Results

F1 had one concentric ring that appeared outward from the inoculum point and green conidia (with dense middle) were spread over the growth media having a compact mycelial growth pattern (Figure 1). In contradiction, F2 showed regular concentric growth rings and fluffy mycelium. Phialide (F1: 4 × 2.6 μm; F2: 3 × 3.2 μm) were hook-shaped in both sp. such as *Trichoderma* sp. (F1, F2) granular mycelial hyphae were aseptate, and conidiophores showed tuft of fertile conidia [F1: globose to subglobose (2.8 × 2.7 μm); F2: globose to ellipsoidal (3.2 × 2.7 μm)] attached at conidiophores (Figure 1). F1 conidiophores (4.5–7.0 × 2.7–2.5 μm) were frequently branched contrary to F2 which had irregularly branched conidiophore (5.0–6.5 × 1.7–2.7 μm) structures (Table 2).

The morphological characterization of bacterial isolates revealed rod-shaped B1 cells, which existed individually as well as in chain-like arrangements. Likewise, B2 cells were also rod-shaped but only appeared as single cells rather than chain or clustered forms (Figure 1, Table 2). Both sp. showed different gram staining projects such as B1 were gram-negative while B2 remained gram-positive as it retained crystal violet dye. In spore testing results, B1 was spore-positive while B2 persisted as negative. Both bacterial isolates were off-white. Similarly, both isolates appeared bright under UV radiations (Table 2).

Extracted DNA bands from pure fungal (F1, F2) cultures were visible over agarose gel (DNA marker size 100 bp) before and after PCR amplification (Supplementary Figure 1). Molecular evolutionary genetics analysis of Trichoderma isolates revealed that F1 was genetically closer (>99.86% likelihood) to F2 as confirmed by NCBI reference sequences analyses. Phylogenetic dendrograms of *Trichoderma* sp. have been presented (Figure 2). Similarly, extracted DNA bands from pure bacteria (B1; B2) cultures appeared by gel electrophoresis (DNA marker size 100 bp) before and after PCR amplification were seen over agarose gel under UV luminescence (Supplementary Figure 1). Molecular evolutionary genetics analysis of B1 with its reference sequences from NCBI confirmed that the isolate had maximum genetic likelihood (92.04%) with an isolate of the same species from China and submitted to NCBI with an accession number KU507053, and 99.93% with another Chinese isolate with accession number JX683725. Likewise, B2 molecular evolutionary genetics analysis with its reference sequences from NCBI has confirmed isolate 99.86% genetic similarity with an isolate of the same species from India and submitted

10.3389/fmicb.2022.990329

TABLE 2 Selected microbial species characterization.

Coding	Name	Culture accession no.	Color	Shape	Gram test	Spore	UV test
Bacteria species							
B1	*P. fluorescence*	FCBP-SB-0188	Off-white	Rod	–	–	Bright
B2	*B. subtilis*	FCBP-SB-0189	Off-white	Rod	+	+	Bright
Coding	**Name**	**Culture accession no.**	**Morphology**	**Micro-metery**			
Fungal species							
F1	*T. harzianum*	FCBP-SF-1277	Rings: Multiple concentric rings and green (dense) middle Colony color: Green Colony texture: Compact, granular Hyphae: Septate Conidia shape: Globose to sub-globose Conidia color: Green Conidiophore: Frequently branched Chlamydospore formation: Infrequent, internal and terminal	Conidia size: 2.8 × 2.7 μm Phialide size: 4 × 2.6 μm Conidiophore size: 4.5 ~ 7.0 × 2.7 ~ 2.5 μm			
F2	*T. viride*	FCBP-SF-644	Rings: Enclosed rings with green conidia throughout or mostly outward Colony color: Green Colony texture: Fluffy, granular Hyphae: Septate Conidia shape: Globose to ellipsoidal Conidia color: Green Conidiophore: long, infrequently and irregularly branched, verticillate Chlamydospore formation: Terminal and intercalary	Conidia size: 3.2 × 2.7 μm Phialide size: 3 × 3.2 μm Conidiophore size: 5.0 ~ 6.5 × 1.7 ~ 2.7 μm			

to NCBI with an accession number MK828386. Phylogenetic dendrograms of B1 and B2 have been given in Figure 2.

Microbial spores inoculated harvested soil analyses revealed the presence of similar fungal (F1, F2) and bacterial isolates (B1, B2) as discussed for pure cultures sp. (Table 2). The following figure (Figure 3) presented the morphological study of microbial sp. isolates from inoculated soil.

There were significant ($p < 0.05$) main and first-order interactions of fungi, bacteria, ZnBC, and FeBC treatments under Cr(VI) stress as shown in Figure 4. Soil post-harvest analyses revealed an increasing rate of DTPA-extractable Cr(VI) concentration of 92%, over time (Figure 4). In WW, the extracted DTPA-Cr(VI) was 2-, 5-, and 7-folds at 20, 30, and 40 DAI, respectively (Figure 4, Table 3). However, the fungal (F1, F2) and bacterial (B1, B2) species as single soil amendments brought significant ($p < 0.05$) metal immobilization *viz.* 31.65% by B1, 14.60% by B2, 40.49% by F1, and 33.86% by F2 at 40 DAI compared to WW (Table 3). Similarly, the BC-mediated soil Cr(VI) retention trend increased with time such as 40 >30 >20 DAI compared to WW (Figure 4). It was observed that B1 + ZnBC 3% brought 92.81% metal immobilization (at 40 DAI), which was the highest among bacterial-BC co-applied treatments (Table 3). Likewise, there was a significant increase of 96.8% in Cr adsorption rate by F2 + FeBC 3% amendment relative to WW at 40 DAI (Figure 4, Table 3).

Langmuir and Freundlich adsorption isotherms were individually applied on ZnBC (1.5 and 3%) and FeBC (1.5 and 3%) against B1, B2, F1, F2 single treatments at 20, 30, and 40 DAI (Table 4). The results demonstrated that the data were highly supported by the Langmuir isotherm adsorption model based on high R^2 ($R^2 = 0.9–1$) values (Table 4). Maximum Cr(VI) adsorption capacity (41 mg g^{-1}) was reported with FeBC 3%

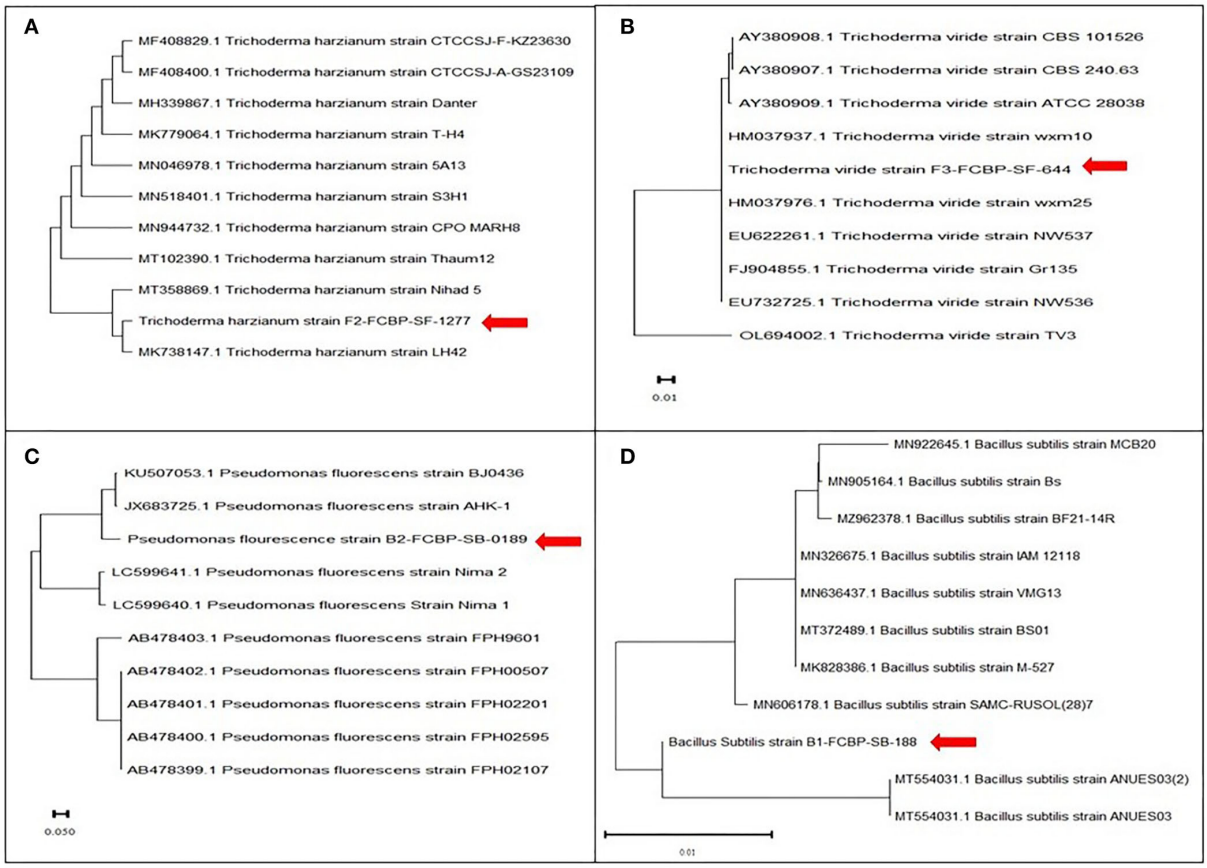

FIGURE 2
Phylogenetic dendogram of **(A)** *T. Harzianum,* **(B)** *T. viride* (sequenced with ITS1 and ITS4 regions), **(C)** *P. fluorescens,* and **(D)** *B. subtilis* (sequenced with 16S ribosomal RNA gene) for identification using sanger sequencing. Phylogenetic tree was constructed using the maximum likelihood method in MEGA version 10 following Tamura and Nei model. Bootstrap value was kept 1,000 replicates.

followed by ZnBC 3% (37.7 mg g^{-1}), which confirmed that 3% input rate enhanced the treatments effectiveness over 1.5% input rate (Table 4).

Data revealed significant ($p < 0.05$) variations in soil pH for main and first-order interaction of fungi, bacteria, ZnBC, and FeBC treatments under Cr(VI) stress from 20 to 40 DAI (Figure 5). The main effects showed enhancement in pH of the soil; particularly, the highest (10.65%) pH increase was observed for B1 relative to WW at 40 DAI. Additionally, all the fungal treatments except F1 + FeBC 1.5% and F2 + FeBC 1.5% caused 16.46% decrease in soil pH value relative to WW at 40 DAI.

The OM content was initially (20 DAI) reported by all the treatments except B2 + ZnBC 3% and F1 + ZnBC 1.5%. The bacterial activity significantly ($p < 0.05$) degraded the OM content with the passage of time, and no OM content was reported eventually among all bacterial treatments at 40 DAI, except B1 + FeBC3% and B2 + FeBC 3% (Figure 6). Similarly, the persistent decrease in OM content was reported in those treatments where both fungal species were applied with Fe and Zn BC. There was a (37.5%) decrease in OM content estimated with F2 + FeBC 3% application, whereas a maximum increase (20%) in OM content with FeBC 1.5% was observed compared to WW at 40 DAI.

There was an increase in EC observed among first-order interaction of all the treatments at 20 DAI relative to WW; however, a significant ($p < 0.05$) reduction in EC values was obtained at 40 DAI (Figure 7). The maximum (19.4%) increase in EC value turned out to be with ZnBC1.5% treatment relative to WW, at 40 DAI. However, FeBC1.5% interaction with B1 resulted in the highest EC reduction (55.6%) among all the treatments relative to WW at 40 DAI (Figure 7).

Soil CEC of first-order interaction treatments significantly ($p<0.05$) increased relative to WW, from 20 to 40 DAI. ZnBC 3% as alone and along with B2 treatment caused the highest soil CEC (2-folds) relative to WW at 40 DAI (Figure 8). However, the B2 with FeBC 3% rate contributed only 1-fold (least among

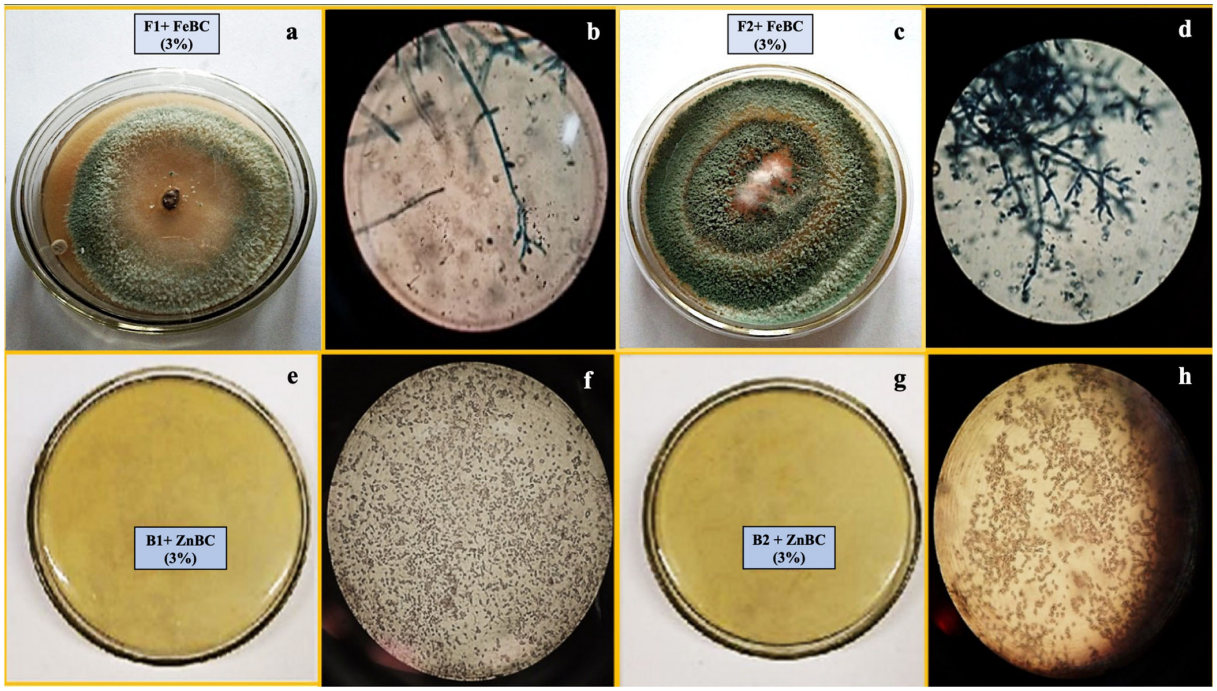

FIGURE 3
Images of *T. harzianum* fungal sp. from harvested soil **(a)** growth pattern **(b)** microscopic study and *T. viride* soil inoculated plate **(c)** growth pattern **(d)** microscopic study; images of *P. fluorescence* bacterial sp. from harvested soil **(e)** growth pattern **(f)** microscopic study and *B. subtilis* sp. from harvested soil **(g)** growth pattern **(h)** microscopic study.

first-order interaction treatments) CEC rise in treated soil. It was observed that all fungal sp. applied soil samples showed lower CEC compared to bacterial appended first-order treatments relative to WW, at 40 DAI (Figure 8).

Principal component analyses segregated the ZnBC-bacterial while FeBC-fungal combinations as effective Cr(VI) immobilizers with >70% data variance at 40 DAI (Figure 9). ZnBC and FeBC treatments variability under Cr(VI), pH, OM, EC, and CEC parameters were visible across 20(F > 75%), 30(F > 56%), and 40(F > 76%) DAI (Figure 9). Similarly, the analyzed parameters (PCA active variables) also depicted the shifting trend by occupying the biplot position relative to significantly influenced treatments (active observations). Heat map data analyses visually presented a gradual increase in variability of treatments and parameters. The contrasting colors in the map depicted the variability, while less distinguishable colors showed homogeneity in variables/treatments (Figure 9B). Analyses of ZnBC and FeBC treatments through PCA biplot demonstrated that treatment-added soil Cr(VI) adsorption was increasing gradually; furthermore, the OM, EC, and pH values showed a reduction after 40 DAI. However, the treatments-applied soil CEC value increment was evident by 76.28% data variance (Figure 9).

Discussion

Soil Cr(VI) adsorption was time- and rate-dependent

The soil Cr(VI) adsorption followed a decreasing trend as 40 DAI > 30 DAI > 20 DAI in WW (Table 3). The significant ($p < 0.05$) metal adsorption and gradual Cr(VI) immobilization were attained by F2 + FeBC 3% (96.8%) and B1 + ZnBC 3% (92.81%) compared to WW at 40 DAI (Figure 4, Table 3). Different scientists mentioned the maximum Cr adsorption at high rates of enriched biochar, such as Liu et al. (2019a) reported that an 8% rate of Fe-enriched rice husk-BC removed 99% Cr(VI) within 2 h from soil containing 795 mg kg^{-1} Cr(VI) concentration. In another study, sheep manure Fe-enriched BC 5% w/w application to soil [100 mg kg^{-1} Cr(VI)] remediated 55% Cr concentration relative to WW within 30 days (Mandal et al., 2017). Similarly, Li et al. (2018) reported that 0.04 g Zn-enriched carbonaceous BC enhanced 91.2% metal removal from Cr(VI) solution (50–100 ppm) relative to WW within 24 h. The previous studies reported the doped BC input rate as >3% (Liu et al., 2019a, 2020); similarly, in our study, 3% BC rates with microbial application remarkably enhanced the Cr(VI) immobilization in WW-affected soil relative to all

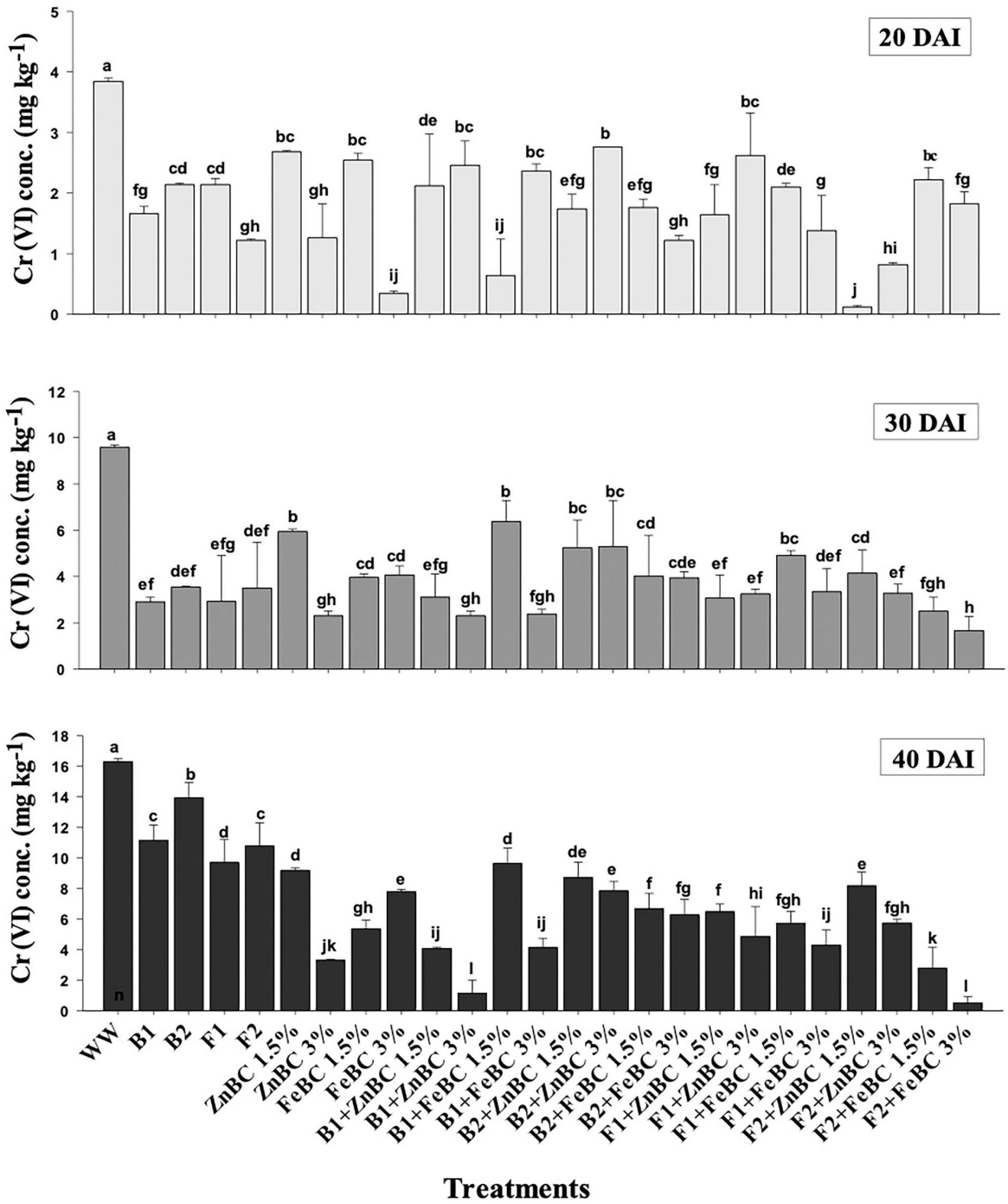

FIGURE 4
DTPA-extractable Cr(VI) concentration (Mean ± S.D) for ZnBC (1.5, 3%) and FeBC (1.5 and 3%) treatments at 20, 30, and 40 DAI periodic assessments.

other treatments (Figure 4, Table 3). Microbes cannot break heavy metals; instead, they bring metal immobilization through surface binding and enzymatic reactions (Wang et al., 2017a). It was examined that F2 exhibited high metal sorption compared to bacterial isolates (Figure 4); thus, they remained potential candidates for hexavalent Cr decontamination by enhancing

TABLE 3 Percentage (%) change in metal adsorption (R = 3 mean) after 20, 30, and 40 days of soil metal-spiking.

Treatments	Cr (VI) mg kg^{-1}					
	20 DAI Mean ± S.D	Percentage change in Cr(VI) adsorption	30 DAI Mean ± S.D	Percentage change in Cr (VI) adsorption	40 DAI Mean ± S.D	Percentage change in Cr(VI) adsorption
Soil	0.02 ± 0.001	–	0.021 ± 0.01	–	0.0243 ± 0.01	–
WW	3.84 ± 0.06	+191%	9.58 ± 0.09	+455%	16.3 ± 0.18	+670%
B1	1.66 ± 0.12	−56.77%	2.9 ± 0.2	−69.72%	11.14 ± 1	−31.65%
B2	2.14 ± 0.02	−44.27%	3.54 ± 0.04	−63.04%	13.92 ± 1	−14.60%
F1	2.14 ± 0.1	−44.27%	2.92 ± 2	−69.51%	9.7 ± 1.5	−40.49%
F2	1.22 ± 0.02	−68.22%	3.5 ± 1.98	−63.46%	10.78 ± 1.5	−33.86%
ZnBC 1.5%	2.68 ± 0.02	−30.20%	5.94 ± 0.12	−37.99%	9.18 ± 0.16	−43.6%
ZnBC 3%	1.26 ± 0.56	−67.18%	2.3 ± 0.2	−75.99%	3.32 ± 0.04	−79.63%
FeBC 1.5%	2.54 ± 0.12	−33.85%	3.96 ± 0.14	−58.66%	5.36 ± 0.58	−67.11%
FeBC 3%	0.34 ± 0.04	−91.14%	4.06 ± 0.4	−57.62%	7.8 ± 0.12	−52.14%
B1 + ZnBC 1.5%	2.12 ± 0.86	−44.79%	3.1 ± 1	−67.64%	4.08 ± 0.09	−74.96%
B1 + ZnBC 3%	2.46 ± 0.4	−35.93%	2.3 ± 0.2	−75.99%	1.16 ± 0.86	**−92.81%**
B1 + FeBC 1.5%	0.64 ± 0.6	−83.33%	6 ± 0.9	−37.36%	9.64 ± 1	−40.85%
B1 + FeBC 3%	2.36 ± 0.12	−38.54%	2.38 ± 0.2	−75.15%	4.14 ± 0.6	−74.601%
B2 + ZnBC 1.5%	1.74 ± 0.24	−54.68%	5.24 ± 1.2	−45.30%	8.72 ± 1	−46.50%
B2 + ZnBC 3%	2.76 ± 0.26	−28.12%	5.3 ± 1.98	−44.67%	7.84 ± 0.6	−51.98%
B2 + FeBC 1.5%	1.76 ± 0.14	−54.16%	4.02 ± 1.76	−58.03%	6.68 ± 1	−59%
B2 + FeBC 3%	1.22 ± 0.08	−68.22%	3.94 ± 0.26	−58.87%	6.28 ± 1	−61.47%
F1 + ZnBC 1.5%	1.64 ± 0.5	−57.29%	3.06 ± 1	−68.05%	6.48 ± 0.5	−60.24%
F1 + ZnBC 3%	2.62 ± 0.7	−31.77%	3.24 ± 0.2	−66.17%	4.86 ± 1.9	−70.18%
F1 + FeBC 1.5%	2.1 ± 0.06	−45.31%	4.92 ± 0.2	−48.64%	5.72 ± 0.78	−64.90%
F1 + FeBC 3%	1.38 ± 0.58	−64.06%	3.34 ± 1	−65.13%	4.3 ± 1	−73.61%
F2 + ZnBC 1.5%	0.12 ± 0.02	−96.87%	4.14 ± 1	−56.78%	8.18 ± 0.88	−49.81%
F2 + ZnBC 3%	0.82 ± 0.03	−78.64%	3.28 ± 0.39	−65.76%	5.74 ± 0.24	−64.78%
F2 + FeBC 1.5%	2.22 ± 0.2	−42.18%	2.5 ± 0.6	−73.90%	2.78 ± 1.38	−82.94%
F2 + FeBC 3%	1.82 ± 0.2	−52.60%	1.66 ± 0.6	−82.67%	0.52 ± 0.4	**−96.8%**

All the treatments have been compared with wastewater (WW) while WW has been compared with soil Cr (VI) content.
The values remained bold to distinguish them from the rest of the treatments. DAI, Day after incubation; SD, Standard deviation.

the chelation (Gan et al., 2015) and accumulation mechanisms (Zhang et al., 2020; Yu et al., 2021). Microbial function as symbionts with metals solubilization potential supports their usage in agronomic fields and for contaminated soils rehabilitation (Alam et al., 2019).

Adsorbents Cr(VI) retention potential (isotherms analyses)

Chromium [Cr(VI)] adsorption rate by ZnBC and FeBC (1.5 and 3%) with their microbial mixes at 20, 30, and 40 DAI was checked by kinetic isotherm models (Table 4). Langmuir isotherm was recommended as the best-fitted model as most of their R^2-values remained ∼1. Similarly, FeBC 3% had maximum Cr(VI) adsorption capacity (Qmax) 41.6 mg g^{-1} followed by ZnBC 3% (38.31 mg g^{-1}) at 40 DAI (Table 4). Basically, Langmuir isotherm suggested a monolayer Cr(VI) adsorption pattern with functional groups (COOH-, OH-) and minerals (Fe/Zn) over BC surface in soil solution (Babu and Gupta, 2008; Manzoor et al., 2013; Dad et al., 2020). Likewise, it is supposed that ZnBC and FeBC 3% dose rate contributed an increase in the number of functional groups and minerals (Fe/Zn) magnetism played a crucial role in enhanced soil Cr(VI) retention (Table 4). In a study, the Cr(VI) adsorption capacity of Zedarach (Chinaberry) wood Magnetic BC was recorded as 25.27 mg g^{-1} by Zhang et al. (2018b). Zhu et al. (2018) also applied adsorption isotherms and mentioned the

TABLE 4 FeBC and ZnBC metal adsorption capacity (20, 30, and 40 days) determined by Langmuir and Freundlich isotherms.

Langmuir adsorption isotherm					Freundlich adsorption isotherm			
	Q (max) or Xm (mg g^{-1})	k (*l*)	R (*l*)	R^2		Qe (mg g^{-1})	$1/n$ = m (slope)	R^2
WW (20)	1	0.547	0.11	0.98	WW (20)	15.84	0.9	0.97
WW (30)	14	0.05	0.005	1	WW (30)	5.370	0.86	1
WW (40)	4.1	0.36	0.02	0.995	WW (40)	2.51	0.4	0.9995
ZnBC 1.5% (20)	1.06	0.77	0.157	0.9013	ZnBC 1.5% (20)	3.16	0.292	0.7782
ZnBC 1.5% (30)	9.09	0.704	0.006	0.9778	ZnBC 1.5% (30)	5.52701	0.84	0.9765
ZnBC 1.5% (40)	27.7	0.023	0.001	0.983	ZnBC 1.5% (40)	7.6	0.67	0.9696
ZnBC 3% (20)	0.672	0.066	0.01	0.9946	ZnBC 3% (20)	4.07	0.843	0.9616
ZnBC 3% (30)	11	0.067	0.005	0.9824	ZnBC 3% (30)	15.84	0.740	0.9595
ZnBC 3% (40)	38.31	0.01	0.001	0.9714	ZnBC 3% (40)	19.95	0.2	0.8632
FeBC 1.5% (20)	1.09	0.636	0.131	0.8309	FeBC 1.5% (20)	3.845	0.584	0.9202
FeBC 1.5% (30)	7.87	0.07	0.007	0.9348	FeBC 1.5% (30)	13.983	0.82	0.9147
FeBC 1.5% (40)	27.47	0.023	0.001	0.9564	FeBC 1.5% (40)	17.93	0.539	0.8853
FeBC 3% (20)	1.408	0.673	0.139	0.8631	FeBC 3% (20)	3.73	0.388	0.8268
FeBC 3% (30)	15.03	0.054	0.004	0.9931	FeBC 3% (30)	14.79	0.406	0.9756
FeBC 3% (40)	41.6	0.016	0.0009	0.9673	FeBC 3% (40)	21.35	0.198	0.8167

Langmuir isotherm as the best-fitted model determining the Cr(VI) adsorption potential of 48.82 mg g^{-1} by Fe-enriched wetland reed BC.

Variation in soil physicochemical parameters (pH and OM) with Cr(VI) stress under bacterial/fungal and Zn/Fe BC amendments

The experimental soil pH was 7.8 that reduced (7.4%) with the WW application at 20 DAI. Virtually, the heterogeneity of pH values increased across the treatments after 40 DAI (Figure 5). The FeBC original pH (3.67) had an acidic effect on soil pH as FeBC applied soil samples showed a pH range of 6.01–6.9. Different treatments such as F1 + FeBC 1.5% and F2 + FeBC 1.5% caused a similar reduction (16.46%) in soil pH compared to WW at 40 DAI (Figure 5). The reason for this reduction trend might be the oxidation potential of FeBC, which enhanced the exposure of Fe and acidic (carbonyl, carboxyl) functional groups, under aerobic conditions (Abrishamkesh et al., 2015). According to Kumar et al. (2007), $HCrO_4^-$ ions are readily adsorbed over the soil surface by electrostatic attraction under acidic conditions, as the probability of H^+ ions exchange increases with negatively charged ions. However, ZnBC (pH 4.7)-added soil samples exhibited a 6.9–7.25 pH range (Figure 5). The Cr(VI) translocation and mobilization majorly depend on its oxidative state and medium pH (Attah and Melkamu, 2013). Furthermore, acidic to neutral pH might induce different metal immobilization mechanisms such as reduction, ion exchange, precipitation, and metabolic metal transformations (Palansooriya et al., 2020). The highly effective F2 + FeBC3% and B1 + ZnBC3% treatments had pH values of 6.03 and 6.97, respectively. Thus, the treatments exclusively contributed in setting the medium pH which influences microbial viability, Cr(VI) oxidative state, and minerals/OM availability.

There was no OM content reported in all bacterial treatments at 40 DAI except B1 + FeBC3% and B2 + FeBC 3% (Figure 6). Organic matter oxidation, microbial metabolic activities, and metal reduction might be the reasons for OM content variation with time (Huang et al., 2017; Liu et al., 2020). Bacteria with fast metabolic activity might consume soil OM at a faster rate compared to fungi (Figure 6). However, OM was present in all fungal applied BC (ZnBC, FeBC) treatments, except F1 + ZnBC 1.5% at 40 DAI. Fungi mycelium grows slowly and retains OM, which contributes to carbon balance and metal particles retention in soil (Xu et al., 2018). Thus, FeBC-fungi inoculated soil had a high potential for metal immobilization, carbon sequestration (high organic content observed), and long-term soil minerals management. With FeBC 1.5%, the maximum increase (20%) in OM content was observed compared to WW at 40 DAI (Figure 6). The variability can be attributed to aerobic experimental conditions and subsequent relative exposure to air.

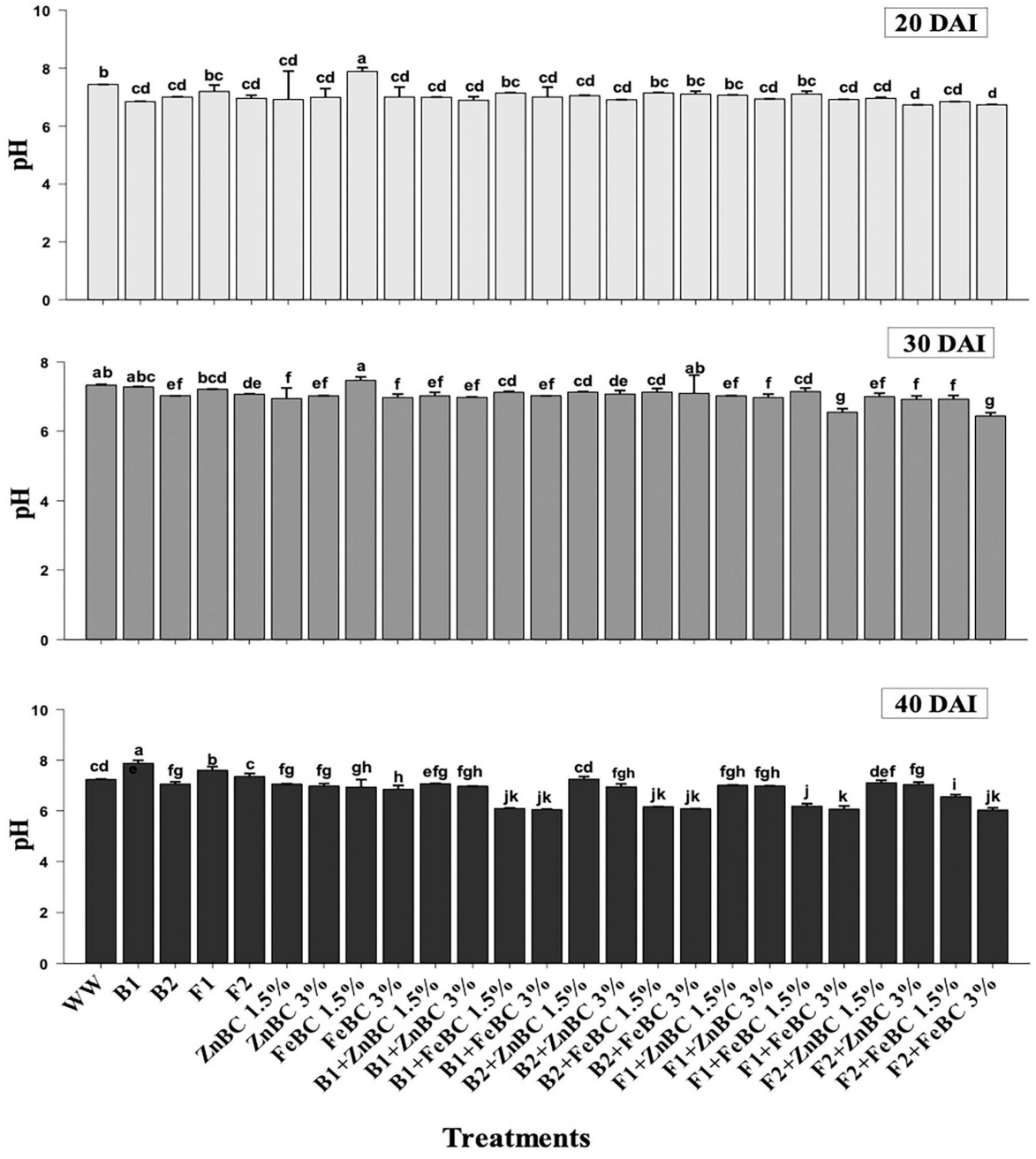

FIGURE 5
Comparative analyses of pH for treatments (Mean ± S.D) at 20, 30, and 40 DAI periodic assessments.

Variation in soil physicochemical parameters (EC and CEC) with Cr(VI) stress applied under bacterial/fungal and Zn/Fe BC amendments

In this study, the soil EC ~0.8 dS/m was reported before commencing the experiment, whereas the optimal EC ranges between 1.10 and 5.70 dS/m for fertile soil (Ghorbani et al., 2019). The WW application significantly ($p < 0.05$) reduced (97.73%) the soil EC as compared to the natural soil (Figure 7). However, the EC value of the soil increased for the main effects of all treatments as we moved from 20 to 40 DAI, while it remained unchanged or lower for the combined BC and microbial treatments over time (20–40 DAI) (Figure 7).

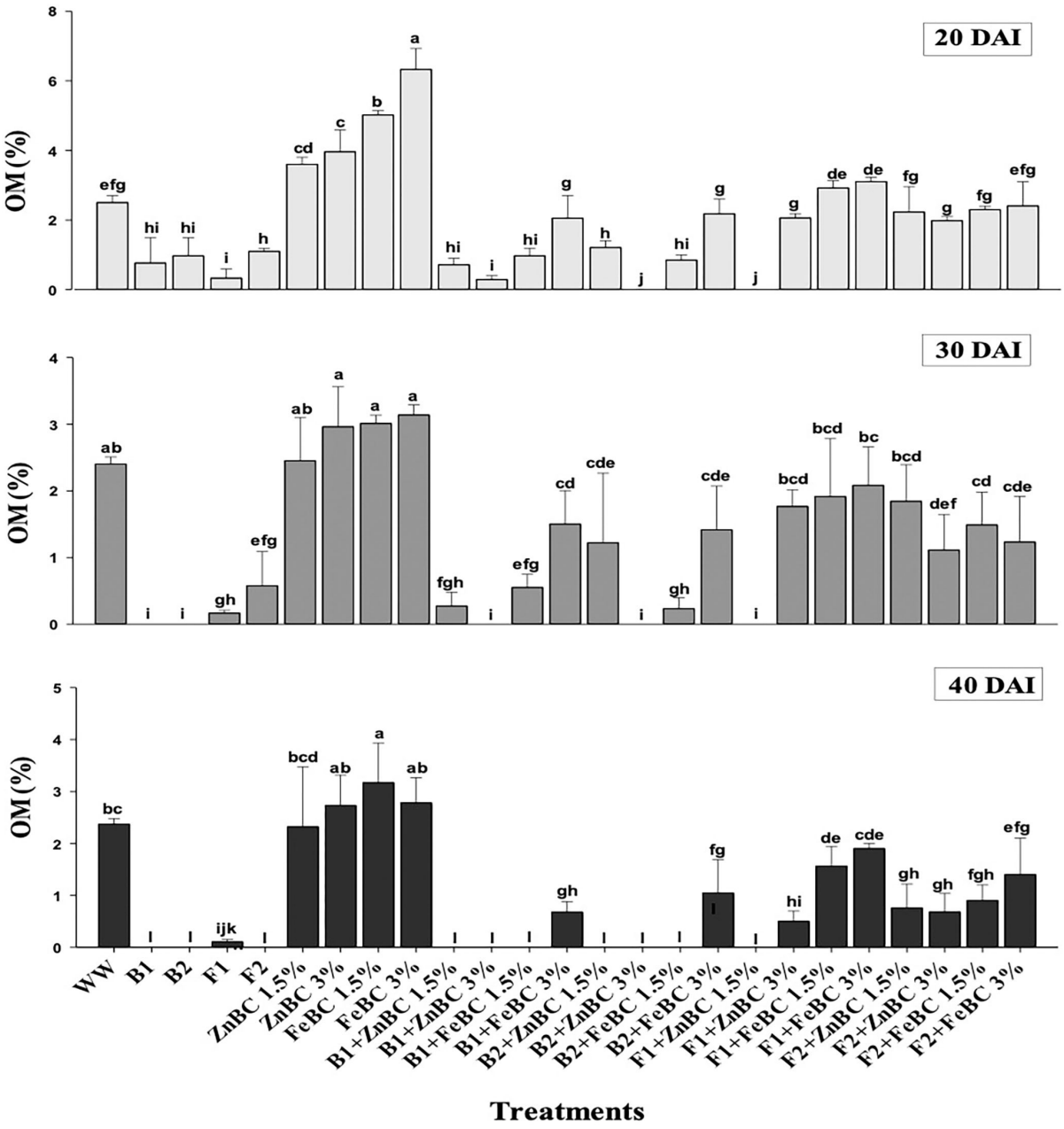

FIGURE 6
Comparative analyses of OM% content for treatments (Mean ± S.D) at 20, 30, and 40 DAI periodic assessments.

Few research studies already reported a rise in soil EC with time as enriched BC application might acquire high reaction kinetics (Masulili et al., 2010; Ghorbani and Amirahmadi, 2018). Contrarily, few studies mentioned non-significant changes in EC value of soil even after the addition of organic amendments (Jien and Wang, 2013; Mavi et al., 2018). The EC of F2 + FeBC 3% and B1 + ZnBC 3% treatments was reduced by 27.1 and 33.3%, relative to WW at 40 DAI, respectively (Figure 7). Low EC represents the less availability of nutrients, while high EC value indicated the presence of excessive nutrients (Liu et al., 2020). Microbial metabolic activities and carbon/nitrogen turnover directly influence the nutrients balance of soil (Muniz et al., 2014; Chen et al., 2017, 2021). Varied and low EC value range (relative to WW) for all ZnBC/FeBC microbial combinations might be due to an increase in metal-salt-OH groups or ionic and electrostatic interactions (Saffari et al.,

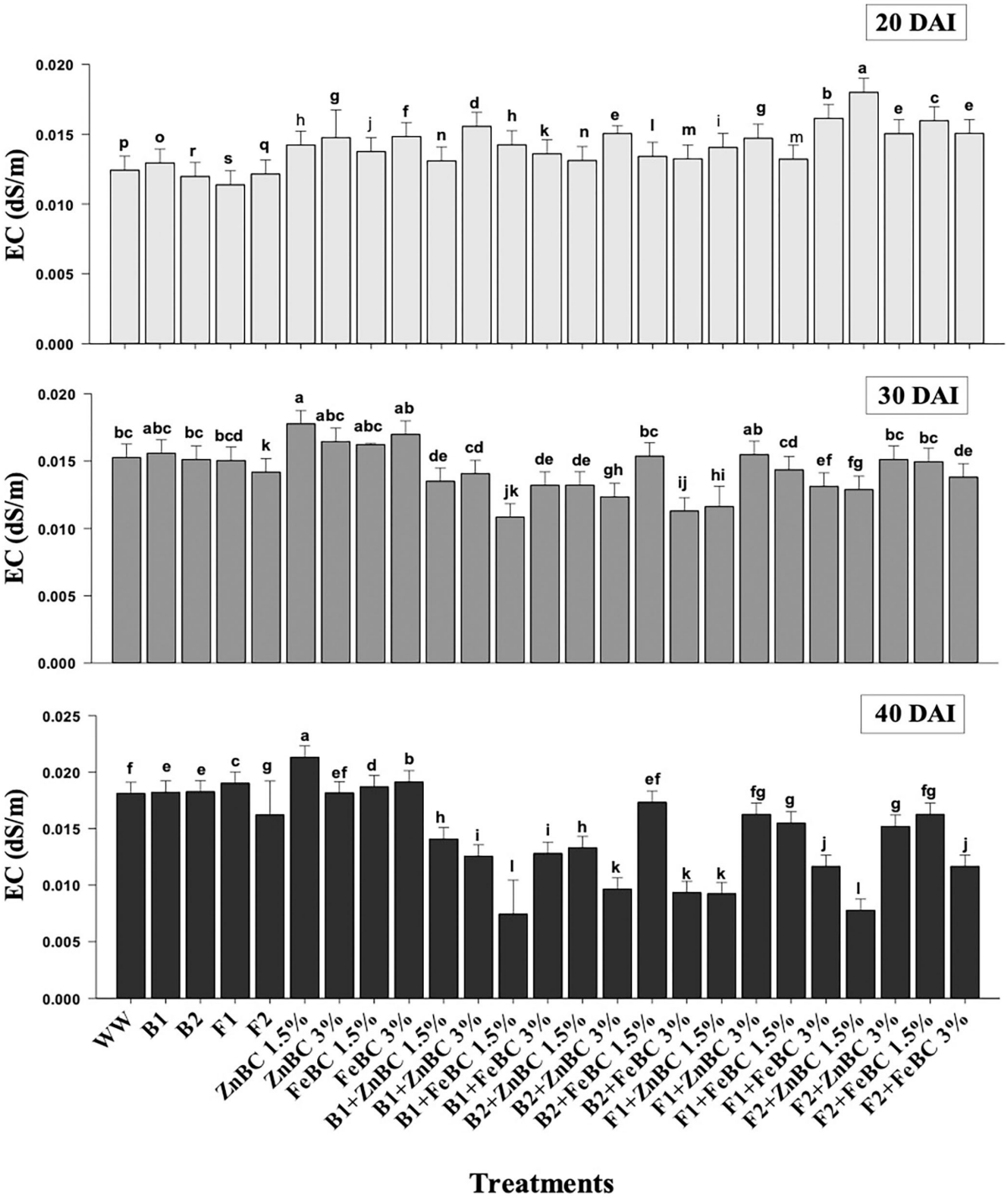

FIGURE 7
Comparative analyses of EC (dS/m) for treatments (Mean ± S.D) at 20, 30, and 40 DAI periodic assessments.

2016; Liu et al., 2020). According to PCA, the EC value was significantly (F = 76.28% for ZnBC; F = 78.23% for FeBC) and positively co-related to DTPA-extractable Cr(VI) content of soil (Figure 9).

The optimal soil CEC has a range of ~4.5–5 cmol(+)/kg for sandy loam soil (Olorunfemi et al., 2016). The WW application significantly ($p < 0.05$) reduced (86.5%) the soil CEC value (Figure 8). This reduction might be attributed to

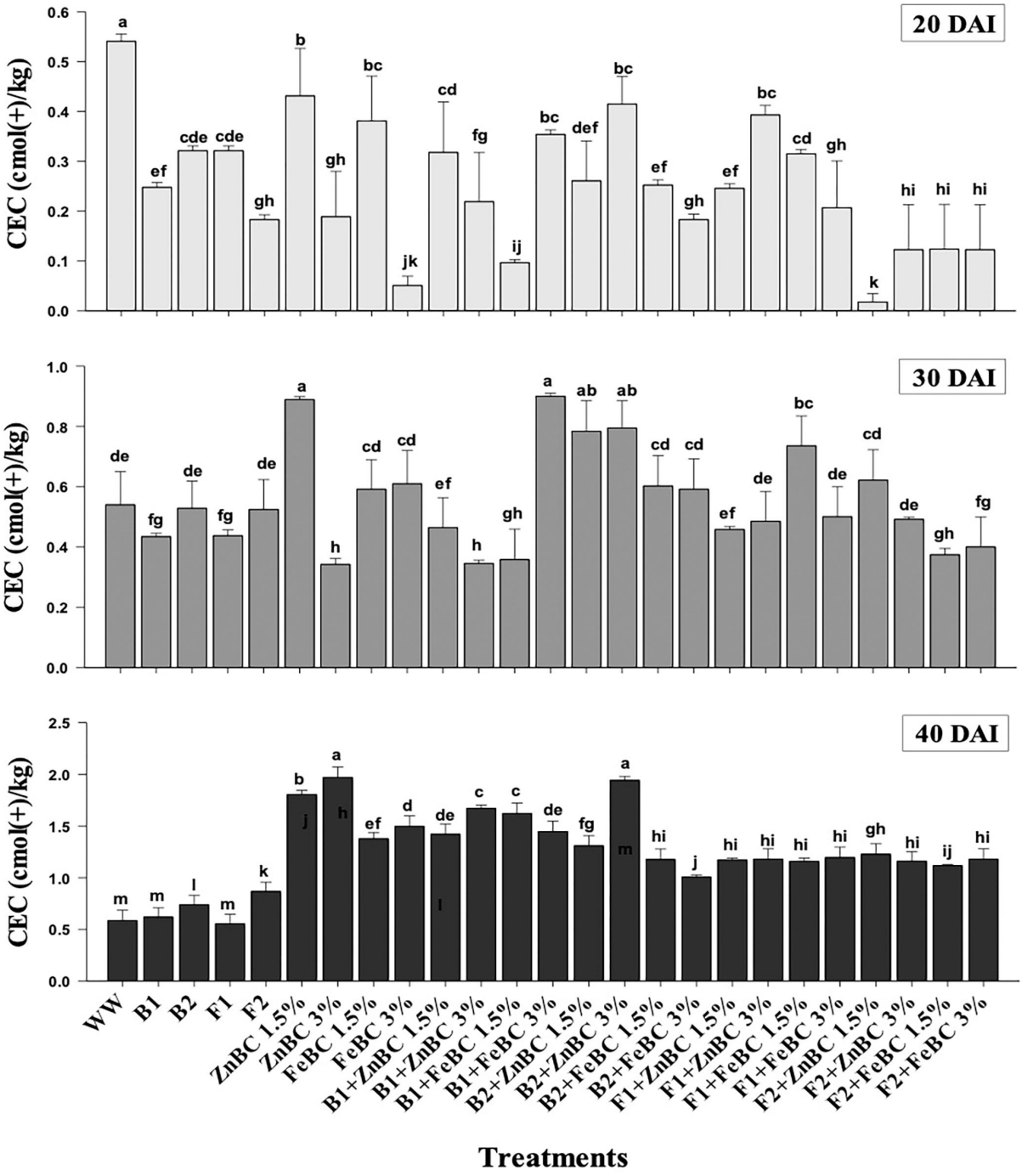

FIGURE 8
Comparative analyses of CEC [cmol (+)/kg] for treatments (Mean ± S.D) at 20, 30, and 40 DAI assessment periods.

Cr(VI) adsorption mechanism at the initial days (20 DAI) (Liu et al., 2020); however, microbial application with BC (first-order interaction) showed a gradual increment in soil CEC. After 40 DAI, there was a 2-fold increment in the CEC value observed for B2 + ZnBC 3% relative to WW (Figure 8). Different scientists have proposed different reasons such as it could be due to oxidation of BC functional groups, increased mobility of Cr(VI) due to microbial activity, competition between OH^- groups and metal anions and disassociation of mineral and metal components (Wang et al., 2017a,b; Liu et al., 2020; Yu

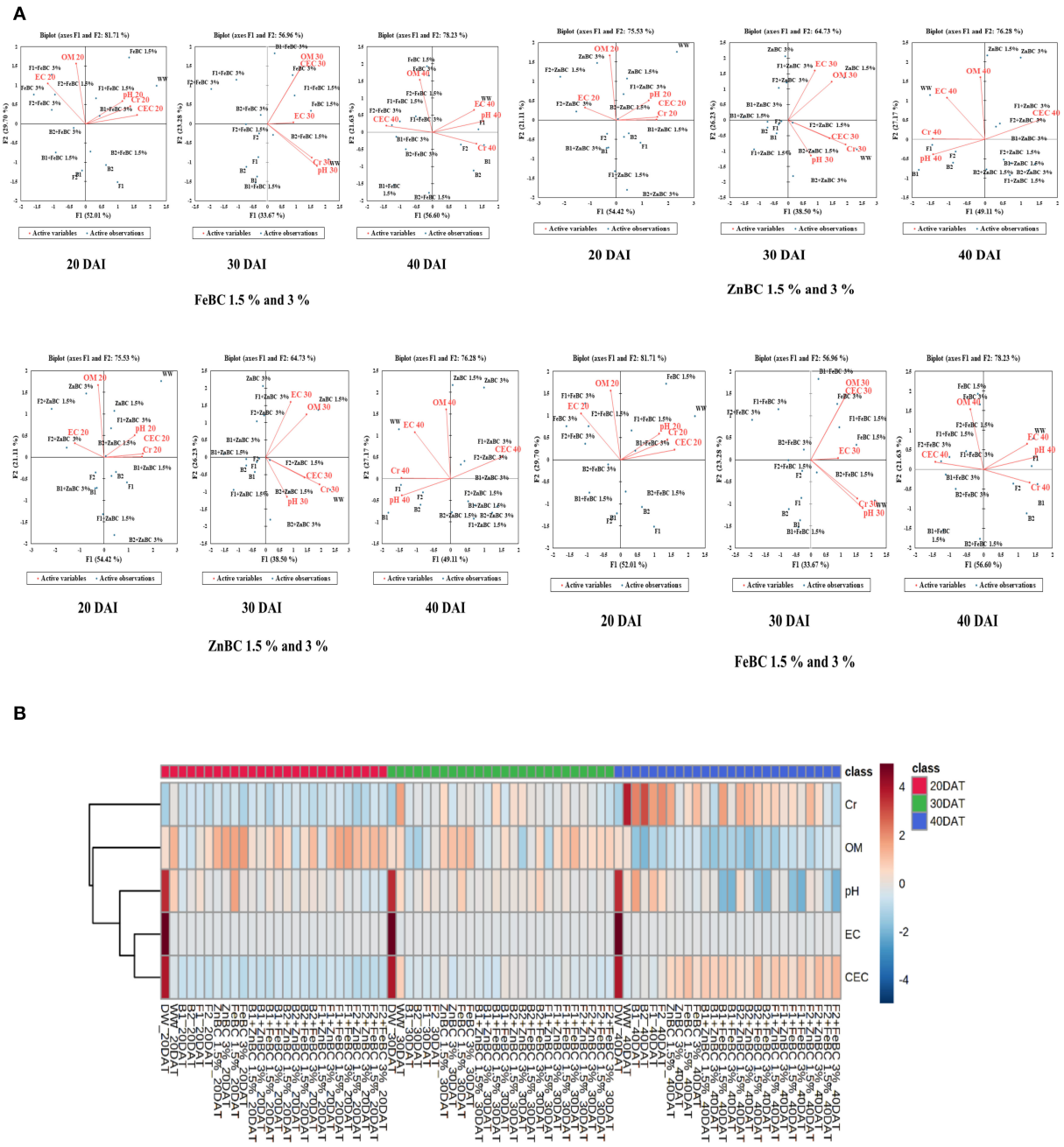

FIGURE 9
(A) Principal component analysis (PCA) for FeBC and ZnBC presenting data distribution co-linearity and variables co-association. **(B)** Heat map showing increasing distinction among variable values over time period of 40 days.

et al., 2021). Furthermore, alterations in H^+ ions balance, metal transformation (precipitation), DOC bioavailability, microbial mobility, and metabolic activity rate (polyphenol oxidase, dehydrogenase, catalase) in soil matrix might be other influential factors for CEC variation (Bandara et al., 2017). Biochar (BC) was approved to be an effective soil conditioner that extracted Cr from the soil solution and thus subsequently improved the soil CEC (Figure 8). Jien and Wang (2013) also reported an increment in the soil CEC value by application of BC having high porosity and large surface area. The sandy loam contains low mineral contents due to lesser silt and clay fractions; thus, BC acquires a high surface charge in sandy loam soil compared to clay soil (Aljoumani et al., 2017). Similarly, the CEC percentage increase was higher for sandy loam than clay, as reported by Ghorbani et al. (2019). Increasing CEC indicates soil nutrients holding capacity, which ultimately depends on

soil biota, adsorbents, moisture content, and texture (Hao et al., 2014). CEC and OM values for tested soil samples depicted the positive co-relations that pointed out OM as a reactive material affecting the soil Cr(VI) adsorption kinetics and CEC (Figure 9). PCA segregated ZnBC/FeBC-fungal assemblages applied soil samples with high CEC and OM values. The above-mentioned factors might be the reason for significantly ($p < 0.05$) enhanced metal immobilization (96.2%) by F2 + FeBC3% treatment applied to the soil which had high CEC (85.7%) and low pH value (11.7%) relative to WW and viable OM content at 40 DAI (Figures 9A,B).

Conclusion

Both fungal sp. with enriched BC (Zn/Fe) proved to be an excellent combination for soil Cr immobilization and showed slow OM oxidation relative to bacterial sp. Thus, FeBC3% + F2 application remained the best treatment for Cr(VI) immobilization as 96.8% soil Cr(VI) adsorption was achieved relative to WW. Similarly, soil Cr(VI) adsorption increased to 92.81% with ZnBC 3%+ B1 relative to WW. Langmuir adsorption isotherm gave FeBC 3% group treatments maximum Cr(VI) adsorption capacity (Qmax) 41.6 mg g^{-1} followed by ZnBC 3% group treatments as 38.31 mg g^{-1} at 40 DAI. Soil pH turned slightly acidic with FeBC and remained neutral with ZnBC promoting the Cr(VI) reduction and speciation processes. We concluded that combined application gave better metal remediation outcomes relative to amendments single application. Biochar was enriched with Fe and Zn minerals because these minerals are deficient in soils of Pakistan and also have nutritional value. This is the first study to report the use of zinc-enriched BC with microbial cultures. Similarly, limited studies were found on Fe-enriched BC co-application with microbial amendments. Mostly, the literature was available on enriched BC and microbial individual or sole applications. Under the comparative analyses' framework, we tried to find out how the combined application was beneficial for soil health and what alterations are occurred in physicochemical properties.

Eventually, this study implies that microbes along with Zn/Fe doped BC resulted in low pH, high OM, and CEC, which ultimately played a role in maximum Cr(VI) adsorption from WW applied soil. However, study can further be extended to determine the soil physicochemical characteristics optimization to promote soil structural stability and high crop productivity with biochar-microbial application. Additionally, plant growth variables can be assessed under the set of these remedial approaches.

Data availability statement

The original contributions presented in the study are included in the article/Supplementary material, further inquiries can be directed to the corresponding author/s.

Author contributions

W-u-DK conceived the idea of this research paper. MB, W-u-DK, MA, and FN designed the methodology of this research paper. MB conducted this research with the help of W-u-DK, MA, MH, and MNA. SR, ZD, FN, and MNA revised and critically reviewed the manuscript. All authors contributed to the subsequent development and approved the final manuscript.

Funding

The authors acknowledge the financial support provided by the National Key R&D program of China (2021YFD1700900), Central Public interest Scientific Institution Basal Research Fund (Y2022GH10), and the Agricultural Science and Technology Innovation Program of the Chinese Academy of Agricultural Sciences (Grant No. CAAS-ASTIP202101).

Conflict of interest

The authors declare that the research was conducted in the absence of any commercial or financial relationships that could be construed as a potential conflict of interest.

The reviewer MM declared a shared affiliation with the author MH to the handling editor at the time of review.

Publisher's note

Supplementary material

The Supplementary Material for this article can be found online at: https://www.frontiersin.org/articles/10.3389/fmicb.2022.990329/full#supplementary-material

SUPPLEMENTARY FIGURE 1
Pure cultures fungal (F1: 1; F2: 2) DNA bands appeared by gel electrophoresis **(a)** before PCR amplification **(b)** after PCR amplification (1 denotes to T.harzianum while 2 denotes to T.viride species; the alphabets show sample replicates); Pure cultures bacteria (B1: 1; B2: 2) DNA bands appeared by gel electrophoresis **(c)** before PCR amplification **(d)** after gel electrophoresis (1 denotes to P. fluorscence while 2 denotes to B. subtilis; the alphabets show sample replicates).

SUPPLEMENTARY FIGURE 2
Changes in soil physicochemical properties under organic and microbial amendments over time period of 40 days.

References

Abrishamkesh, S., Gorji, M., Asadi, H., Bagheri, M., and Pourbabaee, A. A. (2015). Effects of rice husk biochar application on the properties of alkaline soil and lentil growth. *Plant Soil Environ*. 61, 475–482. doi: 10.17221/117/2015-PSE

Abriz, F. S., and Golezani, G. K. (2021). Changes in soil properties and salt tolerance of safflower in response to biochar-based metal oxide nanocomposites of magnesium and manganese. *Ecotoxicol. Environ. Saf.* 211, 111904. doi: 10.1016/j.ecoenv.2021.111904

Ahmad, A., Muneer, B., and Shakoor, A. R. (2012). Effect of chromium, cadmium and arsenic on growth and morphology of HeLa cells. *J. Basic Appl. Sci*. 8, 53–58. doi: 10.6000/1927-5129.2012.08.01.17

Alam, M. Z., McGee, R., Hoque, M. A., Ahammed, G. J., and Carpenter, B. L. (2019). Effect of arbuscular mycorrhizal fungi, selenium, and biochar on photosynthetic pigments and antioxidant enzyme activity under arsenic stress in mung bean (*Vigna radiata*). *Front. Physiol*. 10, 193. doi: 10.3389/fphys.2019.00193

Aljoumani, B., Snchez, E. J., Canameras, N., Wessolek, G., and Josa, R. (2017). Transfer function and time series outlier analysis: modelling soil salinity in loamy sand soil by including the influences of irrigation management and soil temperature. *Irrig. Drain*. 67, 282–294. doi: 10.1002/ird.2187

Alotaibi, B. S., Khan, M., and Shamim, S. (2021). Unraveling the underlying heavy metal detoxification mechanisms of *Bacillus* species. *Microorganisms* 9, 1628. doi: 10.3390/microorganisms9081628

Ao, M., Chen, X., Deng, T., Sun, S., Tang, Y., and Morel, J. L., et al. (2022). Chromium biogeochemical behaviour in soil-plant systems and remediation strategies: a critical review. *J. Hazard. Mater*. 424, 127233. doi: 10.1016/j.jhazmat.2021.127233

Attah, L. E., and Melkamu, B. R. (2013). Assessment of heavy metals, pH, and EC in effluent run-off, river, and adjacent soil around a floriculture industry in Holeta, Welmera District, Ethiopia. *Ethiop. J. Environ. Stud. Manage.* 6, 620–628. doi: 10.4314/ejesm.v6i6.5

Azeez, N. A., Dash, S. S., Gummadi, S. N., and Deepa, V. S. (2021). Nano-remediation of toxic heavy metal contamination: hexavalent chromium [Cr(VI)]. *Chemosphere* 266, 129204. doi: 10.1016/j.chemosphere.2020.129204

Babu, B. V., and Gupta, S. (2008). Adsorption of Cr using activated neem leaves: kinetic studies. *Adsorption* 14, 85–92. doi: 10.1007/s10450-007-9057-x

Bandara, T., Indika, H., Prasanna, K., Mihiri, S., Gamini, S., and Nishanta, R. (2017). Role of woody biochar and fungal-bacterial co-inoculation on enzyme activity and metal immobilization in serpentine soil. *J. Soils Sediments* 17, 665–673. doi: 10.1007/s11368-015-1243-y

Baral, D., Roy, A., Thapa, S., and Chettri, D. (2018). Selection of culture media and monokaryotic isolates of *Pleurotus flabellate* and *P. majorcaju* for their dikaryotization followed by performance testing of dikaryotic isolates on malt extract agar medium. *Curr. J. Appl. Sci. Technol*. 26, 1–10. doi: 10.9734/CJAST/2018/40423

Batool, M., Khan, W. U. D., Hamid, Y., Farooq, M. A., Naeem, N. A., and Nadeem, F. (2022). Interaction of pristine and mineral engineered biochar with the microbial community in attenuating the heavy metals toxicity: a review. *Appl. Soil Ecol.* 175, 104444. doi: 10.1016/j.apsoil.2022.104444

Chen, H., Teng, Y., Lu, S., Wang, Y., and Wang, J. (2015). Contamination features and health risk of soil heavy metals in China. *Sci. Total Environ*. 512–513, 143–153. doi: 10.1016/j.scitotenv.2015.01.025

Chen, Y., Liu, Y., Li, Y., Wu, Y., Chen, Y., and Zeng, G. (2017). Influence of biochar on heavy metals and microbial community during composting of river sediment with agricultural wastes. *Bioresour. Technol.* 243, 347–355. doi: 10.1016/j.biortech.2017.06.100

Chen, Y., Wu, H., Sun, P., Liu, J., Qiao, S., and Zhang, D. (2021). Remediation of chromium-contaminated soil based on *Bacillus cereus* WHX-1 immobilized on biochar: Cr transformation and functional microbial enrichment. *Front. Microbiol.* 12, 641913. doi: 10.3389/fmicb.2021.641913

Choo, H., Choi, Y., Lee, W., and Lee, C. (2020). Effect of pH variations on the yield stress of calcium bentonite slurry treated with pH-responsive polymer. *Materials* 13, 2525. doi: 10.3390/ma13112525

Dad, F. P., Khan, W. U. D., Tanveer, M., Ramzani, P. M. A., Shaukat, R., and Muktadir, A. (2020). Influence of iron-enriched biochar on Cd sorption, its ionic concentration and redox regulation of radish under cadmium toxicity. *Agriculture* 11, 1. doi: 10.3390/agriculture11010001

Dai, L., Wenkun, Z., Li, H., Furong, T., Nengmin, T., and Qin, Z. (2018). Calcium-rich biochar from crab shell: an unexpected super adsorbent for dye removal. *Bioresour. Technol.* 267, 510–516. doi: 10.1016/j.biortech.2018.07.090

David, B., and Davidson, C. E. (2014). Estimation method for serial dilution experiments. *J. Microbiol. Methods* 107, 214–221. doi: 10.1016/j.mimet.2014.08.023

Doyle, J. J., and Doyle, J. L. (1987). A rapid DNA isolation procedure for small quantities of fresh leaf tissue. *Phytochem. Bull*. 19, 11–15.

Ellen, B., Ostrofsky, J. B., Robinson, S. J., and Traina, O. H. (2001). Effect of the cyanuric acid amendment on atrazine mineralization in surface soils and detection of the s-triazine ring-cleavage gene trzD. *Soil Biol. Biochem*. 33, 1539–1545. doi: 10.1016/S0038-0717(01)00072-4

FAO (1990). *Management of Gypsiferous Soils. Soils Bull. No. 62*. Rome: Food and Agriculture Organization.

Gan, C., Liu, Y., Tan, X., Wang, S., Zeng, G., and Zheng, B. (2015). Effect of porous zinc–biochar nanocomposites on Cr adsorption from aqueous solution. *RSC Adv*. 5, 35107–35115. doi: 10.1039/C5RA04416B

Gee, G. W., and Or, D. (2002). Particle-size analysis. *Methods Soil Anal*. 4, 255–293. doi: 10.2136/sssabookser5.4.c12

Ghorbani, M., and Amirahmadi, E. (2018). Effect of rice husk biochar (RHB) on some of the chemical properties of acidic soil and the absorption of some nutrients. *J. Appl. Sci. Environ. Manage*. 22, 313–317. doi: 10.4314/jasem.v22i3.4

Ghorbani, M., Asadi, H., and Abrishamkesh, S. (2019). Effects of rice husk biochar on selected soil properties and nitrate leaching in loamy sand and clay soil. *Int. Soil Water Conserv. Res.* 7, 258–265. doi: 10.1016/j.iswcr.2019.05.005

Gomes, S. M. (2016). *Isolation and Characterization of Chromium Resistant Enterobacter aerogenes From Marine Soil*. BRAC University, Department of Pharmacy Dhaka, Bangladesh. Project Report 50–54. Available online at: http://hdl.handle.net/10361/8334.

Haider, F. U., Coulter, J. A., Cheema, S. A., Farooq, M., Wu, J., and Zhang, R., et al. (2021). Co-application of biochar and microorganisms improves soybean performance and remediate cadmium-contaminated soil. *Ecotoxicol. Environ. Saf.* 214, 112112. doi: 10.1016/j.ecoenv.2021.112112

Han, Y., Cao, X., Ouyang, X., Sohi, S. P., and Chen, J. (2016). Adsorption kinetics of magnetic biochar derived from peanut hull on the removal of Cr (VI) from aqueous solution: Effects of production conditions and particle size. *Chemosphere* 145. 336–341. doi: 10.1016/j.chemosphere.2015.11.050

Hao, Y., Xin, H., Jianguo, N., Baolin, Z., and Yin, C. (2014). Effect of cation exchange capacity of soil on stabilized soil strength. *Soils Found*. 54, 1236–1240. doi: 10.1016/j.sandf.2014.11.016

Hashem, A., Tabassum, B., and Allah, E. F. (2019). Bacillus subtilis: a plant-growth-promoting rhizobacterium that also impacts biotic stress. *Saudi J. Biol. Sci.* 26, 1291–1297. doi: 10.1016/j.sjbs.2019.05.004

He, J., Zhang, Q., and Achal, V. (2020). Heavy metals immobilization in soil with plant-growth-promoting precipitation in support of radish growth. *Microbiol. Biotechnol. Lett*. 48, 223–229. doi: 10.4014/mbl.1912.12011

Hesse, R. (1971). *A Textbook of Soil Chemical Analysis*. New York, NY: Chemical Publishing Company.

Holben, W. E. (1994). Isolation and purification of bacterial DNA from the soil. Methods of soil analysis part 2. Microbiological and biochemical properties. *Soil Sci. Soc. Am.* 5, 727–751. doi: 10.2136/sssabookser5.2.c35

Howard, D. (1956). The preservation of bacteria by freezing in glycerol broth. *J. Bacteriol.* 71, 625–625. doi: 10.1128/jb.71.5.625-625.1956

Huang, D., Liu, L., Zeng, G., Xu, P., Huang, C., and Deng, L. (2017). The effects of rice straw biochar on indigenous microbial community and enzymes activity in heavy metal-contaminated sediment. *Chemosphere* 174, 545–553. doi: 10.1016/j.chemosphere.2017.01.130

Inglis, P. W., Pappas, M. D. C. R., Resende, L. V., and Grattapaglia, D. (2018). Fast and inexpensive protocols for consistent extraction of high-quality DNA and RNA from challenging plant and fungal samples for high throughput SNP genotype and sequencing applications. *PLoS ONE* 13, e0206085. doi: 10.1371/journal.pone.0206085

Jien, S. H., and Wang, C. S. (2013). Effects of biochar on soil properties and erosion potential in a highly weathered soil. *Catena* 110, 225–233. doi: 10.1016/j.catena.2013.06.021

Khan, M. A., Rahman, M., Ramzani, P. M. A., Zubair, M., Rassol, B., and Khan, M. K. (2020). Associative effects of lignin-derived biochar and arbuscular mycorrhizal fungi applied to soil polluted from Pb-acid batteries effluents on barley grain safety. *Sci. Total Environ.* 710, 136294. doi: 10.1016/j.scitotenv.2019.136294

Kumar, P. A., Ray, M., and Chakraborty, S. (2007). Hexavalent chromium removal from wastewater using aniline formaldehyde condensate coated silica gel. *J. Hazard. Mater.* 143, 24–32. doi: 10.1016/j.jhazmat.2006.08.067

Lagree, M. K., Desai, J. V., Finkel, J. S., and Lanni, F. (2018). Microscopy of fungal biofilms. *Curr. Opin. Microbiol.* 43, 100–107. doi: 10.1016/j.mib.2017.12.008

Lederberg, J., and Lederberg, E.M. (1952). Replica plating and indirect selection of bacterial mutants. *J. Bacteriol.* 63, 399–406. doi: 10.1128/jb.63.3.399-406.1952

Li, C., Zhang, L., Gao, Y., and Li, A. (2018). Facile synthesis of nano ZnO/ZnS modified biochar by directly pyrolyzing of zinc contaminated corn stover for Pb(II), Cu(II), and Cr removals. *Waste Manage.* 79, 625–637. doi: 10.1016/j.wasman.2018.08.035

Li, Q., Xing, Y., Fu, X., Ji, L., Li, T., and Wang, J. (2021). Biochemical mechanisms of rhizospheric *Bacillus subtilis*-facilitated phytoextraction by alfalfa under cadmium stress—microbial diversity and metabolomics analyses. *Ecotoxicol. Environ. Saf.* 212, 112016. doi: 10.1016/j.ecoenv.2021.112016

Lindsay, W. L., and Norvell, W. A. (1978). Development of a DTPA soil test for zinc, iron, manganese, and copper. *Soil Sci. Soc. Am. J.* 42, 421–428. doi: 10.2136/sssaj1978.03615995004200030009x

Liu, J., Jiang, J., Meng, Y., Aihemaiti, A., Xu, Y., and Xiang, Y. H. (2020). Preparation, environmental application and prospect of biochar-supported metal nanoparticles: a review. *J. Hazard. Mater.* 388, 122026. doi: 10.1016/j.jhazmat.2020.122026

Liu, X., Yang, L., Zhao, H., and Wang, W. (2019a). Pyrolytic production of zerovalent iron nanoparticles supported on rice husk-derived biochar: simple, in situ synthesis and use for remediation of Cr-polluted soils. *Sci. Total Environ.* 708, 134479. doi: 10.1016/j.scitotenv.2019.134479

Liu, Y., Sohi, S. P., Liu, S., Guan, S. J., Zhou, J., and Chen, J. (2019b). Adsorption and reductive degradation of Cr and TCE by a simply synthesized zero-valent iron magnetic biochar. *J. Environ. Manage.* 235, 276–281. doi: 10.1016/j.jenvman.2019.01.045

Lopez, A., Lazaro, N., Priego, J. M., Laboratori, A. M., and Microbiologia, D. (2000). Effect of pH on the biosorption of nickel and other heavy metals by pseudomonas fluorescens 4F39. *J. Ind. Microbiol. Biotechnol.* 24, 146–151. doi: 10.1038/sj.jim.2900793

Loutfi, H., Pellen, F., Jeune, B. L., Lteif, R., Kallassy, M., and Brun, G. L. (2020). Interpretation of the bacterial growth process based on the analysis of the speckle field generated by calibrated scattering media. *Opt. Express.* 28, 28648–28655. doi: 10.1364/OE.400909

Lyu, H., Zhao, H., Tang, J., Gong, Y., Huang, Y., and Wu, Q. (2018). Immobilization of hexavalent chromium in contaminated soils using biochar supported nanoscale iron sulfide composite. *Chemosphere* 194, 360–369. doi: 10.1016/j.chemosphere.2017.11.182

Mandal, S., Sarkar, B., Bolan, N., Ok, Y. S., and Naidu, R. (2017). Enhancement of chromate reduction in soils by surface-modified biochar. *J. Environ. Manage.* 186, 277–284. doi: 10.1016/j.jenvman.2016.05.034

Manzoor, Q., Nadeem, R., Iqbal, M., Saeed, R., and Ansari, T. M. (2013). Organic acids pretreatment effect on *Rosa bourbonia* phyto-biomass for removal of Pb (II) and Cu (II) from aqueous media. *Bioresoure Technol.* 132, 446–452. doi: 10.1016/j.biortech.2013.01.156

Masulili, A., Utomo, W. H., and Syechfani, M. (2010). Rice husk biochar for rice-based cropping system in acid soil 1. The characteristics of rice husk biochar and its influence on the properties of acid sulfate soils and rice growth in West Kali- mantan, Indonesia. *J. Agric. Sci.* 2, 39. doi: 10.5539/jas.v2n1p39

Mavi, S., Singh, M. G., Singh, B. P., Singh, S. B., Choudhary, O. P., and Sagi, S. (2018). Interactive effects of rice-residue biochar and N-fertilizer on soil functions and crop biomass in contrasting soils. *J. Soil Sci. Plant Nutr.* 18, 41–59. doi: 10.4067/S0718-95162018005000201

Meki, K., Liu, Q., Wu, S., and Yuan, Y. (2022). Plant- and microbe-assisted biochar amendment technology for petroleum hydrocarbon remediation in saline-sodic soils: a review. *Pedosphere* 32, 211–221. doi: 10.1016/S1002-0160(21)60041-3

Moradi, S., Sadaghiani, R. M. H., and Sepehr, E. (2019). Soil nutrients status is affected by simple and enriched biochar application under salinity conditions. *Environ. Monit. Assess.* 191, 257. doi: 10.1007/s10661-019-7393-4

Moyes, R., Reynolds, J., and Breakwell, D. (2009). Differential staining of bacteria: gram St ain. *Curr. Protoc. Microbiol.* 15. doi: 10.1002/9780471729259.mca03cs15s

Muniz, S., Lacarta, J., Pata, M., Jiménez, J., and Navarro, E. (2014). Analysis of the diversity of substrate utilisation of soil bacteria exposed to Cd and earthworm activity using generalised additive models. *PLoS ONE* 9, e85057. doi: 10.1371/journal.pone.0085057

Naggar, N. E. A., El-khateeb, A. Y., and Ghoniem, A. A. (2020). Innovative low-cost biosorption process of Cr^{6+} by *Pseudomonas alcaliphila* NEWG-2. *Sci. Rep.* 10, 14043. doi: 10.1038/s41598-020-70473-5

Nelson, D. W., and Sommers, L. E. (1996). Total carbon, organic carbon, and organic matter. Methods of soil analysis part 3—chemical methods(methodsofsoilan3). *Am. Soc. Agron.* 5, 961–1010. doi: 10.2136/sssabookser5.3.c34

Olorunfemi, I., Fasinmirin, J., and Ojo, A. (2016). Modeling cation exchange capacity and soil water holding capacity from basic soil properties. *Eurasian J. Soil Sci.* 5, 266–274. doi: 10.18393/ejss.2016.4.266-274

Palansooriya, K. N., Shaheen, S. M., Chen, S. S., Tsang, D. C., Hashimoto, Y., and Hou, D. (2020). Soil amendments for immobilization of potentially toxic elements in contaminated soils: a critical review. *Environ. Int.* 134, 105046. doi: 10.1016/j.envint.2019.105046

Pariyar, P., Kumari, K., Kumar, M. J., and Jadhao, P. S. (2019). Evaluation of change in biochar properties derived from different feedstock and pyrolysis temperature for environmental and agricultural application. *Sci. Total Environ.* 713, 136433. doi: 10.1016/j.scitotenv.2019.136433

Quintieri, L., Fanelli, F., Zuhlke, D., Caputo, L., Logrieco, A. F., and Albrecht, D., et al. (2020). Biofilm and pathogenesis-related proteins in the foodborne *P. fluorescens* ITEM 17298 with distinctive phenotypes during cold storage. *Front Microbiol.* 11, 991. doi: 10.3389/fmicb.2020.00991

Rhoades, J. D. (1996). Salinity electrical conductivity and total dissolved solids. Methods of soil analysis, Part 3: chemical methods. SSSA Book series Number 5. *Soil Sci. Soc. Am.* 5, 417–435. doi: 10.2136/sssabookser5.3.c14

Richards, L. A. (1954). *Diagnosis and Improvement of Saline and Alkali Soils*. Washington, DC: USDA Agric. Handbook 60.

Riffiani, R., Sulistinah, N., and Sunarko, B. (2015). Comparison of three DNA isolation and purification methods of bacterial DNA. *KnE Life Sci.* 2, 491. doi: 10.18502/kls.v2i1.199

Saffari, M., Reza, V., Aliabadi, M., Jafari, M., and Masomeh, M. (2016). Influence of organic and inorganic amendments on cadmium sorption in calcareous soil. *Main Group Metal Chem.* 39, 195–207. doi: 10.1515/mgmc-2016-0028

Seleiman, M. F., Majed, A., Bushra, A., Basmah, A., Yahya, R., and Shimaa, B. (2020). Effects of ZnO nanoparticles and biochar of rice straw and cow manure on characteristics of contaminated soil and sunflower productivity, oil quality, and heavy metals uptake. *Agronomy* 10, 790. doi: 10.3390/agronomy10060790

Sempere, F., and Santamarina, M. (2011). Cryo-scanning electron microscopy and light microscopy for the study of fungi interactions. *Microsc. Res. Tech.* 74, 207–211. doi: 10.1002/jemt.20893

Shah, A. N., Tanveer, M., Hussain, S., and Yang, G. (2016). Beryllium in the environment: whether fatal for plant growth? *Rev. Environ. Sci. Biotechnol.* 15, 549–561. doi: 10.1007/s11157-016-9412-z

Shahid, M., Shamshad, S., Rafiq, M., Khalid, S., Bibi, I., and Niazi, N. K., et al. (2017). Chromium speciation, bioavailability, uptake, toxicity and detoxification in soil-plant system: a review. *Chemosphere* 178, 513–533. doi: 10.1016/j.chemosphere.2017.03.074

Shakya, M., Sharma, P., Meryem, S., Mahmood, Q., and Kumar, A. (2016). Heavy metal removal from industrial wastewater using fungi: uptake mechanism and biochemical aspects. *J Environ Eng.* 142, 1–18. doi: 10.1061/(ASCE)EE.1943-7870.0000983

Smith, A. C., and Hussey, M. A. (2005). *Gram Staining Protocols*. Washington, DC: American Society of Microbiology.

Srivastava, D., Madhu, T., Prasanna, D., Puja, S., Khushboo, C., and Monica, K., et al. (2021). Chromium stress in plants: toxicity, tolerance and phytoremediation. *Sustainability* 13, 4629. doi: 10.3390/su13094629

Su, Y., Liu, C., and Fang, H. (2020). Bacillus subtilis: a universal cell factory for industry, agriculture, biomaterials and medicine. *Microb. Cell Fact.* 19, 173. doi: 10.1186/s12934-020-01436-8

Syuhadah, N. S., Muslim, N. Z., and Rohasliney, H. (2015). Determination of heavy metal contamination from batik factory effluents to the surrounding area. *Int. J. Chem. Environ. Biol. Sci.* 3, 2320–4087. doi: 10.1007/978-981-4560-70-2_52

Taqdees, Z., Khan, J., Khan,. W.-,u,-D., Kausar, S., Afzaal, M., and Akhtar, I. (2022). Silicon and zinc nanoparticles-enriched miscanthus biochar enhanced seed germination, antioxidant defense system, and nutrient status of radish under NaCl stress. *Crop Pasture Sci.* 73, 556–572. doi: 10.1071/CP21342

Wang, M., Zhu, Y., Cheng, L., Andserson, B., Zhao, X., and Wang, D. (2017a). Review on utilization of biochar for metal-contaminated soil and sediment remediation. *J. Environ. Sci.* 63, 1. doi: 10.1016/j.jes.2017.08.004

Wang, P., Tang, L., Wei, X., Zeng, G., Zhou, Y., and Deng, Y. (2017b). Synthesis and application of iron and zinc doped biochar for removal of p-nitrophenol in

wastewater and assessment of the influence of co-existed Pb (II). *Appl. Surf. Sci.* 392, 391–401. doi: 10.1016/j.apsusc.2016.09.052

Wang, T., Sun, H., Mao, H., Zhang, Y., Wang, C., and Zhang, Z. (2014). The immobilization of heavy metals in soil by bioaugmentation of a UV-mutant *Bacillus subtilis* 38 assisted by NovoGro biostimulation and changes of soil microbial community. *J. Hazard. Mater.* 278, 483–490. doi: 10.1016/j.jhazmat.2014.06.028

Wang, Y., Liu, Y., Zhan, W., Zheng, K., and Wan, J. (2020). Stabilization of heavy metal-contaminated soils by biochar: challenges and recommendations. *Sci. Total Environ.* 729, 139060. doi: 10.1016/j.scitotenv.2020.139060

Wei, Y., Usman, M., Farooq, M., Adeel, M., Haider, F. U., Pan, Z., et al. (2022). Removing hexavalent chromium by nano zero-valent iron loaded on attapulgite. *Water Air Soil Pollution* 233, 48. doi: 10.1007/s11270-022-05513-z

Xia, S., Song, Z., Jeyakumar, P., Bolan, N., and Wang, H. (2019). Characteristics and applications of biochar for remediating Cr-contaminated soils and wastewater. *Environ. Geochem. Health* 42, 1543–1567. doi: 10.1007/s10653-019-00445-w

Xu, Y., Seshadri, B., and Sarkar, B. (2018). Biochar modulates heavy metal toxicity and improves microbial carbon use efficiency in soil. *Sci. Total Environ.* 621, 148–159. doi: 10.1016/j.scitotenv.2017.11.214

Yu, Y., An, Q., Jin, L., Luo, N., Li, Z., and Jiang, J. (2021). Unraveling sorption of Cr (VI) from aqueous solution by FeCl3 and ZnCl2-modified corn stalks biochar: implicit mechanism and application. *Bioresour. Technol.* 297, 122466. doi: 10.1016/j.biortech.2019.122466

Zhang, S., Lyu, H., Tang, J., Song, B., Zhen, M., and Liu, X. (2018a). Novel biochar supported CMC stabilized nano zero-valent iron composite for hexavalent chromium removal from water. *Chemosphere* 217, 686–694. doi: 10.1016/j.chemosphere.2018.11.040

Zhang, X., Lv, L., Qin, Y., Xu, M., Jia, X., and Chen, Z. (2018b). Removal of aqueous Cr by magnetic biochar derived from *Melia azedarach* wood. *Bioresour. Technol.* 256, 1–10. doi: 10.1016/j.biortech.2018.01.145

Zhang, Y., Jiao, X., Liu, N., Lv, J., and Yang, Y. E. (2020). Enhanced removal of aqueous Cr by green synthesized nanoscale zero-valent iron supported on oak wood biochar. *Chemosphere* 245, 125542. doi: 10.1016/j.chemosphere.2019.125542

Zhu, S., Huang, X., Wang, D., Wang, L., and Ma, F. (2018). Enhanced hexavalent chromium removal performance and stabilization by magnetic iron nanoparticles assisted biochar in aqueous solution: mechanisms and application potential. *Chemosphere* 207, 50–59. doi: 10.1016/j.chemosphere.2018.05.046

frontiers | Frontiers in Microbiology

TYPE Original Research
PUBLISHED 16 September 2022
DOI 10.3389/fmicb.2022.1001464

OPEN ACCESS

EDITED BY
Adnan Mustafa,
Brno University of Technology,
Czechia

REVIEWED BY
Mariella Rivas,
University of Antofagasta, Chile
Luis Antonio Rojas,
Catholic University of the North, Chile

*CORRESPONDENCE
Wen-Chieh Cheng
w-c.cheng@xauat.edu.cn

SPECIALTY SECTION
This article was submitted to Microbiological Chemistry and Geomicrobiology, a section of the journal Frontiers in Microbiology

RECEIVED 23 July 2022
ACCEPTED 29 August 2022
PUBLISHED 16 September 2022

CITATION
Xue Z-F, Cheng W-C, Wang L and Xie Y-X (2022) Catalyzing urea hydrolysis using two-step microbial-induced carbonate precipitation for copper immobilization: Perspective of pH regulation.
Front. Microbiol. 13:1001464.
doi: 10.3389/fmicb.2022.1001464

Catalyzing urea hydrolysis using two-step microbial-induced carbonate precipitation for copper immobilization: Perspective of pH regulation

Zhong-Fei Xue[1,2], Wen-Chieh Cheng[1,2]*, Lin Wang[1,2] and Yi-Xin Xie[1,2]

[1]School of Civil Engineering, Xi'an University of Architecture and Technology, Xi'an, China, [2]Shaanxi Key Laboratory of Geotechnical and Underground Space Engineering (XAUAT), Xi'an, China

Microbial induced carbonate precipitation (MICP) has recently applied to immobilize heavy metals toward preventing their threats to public health and sustainable development of surrounding environments. However, for copper metallurgy activities higher copper ion concentrations cause the ureolytic bacteria to lose their activity, leading to some difficulty in forming carbonate precipitation for copper immobilization (referred to also as "biomineralization"). A series test tube experiments were conducted in the present work to investigate the effects of bacterial inoculation and pH conditions on the copper immobilization efficiency. The numerical simulations mainly aimed to compare with the experimental results to verify its applicability. The copper immobilization efficiency was attained through azurite precipitation under pH in a 4–6 range, while due to Cu^{2+} migration and diffusion, it reduced to zero under pH below 4. In case pH fell within a 7–9 range, the immobilization efficiency was attained via malachite precipitation. The copper-ammonia complexes formation reduced the immobilization efficiency to zero. The reductions were attributed either to the low degree of urea hydrolysis or to inappropriate pH conditions. The findings shed light on the necessity of securing the urease activity and modifying pH conditions using the two-step biomineralization approach while applying the MICP technology to remedy copper-rich water bodies.

KEYWORDS

microbial-induced carbonate precipitation, ureolytic bacteria, copper metal, two-step biomineralization, copper-ammonia complex

Introduction

Copper (Cu) is an indispensable trace element for human health, plant and animal growth, and it has an activating effect on some key enzymes in cellular metabolism (Facchin et al., 2013). However, it can impose serious threats to organisms if the concentration exceeds the legal limit (Elalfy et al., 2021; Guo et al., 2021). Most of the copper in nature exists as compounds (i.e., copper minerals), and in China, the development of copper mining, smelting, and processing has raised the potential of their migration and diffusion in surrounding environments (Bai et al., 2021b,c; Hu et al., 2021a, 2022a,b; Wang et al., 2022b; Xue et al., 2021; Yu et al., 2021). Nowadays there are various physical and chemical measures available for remedying copper-rich water bodies. However, these methods are time-consuming, costly, and not environmental-friendly (Qdais and Moussa, 2004; Wei et al., 2005; Fu and Wang, 2011; You et al., 2018; Chen et al., 2022a,b; Li et al., 2022; Wang et al., 2022a). In recent years, the microbial-induced carbonate precipitation (MICP) technology has attracted extensive attention as an alternative to traditional measures (Achal et al., 2012a; Chen and Achal, 2019; Ye et al., 2021; Xue et al., 2022a,b).

The MICP technology can precipitate carbonates between soil particles and has been widely applied to calcareous sand reinforcement (Jiang et al., 2019; Lai et al., 2020; Rahman et al., 2020; Zhang et al., 2020; Cui et al., 2021; Xiao et al., 2021; Yang et al., 2022), while studies on the remediation of heavy metals using the MICP technology are markedly limited (Kang et al., 2015; Li et al., 2021; Wang et al., 2022e,f). The principle of the MICP technology is to catalyze urea hydrolysis through secreting the urease using the ureolytic bacteria, discharging hydroxide and ammonium ions (see Eqs. 1–3) and subsequently yielding carbonates. Heavy metal ions and calcium ions could co-precipitate with bacteria as nucleation sites in the biomineralization process (see Eqs. 4–7) (Li et al., 2013). As a result, the "net" effect of such a reaction corresponds to an increase in surrounding pH (Schwantes-Cezario et al., 2017; Cui et al., 2022). The use of carbonates aims to capsulize heavy metal ions by forming carbonate precipitation (termed immobilization of heavy metals hereafter), preventing their migration and diffusion (Achal et al., 2011; Achal et al., 2012b; Jiang and Soga, 2019; Chen and Achal, 2019; Schwantes-Cezario et al., 2020; Liu et al., 2021; Mujah et al., 2021; Zeng et al., 2021). Ali et al. (2022) reported that strain *B. diminuta* isolated from soil could immobilize Cd^{2+} and Zn^{2+} in solution by co-precipitation. In addition, extracellular polymers (EPS) secreted by bacteria can provide nucleation sites and promote bacteria to immobilize heavy metal ions in solution (Chen et al., 2016; Casas et al., 2020; Qiao et al., 2021; Kim et al., 2021).

$$CO(NH_2)_2 + H_2O \rightarrow 2NH_3 + CO_2 \quad (1)$$

$$2NH_3 + 2H_2O \leftrightarrow 2NH_4^+ + 2OH^- \quad (2)$$

$$CO_2 + 2OH^- \leftrightarrow HCO_3^- + OH^- \leftrightarrow CO_3^{2-} + H_2O \quad (3)$$

$$Ca^{2+} + Cell \rightarrow Cell - Ca^{2+} \quad (4)$$

$$M^{2+} + Cell \rightarrow Cell - M^{2+} \quad (5)$$

$$Cell - Ca^{2+} + CO_3^{2-} \rightarrow Cell - CaCO_3(s) \quad (6)$$

$$Cell - M^{2+} + CO_3^{2-} \rightarrow Cell - MCO_3(s) \quad (7)$$

Recent studies indicated that the copper immobilization efficiency generally maintains at low levels compared to other heavy metals (Achal et al., 2011; Li et al., 2013; Mugwar and Harbottle, 2016; Bai et al., 2019, 2021a; Hu et al., 2021b; Wang et al., 2022c,d). It is due to the fact that copper ions bind to the functional groups of the urease, and as a result, its spatial structure is badly modified causing its denaturation and inactivation (Krajewska, 2008; Seplveda et al., 2021). Among all the positive divalent heavy metals, copper has the highest toxicity on the urease activity except mercury, and securing the urease activity against copper metal is deemed a challenging task while introducing the MICP technology (Zaborska et al., 2004; Jiang et al., 2019). Increasing the initial urea concentration may improve the resistance of the urease against copper metal. However, the higher the urea concentration, the higher the surrounding pH, and the higher the potential of forming complexes unfavorable for the immobilization of copper metal (Ferris et al., 2004; Torres-Aravena et al., 2018; Duarte-Nass et al., 2020; Liu et al., 2020; Seplveda et al., 2021; Tarach et al., 2021; Chen et al., 2022a,c; Xue et al., 2022c).

Conducting a closer look to the literature on the biomineralization, however, reveals a number of gaps and shortcomings. To this end, the present work proposes a two-step biomineralization approach; the first step allows the ureolytic bacteria hydrolyze urea to discharge the amount of carbonate and hydroxyl ions necessary for forming carbonates in the second step. The second step mainly aims to use the ureolytic bacteria as nucleation sites to precipitate carbonate, capsulizing copper metal (Torres-Aravena et al., 2018; Duarte-Nass et al., 2020). Prior to the second step where the urease is inoculated to the medium containing copper metal, the amount of carbonate and ammonia ions necessary for forming carbonates in the second step is already yielded in the first step, mitigating the effect of Cu^{2+} toxicity. In addition, different inoculation proportions may consider in the second step to modify the surrounding pH, thus preventing the formation of complexes unfavorable for securing the copper immobilization efficiency. The objectives of this study are: (1) To conduct test tube experiments to investigate the effects of bacterial inoculation and pH surrounding conditions, (2) to highlight the necessity of modifying pH and distinguish the speciation of precipitation against different pH ranges using the numerical simulations, and (3) to propose the two-step biomineralization approach to secure the immobilization efficiency.

Materials and methods

Ureolytic bacteria culture

Sporosarcina pasteurii, a basophilic ureolytic bacterium, was used in the present work. It was activated in a sterile liquid medium, which consists of 20 g/L yeast extract, 10 g/L NH_4Cl, 20 g/L urea, 10 mg/L $MnSO_4{\cdot}H_2O$, 24 mg/L $NiCl_2{\cdot}6H_2O$. The surrounding pH for the sterile liquid medium was adjusted to 8.8 using 1 M solution of NaOH. The activated ureolytic bacteria were mixed with glycerol using a ratio of 7:3 and stored at −20 °C. They were subjected to shaking culture at 30 °C and 180 rpm for 30 h. Further, the chemicals of urea, $MnSO_4{\cdot}H_2O$, $NiCl_2{\cdot}6H_2O$, NaOH, and $Cu(NO_3)_2{\cdot}3H_2O$ were diluted to given concentrations, respectively, and applied to the subsequent test tube experiments.

Urease activity measurement

The urease activity (termed UA hereafter) under different bacterial inoculation proportions was measured in Cu^{2+} contained 0.5 M urea solution, which aims to evaluate the effect of Cu^{2+} toxicity on the ureolytic bacteria and urease activity. The concentration of Cu^{2+} and the bacterial inoculation proportion were 5, 10, and 20 mM, and 1:9, 1:3, and 1:1, respectively.

pH, EC (electric conductivity), and UA, while catalyzing urea hydrolysis, were measured using a benchtop pH meter (Hanna Instruments Inc. HI2003) and a benchtop conductivity meter (Hanna Instruments Inc. HI2314), respectively. UA was measured on a basis of the ureolysis rate, as recommended by Whiffin et al. (2007); 2 mL final reaction solution is mixed with 18 mL 1.11 M urea, and EC is measured at 0 min and 5 min after the mixing. UA can be evaluated using the equation below:

$$\mathrm{UA} = \frac{\mathrm{EC}_5 - \mathrm{EC}_0}{5} \times 10 \times 1.11 (\mathrm{mM\ Urea\ min^{-1}}) \quad (8)$$

where EC_0 and EC_5 are electrical conductivity at 0 and 5 min, respectively. NH_4^+ concentration of the final reaction solution is measured at 0, 24 and 48 h, respectively, and the method for measuring NH_4^+ concentration corresponds to the modified Nessler method (Whiffin et al., 2007). There were three replicates for each test set.

TABLE 2 Scheme applied to the test tube experiments.

Parameters applied to the first step	Parameters applied to the second step	Concentration of $Cu(NO_3)_2$ (mM)
Urea at 333 mM NH_4Cl at 187 mM	1:9	20, 40, 60
	1:3	20, 40, 60
	1:1	0–50

Numerical simulations

To evaluate the effect of Cu^{2+} concentration and pH on the speciation of precipitation and copper immobilization efficiency, the biomineralization process was reproduced using the Visual MINTEQ software package, although the process of urea hydrolysis has been neglected. The initial concentration for NH_4^+ and CO_3^{2-} was calculated in accordance with the bacterial inoculation proportion. **Table 1** summarize the parameters applied to the numerical simulations.

Test tube experiments

This part aims to elaborate more about the details applied to the test tube experiments. First, a $Cu(NO_3)_2$ solution at concentrations varying in a 0–60 mM range was prepared, while the ureolytic bacteria were cultivated with yeast extract and ammonia nitrogen, during which time urea at 333 mM was also added to the culture medium. Second, the urea hydrolysis proceeded with the bacterial inoculation proportions of 1:9, 1:3, and 1:1, respectively, for 48 consecutive hours. The aforesaid two-step biomineralization approach is the first proposed by the authors and primarily aims not only to discharge NH_4^+ and OH^- preventing not only the effect of Cu^{2+} toxicity but the formation of complexes unfavorable for securing the copper immobilization efficiency. NH_4^+ and Cu^{2+} concentrations were measured at 0, 24, and 48 h, respectively. An atomic

TABLE 1 Parameters applied to the numerical simulations of the copper immobilization efficiency against $Cu(NO_3)_2$ concentration and pH considering bacterial inoculation proportions of 1:9, 1:3, 1:1, and 3:1, respectively.

Bacterial inoculation proportion	Ion concentration (mM)					pH
	Cu^{2+}	NO_3^-	NH_4^+	CO_3^{2-}	Cl^-	
1:9	5, 20, 40, 60, 80	10, 40, 80, 120, 160	85.3	33.3	18.7	0–13
1:3			213.25	83.25	46.75	
1:1			426.5	166.5	93.5	
3:1			639.75	249.75	140.25	

spectrophotometer (Beijing Purkinje General Instrument TAS-990) was responsible for the Cu^{2+} concentration measurements. The copper immobilization efficiency can be evaluated as follows:'

$$\text{Immobilization efficiency} = ((C_0 - C_1)/C_0) \times 100\% \quad (9)$$

where C_0 and C_1 are Cu^{2+} ions concentration before and after remediation, respectively. **Table 2** summarize the scheme applied to the test tube experiment. There were three replicates for each test set.

Results and discussion

Test tube experiments

Effect of bacterial inoculation

UA is an important indicator that determines the growth and reproduction of the ureolytic bacteria during the biomineralization process. Furthermore, the higher the UA, the higher the resistance of the ureolytic bacteria against copper metal (Song et al., 2017). Considering copper metal can significantly impede the bacteria's growth and reproduction (Zaborska et al., 2004), the degradation mechanism is summarized as copper metal binding to the functional groups of the urease and modifying its spatial structure, thus causing its denaturation and inactivation (Krajewska, 2008). Duarte-Nass et al. (2020) suggested that increasing the initial urea concentration could improve the resistance of ureolytic bacteria against Cu^{2+} toxicity. Despite that, such high initial urea concentration, however, turns the surrounding pH into alkaline environments promoting the formation of copper-ammonia complexes unfavorable for securing the copper immobilization efficiency (Liu et al., 2018; Duarte-Nass et al., 2020).

When subjected to 20 mM Cu^{2+}, UA goes into a decline for the bacterial inoculation proportion = 1:1, while for the bacterial inoculation proportions = 1:3 and 1:9, it shows a smaller change (see **Figure 1A**). UA for all the bacterial inoculation proportions reduces to approximately zero 4 h after the beginning of bacterial inoculation, indicating that the effect of Cu^{2+} toxicity depresses the growth and reproduction of the ureolytic bacteria and causes some difficulty in catalyzing urea hydrolysis. For this reason, the measurements of EC and NH_4^+ show a small change because of a small number of NH_4^+ and OH^- discharged, as depicted in **Figures 1B,C**. UA for the

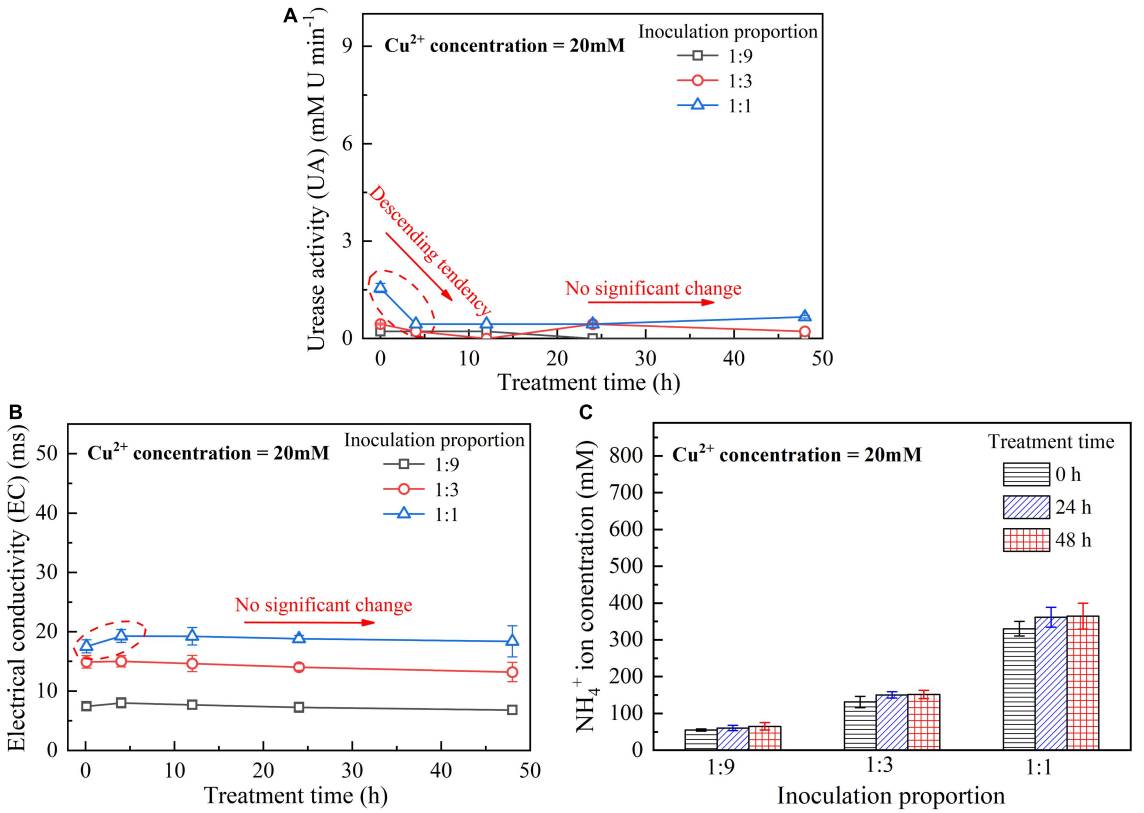

FIGURE 1
(A) UA vs. treatment time relationship, **(B)** EC vs. treatment time relationship, and **(C)** NH_4^+ vs. treatment time relationship when subjected to Cu^{2+} concentration at 20 mM.

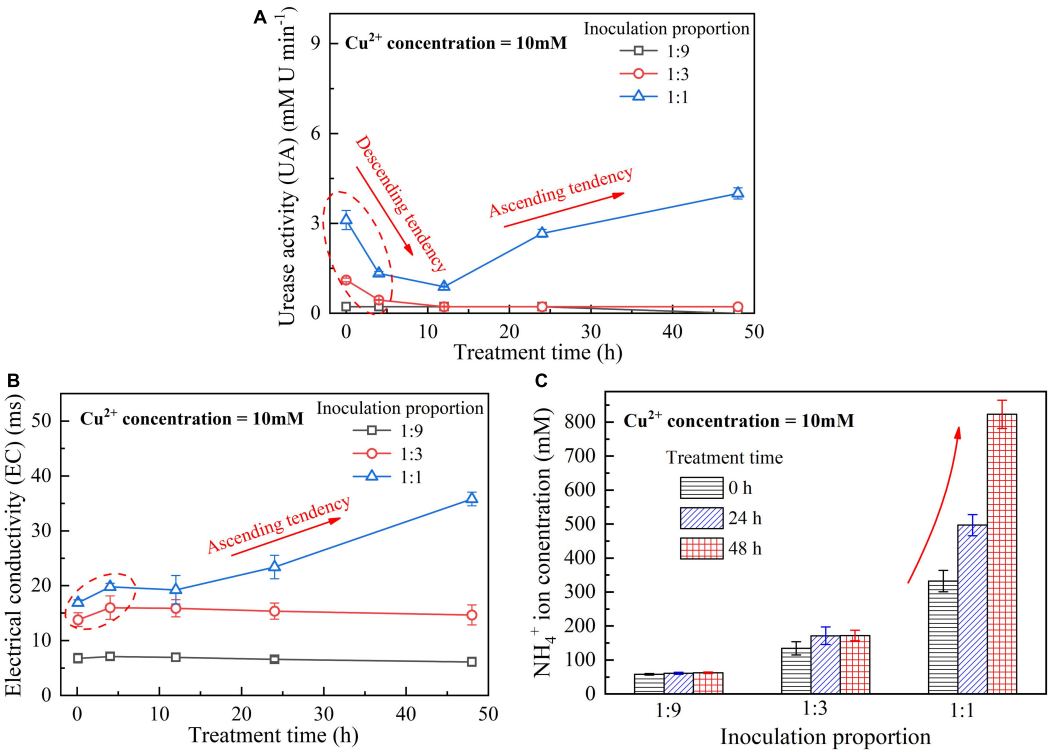

FIGURE 2
(A) UA vs. treatment time relationship, **(B)** EC vs. treatment time relationship, and **(C)** NH_4^+ vs. treatment time relationship when subjected to Cu^{2+} concentration at 10 mM.

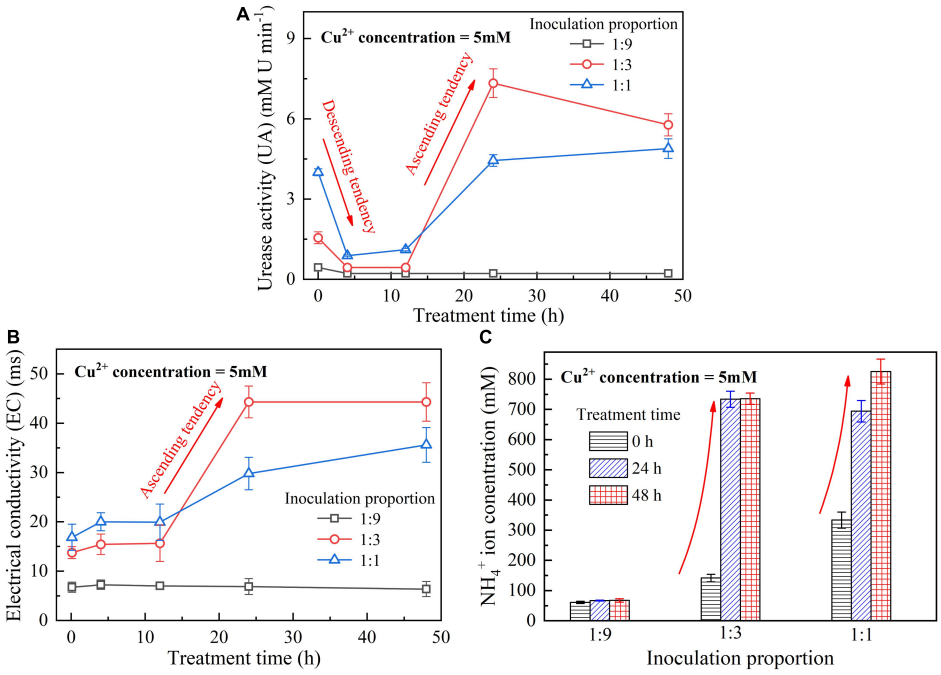

FIGURE 3
(A) UA vs. treatment time relationship, **(B)** EC vs. treatment time relationship, and **(C)** NH_4^+ vs. treatment time relationship when subjected to Cu^{2+} concentration at 5 mM.

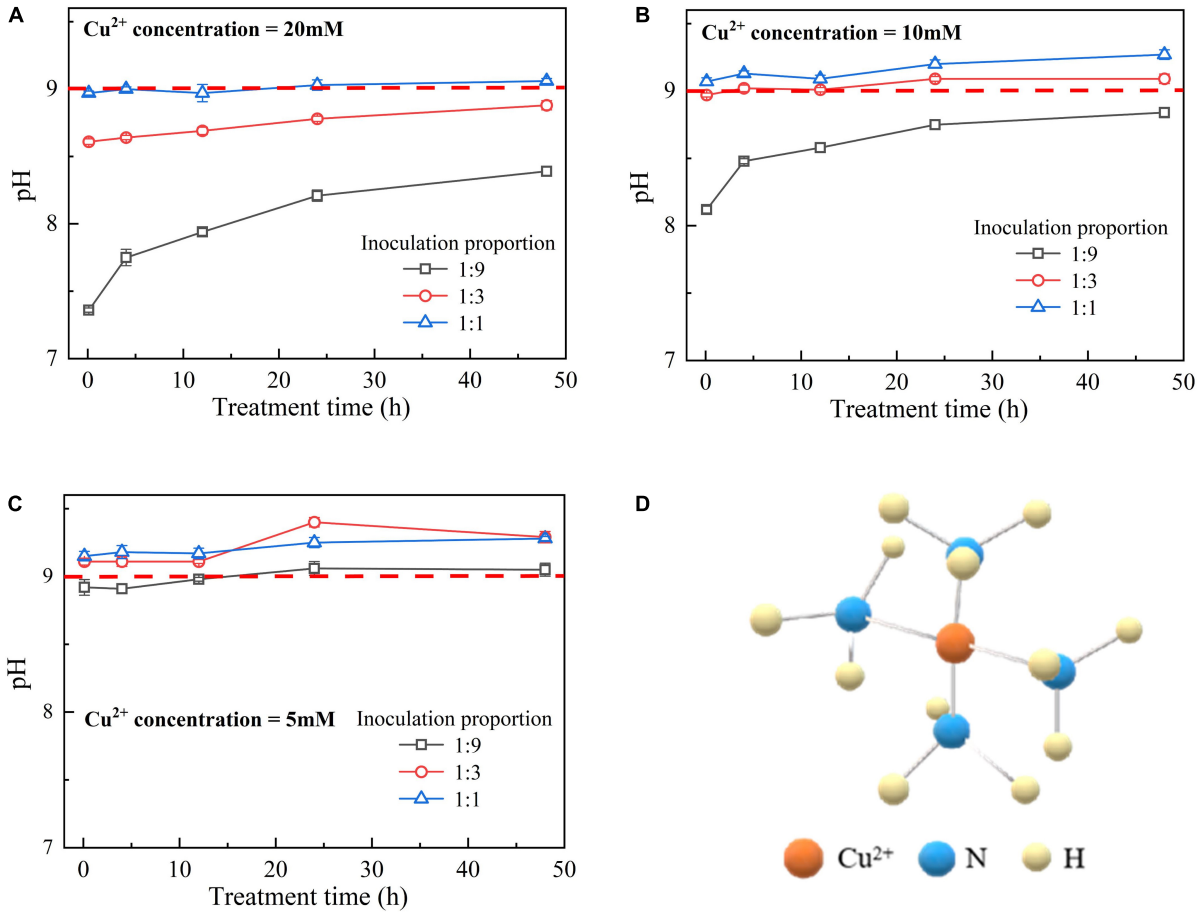

FIGURE 4
(A) pH vs. treatment time relationship under Cu^{2+} concentration at 20 mM, **(B)** pH vs. treatment time relationship under Cu^{2+} concentration at 10 mM, **(C)** pH vs. treatment time relationship under Cu^{2+} concentration at 5 mM, and **(D)** schematical illustration of copper-ammonia complex.

bacterial inoculation proportion = 1:1 goes into a decline at the very beginning of bacterial inoculation when subjected to 10 mM Cu^{2+}, and goes up 12 h following the commencement of bacterial inoculation, as shown in Figure 2A. In contrast, UA for the other two inoculation proportions presents a negligible change all long. These results indicate that the ureolytic bacteria for the bacterial inoculation proportion = 1:1 could remain its activity when subjected to 10 mM Cu^{2+}, and for the other two inoculation proportions, the effect of Cu^{2+} toxicity depresses the growth and reproduction of the ureolytic bacteria reducing the secretion of the urease. The measurements of EC and NH_4^+ provide testimony of the above argument, as shown in Figures 2B,C. Given the inoculation proportion = 1:1, UA going up 12 h after the beginning of bacterial inoculation is attributed to the reduction in the effect of Cu^{2+} toxicity, induced by the formation of copper-ammonia complexes. In other words, the formation of copper-ammonia complexes causes an inability of depressing the growth of the ureolytic bacteria and enhances the resistance of the urease against Cu^{2+} toxicity. When subjected to 5 mM Cu^{2+}, the behavior can also be recognized as UA going down rapidly and going up till the end of the process and becomes more distinct compared to 10 mM Cu^{2+}. UA for the inoculation proportion = 1:3 even surpasses that for the inoculation proportion = 1:1 12 h after the commencement of bacterial inoculation. The relatively higher urea concentration for the inoculation proportion = 1:3 may be considered as the main cause leading to such phenomenon. EC and NH_4^+ measurements give testimony to the argument made, as shown in Figures 3B,C.

On the whole, when subjected to 20 mM Cu^{2+}, either for higher inoculation proportions or lower inoculation proportions the majority of the ureolytic bacteria lose their activity in the first 4 h because of the effect of Cu^{2+} toxicity. For this reason, a small number of NH_4^+ and OH^- are discharged and EC, therefore, shows a small increase. The effect of Cu^{2+} toxicity badly depresses the growth and reproduction of the ureolytic bacteria for the subsequent 8 h. The ureolytic bacteria that remain active 12 h after the

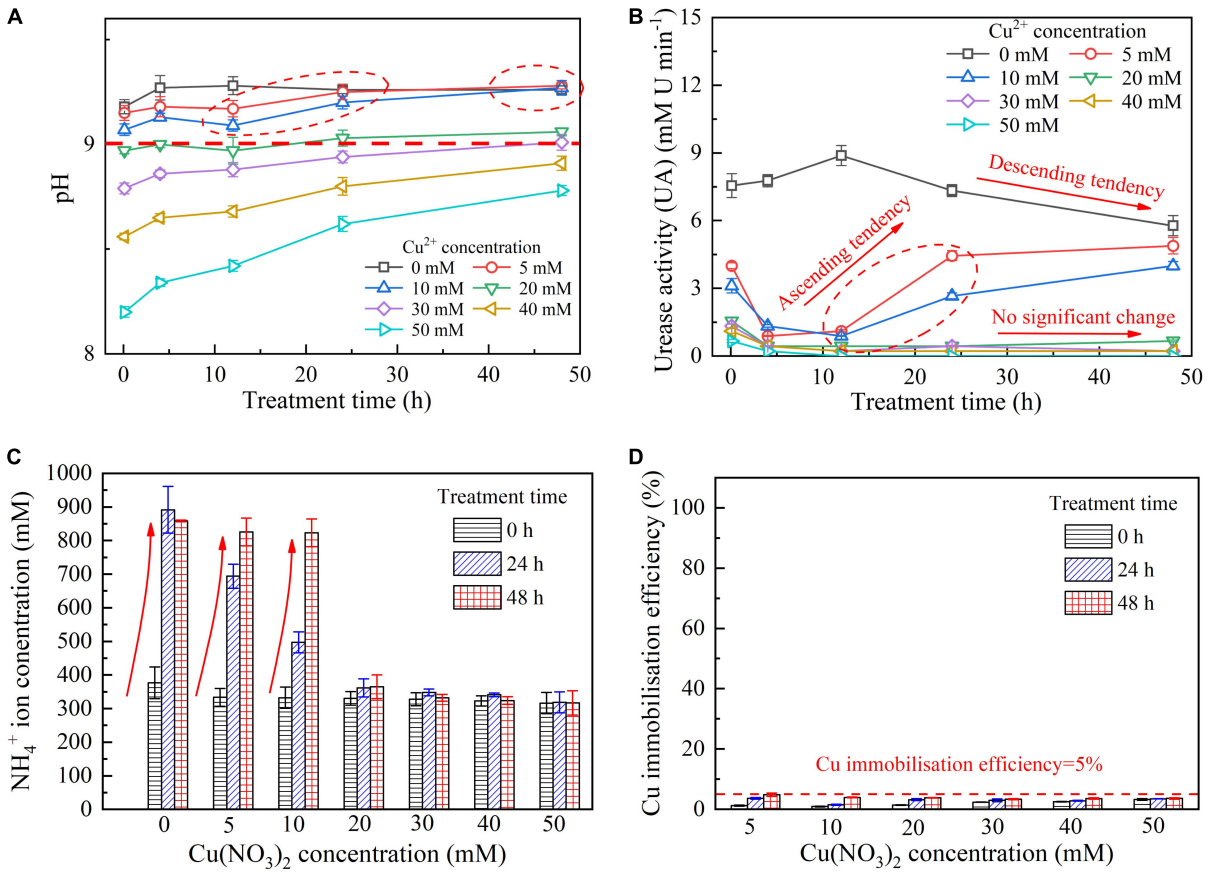

FIGURE 5
(A) pH vs. treatment time relationship, **(B)** UA vs. treatment time relationship, **(C)** NH_4^+ vs. $Cu(NO_3)_2$ concentration relationship and, **(D)** copper immobilization efficiency vs. $Cu(NO_3)_2$ concentration relationship for the bacterial inoculation proportion = 1:1.

commencement of bacterial inoculation begin showing their resistance against Cu^{2+} toxicity. The formation of copper-ammonia complexes reduces the effect of Cu^{2+} toxicity on the ureolytic bacteria and UA. This phenomenon becomes more pronounced when subjected to lower Cu^{2+} concentrations and higher bacterial inoculation proportions (e.g., 1:3 and 1:1). When subjected to 10 mM Cu^{2+}, the ureolytic bacteria remain active only when the bacterial inoculation proportion is raised to 1:1, whereas the ureolytic bacteria, when subjected to 5 mM Cu^{2+}, remain active even when the inoculation proportion is reduced to 1:3. These results lead us to summarize that although higher inoculation proportions can improve the resistance of the ureolytic bacteria against Cu^{2+} toxicity and promote the secretion of the urease, their use is accompanied by discharging more OH^- throughout the biomineralization process, turning surrounding environments into alkaline conditions and promoting the copper-ammonia complexes formation. The copper-ammonia complexes largely raise the potential of Cu^{2+} migration and diffusion, causing an inability of securing the copper immobilization efficiency. As indicated by **Figure 3C**, an improvement in EC and NH_4^+ may cause misleading interferences concerning the use of high inoculation proportion of 1:1 for improving the copper immobilization efficiency. Therefore, it is argued that higher inoculation proportions pave the way to secure copper immobilization efficiency. In addition to UA, particular attention to the surrounding pH conditions should also be given, preventing a reduction in the copper immobilization efficiency by the copper-ammonia complexes formation.

Effect of surrounding pH conditions

The temporal relationships of pH against the bacterial inoculation proportion = 1:9, 1:3, and 1:1 when subjected to 20, 10, and 5 mM Cu^{2+} are shown in **Figures 4A–C**, respectively. The results from the previous section indicate that when subjected to 10 mM Cu^{2+}, the ureolytic bacteria remaining active is present only when the inoculation proportion is raised to 1:1, while the bacteria that remain active, when subjected to 5 mM Cu^{2+}, presents even when the inoculation proportion is as low as 1:3. The value of surrounding pH corresponding to the these results, however, exceeds 9 (Duarte-Nass et al., 2020). As discussed, the ureolytic bacteria can be characterized

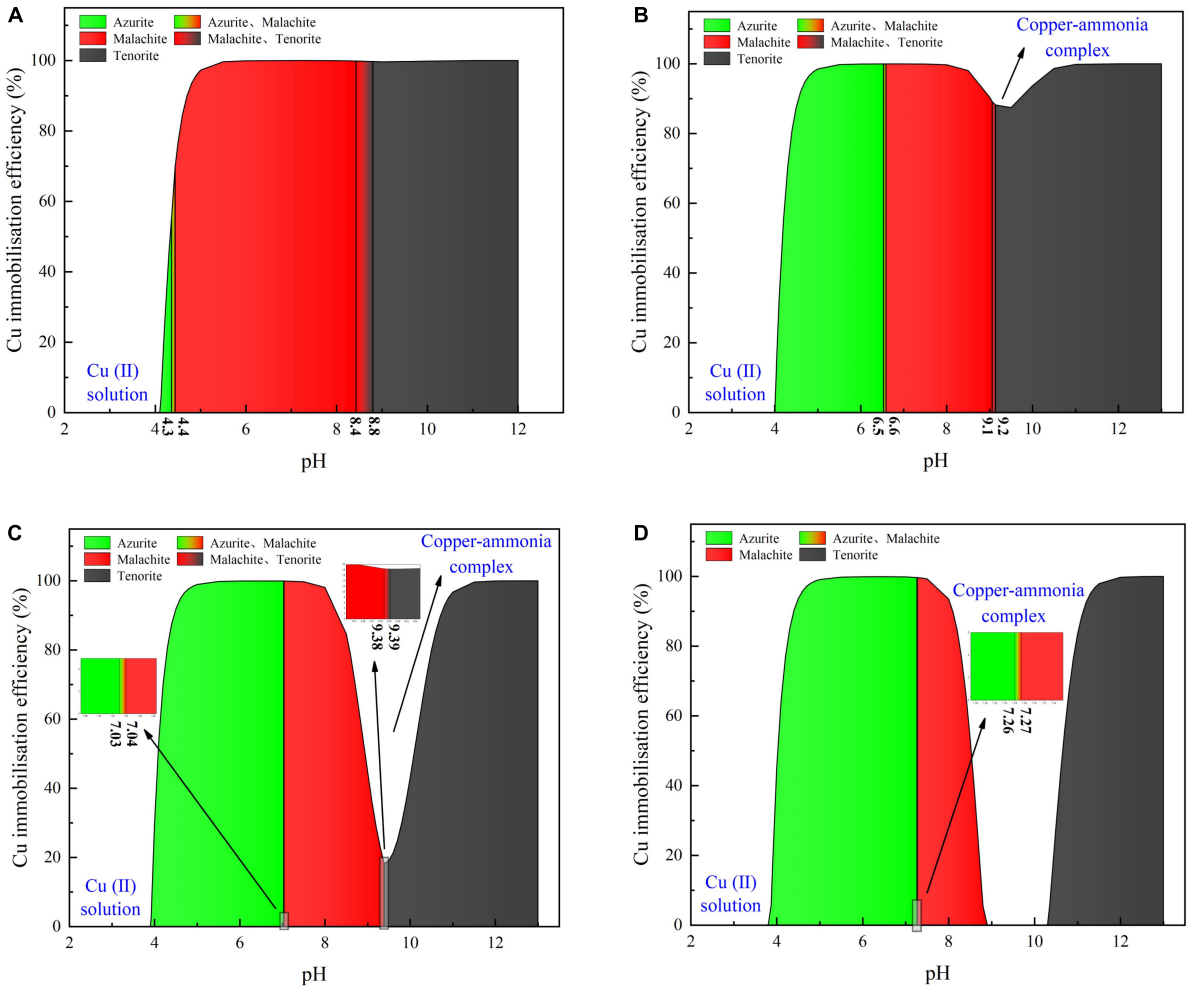

FIGURE 6
(A) copper immobilization efficiency vs. pH relationship for the inoculation proportion = 1:9, **(B)** copper immobilization efficiency vs. pH relationship for the inoculation proportion = 1:3, **(C)** copper immobilization efficiency vs. pH relationship for the inoculation proportion = 1:1, and **(D)** copper immobilization efficiency vs. pH relationship for the inoculation proportion = 3:1 [$Cu(NO_3)_2$ concentration = 40 mM].

as UA going down in the first 4 h after the commencement of bacterial inoculation, and UA going up since after 12 h (see Figures 2A, 3A). The bacteria that remain active 12 h after the commencement of bacterial inoculation can reproduce and catalyze urea hydrolysis, discharging NH_4^+ and OH^-. This is deemed as the main cause leading to the value of pH in excess of 9.

pH below 9 is attained using 20–50 mM Cu^{2+} where the effect of Cu^{2+} toxicity can depress the growth and reproduction of the ureolytic bacteria (see Figures 5A,B). The ureolytic bacteria remain active when subjected to 0–10 mM Cu^{2+}, discharging NH_4^+ throughout the biomineralization process (see Figure 5C). It is worth to note that the copper immobilization efficiency could be as low as 5% under the inoculation proportion being 1:1, and such low copper immobilization efficiency still holds true when Cu^{2+} concentration decreases to 5 mM (see Figure 5D). These results conflict with our consensus that lower Cu^{2+} concentrations can ease the effect of Cu^{2+} toxicity on the ureolytic bacteria and promote the secretion of the urease by the ureolytic bacteria, thus improving the degree of urea hydrolysis and subsequently the copper immobilization efficiency. There are two underlying mechanisms revealed by the present work. Although the ureolytic bacteria remain active when subjected to 0–10 mM Cu^{2+}, the highest inoculation proportion of 1:1 not only eases the effect of Cu^{2+} toxicity on the ureolytic bacteria and UA but turns the surrounding pH into alkaline conditions (pH > 9), promoting the formation of copper-ammonia complexes. The copper-ammonia complexes raise the potential of Cu^{2+} migration and diffusion and reduce the copper immobilization efficiency to as low as 5%. Furthermore, despite pH below 9 and no copper-ammonia complex formation, the

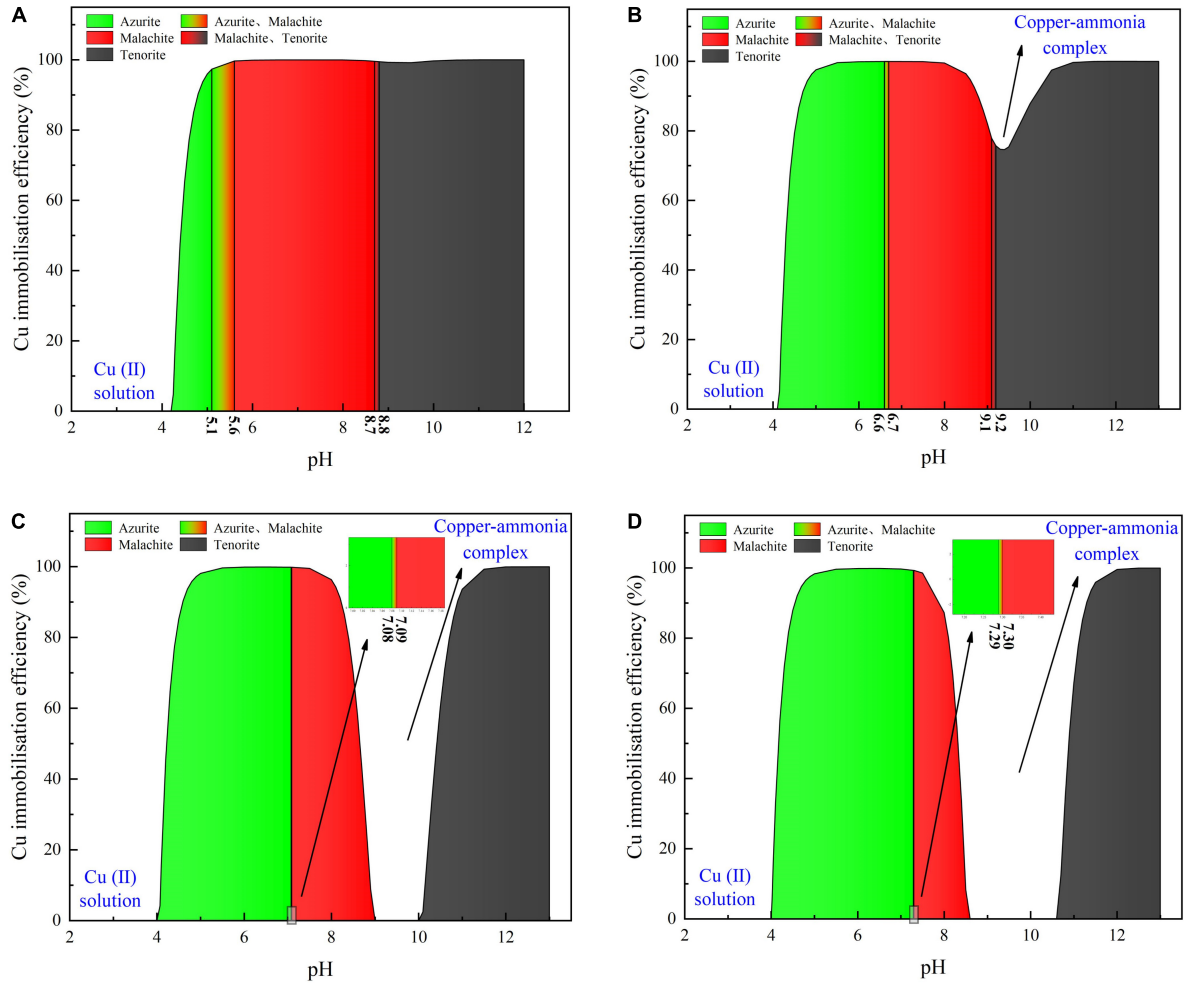

FIGURE 7
(A) copper immobilization efficiency vs. pH relationship for the inoculation proportion = 1:9, **(B)** copper immobilization efficiency vs. pH relationship for the inoculation proportion = 1:3, **(C)** copper immobilization efficiency vs. pH relationship for the inoculation proportion = 1:1, and **(D)** copper immobilization efficiency vs. pH relationship for the inoculation proportion = 3:1 [$Cu(NO_3)_2$ concentration = 20 mM].

effect of Cu^{2+} toxicity badly depresses the ureolytic bacteria and UA when subjected to a range of 20–50 mM Cu^{2+}, reducing the degree of urea hydrolysis. The lower the degree of urea hydrolysis, the lesser the carbonate precipitated, and the lower the copper immobilization efficiency. The reduction in the degree of urea hydrolysis reduces the copper immobilization efficiency to approximately 5%.

Numerical simulations

Considering harsh pH conditions and the precipitation speciation have been neglected in the test tube experiments, they are interpreted a step further using a series of numerical simulations. Given 40 mM $Cu(NO_3)_2$, the relationships of the copper immobilization efficiency vs. the surrounding pH against the inoculation proportions of 1:9, 1:3, 1:1, and 3:1 are shown in Figure 6. Under the inoculation proportion = 1:9, there are three speciations of carbonate precipitation, including azurite [$(Cu_3(OH)_2(CO_3)_2]$, malachite [$Cu_2(OH)_2CO_3$], and tenorite (CuO), when pH remains above 4 (see Figure 6A). The copper immobilization efficiency increases notably when pH is increased from 4.0 to 4.5. It reaches approximately 100% when pH falls within a 5–12 range, with the exception of pH surrounding 9 where a reduction in the copper immobilization efficiency occurs. When pH is below 4, Cu^{2+} are present in a free state and no carbonate precipitation is found, reducing the copper immobilization efficiency to zero. The aforesaid three speciations of carbonate precipitation are also present under the inoculation proportion = 1:3 (see Figure 6B). Similarly, Cu^{2+} are present in a free state when pH remains below 4. Except pH surrounding 9, the copper immobilization efficiency reaches nearly 100% as pH falls within a 5–12 range. Such reduction in the copper immobilization efficiency under the

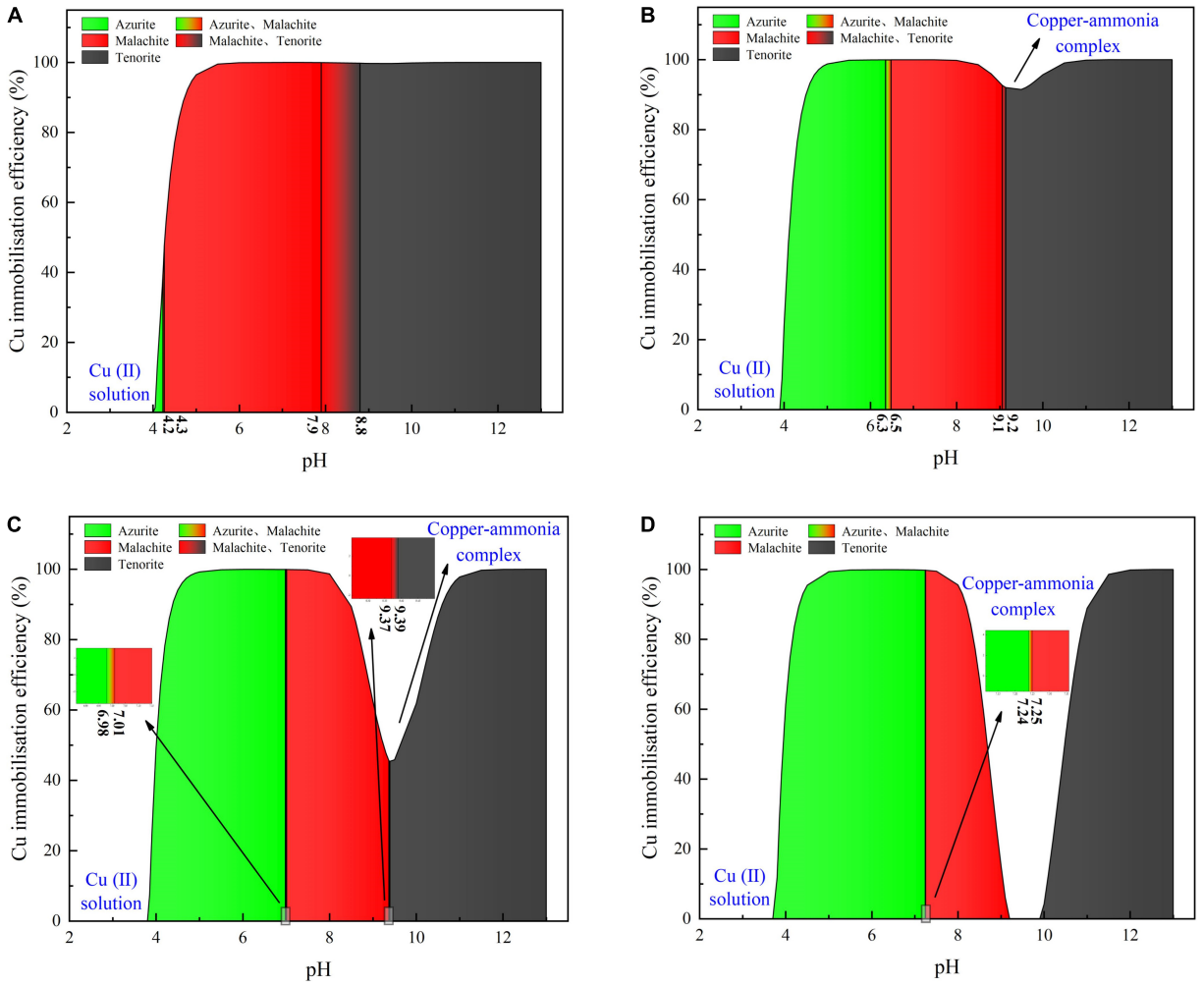

FIGURE 8
(A) copper immobilization efficiency vs. pH relationship for the inoculation proportion = 1:9, **(B)** copper immobilization efficiency vs. pH relationship for the inoculation proportion = 1:3, **(C)** copper immobilization efficiency vs. pH relationship for the inoculation proportion = 1:1, and **(D)** copper immobilization efficiency vs. pH relationship for the inoculation proportion = 3:1 [$Cu(NO_3)_2$ concentration = 60 mM].

inoculation proportion = 1:1 and 3:1, respectively, is also noted (see Figures 6C,D). It is also present when subjected to 20 mM and 60 mM $Cu(NO_3)_2$, respectively (see Figures 7, 8). In this situation (pH approximately 9) precipitation even disappears under the inoculation proportion = 3:1. Taking a close look at the variations of the copper immobilization efficiency shown in Figures 6–8, higher Cu^{2+} concentrations narrow pH ranges that are associated with the formation of copper-ammonia complexes. For example, pH corresponding to the formation of copper-ammonia complexes is narrowed from 8.2 to 10.2 range when subjected to 20 mM Cu^{2+} to 8.6–10 range when subjected to 60 mM Cu^{2+}. In other words, there is a higher possibility for the copper-ammonia complexes to form when subjected to lower Cu^{2+} concentrations. These phenomena are due to the fact that lower Cu^{2+} concentrations in fact turn surrounding environments into alkaline conditions favorable for forming the copper-ammonia complexes. In contrast, higher Cu^{2+} concentrations provide acidic environments.

In acidic environments, the hydrolysis of CO_3^{2-} is going forward and ammonia is present in NH_4^+ form. Considering HCO_3^- and H_2CO_3 as well as NH_4^+ are not going to react with Cu^{2+}, the majority of Cu^{2+} is present in a free state and the remaining is biomineralized with CO_3^{2-}, thereby forming azurite precipitation (see Figures 6–8). Under pH below 4, Cu^{2+} in a free state raises its migration and diffusion potential and is deemed as the main contributor to the reduction in the copper immobilization efficiency. In short, under pH in a 4–6 range (in most cases), the copper immobilization efficiency is attained through azurite precipitation. The copper immobilization efficiency drops sharply to zero under pH below 4 due to Cu^{2+} migration and diffusion. In contrast, the hydrolysis of CO_3^{2-} is going backward in alkaline environments, and ammonia is, in

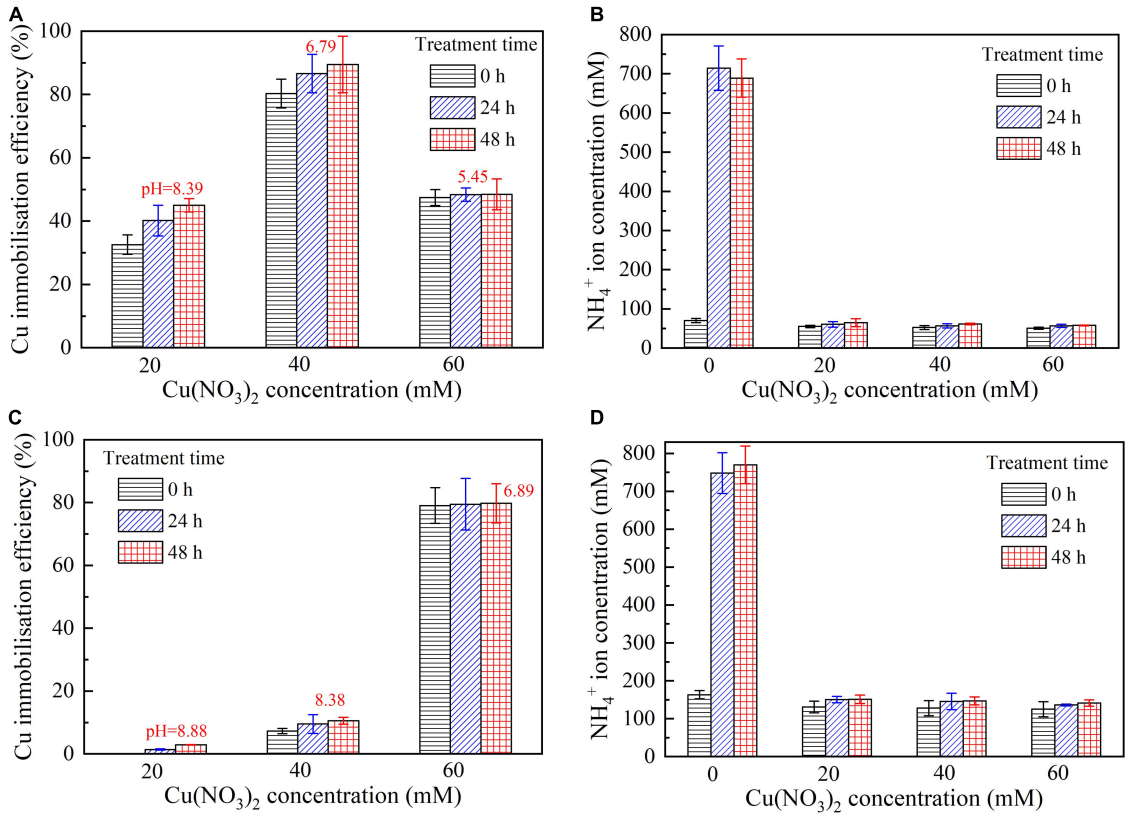

FIGURE 9
(A) copper immobilization efficiency vs. $Cu(NO_3)_2$ concentration relationship and **(B)** NH_4^+ concentration vs. $Cu(NO_3)_2$ concentration relationship for the inoculation proportion = 1:9; **(C)** copper immobilization efficiency vs. $Cu(NO_3)_2$ concentration relationship and **(D)** NH4 + concentration vs. $Cu(NO_3)_2$ concentration relationship for the inoculation proportion = 1:3.

turn, present in NH_3 form. NH_3 is going to react with Cu^{2+}, forming the copper-ammonia complexes. The remaining is going to precipitate with CO_3^{2-} to form malachite precipitation (see **Figures 6–8**). It is noteworthy that tenorite is precipitated under pH above 10, corresponding to a copper immobilization efficiency of approximately 100%. Notwithstanding that, its chemical and thermodynamic properties are not as good as the other two carbonates (i.e., azurite and malachite) because it dissolves under harsh pH and temperature conditions, causing an inability of preventing Cu^{2+} migration and diffusion. To summarize, under pH surrounding 9, the copper-ammonia complexes notably reduce the copper immobilization efficiency to zero by promoting Cu^{2+} migration and diffusion. In case pH falls within a 7–9 range (in most cases), the copper immobilization efficiency is attained through malachite precipitation.

Copper immobilization efficiency

This part aims not only to verify the applicability of the numerical simulations applied to the present work but to investigate further the effect of Cu^{2+} concentration on the immobilization efficiency under a given pH value (Mugwar and Harbottle, 2016). It can be observed that for the inoculation proportion = 1:9, the copper immobilization efficiency being approximately 90% is the highest under $Cu(NO_3)_2$ concentration at 40 mM, corresponding to pH = 6.79 (see **Figures 9B,D**). Further, the copper immobilization efficiency approximately 45% is the lowest when subjected to $Cu(NO_3)_2$ concentration at 20 mM, which corresponds to pH = 8.39. These results are in line with the simulated results, thereby verifying the applicability of the numerical simulations (see **Figures 6–8**). The reductions in the copper immobilization efficiencies, when subjected to $Cu(NO_3)_2$ = 20 mM and 60 mM, appear to be attributed to the effect of pH conditions. Although the majority of the ureolytic bacteria lose their activity in the second step of the two-step biomineralization, the discharge of OH^- (relevant to bacterial inoculation proportion) in the first step determine not only pH conditions but also the speciation of carbonate precipitation. pH = 8.88, induced by the inoculation proportion = 1:3, gives alkaline environments when subjected to 20 mM $Cu(NO_3)_2$ and promotes the formation of copper-ammonia complexes,

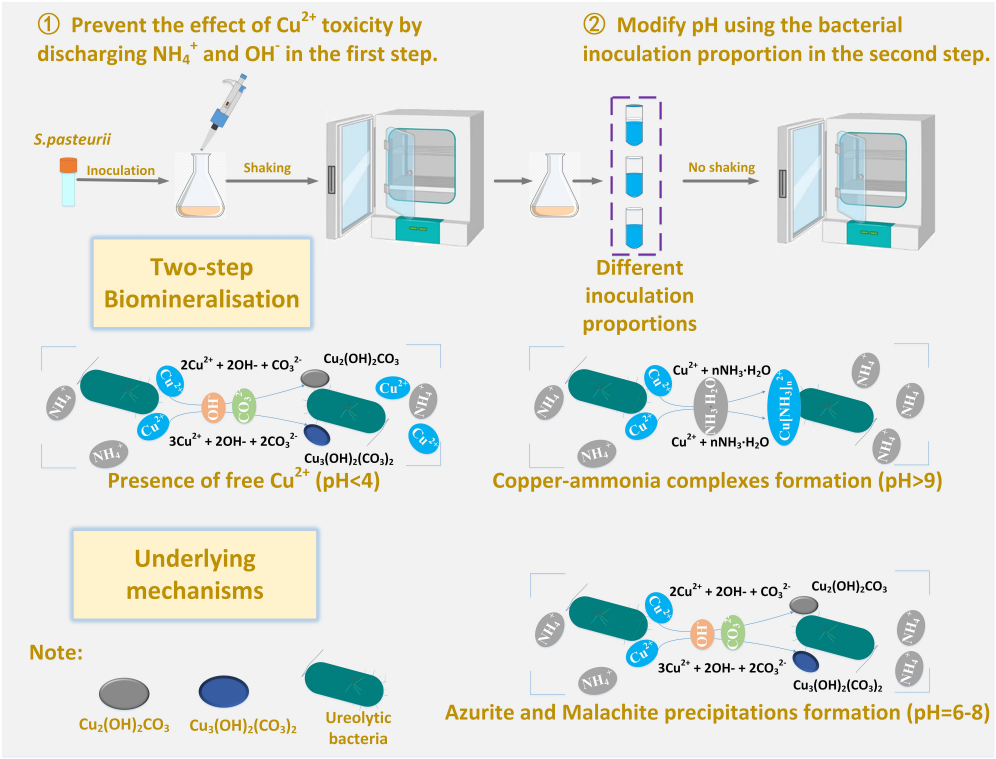

FIGURE 10
Schematic illustration of the underlying mechanisms affecting the copper immobilization efficiency.

yielding the copper immobilization efficiency way below 10% (see Figures 9C,D). In contrast, when subjected to 60 mM $Cu(NO_3)_2$, pH = 6.89, resulting from the inoculation proportion = 1:3, gives acidic environments and then prevent the formation of copper-ammonia complexes, corresponding to the copper immobilization efficiency approximately 80%. In most cases the copper immobilization efficiency using the two-step biomineralization approach higher than 45% is much higher than that using the ordinary biomineralization approach despite a discrepancy in the bacterial inoculation proportion (see Figure 5D). That is to say, the two-step biomineralization approach elevates the copper immobilization efficiency and such improvement is especially pronounced when subjected to higher $Cu(NO_3)_2$ concentrations. However, the copper immobilization efficiency way below 10% under the bacterial inoculation proportion = 1:3 appears when subjected to 20 mM $Cu(NO_3)_2$. Modification concerning pH conditions may consider by reducing the inoculation proportion to 1:9 to prevent the reduction in the copper immobiliztion efficiency. To conclude, the two-step biomineralization approach prevents the effect of Cu^{2+} toxicity by discharging NH_4^+ and OH^- prior to inoculating the ureolytic bacteria to the liquid medium containing $Cu(NO_3)_2$. Discharging NH_4^+ and OH^- while cultivating the ureolytic bacteria is deemed as the first step (see Figure 10). To prevent the formation of copper-ammonia complexes, pH conditions are modified by reducing the inoculation proportion, referred to also as the second step. As a result, the copper immobilization efficiency remains very high when even subjected to higher $Cu(NO_3)_2$ concentrations. The use of the two-step biomineralization to secure the urease activity and also to modify pH conditions is considered of great necessity while applying the MICP technology to remedy copper-rich water bodies.

Conclusion

The proposed two-step biomineralization approach to secure the urease activity and also to modify pH conditions to prevent the copper-ammonia complexes formation was applied to copper immobilization. Based on the results and discussion, some main conclusions can be drawn as follows:

(1) The copper immobilization efficiency way below 10% for the bacterial inoculation proportion = 1:1 is attained and still holds true even when $Cu(NO_3)_2$ concentration is reduced to 5 mM. Although higher inoculation proportions can improve the resistance of the ureolytic bacteria against Cu^{2+} toxicity, their use is accompanied by discharging more OH^-, turning

surrounding environments into alkaline conditions and promoting the formation of copper-ammonia complexes. For this reason, the potential of Cu^{2+} migration is raised, causing an inability of securing the copper immobilization efficiency.

(2) 20–50 mM $Cu(NO_3)_2$ can badly depress the ureolytic bacteria and then reduces the degree of urea hydrolysis. The lower the degree of urea hydrolysis, the lesser the carbonate precipitated, and the lower the copper immobilization efficiency. The lack of CO_3^{2-}, induced by the reduction in the degree of urea hydrolysis, is considered to be the main cause leading to the copper immobilization efficiency way below 10% when subjected to 20–50 mM $Cu(NO_3)_2$.

(3) Under pH in a 4–6 range (in most cases), the copper immobilization efficiency is attained through azurite precipitation. The copper immobilization efficiency drops to zero under pH below 4 due to Cu^{2+} migration and diffusion. Under pH surrounding 9, the copper-ammonia complexes reduce the copper immobilization efficiency to zero. In case pH falls within a 7–9 range (in most cases), the copper immobilization efficiency is attained through malachite precipitation. The findings shed light on the necessity of securing the urease activity and modifying pH conditions while applying the MICP technology to remedy copper-rich water bodies.

Data availability statement

The original contributions presented in this study are included in the article/supplementary material, further inquiries can be directed to the corresponding author/s.

Author contributions

Z-FX: data curation, formal analysis, validation, software, and writing—original draft. W-CC: conceptualization, methodology, writing—review and editing, supervision, and funding acquisition. LW: writing—review and editing. Y-XX: writing—review and editing. All authors contributed to the article and approved the submitted version.

Funding

This manuscript was based upon work supported by the Shaanxi Educational Department under Grant No. 2020TD-005 through the innovative ability support scheme.

Conflict of interest

The authors declare that the research was conducted in the absence of any commercial or financial relationships that could be construed as a potential conflict of interest.

Publisher's note

All claims expressed in this article are solely those of the authors and do not necessarily represent those of their affiliated organizations, or those of the publisher, the editors and the reviewers. Any product that may be evaluated in this article, or claim that may be made by its manufacturer, is not guaranteed or endorsed by the publisher.

References

Achal, V., Pan, X. L., Fu, Q. L., and Zhang, D. Y. (2012a). Biomineralization based remediation of As (III) contaminated soil by Sporosarcina ginsengisoli. *J. Hazard. Mater.* 20, 178–184. doi: 10.1016/j.jhazmat.2011.11.067

Achal, V., Pan, X. L., Zhang, D. Y., and Fu, Q. L. (2012b). Bioremediation of Pb-Contaminated Soil Based on Microbially Induced Calcite Precipitation. *J. Microbiol. Biotechnol.* 22, 244–247. doi: 10.4014/jmb.1108.08033

Achal, V., Pan, X. L., and Zhang, D. Y. (2011). Remediation of copper-contaminated soil by Kocuria flava CR1, based on microbially induced calcite precipitation. *Ecol. Eng.* 37, 1601–1605. doi: 10.1016/j.ecoleng.2011.06.008

Ali, A., Li, M., Su, J., Li, Y., Wang, Z., Bai, Y., et al. (2022). Brevundimonas diminuta isolated from mines polluted soil immobilized cadmium (Cd^{2+}) and zinc (Zn^{2+}) through calcium carbonate precipitation: Microscopic and spectroscopic investigations. *Sci. Total Environ.* 813:152668. doi: 10.1016/j.scitotenv.2021.152668

Bai, B., Rao, D., Chang, T., and Guo, Z. (2019). A nonlinear attachment-detachment model with adsorption hysteresis for suspension-colloidal transport in porous media. *J. Hydrol.* 578:124080. doi: 10.1016/j.jhydrol.2019.124080

Bai, X. D., Cheng, W. C., and Li, G. (2021b). A comparative study of different machine learning algorithms in predicting EPB shield behaviour: A case study at the Xi'an metro, China. *Acta Geotech.* 16, 4061–4080. doi: 10.1007/s11440-021-01383-7

Bai, X. D., Cheng, W. C., Sheil, B. B., and Li, G. (2021c). Pipejacking clogging detection in soft alluvial deposits using machine learning algorithms. *Tunn. Undergr. Space Technol.* 113, 103908. doi: 10.1016/j.tust.2021.103908

Bai, B., Nie, Q., Zhang, Y., Wang, X., and Hu, W. (2021a). Cotransport of heavy metals and SiO_2 particles at different temperatures by seepage. *J. Hydrol.* 597:125771. doi: 10.1016/j.jhydrol.2020.125771

Casas, C. C., Graf, A., Brüggemann, N., Schaschke, C. J., and Jorat, M. E. (2020). Dolerite Fines Used as a Calcium Source for Microbially Induced Calcite Precipitation Reduce the Environmental Carbon Cost in Sandy Soil. *Front. Microbiol.* 2020:557119. doi: 10.3389/fmicb.2020.557119

Chen, L., Zhou, M., Wang, J., Zhang, Z., Duan, C., Wang, X., et al. (2022a). A global meta-analysis of heavy metal(loid)s pollution in soils near copper mines: Evaluation of pollution level and probabilistic health risks. *Sci. Total Environ.* 835:155441. doi: 10.1016/j.scitotenv.2022.155441

Chen, L., Beiyuan, J., Hu, W., Zhang, Z., Duan, C., Cui, Q., et al. (2022b). Phytoremediation of potentially toxic elements (PTEs) contaminated soils using alfalfa (*Medicago sativa L.*): A comprehensive review. *Chemosphere* 293:133577. doi: 10.1016/j.chemosphere.2022.133577

Chen, L., Wang, J. Z., Beiyuan, J. Z., Guo, X. T., Wu, H., and Fang, L. C. (2022c). Environmental and health risk assessment of potentially toxic trace elements in soils near uranium (U) mines: A global meta-analysis. *Sci. Total Environ.* 816:151556. doi: 10.1016/j.scitotenv.2021.151556

Chen, X. Y., and Achal, V. (2019). Biostimulation of carbonate precipitation process in soil for copper immobilization. *J. Hazard. Mater.* 368, 705–713. doi: 10.1016/j.jhazmat.2019.01.108

Chen, Z., Pan, X. H., Chen, H., Guan, X., and Lin, Z. (2016). Biomineralization of Pb(II) into Pb- hydroxyapatite induced by Bacillus cereus 12-2 isolated from Lead-Zinc mine tailings. *J. Hazard. Mater.* 301, 531–537. doi: 10.1016/j.jhazmat.2015.09.023

Cui, M. J., Lai, H. J., Hoang, T., and Chu, J. (2021). One-phase-low-pH enzyme induced carbonate precipitation (EICP) method for soil improvement. *Acta Geotech.* 16, 481–489. doi: 10.1007/s11440-020-01043-2

Cui, M. J., Teng, A., Chu, J., and Cao, B. (2022). A quantitative, high-throughput urease activity assay for comparison and rapid screening of ureolytic bacteria. *Environ. Res.* 208:112738. doi: 10.1016/j.envres.2022.112738

Duarte-Nass, C., Rebolledo, K., Valenzuela, T., Kopp, M., Jeison, D., Rivas, M., et al. (2020). Application of microbe-induced carbonate precipitation for copper removal from copper-enriched waters: Challenges to future industrial application. *J. Environ. Manag.* 256:109938. doi: 10.1016/j.jenvman.2019.109938

Elalfy, M., Abomosallam, M., Elhadidy, M. G., and Sleem, F. (2021). Copper and copper containing pesticide as copper oxychloride toxicity and its adverse effects on animal and human health. *Med. Res. Chron.* 8, 89–98. doi: 10.26838/MEDRECH.2021.8.2.486

Facchin, V., Cavinato, C., Fatone, F., Pavan, P., Cecchi, F., and Bolzonella, D. (2013). Effect of trace element supplementation on the mesophilic anaerobic digestion of foodwaste in batch trials: The influence of inoculum origin. *Biochem. Eng. J.* 70, 71–77. doi: 10.1016/j.bej.2012.10.004

Ferris, F. G., Phoenix, V., Fujita, Y., and Smith, R. W. (2004). Kinetics of calcite precipitation induced by ureolytic bacteria at 10 to 20°C in artificial groundwater. *Geochim. Cosmochim. Acta.* 67, 1701–1722. doi: 10.1016/S0016-7037(03)00503-9

Fu, F. L., and Wang, Q. (2011). Removal of heavy metal ions from wastewaters: A review. *J. Environ. Manag.* 92, 407–418. doi: 10.1016/j.jenvman.2010.11.011

Guo, H. R., Ouyang, Y. J., Wang, J. Q., Cui, H. M., Deng, H. D., Zhong, X. Y., et al. (2021). Cu-induced spermatogenesis disease is related to oxidative stress-mediated germ cell apoptosis and DNA damage. *J. Hazard. Mater.* 416:125903. doi: 10.1016/j.jhazmat.2021.125903

Hu, W., Cheng, W. C., and Wen, S. (2022a). Investigating the effect of degree of compaction, initial water content, and electric field intensity on electrokinetic remediation of an artificially Cu- and Pb-contaminated loess. *Acta Geotech.* doi: 10.1007/s11440-022-01602-9 [Epub ahead of print].

Hu, W., Cheng, W. C., Wang, L., and Xue, Z. F. (2022b). Micro-structural characteristics deterioration of intact loess under acid and saline solutions and resultant macro-mechanical properties. *Soil Tillage Res.* 220:105382. doi: 10.1016/j.still.2022.105382

Hu, W., Cheng, W. C., Wen, S., and Rahman, M. M. (2021a). Effects of chemical contamination on microscale structural characteristics of intact loess and resultant macroscale mechanical properties. *CATENA* 203:105361. doi: 10.1016/j.catena.2021.105361

Hu, W., Cheng, W. C., Wen, S., and Yuan, K. (2021b). Revealing enhancement and degradation mechanisms affecting calcite precipitation in EICP process. *Front. Bioeng. Biotechnol.* 9:750258. doi: 10.3389/fbioe.2021.750258

Jiang, N.-J., Liu, R., Du, Y.-J., and Bi, Y.-Z. (2019). Microbial induced carbonate precipitation for immobilizing Pb contaminants: Toxic effects on bacterial activity and immobilization efficiency. *Sci. Total Environ.* 672, 722–731. doi: 10.1016/j.scitotenv.2019.03.294

Jiang, N.-J., and Soga, K. (2019). Erosional Behavior of Gravel-Sand Mixtures Stabilized by Microbial Induced Calcite Precipitation (MICP). *Soils Found.* 59, 699–709. doi: 10.1016/j.sandf.2019.02.003

Kang, C. H., Oh, S. J., Shin, Y., Han, S. H., Nam, I. H., and So, J. S. (2015). Bioremediation of lead by ureolytic bacteria isolated from soil at abandoned metal mines in South Korea. *Ecol. Eng.* 74, 402–407. doi: 10.1016/j.ecoleng.2014.10.009

Kim, Y., Kwon, S., and Roh, Y. (2021). Effect of Divalent Cations (Cu, Zn, Pb, Cd, and Sr) on Microbially Induced Calcium Carbonate Precipitation and Mineralogical Properties. *Front. Microbiol.* 2021:646748. doi: 10.3389/fmicb.2021.646748

Krajewska, B. (2008). Mono- (Ag, Hg) and di- (Cu, Hg) valent metal ions effects on the activity of jack bean urease. Probing the modes of metal binding to the enzyme. *J. Enzyme Inhib. Med. Chem.* 23, 535–542. doi: 10.1093/emboj/cdg128

Lai, Y., Yu, J., Liu, S., and Dong, B. (2020). Experimental study to improve the mechanical properties of iron tailings sand by using MICP at low pH. *Constr. Build. Mater.* 273:121729. doi: 10.1016/j.conbuildmat.2020.121729

Li, M., Cheng, X. H., and Guo, H. X. (2013). Heavy metal removal by biomineralization of urease producing bacteria isolated from soil. *Int. Biodeterior. Biodegradation* 76, 81–85. doi: 10.1016/j.ibiod.2012.06.016

Li, Q., Wang, Y. H., Li, Y. C., Li, L. F., Tang, M. D., Hu, W. F., et al. (2022). Speciation of heavy metals in soils and their immobilization at micro-scale interfaces among diverse soil components. *Sci. Total Environ.* 825:153862. doi: 10.1016/j.scitotenv.2022.153862

Li, W. L., Fishman, A., and Achal, V. (2021). Ureolytic bacteria from electronic waste area, their biological robustness against potentially toxic elements and underlying mechanisms. *J. Environ. Manag.* 289:112517. doi: 10.1016/j.jenvman.2021.112517

Liu, F., Zhou, K. G., Chen, Q. Z., Wang, A. H., and Chen, W. (2018). Application of magnetic ferrite nanoparticles for removal of Cu (II) from copper-ammonia wastewater. *J. Alloys Compd.* 773:240. doi: 10.1016/j.jallcom.2018.09.240

Liu, K. W., Jiang, N.-J., Qin, J. D., Wang, Y. J., Tang, C. S., and Han, X. L. (2021). An experimental study of mitigating coastal sand dune erosion by microbial- and enzymatic-induced carbonate precipitation. *Acta Geotech.* 16, 467–480. doi: 10.1007/s11440-020-01046-z

Liu, P., Hu, W. Y., Tian, K., Huang, B., Zhao, Y. C., Wang, X. K., et al. (2020). Accumulation and ecological risk of heavy metals in soils along the coastal areas of the Bohai Sea and the Yellow Sea: A comparative study of China and South Korea. *Environ. Int.* 137:105519. doi: 10.1016/j.envint.2020.105519

Mugwar, A. J., and Harbottle, M. J. (2016). Toxicity effects on metal sequestration by microbially-induced carbonate precipitation. *J. Hazard Mater.* 314, 237–248. doi: 10.1016/j.jhazmat.2016.04.039

Mujah, D., Shahin, M. A., Cheng, L., and Karrech, A. (2021). Experimental and Analytical Study on Geomechanical Behavior of Biocemented Sand. *Int. J. Geomech.* 21:0002105. doi: 10.1061/(ASCE)GM.1943-5622.0002105

Qdais, H. A., and Moussa, H. (2004). Removal of heavy metals from wastewater by membrane processes: A comparative study. *Desalination* 164, 105–110. doi: 10.1016/S0011-9164(04)00169-9

Qiao, S., Zeng, G., Wang, X., Dai, C., Sheng, M., Chen, Q., et al. (2021). Multiple heavy metals immobilization based on microbially induced carbonate precipitation by ureolytic bacteria and the precipitation patterns exploration. *Chemosphere* 274:129661. doi: 10.1016/j.chemosphere.2021.129661

Rahman, M. M., Hora, R. N., Ahenkorah, I., Beecham, S., Karim, M. R., and Iqbal, A. (2020). State-of-the-art review of microbial-induced calcite precipitation and its sustainability in engineering applications. *Sustainability* 12:6281. doi: 10.3390/su12156281

Schwantes-Cezario, N., Camargo, G., Couto, L., Porto, M. F., and Toralles, B. M. (2020). Mortars with the addition of bacterial spores: Evaluation of porosity using different test methods. *J. Build. Eng.* 30:101235. doi: 10.1016/j.jobe.2020.101235

Schwantes-Cezario, N., Medeiros, L. P., Oliveira, A. D., Nakazato, G., Renata, K., and Toralles, B. M. (2017). Bioprecipitation of calcium carbonate induced by bacillus subtilis isolated in brazil. *Int. Biodeterior. Biodegradation* 123, 200–205. doi: 10.1016/j.ibiod.2017.06.021

Seplveda, S., Duarte-Nass, C., Rivas, M., Azcar, L., Ramrez, A., Toledo-Alarcn, J., et al. (2021). Testing the Capacity of Staphylococcus equorum for Calcium and Copper Removal through MICP Process. *Minerals* 11:905. doi: 10.3390/min11080905

Song, B., Zeng, G. M., Gong, J. L., Liang, J., Xu, P., Liu, Z. F., et al. (2017). Evaluation methods for assessing effectiveness of in situ remediation of soil and sediment contaminated with organic pollutants and heavy metals. *Environ. Int.* 105, 43–55. doi: 10.1016/j.envint.2017.05.001

Tarach, K. A., Jabońska, M., Pyra, K., Liebau, M., and Góra-Marek, K. (2021). Effect of zeolite topology on NH_3-SCR activity and stability of Cu-exchanged zeolites. *Appl. Catal. B* 2021:119752. doi: 10.1016/j.apcatb.2020.119752

Torres-Aravena, A. E., Duarte-Nass, C., Azcar, L., Mella-Herrera, R., Rivas, M., and Jeison, D. (2018). Can Microbially Induced Calcite Precipitation (MICP) through a Ureolytic Pathway Be Successfully Applied for Removing Heavy Metals from Wastewaters? *Crystals* 8:438. doi: 10.3390/cryst8110438

Wang, L., Cheng, W. C., and Xue, Z. F. (2022b). Investigating microscale structural characteristics and resultant macroscale mechanical properties of loess exposed to alkaline and saline environments. *Bull. Eng. Geol. Environ.* 81:146. doi: 10.1007/s10064-022-02640-z

Wang, H., Yun, H., Ma, X. D., Li, M. H., Qi, M. Y., Wang, L., et al. (2022a). Bioelectrochemical catabolism of triclocarban through the cascade acclimation of triclocarban-hydrolyzing and chloroanilines-oxidizing microbial communities. *Environ. Res*. 210:112880. doi: 10.1016/j.envres.2022.112880

Wang, Z., Su, J. F., Ali, A., Sun, Y., Li, Y. F., Wang, W. S., et al. (2022e). Enhanced removal of fluoride, nitrate, and calcium using self-assembled fungus-flexible fiber composite microspheres combined with microbially induced calcium precipitation. *Chemosphere* 302:134848. doi: 10.1016/j.chemosphere.2022.134848

Wang, Z., Su, J. F., Ali, A., Yang, W. S., Zhang, R. J., Li, Y. F., et al. (2022f). Chitosan and carboxymethyl chitosan mimic biomineralization and promote microbially induced calcium precipitation. *Carbohydr. Polym.* 287:119335. doi: 10.1016/j.carbpol.2022.119335

Wang, L., Cheng, W. C., and Xue, Z. F. (2022c). The effect of calcium source on Pb and Cu remediation using enzyme-induced carbonate precipitation. *Front. Bioeng. Biotechnol.* 10:849631. doi: 10.3389/fbioe.2022.849631

Wang, L., Cheng, W. C., Xue, Z. F., and Hu, W. (2022d). Effects of the urease concentration and calcium source on enzyme-induced carbonate precipitation for lead remediation. *Front. Chem.* 10:892090. doi: 10.3389/fchem.2022.892090

Wei, S. H., Zhou, Q. X., and Wang, X. (2005). Identification of weed plants excluding the uptake of heavy metals. *Environ. Int*. 31, 829–834. doi: 10.1016/j.envint.2005.05.045

Whiffin, V. S., van Paassen, L. A., and Harkes, M. P. (2007). Microbial carbonate precipitation as a soil improvement technique. *Geomicrobiol. J*. 24, 417–423. doi: 10.1080/01490450701436505

Xiao, Y., Wang, Y., Wang, S., Matthew Evans, T., Stuedlein, A. W., Chu, J., et al. (2021). Homogeneity and mechanical behaviors of sands improved by a temperature-controlled one-phase MICP method. *Acta Geotech*. 16, 1417–1427. doi: 10.1007/s11440-020-01122-4

Xue, Z. F., Cheng, W. C., Wang, L., and Hu, W. L. (2022a). Effects of bacterial inoculation and calcium source on microbial-induced carbonate precipitation for lead remediation. *J. Hazard. Mater*. 426:128090. doi: 10.1016/j.jhazmat.2021.128090

Xue, Z. F., Cheng, W. C., Wang, L., and Song, G. Y. (2021). Improvement of the shearing behaviour of loess using recycled straw fiber reinforcement. *KSCE J. Civ. Eng.* 25, 3319–3335. doi: 10.1007/s12205-021-2263-3

Xue, Z. F., Cheng, W. C., Wang, L., Qin, P., and Zhang, B. (2022c). Revealing degradation and enhancement mechanisms affecting copper (Cu) immobilization using microbial-induced carbonate precipitation (MICP). *J. Environ. Chem. Eng.* 10:108479. doi: 10.1016/j.jece.2022.108479

Xue, Z. F., Cheng, W. C., Wang, L., and Wen, S. J. (2022b). Effects of Bacterial Culture and Calcium Source Addition on Lead and Copper Remediation Using Bioinspired Calcium Carbonate Precipitation. *Front. Bioeng. Biotechnol.* 10:889717. doi: 10.3389/fbioe.2022.889717

Yang, Y., Chu, J., Liu, H., and Cheng, L. (2022). Improvement of uniformity of biocemented sand column using CH3COOH-buffered one-phase-low-pH injection method. *Acta Geotech.* 228. doi: 10.1007/s11440-022-01576-8

Ye, X. Y., Zheng, X. X., Zhang, D. Q., Niu, X. J., Fan, Y. M., Deng, W. D., et al. (2021). The efficient biomineralization and adsorption of cadmium (Cd^{2+}) using secretory organo-biominerals (SOBs) produced by screened Alcaligenes faecalis K2. *Environ. Res.* 2021:111330. doi: 10.1016/j.envres.2021.111330

You, S. Z., Hu, Y., Liu, X. C., and Wei, C. H. (2018). Synergetic removal of Pb(II) and dibutyl phthalate mixed pollutants on Bi_2O_3-TiO_2 composite photocatalyst under visible light. *Appl. Catal. B Environ.* 232, 288–298. doi: 10.1016/j.apcatb.2018.03.025

Yu, D. Y., Wang, J. R., Wang, Y. H., Du, X. L., Li, G. C., and Li, B. (2021). Identifying the Source of Heavy Metal Pollution and Apportionment in Agricultural Soils Impacted by Different Smelters in China by the Positive Matrix Factorization Model and the Pb Isotope Ratio Method. *Sustainability* 13:6526. doi: 10.3390/su13126526

Zaborska, W., Krajewska, B., and Olech, Z. (2004). Heavy Metal Ions Inhibition of Jack Bean Urease: Potential for Rapid Contaminant Probing. *J. Enzyme Inhib. Med. Chem*. 19, 65–69. doi: 10.1118/1.1624755

Zeng, C., Veenis, Y., Hall, C. A., Young, E. S., van der Star, W. R. L., Zheng, J. J., et al. (2021). Experimental and Numerical Analysis of a Field Trial Application of Microbially Induced Calcite Precipitation for Ground Stabilization. *J. Geotech. Geoenviron. Eng.* 147:05021003. doi: 10.1061/(ASCE)GT.1943-5606.0002545

Zhang, K. J., Xue, Y. W., Zhang, J. Q., and Hu, X. L. (2020). Removal of lead from acidic wastewater by bio-mineralized bacteria with pH self-regulation. *Chemosphere* 241:125041. doi: 10.1016/j.chemosphere.2019.125041

frontiers | Frontiers in Microbiology

TYPE Original Research
PUBLISHED 26 September 2022
DOI 10.3389/fmicb.2022.958300

OPEN ACCESS

EDITED BY
Adnan Mustafa,
Brno University of Technology,
Czechia

REVIEWED BY
Shah Fahad,
The University of Haripur, Pakistan
Anis Ali Shah,
University of Education Lahore,
Pakistan

*CORRESPONDENCE
Walid Janati
walid.janati@usmba.ac.ma

SPECIALTY SECTION
This article was submitted to Microbe and Virus Interactions with Plants, a section of the journal Frontiers in Microbiology

RECEIVED 31 May 2022
ACCEPTED 30 August 2022
PUBLISHED 26 September 2022

CITATION
Janati W, Mikou K, El Ghadraoui L and Errachidi F (2022) Isolation and characterization of phosphate solubilizing bacteria naturally colonizing legumes rhizosphere in Morocco.
Front. Microbiol. 13:958300.
doi: 10.3389/fmicb.2022.958300

Isolation and characterization of phosphate solubilizing bacteria naturally colonizing legumes rhizosphere in Morocco

Walid Janati *, Karima Mikou, Lahsen El Ghadraoui and Faouzi Errachidi

Functional Ecology and Environment Engineering Laboratory, Faculty of Science and Technology, Sidi Mohamed Ben Abdellah University, Fez, Morocco

Low-cost and environmentally friendly agricultural practices have received increasing attention in recent years. Developing microbial inoculants containing phosphate (P) solubilizing bacteria (PSB) represents an emerging biological solution to improve rhizosphere P availability. The present study aims to explore PSB strains isolated from soils located at different bioclimatic stages in Morocco and present in various legumes rhizosphere to improve agronomic microbial fertilizer's effectiveness. It was also aimed to test the isolated strains for their ability to solubilize P in NBRIP medium with Tricalcium P (Ca_3 $(PO_4)_2$) (TCP), rock phosphate (RP), and their combination as a source of phosphorus, by (2^2) experiment design. Bacterial strains with a high P solubility index (PSI) were selected, characterized, and compared to commercial control. The vanadate-molybdate method was used to estimate P solubilization activity. Stress tolerance to salinity, acidity, drought, and temperature was tested. From all isolated strains (64), 12 were screened as promising biotechnological interest because of their P solubilization and their good resistance to different drastic conditions. Besides, the strain WJEF15 showed the most P solubility efficiency in NBRIP solid medium with a PSI of 4.1; while the WJEF61 strain was located as the most efficient strain in NBRIP-TCP liquid medium by releasing 147.62 $mg.l^{-1}$ of soluble P. In contrast, in the NBRIP-RP medium, the strain WJEF15 presented maximum solubilization with 25.16 $mg.l^{-1}$. The experiment design showed that a combination of RP and TCP with max level progressively increases P solubilization by 20.58%, while the WJEF63 strain has the most efficient concentration of 102.69 $mg.l^{-1}$. Indeed, among the selected strains, four strains were able to limit tested fungi growth. Thus, results reveal a potential effect of selecting PSBs to support cropping cultures as plant growth-promoting rhizobacteria (PGPR).

KEYWORDS

microbial fertilizers, rock phosphate, stress tolerance, sustainability, antifungal acitivity, TCP

Introduction

Phosphorus (P) is one of the main essential macronutrient compounds for growth and plant development. It is involved in central plant metabolic processes such as cellular energy storage, photosynthesis, and respiration (Balemi and Negisho, 2012; Razaq et al., 2017; Sanz-Sáez et al., 2017; Malhotra et al., 2018). Depending on the environmental and biological factors, it can be the primary growth-limiting nutrient factor (Alok et al., 2013; Rajkumar and Kurinjimalar, 2021). However, the amount of soluble P in soil is generally low (0.4–1.2 $g.kg^{-1}$) (Fernández et al., 2014; Joe et al., 2018). Most parts of soil P (approximately 95–99%) are present in insoluble forms, and therefore they cannot be easily used by plants (Mara et al., 2014). Traditionally, organic and inorganic fertilizers applied to farm fields have been used to correct nutrient deficiencies and maintain nutrient balances (Liu et al., 2020; Tiwari et al., 2020). Soil P is characterized by its restricted mobility when compared to other important nutrients such as nitrogen or potassium and plant nutrient models have long shown that slow diffusion of inorganic phosphate (Pi) is a major limitation to P acquisition by plants (Barber, 1995). This suggests that plants need additional mechanisms to acquire Pi under low P conditions, as their roots have access to a rather small fraction of total soil P. Even if chemical fertilizers are supplied to soils, plants can only use small amounts of P fertilizer because of P complexities in growing weak soil structures. A large quantity of P applied as chemical fertilizer goes out of the plant-soil system through complexity with Ca^{2+} in calcareous soils, and Al^{3+} and Fe^{3+} in acidic soils (Gyaneshwar et al., 2002; Izhar Shafi et al., 2020), therefore, approximately 80% of applied P become unavailable to plant (Salvagiotti et al., 2017). Nevertheless, the negative environmental impact could result from excessive and irrational nutrient application in agroecosystems, which has attracted attention from stakeholders along the food value chain (Choudhury and Kennedy, 2005). According to FAO, more than 175.5 million tons of chemical fertilizers are used in agriculture to obtain the highest crop yield to meet increasing habitat demands.

Most phosphate fertilizers are manufactured using rock phosphate (RP) as the principal source of P_2O_5. While demand continues to increase, the supply of rock phosphate is limited worldwide (Suleman et al., 2018). The extremely poor solubility of RP is the only constraint in its direct use as a soil amendment (Baig et al., 2012). However, insoluble P forms such as tricalcium P [Ca_3 $(PO_4)_2$], aluminum P ($AlPO_4$), and iron P ($FePO_4$) can be solubilized by organic acids, phosphatase enzymes, and complexing agents produced by soil microorganisms inhabiting different soil ecosystems (Vaishampayan et al., 2001). Several studies have reported the usage of microorganisms to solubilize insoluble phosphate compounds as an alternative strategy to phosphate fertilizers (Adnan et al., 2020). Indeed, using these telluric competent strains is an agroecological strategy for improving agricultural fertility and reducing farmers' dependency on inorganic fertilizers to enhance soil health (Janati et al., 2021). For several decades, agricultural microbiologists have studied the ability of certain bacteria to dissolve P fertilizers and P chelated in soil according to sustainability tendency. For this purpose, Behera et al. (2017) noted that PSB's ability to solubilize P from soil or fertilization activities in many agricultural fields is highly dependent on their secretion of organic acids such as citric, formic, oxalic, lactic, acetic, and malic acids. Moreover, PSBs can increase plant P availability by modifying soil processes in the rhizosphere, providing essential nutrients to plants and generating other regulators' growth in various production systems (Adnan et al., 2020; Islam et al., 2021). Likewise, PSBs can produce growth-promoting hormones such as Gibberellins and Indol Acetic Acid (IAA), which are beneficial for plant growth (Bahadur et al., 2016; Linu et al., 2019; Khan et al., 2020; Kour et al., 2020). Currently, most bacteria classified as PSBs belong to *Pseudomonas*, *Serratia*, *Burkholderia*, *Achromobacter*, *Agrobacterium*, *bacillus*, *rhizobia*, *Micrococcus*, *Aerobacter*, *Flavobacterium*, *Acinetobacter*, and *Pantoea* genera (Castagno et al., 2011; Chauhan A. et al., 2015; Adnan et al., 2019; Seenivasagan and Babalola, 2021).

Morocco covers a significant share of world P reserves; it contains 75% of planetary P and is the leading exporter of P and its derivatives. So the global market country's contribution is more than 30% (Hakkou et al., 2016). This advantageous position of Morocco on commercial and technical levels of P extraction remains very far from a bio-industry that accompanies the sector of biotechnology. The latter could open up possibilities for the maximum valorization of soil P. Although PSBs can provide agronomic benefits, they are not always abundant enough in the soil to compete with other indigenous microorganisms (Acevedo et al., 2014). For this reason, these telluric bacteria should be promising at the same time crop productivity and economic-environmental sustainability need to be selected, characterized, and identified to establish sustainable cropping systems.

Considering the above facts, the present study focused on the effect of several tolerant PSBs on different abiotic stresses to promote P solubilization from RP and TCP as the only P source in the context of biological fertilization and sustainable agricultural strategy. We isolated and characterized PSBs from legumes rhizosphere located at various bioclimatic stages and we detected their optimal resistance under different growth and environmental stress conditions (salinity, pH, drought, and temperature). The findings of this study could provide an effective approach for agronomic improvement of microbial inoculants to enhance soil P mobilization for plant growth, either in intensive production or in agroecological applications in Morocco.

Materials and methods

Soil sample collection and analysis

Soil samples were taken from different rhizospheres of cultivated legumes, cereals, and spontaneous plants from different localities in Fes-Meknes regions. Plantations are located at different bioclimatic stages in four stations, namely Tafrant, Ait Saleh, Dayt Al Amira, and Ait Yaakoub. These locations are characterized by:

- Tafrant: Climate is warm and temperate, with less rainfall in winter. The average annual temperature is 18.1°C and average annual rainfall is 866 mm.
- Ait Saleh: Climate is warm and temperate. Rain falls mainly in winter, with relatively little rain in summer. It has an average annual temperature of 15.5°C and an average annual rainfall of 651 mm.
- Dayt Al Amira: Climate is warm and temperate. Rainfall is high even in the driest months. The average annual temperature is 12.1°C and the average annual rainfall is 683 mm.
- Ait Yaakoub: Climate is warm and temperate. In winter, rainfall is much higher than in summer. The average annual temperature is 17.8°C and the average annual rainfall is 549 mm (Climate-data.org, 2022).

Rhizospheric soil samples were carefully collected, placed in labeled sterile plastic bags, analyzed for physico-chemical characteristics and stored at −20°C before rhizobacteria isolation.

Isolation and purification of phosphate solubilizing bacteria

A soil suspension was prepared to isolate PSBs from a dilution cascade. For this purpose, 10 g of soil were suspended in 100 mL of sterile phosphate-buffered saline (PBS) solution (pH 7.2) and shaken at 190 rpm for 45 min. Subsequently, serial dilutions were prepared to 10^{-6}. About 100 µL of each dilution was placed on NBRIP agar plates (National Botanical Research in P medium), which has as composition: glucose 10 g, $(NH_4)_2SO_4$ 0.1 g, $MgSO_4.7H_2O$ 0.25 g, KCl 0.2 g, and agar 15 g, supplemented with 5 g RP from Khouribga phosphate mine and dissolved in 1,000 ml distilled water, and the medium is stabilized to pH 6.8 (Nautiyal, 1999). The NBRIP medium was then complemented with cycloheximide to inhibit fungal growth. NBRIP agars plates were incubated for 6 days at 28 ± 2°C. During this incubation, clear zones of solubilization surrounding the colony allowed the detection of PSBs. Every different morphological colony types were isolated, purified, and retested by restricting them from a single colony (five times) for purification on NBRIP plates and finally preserved in Tryptic Soy Agar (TSA) medium before cryopreservation in sterile glycerine (20%) at −80°C.

Quantitative estimation of phosphate solubilization indice

Colony diameter and visible halos were evaluated between 3 and 9 days after inoculation to calculate the P solubilization index (PSI) (Nautiyal, 1999). Halo and colony diameters were measured after 9 days of incubation on NBRIP plates' at 28 ± 2°C. Bacteria's ability to solubilize insoluble P was described by the solubilization index formula (Equation 1):

$$\mathbf{PSI} = \frac{CD+HD}{CD} \quad (1)$$

CD: Colony Diameter.
HD: Halo zone Diameter.

Quantitative estimation of phosphate solubilization using tricalcium phosphate, rock phosphate, and their combination

Phosphate solubilizing assessment

Phosphate solubilizing bacteria's quantitative solubilization capacity of TCP, RP, and their combination was done in a liquid NBRIP medium. For this purpose, overnight pre-culture in TSA medium was prepared and then moved to NBRIP medium. After 7 days of incubation at 28°C under shaking to 150 rpm, 20 ml of bacterial suspensions were taken and centrifuged (12,000 g for 15 min). Supernatants were recovered and analyzed for their assimilable P content and pH measurements. Assimilable P content was carried out by the ascorbic acid colorimetric method (Murphy and Riley, 1962). About 1 mL of supernatant is mixed with 160 µL of a reaction solution and the OD (optical density) was then measured at 880 nm after a few minutes of incubation at room temperature. Phosphate soluble content was calculated based on a standard P solution of KH_2PO_4 (concentrations ranging from 0 to 1 $mg.l^{-1}$).

TABLE 1 Factors' levels (X1 and X2) involved in P solubilization.

	Min level	Max level
	−1	+1
X_1 : RP	1%	2.5%
X_2 : TCP	1%	2.5%

Optimization study of combined rock phosphate and tricalcium phosphate solubilization system

Optimization strategy to reveal and quantify the influence of PSBs effect on the solubilization process of two combined phosphate sources (RP and TCP) was conducted following a two-level experimental design (2^2 = 4 experiments). Experimental domain of both factors [X_1 = (RP) and X_2 = (TCP)] are presented in Table 1. The experimental design was developed to study the effects of the two factors (X_1 and X_2) and their interaction (X_1*X_2) on the concentration of P solubilized and pH medium (Table 2).

Factors and their mathematical modeling interaction

The matrix analysis model of experimental design (Table 2) results in response functions indicating the coded factors' effects (X1 and X2) and their interaction, which has the following formula (Equation 2):

$$Y = a_0 + a_1X_1 + a_2X_2 + a_{12}X_1X_2 \quad (2)$$

$\mathbf{a_0}$: Coefficient model.

$\mathbf{a_1}$ and $\mathbf{a_2}$: Coefficients of the linear part of the mathematical model.

$\mathbf{a_{12}}$: Interaction coefficient of the two factors.

Mathematical analysis interactions between factors (X_1 and X_2) provide response surfaces and allow us to define the domains where there is a maximum or minimum response of the studied response functions ($Y_{P[C]}$ and Y_{pH}) experimentally.

Morphological and biochemical characterization

Phosphate solubilizing bacteria were characterized as described in Bergey's Manual (Systematic Bacteriology, 2nd ed., vol. 5, eds., 2012), and cells morphology, motility test, and Gram staining were performed (Aneja, 2007). Isolates were also tested for catalase, gelatinase, and urease activities (Graham and Parker, 1964; Aneja and Wilkes, 2003). Experiments were repeated three times for each isolate. To determine PSBs' capability to use starch as a source of carbon (Salgaonkar et al., 2018), PSBs were inoculated on starch agar media and incubated at 28°C ± 2°C for 24 h. Citrate utilization by the isolates was observed by growth on YEM agar containing sodium citrate in place of mannitol and supplemented with 1 ml of bromothymol blue (BTB) solution (1%) and incubated at 30°C. After incubation (7 days), a distinct change in color, from green

TABLE 2 Experimental design developed to study the effects of factors (X1: RP and X2: TCP) and their interaction (X1*X2) on pH medium and P concentration.

Experiment	X_0	X_1	X_2	X_{1*2}	$Y_{P[C]}$	Y_{pH}
1	+1	−1	−1	+1	–	–
2	+1	−1	+1	−1	–	–
3	+1	+1	−1	−1	–	–
4	+1	+1	+1	+1	–	–

$Y_{P[C]}$: concentration of P solubilized response function. Y_{pH}: pH medium response function.

TABLE 3 Physico-chemical and PSBs analysis of the studied soil samples.

Sites	Tafrant	A. Yaakoub	D.A. Amira	A. Saleh
Coordinates	Y −5.112751,X 34.615013	Y −4.950365,X 33.975209	Y −5.019709,X 33.692496	Y −4.992072,X 33.791152
Altitude (m)	312.5	566	1548	922
T.avg/year (°C)	18.1	17.8	12.1	15.5
P.avg/year (mm)	866	549	683	651
PSBs load (Cells / g of soil)	$5.95*10^3$	$1.98*10^5$	$1.04*10^6$	$3.16*10^7$
pH-water	8.26	8.323	8.067	8.273
Electrical conductivity 1/5 (ds/m)	187.033	300.333	241.233	173.2
Cation exchange capacity (cmol+/kg)	40.987	32.28	37.227	31.563
Organic matter (%)	2.573	5.103	5.64	4.38
N total (%)	0.126	0.255	0.324	0.174
$N\text{-}NH_4$ + $N\text{-}NO_3$ (mg/kg N)	7.383	8.867	8.167	7.4
P_2O_5 (mg/kg)	10	46.7	98.7	23.3
K_2O (mg/kg)	432	846.3	990.7	373
CaO (mg/kg)	9,450	8,550	5,250	6,375
MgO (mg/kg)	410.667	854	1213.333	917.333

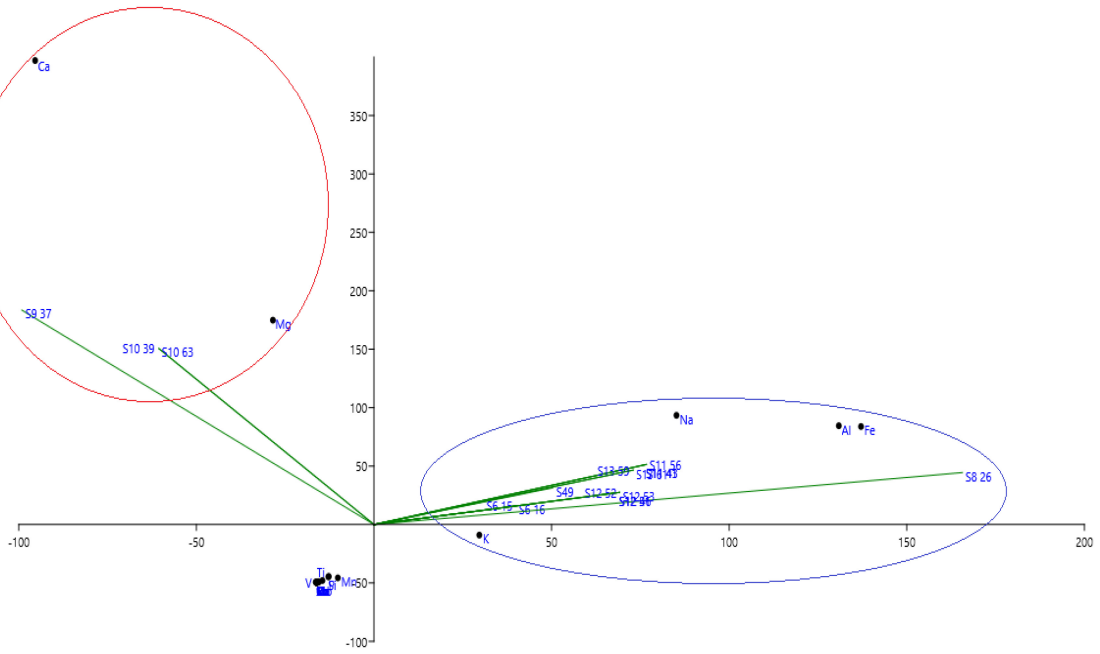

FIGURE 1
Principal component analysis of different soil in the function of mineralogical composition.

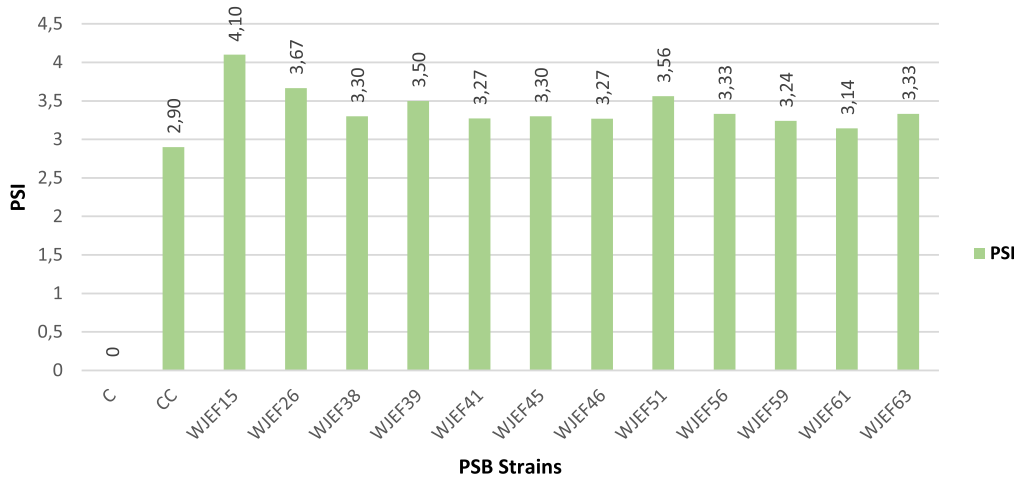

FIGURE 2
Phosphate solubilization index (PSI) of isolated strains on solid NBRIP medium.

to blue, refers to as a positive test. A glucose peptone agar (GPA) assay was performed to determine PSB's capability to use glucose as the sole source of carbon and energy for growth (Amela et al., 2018). Similarly, a lactose assay was performed (Paudyal et al., 2021).

Bacterial stress tolerance

Isolates salinity tolerance evaluation was done onto a liquid rich medium (TSA) containing different NaCl concentrations (0.2, 0.4, 0.6, 0.8, 1, 1.2, 1.6, and 2 M). Incubation was carried out at 28°C ± 2°C for 48 h. Then, absorbance was measured at 620 nm (Singh et al., 2015). As solubilization is strongly related to pH medium changes, isolates were inoculated on a solid TSA medium at different pH values starting from 3 to 13 and incubated at 28°C ± 2°C for 48 h. This test allows isolates selection that can grow over a wide range of soil pH (acid, neutral, and alkaline). Phosphate solubilizing bacteria isolates were also cultured onto a solid rich agar

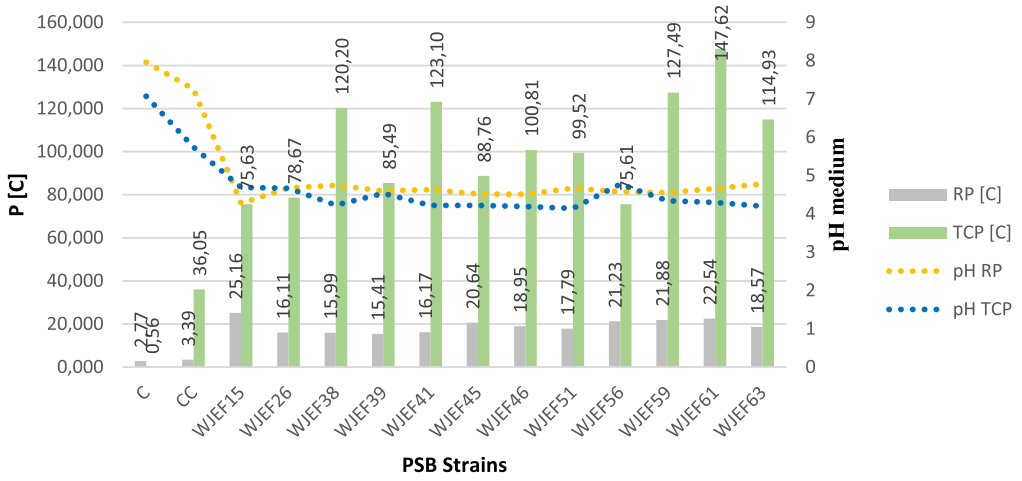

FIGURE 3
PSBs solubilization capacity of TCP and RP after 7 days in liquid medium.

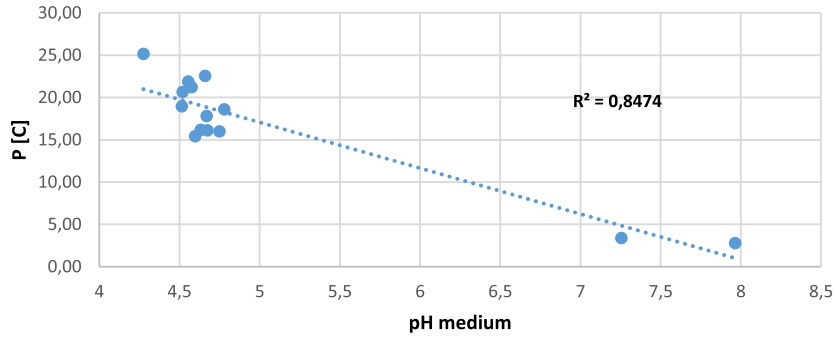

FIGURE 4
Negative correlation between pH medium and solubilization concentration.

medium (TSA) and incubated at 37, 48, and 55°C for 48 h to assess isolates' temperature tolerance through bacterial growth. In addition, drought tolerance of PSBs was assessed on a liquid medium (TSA) containing different concentrations of polyethylene glycol 6000 (PEG) (10, 20, and 30%). Incubation was carried out at 28°C ± 2°C for 24 h, after that absorbance assessment was done at 620 nm.

Antifungal effect of phosphate solubilizing bacteria strains

All 12 bacterial isolates were tested for their antagonistic effect against six fungal strains isolated from strawberry fruit and grown in a PDA medium. To assess antagonism, a 5-mm block (growing mycelium + medium) was placed in the middle of the Petri dish. Tested bacteria were placed in four different positions around the block. After incubation at 26°C ± 2°C for 24 h, a zone of inhibition between colonies and fungal strains indicates antagonism presence. Finally, isolates producing more than 15 mm of inhibition zone were selected. The inhibition rate of fungal growth was determined using the percentage of inhibited radial growth (% IRG) according to the following formula (Equation 3):

$$\%\ \mathrm{IRG} = \frac{\mathrm{R1} - \mathrm{R2}}{\mathrm{R1}} * 100 \quad (3)$$

$\mathbf{R}_1$ radial growth of control mycelium.
$\mathbf{R}_2$ radial growth of treated mycelium.

Statistical analysis

Data were analyzed using SPSS software, and the results were expressed as the means ± standard deviation of three replicates. Data were examined by ANOVA I analysis, and mean comparison was performed by Duncan's multiple range test at $p \leq 0.05$. Dimensional analysis done by principal component analysis (PCA) has been used to give a summarizing view of obtained results. For the design of the experiment

trial, all experiments were done in four replicates, and data were analyzed using JMP 4 software. Response surface of experimental design response functions (Y_{pH} and $Y_{P[C]}$) were done by Maple 9 software.

Results

Soil physico-chemical analysis

Soil samples' physico-chemical and PSBs contents are listed in Table 3. Agricultural legume soils analyzed contained, on average, 4.4% of Organic Matter, 7.9 (mg/Kg) of nitrogen, 44.65 (mg/Kg) of P_2O_5, 660.5 of K_2O (mg/Kg), 7,406.25 of CaO (mg/Kg), and 848.83 (mg/Kg) of MgO. Maximum electrical conductivity, reflecting soil salinity, was recorded in the Ait Yaakoub soil sample with an average of 300.33 (ds/m). In terms of soil pH, it was close to neutral or slightly basic (pH = 8.2 on average).

The mineralogical compositions of different analyzed sites with ICP are presented, respectively, in Figure 1. We notice that Al, Ca, Fe, K, Mg, Na, and P are the most important minerals in the studied sites. Based on principal component analysis of different sites in terms of mineralogical composition, we find that sites S9 (Dayt Al Amira) and S10 (Ait Saleh) are controlled by both Mg and Ca minerals, while all the other sites are controlled by Al, Fe, K, and Na minerals.

Selection and purification of phosphate solubilizing bacteria

Soil samples collected from different sites were used to study the PSB bacteria. Strains were selected based on colonies' morphological difference and halo resulting from TCP solubilization. Although, halo formation around colonies provides the first qualitative indication of PSB. Colonies that grew without forming a halo were also isolated to test their solubilization capacity. Initially, 134 isolates were selected; these isolates were transplanted onto the NBRIP medium three times to guarantee their efficiency and stability. Among 134 isolates, 64 were designated as PSB based on their solubilization of P on NBRIP liquid medium, and only 12 isolates were screened as promising biotechnological interest.

Quantitative estimation of phosphate solubilization indice

The appearance of the halo zone in all strains was noticed after 4th day of incubation, solubilization index ranged from 3.14 cm to 4.1 on average. Isolate WJEF15 showed a maximum solubilization index with PSI = 4.1 (Figure 2). Thus, a significant difference was found for all strains tested. We notice the existence of a correlation between incubation time and halo zone size, whereby the halo zone size of each isolate increases with incubation time.

Quantitative estimation of phosphate solubilization using tricalcium phosphate and rock phosphate

Soluble P and pH variations are presented in Figure 3. The solubilization of TCP, RP, and their combination in liquid NBRIP medium by tested strains was accompanied by a significant pH decrease. NBRIP-TCP soluble P concentration varied between 75.61 and 147.62 $mg.l^{-1}$, whereas NBRIP-RP soluble P concentration varied between 15.41 and 25.16 $mg.l^{-1}$ with significant variations between all strains when compared to control ($p \leq 0.05$). However, maximum solubilization in NBRIP-TCP liquid medium was observed for isolate WJEF61 (147.62 $mg.l^{-1}$). In contrast, for the NBRIP-RP medium, strain WJEF15 presented maximum solubilization with 25.16 $mg.l^{-1}$. On the other hand, commercial control solubilized only 36.05 $mg.l^{-1}$ of P with TCP and 3.39 $mg.l^{-1}$ with RP. Besides, NBRIP medium pH inoculated with selected strains strongly decreased from 7.06 to 4.145 (TCP) and from 7.97 to 4.28 (RP) after 7 days of incubation. Compared to the commercial control, it decreased to 5.74 and 7.26, respectively.

Correlation between pH medium and solubilization concentration

The correlation between P[C] and pH was positive in all strains with high P solubility. Correlation coefficients (R) were greater than 0.84 for P [C] vs. pH medium. However, in several applications, regression equations for P [C] vs. pH medium were linear models (Figure 4).

Design of experiments method to study tricalcium phosphate and rock phosphate interaction

Experimental matrix analysis design (Tables 4, 5) results (response functions) present coded factors' effects (X_1 and X_2) and their interaction ($X_1{*}X_2$) (Equation 2). The control (non-inoculated) was introduced to evaluate the chemical reaction of the medium.

Phosphate solubilization and pH medium results obtained by WJEF26 isolate according to the experimental design are summarized in Table 6. The values correspond to the mean of four replicates.

The main factors' effects (X_1 and X_2) and their interaction (X_1*X_2) of the WJEF26 strain, for example, are summarized in Figures 5A,B. We notice that factors' interaction on pH medium and P [C] have a positive effect in comparison to each factor alone.

For the strain WJEF63, P solubilization and pH medium results obtained according to the designed experiment are summarized in Table 7. Values correspond to the four replicates' mean.

Factors' effects (X_1 and X_2) and their interaction (X_1*X_2) of WJEF63 isolate are summarized in Figures 5C,D. We notice that factors' interaction on P [C] has a positive effect on the contract of each factor alone. On the other hand, the effect of factors alone or in interaction on pH medium have the same activity.

TABLE 4 Effect of phosphorus source (RP and TCP) on culture medium acidification.

Isolates	Model coefficient	RP effect	TCP effect	Interaction RP/TCP
Coefficients	a_0	a_1	a_2	a_{12}
Control	1.931	0.013	0.055	−0.016
Commercial control	0.335	−0.025	−0.079	0.016
WJEF15	3.278	−0.034	0.029	0.047
WJEF56	2.793	0.042	−0.019	−0.101
WJEF26	2.921	−0.020	−0.138	−0.019
WJEF38	3.237	0.063	0.047	−0.129
WJEF41	3.193	0.020	0.075	−0.143
WJEF45	3.222	0.011	0.146	−0.123
WJEF46	3.209	0.057	0.104	−0.076
WJEF51	3.261	0.009	0.101	−0.149
WJEF59	3.089	0.084	0.100	−0.115
WJEF61	3.237	0.051	0.092	−0.109
WJEF63	3.199	0.085	0.140	−0.161

TABLE 5 Impact of phosphorus source (RP and TCP) on P solubilization in culture medium.

Isolates	Model coefficient	RP effect	TCP effect	Interaction RP/TCP
Coefficients	a_0	a_1	a_2	a_{12}
Control	0.481	−0.055	−0.031	−0.049
Commercial control	1.076	−0.030	0.178	−0.037
WJEF15	14.637	−0.598	8.050	−0.405
WJEF56	10.102	0.228	4.623	−1.197
WJEF26	10.865	−2.116	3.722	−0.898
WJEF38	15.491	−1.406	7.430	−0.873
WJEF41	14.208	0.570	8.394	−2.034
WJEF45	14.513	0.912	8.628	−1.993
WJEF46	14.738	0.966	8.768	−1.774
WJEF51	16.397	−0.182	8.601	−1.119
WJEF59	16.196	0.008	7.785	−1.589
WJEF61	16.802	0.713	8.019	−1.779
WJEF63	16.574	1.452	8.743	−1.094

TABLE 6 Experimental design results done after P solubilization by isolate WJEF26.

Experiments	X_1	X_2	X_{12}	Y_{pH}	$Y_{P[C]}$
1	−1	−1	+1	4.3	33.442
2	+1	−1	−1	4.7725	23.696
3	−1	+1	−1	5.1175	70.405
4	+1	+1	+1	5.165	46.289

Y_{pH}: Function response of pH medium during P solubilization. $Y_{P[C]}$: Function response of P solubilization ($mg.l^{-1}$).

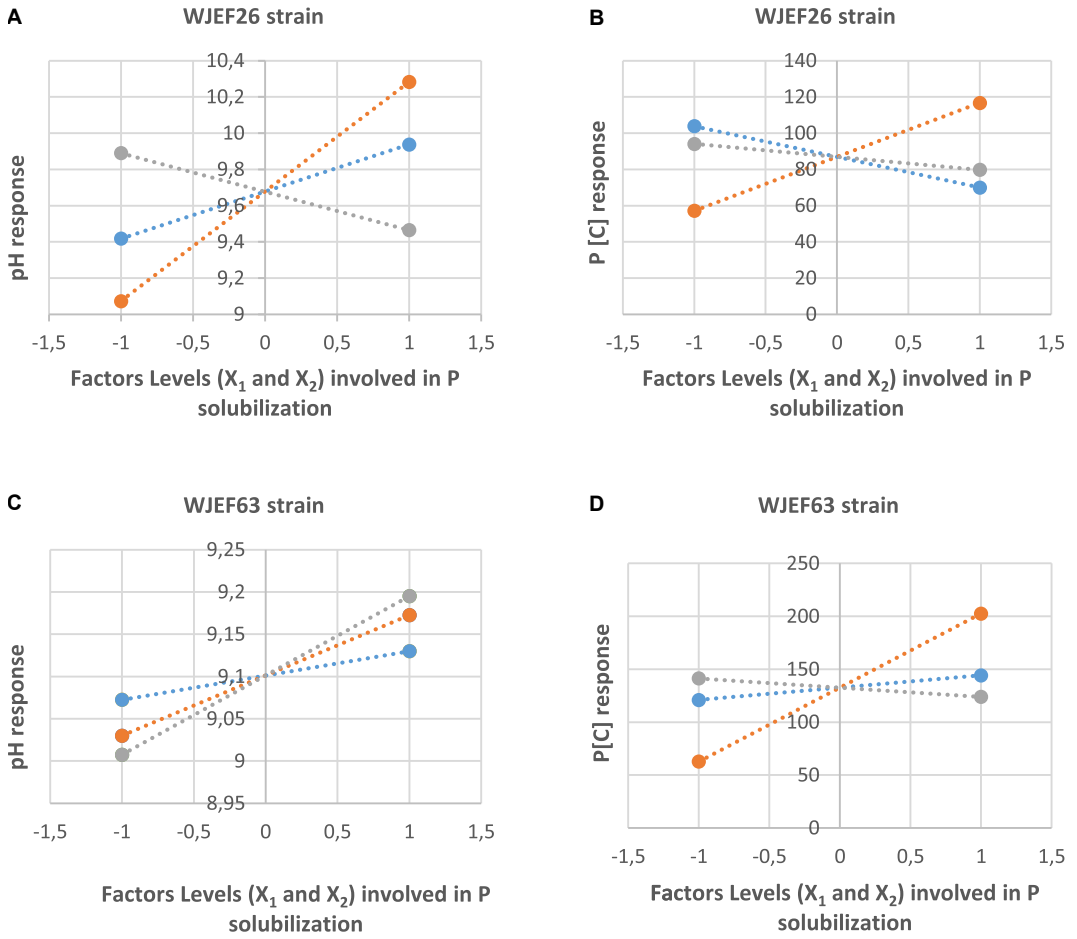

FIGURE 5
(A) Effects of studied factors (X_1 and X_2) and their interaction on pH medium in the presence of WJEF26 strain. **(B)** Effects of studied factors (X_1 and X_2) and their interaction on P[C] in the presence of WJEF26 strain. **(C)** Effects of studied factors (X_1 and X_2) and their interaction on pH medium in the presence of WJEF63 strain. **(D)** Effects of studied factors (X_1 and X_2) and their interaction on P[C] in the presence of WJEF63 strain.

TABLE 7 Experimental design results done after P solubilization by isolate WJEF63.

Experiments	X_1	X_2	X_{12}	Y_{pH}	$Y_{P[C]}$
1	−1	−1	+1	4.547	21.144
2	+1	−1	−1	4.482	41.505
3	−1	+1	−1	4.525	99.836
4	+1	+1	+1	4.647	102.699

Y_{pH}: Function response of pH medium during P solubilization. $Y_{P[C]}$: Function response of P solubilization ($mg.l^{-1}$).

Factor interaction is presented in Figure 6, where we observe the response surface according to coded variables (RP medium and TCP) which delimits the experimental domain. Figure 6A shows that the pH medium is maximal when RP is at the lowest level and TCP is at the highest level (1 and 2.5%, respectively). On the opposite, Figure 6B shows that P[C] is maximal when both factors X_1 and X_2 are at the highest level (2.5 and 2.5%, respectively).

The second example was done with the WJEF63 strain. The interaction of studied factors is presented in Figures 6C,D, where we observe the response surface according to coded variables (RP medium and TCP) which delimits the experimental domain. The figure shows that pH medium and P [C] is maximal when RP is at the lowest level and TCP is at the highest level (1 and 2.5%, respectively). From response surface function, we notice that strains' metabolic response depends on the nature of the used microorganisms.

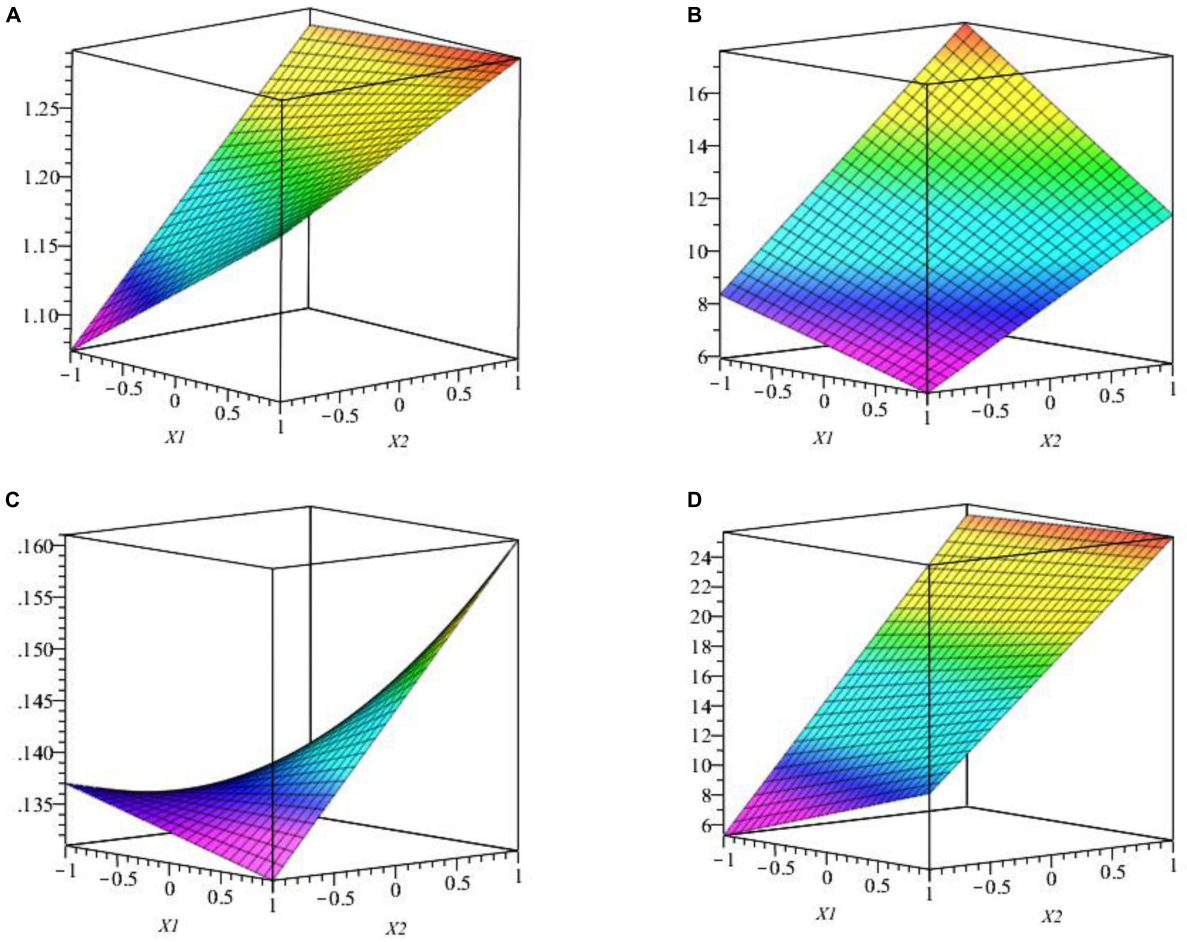

FIGURE 6
(A) The effect of studied factors (X_1 and X_2) and their interaction on pH surface response by WJEF26 strain. **(B)** The effect of studied factors (X_1 and X_2) and their interaction on the response surface of P[C] by WJEF26 strain. **(C)** Effect of studied factors (X_1 and X_2) and their interaction on response surface of pH with WJEF63 strain. **(D)** Effect of studied factors (X_1 and X_2) and their interaction on response surface of P[C] with WJEF63 strain.

Morphological and biochemical characteristics

The morphological profile of studied strains shows a whole appearance; irregular edges, white, off-white, or yellow color, and a mucoid or viscous texture. Cell structures show rod and coccobacillus shapes with an arrangement of single pairs, chain rods, and solitaires. Gram reaction indicates that all isolates were Gram-negative with the exception of five strains (WJEF15, WJEF38, WJEF41, WJEF45, and WJEF59). Cell motility test and catalase activity is positive for all selected strains (Table 8). Similarly, all strains grew on GPA with glucose or lactose as a source of carbon. The same results were obtained from the starch hydrolysis test except for WJEF61, WJEF52, and WJEF56 strains. After submitting inoculated plates to iodine vapor, clear areas around colonies were observed and the colonies turned yellow, while blue color occurs on growth-free areas. This indicates that two strains (WJEF56 and WJEF61) have the potential to hydrolyze starch present in the medium.

Bacterial tolerance to stresses

According to the results in Table 9, it is evident that selected strains are tolerant to considerable variations in terms of alkalinity, acidity, salinity, dryness, and temperature. All strains present tolerate temperatures between 24 and 37°C, except the strain WJEF56. Also, strains WJEF45, WJEF46, WJEF51, WJEF61, and WJEF63 were able to grow at temperatures up to 55°C. In addition, these isolates were able to grow and survive over a wide pH range (3–13). Moreover, among all tested isolates, only WJEF45, WJEF51, WJEF59, and WJEF61 were able to successfully resist higher NaCl concentrations (2M) g/L (Table 9).

TABLE 8 Morphological and biochemical characteristics of selected strains.

PSB strains/characteristics		Commercial control	WJEF15	WJEF26	WJEF38	WJEF39	WJEF41	WJEF45	WJEF46	WJEF51	WJEF56	WJEF59	WJEF61	WJEF63
Colony morphology	Margin	I	E	E	E	E	I	E	I	E	I	I	E	E
	Color	W	Y	Y	OW	Y	OW	OW	OW	OW	Y	Y	OW	OW
	Texture	D	V	V	V	V	M	V	M	V	M	M	V	V
Cells morphology	Shape	R	R	R	C	R	C	C	C	C	C	C	C	CB
	Arrangement	S	S	CR	S	S	S	S	S	SP	S	S	S	S
Physiological tests	Gram staining	+	+	−	+	−	+	+	−	−	−	+	−	−
	Catalase	+	+	+	+	+	+	+	+	+	+	+	+	+
	Motility	+	+	+	+	+	+	+	+	+	+	+	+	+
	Gelatin hydrolysis	−	+	+	−	+	−	−	−	−	+	+	−	−
	Urea hydrolysis	−	−	−	+	−	−	−	−	−	−	−	−	−
	GPA (Glucose)	+	+	+	+	+	+	+	+	+	+	+	+	+
	GPA (Lactose)	+	+	+	+	+	+	+	+	+	+	+	+	+
	Starch	−	−	−	−	−	−	−	−	−	+	−	+	−

Tested positive, utilized substrate; tested negative, not utilized substrate. E, entire; I, irregular; Y, yellow; W, white; OW, off-white; D, Dry; V, viscid; M, mucoid; R, rod; C, cocci; CB, coccobacillus; SP, single pairs; CR, chain rods; and S, solitaire.

TABLE 9 Physiological characteristics of selected isolates under temperature, pH, and salinity pressure.

PSB strains/pressures		Commercial control	WJEF15	WJEF26	WJEF38	WJEF39	WJEF41	WJEF45	WJEF46	WJEF51	WJEF56	WJEF59	WJEF61	WJEF63
GT	24°C	1	1	1	1	1	1	1	1	1	1	1	1	1
	37°C	1	1	1	1	1	1	1	1	1	−1	1	1	1
	48°C	1	−1	−1	1	1	1	1	1	1	1	1	1	1
	55°C	−1	−1	−1	−1	−1	−1	1	1	1	−1	−1	1	1
G pH	pH 3	−1	1	1	1	1	1	1	1	1	1	1	1	1
	pH 5	1	1	1	1	1	1	1	1	1	1	1	1	1
	pH 7	1	1	1	1	1	1	1	1	1	1	1	1	1
	pH 9	1	1	1	1	1	1	1	1	1	1	1	1	1
	pH 11	1	1	1	1	1	1	1	1	1	1	1	1	1
	pH 13	−1	1	1	1	1	1	1	1	1	1	1	1	1
GS	1.6M	1	1	1	−1	1	1	1	1	1	−1	1	1	1
	2M	−1	−1	−1	−1	−1	−1	1	−1	1	−1	1	1	−1

GT, growth temperature; GpH, growth pH; GS, growth salinity. Tested positive/utilized as substrate; tested negative/not utilized substrate.

10.3389/fmicb.2022.958300

To quantify tested PSBs' tolerance to high salt concentrations, we incubated PSBs in a nutrient-liquid medium, and after 24 h, we measured biomass formation expressed by absorbance. Log (AB) as a function of salt concentrations revealed that all strains significantly decreased at 1.5M NaCl concentration, except WJEF15, WJEF26, and WJEF39 strains, which resist and show positive growth (**Figure 7**).

Regarding drought tolerance, all 12 isolates show the same behavior under increasing PEG-6000 concentrations (10, 20, and 30%). PSB isolates exhibit a decline in cell numbers and absorbance value. However, the WJEF61 strain presented an optimal resistance, with an absorbance value higher than those of the other isolates and commercial control to all PEG levels (**Figure 8**).

Based on the principal correspondence analysis of tested strains on physico-chemical pressure, we notice that we have two major groups of strains, the first one is correlated with temperature and the second group is correlated with alkalinity, acidity, and salinity (**Figure 9**).

Antifungal effect of phosphate solubilizing bacteria strains

Fungal growth inhibitory of isolated PSBs was tested on six plant pathogenic fungi: *Aspergillus Niger, Fusarium Culmorum, Fusarium Oxysporum, Penicillium Digitatum, Penicillium Notatum*, and *Rhizopus Stolonifer* (**Table 10**). The antifungal activity showed that of the 12 bacteria, 3 (WJEF26, WJEF56, and WJEF61) were able to inhibit fungal growth of at least 4 fungi tested (**Table 10**). In addition, the best antagonist against tested fungi was located in the WJEF61 strain with an IRG percentage of 49.15, 23.51, 32.76, and 32.92% against *Aspergillus Niger*, *Fusarium Culmorum*, *Fusarium Oxysporum*, and *Rhizopus Stolonifer*, respectively. The WJEF59 strain has an antagonistic effect only against *R. Stolonifer* with a % IRG of 36.54% which presents a specific character (**Table 10**).

Discussion

The present study focused on the effect of several tolerant PSBs on different abiotic stresses to promote P solubilization from RP and TCP as the only P source in the context of biological fertilization and sustainable agricultural strategy. Increasing soil P concentrations *via* inorganic and organic soil P mobilization pools involve changes in pH and the release of P-mobilizing compounds such as carboxylates and phosphatases, which are exuded by the roots themselves or by micro-organisms in the rhizosphere. However, the selection of an efficient PSB is crucial, as it practically increases P in the plant rhizosphere (Aliyat et al., 2020). Phosphate solubilization capacity is considered a key factor in isolating highly efficient PSBs from agricultural soils (Aliyat et al., 2020). Among 134 PSB strains from different leguminous plants' rhizosphere in the Fez-Meknes region, only 12 (12) PSBs show phenotypic stability of P solubilization after five successive subcultures in the NBRIP-RP plates.

The solubility index (**Figure 2**) indicates a PSI of TCP in agreement with previous studies conducted on different plants' rhizosphere, where the PSBs solubility index ranges from 2 to 5.1 (Sadik et al., 2013; Rfaki et al., 2014; Manzoor et al., 2017). The PSB isolated strains used in this work were able to increase P availability in NBRIP liquid medium containing RP or TCP as a source of P, also a combination of RP * TCP. Our results support the idea that PSBs are characterized by their ability to easily and efficiently solubilize inorganic P (Elkoca et al., 2008; Anand et al., 2016; Adnan et al., 2019). This is confirmed with the use of *Bacillus subtilis* DSM 10, which improved the P nutrition of common beans in hydroponic experiments when plants were inoculated with *Rhizobium tropici* and grown with one of the two P sources (Pi or phytate) and co-inoculated with *B. subtilis* (Maougal et al., 2014). Our results show that soluble P concentration in the medium containing RP was between 16.11 $mg.l^{-1}$ and 25.16 $mg.l^{-1}$, while the medium containing TCP was between 75.61 $mg.l^{-1}$ and 147.62 $mg.l^{-1}$ (**Figure 3**). These results are in agreement with other studies done by Zaidi and El Naqa (2010) and Anand et al. (2016), who report that PSBs can solubilize insoluble inorganic P compounds, such as TCP, dicalcium P (DCP), hydroxyapatite, and RP. Phosphate solubilization is accompanied by a pH medium decrease when compared to control, both in media containing RP and TCP. Furthermore, we note that as pH values decrease, the P concentration increases. This is noted by Batool and Iqbal (2019), who indicate a strong correlation between P solubilization and pH decrease. Changes in pH value in the rhizosphere, caused by roots or microorganisms, can influence the surface charges on metal oxide particles and thus Pi availability (Hinsinger et al., 2009), ultimately leading to Pi release that is available to plants. P mobilization in the rhizosphere is largely due to pH changes induced by roots and/or associated microorganisms and to carboxylate exudation (Hinsinger et al., 2011). Soil pH is critical in determining the availability of inorganic forms of P (Hinsinger et al., 2009; Adnan et al., 2018), and it can also influence the fate of organic P through its impact on enzymatic activities. In neutral to alkaline soils, Pi occurs largely in various forms of Ca phosphate (mainly apatites) whereas, in acidic and deeply weathered soils, such as those abundant in the tropics, much of the soil Pi occurs as bound to and/or occluded in Fe and Al oxy (hydr) oxides (Jones and Oburger, 2011). As the positive charges on these minerals become increasingly positive with decreasing pH, greater amounts of P can be adsorbed at low rather than high pH. In addition, Ca-phosphates solubility is strongly increased with decreasing pH. Devau et al. (2011) showed that both increasing and decreasing pH could lead to an increase in soil

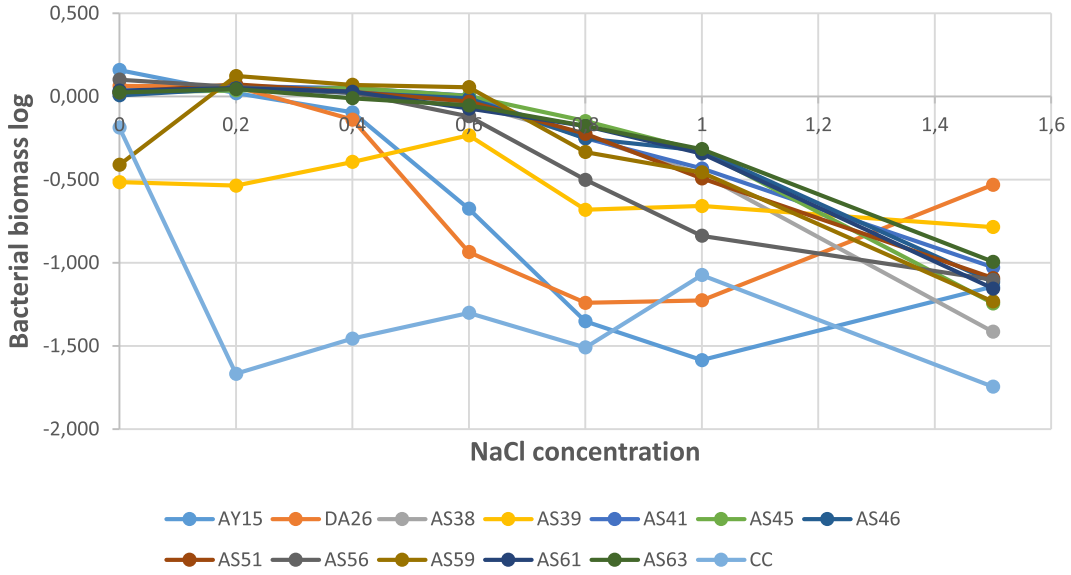

FIGURE 7
Biomass in function of salt concentrations g/L.

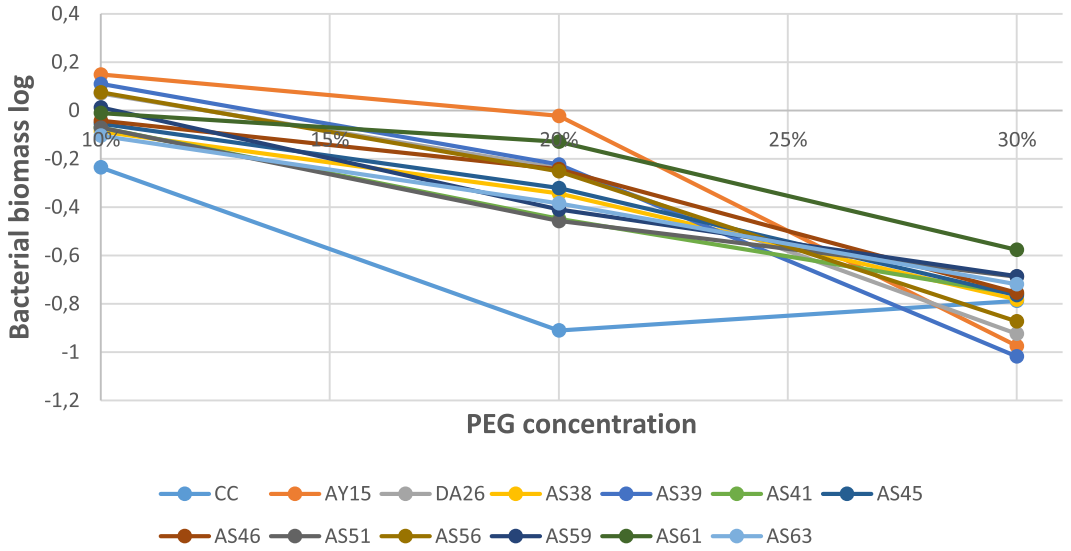

FIGURE 8
Biomass in the function of PEG concentrations.

P availability, which was consistent with the findings of previous studies, as reviewed by Hinsinger et al. (2009). Similarly, Alori et al. (2017) observed a negative correlation between the amount of P solubilized by *B. cepacia* (SCAUK0330) and decreasing pH, leading to increased solubilization of P. As proposed by Batool and Iqbal (2019), the decrease in pH can be explained by organic acid production and H^+ secretion. Several studies support this argument and indicate that the main mechanism of mineral P solubilization is lowering soil pH by microbial organic acid production (Rodríguez and Fraga, 1999; Khan et al., 2010; Sharma et al., 2013; Anand et al., 2016). The excretion of organic acids that promote Pi solubilization is a trait found in many P-solubilizing microorganisms. Rodríguez et al. (2007) listed several bacterial genes involved in gluconic acid oxidation, which is a major mechanism of mineral P solubilization in Gram-negative bacteria (Chauhan H. et al., 2015).

Experimental design results of P solubilization and pH medium are highly significant and show that pH medium and P[C] is maximal when RP and TCP are at the highest level (2.5 and 2.5%) (**Tables 6**, 7). However, Bashan et al. (2013)

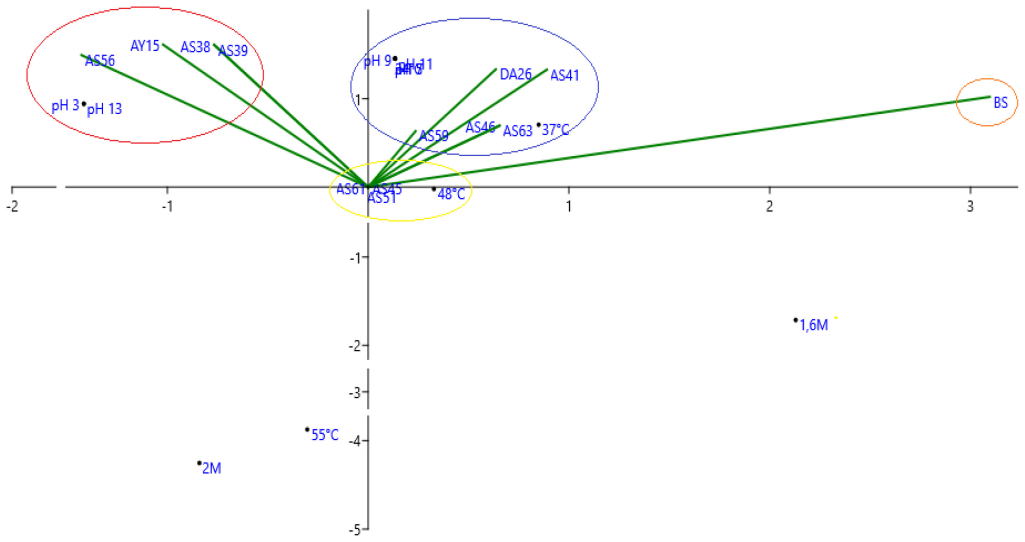

FIGURE 9
Principal correspondence analysis of tested isolates on physico-chemical pressure.

pointed out that the most commonly used source of insoluble Pi, tricalcium phosphate (TCP), is unreliable and insufficient; And also suggested that a combination of two or three metal-P compounds is used together or in tandem, depending on the type of soil and final use of screened bacteria. This would result in a significant reduction in potential PSBs and would also maximize the chances of selecting the most efficient strains capable of contributing to plant P nutrition. Our experiments show an increase in P solubilization accompanied by a decrease in pH, increasing as RP and TCP concentration increase (**Figures 5**, **6**). Similarly, Yadav et al. (2017) use organic compost with RP at different concentrations to optimize P solubilization by PSBs. They found that the 75:25 ratio of RP and compost showed maximum soluble P accompanied by higher plant growth when compared to plants fertilized with normal compost and rock phosphate. Our result can explain the Pi solubilization process by micro-organisms due to carboxylates and organic acids production. Concerning the free extracellular phosphatase enzymes, although it is difficult to differentiate their origin (Burns et al., 2013), several examples show that microbial enzymes are predominant in soil (Gao et al., 2019), and these present a higher efficiency for Pi release (Adnan et al., 2019). Different types of phosphatases can be found, including phosphomonoesterases, which have been most studied, especially for P-solubilizing microorganisms (Jones and Oburger, 2011).

On the other hand, as discussed by Khan et al. (2010), although there is a clear potential for the development of inoculants with PSBs, their widespread application remains limited by a poor understanding of microbial ecology, dynamics population in soil, and inconsistent performance in a range of environmental factors. However, although PSBs are present in the majority of soils, their performance is strongly influenced by environmental factors such as soil type, temperature, salinity, cation exchange capacity, pH, organic matter, and availability of substances in soils (Rfaki et al., 2018; Masdariah et al., 2019). Similarly, Namli et al. (2017) stated that resistance to extreme environmental conditions is an important characteristic that allows inoculant bacteria to survive and maintain optimal population numbers throughout a specific crop life cycle. Resistance to intrinsic and extrinsic stresses is an important factor for the proliferation, development, and survival of microorganisms in rhizospheric soils. In our study, to have a more appropriate approach for competent strains selection of PSB that could increase the chances of successful field inoculation and significantly improve plants' P status, all selected strains showed good tolerance to various environmental stresses such as increased temperature from 37 to 55°C, salinity ranging from 0.2 to 2 M, pH between 3 and 13 (**Table 9**), and drought variation of PEG-600 from 10 to 30% (**Figure 8**). Therefore, these microorganisms that survive under drastic conditions could be used in different cultural practices to improve agricultural production. Moreover, isolated PSBs showed a strong ability to inhibit different fungal species (**Table 10**). These results were confirmed by the findings of Muleta et al. (2009), who reported that several *Pseudomonas* strains which could inhibit phytopathogenic strain *Fusarium oxysporum* possess the ability to produce HCN, siderophores, and antibiotics.

Furthermore, Gram staining indicates a group of Gram-negative and Gram-positive strains, with an advantage for Gram-negatives (**Table 8**). Besides, previous observations have

10.3389/fmicb.2022.958300

TABLE 10 Fungal inhibited radial growth behavior of tested PSB.

PSB strains/Fungal strains	Commercial control	WJEF15	WJEF26	WJEF38	WJEF39	WJEF41	WJEF45	WJEF46	WJEF51	WJEF56	WJEF59	WJEF61	WJEF63
A. niger	21.31	–	23.21	–	–	–	–	–	21.42	–	49.15	–	–
F. culmorum	–	20.44	–	18.97	–	–	18	24	18.36	–	23.51	22.44	–
F. oxysporum	18.64	–	21.15	–	22.92	–	–	16.67	–	–	32.76	–	–
P. digitatum	26.92	–	–	–	–	33.89	–	–	20.33	–	–	–	–
P. notatum	25.53	–	16.03	–	–	–	–	–	18	–	–	–	–
R. stolonifer	–	23.07	21.15	17.31	26.93	30.77	25	–	–	36.54	32.92	19.23	21.42

shown that several plants' rhizosphere selects more Gram-negative than Gram-positive rhizobacteria (Muleta et al., 2009). The cell motility test indicates that all selected strains were motile (**Table 8**). Moreover, bacterial motility is considered to be an essential element for successful root colonization and P transfer in soil (Shahid et al., 2015). In addition, it has been reported that motile bacteria have better access to root exudates in the rhizospheric zone through chemotaxis (Shahid et al., 2015; Manzoor et al., 2017). Motility can potentially enhance the rhizoplane competence in terms of movement, both from bulk soil to root and along roots (Dutta and Podile, 2010), leading to heterogeneous colonization of host plant roots by the PGPR. After root surface colonization, PGPR can stimulate plant growth through several mechanisms impacting plant nutrition and, in some cases, also improving its resistance to pathogens (Pérez-Montaño et al., 2014).

However, PSB biotechnology offers an excellent opportunity to develop durable biofertilizers to be used as supplements and/or alternatives to chemical fertilizers to overcome agricultural challenges imposed by an ever-increasing food demand (Sharma et al., 2013). Moreover, with readily available carbon resources, free-living soil bacteria can rapidly mineralize P from soil organic matter and incorporate it into their biomass. Microbial P thus represents not only an important P sink in soil and terrestrial ecosystems but also a possible source of available P for plants (Xu et al., 2013). In addition to chemical fertilizers, PSBs application as biofertilizers could also promote plant growth with large amounts of soluble P (Pi, polyphosphates, and organic P) released from lysed bacterial cells following rewetting of dry soils or during freeze-thaw cycles at the beginning of the growing season. For example, Turner et al. (2003) showed that the potential contribution of bacterial cell lysis to water-extractable phosphorus following soil drying varied between 88 and 95% in two Australian pasture soils. In general, the selection of a competent strain of PSBs as an inoculant and their qualification as a biofertilizer should not only be based on laboratory and greenhouse experiments but also on field experiments.

Conclusion

The main objective of this study was to assess several PSB strains' ability to enhance solubilization activity from RP, TCP, and their combination. As a problem, inorganic P fixation into insoluble complexes renders these compounds inaccessible for plant absorption. The use of biofertilizers such as microorganisms can help in this regard by sustainably enhancing plant growth. Based on the mentioned results, we find that the isolated PSB strains have an antifungal effect of up

to 49.15% inhibition as well as a high capacity to resist intrinsic and extrinsic stress. In addition, we note that P solubilization significantly increased by 20.58% when RP and TCP percentages in combination are at the max level. By analyzing all the different orientations of this study, we recommended the use of PSBs strains with high potential as microbial fertilizers in the agronomic field. To exploit the full potential of these telluric bacteria, more studies are need to be investigated on the genetic mechanisms level and microbial-mineral interfaces. Further innovative research should focus on the application concepts of microbial biotechnology in agriculture to identify more PSBs for their usage in a consortium to have competent microbial inoculants in sustainable cultures' production systems under various conditions.

Data availability statement

The original contributions presented in this study are included in the article/supplementary material, further inquiries can be directed to the corresponding author/s.

Author contributions

All authors listed have made a substantial, direct, and intellectual contribution to the work, and approved it for publication.

Conflict of interest

The authors declare that the research was conducted in the absence of any commercial or financial relationships that could be construed as a potential conflict of interest.

Publisher's note

All claims expressed in this article are solely those of the authors and do not necessarily represent those of their affiliated organizations, or those of the publisher, the editors and the reviewers. Any product that may be evaluated in this article, or claim that may be made by its manufacturer, is not guaranteed or endorsed by the publisher.

References

Acevedo, E., Galindo-Castañeda, T., Prada, F., Navia, M., and Romero, H. M. (2014). Phosphate-solubilizing microorganisms associated with the rhizosphere of oil palm (*Elaeis guineensis* Jacq.) in Colombia. *Appl. Soil Ecol.* 80, 26–33. doi: 10.1016/j.apsoil.2014.03.011

Adnan, M., Fahad, S., Khan, I. A., Saeed, M., Ihsan, M. Z., Saud, S., et al. (2019). Integration of poultry manure and phosphate solubilizing bacteria improved availability of Ca bound P in calcareous soils. *3 Biotech* 9:368. s doi: 10.1007/s13205-019-1894-2

Adnan, M., Fahad, S., Zamin, M., Shah, S., Mian, I. A., Danish, S., et al. (2020). Coupling phosphate-solubilizing bacteria with phosphorus supplements improve maize phosphorus acquisition and growth under lime induced salinity stress. *Plants* 9:900. doi: 10.3390/plants9070900

Adnan, M., Shah, Z. Prof Dr, Sharif, M. N., and Rahman, H. (2018). Liming induces carbon dioxide (CO_2) emission in PSB inoculated alkaline soil supplemented with different phosphorus sources. *Environ. Sci. Pollut. Res.* 25, 9501–9509. doi: 10.1007/s11356-018-1255-4

Aliyat, F. Z., Maldani, M., El Guilli, M., Nassiri, L., and Ibijbijen, J. (2020). Isolation and characterization of phosphate solubilizing bacteria from phosphate solid sludge of the moroccan phosphate mines. *Open Agric. J.* 14, 16–24. doi: 10.2174/1874331502014010016

Alok, S., Jain, S. K., Verma, A., Kumar, M., Mahor, A., and Sabharwal, M. (2013). Plant profile, phytochemistry and pharmacology of *Asparagus racemosus* (Shatavari): A review. *Asian Pac. J. Trop. Dis.* 3, 242–251. doi: 10.1016/S2222-1808(13)60049-3

Alori, E. T., Glick, B. R., and Babalola, O. O. (2017). Microbial phosphorus solubilization and its potential for use in sustainable agriculture. *Front. Microbiol.* 8:971. doi: 10.3389/fmicb.2017.00971

Amela, B., Tellah, S., Faiza, O., and Ounane, S. (2018). Characterization of rhizobia from root nodule and rhizosphere of *Vicia faba* in Algeria. *Legume Res.* 41, 624–628. doi: 10.18805/LR-399

Anand, K., Kumari, B., and Mallick, M. A. (2016). Phosphate solubilizing microbes: An effective and alternative approach as biofertilizers. *Int. J. Pharm. Pharm. Sci.* 8, 37–40.

Aneja, A., and Wilkes, G. L. (2003). A systematic series of 'model' PTMO based segmented polyurethanes reinvestigated using atomic force microscopy. *Polymer* 44, 7221–7228. doi: 10.1016/j.polymer.2003.07.007

Aneja, K. R. (2007). *Experiments in microbiology, plant pathology and biotechnology*. New Delhi: New Age International.

Bahadur, I., Maurya, B. R., Meena, V. S., Saha, M., Kumar, A., and Aeron, A. (2016). Mineral release dynamics of tricalcium phosphate and waste muscovite by mineral-solubilizing rhizobacteria isolated from indo-gangetic plain of India. *Geomicrobiol. J.* 34, 1–13. doi: 10.1080/01490451.2016.1219431

Baig, K. S., Arshad, M., Shaharoona, B., Khalid, A., and Ahmed, I. (2012). Comparative effectiveness of *Bacillus* spp. Possessing either dual or single growth-promoting traits for improving phosphorus uptake, growth and yield of wheat (*Triticum aestivum* L.). *Ann. Microbiol.* 62, 1109–1119.

Balemi, T., and Negisho, K. (2012). Management of soil phosphorus and plant adaptation mechanisms to phosphorus stress for sustainable crop production: A review. *J. Soil Sci. Plant Nutr.* 12, 547–562. doi: 10.4067/S0718-95162012005000015

Barber, S. A. (1995). *Soil nutrient bioavailability: A mechanistic approach*. Hoboken, NJ: John Wiley & Sons.

Bashan, Y., Kamnev, A. A., and de-Bashan, L. E. (2013). Tricalcium phosphate is inappropriate as a universal selection factor for isolating and testing phosphate-solubilizing bacteria that enhance plant growth: A proposal for an alternative procedure. *Biol. Fertil. Soils* 49, 465–479. doi: 10.1007/s00374-012-0737-7

Batool, S., and Iqbal, A. (2019). Phosphate solubilizing rhizobacteria as alternative of chemical fertilizer for growth and yield of *Triticum aestivum* (Var. Galaxy 2013). *Saudi J. Biol. Sci.* 26, 1400–1410. doi: 10.1016/j.sjbs.2018.05.024

Behera, B. C., Yadav, H., Singh, S. K., Mishra, R. R., Sethi, B. K., Dutta, S. K., et al. (2017). Phosphate solubilization and acid phosphatase activity of *Serratia* sp. Isolated from mangrove soil of Mahanadi river delta, Odisha, India. *J. Genet. Eng. Biotechnol.* 15, 169–178. doi: 10.1016/j.jgeb.2017.01.003

Burns, R. G., DeForest, J. L., Marxsen, J., Sinsabaugh, R. L., Stromberger, M. E., Wallenstein, M. D., et al. (2013). Soil enzymes in a changing environment: Current knowledge and future directions. *Soil Biol. Biochem.* 58, 216–234.

Castagno, L. N., Estrella, M. J., Sannazzaro, A. I., Grassano, A. E., and Ruiz, O. A. (2011). Phosphate-solubilization mechanism and in vitro plant growth promotion activity mediated by *Pantoea eucalypti* isolated from *Lotus tenuis* rhizosphere in the salado river basin (Argentina): Phosphate-solubilization and plant growth promotion. *J. Appl. Microbiol.* 110, 1151–1165. doi: 10.1111/j.1365-2672.2011.04968.x

Chauhan, A., Bharti, P. K., Goyal, P., Varma, A., and Jindal, T. (2015). Psychrophilic *Pseudomonas* in antarctic freshwater lake at stornes peninsula, larsemann hills over east Antarctica. *Springerplus* 4:582. doi: 10.1186/s40064-015-1354-3

Chauhan, H., Bagyaraj, D. J., Selvakumar, G., and Sundaram, S. P. (2015). Novel plant growth promoting rhizobacteria—Prospects and potential. *Appl. Soil Ecol.* 95, 38–53. doi: 10.1016/j.apsoil.2015.05.011

Choudhury, A., and Kennedy, I. (2005). Nitrogen fertilizer losses from rice soils and control of environmental pollution problems. *Commun. Soil Sci. Plant Anal.* 36, 1625–1639. doi: 10.1081/CSS-200059104

Devau, N., Hinsinger, P., Le Cadre, E., Colomb, B., and Gérard, F. (2011). Fertilization and pH effects on processes and mechanisms controlling dissolved inorganic phosphorus in soils. *Geochim. Cosmochim. Acta* 75, 2980–2996. doi: 10.1016/j.gca.2011.02.034

Dutta, S., and Podile, A. R. (2010). Plant Growth Promoting Rhizobacteria (PGPR): The bugs to debug the root zone. *Crit. Rev. Microbiol.* 36, 232–244. doi: 10.3109/10408411003766806

Elkoca, E., Kantar, F., and Sahin, F. (2008). Influence of nitrogen fixing and phosphorus solubilizing bacteria on the nodulation, plant growth, and yield of chickpea. *J. Plant Nutr.* 31, 157–171. doi: 10.1080/01904160701742097

Fernández, V., Guzmán, P., Peirce, C. A. E., McBeath, T. M., Khayet, M., and McLaughlin, M. J. (2014). Effect of wheat phosphorus status on leaf surface properties and permeability to foliar-applied phosphorus. *Plant Soil* 384, 7–20. doi: 10.1007/s11104-014-2052-6

Gao, S., DeLuca, T. H., and Cleveland, C. C. (2019). Biochar additions alter phosphorus and nitrogen availability in agricultural ecosystems: A meta-analysis. *Sci. Total Environ.* 654, 463–472. doi: 10.1016/j.scitotenv.2018.11.124

Graham, P. H., and Parker, C. A. (1964). Diagnostic features in the characterisation of the root-nodule bacteria of legumes. *Plant Soil* 20, 383–396.

Gyaneshwar, P., Kumar, G. N., Parekh, L. J., and Poole, P. S. (2002). Role of soil microorganisms in improving P nutrition of plants. *Plant Soil* 245, 133–143.

Hakkou, R., Benzaazoua, M., and Bussière, B. (2016). Valorization of phosphate waste rocks and sludge from the moroccan phosphate mines: Challenges and perspectives. *Procedia Eng.* 138, 110–118. doi: 10.1016/j.proeng.2016.02.068

Hinsinger, P., Bengough, A. G., Vetterlein, D., and Young, I. M. (2009). Rhizosphere: Biophysics, biogeochemistry and ecological relevance. *Plant Soil* 321, 117–152. doi: 10.1007/s11104-008-9885-9

Hinsinger, P., Betencourt, E., Bernard, L., Brauman, A., Plassard, C., Shen, J., et al. (2011). Focus issue on phosphorus plant physiology: P for two, sharing a scarce resource: Soil phosphorus acquisition in the rhizosphere of intercropped species. *Plant Physiol.* 156, 1078–1086. doi: 10.1104/pp.111.175331

Islam, M. S., Fahad, S., Hossain, A., Chowdhury, M., Iqbal, M. A., Dubey, D.-A., et al. (2021). "Legumes under drought stress: Plant responses, adaptive mechanisms and management strategies in relation to nitrogen fixation," in *Engineering tolerance in crop plants against abiotic stress*, eds S. Fahad, et al., (Boca Raton: CRC Press), 336. doi: 10.1201/9781003160717-9

Izhar Shafi, M., Adnan, M., Fahad, S., Wahid, F., Khan, A., Yue, Z., et al. (2020). Application of single superphosphate with humic acid improves the growth, yield and phosphorus uptake of wheat (*Triticum aestivum* L.) in calcareous soil. *Agronomy* 10:1224. doi: 10.3390/agronomy10091224

Janati, W., Benmrid, B., Elhaissoufi, W., Youssef, Z., Nasielski, J., and Adnane, B. (2021). Will P bio-solubilization stimulate biological N2 fixation in grain legumes? *Front. Agron.* 3:637196. doi: 10.3389/fagro.2021.637196

Joe, M. M., Deivaraj, S., Benson, A., Henry, A. J., and Narendrakumar, G. (2018). Soil extract calcium phosphate media for screening of phosphate-solubilizing bacteria. *Agric. Nat. Resour.* 52, 305–308. doi: 10.1016/j.anres.2018.09.014

Jones, D., and Oburger, E. (2011). "Solubilization of phosphorus by soil microorganisms," in *Phosphorus in action*, Vol. 26, eds E. Bunemann, A. Oberson, and E. Frossard (Berlin: Springer Science and Business Media), 169–198. doi: 10.1007/978-3-642-15271-9_7

Khan, M. A., Asaf, S., Khan, A. L., Jan, R., Kang, S.-M., Kim, K.-M., et al. (2020). Thermotolerance effect of plant growth-promoting *Bacillus cereus* SA1 on soybean during heat stress. *BMC Microbiol.* 20:175. doi: 10.1186/s12866-020-01822-7

Khan, M. S., Zaidi, A., Ahemad, M., Oves, M., and Wani, P. A. (2010). Plant growth promotion by phosphate solubilizing fungi – Current perspective. *Arch. Agron. Soil Sci.* 56, 73–98. doi: 10.1080/03650340902806469

Kour, D., Rana, K. L., Yadav, A. N., Yadav, N., Kumar, M., Kumar, V., et al. (2020). Microbial biofertilizers: Bioresources and eco-friendly technologies for agricultural and environmental sustainability. *Biocatal. Agric. Biotechnol.* 23:101487. doi: 10.1016/j.bcab.2019.101487

Linu, M. S., Asok, A. K., Thampi, M., Sreekumar, J., and Jisha, M. S. (2019). Plant growth promoting traits of indigenous phosphate solubilizing *Pseudomonas aeruginosa* isolates from chilli (*Capsicum annuum* L.) rhizosphere. *Commun. Soil Sci. Plant Anal.* 50, 444–457. doi: 10.1080/00103624.2019.1566469

Liu, L., Li, C., Zhu, S., Xu, Y., Li, H., Zheng, X., et al. (2020). Combined application of organic and inorganic nitrogen fertilizers affects soil prokaryotic communities compositions. *Agronomy* 10:132. doi: 10.3390/agronomy10010132

Malhotra, H., Vandana, Sharma, S., and Pandey, R. (2018). "Phosphorus nutrition: Plant growth in response to deficiency and excess," in *Plant nutrients and abiotic stress tolerance*, eds M. Hasanuzzaman, M. Fujita, H. Oku, K. Nahar, and B. Hawrylak-Nowak (Singapore: Springer), 171–190. doi: 10.1007/978-981-10-9044-8_7

Manzoor, M., Abbasi, M. K., and Sultan, T. (2017). Isolation of phosphate solubilizing bacteria from maize rhizosphere and their potential for rock phosphate solubilization–mineralization and plant growth promotion. *Geomicrobiol. J.* 34, 81–95. doi: 10.1080/01490451.2016.1146373

Maougal, R. T., Adnane, B., Sahel, C., Amenc, L., Abdelhamid, D., Plassard, C., et al. (2014). Localization of the *Bacillus subtilis* beta-propeller phytase transcripts in nodulated roots of *Phaseolus vulgaris* supplied with phytate. *Planta* 239, 901–908. doi: 10.1007/s00425-013-2023-9

Mara, P. R., Isabel, C. M. C. J., Luiz, C. R., dos, S., Marcos, A. S., Flvia, D. P., et al. (2014). Phosphate solubilization and phytohormone production by endophytic and rhizosphere *Trichoderma* isolates of guanandi (*Calophyllum brasiliense* Cambess). *Afr. J. Microbiol. Res.* 8, 2616–2623. doi: 10.5897/AJMR2014.6633

Masdariah, Sembiring, M., Mukhlis, and Rosneli. (2019). The increasing of phosphorus availability and corn growth (Zea mays l.) With the application of phosphate solubilizing microbes and some sources of organic materials on andisol. *IOP Conf. Ser. Earth Environ. Sci.* 260:012166. doi: 10.1088/1755-1315/260/1/012166

Muleta, D., Assefa, F., Hjort, K., Roos, S., and Granhall, U. (2009). Characterization of rhizobacteria isolated from wild *Coffea arabica* L. *Eng. Life Sci.* 9, 100–108. doi: 10.1002/elsc.200700031

Murphy, J., and Riley, J. P. (1962). A modified single solution method for the determination of phosphate in natural waters. *Anal. Chim. Acta* 27, 31–36. doi: 10.1016/S0003-2670(00)88444-5

Namli, A., Mahmood, A., Sevilir, B., and Özkir, E. (2017). Effect of phosphorus solubilizing bacteria on some soil properties, wheat yield and nutrient contents. *Eurasian J. Soil Sci.* 6, 249–258. doi: 10.18393/ejss.293157

Nautiyal, C. S. (1999). An efficient microbiological growth medium for screening phosphate solubilizing microorganisms. *FEMS Microbiol. Lett.* 170, 265–270.

Paudyal, S. P., Kunwar, B., Paudel, N., and Das, B. D. (2021). Isolation and characterization of rhizobia from the root nodule of some cultivated legume crops. *Eur. J. Biol. Res.* 11, 294–306.

Pérez-Montaño, F., Alías-Villegas, C., Bellogín, R. A., del Cerro, P., Espuny, M. R., Jiménez-Guerrero, I., et al. (2014). Plant growth promotion in cereal and leguminous agricultural important plants: From microorganism capacities to crop production. *Microbiol. Res.* 169, 325–336. doi: 10.1016/j.micres.2013.09.011

Rajkumar, R., and Kurinjimalar, C. (2021). "Microbes and plant mineral nutrition," in *Microbiological activity for soil and plant health management*, eds R. Soni, D. C. Suyal, P. Bhargava, and R. Goel (Berlin: Springer), 111–132. doi: 10.1007/978-981-16-2922-8_5

Razaq, M., Zhang, P., Shen, H., and Salahuddin. (2017). Influence of nitrogen and phosphorous on the growth and root morphology of *Acer mono*. *PLoS One* 12:e0171321. doi: 10.1371/journal.pone.0171321

Rfaki, A., Nassiri, L., and Ibijbijen, J. (2014). Phosphate-solubilizing bacteria in the rhizosphere of some cultivated legumes from Meknes region, Morocco. *Br. Biotechnol. J.* 4, 946–956. doi: 10.9734/BBJ/2014/12387

Rfaki, A., Zennouhi, O., Nassiri, L., and Ibijbijen, J. (2018). Soil properties related to the occurrence of rock phosphate-solubilizing bacteria in the rhizosphere soil of faba bean (*Vicia faba* L.) in Morocco. *Soil Syst.* 2:31. doi: 10.3390/soilsystems2020031

Rodríguez, H., Fraga, R., Gonzalez, T., and Bashan, Y. (2007). Genetics of phosphate solubilization and its potential applications for improving plant growth-promoting bacteria. *Dev. Plant Soil Sci.* 287, 15–21.

Rodríguez, H., and Fraga, R. (1999). Phosphate solubilizing bacteria and their role in plant growth promotion. *Biotechnol. Adv.* 17, 319–339. doi: 10.1016/S0734-9750(99)00014-2

Sadik, J. A., Demelash, B., and Gizaw, M. (2013). Hydration kinetics of teff grain. *Agric. Eng. Int. J.* 15, 124–130.

Salgaonkar, M., Nadar, S. S., and Rathod, V. K. (2018). Combi-metal organic framework (Combi-MOF) of α-amylase and glucoamylase for one pot starch hydrolysis. *Int. J. Biol. Macromol.* 113, 464–475. doi: 10.1016/j.ijbiomac.2018.02.092

Salvagiotti, F., Prystupa, P., Ferraris, G., Couretot, L., Magnano, L., Dignani, D., et al. (2017). N:P:S stoichiometry in grains and physiological attributes associated with grain yield in maize as affected by phosphorus and sulfur nutrition. *Field Crops Res.* 203, 128–138. doi: 10.1016/j.fcr.2016.12.019

Sanz-Sáez, Á, Koester, R. P., Rosenthal, D. M., Montes, C. M., Ort, D. R., and Ainsworth, E. A. (2017). Leaf and canopy scale drivers of genotypic variation in soybean response to elevated carbon dioxide concentration. *Glob. Change Biol.* 23, 3908–3920. doi: 10.1111/gcb.13678

Seenivasagan, R., and Babalola, O. O. (2021). Utilization of microbial consortia as biofertilizers and biopesticides for the production of feasible agricultural product. *Biology* 10:1111. doi: 10.3390/biology10111111

Shahid, M., Hameed, S., Tariq, M., Zafar, M., Ali, A., and Ahmad, N. (2015). Characterization of mineral phosphate-solubilizing bacteria for enhanced sunflower growth and yield-attributing traits. *Ann. Microbiol.* 65, 1525–1536. doi: 10.1007/s13213-014-0991-z

Sharma, S. B., Sayyed, R. Z., Trivedi, M. H., and Gobi, T. A. (2013). Phosphate solubilizing microbes: Sustainable approach for managing phosphorus deficiency in agricultural soils. *Springerplus* 2:587. doi: 10.1186/2193-1801-2-587

Singh, R. P., Jha, P., and Jha, P. N. (2015). The plant-growth-promoting bacterium *Klebsiella* sp. SBP-8 confers induced systemic tolerance in wheat (*Triticum aestivum*) under salt stress. *J. Plant Physiol.* 184, 57–67. doi: 10.1016/j.jplph.2015.07.002

Suleman, M., Yasmin, S., Rasul, M., Yahya, M., Atta, B. M., and Mirza, M. S. (2018). Phosphate solubilizing bacteria with glucose dehydrogenase gene for phosphorus uptake and beneficial effects on wheat. *PLoS One* 13:e0204408. doi: 10.1371/journal.pone.0204408

Tiwari, S., Patel, A., Pandey, N., Raju, A., Singh, M., and Prasad, S. M. (2020). "Deficiency of essential elements in crop plants," in *Sustainable solutions for elemental deficiency and excess in crop plants*, eds K. Mishra, P. K. Tandon, and S. Srivastava (Berlin: Springer), 19–52. doi: 10.1007/978-981-15-8636-1_2

Turner, B. L., Driessen, J. P., Haygarth, P. M., and Mckelvie, I. D. (2003). Potential contribution of lysed bacterial cells to phosphorus solubilisation in two rewetted Australian pasture soils. *Soil Biol. Biochem.* 35, 187–189. doi: 10.1016/S0038-0717(02)00244-4

Vaishampayan, A., Sinha, R. P., Häder, D.-P., Dey, T., Gupta, A. K., Bhan, U., et al. (2001). Cyanobacterial biofertilizers in rice agriculture. *Bot. Rev.* 67, 453–516.

Xu, X., Thornton, P., and Post, W. (2013). A global analysis of soil microbial biomass carbon, nitrogen and phosphorus in terrestrial ecosystems. *Glob. Ecol. Biogeogr.* 22, 737–749. doi: 10.1111/geb.12029

Yadav, H., Fatima, R., Sharma, A., and Mathur, S. (2017). Enhancement of applicability of rock phosphate in alkaline soils by organic compost. *Appl. Soil Ecol.* 113, 80–85. doi: 10.1016/j.apsoil.2017.02.004

Zaidi, H., and El Naqa, I. (2010). PET-guided delineation of radiation therapy treatment volumes: A survey of image segmentation techniques. *Eur. J. Nucl. Med. Mol. Imaging* 37, 2165–2187. doi: 10.1007/s00259-010-1423-3

frontiers | Frontiers in Microbiology

TYPE Original Research
PUBLISHED 29 September 2022
DOI 10.3389/fmicb.2022.958522

OPEN ACCESS

EDITED BY
Muhammad Zahid Mumtaz,
The University of Lahore, Pakistan

REVIEWED BY
Fasih Ullah Haider,
South China Botanical Garden (CAS), China
Muhammad Baqir Hussain,
MNS University of Agriculture, Multan, Pakistan
Sudhir K. Upadhyay,
Veer Bahadur Singh Purvanchal University, India

*CORRESPONDENCE
Sajid Mahmood Nadeem
smnadeem@uaf.edu.pk
Muhammad Sohaib
msohaib@ksu.edu.sa

†These authors have contributed equally to this work and share first authorship

SPECIALTY SECTION
This article was submitted to Terrestrial Microbiology, a section of the journal Frontiers in Microbiology

RECEIVED 31 May 2022
ACCEPTED 26 August 2022
PUBLISHED 29 September 2022

CITATION
Khan MY, Nadeem SM, Sohaib M, Waqas MR, Alotaibi F, Ali L, Zahir ZA and Al-Barakah FNI (2022) Potential of plant growth promoting bacterial consortium for improving the growth and yield of wheat under saline conditions.
Front. Microbiol. 13:958522.
doi: 10.3389/fmicb.2022.958522

Potential of plant growth promoting bacterial consortium for improving the growth and yield of wheat under saline conditions

Muhammad Yahya Khan[1†], Sajid Mahmood Nadeem[1*†], Muhammad Sohaib[2*], Muhammad Rashid Waqas[1], Fahad Alotaibi[2], Liaqat Ali[1], Zahir Ahmad Zahir[3] and Fahad N. I. Al-Barakah[2]

[1]Sub-Campus Burewala-Vehari, University of Agriculture, Faisalabad, Pakistan, [2]Department of Soil Sciences, College of Food and Agricultural Sciences, King Saud University, Riyadh, Saudi Arabia, [3]Institute of Soil and Environmental Sciences, University of Agriculture, Faisalabad, Pakistan

Owing to inconsistent results of a single bacterial strain, co-inoculation of more than one strain under salinity stress could be a more effective strategy to induce salt tolerance. Co-inoculation of more than one bacterial strain could be more effective due to the presence of several growths promoting traits. This study was conducted to evaluate the effectiveness of multi-strains bacterial consortium to promote wheat growth under salinity stress. Several plant growth promoting rhizobacteria (PGPR) had been isolated and tested for their ability to grow in increasing concentrations of sodium chloride (NaCl). Those rhizobacterial strains having tolerance against salinity were screened to evaluate their ability to promote wheat growth in the presence of salinity by conducting jar trials under axenic conditions. The rhizobacteria with promising results were tested for their compatibility with each other before developing multi-strain inoculum of PGPR. The compatible PGPR strains were characterized, and multi-strain inoculum was then evaluated for promoting wheat growth under axenic conditions at different salinity levels, i.e., 2.1 (normal soil), 6, 12, and 18 dS m^{-1}. The most promising combination was further evaluated by conducting a pot trial in the greenhouse. The results showed that compared to a single rhizobacterial strain, better growth-promoting effect was observed when rhizobacterial strains were co-inoculated. The multi-strain consortium of PGPR caused a significant positive impact on shoot length, root length, shoot fresh weight, and root fresh weight of wheat at the highest salinity level in the jar as well as in the pot trial. Results showed that the multi-strain consortium of PGPR caused significant positive effects on the biochemical traits of wheat by decreasing electrolyte leakage and increasing chlorophyll contents, relative water contents (RWC), and K/Na ratio. It can be concluded that a multi-strain consortium of PGPR (*Ensifer adhaerens* strain BK-30,

Pseudomonas fluorescens strain SN5, and *Bacillus megaterium* strain SN15) could be more effective to combat the salinity stress owing to the presence of a variety of growth-promoting traits. However, further work is going on to evaluate the efficacy of multi-strain inoculum of PGPR under salt-affected field conditions.

KEYWORDS

salinity, rhizobacteria, multi-strain, wheat, tolerance

Introduction

In the soil environment, a plant faces both biotic and abiotic stresses, which cause a harmful impact on plant growth and development. In many areas of the world, including Pakistan, salinity is one of the most serious problems hampering agricultural production. About 40,000 ha of land is lost annually to cultivation due to salinity, and therefore causes a significant impact on the country's economy (Aslam and Prathapar, 2006; Qadir et al., 2014). Salinity is considered a major cause of desertification and effect almost one-fourth of the world's cultivated land (Machado and Serralheiro, 2017).

Under salinity stress, the plant faces a nutritional and hormonal imbalance as well as ion toxicity, and a huge amount of energy is required to modify the environment to accommodate the plant. Increased concentration of Na^+ caused an increased uptake of Na^+ and a decrease in K^+ and Ca^{2+} contents of the plant (Abrar et al., 2020; Ndiate et al., 2021, 2022). Similarly, a significant quantity of ethylene produced under stress can damage the plants due to its negative impact on roots growth, and it can also cause epinasty and premature senescence (Nadeem et al., 2010). Soil microbial functioning has also been significantly affected by the influence of soil salinity stress (Liu et al., 2019).

Many efforts have been channelized to understand the mechanisms of stress tolerance and to enhance plant resistance against salinity stress. Among these, an environmentally sound and cost-effective option is the use of beneficial microbes for providing assistance to plants (Nazli et al., 2020). These beneficial bacteria including plant growth promoting rhizobacteria (PGPR) have been widely reported to help crop plants in various kinds of stresses under varying environmental conditions (Khan et al., 2013; Raza et al., 2021; Nadeem et al., 2022; Rafique et al., 2022). These PGPR protect the plant from the negative impact of salinity through a number of their direct and indirect mechanisms and therefore enable it to withstand stress environment (Zahir et al., 2009, 2019; Fu et al., 2010; Glick, 2013; Nadeem et al., 2016; Ullah et al., 2017; Al-Barakah and Sohaib, 2019; Rafique et al., 2021; Saeed et al., 2021; Singh P. et al., 2022; Upadhyay and Chauhan, 2022; Upadhyay et al., 2022). However, under certain stresses, the results obtained in axenic conditions could not be reproduced in the field (Smyth et al., 2011). This might be occurred due to the low quality of the inoculums and/or the inability of the bacteria to compete with the indigenous population (Catroux et al., 2001). The reasons for the poor performance of agricultural bio-inocula in natural environments and in the rhizosphere of host plants could be the use of a single bacterial strain (Van Veen et al., 1997). Therefore, instead of using a single bacterial strain with single trait/multiple traits for inoculation of seeds/seedlings, multiple microbial consortia could be used for multiple benefits. The preparation of a multi-strain bacterial consortium by keeping in view their compatibility enables the bacterial strain to communicate synergistically with each other by decreasing inhibitory products and providing more balanced plant nutrition improve plant growth and development in variable environments (Wani et al., 2007). In certain cases, single strain inoculation fails to compete with indigenous soil microflora due to its low root colonization percentage and poor survival efficiency (Bashan, 1998; Elkoca et al., 2010) significant positive results are not obtained (Smyth et al., 2011). Compared to a single strain, a multi-strain consortium improves plant growth through the cumulative effect of various mechanisms adopted by different microbial strains (Khan and Zaidi, 2007). Jha and Saraf (2012) observed that the growth of the Jatropha plant (*Jatropha curca*) improved maximally in greenhouse and field experiments when three strains were applied together. Similarly, the consortia of three strains gave the best performance in terms of growth parameters of *Lycopersicum esculentus* (Nicolaus et al., 1999). They demonstrated that the use of combined biofertilizers containing consortia of bacteria was an excellent inoculant for the growth performance of the plants.

As far as growth under stress environment is concerned, Annapurna et al. (2011) studied the effectiveness of PGPR separately and in combination for reducing the impact of salinity on wheat growth. They found that single and dual inoculations of PGPR strains showed variations in their effect to enhance the crops' tolerance to salt. The bacterial consortium was more effective in inducing salinity tolerance in wheat plants. They considered it as an acceptable and environment-friendly technology to improve plant performance and development under stress environments. The results of their study indicated

that co-inoculation with *Bacillus subtilis* and *Arthrobacter* sp. could alleviate the adverse effects of soil salinity on wheat growth. The use of multi-strain bacterial consortia in agriculture has become an area of interest because of its positive impact on plant growth compared to single inoculation. The positive interactions between rhizobacteria could be helpful in better colonization and combating stress-induced negative impact.

Some recent studies show that the effectiveness of bacterial consortia for enhancing plant growth over a single bacterial strain (Moronta-Barrios et al., 2018; Chandra et al., 2019; Olanrewaju and Babalola, 2019). However, most of this work has been conducted under normal conditions or plant protection against biotic stress. Furthermore, some preliminary studies also indicate that multi-strain bacterial consortium offers more sustainable plant growth improvement (Khan et al., 2017; Irfan et al., 2019; Sohaib et al., 2020). Limited work has been conducted under salinity stress therefore the application of multi-strains bacterial consortium over single inoculation could be an effective approach for reducing the harmful impact of salinity stress on plant growth, which is one of the major growth limiting factors in arid and semi-arid regions. Therefore, this study was undertaken with the objective to evaluate the effectiveness of multi-strain bacterial consortium for improving the growth and development of wheat under salt stress condition.

Materials and methods

Isolation of plant growth promoting rhizobacteria and salinity tolerance assay

A total of 55 samples of rhizosphere soil samples were collected from the salt-affected fields of wheat (30°14′35.9"N 72°43′19.7" E). The rhizosphere sample was collected by following the procedure adopted by Khan et al. (2017). The rhizosphere soil adhering to the roots was collected and soil suspension obtained was used to isolate rhizobacteria by dilution plate method by using DF minimal salt medium (Dworkin and Foster, 1958) containing ACC as a sole source of nitrogen (Jacobson et al., 1994). The isolated rhizobacterial strains were purified by further 2–3 times streaking on freshly prepared DF minimal salt medium and pure colonies were used for further screening.

A total of 50 isolated bacterial strains including two previously characterized PGPR strains, i.e., *Pseudomonas fluorescens* strain SN5 (Accession Number; JN858098) and *Bacillus megaterium* strain SN15 (Accession Number; JN858088) were examined for their ability to tolerate salinity. For this purpose, tryptic soya broth (TSB) with 2.5, 5, and 7.5% sodium chloride (NaCl) were prepared and inoculated with respective strains. For each isolate, triplet test tubes at each salinity level were inoculated with 0.5 mL inoculum of OD 0.5 ($>10^8$ cell mL^{-1}) and incubated for 72 h at 28 ± 1°C, shaking at 100 rpm. PGPR isolates showing high optical density (OD) at 600 nm under salinity were considered salinity tolerant.

Screening of plant growth promoting rhizobacteria for promoting wheat growth under salinity stress

The 20 bacterial isolates selected on the basis of salinity tolerance assay were evaluated for their growth promoting potential For this purpose, a jar experiment was conducted under axenic conditions. Four salinity levels, i.e., original, 6, 12, and 18 dS m^{-1} were used. Salinity levels were developed by NaCl salt in sterilized half-strength Hoagland solution (Machado and Serralheiro, 2017). Two sterilized filter paper sheets were soaked and saturated with respective inoculum. Four surface-sterilized wheat seeds were sandwiched between these two sterilized filter papers, which were rolled and placed in the glass jars (Asghar et al., 2002). Seeds were surface sterilized by dipping in 70% ethanol for 1 min and 3.5% sodium hypochlorite for 3–5 min and followed by 3–4 washings with autoclaved distilled water (Long et al., 2008). Jars were arranged using a completely randomized design with four replications for each treatment. Jars were placed in a growth chamber at 25 ± 1°C, adjusted to 16 h of light (supplied by a mixture of incandescent and fluorescent lamps at an intensity range of 200–225 μE $m^{-2}s^{-1}$), and an 8 h dark period. After 3 weeks, four plants were harvested and data regarding shoot/root length, shoot\root fresh weight, and shoot/root dry weight were recorded.

Compatibility test

On the basis of the results of the axenic trial, 10 most promising strains (DG-18, DG-34, BK-6, BK-30, BK-46, BK-50, UA-3, UA-46, SN5, and SN15) were tested for their compatibility with each other in all possible combination by cross streak assay on nutrient agar medium (Raja et al., 2006). One bacterial strain was streaked on the solidified nutrient agar plate and incubated at 28 ± 1°C for 24 h for growth. The counter bacterial strain was streaked vertically to the growth of the already streaked bacterial strain. The plates were incubated at 28 ± 1°C for 48 h and bacterial growth was observed. The growth suppression of counter bacterial strain by already streaked bacterial strain was considered as un-compatible and mixing of bacterial growth of both strains was considered as compatible. Among these strains, six strains (DG-34, BK-30, UA-3, UA-46, SN5, and SN15) showed compatibility when used in various combinations.

Characterization of compatible strains

The six strains showed compatibility in various combinations and were characterized by their plant growth

promoting traits. The ACC-deaminase activities of the strains were measured quantitively by determining the amount of α-ketobutyrate produced when the enzyme cleaved ACC into ammonia and α-ketobutyrate according to the method of Penrose and Glick (2003). All measurements were carried out in triplicate and ACC-deaminase activity was calculated as μmol α-ketobutyrate mg^{-1} protein h^{-1}. Exopolysaccharides production was measured qualitatively according to the method of Nicolaus et al. (1999). For this purpose, strains were grown in a culture medium, and supernatants were collected by centrifuging at 1,000 rpm. The formation of the precipitate by the addition of cold absolute ethanol dropwise was an indication of the production of exopolysaccharides.

Phosphate solubilization was determined qualitatively by using the National Botanical Research Institute (NBRI) growth medium according to Mehta and Nautiyal (2001). Individual bacterial isolates were cultured, and spot inoculated in the center of the agar plates. Colonies showing the formation of clear zones after incubating at 28°C for 5 days were considered positive for phosphate solubilization, and the diameter of the clear halo zone was measured. Siderophore production of the strains was assayed qualitatively according to the universal method of Schwyn and Neilands (1987). Fresh cultures of each strain were inoculated into a modified MM9 medium (low iron medium). The cultures were centrifuged after incubation at 28°C for 48 h. The supernatant was then mixed with the chrome azurol S (CAS) solution. The change of color from blue to orange indicated the presence of siderophores in the solution.

Indole acetic acid production of the selected six isolates was determined colorimetrically as used by Sarwar et al. (1992). For this purpose, 5 mL of filter sterilized 0.5% l-tryptophan solution was added to the flask and inoculated with a particular strain, and then incubated at 28°C for 48 h on a horizontal shaker at 100 rev min^{-1}. Un-inoculated control was also kept for comparison. After incubation, the contents were filtered, and 3 mL of the filtrate was mixed with 2.0 mL of Salkowski reagent and allowed to stand for 30 min for color development. Auxin compounds expressed as IAA equivalents were determined by spectrophotometer (Sarwar et al., 1992).

Screening of multi-strain consortium for promoting wheat growth under salinity stress

Six rhizobacterial strains showed compatibility with each other and were used in various combinations as co-inoculation and multi-strain inoculum. These combinations were DG-34 × BK30, UA-3 × UA-46, UA-3 × SN5, UA-46 × SN15, BK-30 × SN5, UA-3 × SN15, BK-30 × SN15, UA-3 × SN15 × UA-46, and BK-30 × SN5 × SN15. These combinations were tested for evaluating their ability to promote wheat growth under salinity stress. The inoculum of each strain was prepared as described above. For inoculating the sterilized wheat seed with multi-strain inoculum, broth cultures of desired bacterial strains were mixed in equal proportion and vortexed for 5 min to ensure homogenized cell density of different bacterial strains before seed dipping. Surface sterilized seeds of wheat were placed in sterilized Petri plates enfolded in two sheets of filter paper moistened with sterilized distilled water. These Petri plates were incubated at 25 ± 1°C for germination in an incubator under darkness for 2 days. Fully sprouted seeds of wheat and maize were dipped for 10 min in broth culture of the required bacterial population (10^7–10^8 cfu mL^{-1}). Four salinity levels, i.e., 0, 6, 12, and 18, as described above were prepared.

Salinity levels were developed by NaCl salt in the sterilized Hoagland solution (Machado and Serralheiro, 2017) of half-strength. The actual salinity levels obtained after developing salinity were 0.8, 6.2, 12.5, and 17.4 dS m^{-1}. Jars were arranged using completely randomized design with four replications for each treatment. Jars were placed in a growth chamber at 25 ± 1°C, adjusted to 16 h light (supplied by a mixture of incandescent and fluorescent lamps at an intensity range of 200–225 μE $m^{-2}s^{-1}$) and an 8 h dark period. After 3 weeks, plants were harvested and data regarding shoot/root length, shoot\root fresh weight, and shoot/root dry weight were recorded and analyzed statistically.

Root colonization assay

The root colonization ability of bacterial isolates was determined by the modified method of Simons et al. (1996). After 1 week of starting the jar experiment, the plant from one replication was harvested and rinsed with distilled water, and blotted to dryness. The root tips (0.2 g) were removed and put into a flask containing 5 mL of sterilized distilled water. The root samples were shaken vigorously for 30 min using an orbital shaker (Memmert, Schwabach, Germany). Serial dilutions of bacterial suspensions were prepared and 1 mL of each dilution was spread on already prepared tryptic soya agar plates (TSA). All treatments in the colonization experiment were replicated three times. The average number of colony-forming units (cfu) per gram root was determined after 24 h of incubation at 28 ± 2°C using a digital colony meter (J.P Selecta, Barcelona, Spain).

Pot trial

From the results of the axenic trial, the two combinations (UA-3 + SN15 + UA-46 and BK-30 + SN5 + SN15) were selected on the basis of their better performance by promoting growth at the highest salinity level. A third combination having a consortium of two strains, i.e., UA-46 + SN15 was also selected for comparison. There were four treatments, i.e., T_1 (Control),

T_2 (UA-46 + SN15), T_3 (UA-3 + SN15 + UA-46), and T_4 (BK-30 + SN5 + SN15). For developing a multi-strain consortium, a fresh inoculum of each strain was prepared in sterilized broth separately as described earlier. Before inoculating the wheat seeds, an optical density (OD) of 0.5 was developed to maintain a population density of 10^7–10^8 cfu mL^{-1}.

For conducting a pot trial, the soil was ground and passed through a 2 mm sieve. The electrical conductivity (EC) of soil was 2.1 dS m^{-1}. The required salinity levels, i.e., 6, 12, and 18 dS m^{-1} were developed by thoroughly mixing the calculated amount of NaCl in the sieved soil.

After developing salinity, each pot was filled with 12 kg of soil and was arranged according to a complete randomized design with three replications. For inoculating wheat seed, a consortium of three strains were prepared by mixing equal proportion (at a ratio of 1:1:1 having 4 mL inoculum of each strain) and a consortium of two strains was prepared by mixing equal proportion (at a ratio of 1:1 having 6 mL inoculum of each strain). Surface-disinfected wheat seeds were inoculated with sterilized (autoclaved) peat mixed with 10% sterilized sugar solution (1:1 w/w inoculum to peat ratio).

Five wheat seeds were sown in each pot at an equal distance. The pots of each treatment were arranged randomly and NPK at the rate of 120:90:60 kg ha^{-1} were used as urea, diammonium phosphate, and muriate of potash fertilizers. Good quality canal water (EC = 0.7 dS m^{-1}, SAR = 0.5 (mmol $L^{-1})^{1/2}$ and RSC = 0.05 mmolc L^{-1}) meeting the irrigation quality criteria of the crops (Ayers and Westcot, 1985) was used for irrigation. Twenty days after germination, a uniform plant population of two seedlings per pot was maintained by thinning. In all these experiments, wheat crop variety Faisalabad-2008 (Approved by Punjab Seed Corporation (PSC), Pakistan in September, 2008) was used as a test wheat variety.

Data collection and physiological analysis

Seventy days after sowing, plant leaf samples were collected for analyzing some chemical and biochemical parameters like sodium, potassium, chlorophylls (a and b), relative water content (RWC), membrane stability, and proline contents. At maturity, data regarding plant height, number of tillers per pot, number of spikelets per spike, grain yield per pot, root length, and 1,000-grain weight were collected. Wheat shoot and grain samples were analyzed for nitrogen and phosphorus content.

For determining chlorophyll contents, 0.5 g of leaf sample was collected from each treatment and homogenized with 80% acetone (v/v). The homogenate was filtered through filter paper. The absorbance of the resulting solution was read by spectrophotometer at 663 and 645 nm for chlorophylls a and b, respectively (Arnon, 1949). Chlorophylls a and b were calculated using the following formula and results were mentioned as total chlorophyll content, i.e., Chlorophyll a + b:

$$\text{Chl 'a'}\ (\text{mg/g fresh weight}) = [\{(12.7 \times \text{OD663}) - (2.69 \times \text{OD645})\} \times \frac{\text{V}}{1000} \times \text{W}]$$

$$\text{Chl 'b'}\ (\text{mg/g fresh weight}) = [\{(22.9 \times \text{OD645}) - (4.68 \times \text{OD663})\} \times \frac{\text{V}}{1000} \times \text{W}]$$

where,

$$\text{OD663} = \text{OpticalDensityatawavelengthof663 nm}$$

$$\text{OD645} = \text{OpticalDensityatawavelengthof645 nm}$$

$$V = \text{Volumeofthesample},$$

$$W = \text{Weightoffreshtissue}$$

RWC was determined by using the following formula as described by Mayak et al. (2004):

$$\text{RWC}\ (\%) = \frac{(\text{FW} - \text{DW})}{(\text{FTW} - \text{DW})} \times 100 \quad (1)$$

where,

$$\text{RWC} = \text{RelativeWaterContents}$$

$$\text{FW} = \text{Freshweight}$$

$$\text{DW} = \text{Dryweight}$$

$$\text{FTW} = \text{Fullyturgidweight}$$

The fully turgid weight (FTW) is defined as the weight of the leaf after it was held in 100% humidity conditions in the dark at 4°C for 48 h.

Membrane stability was determined by calculating electrolyte leakage according to the method described by Lutts et al. (1996). One young leaf was collected from two plants from each treatment and washed thoroughly with deionized water to remove surface-adhered electrolytes.

The samples were placed in closed vials with deionized water and incubated on a rotary shaker for 24 h at 25°C. The EC of the solution (Lt) was determined by a conductivity meter. Samples were then autoclaved at 120°C for 20 min and the final EC of the solution (L0) was measured after cooling. The electrolyte leakage was determined by the formula:

$$\text{EL}\ (\%) = \left(\frac{\text{Lt}}{\text{L0}}\right) \times 100$$

Free proline content was determined according to the method described by Bates et al. (1973). One gram leaf sample was homogenized in 3% sulphosalyclic acid and then filtered through Whatman filter paper No. 2. After the addition of acid ninhydrin and glacial acetic acid, the mixture was heated at 100°C for 1 h in a water bath and the reaction was

stopped using an ice bath. The mixture was extracted with toluene and the absorbance was read at 520 nm. Proline concentration was determined using a standard curve and was expressed as μmol g^{-1}.

Plant analyses

The grain samples of wheat were first digested for determining nitrogen and phosphorus according to the method of Wolf (1982). The sample was digested with conc. H_2SO_4 and H_2O_2 (35% A. R. grade extra pure) at 350°C. After digestion, nitrogen was determined by the Kjeldahl method. The phosphorus-digested sample was mixed with Barton reagents and phosphorus was determined by spectrophotometer using a standard curve.

Identification of rhizobacterial strains

Rhizobacterial isolates were identified based on the *16S ribosomal RNA* (*16S rRNA*) gene sequencing. Pure colonies of efficient bacterial isolates (DG-34, BK-30, UA-3, and UA-46) were sent to Macrogen Inc., Korea for getting sequences of the target gene. The BlastN tool of the NCBI database[1] was used to compare with the known nucleotide sequences of *16S rRNA* genes. Bacterial isolates were given names as *Atlantibacter hermannii* strain DG-34 (Accession Number; OP204096), *Ensifer adhaerens* strain BK-30 (Accession Number; OP204097), *Stenotrophomonas maltophilia* strain UA-3 (Accession Number; OP295490), and *Atlantibacter hermannii* strain UA-46 (Accession Number; OP295491) based on the maximum similarity with known bacteria.

Statistical analyses

Standard errors (SE) were estimated using Microsoft Excel 2016® (Microsoft Cooperation, USA), and the Student's *t*-test was applied for the level of significance ($P < 0.05$). Data were statistically analyzed using the statistical software (Statistix-8.1®; Analytical Software, Tallahassee, USA).

Results

Salinity tolerance of isolated strains

A total number of 50 isolated strains were evaluated for their ability to tolerate saline conditions. The results show that strains had great variability regarding their growth under saline conditions. The optical density values of certain strains remained very low with increasing levels of salinity that show their limited growth in the saline environment (Figure 1). At normal condition (0% NaCl), 26 strains (52%) showed 6–8 optical density and 16 strains (32%) showed optical density value of more than 8. With increasing salinity, the optical density decreased. At 2.5% NaCl, 9 (18%) and 31 (62%) strains showed optical density values in the range of 6–8 and > 8, respectively. At 5% NaCl, only three strains (6%) showed optical density value > 8. However, no strain showed this optical density value (> 8) at saline media containing 7.5% NaCl. Twenty strains, i.e., 40% showed optical density values in the range of 6–8. This indicates the ability of these strains to tolerate high salinity.

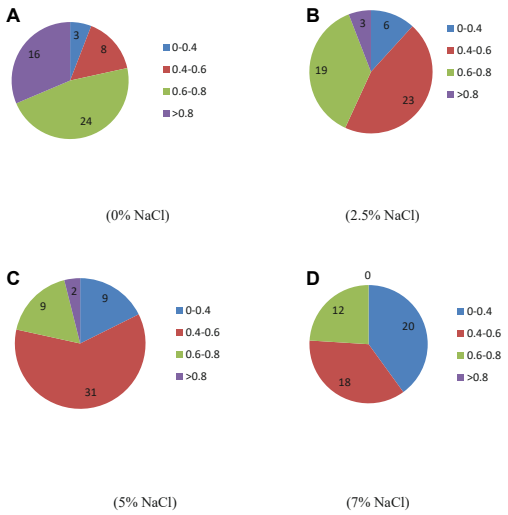

FIGURE 1
Impact of different salinity levels on optical density (600 nm) of isolates. **(A–D)** Different levels of salinity.

Screening of plant growth promoting rhizobacteria for promoting wheat growth under salinity stress

Out of these 50 strains used to evaluate their growth in a saline environment, 20 strains were selected based on their ability to tolerate salinity. These 20 strains were further evaluated for their efficacy to promote wheat growth by conducting jar trials under salinity stress conditions. The data regarding shoot and root parameters were recorded.

Our results indicated that bacterial inoculation enhanced the shoot length at all salinity levels (Supplementary Table 1). This impact was more pronounced at high salinity levels 12 and 18 dSm^{-1}. At 6 dSm^{-1} strain, DG-48 showed a maximum increase in shoot length by 55%, and at this level, strains UA-46,

1 http://www.ncbi.nlm.nih.gov/BLAST

UA-1, and BK-50 increased shoot length up to 47, 48, and 42%. Similarly, at salinity level 12 dSm^{-1} strains DG-18 and UA-3 gave maximum shoot length and increased the shoot length up to 69 and 61%. At higher salinity (18 dSm^{-1}) maximum shoot length was showed by strain DG-18 followed by strain UA-3, which increased shoot length up to 140% as compared to the un-inoculated control. Data predicted in **Supplementary Table 2** showed that strains DG-52 and BK-50 increased shoot fresh weight up to 13% at 6 dSm^{-1}, followed by the strains UA-1, BK-23, DG-18, and DG-48. At 12 dSm^{-1}, UA-1 gave the best results and caused an increase in shoot fresh weight of wheat seedling up to 18%, and strains DG-12, BK-50, BK-28, and UA-44 were the next most effective strains. Strains BK-6 and BK-30 showed good results at EC 18 dSm^{-1} and increased shoot fresh weight up to 60% compared to the un-inoculated control. The data regarding shoot dry weight showed that at 6 dSm^{-1}, DG-48 performed better and increased shoot dry weight up to 96%. At 12 and 18 dSm^{-1}, strains SN5 and UC-14 increased shoot dry weight by 100 and 200% over un-inoculated control followed by UA-44 and UA-46 (**Supplementary Table 3**).

Supplementary Table 4 indicated that strains had variable responses regarding root length. All strains increased the root length of wheat in the case where no salt was added (normal). At 6 dSm^{-1}, the highest root length was observed by BK-46, while strain DG-18 exhibited a maximum increase in root length at EC level 12 dS m^{-1}. At higher salinity levels, i.e., 18 dS m^{-1} strain BK-33 was found to increase root length up to 177%. Inoculation of wheat seeds caused a significant increase in root fresh weight at different salinity levels (**Supplementary Table 5**). At 6 dS m^{-1}, strains UA-1 and SN5 resulted in a maximum increase in fresh weight that was 29 and 28% higher than the uninoculated control. BK-46 caused a 20% increase in root fresh weight at salinity level 12 dS m^{-1}. At high salinity level (18 dS m^{-1}), strains UA-44 and SN15 performed better and increase root fresh weight by 45 and 42%. The effect of bacterial inoculation on root dry weight is presented in **Supplementary Table 6**. At 6 dS m^{-1}, the strain SN15 caused an increase up to 46%, while an increase of 146% was observed due to strain DG-8 at EC level 12 dS m^{-1}. At higher salinity level, i.e., 18 dS m^{-1}, maximum root dry weight was shown by DG-8, DG-34, BK-30, UA-44, and SN15, which cause an increase up to 166% as compared to their respective controls.

Multi-strain grouping

Out of 20 strains tested in the jar experiment, the strains that gave promising results were examined for their compatibility with each other. On the basis of the compatibility test, six strains were selected and then used in different combinations to prepare a multi-strain bacterial consortium for enhancing salinity tolerance in wheat.

Screening of multi-strain consortium for promoting wheat growth under salinity stress

A further jar experiment was conducted to evaluate the efficacy of bacterial consortium for promoting the growth of wheat grown under salinity stress conditions. Obtained results showed that multi-strain inoculum promoted wheat growth significantly more than dual inoculation.

Results regarding the shoot length of wheat seedlings presented in **Figure 2** demonstrated that salinity decreased the shoot length compared to normal (non-saline). The reduction in shoot length was more at high salinity levels (12 and 18 dS m^{-1}) as compared to low-salinity level. However, inoculation with different strains enhanced the shoot length at all salinity levels, i.e., normal, 6, 12, and 18 dS m^{-1}. Under axenic conditions, shoot length was significantly improved when the strains were used in different combinations. At 6 dS m^{-1}, the dual combinations of UA-3 × SN5 and DG-34 × BK-30 enhanced shoot length up to 19 and 17%. At high salinity levels, i.e., 12 dS m^{-1} the combination UA-3 × UA-46 increased the shoot length by 49%. However, at 18 dS m^{-1}, multi-strain inoculation was used, and the combination UA-3 × SN15 × UA-46 increased the shoot length up to 51%. Inoculation with strains improved the shoot fresh weight at low (normal and 6 dS m^{-1}) and high (12 and 18 dS m^{-1}) salinity levels as compared to respective uninoculated control (**Figure 3**). Shoot fresh weight significantly increased when combinations of UA-46 × SN15 were used, which increased fresh weight up to 12% at 6 dS m^{-1}. At 12 dS m^{-1}, the combinations of BK-30 × SN5 and at 18 dS m^{-1}, BK-30 × SN5 × SN15 caused a 41 and 47% increase in shoot fresh weight, respectively. The effect of various salinity levels on shoot dry weight of wheat seedlings and comparative efficacy of co-inoculation and multi-strain inoculation for improving shoot weight is presented in **Figure 4**. Results showed that the response of co-inoculation and multi-strain inoculation was significantly better than the un-inoculated control. An increase of 25% was observed in the combination of UA-3 × UA-46 when EC was 6 dS m^{-1}. At higher salinity, the combination of UA-3 × SN15 × UA-46 increased shoot dry weight up to 56% as compared to the un-inoculated control.

Root length was increased due to inoculation with different strains at low (normal) and high (12 and 18 dS m^{-1}) salinity levels (**Figure 2**). At normal, the combinations of UA-46 × SN15 and BK-30 × SN5 enhanced root length up to 39 and 34%, respectively. The combination of UA-3 × SN5 caused an increase up to 57% at 6 dS m^{-1}. At higher salinity levels (i.e., 12 and 18 dS m^{-1}), the co-inoculation of UA-3 × SN15 × UA-46 exhibited an increase up to 61 and 83%. Data given in **Figure 3** indicate that different salinity levels (6, 12, and 18 dS m^{-1}) had posed a significant reduction in root fresh weight of wheat seedlings as compared to normal. It is clearly evident

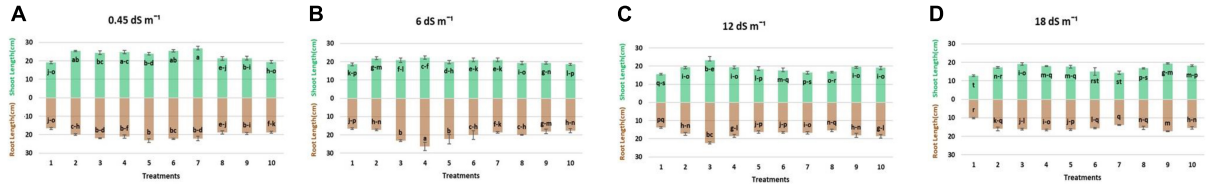

FIGURE 2
Effect of multi-strains inoculum on shoot length (cm plant^{-1}) and root length (cm plant^{-1}) of wheat in the presence of salinity under the axenic condition. **(A–D)** Different levels of salinity.

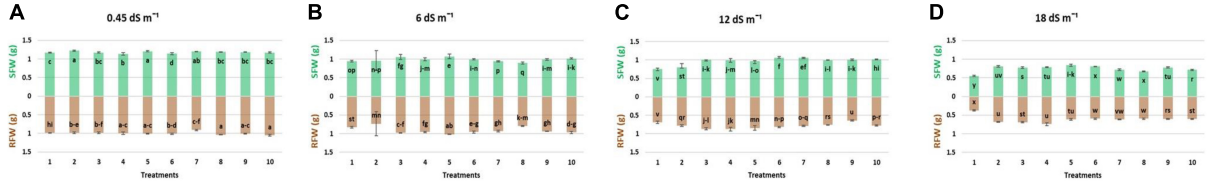

FIGURE 3
Effect of multi-strains inoculum on shoot fresh weight: SFW (g plant^{-1}) and shoot fresh weight: RWF (g plant^{-1}) of Wheat in the presence of salinity under the axenic condition. **(A–D)** Different levels of salinity.

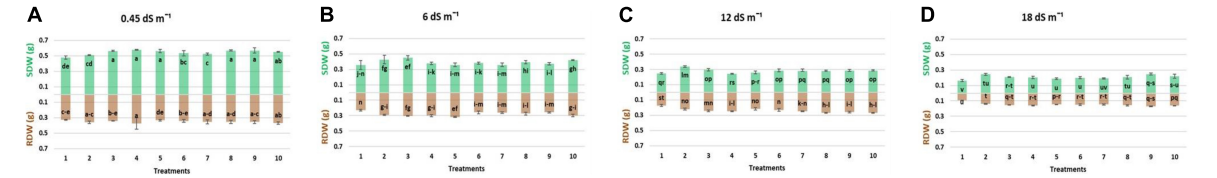

FIGURE 4
Effect of multi-strains inoculum on shoot dry weight: SDW (g plant^{-1}) and root dry weight: RDW (g plant^{-1}) of wheat in the presence of salinity under the axenic condition. **(A–D)** Different levels of salinity.

from the results that inoculation reduced the salinity impact on wheat seedlings and improved the root fresh weight as compared to their respective controls. All co-inoculation and multi-strain inoculation caused an improvement in root fresh weight. At 6 dS m^{-1}, the combination of UA-46xSN15 caused an increase of up to 22%. At 12 dS m^{-1}, the combination of BK-30 × SN5 × SN15 posed an increase up to 100%, whereas at 18 dSm^{-1}, UA-3 × UA-16 × UA-46 caused up to 72% increase in root fresh weight. Salinity stress significantly decreased the root dry weight at all salinity levels (6, 12, and 18 dS m^{-1}) as compared to normal (Figure 4). However, various strains well supported the wheat seedlings to tolerate the salinity stress by improving root dry weight. An increase of 39% was observed when co-inoculation of UA-46 × SN15 was done at 6 dS m^{-1}. At 12 dS m^{-1}, the combination of BK-30 × SN5 × SN15 showed statistically similar results and caused up to a 58% increase in root dry weight as compared to their respective un-inoculated controls. The combination of BK-30 × SN5 × SN15 gave significant results and caused up to a 180% increase at 18 dSm^{-1}.

Plant growth promoting characteristics of strains

The selected strains were characterized by certain growth promoting traits (Table 1). The results of characterization assays showed that all six strains (DG-34, BK-30, UA-3, UA-46, SN5, and SN15) were positive for ACC-deaminase. UA-16 was highest in ACC-deaminase activity followed by UA-3 and UA-46. DG-34 showed the lowest ACC-deaminase activity compared to other strains. All strains for positive for phosphate solubilization and exopolysaccharides activity except DG-34, which was due to the lack of exopolysaccharides production. DG-34, UA-3, SN5, and SN15 were found positive for siderophores production.

Root colonization assay

Data regarding root colonization showed that all selected strains efficiently colonized wheat roots (Table 2). Maximum root colonization was observed in the case of SN15, which was

TABLE 1 Characterization and identification of the rhizobacterial strains.

PGPR strain	Identification	Accession number (NCBI database)	Exopolysaccharides activity	ACC-deaminase activity (μ mol kg^{-1} h^{-1})	Phosphate solubilization	Siderophores	Indole acetic acid (μ g mL^{-1})
DG-34	*Atlantibacter hermannii*	OP204096	+	96	+	+	13.4
BK-30	*Ensifer adhaerens*	OP204097	+	102	+	–	15.2
UA-3	*Stenotrophomonas maltophilia*	OP295490	+	176	+	+	12.7
UA-46	*Atlantibacter hermannii*	OP295491	+	135	+	–	17.2
SN5	*Pseudomonas fluorescens*	JN858098	+	110	+	+	16.3
SN15	*Bacillus megaterium*	JN858088	+	221	+	+	15.5

TABLE 2 Root colonization ability of bacterial strains.

Bacterial strains	DG-34	BK-30	UA-3	UA-46	SN5	SN15
Root colonization (cfu g^{-1})	3.46×10^4	4.10×10^4	3.45×10^5	4.61×10^4	3.31×10^5	5.21×10^5

5.21×10^5 followed by UA-3 (3.45×10^5) and SN5 (3.31×10^5). UA-46 and BK-30 were the next effective strains regarding root colonization ability. Strain DG-34 showed less root colonization ability (3.46×10^4) compared to other strains.

Pot trial

The multi-strain bacteria caused a significant impact on the growth and yield parameters of wheat. The results of the pot trail are described below.

Data in Table 3 show that the plant height of wheat seedlings increased significantly due to inoculation with the multi-strain bacterial consortium. Maximum increase (up to 33% over un-inoculated control) in plant height was recorded by inoculation with T_4 at EC 17.5 dS m^{-1}, which was statistically similar to T_2 and T_3. High salinity level (17.5 dS m^{-1}) affected the number of tillers to a great extent; however, inoculation with multi-strain consortia mitigate this negative effect (Table 3). A maximum number of tillers at this EC (17.5 dS m^{-1}) was obtained by T_4, which was 128% more than the control. T_2 and T_3 were the next effective combinations. These two combinations were statistically similar to each other and caused up to an 86% increase in the number of tillers compared to the control.

Data regarding the number of spikelets per spike of wheat under salinity stress indicated that with an increase in salinity, the number of spikelets per spike of wheat decreased except for T_4 at 12.1 dS m^{-1} (Table 4). At high salinity, i.e., 17.5 dSm^{-1} again T_4 caused a significant increase in the number of spikelets over control, which was 35% more than the un-inoculated control. Data regarding root length revealed that in most of the cases, the statistically similar increase was observed by inoculation with selected PGPR strains that differed significantly from the un-inoculated control (Table 4). Consortium T_4 performed better than other strains and caused 35, 44, and 66% increases over un-inoculated control at 5.8, 12.1, and 17.5 dS m^{-1}, respectively. Inoculation with multi-strain bacterial consortium caused a significant increase in the grain yield of wheat compared to the un-inoculated control (Table 5). At higher salinity levels (12.1 and 17.5 dS m^{-1}), T_4 performed significantly better than other groups and increased grain yield up to 56 and 50%, respectively, over the un-inoculated control. Similarly, data regarding 1,000 grain weight at a high salinity level, i.e., 17.5 dSm^{-1} T_4 again showed a maximum 1,000 grain weight that was 36% more than the un-inoculated control (Table 5).

Physiological parameters

Data regarding chlorophyll contents in Table 6 revealed that inoculation effect was significant at different salinity levels. At low- and medium-salinity levels (5.8 and 12.1 dSm^{-1}), T_3 caused a maximum increase in chlorophyll content. Up to 127% increase in chlorophyll contents was observed with T4 at 17.5 dSm^{-1} followed by T_3. As compared to higher salinity levels, no significant impact of inoculation was observed on electrolyte leakage at low salinity (Table 6). At 12.1 dS m^{-1}, bacterial consortium T_4 caused a maximum increase in membrane stability, i.e., 16% more than un-inoculated control. At 17.5 dS m^{-1}, T_4 performed better and increased the membrane stability of wheat leaf, which was 26% higher than the un-inoculated control.

At a high salinity level of 17.5 dS m^{-1}, the inoculated plants showed more proline contents compared to un-inoculated (Table 7). The plant inoculated with bacterial consortium T_4 showed the highest proline contents (12% more than the un-inoculated control). However, the strains were statistically

TABLE 3 Effect of inoculation with multi-strain bacterial consortium on plant height (cm plant^{-1}) and the number of tillers of wheat at different salinity levels in a pot trial.

Strain	Plant height				Number of tillers			
	Salinity (dS m^{-1})				Salinity (dS m^{-1})			
	2.1	6	12	18	2.1	6	12	18
T_1	63.3 cd	60.3 de	49.7 g	42.0 h	4.67 bcd	4.67 bcd	3.33 de	2.33 e
T_2	74.0 a	67.3 bc	60.7 de	53.7 fg	6.33 a	5.33 abc	4.33 cd	4.33 cd
T_3	71.7 ab	68.0 bc	64.7 cd	55.0 f	6.33 a	5.33 abc	5.33 abc	4.33 cd
T_4	70.7 ab	72.0 ab	62.0 d	56.0 ef	6.33 a	6.00 ab	5.33 abc	5.33 abc
LSD (5%)	5.164				0.656			

Means sharing the same letter(s) are statistically non-significant according to Duncan's multiple range test ($p < 0.05$).
T_1 (Control), T_2 (UA-46 + SN15), T_3 (UA-3 + SN15 + UA-46), T_4 (BK-30 + SN5 + SN15).

TABLE 4 Effect of inoculation with multi-strain bacterial consortium on a number of spikelets per spike of wheat at different salinity levels in a pot trial.

Strain	Number of spikelets per spike				Root length			
	Salinity (dS m^{-1})				Salinity (dS m^{-1})			
	2.1	6	12	18	2.1	6	12	18
T_1	17.3 abc	14.6 de	13.3 ef	11.3 f	18.7 bc	13.6 cdef	13.0 efg	8.00 g
T_2	18.6 a	17.3 abc	15.3 cde	13.3 ef	21.0 a	17.3 bcde	14.6 cdef	12.0 fg
T_3	18.3 ab	16.0 bcd	15.3 cde	14.3 de	20.3 ab	17.3 bcde	17.6 bcde	11.6 fg
T_4	18.0 ab	15.0 cde	17.3 abc	15.3 cde	20.3 ab	18.3 bcd	18.7 bc	13.3 def
LSD (5%)	2.47				5.07			

Means sharing the same letter(s) are statistically non-significant according to Duncan's multiple range test ($p < 0.05$).
T_1 (Control), T_2 (UA-46 + SN15), T_3 (UA-3 + SN15 + UA-46), T_4 (BK-30 + SN5 + SN15).

TABLE 5 Effect of inoculation with multi-strain bacterial consortium on grain yield (g pot^{-1}) and 1,000-grain weight of wheat at different salinity levels in a pot trial.

Strain	Grain yield				1,000 grain weight			
	Salinity (dS m^{-1})				Salinity (dS m^{-1})			
	2.1	6	12	18	2.1	6	12	18
T_1	11.87 b	9.67 c	6.00 ef	5.03 f	3.63 defg	3.40 g	2.91 h	2.69 h
T_2	13.10 ab	12.27 b	9.07 cd	7.13 e	3.74 cde	3.82 bcde	3.66 def	3.42 fg
T_3	14.60 a	12.93 ab	9.30 c	7.30 de	4.06 ab	4.11 a	3.68 de	3.57 efg
T_4	14.70 a	12.73 b	9.37 c	7.56 d	3.96 abc	3.84 bcd	3.72 cde	3.66 def
LSD (5%)	1.827				0.253			

Means sharing the same letter(s) are statistically non-significant according to Duncan's multiple range test ($p < 0.05$).
T_1 (Control), T_2 (UA-46 + SN15), T_3 (UA-3 + SN15 + UA-46), T_4 (BK-30 + SN5 + SN15).

similar to each other. Similar to proline content, the inoculation effect regarding RWC was non-significant at low salinity levels (5.8 and 12.1 dS m^{-1}). Up to a 19% increase in RWCs was recorded due to inoculation with different bacterial consortiums (Table 7). At a high salinity level (17.5 dS m^{-1}), all three bacterial consortia significantly increased RWC over the un-inoculated control. Bacterial consortium T_4 was the most effective for increasing RWC (19% more than the un-inoculated control).

Data regarding sodium and potassium revealed that inoculation with bacterial consortium had variable effects on Na^+ and K^+ uptake by wheat plants. A significant decrease in Na^+ concentration in the leaf sap at high salinity levels was observed due to inoculation with bacterial strains. However, more K^+ concentration was observed in the leaf sap in inoculated treatments compared to the un-inoculated control, which resulted in a high K^+/Na^+ ratio in inoculation treatments compared to the un-inoculated control (Table 8). At a high salinity level (17.5 dS m^{-1}), the highest increase in K^+/Na^+ was observed by inoculation with consortium T_4 that was 31% more than the un-inoculated control.

TABLE 6 Effect of inoculation with multi-strain bacterial consortium on chlorophyll content (mg/g fresh weight) and membrane stability index of wheat at different salinity levels in a pot trial.

Strain	Chlorophyll content				Electrolyte leakage			
	Salinity (dS m^{-1})				Salinity (dS m^{-1})			
	2.1	6	12	18	2.1	6	12	18
T_1	4.49 abc	4.14 def	2.65 g	1.11 i	41.3 f	40.7 f	46.6 def	55.16 bc
T_2	4.56 ab	4.21 def	3.99 f	2.33 h	42.9 ef	41.9 ef	47.2 def	60.03 b
T_3	4.50 abc	4.35 bcd	4.20 def	2.35 h	42.9 ef	44.1 ef	49.3 cde	56.80 bc
T_4	4.62 a	4.29 cde	4.09 ef	2.52 gh	44.1 ef	43.4 ef	54.1 bcd	69.53 a
LSD (5%)	0.247				7.542			

Means sharing the same letter(s) are statistically non-significant according to Duncan's multiple range test ($p < 0.05$).
T_1 (Control), T_2 (UA-46 + SN15), T_3 (UA-3 + SN15 + UA-46), T_4 (BK-30 + SN5 + SN15).

TABLE 7 Effect of inoculation with multi-strain bacterial consortium on proline (μmole g^{-1}) and relative water content of wheat at different salinity levels in a pot trial.

Strain	Proline				Relative water content			
	Salinity (dS m^{-1})				Salinity (dS m^{-1})			
	2.1	6	12	18	2.1	6	12	18
T_1	0.70 e	0.86 d	1.17 c	1.26 bc	76.0 abc	68.5 de	62.1 fg	51.7 h
T_2	0.64 e	0.99 d	1.18 c	1.39 ab	78.0 ab	70.2 cd	63.3 efg	59.1 g
T_3	0.65 e	1.00 d	1.31 abc	1.41 a	78.4 a	72.0 bcd	62.8 efg	59.8 g
T_4	0.64 e	0.94 d	1.31 abc	1.42 a	77.7 ab	71.8 bcd	66.4 def	61.4 ef
LSD (5%)	0.147				6.31			

Means sharing the same letter(s) are statistically non-significant according to Duncan's multiple range test ($p < 0.05$).
T_1 (Control), T_2 (UA-46 + SN15), T_3 (UA-3 + SN15 + UA-46), T_4 (BK-30 + SN5 + SN15).

Data regarding nitrogen contents of wheat grain showed that inoculation significantly increased the nitrogen content at low as well as high salinity levels; however, strains had variable effects (Table 9). Up to a 17% increase in nitrogen content was observed with T_4 at low salinity levels (5.8 dS m^{-1}). At 12.1 and 17.5 dS m^{-1}, T_3 and T_4 caused a maximum increase in nitrogen content, respectively. The wheat straw sample analyzed for phosphorus showed variable effects on the phosphorus contents of wheat grain (Table 9). At low-salinity levels (original and 5.8 dS m^{-1}), inoculation with consortium T_4 caused a maximum increase in phosphorus contents. At 12.1 and 17.5 dS m^{-1}, inoculation showed the non-significant difference. Inoculation with bacterial consortium T_4 showed maximum phosphorus contents (64% more than the un-inoculated control), which were statistically similar with T_2 and T_3.

TABLE 8 Effect of inoculation with multi-strain bacterial consortium on K/Na of wheat at different salinity levels in a pot trial.

Strain	Salinity (dS m^{-1})			
	2.1	6	12	17
T_1	1.95 cd	1.90 d	1.60 gh	1.30 j
T_2	2.11 b	1.98 cd	1.66 fgh	1.46 j
T_3	2.23 a	2.04 c	1.80 e	1.67 fgh
T_4	1.99 c	2.06 c	1.73 efg	1.57 hi
LSD (5%)	0.11			

Means sharing the same letter(s) are statistically non-significant according to Duncan's multiple range test ($p < 0.05$).
T_1 (Control), T_2 (UA-46 + SN15), T_3 (UA-3 + SN15 + UA-46), T_4 (BK-30 + SN5 + SN15).

Discussion

Salinity is a major constraint for agricultural production, especially in arid and semi-arid regions of the world. The problem of salinity is also increasing due to the use of poor quality of underground water because of the non-availability of canal water. There are various approaches to combat the problem of salinity. The biological approach used in this study is also one of the emerging approaches. Although a number of studies have been conducted for promoting plant growth through PGPR inoculation; however, due to inconsistent results of single bacterial strain, the multi-strains consortium has been made to reduce the uncertainties related to this approach.

The results of the salinity tolerance assay showed that all strains were not equally effective to maintain their growth in saline environments. Some strains maintain their growth even at high concentrations of salts. This ability of a strain to maintain its growth at high salt concentration might be due to some of its particular mechanisms. These include the production

TABLE 9 Effect of inoculation with multi-strain bacterial consortium on nitrogen and phosphorus content (%) of wheat grain at different salinity levels in a pot trial.

Strain	Nitrogen				Phosphorus			
	Salinity (dS m^{-1})				Salinity (dS m^{-1})			
	2.1	6	12	18	2.1	6	12	18
T_1	1.23 cd	1.20 cd	1.17 de	0.91 f	0.23 c-g	0.22 efgh	0.20 fghi	0.14 j
T_2	1.60 ab	1.22 cd	1.22 cd	1.26 cd	0.27 bcd	0.26 bcd	0.23 d-h	0.19 ghi
T_3	1.53 ab	1.22 cd	1.41 bc	1.11 de	0.30 ab	0.27 bcde	0.24 c-g	0.18 hi
T_4	1.69 a	1.41 bc	1.31 cd	1.30 cd	0.32 a	0.28 abc	0.24 cdef	0.23 d-h
LSD (5%)	0.199				0.052			

Means sharing the same letter(s) are statistically non-significant according to Duncan's multiple range test ($p < 0.05$).
T_1 (Control), T_2 (UA-46 + SN15), T_3 (UA-3 + SN15 + UA-46), T_4 (BK-30 + SN5 + SN15).

of osmolytes and polysaccharides like exopolysaccharides. For example, to maintain growth in a saline environment, the bacteria establish and develop their internal pressure above the surrounding environment, and they generally achieve this by the accumulation of osmolytes in their body (Rhodes and Hanson, 1993). The survival of *Pseudomonas aeruginosa* in the sea by the accumulation of glycine and betaine is an example of this mechanism (Bakhrouf et al., 1991). Betaine is also involved in the biosynthesis of cyclopropane fatty acids to increase the membrane stability of *Pseudomonas halosaccharolytica* under extreme salty conditions (Monteoliva-Sanchez et al., 1993). Similarly, the production of exopolysaccharides may also protect the microbes from sodium toxicity, because these polysaccharides have the ability to bind Na^+ and thus reduced their mobility (Upadhyay et al., 2011). Exopolysaccharide's production character of bacterial strain is an important characteristic that protects the plant from the negative impact of stress. Shultana et al. (2020) observed that salt-tolerant PGPR strains containing exopolysaccharides caused a positive effect on the growth and yield of rice grown on salt-affected soils.

For better performance of bacterial strains when these are used in combination, the compatibility of strains with each other is a pre-requisite so better results can be achieved. In certain cases, a multi-strain microbial consortium is prepared by mixing microbes without taking antagonistic interactions that occur among the strains and therefore reduces their efficacy (Sarma et al., 2015). In this study, before preparing a multi-strain consortium, bacterial strains were checked for their compatibility with each other. It has been observed that some strains did not show compatibility with each other. This might be due to the reason for the production of certain compounds like cyanide that cause a negative impact on the growth of living organisms. The production of cyanide is a common characteristic of certain bacterial strains (Bakker and Schippers, 1987). Keeping in view the drawback of non-compatible strains, only the compatible strains were evaluated for their ability to promote plant growth under stress conditions.

Results of jar and pot trials indicated that the growth of wheat was affected by salinity stress. The effect of different salinity levels was variable on the growth parameters of wheat. All the growth parameters of wheat, i.e., shoot length, root length, shoot fresh weight, shoot dry weight, root fresh weight, and root dry weight were decreased due to salinity stress. Hindrance in plant growth and development in saline conditions might be due to the osmotic effect of salts and/or due to the toxic effect of salts within the plant (Munns and Tester, 2008). A decrease in plant growth might also be attributable to impaired mineral nutrient absorption and their translocation within the plant (Glenn et al., 1999). Moreover, root growth might reduce due to excessive biosynthesis of stress-induced ethylene (Mayak et al., 2004; Nadeem et al., 2007, 2010; Ahmad et al., 2013). Ethylene biosynthesis is increased due to salinity stress, which might be a key factor in the inhibition of root growth (Zahir et al., 2012). All these factors may be collectively responsible for decreased growth of wheat in salinity stress. All the growth parameters of wheat were improved due to inoculation with PGPR. This improvement in the growth of wheat at all salinity levels very likely be due to one or more growth-promoting activities of selected PGPR strains. But, most importantly this increase in growth of wheat seedlings in salinity stress might be due to the lowering of salinity-induced biosynthesis of ethylene in roots by ACC-deaminase activity of PGPR strains, which ultimately resulted in more root length (Glick et al., 1999; Mayak et al., 2004). In general, biosynthesis of ethylene is regulated by PGPR-containing ACC-deaminase, and they maintain its concentration below the growth inhibition level (Glick et al., 2007). The improvement in shoot length and shoot fresh and dry weight under salinity stress might be due to this increase in root length because an extensive root system is primarily important for better plant growth and development as plant vigor is directly related to the better root system (Doty et al., 2007). Furthermore, root and shoot growth of wheat might increase due to a decline in the concentration of Na^+ ion within the plant before toxic limits by inoculation

with PGPR strains possibly due to exopolysaccharides activity which may bind it and decrease its availability for plant uptake (Ashraf et al., 2004), as PGPR strains were positive for exopolysaccharide production. Moreover, Zhang et al. (2008) reported that bacterial inoculation with *Bacillus subtilis* GB03 decreases Na^+ concentration within plants due to tissue-specific down- and upregulation of high-affinity K^+ transporter (HKT1) in roots and shoots, respectively, which controls Na^+ uptake and transport in plants. The better growth of wheat under salinity stress might also be a result of better protection against oxidative stress by PGPR-containing ACC-deaminase activity (Upadhyay et al., 2012).

In this study, salinity stress caused a negative impact on physiological parameters of wheat including chlorophyll content, electrolyte leakage, proline content, and RWCs. It has been observed that salinity enhanced the electrolyte leakage; however, a significant decrease in electrolyte leakage was observed in treatments where a multi-strain consortium was applied. Similarly, increasing the order of salinity caused a significant decrease in RWC. Other studies also mentioned the decrease in RWC in the presence of salinity (Yildrim et al., 2008; Yasin et al., 2018). The application of bacterial strains alone or in combination mitigated this negative impact of salinity relative to water content; however, the effect was more pronounced where multi-strain microbial consortium was applied. The increase in RWC and decrease in electrolyte leakage at varying levels of salinity has been observed by other workers by the application of effective strains of bacteria (Shultana et al., 2020).

Salinity also negative impact on chlorophyll contents of wheat and this effect was more pronounced at high salinity concentration. It has already been described by various researchers that salinity causes a decline a chlorophyll contents that ultimately affect the photosynthesis rate of the plant (Aquino et al., 2007; Silva et al., 2019). However, in present study, it has been observed that under salinity stress, the application of multi-strain bacterial consortium was found to be an effective strategy to improve the photosynthetic pigments that ultimately improve the photosynthesis rate of the plant. Sapre et al. (2018) also reported an increase in chlorophyll content of oat seedlings under salinity stress due to the application of *Klebsiella* sp.

Proline is a biochemical marker of salinity stress. Proline accumulation plays an osmoregulatory role to protect the plant from salt stress (Kavi Kishor et al., 2005). A multi-strain bacterial consortium of *Bacillus* sp. *Azospirillum brasilense, and Azosprillum lippferum* improved the biomass of wheat. The consortium also decreases electrolyte leakage and enhanced the chlorophyll content, RWC, proline content, amino acid, and antioxidant enzymes Akhtar et al. (2021).

A study conducted by Numan et al. (2018) demonstrated that improved plant growth under salinity stress was due to stimulation of osmoprotectants utilizing the microbial population for inducing salt tolerance rice. They further reported that it was due to ACC deaminase activity of inoculated strain, better root colonization, and enhancing chlorophyll and proline content. *Bacillus spp*. alleviated the harmful impact of salinity on pepper and improved growth by inducing salinity tolerance through the accumulation of proline (Wang et al., 2018). Similarly, He et al. (2018) also reported the more accumulation of proline content in *Haloxylon amodendron* inoculated ryegrass that induces salinity tolerance in said plant.

It is a well-documented effect that a high concentration of Na^+ not causes a toxic effect on plant growth but also decreases the uptake of other essential nutrients, therefore, causing nutritional imbalances (Hirpara et al., 2005; da Costa and de Medeiros, 2018; Bekmirzaev et al., 2020). Sodium (Na^+) and potassium (K^+) play a major role in plant physiology under salinity stress. A high K/Na ratio is considered as one of the prerequisites for plant salinity tolerance. In this study, it has been observed that a significant decrease in K^+ content occurred under salinity stress, particularly in un-inoculated treatments. Maximum Na content was observed in un-inoculated control treatments. Shahzad et al. (2019) also reported a high concentration of Na in plant tissue with an increase in salinity levels. The application of a multi-strain bacterial consortium mitigates this negative effect on K uptake. A decrease in Na uptake and an increase in K content have been observed that result in a high K/Na ratio. Other workers also reported the reduced uptake of Na^+ and enhanced uptake of K^+ by the application of bacterial strains (Khan et al., 2019). Recently, Shultana et al. (2020) while working on rice varieties having different salt tolerant abilities observed that inoculation with *Bacillus* spp. caused a significant decrease in the Na/K ratio under saline conditions.

Better plant growth is dependent on the availability of nutrients (Glick, 1995) and better uptake of essential plant nutrients, such as N, P, and K, with PGPR application, play an important role in plant growth (Hassan et al., 2015 p. 38). Multi-strain microbial inoculation also improved the plant nutrition by enhancing the uptake of nitrogen, phosphorus, and potassium. The improvement in the physiological parameters of the plant could be the reason for the enhanced uptake of essential nutrients. This better nutrition of wheat in salinity stress could be due to the production of siderophores (Singh R. K. et al., 2022) by these PGPR. Other reason could be the production of exopolysaccharides that play a significant role in biofilm formation that enhances the bacterial colonization on plant root (Chen et al., 2013) and restrict Na^+ under saline conditions (Ashraf and Harris, 2004). Therefore, the ability of microbial strains to bind Na^+ due to the production of exopolysaccharides decreases the availability of Na^+ near the root environment, which ultimately reduces the antagonistic effect of Na^+ on other essential plant nutrients.

Comparatively, better growth of wheat in salinity stress due to co-inoculations and multi-strain inoculation might be owing to improved colonization potential and sustainability

of inoculants as compared to single strain inoculation (Raja et al., 2006). This is more likely to be successful survival and maintenance of different PGPR strains in communities (Andrews, 1991). Microbial studies performed without plants indicated that some combinations allow the bacteria to interact with each other synergistically, provide nutrients, remove inhibitory products, and stimulate each other through physical and biochemical activities that may enhance some beneficial aspects of their physiology (Bashan, 1998). Rajasekar and Elango (2011) studied the effectiveness of *Azospirillum*, *Azotobacter*, *Pseudomonas,* and *Bacillus* separately and in combination on the ashwagandha plant (*Withania somniferous*) for two consecutive years. They observed that PGPR consortia significantly increased plant height, root length, and alkaloid content in *Withania somnifera* when compared to the un-inoculated control and single inoculation. Jha et al. (2012) observed that growth of Jatropha plant improved maximally in greenhouse and field experiments when four strains were applied together. Co-inoculation provides the largest and most consistent increases in shoot weight, root weight, total biomass, shoot and root length, total chlorophyll, shoot width, and grain yield. In certain soil conditions, single strain inoculation does not provide the desired result due to the reason that inoculating strain could not compete with soil microflora. Poor root colonization and survival efficiency as well as soil factors, such as pH, temperature, humidity, etc., affect the performance of inoculating strain (Elkoca et al., 2010). However, in the case of a multi-strain microbial consortium, owing to their compatibility with each other, the microbial strain communicates synergistically with each other and enhances plant growth and development (Wani et al., 2007) as has been observed in this study.

Conclusion

On an overall basis, it can be concluded that no doubt the single inoculation also caused a significant increase in wheat under salinity stress; however, this improvement was further enhanced due to the application of multi-strains inoculum. These preliminary studies that are conducted under laboratory and greenhouse conditions show the significant effectiveness of multi-strain compared to single strain inoculation; however, the effectiveness of this multi-strains consortium in a natural soil environment will further validate the results.

Data availability statement

The data presented in this study can be found in the article/**Supplementary material**.

Author contributions

MK, SN, ZZ, and FA-B contributed to conception and design of the study. MK, MS, MW, and LA organized the database. MK, FA, and MS performed the statistical analysis. MK and SN wrote the first draft of the manuscript. FA and MS wrote sections of the manuscript. All authors contributed to manuscript revision, read, and approved the submitted version.

Funding

The authors are thankful to the Higher Education Commission (HEC) of Pakistan for financial support to conduct this research (No. 20-2745/NRPU/R&D/HEC/13/7054).

Acknowledgments

We extend their sincere appreciation to the Deanship of Scientific Research (DSR) at King Saud University for funding and supporting the work through the College of Food and Agriculture Sciences Research Center.

Conflict of interest

The authors declare that the research was conducted in the absence of any commercial or financial relationships that could be construed as a potential conflict of interest.

Publisher's note

Supplementary material

The Supplementary Material for this article can be found online at: https://www.frontiersin.org/articles/10.3389/fmicb.2022.958522/full#supplementary-material

References

Abrar, M. M., Saqib, M., Abbas, G., Atiq-ur-Rahman, M., Mustafa, A., Shah, S. A. A., et al. (2020). Evaluating the contribution of growth, physiological, and ionic components towards salinity and drought stress tolerance in Jatropha curcas. *Plants* 9:1574. doi: 10.3390/plants9111574

Ahmad, M., Zahir, Z. A., Khalid, M., Nazli, F., and Arshad, M. (2013). Efficacy of *Rhizobium* and *Pseudomonas* strains to improve physiology, ionic balance and quality of mung bean under salt affected conditions on farmer's fields. *Plant Physiol. Biochem.* 63, 170–176. doi: 10.1016/j.plaphy.2012.11.024

Akhtar, N., Ilyas, N., Hayat, R., Yasmin, H., Noureldeen, A., and Ahmad, P. (2021). Synergistic effects of plant growth promoting rhizobacteria and silicon dioxide nano-particles for amelioration of drought stress in wheat. *Plant Physiol. Biochem.* 166, 160–176.

Al-Barakah, F. N., and Sohaib, M. (2019). Evaluating the germination response of *Chenopodium quinoa* seeds to bacterial inoculation under different germination media and salinity conditions. *Seed Sci. Technol.* 47, 161–169. doi: 10.15258/sst.2019.47.2.05

Andrews, J. H. (1991). *Comparative Ecology of Microorganisms and Macroorganisms*. New York, NY: Springer Verlag. doi: 10.1007/978-1-4612-3074-8

Annapurna, D. R., Vithal, L., and Bose Sajad, P. (2011). "PGPR bioinoculants for ameliorating biotic and abiotic stresses in crop production K," in *Proceedings of the 2nd Asian PGPR Conference August* (Beijing) 21-24.

Aquino, A. J. S., Lacerda, C. F., Bezerra, M. A., Gomes-Filho, E., and Co1sta, R. N. T. (2007). Crescimento, partição de matéria seca e retenção de Na+ e Cl- em dois genótipos de sorgo irrigados com águas salinas. *Rev. Bras. Ciênc. Solo* 31, 961–971. doi: 10.1590/S0100-06832007000500013

Arnon, D. I. (1949). Copper enzymes in isolated chloroplasts. Polyphenol oxidase in *Beta vulgaris*. *Plant Physiol.* 24, 11–15.

Asghar, H. N., Zahir, Z. A., Arshad, M., and Khaliq, A. (2002). Relationship between in vitro production of auxins by rhizobacteria and their growth promoting activities in *Brassica juncea L. Biol. Fertil. Soils* 35, 231–237. doi: 10.1007/s00374-002-0462-8

Ashraf, M., Berge, S. H., and Mahmood, O. T. (2004). Inoculating wheat seedling with exopolysaccharide-producing bacteria restricts sodium uptake and stimulates plant growth under salt stress. *Biol. Fertil. Soils*. 40, 157–162. doi: 10.1007/s00374-004-0766-y

Ashraf, M. P. J. C., and Harris, P. J. C. (2004). Potential biochemical indicators of salinity tolerance in plants. *Plant Sci.* 166, 3–16.

Aslam, M., and Prathapar, S. A. (2006). *Strategies to Mitigate Secondary Salinization in the Indus Basin of Pakistan: A Selective Review*. Research Report 97 Colombo: IWMI.

Ayers, R. S., and Westcot, D. W. (1985). *Water quality for agriculture*, Vol. 29. Rome: Food and Agriculture Organization of the United Nations.

Bakhrouf, A., Jeddi, M., Bouddabous, A., and Gauthier, M. J. (1991). Survie du *Salmonella* paratyphi B et du *Pseudomonas aeruginosa* dans l'eau de mer après incubation ou lavage en presence d'osmolytes. *Can. J. Microbiol.* 38, 690–693. doi: 10.1139/m92-112

Bakker, A. W., and Schippers, B. (1987). Microbial cyanide production in the rhizosphere in relation to potato yield reduction and *Pseudomonas* SPP-mediated plant growth-stimulation. *Soil Biol. Biochem.* 19, 451–457. doi: 10.1016/0038-0717(87)90037-X

Bashan, Y. (1998). Inoculants of plant growth promoting bacteria for use in agriculture. *Biotechnol. Adv.* 16, 729–770. doi: 10.1016/S0734-9750(98)00003-2

Bates, L. S., Waldren, R. P., and Teare, I. D. (1973). Rapid determination of free proline for water stress studies. *Plant Soil* 39, 205–209.

Bekmirzaev, G., Ouddane, B., Beltrao, J., and Fujii, Y. (2020). The impact of salt concentration on the mineral nutrition of tetragonia tetragonioides. *Agriculture* 10:238.

Catroux, G., Hartmann, A., and Revellin, C. (2001). Trends in rhizobial inoculant production and use. *Plant Soil* 230, 21–30. doi: 10.1023/A:1004777115628

Chandra, D., Srivastava, R., Gupta, V. V., Franco, C. M., and Sharma, A. K. (2019). Evaluation of ACC-deaminase-producing rhizobacteria to alleviate water-stress impacts in wheat (Triticum aestivum L.) plants. *Can. J. Microbiol.* 65, 387–403. doi: 10.1139/cjm-2018-0636

Chen, Y., Yan, F., Chai, Y., Liu, H., Kolter, R., Losick, R., et al. (2013). Biocontrol of tomato wilt disease by *Bacillus subtilis* isolates from natural environments depends on conserved genes mediating biofilm formation. *Environ. Microbiol.* 15, 848–864.

da Costa, A. R. F. C., and de Medeiros, J. F. (2018). Nitrogen, phosphorus and potassium accumulation in watermelon cultivars irrigated with saline water. *Engenharia Agríc.* 38, 343–350. doi: 10.1590/1809-4430-Eng.Agric.v38n3p343-350/2018

Doty, S. L., James, C. A., Moore, A. L., Vajzovic, A., Singleton, G. L., Ma, C., et al. (2007). Enhanced phytoremediation of volatile environmental pollutants with transgenic trees. *Proc. Natl. Acad. Sci.* 104, 16816–16821. doi: 10.1073/pnas.0703276104

Elkoca, E., Turan, M., and Donmez, M. F. (2010). Effects of single, dual and triple inoculations with *Bacillus subtilis*, *Bacillus megaterium* and *Rhizobium leguminosarum* bv. phaseoli on nodulation, nutrient uptake, yield and yield parameters of common bean (*Phaseolus vulgaris* L. cv. 'Elkoca-05'). *J. Plant Nutr.* 33, 2104–2119.

Dworkin, M., and Foster, J. (1958). Experiments with some microorganism which utilizes ethane and hydrogen. *J. Bacteriol.* 75, 592–601.

Fu, Q., Liu, C., Ding, N., Lin, Y., and Guo, B. (2010). Ameliorative effects of inoculation with the plant growth-promoting rhizobacterium *Pseudomonas* sp. DW1 on growth of eggplant (*Solanum melongena* L.) seedlings under salt stress. *Agric. Water Manag.* 97, 1994–2000. doi: 10.1016/j.agwat.2010.02.003

Glenn, E. P., Brown, J. J., and Blumwald, E. (1999). Salt tolerance and crop potential of halophytes. *Crit. Rev. Plant Sci.* 18, 227–255. doi: 10.1080/07352689991309207

Glick, B. R. (1995). The enhancement of plant-growth by free-living bacteria. *Can. J. Microbiol.* 41, 109–117. doi: 10.1139/m95-015

Glick, B. R. (2013). Bacteria with ACC deaminase can promote plant growth and help to feed the world. *Microbiol. Res.* 169, 30–9. doi: 10.1016/j.micres.2013.09.009

Glick, B. R., Patten, C. L., Holgiun, G., and Penrose, D. M. (1999). *Biochemical and Genetic Mechanisms used by Plant Growth-Promoting Bacteria*. London: Imperial College Press. doi: 10.1142/p130

Glick, B. R., Todorovic, B., Czarny, J., Cheng, Z., Duan, J., and McConkey, B. (2007). Promotion of plant growth by bacterial ACC deaminase. *Crit. Rev. Plant Sci.* 26, 227–242. doi: 10.1080/07352680701572966

Hassan, W., Hussain, M., Bashir, S., Shah, A. N., Bano, R., and David, J. (2015). ACC-deaminase and/or nitrogen fixing rhizobacteria and growth of wheat (*Triticum aestivum* L.). *J. Soil Sci. Plant Nutr.* 15, 232–248.

He, A. L., Niu, S. Q., Zhao, Q., Li, Y. S., Gou, J. Y., Gao, H. J., et al. (2018). Induced salt tolerance of perennial ryegrass by a novel bacterium strain from the rhizosphere of a desert shrub *Haloxylon ammodendron*. *Int. J. Mol. Sci.* 19, 469.

Hirpara, K. D., Ramoliya, P. J., Patel, A. D., and Pandey, A. N. (2005). "Effect of salinisation of soil on growth and macro-and micro-nutrient accumulation in seedlings of *Butea monosperma* (Fabaceae)," in *Anales de biología*, (Murcia: Servicio de Publicaciones de la Universidad de Murcia), 3–14.

Hoagland, D.R. and Arnon, D. I. (1950). The water-culture method for growing plants without soil. *Circular. Cal. Agric. Exp. Station* 347:32.

Ibiene, A. A., Agogbua, J. U. I, Okonko, O., and Nwachi, G. N. (2012). Plant growth promoting rhizobacteria (PGPR) as biofertilizer: Effect on growth of *Lycopersicum esculentus* J. *Am. Sci.* 8, 318–324.

Irfan, M., Zahir, Z. A., Asghar, H. N., Khan, M. Y., Ahmad, H. T., and Ali, Q. (2019). Effect of multi-strain bacterial inoculation with different carriers on growth and yield of maize under saline conditions. *Int. J. Agricult. Biol.* 22, 1407–1414.

Jacobson, C. B., Pasternak, J. J., and Glick, B. R. (1994). Partial purification and characterization of ACC deaminase from the plant growth-promoting rhizobacterium *Pseudomonas* putida GR12-2. *Can. J. Microbiol* 40, 1019–1025. doi: 10.1139/m94-162

Jha, B., Gontia, I., and Hartmann, A. (2012). The roots of the halophyte Salicornia brachiata are a source of new halotolerant diazotrophic bacteria with plant growth promoting potential. *Plant Soil* 356, 265–277.

Jha, C. K., and Saraf, M. (2012). Evaluation of multispecies plant-growth-promoting consortia for the growth promotion of *Jatropha curcas* L. *J. Plant Growth Regul.* 31, 588–598. doi: 10.1007/s00344-012-9269-5

Kavi Kishor, P. B., Sangam, S., Amrutha, R. N., Sri Laxmi, P., Naidu, K. R., Rao, K. R. S. S., et al. (2005). Regulation of proline biosynthesis, degradation, uptake and transport in higher plants: Its implications in plant growth and abiotic stress tolerance. *Curr. Sci.* 88, 424–438.

Khan, M. A., Asaf, S., Khan, A. L., Adhikari, A., Jan, R., Ali, S., et al. (2019). Halotolerant rhizobacterial strains mitigate the adverse effects of NaCl stress in soybean seedlings. *BioMed Res. Int.* 15:9530963. doi: 10.1155/2019/9530963

Khan, M. S., and Zaidi, A. (2007). Synergistic effects of the inoculation with plant growth-promoting rhizobacteria and an arbuscular mycorrhizal fungus on the performance of wheat. *Turk. J. Agric. For.* 31:355.

Khan, M. Y., Asghar, H. N., Jamshaid, M. U., Akhtar, M. J., and Zahir, Z. A. (2013). Effect of microbial inoculation on wheat growth and phyto-stabilization of chromium contaminated soil. *Pak. J. Bot.* 45, 27–34.

Khan, M. Y., Zahir, Z. A., Asghar, H. N., and Waraich, E. A. (2017). Preliminary investigations on selection of synergistic halotolerant plant growth promoting rhizobacteria for inducing salinity tolerance in wheat. *Pak. J. Bot.* 49, 1541–1551.

Liu, H., Khan, M. Y., Cavalhais, L. C., Delgado Baquerizo, M., Yan, L., Crawford, M., et al. (2019). Soil amendments with ethylene precursor affect the soil microbiome and reverse negative impacts of salinity on soil microbial functions. *Sci. Rep.* 9:6892. doi: 10.1038/s41598-019-43305-4

Long, H. H., Schmidt, D. D., and Baldwin, I. T. (2008). Native bacterial endophytes promote host growth in a species-specific manner; phytohormone manipulations do not result in common growth responses. *PLoS One* 3:e2702. doi: 10.1371/journal.pone.0002702

Lutts, S., Kinet, J. M., and Bouharmont, J. (1996). NaCl-induced senescence in leaves of rice(*Oryza sativa* L.) cultivars differing in salinity resistance. *Ann. Bot.* 78, 389–398.

Machado, R. M. A., and Serralheiro, R. P. (2017). Soil salinity: Effect on vegetable crop growth. management practices to prevent and mitigate soil salinization. *Horticulturae* 3:30. doi: 10.3390/horticulturae3020030

Mayak, S., Tirosh, T., and Glick, B. R. (2004). Plant growth-promoting bacteria confer resistance in tomato plants to salt stress. *Plant Physiol. Biochem.* 42, 565–572. doi: 10.1016/j.plaphy.2004.05.009

Mehta, S., and Nautiyal, C. S. (2001). An efficient method for screening phosphate solubilizing bacteria. *Curr. Microbiol.* 43, 57–58.

Monteoliva-Sanchez, M., Ramos-Cormenzana, A., and Russell, N. J. (1993). The effect of salinity and compatible solutes on the biosynthesis of cyclopropane fatty acids in *Pseudomonas* halosaccharolytica. *J. General Microbiol.* 139, 1877–1884. doi: 10.1099/00221287-139-8-1877

Moronta-Barrios, F., Gionechetti, F., Pallavicini, A., Marys, E., and Venturi, V. (2018). Bacterial microbiota of rice roots: 16s-based taxonomic profiling of endophytic and rhizospheric diversity, endophytes isolation and simplified endophytic community. *Microorganisms* 6:14. doi: 10.3390/microorganisms6010014

Munns, R., and Tester, M. (2008). Mechanisms of salinity tolerance. *Annu. Rev. Plant Biol.* 59, 651–681. doi: 10.1146/annurev.arplant.59.032607.092911

Nadeem, S. M., Hanif, A., Khan, M. Y., Waqas, M. R., Ahmad, Z., Ashraf, M. R., et al. (2022). Elemental sulphur with sulphur oxidizing bacteria enhances phosphorus availability and improves growth and yield of wheat in calcareous soil. *Arch. Agron. Soil Sci.* 1–9. doi: 10.1080/03650340.2022.2099541

Nadeem, S. M., Naveed, M., Ayyub, M., Khan, M. Y., Ahmad, M., and Zahir, Z. A. (2016). Potential, limitations and future prospects of *Pseudomonas* spp. for sustainable agriculture and environment: A Review. *Soil Environ.* 35, 106–145.

Nadeem, S. M., Zahir, Z. A., Naveed, M., and Arshad, M. (2007). Preliminary investigation on inducing salt tolerance in maize through inoculation with rhizobacteria containing ACC-deaminase activity. *Can. J. Microbiol.* 53, 1141–1149. doi: 10.1139/W07-081

Nadeem, S. M., Zahir, Z. A., Naveed, M., Asghar, H. N., and Arshad, M. (2010). Rhizobacteria capable of producing ACC-deaminase may mitigate salt stress in wheat. *Soil Sci. Soc. Am. J.* 74, 533–542. doi: 10.2136/sssaj2008.0240

Nazli, F., Najm-ul-Seher, Khan, M. Y., Jamil, M., Nadeem, S. M., and Ahmad, M. (2020). "Soil Microbes and Plant Health," in *Plant Disease Management Strategies for Sustainable Agriculture through Traditional and Modern Approaches*, Vol. 13, eds I. Ul Haq and S. Ijaz (Cham: Springer). doi: 10.1007/978-3-030-35955-3_6

Ndiate, N. I, Saeed, Q., Haider, F. U., Liqun, C., Nkoh, J. N., and Mustafa, A. (2021). Co-Application of Biochar and Arbuscular mycorrhizal Fungi Improves Salinity Tolerance, Growth and Lipid Metabolism of Maize (*Zea mays* L.) in an Alkaline Soil. *Plants* 10:2490. doi: 10.3390/plants10112490

Ndiate, N. I., Zaman, Q. U., Francis, I. N., Dada, O. A., Rehman, A., Asif, M., et al. (2022). Soil Amendment with Arbuscular Mycorrhizal Fungi and Biochar Improves Salinity Tolerance, Growth, and Lipid Metabolism of Common Wheat (*Triticum aestivum* L.). *Sustainability* 14:3210. doi: 10.3390/su14063210

Nicolaus, B., Lama, L., Esposito, L. E., Manca, M. C., Improta, R., Bellitti, M. R., et al. (1999). Haloarcula spp able to biosynthesize exo- and endopolymers. *J. Ind. Microbiol. Biotechnol.* 23, 489–496.

Numan, M., Bashir, S., Khan, Y., Mumtaz, R., Khan Shinwari, Z., Khan, A. L., et al. (2018). Plant growth promoting bacteria as an alternative strategy for salt tolerance in plants: A review. *Microbiol. Res.* 209, 21–32.

Olanrewaju, O. S., and Babalola, O. O. (2019). Bacterial consortium for improved maize (Zea mays L.) production. *Microorganisms* 7:519. doi: 10.3390/microorganisms7110519

Penrose, D. M., and Glick, B. R. (2003). Methods for isolating and characterizing ACC deaminase-containing plant growth promoting rhizobacteria. *Physiol. Plant.* 118, 10–15.

Qadir, M., Quillérou, E., Nangia, V., Murtaza, G., Singh, M., Thomas, R. J., et al. (2014). November. Economics of salt-induced land degradation and restoration. *Nat. Resour. Forum* 38, 282–295. doi: 10.1111/1477-8947.12054

Rafique, H. M., Khan, M. Y., Asghar, H. N., Zahir, Z. A., Nadeem, S. M., Sohaib, M., et al. (2022). Converging alfalfa (*Medicago sativa* L.) and petroleum hydrocarbon acclimated ACC-deaminase containing bacteria for phytoremediation of petroleum hydrocarbon contaminated soil. *Int. J. Phytoremed.* [Epub ahead of print]. doi: 10.1080/15226514.2022.2104214

Rafique, M., Naveed, M., Mustafa, A., Akhtar, S., Munawar, M., Kaukab, S., et al. (2021). The combined effects of gibberellic acid and rhizobium on growth, yield and nutritional status in chickpea (*Cicer arietinum* L.). *Agronomy* 11:105. doi: 10.3390/agronomy11010105

Raja, P., Uma, S., Gopal, H., and Govindarajan, K. (2006). Impact of bio inoculants consortium on rice root exudates, biological nitrogen fixation and plant growth. *J. Biol. Sci.* 6, 815–823. doi: 10.3923/jbs.2006.815.823

Rajasekar, S., and Elango, R. (2011). Effect of microbial consortium on plant growth and improvement of alkaloid content in *Withania somnifera* (*Ashwagandha*). *Curr. Bot.* 2, 27–30.

Raza, T., Khan, M. Y., Nadeem, S. M., Imran, S., Qureshi, K. N., Mushtaq, M. N., et al. (2021). Biological management of selected weeds of wheat through co-application of allelopathic rhizobacteria and sorghum extract. *Biol. Control* 164:104775. doi: 10.1016/j.biocontrol.2021.104775

Rhodes, D., and Hanson, A. (1993). Quaternary ammonium and tertiary sulfonium compounds in higher plants. *Ann. Rev. Plant Biol.* 44, 357–384. doi: 10.1146/annurev.pp.44.060193.002041

Saeed, Q., Xiukang, W., Haider, F. U., Kuèerik, J., Mumtaz, M. Z., Holatko, J., et al. (2021). Rhizosphere bacteria in plant growth promotion, biocontrol, and bioremediation of contaminated sites: A comprehensive review of effects and mechanisms. *Int. J. Mol. Sci.* 22:10529. doi: 10.3390/ijms221910529

Sapre, S., Gontia-Mishra, I., and Tiwari, S. (2018). Klebsiella sp. confers enhanced tolerance to salinity and plant growth promotion in oat seedlings (*Avena sativa*). *Microbiol. Res.* 206, 25–32. doi: 10.1016/j.micres.2017.09.009

Sarma, B. K., Yadav, S. K., Singh, S., and Singh, H. B. (2015). Microbial consortium-mediated plant defense against phytopathogens: Readdressing for enhancing efficacy. *Soil Biolo. Biochem.* 87, 25–33.

Sarwar, M., Arshad, M., Martens, D. A., and Frankenberger, W. T. Jr. (1992). Tryptophan dependent biosynthesis of auxins in soil. *Plant Soil* 147, 207–215. doi: 10.1007/BF00029072

Schwyn, B., and Neilands, J. B. (1987). Universal chemical assay for the detection and determination of siderophores. *Anal. Biochem.* 160, 47–56.

Shahzad, H., Ullah, S., Iqbal, M., Bilal, H. M., Shah, G. M., Ahmad, S., et al. (2019). Salinity types and level-based effects on the growth, physiology and nutrient contents of maize (*Zea mays*). *Italian J. Agron.* 14, 199–207.

Shultana, R., Kee Zuan, A. T., Yusop, M. R., and Saud, H. M. (2020). Characterization of salt-tolerant plant growth-promoting rhizobacteria and the effect on growth and yield of saline-affected rice. *PLoS One* 15:e0238537. doi: 10.1371/journal.pone.0238537

Silva, M. L. D. S., Sousa, H. G. D., Silva, M. L. D. S., Lacerda, C. F. D., and Gomes-Filho, E. (2019). Growth and photosynthetic parameters of saccharine sorghum plants subjected to salinity. *Acta Sci. Agron.* 41:e42607.

Simons, M., Van der Bij, A. J., Brand, I., De Weger, L. A., Wijffelman, C. A., and Lugtenberg, B. J. J. (1996). Gnotobiotic system for studying rhizosphere colonization by plant growth-promoting *Pseudomonas* bacteria. *Mol. Plant Microbe Interact.* 9, 600–607. doi: 10.1094/MPMI-9-0600

Singh, P., Chauhan, P. K., Upadhyay, S. K., Singh, R. K., Dwivedi, P., Wang, J., et al. (2022). Mechanistic Insights and Potential Use of Siderophores Producing Microbes in Rhizosphere for Mitigation of Stress in Plants Grown in Degraded Land. *Front. Microbiol.* 13:898979. doi: 10.3389/fmicb.2022.898979

Singh, R. K., Singh, P., Sharma, A., Guo, D.-J., Upadhyay, S. K., Song, Q.-Q., et al. (2022). Unraveling Nitrogen Fixing Potential of Endophytic Diazotrophs of Different Saccharum Species for Sustainable Sugarcane Growth. *Int. J.Mol. Sci.* 23:6242. doi: 10.3390/ijms23116242

Smyth, E. M., McCarthy, J., Nevin, R., Khan, M. R., Dow, J. M., Gara, F. O., et al. (2011). *In vitro* analyses are not reliable predictors of the plant growth promotion capability of bacteria; a *Pseudomonas fluorescens* strain that promotes the growth

and yield of wheat. *J. Appl. Microbiol.* 111, 683–692. doi: 10.1111/j.1365-2672.2011.05079.x

Sohaib, M., Zahir, Z. A., Khan, M. Y., Ans, M., Asghar, H. N., Yasin, S., et al. (2020). Comparative evaluation of different carrier-based multi-strain bacterial formulations to mitigate the salt stress in wheat. *Saudi J. Biol. Sci.* 27, 777–787. doi: 10.1016/j.sjbs.2019.12.034

Ullah, S., Hussain, M. B., Khan, M. Y., and Asghar, H. N. (2017). "Ameliorating Salt Stress in Crops through Plant Growth-Promoting Bacteria," in *Plant-Microbe Interactions in Agro-Ecological Perspectives*, eds D. P. Singh, et al. (Singapore: Springer Nature Singapore Pte Ltd), 549–575. doi: 10.1007/978-981-10-5813-4_28

Upadhyay, S. K., and Chauhan, P. K. (2022). Optimization of eco-friendly amendments as sustainable asset for salt-tolerant plant growth-promoting bacteria mediated maize (Zea Mays L.) plant growth, Na uptake reduction and saline soil restoration. *Environ. Res.* 211:113081. doi: 10.1016/j.envres.2022.113081

Upadhyay, S. K., Singh, J. S., Saxena, A. K., and Singh, D. P. (2012). Impact of PGPR inoculation on growth and antioxidant status of wheat under saline conditions. *Plant Biol.* 14, 605–611. doi: 10.1111/j.1438-8677.2011.00533.x

Upadhyay, S. K., Srivastava, A. K., Rajput, V. D., Chauhan, P. K., Bhojiya, A. A., Jain, D., et al. (2022). Root exudates: Mechanistic insight of plant growth promoting rhizobacteria for sustainable crop production. *Front. Microbiol.* 13:916488. doi: 10.3389/fmicb.2022.916488

Upadhyay, S., Singh, J., and Singh, D. (2011). Exopolysaccharide-producing plant growth-promoting rhizobacteria under salinity condition. *Pedosphere* 21, 214–222. doi: 10.1016/S1002-0160(11)60120-3

Van Veen, A. J., Van Overbeek, L. S., and Van Elsas, J. D. (1997). Fate and activity of microorganisms introduced into soil. *Microbiol. Mol. Biol. Rev.* 61, 121–133. doi: 10.1128/mmbr.61.2.121-135.1997

Wang, W., Wu, Z., He, Y., Huang, Y., Li, X., and Ye, B. C. (2018). Plant growth promotion and alleviation of salinity stress in *Capsicum annuum* L. by *Bacillus* isolated from saline soil in Xinjiang. *Ecotox. Environ. Safe* 164, 520–529. doi: 10.1016/j.ecoenv.2018.08.070

Wani, P. A., Khan, M. S., and Zaidi, A. (2007). E_ect of metal tolerant plant growth promoting *Bradyrhizobium* sp. (vigna) on growth, symbiosis, seed yield and metal uptake by green gram plants. *Chemosphere* 70, 36–45.

Wolf, B. (1982). A comprehensive system of leaf analyses and its use for diagnosing crop nutrient status. *Commun. Soil Sci. Plant Anal.* 13, 1035–1059.

Yasin, N. A., Khan, W. U., Ahmad, S. R., Ali, A., Ahmad, A., and Akram, W. (2018). Imperative roles of halotolerant plant growth-promoting rhizobacteria and kinetin in improving salt tolerance and growth of black gram (*Phaseolus mungo*). *Environ. Sci. Pollut. Res.* 25, 4491–4505. doi: 10.1007/s11356-017-0761-0

Yildrim, E., Donmez, M. F., and Turan, M. (2008). Use of bioinoculants in ameliorative effects on radish plants under salinity stress. *J. Plant Nutr.* 31, 2059–2074.

Zahir, Z. A., Akhtar, S. S., Saifullah, M. A., and Nadeem, S. M. (2012). Comparative effectiveness of *Enterobacter aerogenes* and *Pseudomonas fluorescens* for mitigating the depressing effect of brackish water on maize. *Int. J. Agric. Biol.* 14, 337–344.

Zahir, Z. A., Ghani, U., Naveed, M., Nadeem, S. M., and Asghar, H. N. (2009). Comparative effectiveness of *Pseudomonas* and *Serratia* sp. containing ACC deaminase for improving growth and yield of wheat (*Triticum aestivum* L.) under salt-stressed conditions. *Arch. Microbiol.* 191, 415–424. doi: 10.1007/s00203-009-0466-y

Zahir, Z. A., Nadeem, S. M., Khan, M. Y., Binyamin, R., and Waqas, M. R. (2019). "Role of Halotolerant Microbes in Plant Growth Promotion Under Salt Stress Conditions," in *Saline Soil-Based Agriculture by Halotolerant Microorganisms*, eds M. Kumar, H. Etesami, and V. Kumar (Singapore: Springer). doi: 10.1007/978-981-13-8335-9_10

Zhang, H., Kim, M. S., Sun, Y., Dowd, S. E., Shi, H., and Pare, P. W. (2008). Soil bacteria confer plant salt tolerance by tissue-specific regulation of the sodium transporter *HKT1*. *Mol. Plant Microbe Interact.* 21, 737–744. doi: 10.1094/MPMI-21-6-0737

frontiers | Frontiers in Microbiology

TYPE Original Research
PUBLISHED 01 November 2022
DOI 10.3389/fmicb.2022.1024672

OPEN ACCESS

EDITED BY
Muhammad Zahid Mumtaz,
The University of Lahore, Pakistan

REVIEWED BY
Yizhi Sheng,
China University of Geosciences, China
Susana De La Rosa-García,
Universidad Juárez Autónoma de Tabasco, Mexico
Andrea Ceci,
Sapienza University of Rome, Italy

*CORRESPONDENCE
Lifei Yu
lfyu@gzu.edu.cn

SPECIALTY SECTION
This article was submitted to Microbiological Chemistry and Geomicrobiology, a section of the journal Frontiers in Microbiology

RECEIVED 22 August 2022
ACCEPTED 04 October 2022
PUBLISHED 01 November 2022

CITATION
Chen J, Li F, Zhao X, Wang Y, Zhang L, Yan L and Yu L (2022) Change in composition and potential functional genes of microbial communities on carbonatite rinds with different weathering times. *Front. Microbiol.* 13:1024672. doi: 10.3389/fmicb.2022.1024672

Change in composition and potential functional genes of microbial communities on carbonatite rinds with different weathering times

Jin Chen[1], Fangbing Li[1], Xiangwei Zhao[1], Yang Wang[1], Limin Zhang[2], Lingbin Yan[1] and Lifei Yu[1]*

[1]Key Laboratory of Plant Resources Conservation and Germplasm Innovation in Mountainous Region (Ministry of Education), College of Life Sciences and Institute of Agro-Bioengineering, Guizhou University, Guiyang, Guizhou, China, [2]Institute of Guizhou Mountain Resources, Guizhou Academy of Sciences, Guiyang, Guizhou, China

Organisms and time are important factors for rock weathering to form soils. However, weathering time is usually difficult to quantitatively study, and the potential microorganisms involved in rock weathering are difficult to identify qualitatively. Currently, there is no clear conclusion on how ecological strategies of carbonatite weathering rind microorganisms change with weathering time, and how the microbial composition and functional genes involved in element cycling change over two century-scale weathering time. In this study, we selected abandoned carbonate tombstones as the subject and used the date when the tombstones were erected by humans as the onset of weathering. Using metagenome sequencing methods, we investigated the trends in the composition of fungal, bacterial and archaeal communities of carbonate weathering rind and related elemental cycle functional genes during a weathering time of 19 to 213 years. The results showed that: (1) with the increase in weathering time, at the phylum level, microbial taxa gradually shifted from r-strategists (faster turnover rates, higher mortality rates, higher reproduction, lower competition rate) to K-strategists (slower turnover rates, lower mortality rates, lower reproduction, higher competition rate), which correspondingly increased the abundance of functional genes related to C and N cycles. (2) The properties of the parent rock layer determines the colonization and distribution of weathering rind microorganisms (especially prokaryotic microorganisms) and the corresponding functional gene abundance. Our study provides new insights into the weathering process of carbonate rocks.

KEYWORDS

ecological succession, biodeterioration, bioweathering, r strategy, K strategy, functional genes

Introduction

Rock weathering is the result of a combination of physical, chemical, and biological weathering, with organisms, particularly microorganisms, playing an important role in the early rock weathering process. On one hand, biodeterioration of rocks caused by microbial activity has led to extensive destruction of artefacts, and therefore biodeterioration of rocks is considered to be one of the most important factors threatening the safety of stone artefacts and buildings (Liu et al., 2020). On the other hand, in degraded ecosystems (e.g., karstic desertification zones), the interaction of microorganisms with rock minerals produces protons, hydroxyl ions, or metal-chelating metabolic products that alter the dynamics of rock surface reactions (Rogers and Bennett, 2004), facilitate weathering processes and form soils that are important contributors to the ecological restoration of degraded areas. As a result, the biological weathering of rocks has received widespread attention (Warscheid and Braams, 2000; Gaylarde and Gaylarde, 2004; Checcucci et al., 2022; Liu et al., 2022; Wu et al., 2022). The biological deterioration of rocks and lithic artefacts is a complex process of microbial action in which a rich diversity of microorganisms are involved in a variety of biogeochemical cycling processes (Sáiz-Jiménez, 1999; Warscheid and Braams, 2000; Gaylarde and Gaylarde, 2004; Gadd, 2017; Liu et al., 2020). Therefore, the use of microbiomics to decipher the structure and function of microorganisms involved in rock weathering is of great ecological importance.

Bioreceptivity originated from materials science, which is the ability of materials to be colonized by living organisms (Guillitte, 1995). Besides, the bioreceptivity of rocks is affected by environmental conditions (such as temperature, humidity and light, etc.) and rock properties (such as porosity, water permeability and roughness, etc.) (Miller et al., 2012). Differences in the bioreceptivity of rocks allow different kinds of microscopic taxa (such as bacteria, fungi, algae, etc.) to deposit on the rock surface, forming biofilms (Warscheid and Braams, 2000). In the beginning, the structural pores of the rock surface provided suitable niches for the dissemination of airborne microbes for their deposition and capture (Šimonovičová et al., 2004). Due to the very limited availability of nutrients on the rock surface, carbon dioxide in the air is the main carbon source for microbes on the rock surface (Liu et al., 2020). Phototrophs (such as cyanobacteria and algae, etc.) and chemolithoheterotroph (nitrifying bacteria and sulfur-oxidizing fungi, etc.) are major contributors to the assimilation of carbon dioxide into organic form for subsequent bio-colonizers (Salvadori and Municchia, 2016; Vázquez-Nion et al., 2018). Ammonia and ammonia oxides in the air are the main nitrogen sources for the microorganisms on the rock surface, which are utilized by nitrifying bacteria and archaea to produce nitrous oxide and nitric acid, which cause acid corrosion of stone artefacts (Meng et al., 2016, 2017). In addition, sulfur exists in the atmosphere in organic and inorganic forms of various valence states, and in the sulfur cycle, sulfur-oxidizing bacteria and sulfate-reducing bacteria are important factors leading to biocorrosion of rocks (Kusumi et al., 2011, 2013). However, the above studies are mainly aimed at the study of rock surface microorganisms in a certain period of time, and very few studies involve the succession of microbial communities on the surface of carbonate rocks and their correlation with the dissolution characteristics of carbonate rocks on a time scale.

From a soil science perspective, rock biodeterioration is the process of biological decomposition of rock minerals to form soil, which is manifested by surface disintegration (Gleeson et al., 2006), loss of rock hardness, and accumulation of secondary minerals. From an ecological point of view, rock biodeterioration is a process of biological primary succession on the rock surface, manifested by biofilm attachment, covering of the rock surface with green-black stains (Cutler et al., 2013b), and formation of bio-pitting (Piñar et al., 2013), which, in turn, alters the rock surface environment and supports the growth of lichens and bryophytes. Succession theory can be applied to the process of rock succession, and in Odum's related account of plant community succession, r-strategists dominate early in succession, while K-strategists dominate later (Odum, 1969). In a stable environment, the reproduction of organisms is likely to reach the environmental capacity (that is, the saturation density K value in the logistic equation), while in an unstable environment, disturbances often occur, with high reproductive capacity (innate rate of increase) organisms are usually able to adapt (MacArthur, 1960; MacArthur and Wilson, 1967). K-strategists usually have slower growth rate and higher competitive capacity, but r-strategists usually with a faster growth rate and higher turnover rate (Bardgett et al., 2005; Yan et al., 2020). The reproduction rate of bacteria is higher than that of fungi, and the competition rate of fungi is higher than that of bacteria. Therefore, in microbial communities, fungi tend to be K-strategists, while bacteria tend to be r-strategists (Bardgett et al., 2005; Kaiser et al., 2014; Chen et al., 2016). During secondary succession in derelict land, the ratio of fungi to bacteria increases, indicating a gradual increase in the number of K-strategists during secondary succession (Zhou et al., 2017). In addition, within bacterial taxa, Acidobacteria and Actinobacteria are considered K-strategists, while Proteobacteria and Bacteroidetes are considered r-strategists (Fierer et al., 2007; Zechmeister-Boltenstern et al., 2015). Among the fungal taxa, Basidiomycota is considered a K-strategist, while Ascomycota is considered an r-strategist (Bastian et al., 2009; Zumsteg et al., 2012). In archaeal communities, Euryarchaeota are thought to occur early in the succession, while Crenarchaeota are thought to occur later (Zumsteg et al., 2012). Further, the abundance of genes associated with C (for example, *rbcL*, *accA* and *porA* etc.) and N (such as *nifH*, *nifK* and *napA* etc.) cycling has been reported to be greater in late- rather than in the early succession (Blaud et al., 2018; Liu et al., 2018; Yan et al., 2020). However, the strategic shift in microbial taxa and trends in functional genes during weathering of carbonate rocks are not well understood.

Southwest China is a typical karst distribution area, where carbonate rock is widely used as a common building material for tombstones. According to local customs, when a tombstone is built, the time of its erection will be engraved at the same time, which provides us with a relatively accurate weathering start time.

Considering the possible damage caused by sampling, we chose to investigate abandoned tombstones where tomb relocation events have occurred. We calculated the carbonatite weathering duration (2021 minus the engraved year on the tombstone) using the etched date on the abandoned tombstone as the weathering start time. This study investigated the bioweathering patterns of carbonate rocks on a time scale using abandoned carbonate rocks at different times of monument erection, which helps to further our understanding of microbial weathering processes and mechanisms of carbonate rocks. During progressive succession, environmental conditions tend to change from unstable to stable, and from entropy increase to entropy decrease. With the increase of weathering time, the surface of carbonatite is dissolved (Zha et al., 2020), roughness increases (Emmanuel and Levenson, 2014; Levenson and Emmanuel, 2016), and many microhabitats are formed (Jones, 1965), which increases the accumulation ability of organic matter in the atmosphere (Saheb et al., 2016), the environment tends to be stable, and the carbonatite rock rind begins to form. The carbonatite surface gradually became suitable for the r-strategist from the initial suitable for the K-strategist. Therefore, we hypothesized the following: (i) as weathering time increases, the microbial community shifts from r-strategy (i.e., high turnover, low competition) to K-strategy (i.e., high competitiveness, low growth). (ii) With the increase in weathering time, the abundance of functional genes related to C, N, and S cycles gradually increases.

To test the hypotheses, we selected carbonatite tombstones concentrated in a small area, with little disturbance, and different weathering times as the research objects. We used metagenomes to interpret the structure and functional composition of microbial communities to explore the changing trend of microbial community structure and function during bioweathering of carbonate rocks during succession. Our research goal is to better describe and understand the microbial weathering patterns of carbonate rocks during succession.

Materials and methods

Site description and sampling strategy

The study area is located in the karst area of southwest China near the Guiyang City (26°26′46″–26°26′56″, 106°38′06″–106°39′18″), which has a subtropical humid and mild climate, with rain and heat in the same period. The average annual temperature is 15.3°C, the average altitude is about 1,100 m, the average annual rainfall is approximately 1,100–1,300 mm, and the sunshine duration are about 1,000–1,100 h.

We used the tombstone erection time as the onset of weathering (Figure 1A), and among the 18 abandoned tombstones we investigated, the weathering time ranged from 19 to 213 years (Supplementary Table S1). During our investigation, we determined whether the target object was carbonatite based on the results of the "cold acid test" (Ford and Williams, 2013) combined with XRD data (Supplementary Figure S1). Due to local customs, the A, B, C, and D sides of tombstones (Figure 1) are generally disturbed to varying degrees during special festivals (such as the Ching Ming Festival), while the side E is left undisturbed (Figures 1B,C). To ensure rationality of sampling, therefore, we used only the E side of tombstones in our study. In addition, the tombstones were covered with moss and/or lichens, which were carefully removed to prevent contamination of the rock samples. To obtain a true weathered crust sample, we controlled the angle grinder to ensure full contact with the rock until an entire available weathered surface was removed. To prevent cross-contamination, we replaced the grinding disc for each tombstone. For sampling, we laid a sterilized (121°C, 103 kPa for 20 min) rectangular piece of medical surgical wrap flat on the E side directly below to collect sample particles. We measured the available length and height (width) of the E side of the tombstone and recorded it (Supplementary Table S1). Before the formal sampling, we simulated the sampling situation of the angle grinder on the limestone rock surface, and obtained that the angle grinder contacted the rock surface for about 3 s, and the rock surface could be ground off. Sampling was carried out from top to bottom using an angle grinder. To collect the samples, we controlled the angle grinder to touch the E side of the tombstone at a constant speed for approximately 3 s and then moved to the next sampling points until the entire available E side was collected. Finally, the samples that fell onto the wrapping cloth were collected. For specific sampling volume and sampling area, please refer to the Supplementary Table S1. In addition, during sampling, we controlled that the lowest sampling height of the tombstone was 20 ~ 30 cm from the ground, while the highest sampling distance depended on the height of the tombstone. Finally, as a control for the regolith, we took 18 un-weathered samples of each tombstone. We used a geological hammer to knock it off and cut off the weathered part of the rock to get the un-weathered part, which is then ground into powder.

Regolith sampling and measurement

The collected weathering rind samples (n = 18) were divided into two parts, one was passed through a 0.25-mm sieve for Organic carbon (OC), total nitrogen (TN), total phosphorus (TP), and total potassium (TK) tests, and the other was stored at −80°C after removing large sand and plant residues for metagenomic analysis. OC was determined by the H_2SO_4-$K_2Cr_2O_7$ method (Bao, 2000), TN by Kjeldahl (Page, 1982), TP by the H_2SO_4-$HClO_4$ abatement colorimetric method, and TK by flame photometry (Bao, 2000). We used the weathering strength (W_s) (Huang et al., 1996) to measure the degree of weathering relative to the parent rock, and used the mobiles index (I_{mob}) to characterize the element migration of the overweathered layer relative to the parent rock during the carbonatite weathering process (Irfan, 1996). In addition, X-ray fluorescence (XRF) was used to measure the content of major element chemistry of carbonatite, and X-ray diffraction (XRD) was used to determine the rock phase. Prior to this, in order to prevent organic matter content in the sample from

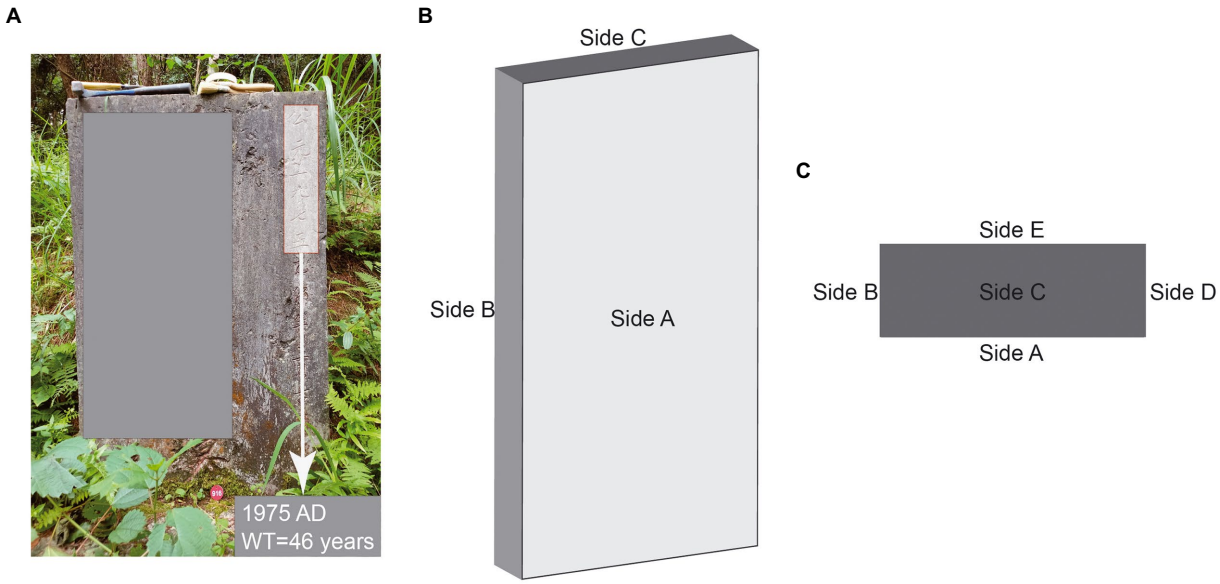

FIGURE 1
Sketch of carbonatite tombstone; **(A)** Entity diagram of carbonatite tombstone, **(B)** Stereogram of carbonatite gravestone, **(C)** Top view of carbonatite tombstone.

affecting the test results, we placed samples in a porcelain crucible and heated them to 950°C to eliminate this effect. Finally, according to the definition of bioreceptivity (Guillitte, 1995), we took the number of all individuals in each sample as the bioreceptivity of the sample.

DNA extraction, library construction, and metagenomic sequencing

Total genomic DNA was extracted from carbonatite regolith samples using the E.Z.N.A.® Soil DNA Kit (Omega Bio-tek, Norcross, GA, U.S.) according to manufacturer's instructions. Concentration and purity of extracted DNA was determined with TBS-380 and NanoDrop 2000, respectively. DNA extract quality was assessed on a 1% (w/v) agarose gel.

DNA samples were fragmented to an average size of about 400 bp using Covaris M220 (Gene Company Limited, China) for paired-end library construction. A paired-end library was constructed using NEXTflex™ Rapid DNA-Seq (Bioo Scientific, Austin, TX, USA). Adapters containing the full complement of sequencing primer hybridization sites were ligated to the blunt-end of fragments. Paired-end sequencing was performed on an Illumina HiSeq Xten instrument (Illumina Inc., San Diego, CA, USA) at Majorbio Bio-Pharm Technology Co., Ltd. (Shanghai, China) using HiSeq X Reagent Kits according to the manufacturer's instructions.[1]

1 www.illumina.com

Sequence quality control and genome assembly

The raw reads from metagenome sequencing were used to generate clean reads by removing adaptor sequences, trimming, and removing low-quality reads (reads with N bases, a minimum length threshold of 50 bp and a minimum quality threshold of 20) using fastp (Chen et al., 2018; Ren et al., 2022, version 0.20.0)[2] on the free online Majorbio Cloud Platform (cloud. majorbio.com). These high-quality reads were then assembled into contigs using MEGAHIT (Li et al., 2015) (parameters: kmer_min = 47， kmer_max = 97， step = 10, version 1.1.2)[3] which makes use of succinct de Bruijn graphs. Contigs equal to or over 300 bp in length were selected as the final assembled result.

Gene prediction, taxonomy, and functional annotation

Open reading frames (ORFs) in contigs were identified using MetaGene (Noguchi et al., 2006).[4] Predicted ORFs equal to or over 100 bp in length were retrieved and translated into amino acid sequences using the NCBI translation table.[5]

2 https://github.com/OpenGene/fastp
3 https://github.com/voutcn/megahit
4 http://metagene.cb.k.u-tokyo.ac.jp
5 http://www.ncbi.nlm.nih.gov/Taxonomy/taxonomyhome.html/index.cgi?chapter=tgencodes#SG1

A non-redundant gene catalog was constructed using CD-HIT (Fu et al., 2012, version 4.6.1)[6] with 90% sequence identity and 90% coverage. After quality control, reads were mapped to the non-redundant gene catalog with 95% identity using SOAPaligner (Li et al., 2008, version 2.21),[7] and gene abundance in each sample was evaluated.

Representative sequences of non-redundant gene catalogs were annotated based on the NCBI NR database using blastp as implemented in DIAMOND v0.9.19 with an e-value cutoff of $1e^{-5}$ using DIAMOND (Buchfink et al., 2015, version 0.8.35)[8] for taxonomic annotations. Cluster of orthologous groups of proteins (COG) annotation for the representative sequences were performed using DIAMOND (Buchfink et al., 2015, version 0.8.35)[9] against the eggNOG database (version 4.5.1) with an e-value cutoff of $1e^{-5}$. KEGG annotations were also generated using DIAMOND (Buchfink et al., 2015, version 0.8.35)[10] against the Kyoto Encyclopedia of Genes and Genomes database (version 94.2)[11] with an e-value cutoff of $1e^{-5}$.

Calculations and statistical analyses

The abundance counts for taxa were converted by multiplying the relative abundance by the minimum total sequence count for all samples, and this method was used to correct for the different sequencing depths of the samples (McMurdie and Holmes, 2014; Weiss et al., 2017). The relative abundance of a bacterial phylum is the ratio of the abundance of each bacterium at the phylum level compared to the total bacterial abundance. In addition, the relative abundance of fungal taxa, archaeal taxa, and functional genes is determined in the same way as bacterial taxa. Functional gene abundance is often used to predict biogeochemical cycle rates (Jha et al., 2017). For example, *nifH* for N2 fixation (Rösch and Bothe, 2005) and *amoA* for nitrification (Wei et al., 2019). We find the relevant KO numbers based on the functional genes associated with a particular biogeochemical cycle process as the corresponding functional genes. For example, in the N cycle, the KO number of *nifH* is K02588, while the *nifK* is K02591, and both K02588 and K02591 are components of N-cycle corresponding functional genes (see Supplementary Table S2 for more details).

The relative abundance of C, N, and S cycle-related genes was calculated as the ratio of C, N, and S cycle-related gene abundance compared to the KEGG Orthology total gene abundance. The relative abundance of C Fixation genes, C Degradation genes, and Methane Metabolism genes were calculated based on the ratios of C Fixation genes, C Degradation genes, and Methane Metabolism genes to the abundance of C cycle genes, respectively. The relative abundance of Calvin cycle genes, Reductive citrate cycle (rTCA) genes, Reductive acetyl-CoA or Wood-Ljungdahl pathway (rAcCoA) genes, 3-Hydroxypropionate bi-cycle (3HP) genes, Hydroxypropionate-hydroxybutylate cycle (3HP/4HB) genes, and Dicarboxylate-hydroxybutyrate cycle (DC/4HB) genes were calculated based on the ratios of each respective gene compared to the abundance of C Fixation genes. Similarly, the relative abundance of Starch Degradation genes, Cellulose Degradation genes, Chintin Degradation genes, Hemicellulose Degradation genes, Lignin Degradation genes, and Aromatics Degradation genes were calculated based on the ratios of each respective gene compared to the abundance of C Degradation genes. Moreover, the relative abundance of Assimilatory N Reduction (ANRA) genes, Dissimilatory N Reduction (DNRA) genes, Nitrification genes, Denitrification genes, N Transport genes, N Fixation genes, and Organic N Metabolism (ONM) genes were also calculated based on the ratios of each respective gene compared to the abundance of N cycle genes. Further, the relative abundance of Assimilatory sulfate reduction (ASR) genes, Dissimilatory sulfate reduction (DSR) genes and Thiosulfate oxidation by SOX complex (SOX) genes were calculated based on the ratios of each respective gene compared to the abundance of S cycle genes.

The meteorological data came from the China Meteorological Administration.[12] To analyze the characteristics of taxa and functional genes with weathering time, the significance of linear models was tested with the built-in function 'lm' in *stat* package of R (version 4.2.1). *p* values were obtained by permutation test when the data did not conform to normal distribution or/and homogeneity of variance. In the Mantel test, taxa data that exist in all samples (n = 18) were selected for analysis. The Bray–Curtis distance algorithm was used to conduct Mantel tests on taxa and functional gene data, and the Euclidean distance algorithm was used to conduct Mantel tests on environmental data. Mantel validation and drawing were performed using the R package *linkET*. When doing regression analysis, composition data were transformed by $\log_{10}(x+x_0)$, where x is the relative abundance, x_0 is a constant, and $x_0 = 0.9 \cdot \min(x)$. The structural equation model (SEM) was evaluated with the built-in 'sem' function in the R package *lavaan* (Rosseel, 2012).

Results

Changes in element content of carbonatite regolith at different weathering times

Because the properties of carbonatite parent rocks at different weathering times are different, the relative changes in the element content of the regolith relative to the parent rock layer can better

6 http://www.bioinformatics.org/cd-hit/
7 http://soap.genomics.org.cn/
8 http://www.diamondsearch.org/index.php
9 http://www.diamondsearch.org/index.php
10 http://www.diamondsearch.org/index.php
11 http://www.genome.jp/keeg/
12 http://www.cma.gov.cn/

reflect the relative changes of the main elements of carbonatite at different weathering times. The XRF results show that, relative to the parent rock, with the increase of the carbonatite weathering time, the Mg, Al, Si, Fe, and Ti in the carbonatite regolith were gradually enriched, and the increment relative to the parent rock layer was significantly reduced (Figure 2). The content of Ca gradually decreased with the increase of weathering time, and the increment of Ca relative to the parent rock decreased significantly with the increase of weathering time (Figure 2).

In addition, the mobiles index decreased significantly with increasing weathering time (Figure 3B), while the weathering strength was reversed (Figure 3A). It shows that with the increase of weathering time, the weathering degree of carbonatite gradually increases, while the element migration rate decreases gradually.

Changes in gene abundance in microorganisms

A total of 6,282,480 non-redundant genes were screened out in the metagenomes of all samples, including 5,207,594 in bacteria, 108,547 in fungi, and 30,221 in archaea. In addition, NR annotation results showed that the ratio of fungal abundance to bacterial abundance decreased significantly with an increase in the weathering time of carbonate rocks, while the ratio of archaeal abundance to bacterial abundance did not change significantly (Supplementary Figure S2). The Shannon–Wiener index showed that the diversity of bacteria decreased significantly with an increase in weathering time, while the diversity of fungi and archaea did not change significantly with an increase in weathering time (Supplementary Figure S3). The bioreceptivity and total diversity first increased and then decreased with the increase in weathering time (Supplementary Figure S2).

Changes in fungal, bacterial, and archaeal diversity and composition at different weathering times

Based on similarities to entries in the NCBI-NR database, among the 18 samples, per sample read counts ranged from 18,326 to 22,469 reads, 97.88% of sequences were classified as Bacteria, 0.41% were classified as Archaea, 1.51% were classified as Eukaryota (among them, 1.21% were classified as Fungi), and 0.03% were classified as Viruses. The phyla Actinobacteria (37.03%) and Proteobacteria (23.07%) dominated carbonate rock rind bacterial communities (Figure 4). The average relative abundance of Actinobacteria significantly increased with the

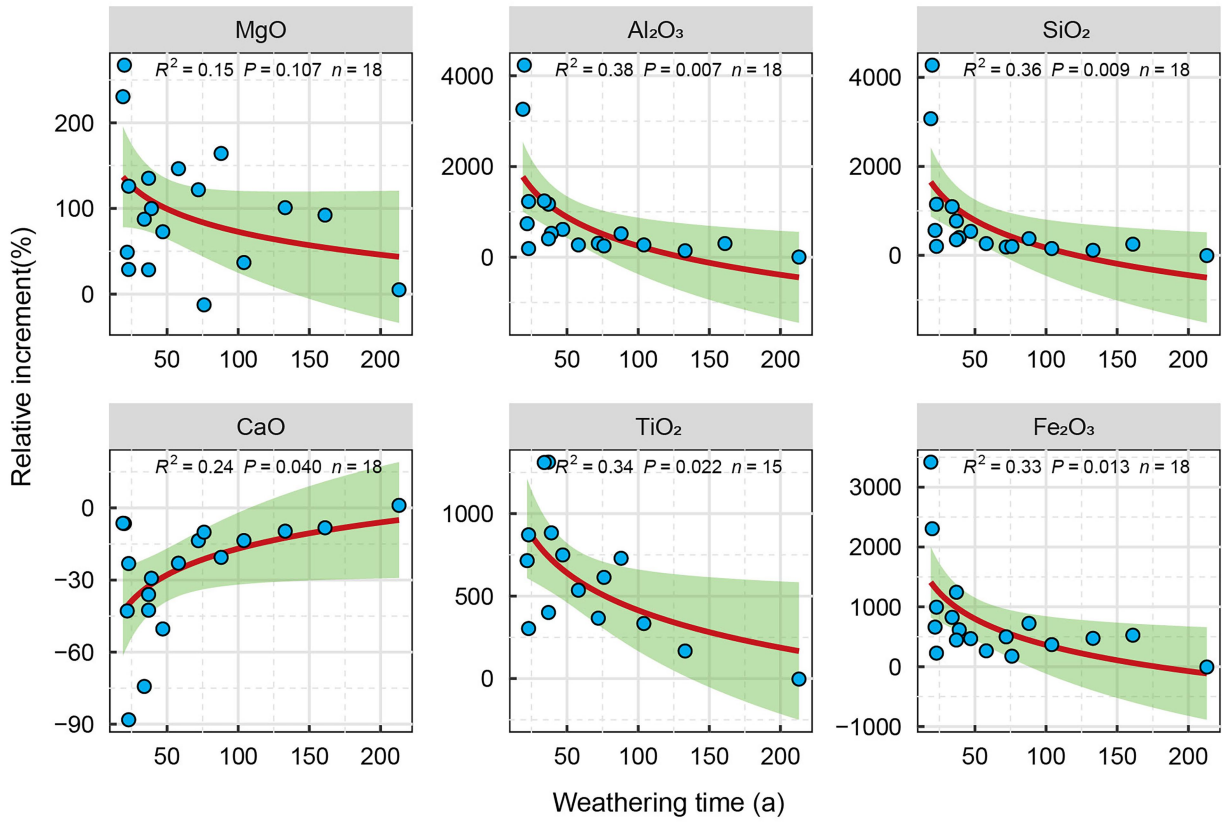

FIGURE 2
Relative variation of elements in carbonatite weathering rind with different weathering years.

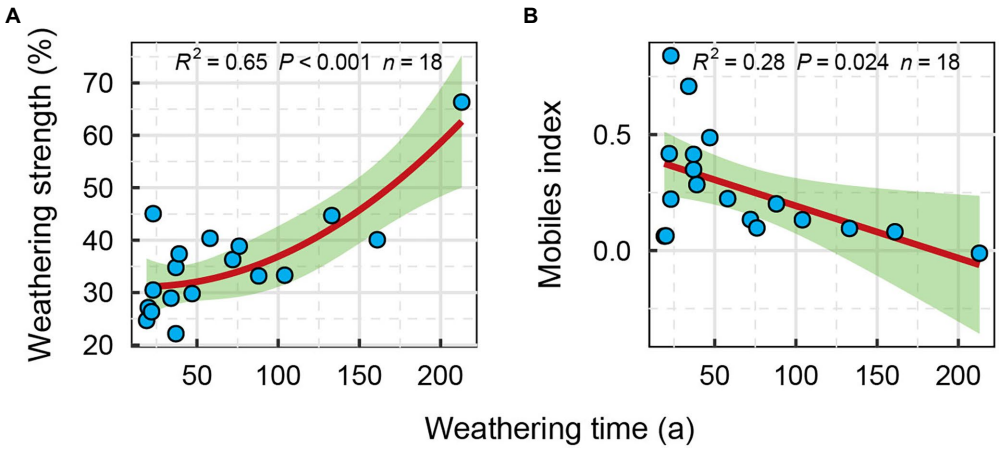

FIGURE 3
Regression fitting between weathering index and weathering time; **(A)** Weathering strength, **(B)** Mobiles index.

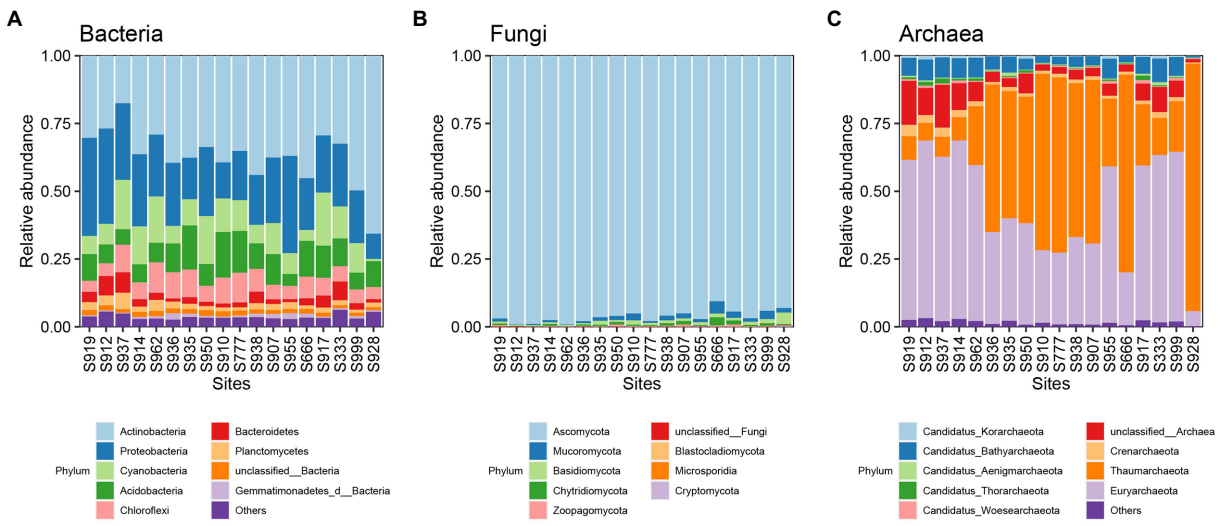

FIGURE 4
The relative abundance of different taxa at the phylum taxonomic level (the top 10 relative abundances are shown); **(A)** Bacteria, **(B)** Fungi and **(C)** Archaea.

increase in weathering time (Table 1). The average relative abundance of Proteobacteria decreased significantly with the increase in weathering time, while the other bacterial phyla with average relative abundance >1% had no significant trend during succession (Table 1). The phyla Ascomycota (96.25%) dominated carbonate rock rind fungal communities (Figure 4). The relative abundance of Ascomycota decreased significantly, while Mucoromycota and Basidiomycota increased significantly during succession (Table 1). The phyla Euryarchaeota (44.28%) and Thaumarchaeota (38.49%) dominated carbonate rock rind archaeal communities (Figure 4). At a threshold of mean relative abundance >1%, Crenarchaeota and Euryarchaeota decreased significantly, while Thaumarchaeota showed no significant change during succession (Table 1).

Potential functional pathways in microorganisms at different weathering times

The corresponding ORFs were annotated according to the KEGG and CAZy databases to quantify the changes of potential functional genes of carbonate rock rind at different weathering times. In total, 450 pathway-associated genes and 552 CAZy genes were screened from all metagenomes. The dominant categories were biosynthesis of secondary metabolites (8.41%), microbial metabolism in diverse environments (5.67%), biosynthesis of amino acids (3.05%), carbon metabolism (2.89%), ABC transporters (2.73%), and quorum sensing (1.8%) of the total KEGG pathway Level 3 annotated genes (Supplementary Table S3).

TABLE 1 The variations of phyla of bacteria, fungi, and archaea over different weathering times (average relative abundance >1%).

Phylum	Slope	*SE*	*p*-param	R^2	Adj R^2	HmV and Normality	*p*-perm	*p*-sign
Acidobacteria	−2.12E-05	7.48E-04	0.978	<0.01	Null	Null	Null	0.978
Actinobacteria	1.41E-03	4.22E-04	0.004	0.41	0.38	No, Non-N	0.005	0.005**
Bacteroidetes	−8.07E-04	1.21E-03	0.516	0.03	Null	Null	Null	0.516
Chloroflexi	−1.18E-03	6.14E-04	0.072	0.19	Null	Null	Null	0.072
Cyanobacteria	−3.20E-03	1.20E-03	0.017	0.31	0.26	No, HtV	0.029	0.029*
Planctomycetes	−1.71E-03	7.60E-04	0.039	0.24	0.19	Yes	Null	0.039*
Proteobacteria	−1.50E-03	5.81E-04	0.020	0.29	0.25	Yes	Null	0.020*
Ascomycota	−1.19E-04	3.60E-05	0.005	0.40	0.37	No, Non-N	0.012	0.012*
Basidiomycota	3.89E-03	7.94E-04	0.000	0.60	0.57	Yes	Null	<0.001***
Mucoromycota	3.59E-03	1.45E-03	0.025	0.28	0.23	Yes	Null	0.025*
Candidatus Bathyarchaeota	−2.39E-03	1.10E-03	0.045	0.23	0.18	No, HtV	0.057	0.057
Crenarchaeota	−2.33E-03	8.72E-04	0.017	0.31	0.27	Yes	0.017	0.017*
Euryarchaeota	−2.44E-03	1.07E-03	0.036	0.25	0.20	No, HtV	0.037	0.037*
Thaumarchaeota	2.12E-03	1.66E-03	0.221	0.09	Null	Null	Null	0.221

The relative abundance of bacterial, fungal, and archaeal phyla were averaged for each sample ($n = 18$).
The variance explained (R^2), regression slope, and parametric *p* value (*p*-param) of the linear regression, normality test, homogeneity test for variance, and permutation test *p* value (*p*-perm) with different weathering times are shown in the table (*indicates $p < 0.05$, ** indicates $p < 0.01$, and ***indicates $p < 0.001$). HmV, homogeneity of variance; HtV, heterogeneity of variance; *p*-sign, significance value of *p*.

In all pathways with average relative abundance >1%, biosynthesis of secondary metabolites, microbial metabolism in diverse environments, biosynthesis of amino acids, carbon metabolism, glyoxylate and dicarboxylate metabolism, and pyruvate metabolism increased significantly with an increase in weathering time (Supplementary Table S3). However, ABC transporters, quorum sensing, and two-component systems significantly decreased with an increase in weathering time, while the other pathways showed no significant changes with weathering time (Supplementary Table S3). Glycoside hydrolases (30.92%) and glycosyl transferases (38.39%) were dominant in the class hierarchy of CAZY-related enzyme genes. However, the mean relative abundance of all class levels did not change significantly with the increase in weathering time (Supplementary Table S4).

Changes in functional genes related to C, N, and S cycle at different weathering times

We identified genes associated with C, N, and S cycles based on the KEGG Orthology database. We identified 2,640,106 genes related to the C cycle, 1,062,634 genes related to the N cycle, and 550,188 genes related to the S cycle in all metagenomes. During succession, we found that the relative abundance of genes related C (from 2.21 to 2.75%) and N (from 0.83 to 1.22%) cycling significantly increased with time (Table 2). However, the relative abundance of genes related to S cycling did not change significantly with time (Table 2). Furthermore, in S cycling, we found that the relative abundance of genes related to ASR (from 90.07 to 98.01%) significantly increased with time, but SOX (from 8.91 to 1.51%) decreased (Table 2). In N cycling, the relative abundance of genes related to denitrification (from 5.58 to 0.43%) and nitrification (3.34 to 0.06%) significantly decreased with time (Table 2), while, the other N cycle processes showed no significant changes with time. In C cycling, the relative abundance of genes related to C degradation (from 17.51 to 10.31%) significantly decreased with time, while genes related to C Fixation and methane metabolism showed no significant trend with time (Table 2). In C Fixation, the relative abundance of genes related to 3HP/4HB (from 25.14 to 21.62%, with the main taxa being Sphingomonadaceae and Rubrobacteraceae; Supplementary Figure S12) and 3HP (from 26.89 to 22.71%, with the main taxa being Rubrobacteraceae and Sphingomonadaceae; Supplementary Figure S11) significantly decreased with time, while genes related to DC/4HB (from 33.93 to 42.54%), rTCA (from 43.55 to 51.97%), and rAcCoA (from 9.34 to 12.18%) significantly increased with time (Table 2). In C Degradation, the relative abundance of genes related to starch degradation (from 30.04 to 46.45%) and aromatics degradation (from 0.34 to 1.65%) significantly increased with time, while genes related to cellulose degradation (from 30.05 to 16.68%) significantly decreased with time (Table 2).

Drivers of microbial biodiversity and biogeochemical cycling genes at different weathering times

To identify the drivers of carbonate rock rind microbes and related gene functions at different weathering times, we correlated differences in taxa composition (present in all 18 samples) and gene function composition (relative abundance of genes mainly related to C, N, and S cycles) with differences in environmental factors (physicochemical factors and oxide molecular ratio of regolith, and parent rock oxide molecular ratio; Figure 5A).

TABLE 2 Variations of the relative abundance of genes related to microbial biogeochemical cycling over different weathering times (mean relative abundance >1%).

Gene function category	Relative abundance % (mean abundance)	HmV and normality	Slope	SE	R^2	p-param	Adj R^2	*p*-perm	*p*-sign
S Cycle	0.49% (30566)	Null	−2.58E-04	1.47E-04	0.16	0.099	Null	Null	Null
N Cycle	0.95% (59035)	No, HtV	8.73E-04	3.31E-04	0.30	0.018*	0.26	0.035	0.035*
C Cycle	2.34% (146672)	No, HtV	1.38E-03	3.85E-04	0.44	0.003**	0.41	0.012	0.012*
C Fixation	76.09% (111643)	Null	1.11E+00	5.51E-01	0.20	0.060	Null	Null	Null
C Degradation	12.70% (18588)	No, HtV	−1.51E+00	4.83E-01	0.38	0.007**	0.34	0.007	0.007**
Methane Metabolism	11.21% (16440)	Null	3.97E-01	3.43E-01	0.08	0.265	Null	Null	Null
ANRA	6.65% (3911)	Null	−1.44E-02	2.20E-02	0.13	0.523	Null	Null	Null
DNRA	4.36% (2592)	Null	1.29E-02	1.20E-02	0.12	0.302	Null	Null	Null
N Fixation	0.21% (122)	Null	1.96E-04	4.79E-03	0.06	0.968	Null	Null	Null
N Transport	5.10% (2990)	Null	1.75E-02	2.93E-02	0.17	0.560	Null	Null	Null
Denitrification	1.39% (804)	Yes	−3.27E-02	1.36E-02	0.55	0.002*	0.49	0.002	0.002**
Nitrification	0.65% (368)	Yes	−2.14E-02	8.12E-03	0.60	<0.001***	0.55	<0.001	<0.001***
ONM	82.14% (48528)	Null	2.15E-02	3.89E-02	0.03	0.588	Null	Null	Null
ASR	93.87% (28648)	Yes	2.16E-02	8.26E-03	0.30	0.019*	0.26	0.019	0.019*
DSR	6.67% (2019)	Null	7.26E-04	4.52E-03	0.00	0.874	Null	Null	Null
SOX	5.47% (1713)	Yes	−2.16E-02	7.60E-03	0.34	0.012*	0.29	0.012	0.012*
Hemicellulose	27.50% (5140)	Null	2.19E-01	7.66E-01	0.01	0.779	Null	Null	Null
Starch	41.47% (7620)	Yes	2.99E+00	1.24E+00	0.27	0.028*	0.22	0.028	0.028*
Aromatics	1.00% (181)	Yes	2.74E-01	1.08E-01	0.29	0.021*	0.24	0.021	0.021*
Chintin	8.04% (1532)	Null	−1.07E+00	7.26E-01	0.12	0.159	Null	Null	Null
Lignin	0.03% (6)	Null	−2.60E-02	1.35E-02	0.19	0.072	Null	Null	Null
Cellulose	21.97% (4109)	Yes	−2.38E+00	1.01E+00	0.26	0.031*	0.21	0.031	0.031*
3HP/4HB	23.86% (26699)	Yes	−1.12E-02	3.96E-03	0.34	0.012*	0.29	0.012	0.012*
3HP	25.78% (28819)	Yes	−1.34E-02	3.73E-03	0.45	0.002**	0.41	0.002	0.002**
DC/4HB	36.16% (40311)	No, HtV	2.05E-02	7.41E-03	0.32	0.014*	0.28	0.029	0.029*
rTCA	45.55% (50766)	No, HtV	1.88E-02	7.46E-03	0.28	0.023*	0.24	0.046	0.046*
rAcCoA	10.89% (12227)	Yes	3.27E-02	1.06E-02	0.39	0.008**	0.31	0.008	0.008**
Calvin cycle	27.87% (31093)	Null	−3.55E-01	2.60E-01	0.10	0.191	Null	Null	Null

The relative abundances of gene function category were averaged for each site ($n = 18$). The variance explained (R^2), regression slope, and parametric *p*-value (*p*-param) of the linear regression, normality test, homogeneity test for variance, and permutation test *p* value (*p*-perm) with different weathering times were shown in the table (* indicates $p < 0.05$, ** indicates $p < 0.01$, and ***indicates $p < 0.001$). HmV, homogeneity of variance; HtV, heterogeneity of variance; p-sign, significance value of *p*.

We found an interesting phenomenon: the composition of gene abundances related to archaeal community, bacterial community, and element cycling is mostly related to the parent rock oxide ratio compared to the regolith oxide molecular ratio and physicochemical factors (Figure 5A). However, fungal community composition was insensitive to these environmental factors. In addition, the organic carbon content of the regolith was significantly correlated with the composition of archaeal and bacterial communities in the carbonatite regolith at different weathering times. Mantel analysis showed that the properties of the parent rock and the organic carbon content of the regolith may be important driving factors affecting the archaea and bacteria of the carbonate rock rind at different weathering times.

We used SEM to investigate the direct and indirect effects of functional genes related to cycling and microbial diversity in carbonate weathering regolith at different weathering times on the degree of carbonate weathering. We found that N cycle-related functional genes had significant direct positive effects on mobiles index and weathering strength. Meanwhile, the OC content of the weathering regolith has a significant direct positive effect on the mobiles index, but the mobiles index has a significant direct negative effect on the weathering strength (Figure 5B). In addition, N cycle-related functional genes had a significant direct negative effect on the Shannon diversity index, while the S cycle had a significant direct positive effect on the Shannon diversity index. Shannon diversity index had a significant direct positive effect on OC, while OC had a significant direct negative effect on C cycling, which had a direct negative effect on migration index (Figure 5B). SEM indicated that the differences in the abundance of N and S cycle-related functional genes may be the driving mechanism for the microbial diversity of carbonate rock rind at different weathering times. Additionally, the differences in the abundance

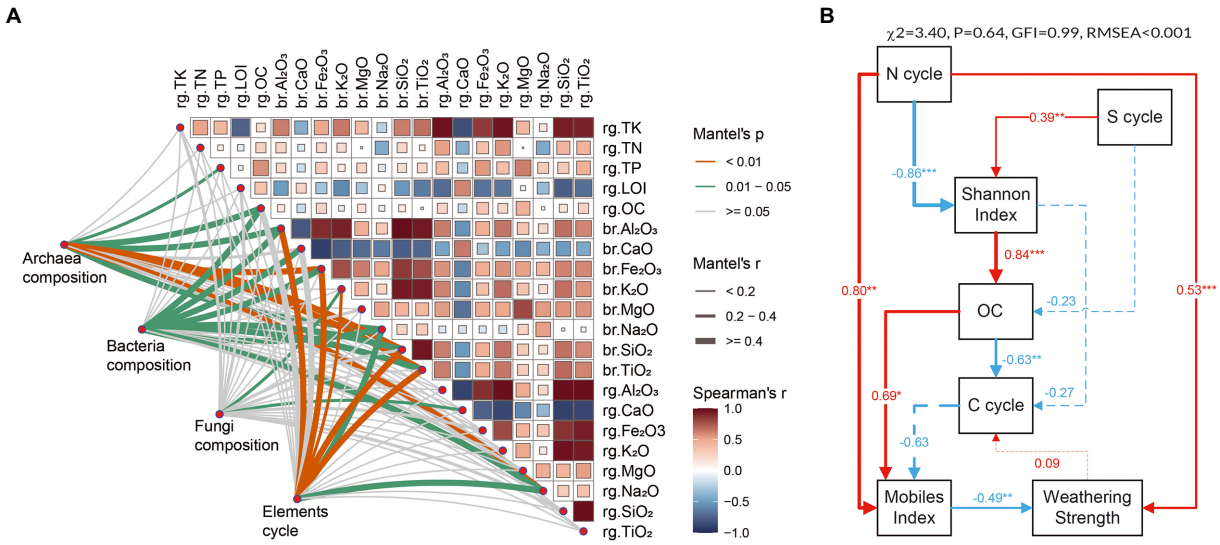

FIGURE 5
Biotic and abiotic drivers of microbial community composition and rock weathering. **(A)** Pairwise comparisons of environmental factors are shown, with a color gradient denoting spearman's correlation coefficints. Taxonomic and functional (based on biochemical KEGG Orthologs) genes composition was related to each environmental factor of Mantel tests. Edge width corresponds to the Mantel's r statistic for the corresponding distance correlations, and edge color denotes the statistical based on 9,999 permutations. **(B)** Structural equation modeling. The rg prefix indicates regolith and the br prefix indicates parent rock. Red and blue arrows represent positive and negative path coefficients, respectively, and dashed arrows represent non-significant paths (p>0.05). The path width is proportional to the absolute value of the path coefficients, and numbers are normalized path coefficients.

of functional genes related to the N cycle may also be the driving mechanism for the natural weathering of carbonate rocks.

Discussion

Variation characteristics of carbonate weathering rind taxa at different weathering times

Despite rapid temperature fluctuations and poor water availability on the rock surface, many species of microorganisms have colonized (Gaylarde et al., 2017a,b; Louati et al., 2020; Ding et al., 2021). In this study, the overall abundance of microbial taxa (about 21,270 on average) was lower than that in forest soils (about 4.6 million on average) and farmland soils (about 2.23 million on average; Yan et al., 2020). In addition, the Shannon index of microbial taxa decreased significantly with the increase of weathering time (Supplementary Figure S3). Previous studies have shown that the large temperature difference on the rock surface, poor energy source and nutrient availability, and strong ultraviolet radiation limit the colonization of microorganisms (Gorbushina, 2007; Miller et al., 2012), which may also lead to a lower abundance of microbial taxa in the carbonatite weathering rinds than in the soil. In addition, the total number of reads obtained in this study was slightly lower than those obtained in previous studies (Louati et al., 2020), which may be related to our sampling location. Our sampling position was perpendicular to the ground, which may not be conducive to microbial colonisation.

The number of individuals first increased and then decreased with weathering time, which is different from previous studies (Nemergut et al., 2007; Zumsteg et al., 2012). This change implies that factors affecting microbial taxa are not only related to weathering time but may also be related to the rock's parent rock composition, climatic conditions (Figure 6), nutrient status, and other factors (Lazzaro et al., 2009). In this study, bioreceptivity, total diversity, and organic carbon content were significantly positively correlated, and total diversity was significantly negatively correlated with weathering strength (Figure 7). This suggests that despite lower weathering, higher weathering rates recruit a greater variety of microorganisms, leading to higher organic carbon production rates (Figure 5B).

Regarding fungal communities, studies have shown that eukaryotic algal and fungal communities on rock surfaces tend to exhibit lower biodiversity compared to natural environments, but fungal communities on rock surfaces are more abundant and heterogeneous (Cutler et al., 2013a). Overall, the fungal community abundance decreased with weathering time. However, in the fungal community, the relative abundance of the r-strategist Ascomycota decreased significantly with weathering time, while the relative abundance of the K-strategist Basidiomycota increased significantly with weathering time; this finding is more consistent with our first hypothesis. In addition, the relative abundance of Mucoromycota also increased significantly with weathering time (Table 1), suggesting that Mucoromycota may be a K-strategist.

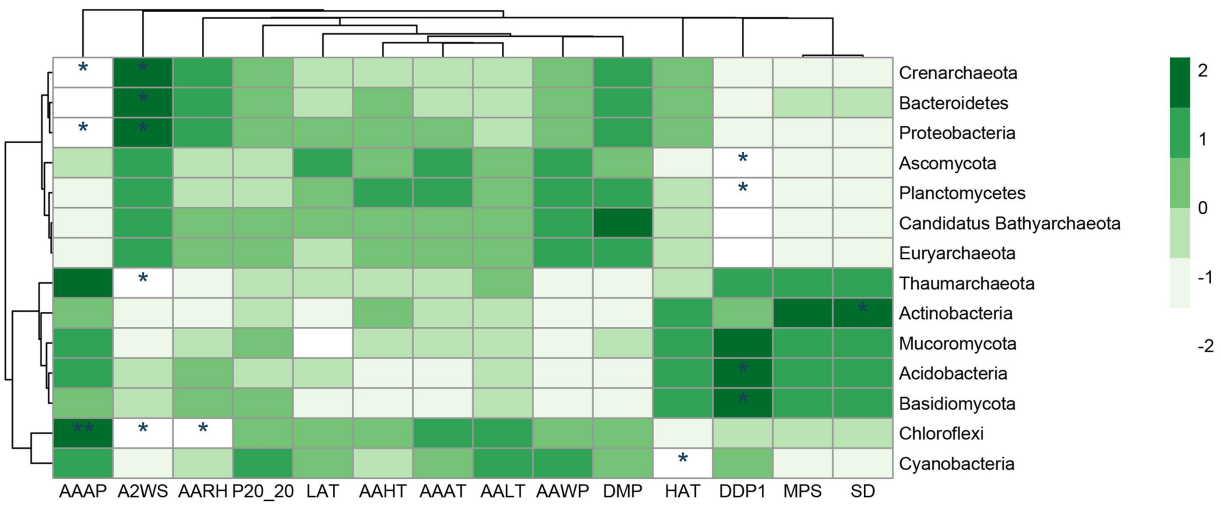

FIGURE 6
Correlation analysis between different taxa and meteorological data at phylum taxa level. AAAP, annual average atmospheric pressure (hPa); A2WS, average 2 min wind speed (m/s); AARH, annual average relative humidity (%); P20-20, recipitation of 20 p.m.–20 p.m. (mm); LAT, the lowest air temperature (°C); AAHT, annual average highest temperature (°C); AAAT, annual average air temperature (°C); AALT, annual average lowest temperature (°C); AAWP, annual average water pressure(hPa); DMP, daily maximum precipitation (mm); HAT, the highest temperature (°C); DDP1, Days with daily precipitation >=0.1 mm (d); MPS, monthly percentage of sunshine (%); SD, sunshine duration (h). *inidicates $p<0.05$, **inidicates $p<0.01$.

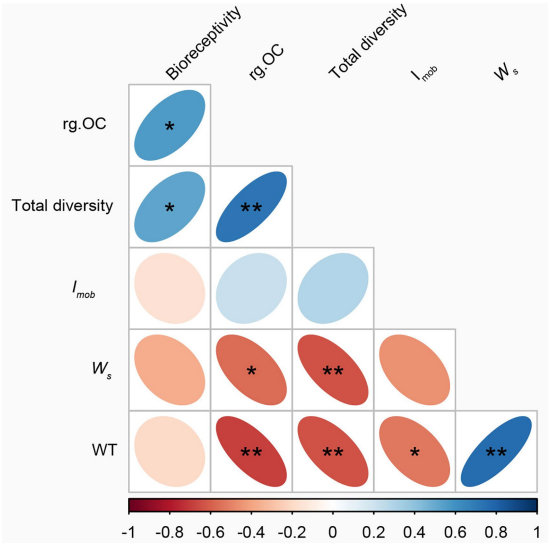

FIGURE 7
Correlation of weathering time with weathering degree, diversity index, and organic carbon. *$p < 0.05$, **$p < 0.01$.

Previous studies (Bastian et al., 2009) have shown that Ascomycota is usually suitable for living in barren environments, and is especially common as a pioneer species in the early succession; while in late succession, it is dominated by the environmental nutrient-dependent Basidiomycota. This may be because the environment is relatively barren in the early stage of carbonatite weathering, and it is more suitable for microbial colonization through nutrient enrichment in the later stage.

For bacterial communities, studies have shown that the selection of bacterial communities by petrochemical elements results in bacterial community structure driven by the chemical composition of minerals (Gleeson et al., 2006). In this study, the bacterial diversity index decreased significantly with increasing weathering time (Supplementary Figure S3). At the phylum level, the K-strategist Actinobacteria significantly increased with increasing carbonatite weathering time, while the r-strategic Proteobacteria decreased significantly with increasing weathering time (Table 1). Studies have shown that Proteobacteria are composed of a large number of phototrophs, photoheterotrophs, and chemolithotrophs, and are at an advantage in initial ecosystems with limited nutrient resources (Hodkinson et al., 2002). Actinobacteria play an important role in the decomposition of lignin and other refractory polymers (Heuer et al., 1997). In this study, Cyanobacteria, Planctomycetes, and Chloroflexi decreased significantly with weathering time, suggesting that they may be r-strategists. Cyanobacteria are photoautotrophs that form lichen symbionts with fungi and were the first to colonize bare rocks (Fermani et al., 2007). The increased C and N inputs of Cyanobacteria colonization provide an important prerequisite for the progressive succession of subsequent heterotrophs (Freeman et al., 2009).

For archaeal communities, most previous studies have reported that archaea are usually found in extreme environments (Bintrim et al., 1997; Chaban et al., 2006). Unlike bacteria and fungi, archaeal community diversity indices showed no significant change with weathering time (Supplementary Figure S3). However, Candidatus Bathyarchaeota, Crenarchaeota, and Euryarchaeota phyla decreased significantly with increasing weathering time (Table 1), which differs from previous studies. Crenarchaeota is usually a

K-strategist and is enriched in late succession, while Euryarchaeota is considered to be an r-strategist and is usually present in barren environments (Zumsteg et al., 2012). Crenarchaeota has been reported to be affected by organic carbon (Zinger et al., 2011). In this study, the organic carbon content was higher in the early stage of weathering than in the later stage, which may be one of the reasons why the abundance of Crenarchaeota in the early stage of weathering was higher than that in the later stage.

Variation characteristics of genes abundance related to C, N, and S cycling in carbonate rind at different weathering times

In this study, we found that the gene abundances of microbial taxa associated with carbonatite regolith C-cycle (the main taxa are Actinobacteria and Proteobacteria; Supplementary Figure S4A) and N-cycle (the main taxa are Actinobacteria, Proteobacteria and Cyanobacterial; Supplementary Figure S5A) increased with weathering time (Table 2), which supports our second hypothesis. The above conclusions are similar to those of the secondary succession process of plant communities (Blaud et al., 2018; Yan et al., 2020).

The abundance of C degradation-related genes decreased significantly with the increase in weathering time, which showed that the abundance of starch-related degradation genes (the main dominant taxa are *Acidobacteria bacterium, Chloroflex bacterium,* and *Kallotenue* sp., see Supplementary Figure S7B) increased significantly, while the abundance of cellulose degradation-related genes (the main dominant taxa is *Acidobacteria bacterium* and *Cellulomonas sp.*, see Supplementary Figure S8B) gradually decreased significantly. This implies that during the carbonatite weathering process, the microbial niche of the carbonatite weathering crust differentiated, and the carbon source for microbial carbon degradation changed from a difficult-to-decompose carbon source (cellulose) to an easily-decomposable carbon source (starch).

In C fixation, both rTCA and rAcCoA increased significantly with weathering time, and the rTCA cycle pathway to fix CO_2 taxa usually exists in anaerobic and sulfur-rich extreme habitats (Campbell and Cary, 2004). In this study, the main taxa of the rTCA cycle pathway were Actinobacteria (mainly include Rubrobacteraceae and Pseudonocardiaceae, see Supplementary Figure S9B), Proteobacteria, Acidobacteria, and Cyanobacteria (Supplementary Figure S9A), which was consistent with previous studies (Hall et al., 2008). In the maize rhizosphere microbial community, *Rhodopseudomonas* and *Stappia* may be the main groups for carbon dioxide fixation through the rAcCoA pathway (Li et al., 2014). In this study, the main taxa in the rAcCoA pathway were Rubrobacteraceae and Pseudonocardiaceae (Supplementary Figure S10). In addition, *Rubrobacter radiotolerans*, which belong to Rubrobacteraceae was γ-irradiation and moderate thermophiles (Suzuki, 2015). Pseudonocardiaceae were found to be the main dominant taxa in the biological degradation of stony artifacts (Stomeo et al., 2008, 2009). Further, 3HP and 3HP/4HB decreased significantly with the increase in weathering time. The main group of 3HP has been reported as *Chloroflexus aurantiacus* (Holo, 1989). Previous studies have shown that 3HP is the main carbon fixation method in oolites (Diaz et al., 2014). The main taxa in the 3HP/4HB pathway are Crenarchaeota and Thaumarchaeota (Bergauer et al., 2013). To sum up, the types of microorganisms involved in the C fixation in carbonatite rock rind are similar to those in the previous studies, which are in line with their respective ecological amplitudes.

N is an essential component of all living things, and its availability depends on the various nitrogen conversion reactions carried out by microorganisms (Kuypers et al., 2018). For N cycling, nitrification, and denitrification decreased significantly with increasing weathering time, which may be related to nutrient availability (Sun and Badgley, 2019). The S-cycle related functional genes did not change significantly with the increase of weathering time, and the main taxa was Sphingomonadaceae and Rubrobacteraceae (Supplementary Figure S6).

Sphingomonadaceae and Rubrobacteraceae were more common on the surfaces of gravestones in all weathering time periods and were closely related to C, N and S cycle processes. Sphingomonadaceae are widespread in almost all types of natural environments and are usually Gram-negative bacteria, mostly containing carotenoids, which are yellow in their natural environment (Glaeser and Kämpfer, 2014). Some genera of Sphingomonadaceae (e.g., *Blastomonas*, *Sandaracinobacter*, etc.) are facultative prototrophs (Glaeser and Kämpfer, 2014). Bacteria able to produce growth factors are called prototrophs (D'Souza et al., 2018; Soto-Martin et al., 2020). These properties suggest that Sphingomonadaceae may be autotrophic and able to survive in extreme environments (e.g., rocky surfaces, polluted water bodies, etc.). In addition, some genera of the Sphingomonadaceae (e.g., *Sphingomonas*) have been found to have nitrogen-fixing functions. Besides, Several species of the genus *Rubrobacter* (Rubrobacteraceae) can tolerate extremely high levels of ionizing radiation and are moderately thermophilic or thermophilic (Albuquerque and da Costa, 2014). These species were primarily isolated mainly from deteriorated stone artefacts. In addition, as well as isolated from arid soils and dry, discolored, and sun-exposed walls (Albuquerque and da Costa, 2014). The species characteristics of Rubrobacteraceae described above all suggest that Rubrobacteraceae are suited to survive in arid, nutrient-poor environments and it is not surprising that they have been found to colonise the surface of tombstones in large numbers.

Conclusion

This study provides new insights into how the ecological succession strategies and functional gene changes of bacterial, archaeal, and fungal communities vary with the time of carbonatite weathering. We have three main conclusions. First, during the weathering of carbonatite over time, microbial taxa gradually shifted from r-strategists to K-strategists, and the abundance of functional genes related to C and N was gradually

increased. Secondly, the properties of carbonatite parent rock determine the colonization and distribution of microorganisms. In the early stage of carbonatite weathering, the weathering potential is large, the weathering rate is fast, and the weathering degree is small. Therefore, in the early stage, there are many kinds of microorganisms, but the abundance of genes related to element cycling is small, and the rate of environmental modification is fast, while the opposite is true in the later stage of weathering. Thirdly, the increase in the abundance of genes related to the N cycle promotes an increase in carbonatite weathering degree and drives the succession of carbonatite rock rind microorganisms. In summary, this study provides a coupling mechanism between carbonatite weathering rind microorganisms and potential functional genes during succession, and at the same time, we also reveal the coupling mechanism between carbonatite weathering degrees and potential functional genes.

Data availability statement

The datasets presented in this study can be found in online repositories. The 36 Sequence data associated with this project have been deposited in the NCBI Short Read Archive database (Accession Number: PRJNA848062). The names of the repository/repositories and accession number(s) can be found in the article/Supplementary material.

Author contributions

LYu conceived the project. JC, FL, XZ, YW, LZ, and LYan collected samples in the field. JC, FL, XZ and LYan performed data analysis; JC, FL, XZ, and YW performed the experiment. JC and LYu wrote the manuscript. All authors contributed to the article and approved the submitted version.

Funding

This work was supported by the Project of National Key Research and Development Program of China (2016YFC0502604); Construction Program of Biology First-class Discipline in Guizhou (GNYL[2017]009); the Postgraduate Education Innovation Program in Guizhou Province (grant number YJSKYJJ[2021]079); and the Natural Science Research Project of Guizhou Provincial Department of Education (Qian Jiao He KY Zi [2018]170).

Acknowledgments

We are grateful to the three reviewers for their constructive comments on this paper, which have greatly improved it. We would like to thank Shiyang Yao, Zhilin Chen, Kun Nie and Daqing Liang for their enthusiastic help. In addition, Jin Chen wants to thank, in particular, the patience, care and support from Yan Yao over the past 9 years.

Conflict of interest

The authors declare that the research was conducted in the absence of any commercial or financial relationships that could be construed as a potential conflict of interest.

Publisher's note

All claims expressed in this article are solely those of the authors and do not necessarily represent those of their affiliated organizations, or those of the publisher, the editors and the reviewers. Any product that may be evaluated in this article, or claim that may be made by its manufacturer, is not guaranteed or endorsed by the publisher.

Supplementary material

The Supplementary material for this article can be found online at: https://www.frontiersin.org/articles/10.3389/fmicb.2022.1024672/full#supplementary-material

References

Albuquerque, L., and da Costa, M. S. (2014). "The family Rubrobacteraceae," in *The prokaryotes: Actinobacteria*. eds. E. Rosenberg, E. F. DeLong, S. Lory, E. Stackebrandt and F. Thompson (Berlin, Heidelberg: Springer Berlin Heidelberg)

Bao, S. (2000). *Soil and Agricultural Chemistry Analysis*. Beijing: China Agriculture Press Co., Ltd.

Bardgett, R. D., Bowman, W. D., Kaufmann, R., and Schmidt, S. K. (2005). A temporal approach to linking aboveground and belowground ecology. *Trends Ecol. Evol.* 20, 634–641. doi: 10.1016/j.tree.2005.08.005

Bastian, F., Bouziri, L., Nicolardot, B., and Ranjard, L. (2009). Impact of wheat straw decomposition on successional patterns of soil microbial community structure. *Soil Biol. Biochem.* 41, 262–275. doi: 10.1016/j.soilbio.2008.10.024

Bergauer, K., Sintes, E., van Bleijswijk, J., Witte, H., and Herndl, G. J. (2013). Abundance and distribution of archaeal acetyl-CoA/propionyl-CoA carboxylase genes indicative for putatively chemoautotrophic archaea in the tropical Atlantic's interior. *FEMS Microbiol. Ecol.* 84, 461–473. doi: 10.1111/1574-6941.12073

Bintrim, S. B., Donohue, T. J., Handelsman, J., Roberts, G. P., and Goodman, R. M. (1997). Molecular phylogeny of archaea from soil. *Proc. Natl. Acad. Sci. U. S. A.* 94, 277–282. doi: 10.1073/pnas.94.1.277

Blaud, A., van der Zaan, B., Menon, M., Lair, G. J., Zhang, D. Y., Huber, P., et al. (2018). The abundance of nitrogen cycle genes and potential greenhouse gas fluxes depends on land use type and little on soil aggregate size. *Appl. Soil Ecol.* 125, 1–11. doi: 10.1016/j.apsoil.2017.11.026

Buchfink, B., Xie, C., and Huson, D. H. (2015). Fast and sensitive protein alignment using DIAMOND. *Nat. Methods* 12, 59–60. doi: 10.1038/nmeth.3176

Campbell, B. J., and Cary, S. C. (2004). Abundance of reverse tricarboxylic acid cycle genes in free-living microorganisms at deep-sea hydrothermal vents. *Appl. Environ. Microbiol.* 70, 6282–6289. doi: 10.1128/AEM.70.10.6282-6289.2004

Chaban, B., Ng, S. Y., and Jarrell, K. F. (2006). Archaeal habitats--from the extreme to the ordinary. *Can. J. Microbiol.*, 52 73–116. doi: 10.1139/w05-147

Checcucci, A., Borruso, L., Petrocchi, D., and Perito, B. (2022). Diversity and metabolic profile of the microbial communities inhabiting the darkened white marble of Florence Cathedral. *Int. Biodeterior. Biodegrad.* 171:105420. doi: 10.1016/j.ibiod.2022.105420

Chen, S., Zhou, Y., Chen, Y., and Gu, J. (2018). Fastp: an ultra-fast all-in-one FASTQ preprocessor. *Bioinformatics* 34, i884–i890. doi: 10.1093/bioinformatics/bty560

Chen, Y. L., Chen, L. Y., Peng, Y. F., Ding, J. Z., Li, F., Yang, G. B., et al. (2016). Linking microbial C:N:P stoichiometry to microbial community and abiotic factors along a 3500-km grassland transect on the Tibetan Plateau. *Glob. Ecol. Biogeogr.*, 25 1416–1427. doi: 10.1111/geb.12500

Cutler, N. A., Oliver, A. E., Viles, H. A., Ahmad, S., and Whiteley, A. S. (2013a). The characterisation of eukaryotic microbial communities on sandstone buildings in Belfast, UK, using TRFLP and 454 pyrosequencing. *Int. Biodeterior. Biodegrad.* 82, 124–133. doi: 10.1016/j.ibiod.2013.03.010

Cutler, N. A., Viles, H. A., Ahmad, S., McCabe, S., and Smith, B. J. (2013b). Algal 'greening' and the conservation of stone heritage structures. *Sci. Total Environ.* 442, 152–164. doi: 10.1016/j.scitotenv.2012.10.050

D'Souza, G., Shitut, S., Preussger, D., Yousif, G., Waschina, S., and Kost, C. (2018). Ecology and evolution of metabolic cross-feeding interactions in bacteria. *Nat. Prod. Rep.* 35, 455–488. doi: 10.1039/c8np00009c

Diaz, M. R., Van Norstrand, J. D., Eberli, G. P., Piggot, A. M., Zhou, J., and Klaus, J. S. (2014). Functional gene diversity of oolitic sands from great Bahama Bank. *Geobiology* 12, 231–249. doi: 10.1111/gbi.12079

Ding, X., Lan, W., Li, Y., Yan, A., Katayama, Y., Koba, K., et al. (2021). An internal recycling mechanism between ammonia/ammonium and nitrate driven by ammonia-oxidizing archaea and bacteria (AOA, AOB, and Comammox). and DNRA on Angkor sandstone monuments. *Int. Biodeterior. Biodegrad.* 165:105328. doi: 10.1016/j.ibiod.2021.105328

Emmanuel, S., and Levenson, Y. (2014). Limestone weathering rates accelerated by micron-scale grain detachment. *Geology* 42, 751–754. doi: 10.1130/G35815.1

Fermani, P., Mataloni, G., and Van de Vijver, B. (2007). Soil microalgal communities on an Antarctic active volcano (Deception Island, south Shetlands). *Polar Biol.* 30, 1381–1393. doi: 10.1007/s00300-007-0299-6

Fierer, N., Bradford, M. A., and Jackson, R. B. (2007). Toward an ecological classification of soil bacteria. *Ecology* 88, 1354–1364. doi: 10.1890/05-1839

Ford, D., and Williams, P. D. (2013). *Karst Hydrogeology and Geomorphology*. New York John Wiley & Sons.

Freeman, K. R., Pescador, M. Y., Reed, S. C., Costello, E. K., Robeson, M. S., and Schmidt, S. K. (2009). Soil CO2 flux and photoautotrophic community composition in high-elevation, 'barren' soil. *Environ. Microbiol.* 11, 674–686. doi: 10.1111/j.1462-2920.2008.01844.x

Fu, L., Niu, B., Zhu, Z., Wu, S., and Li, W. (2012). CD-HIT: accelerated for clustering the next-generation sequencing data. *Bioinformatics* 28, 3150–3152. doi: 10.1093/bioinformatics/bts565

Gadd, G. M. (2017). Geomicrobiology of the built environment. *Nat. Microbiol.* 2:16275. doi: 10.1038/nmicrobiol.2016.275

Gaylarde, C., Baptista-Neto, J. A., Ogawa, A., Kowalski, M., Celikkol-Aydin, S., and Beech, I. (2017a). Epilithic and endolithic microorganisms and deterioration on stone church facades subject to urban pollution in a sub-tropical climate. *Biofouling* 33, 113–127. doi: 10.1080/08927014.2016.1269893

Gaylarde, C., Ogawa, A., Beech, I., Kowalski, M., and Baptista-Neto, J. A. (2017b). Analysis of dark crusts on the church of Nossa Senhora do Carmo in Rio de Janeiro, Brazil, using chemical, microscope and metabarcoding microbial identification techniques. *Int. Biodeterior. Biodegrad.* 117, 60–67. doi: 10.1016/j.ibiod.2016.11.028

Gaylarde, P. M., and Gaylarde, C. C. (2004). Deterioration of siliceous stone monuments in Latin America: microorganisms and mechanisms. *Corros. Rev.* 22, 395–416. doi: 10.1515/CORRREV.2004.22.5-6.395

Glaeser, S. P., and Kämpfer, P. (2014). "The family Sphingomonadaceae," in *The Prokaryotes: Alphaproteobacteria and Betaproteobacteria*. eds. E. Rosenberg, E. F. DeLong, S. Lory, E. Stackebrandt and F. Thompson (Berlin, Heidelberg: Springer Berlin Heidelberg)

Gleeson, D. B., Kennedy, N. M., Clipson, N., Melville, K., Gadd, G. M., and McDermott, F. P. (2006). Characterization of bacterial community structure on a weathered pegmatitic granite. *Microb. Ecol.* 51, 526–534. doi: 10.1007/s00248-006-9052-x

Gorbushina, A. A. (2007). Life on the rocks. *Environ. Microbiol.* 9, 1613–1631. doi: 10.1111/j.1462-2920.2007.01301.x

Guillitte, O. (1995). Bioreceptivity: a new concept for building ecology studies. *Sci. Total Environ.* 167, 215–220. doi: 10.1016/0048-9697(95)04582-L

Hall, J. R., Mitchell, K. R., Jackson-Weaver, O., Kooser, A. S., Cron, B. R., Crossey, L. J., et al. (2008). Molecular characterization of the diversity and distribution of a thermal spring microbial community by using rRNA and metabolic genes. *Appl. Environ. Microbiol.* 74, 4910–4922. doi: 10.1128/AEM.00233-08

Heuer, H., Krsek, M., Baker, P., Smalla, K., and Wellington, E. M. (1997). Analysis of actinomycete communities by specific amplification of genes encoding 16S rRNA and gel-electrophoretic separation in denaturing gradients. *Appl. Environ. Microbiol.* 63, 3233–3241. doi: 10.1128/aem.63.8.3233-3241.1997

Hodkinson, I. D., Webb, N. R., and Coulson, S. J. (2002). Primary community assembly on land-the missing stages: why are the heterotrophic organisms always there first? *J. Ecol.* 90, 569–577. doi: 10.1046/j.1365-2745.2002.00696.x

Holo, H. (1989). Chloroflexus aurantiacus secretes 3-hydroxypropionate, a possible intermediate in the assimilation of CO2 and acetate. *Arch. Microbiol.* 151, 252–256. doi: 10.1007/BF00413138

Huang, Z., Zhang, W., Chen, J., Liu, R., and Li, Z. (1996). *Red Weathering Crust in Southern China* Beijing: China Ocean Press.

Irfan, T. (1996). Mineralogy, fabric properties and classification of weathered granites in Hong Kong. *Q. J. Eng. Geol. Hydrogeol.* 29, 5–35. doi: 10.1144/GSL.QJEGH.1996.029.P1.02

Jha, N., Saggar, S., Giltrap, D., Tillman, R., and Deslippe, J. (2017). Soil properties impacting denitrifier community size, structure, and activity in New Zealand dairy-grazed pasture. *Biogeosciences* 14, 4243–4253. doi: 10.5194/bg-14-4243-2017

Jones, R. J. (1965). Aspects of the biological weathering of limestone pavement. *Proc. Geol. Assoc.* 76:421-IN8. doi: 10.1016/S0016-7878(65)80041-4

Kaiser, C., Franklin, O., Dieckmann, U., and Richter, A. (2014). Microbial community dynamics alleviate stoichiometric constraints during litter decay. *Ecol. Lett.* 17, 680–690. doi: 10.1111/ele.12269

Kusumi, A., Li, X., Osuga, Y., Kawashima, A., Gu, J. D., Nasu, M., et al. (2013). Bacterial communities in pigmented biofilms formed on the sandstone bas-relief walls of the Bayon Temple, Angkor Thom. *Cambodia. Microbes Environ.* 28, 422–431. doi: 10.1264/jsme2.me13033

Kusumi, A., Li, X. S., and Katayama, Y. (2011). Mycobacteria isolated from angkor monument sandstones grow chemolithoautotrophically by oxidizing elemental sulfur. *Front. Microbiol.* 2:104. doi: 10.3389/fmicb.2011.00104

Kuypers, M. M. M., Marchant, H. K., and Kartal, B. (2018). The microbial nitrogen-cycling network. *Nat. Rev. Microbiol.* 16, 263–276. doi: 10.1038/nrmicro.2018.9

Lazzaro, A., Abegg, C., and Zeyer, J. (2009). Bacterial community structure of glacier forefields on siliceous and calcareous bedrock. *Eur. J. Soil Sci.* 60, 860–870. doi: 10.1111/j.1365-2389.2009.01182.x

Levenson, Y., and Emmanuel, S. (2016). Quantifying micron-scale grain detachment during weathering experiments on limestone. *Geochim. Cosmochim. Acta* 173, 86–96. doi: 10.1016/j.gca.2015.10.024

Li, D., Liu, C. M., Luo, R., Sadakane, K., and Lam, T. W. (2015). MEGAHIT: an ultra-fast single-node solution for large and complex metagenomics assembly via succinct de Bruijn graph. *Bioinformatics* 31, 1674–1676. doi: 10.1093/bioinformatics/btv033

Li, R., Li, Y., Kristiansen, K., and Wang, J. (2008). SOAP: short oligonucleotide alignment program. *Bioinformatics* 24, 713–714. doi: 10.1093/bioinformatics/btn025

Li, X., Rui, J., Xiong, J., Li, J., He, Z., Zhou, J., et al. (2014). Functional potential of soil microbial communities in the maize rhizosphere. *PLoS One* 9:e112609. doi: 10.1371/journal.pone.0112609

Liu, X., Koestler, R. J., Warscheid, T., Katayama, Y., and Gu, J.-D. (2020). Microbial deterioration and sustainable conservation of stone monuments and buildings. *Nat Sustain* 3, 991–1004. doi: 10.1038/s41893-020-00602-5

Liu, Y. B., Zhao, L. N., Wang, Z. R., Liu, L. C., Zhang, P., Sun, J. Y., et al. (2018). Changes in functional gene structure and metabolic potential of the microbial community in biological soil crusts along a revegetation chronosequence in the Tengger Desert. *Soil Biol. Biochem.* 126, 40–48. doi: 10.1016/j.soilbio.2018.08.012

Liu, Z., Zhu, H., Wu, M., Li, Y., Cao, H., and Rong, R. (2022). Seasonal dynamics of airborne culturable fungi and its year-round diversity monitoring in Dahuting Han dynasty tomb of China. *Sci. Total Environ.* 838:155990. doi: 10.1016/j.scitotenv.2022.155990

Louati, M., Ennis, N. J., Ghodhbane-Gtari, F., Hezbri, K., Sevigny, J. L., Fahnestock, M. F., et al. (2020). Elucidating the ecological networks in stone-dwelling microbiomes. *Environ. Microbiol.* 22, 1467–1480. doi: 10.1111/1462-2920.14700

MacArthur, R. H. (1960). On the relative abundance of species. *Am. Nat.* 94, 25–36. doi: 10.1086/282106

MacArthur, R. H., and Wilson, E. O. (1967). *The Theory of Island Biogeography*. Princeton: Princeton University Press.

McMurdie, P. J., and Holmes, S. (2014). Waste not, want not: why rarefying microbiome data is inadmissible. *PLoS Comp. Biol.* 10:e1003531. doi: 10.1371/journal.pcbi.1003531

Meng, H., Katayama, Y., and Gu, J.-D. (2017). More wide occurrence and dominance of ammonia-oxidizing archaea than bacteria at three Angkor sandstone temples of Bayon, Phnom Krom and wat Athvea in Cambodia. *Int. Biodeterior. Biodegrad.* 117, 78–88. doi: 10.1016/j.ibiod.2016.11.012

Meng, H., Luo, L., Chan, H. W., Katayama, Y., and Gu, J.-D. (2016). Higher diversity and abundance of ammonia-oxidizing archaea than bacteria detected at the Bayon Temple of Angkor Thom in Cambodia. *Int. Biodeterior. Biodegrad.* 115, 234–243. doi: 10.1016/j.ibiod.2016.08.021

Miller, A. Z., Sanmartín, P., Pereira-Pardo, L., Dionísio, A., Saiz-Jimenez, C., Macedo, M. F., et al. (2012). Bioreceptivity of building stones: a review. *Sci. Total Environ.* 426, 1–12. doi: 10.1016/j.scitotenv.2012.03.026

Nemergut, D. R., Anderson, S. P., Cleveland, C. C., Martin, A. P., Miller, A. E., Seimon, A., et al. (2007). Microbial community succession in an unvegetated, recently deglaciated soil. *Microb. Ecol.* 53, 110–122. doi: 10.1007/s00248-006-9144-7

Noguchi, H., Park, J., and Takagi, T. (2006). MetaGene: prokaryotic gene finding from environmental genome shotgun sequences. *Nucleic Acids Res.* 34, 5623–5630. doi: 10.1093/nar/gkl723

Odum, E. P. (1969). The strategy of ecosystem development: an understanding of ecological succession provides a basis for resolving man's conflict with nature. *Science* 164, 262–270. doi: 10.1126/science.164.3877.262

Page, A. L. (1982). *Methods of Soil Analysis. Part 2. Chemical and Microbiological Properties*, *2nd edn.*. Madison, Wisconsin USA: American Society of Agronomy, Inc. and Soil Science Society of America, Inc..

Piñar, G., Garcia-Valles, M., Gimeno-Torrente, D., Fernandez-Turiel, J. L., Ettenauer, J., and Sterflinger, K. (2013). Microscopic, chemical, and molecular-biological investigation of the decayed medieval stained window glasses of two Catalonian churches. *Int. Biodeterior. Biodegradation* 84, 388–400. doi: 10.1016/j.ibiod.2012.02.008

Ren, Y., Yu, G., Shi, C., Liu, L., Guo, Q., Han, C., et al. (2022). Majorbio cloud: a one-stop, comprehensive bioinformatic platform for multiomics analyses. *iMeta* 1:e12. doi: 10.1002/imt2.12

Rogers, J. R., and Bennett, P. C. (2004). Mineral stimulation of subsurface microorganisms: release of limiting nutrients from silicates. *Chem. Geol.* 203, 91–108. doi: 10.1016/j.chemgeo.2003.09.001

Rösch, C., and Bothe, H. (2005). Improved assessment of denitrifying, N2-fixing, and total-community bacteria by terminal restriction fragment length polymorphism analysis using multiple restriction enzymes. *Appl. Environ. Microbiol.* 71, 2026–2035. doi: 10.1128/aem.71.4.2026-2035.2005

Rosseel, Y. (2012). Lavaan: an R package for structural equation modeling. *J. Stat. Softw.* 48, 1–36. doi: 10.18637/jss.v048.i02

Saheb, M., Chabas, A., Mertz, J. D., Colas, E., Rozenbaum, O., Sizun, J. P., et al. (2016). Weathering of limestone after several decades in an urban environment. *Corros. Sci.* 111, 742–752. doi: 10.1016/j.corsci.2016.06.015

Sáiz-Jiménez, C. (1999). Biogeochemistry of weathering processes in monuments. *Geomicrobiol J.* 16, 27–37. doi: 10.1080/014904599270721

Salvadori, O., and Municchia, A. C. (2016). The role of fungi and lichens in the biodeterioration of stone monuments. *The Open Conf. Proc. J.* 7, 39–54. doi: 10.2174/2210289201607020039

Šimonovičová, A., Gódyová, M., and Ševc, J. (2004). Airborne and soil microfungi as contaminants of stone in a hypogean cemetery. *Int. Biodeterior. Biodegrad.* 54, 7–11. doi: 10.1016/j.ibiod.2003.11.004

Soto-Martin, E. C., Warnke, I., Farquharson, F. M., Christodoulou, M., Horgan, G., Derrien, M., et al. (2020). Vitamin biosynthesis by human gut butyrate-producing bacteria and cross-feeding in synthetic microbial communities. *MBio* 11:e00886-20. doi: 10.1128/mBio.00886-20

Stomeo, F., Portillo, M. C., and Gonzalez, J. M. (2009). Assessment of bacterial and fungal growth on natural substrates: consequences for preserving caves with prehistoric paintings. *Curr. Microbiol.* 59, 321–325. doi: 10.1007/s00284-009-9437-4

Stomeo, F., Portillo, M. C., Gonzalez, J. M., Laiz, L., and Saiz-Jimenez, C. (2008). Pseudonocardia in white colonizations in two caves with Paleolithic paintings. *Int. Biodeterior. Biodegrad.* 62, 483–486. doi: 10.1016/j.ibiod.2007.12.011

Sun, S., and Badgley, B. D. (2019). Changes in microbial functional genes within the soil metagenome during forest ecosystem restoration. *Soil Biol. Biochem.* 135, 163–172. doi: 10.1016/j.soilbio.2019.05.004

Suzuki, K. i. (2015). *Rubrobacter, Bergey's Manual of Systematics of Archaea and Bacteria*, New York John Wiley & Sons

Vázquez-Nion, D., Silva, B., and Prieto, B. (2018). Influence of the properties of granitic rocks on their bioreceptivity to subaerial phototrophic biofilms. *Sci. Total Environ.* 610-611, 44–54. doi: 10.1016/j.scitotenv.2017.08.015

Warscheid, T., and Braams, J. (2000). Biodeterioration of stone: a review. *Int. Biodeterior. Biodegrad.* 46, 343–368. doi: 10.1016/S0964-8305(00)00109-8

Wei, Y., Wu, D., Wei, D., Zhao, Y., Wu, J., Xie, X., et al. (2019). Improved lignocellulose-degrading performance during straw composting from diverse sources with actinomycetes inoculation by regulating the key enzyme activities. *Bioresour. Technol.* 271, 66–74. doi: 10.1016/j.biortech.2018.09.081

Weiss, S., Xu, Z. Z., Peddada, S., Amir, A., Bittinger, K., Gonzalez, A., et al. (2017). Normalization and microbial differential abundance strategies depend upon data characteristics. *Microbiome* 5, 27–18. doi: 10.1186/s40168-017-0237-y

Wu, F., Zhang, Y., Gu, J.-D., He, D., Zhang, G., Liu, X., et al. (2022). Community assembly, potential functions and interactions between fungi and microalgae associated with biodeterioration of sandstone at the Beishiku Temple in Northwest China. *Sci. Total Environ.* 835:155372. doi: 10.1016/j.scitotenv.2022.155372

Yan, B., Sun, L., Li, J., Liang, C., Wei, F., Xue, S., et al. (2020). Change in composition and potential functional genes of soil bacterial and fungal communities with secondary succession in Quercus liaotungensis forests of the loess plateau, western China. *Geoderma* 364:114199. doi: 10.1016/j.geoderma.2020.114199

Zechmeister-Boltenstern, S., Keiblinger, K. M., Mooshammer, M., Peñuelas, J., Richter, A., Sardans, J., et al. (2015). The application of ecological stoichiometry to plant–microbial–soil organic matter transformations. *Ecol. Monogr.* 85, 133–155. doi: 10.1890/14-0777.1

Zha, J., Wei, S., Wang, C., Li, Z., Cai, Y., and Ma, Q. (2020). Weathering mechanism of red discolorations on limestone object: a case study from Lingyan Temple, Jinan, Shandong Province, China. *Heritage Sci.* 8:54. doi: 10.1186/s40494-020-00394-z

Zhou, Z., Wang, C., Jiang, L., and Luo, Y. (2017). Trends in soil microbial communities during secondary succession. *Soil Biol. Biochem.* 115, 92–99. doi: 10.1016/j.soilbio.2017.08.014

Zinger, L., Lejon, D. P., Baptist, F., Bouasria, A., Aubert, S., et al. (2011). Contrasting diversity patterns of crenarchaeal, bacterial and fungal soil communities in an alpine landscape. *PLoS One* 6:e19950. doi: 10.1371/journal.pone.0019950

Zumsteg, A., Luster, J., Göransson, H., Smittenberg, R. H., Brunner, I., Bernasconi, S. M., et al. (2012). Bacterial, archaeal and fungal succession in the forefield of a receding glacier. *Microb. Ecol.* 63, 552–564. doi: 10.1007/s00248-011-9991-8

Frontiers in Microbiology

Explores the habitable world and the potential of microbial life

The largest and most cited microbiology journal which advances our understanding of the role microbes play in addressing global challenges such as healthcare, food security, and climate change.

Discover the latest Research Topics

See more →

Frontiers

Avenue du Tribunal-Fédéral 34
1005 Lausanne, Switzerland
frontiersin.org

Contact us

+41 (0)21 510 17 00
frontiersin.org/about/contact